

Copper-catalyzed Enantioselective Allylic Substitutions and Conjugate Additions Promoted by Chiral Sulfonate- or Alkoxy-containing N-heterocyclic Carbenes:

Author: Ying Shi

Persistent link: <http://hdl.handle.net/2345/bc-ir:107648>

This work is posted on [eScholarship@BC](#),
Boston College University Libraries.

Boston College Electronic Thesis or Dissertation, 2017

Copyright is held by the author, with all rights reserved, unless otherwise noted.

Boston College
The Graduate School of Arts and Sciences
Department of Chemistry

**COPPER-CATALYZED ENANTIOSELECTIVE ALLYLIC
SUBSTITUTIONS AND CONJUGATE ADDITIONS
PROMOTED BY CHIRAL SULFONATE- OR ALKOXY-
CONTAINING N-HETEROCYCLIC CARBENES**

A Dissertation

By

YING SHI

Submitted in partial fulfillment of the requirements

For the degree of

Doctor of Philosophy

Nov 2017

©copyright by YING SHI

2017

**COPPER-CATALYZED ENANTIOSELECTIVE ALLYLIC
SUBSTITUTIONS AND CONJUGATE ADDITIONS
PROMOTED BY CHIRAL SULFONATE- OR ALKOXY-
CONTAINING N-HETEROCYCLIC CARBENES**

Ying Shi

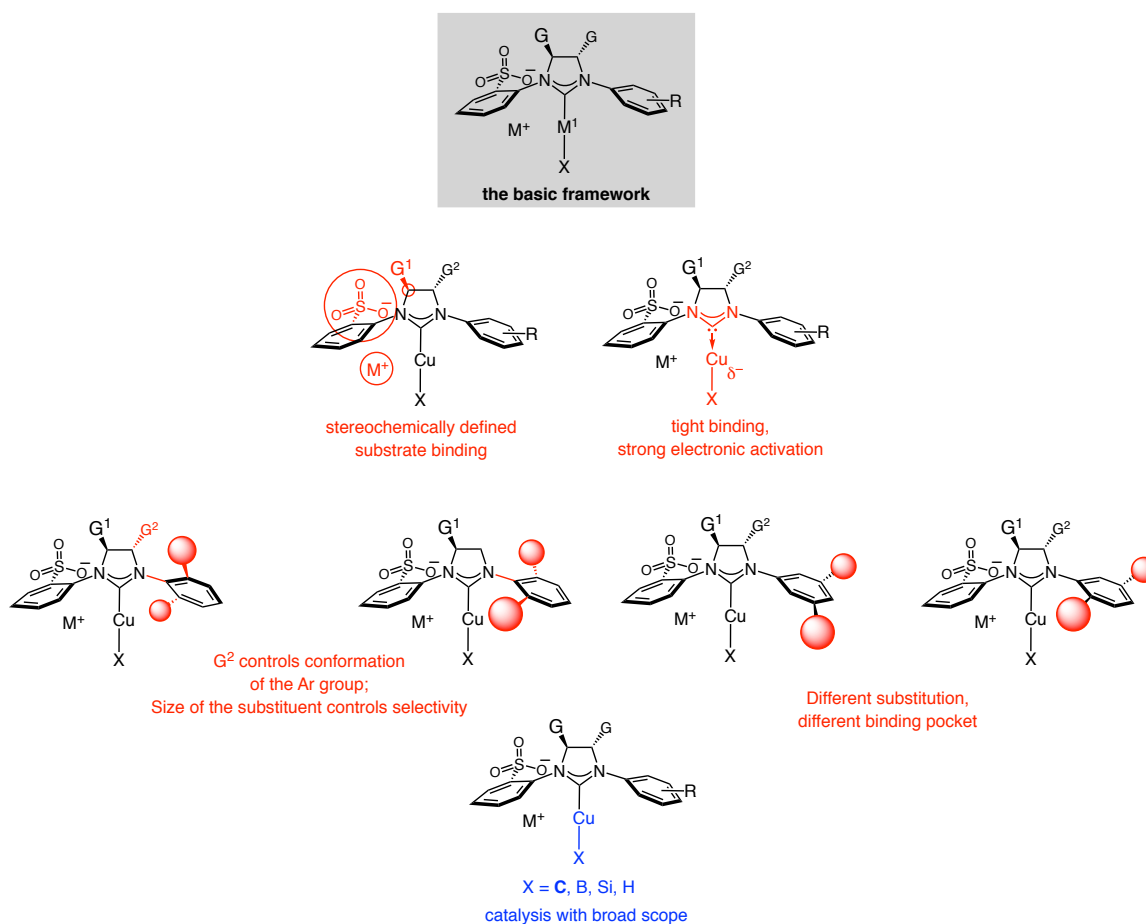
Thesis Advisor: Professor Amir H. Hoveyda

Abstract

■ **Chapter 1. A Review of Sulfonate-Containing NHC Ligands in Copper-Catalyzed Enantioselective Transformations—Maneuvering Selectivities in Tight Space.** A comprehensive review of enantioselective copper-catalyzed transformations, which are promoted by a chiral N-heterocyclic carbene metal complex that features a unique sulfonate motif, is provided in this chapter. Reactions have been categorized into four sets: allylic substitutions conjugate additions, Cu-B additions alkenes and multicomponent reactions. The mechanistic scenarios provided by DFT calculations accounts for their uniquely reaction profile in enantioselective allylic substitutions (EAS), enantioselective conjugate additions (EAS) and enantioselective Cu-B additions to alkenes. Mechanistic investigations (density functional theory calculations and deuterium labeling) point to a bridging function for an alkali metal cation connecting the sulfonate anion and a substrate' s phosphate group to form the branched addition products as the

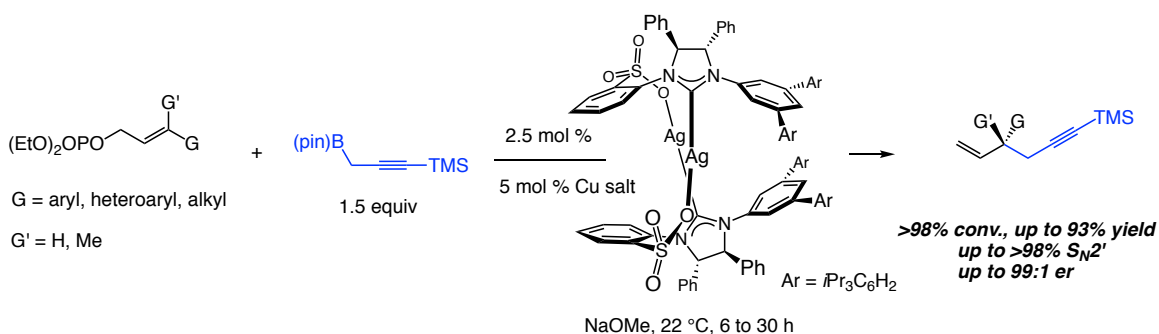
dominant isomers via Cu(III) π -allyl intermediate complexes in EAS reactions.

Sulfonate-bearing NHC ligand with different substitution patterns promote EAS reactions with different reactivity and enantioselectivity. We also developed a guideline to follow to choose the proper sulfonate-based NHC ligands according to the combination of the substrates and the nucleophiles.



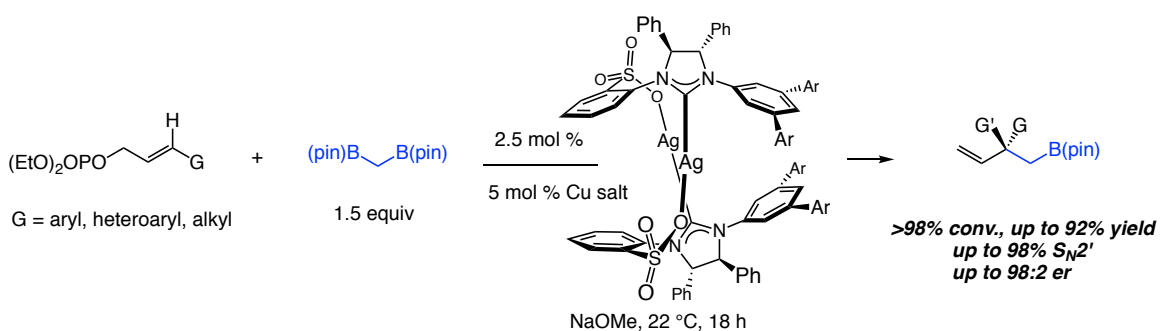
■ **Chapter 2. NHC–Cu-Catalyzed Enantioselective Allylic Substitutions with Silyl-protected Propargyl Boron Reagent to Generate Tertiary and Quaternary Carbon Stereogenic Centers.** Catalytic allylic substitution reactions involving a propargylic nucleophilic component are presented; reactions are facilitated by 5.0 mol % of a catalyst

derived from a chiral N-heterocyclic carbene (NHC) and a copper chloride salt. A silyl-containing propargylic organoboron compound, easily prepared in multi-gram quantities, serves as the reagent. Aryl- and heteroaryl-substituted disubstituted alkenes within allylic phosphates and those with an alkyl or a silyl group can be used. Functional groups typically sensitive to hard nucleophilic reagents are tolerated, particularly in the additions to disubstituted alkenes. Reactions may be performed on the corresponding trisubstituted alkenes, affording quaternary carbon stereogenic centers. Incorporation of the propargylic group is generally favored (vs allenyl addition; 89:11 to >98:2 selectivity); 1,5-enynes can be isolated in 75–90% yield, 87:13 to >98:2 S_N2' : S_N2 (branched/linear) selectivity and 83:17–99:1 enantiomeric ratio. Utility is showcased by conversion of the alkynyl group to other useful functional units. Application to stereoselective synthesis of the acyclic portion of antifungal agent plakinic acid A, containing two remotely positioned stereogenic centers, by sequential use of two different NHC–Cu-catalyzed enantioselective allylic substitution (EAS) reactions further highlights utility.



Chapter 3. NHC–Cu-Catalyzed Enantioselective Allylic Substitutions with Methyleneboron to Generate Tertiary and Quaternary Carbon Stereogenic

Centers. A catalytic EAS method for the site- and enantioselective addition of commercially available di-B(pin)-methane to disubstituted allylic phosphates is introduced. Transformations are facilitated by a sulfonate-containing NHC–Cu complex and products are obtained in 63–95% yield, 88:12 to >98:2 S_N2'/S_N2 selectivity, and 85:15–99:1 enantiomeric ratio. The utility of the approach is highlighted by its application to the formal synthesis of the cytotoxic natural product rhopaloic acid A, in an all-catalytic-method synthesis route. Catalytic EAS methods of the di-B(pin) methane to *Z*-trisubstituted allylic phosphates are also disclosed and DFT calculations provide insights to the stereochemical models for those transformations and rationales for the choice of *Z*-trisubstituted allylic phosphates as the starting materials.



Chapter 4. Enantioselective NHC–Cu-Catalyzed Prenyl Conjugate Additions to Enoates to Generate Tertiary Carbon Stereogenic Centers. An efficient catalytic protocol for generation of prenyl-bearing tertiary carbon stereogenic centers from aryl-substituted enoates was achieved in the presence of a chiral alkoxy-based NHC–Cu complex. A range of aryl and heteroaryl-substituted substrate were suitable substrates, the corresponding prenyl conjugate addition products were generated in up to 94% yield and 95:5 enantioselectivity. The utility of the current method has been shown in the

application to the synthesis of a selective integrin antagonist. DFT calculations provided a stereochemical model for the ECA reaction employing alkoxy-containing NHC–Cu catalyst.

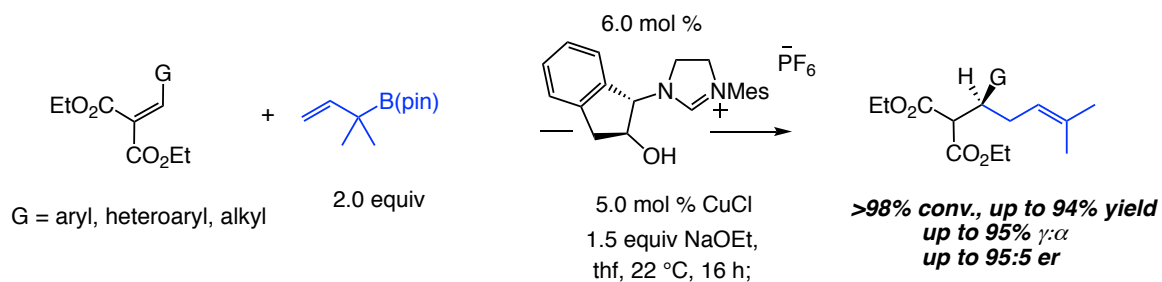


Table of Contents

Chapter 1. A Review of Sulfonate-Containing NHC Ligands in Copper-Catalyzed Enantioselective Transformations—Maneuvering Selectivities in Tight Space

1.1. Introduction	1
1.2. Catalytic Enantioselective Allylic Substitutions	3
1.2.1. Catalytic Enantioselective Allylic Substitutions with Zn- and Al-Based Reagents	3
1.2.2. Catalytic Enantioselective Allylic Substitutions with B-Based Reagents	10
1.2.3. Mechanistic Studies Assisted by DFT Calculations	15
1.2.3.1. Elucidation of the Coordination Sphere of the Sulfonate-Based NHC–Cu Complexes	16
1.2.3.2. Stereochemical Models for EAS Reactions Promoted by Sulfonate-Containing NHC Ligands with Ortho and Meta Substitution Patterns	24
1.3. Catalytic Enantioselective Conjugate Additions	32
1.3.1. Stereochemical Model for Cyclic Enones	32
1.3.2. The Bridging Metal Species Is important	36
1.4. Catalytic Enantioselective Cu–B Additions	38
1.5. Catalytic Enantioselective Multicomponent Reactions	39
1.6. Conclusions	41

Chapter 2. NHC–Cu-Catalyzed Enantioselective Allylic Substitutions with a Silyl-protected Propargyl Boron Reagent to Generate Tertiary and Quaternary Carbon Stereogenic Centers

2.1. Introduction	43
2.2. Background	46
2.3. Catalytic Enantioselective Allylic Substitutions with a Silyl-Protected Propargyl Boron Reagent	47
2.3.1. An Easily Accessible Propargyl Pinacolboron Reagent	47

2.3.2. Synthesis of Propargyl-Substituted Tertiary Carbon Stereogenic Centers: Additions to Allylic Phosphates that Contain a Disubstituted Alkene	48
2.3.3. Synthesis of Propargyl-Substituted Quaternary Carbon Stereogenic Centers: Additions to Allylic Phosphates that Contain a Trisubstituted Alkene	55
2.3.4. Mechanistic Studies	59
2.3.5. Functionalizations and Application to the Synthesis of Plakinic Acid A	60
2.4. Development of New Sulfonate-Containing NHC Ligands Assisted by DFT Calculations—A New NHC Ligand Bearing a 2,5-Disubstituted N-Aryl Group	65
2.4.1. Development of a New NHC Ligand with 2,5-Substitution Pattern for EAS Reactions Employing 1,2-Disubstituted Allylic Phosphates	66
2.4.2. Application of the New NHC Ligand with 2,5-Substitution for Enantioselective S_N2'' Addition to Alkenyl-Substituted Allylic Phosphates	71
2.5. Conclusions	73
2.6. Experimentals	74

Chapter 3. NHC–Cu-Catalyzed Enantioselective Allylic Substitutions with Methylenediboron to Generate Tertiary and Quaternary Carbon Stereogenic Centers

3.1. Introduction	249
3.2. Background	252
3.3. Catalytic Enantioselective Allylic Substitutions with Methylenediboron	257
3.3.1. Screening of Reaction Conditions for Methyleneboryl Additions to 1,2-Disubstituted Allylic Phosphates	257
3.3.2. Application to the Synthesis of Rhopaloic Acid A	261
3.3.3. Screening of Reaction Conditions for the Methyleneboryl Additions to Trisubstituted Allylic Phosphates and DFT Calculations	263
3.4. Conclusions	268
3.5. Experimentals	269

Chapter 4. Enantioselective NHC–Cu-Catalyzed Prenyl Conjugate Additions

to Enoates

4.1. Introduction	329
4.2. Background	331
4.2.1. Catalytic Enantioselective Allyl Conjugate Additions to Cyclic α,β -Unsaturated Diesters	331
4.2.2. Catalytic Enantioselective Allyl Conjugate Additions to Acyclic α,β -Unsaturated Diesters	332
4.2.3. Catalytic Enantioselective Conjugate Additions to Acyclic α,β -Unsaturated Diesters with Boron-Based Nucleophiles	333
4.3. Cu-Catalyzed Enantioselective Prenyl Conjugate Additions to Acyclic α,β-Unsaturated Diesters	335
4.3.1. Catalyst Screening and Reaction Optimizations	335
4.3.2. Scope of Enantioselective Prenyl Conjugate Additions	338
4.3.3. Functionalization and Application to the Synthesis of a Selective Integrin Antagonist	343
4.3.4. Stereochemical Models by DFT Calculations	344
4.4. Conclusions	345
4.5. Experimentals	346

Chapter One

A Review of Sulfonate-Containing NHC Ligands in Copper-Catalyzed Enantioselective Transformations—Maneuvering Selectivities in Tight Space

1.1. Introduction

Copper-catalyzed enantioselective allylic substitution (EAS)¹ and conjugate additions (ECA)² are two extensively-explored reactions for the construction of enantiomerically enriched compounds. Such transformations afford either a stereogenic center adjacent to an alkene, or at the β -position to a carbonyl group. These motifs can be found in natural products and pharmaceuticals, and are amenable to further manipulations

(1) For reviews on allylic substitution reactions catalyzed by other transition metals and with “soft” nucleophiles, see: (a) Trost, B. M.; Lee, C. In *Catalytic Asymmetric Synthesis*; Ojima, I., Ed.; Wiley-VCH: Weinheim, Germany, 2000; Chapter 8E. (b) Trost, B. M.; Crawley, M. L. *Chem. Rev.* **2003**, *103*, 2921–2944. (c) Stanley, L. M.; Hartwig, J. F. *Acc. Chem. Res.* **2010**, *43*, 1461–1475. (d) Trost, B. M. *Org. Process Res. Dev.* **2012**, *16*, 185–194. (e) Tosatti, P.; Nelson, A.; Marsden, S. P. *Org. Biomol. Chem.* **2012**, *10*, 3147–3163. For reviews on Cu-catalyzed allylic alkylation reactions that involve “hard” alkyl- or arylmetal-based reagents, see: (f) Hoveyda, A. H.; Hird, A. W.; Kacprzynski, M. A. *Chem. Commun.* **2004**, 1779–1785. (g) Yorimitsu, H.; Oshima, K. *Angew. Chem., Int. Ed.* **2005**, *44*, 4435–4439. (h) Falcicola, C. A.; Alexakis, A. *Eur. J. Org. Chem.* **2008**, 3765–3780. (i) Alexakis, A.; Bäckvall, J.-E.; Krause, N.; Pàmies, O.; Diéguez, M. *Chem. Rev.* **2008**, *108*, 2796–2823. (j) Harutyunyan, S. R.; den Hartog, T.; Geurts, K.; Minnaard, A. J.; Feringa, B. L. *Chem. Rev.* **2008**, *108*, 2824–2852. (k) Lu, Z.; Ma, S. *Angew. Chem., Int. Ed.* **2008**, *47*, 258–297. (l) Langlois, J. -B.; Alexakis, A. *Topics in Organometallic Chemistry* **2012**, *38*, 235–268.

(2) (a) Krause, N.; Hoffmann-Röder, A. *Synthesis* **2001**, 171–196. (b) Alexakis, A.; Benhaim, C. *Eur. J. Org. Chem.* **2002**, 3221–3236. (c) Feringa, B. L.; Naasz, R.; Imbos, R.; Arnold, L. A. In *Modern Organocopper Chemistry*, Krause, N. Ed.; Wiley-VCH, Weinheim, 2002, pp. 224–258. (d) Alexakis, A.; Bäckvall, J. E.; Krause, N.; Pàmies, O.; Diéguez, M. *Chem. Rev.* **2008**, *108*, 2796–2823. (e) Quasdorf, K. W.; Overman, L. E. *Nature*, **2014**, *516*, 181–191.

that yield higher desirable structural units, such as alkylboranes²⁴, carboxylic acids³.

Ever since the first example of enantioselective allylic substitutions utilizing Grignard reagents was reported by Bäckvall et al,⁴ the field has received a tremendous amount of interest in the past two decades. As the interest in enantioselective catalysis grows, a number of catalyst systems have also been devised to address problems in Cu-catalyzed EAS reactions. Phosphine-⁵ and amino acid-⁶ based copper complexes are two of the most prominent catalyst classes in promoting EAS reactions with alkyl Grignard or zinc reagents. Additionally, over the last decade, N-heterocyclic carbenes (NHC), have been introduced as chiral ligands for Cu to facilitate EAS reactions and have been of great interest ever since.

In 2004 and 2005, our group developed two types of phenoxide-based NHC ligands, derived from binol⁷ or with an optically pure biphenylethylene diamine as the backbone (Scheme 1.1).⁸ The corresponding copper complexes exhibited superior reactivity and selectivity profiles compared to those that contain an amino acid-based chiral ligand. Another type of carbene containing an alkoxy chelating group was reported by Mauduit et al⁹ with its application as a monodentate NHC–Cu complex capable of

(3) May, T. L.; Dabrowski, J. A.; Villaume, M. T.; Hoveyda, A. H. *Angew. Chem., Int. Ed.* **2013**, *52*, 8156–8159.

(4) van Klaveren, M.; Persson, E. S. M.; Grove, D. M.; Bäckvall, J. E.; van Koten, G. *Tetrahedron Lett.* **1995**, *36*, 3059–3062.

(5) ref. 1(f)–(l). For an additional review dedicated to widely used phosphoramidite ligands, see: (b) Teichert, J. F.; Feringa, B. L. *Angew. Chem., Int. Ed.* **2010**, *49*, 2486–2528.

(6) (a) Luchaco-Cullis, C.; Mizutani, H.; Murphy, K. E.; Hoveyda, A. H. *Angew. Chem., Int. Ed.* **2001**, *40*, 1456–1460. (b) Murphy, K. E.; Hoveyda, A. H. *J. Am. Chem. Soc.* **2003**, *125*, 4690–4691. (c) Kacprzynski, M. A.; Hoveyda, A. H. *J. Am. Chem. Soc.* **2004**, *126*, 10676–10681. (d) Murphy, K. E.; Hoveyda, A. H. *Org. Lett.* **2005**, *7*, 1255–1258.

(7) Larsen, A. O.; Leu, W.; Oberhuber, C. N.; Campbell, J. E.; Hoveyda, A. H. *J. Am. Chem. Soc.* **2004**, *126*, 11130–11131.

(8) Van Veldhuizen, J. J.; Campbell, J. E.; Guidici, R. E.; Hoveyda, A. H. *J. Am. Chem. Soc.* **2005**, *127*, 6877–6882.

(9) (a) Martin, D.; Kehrli, S.; d'Augustin, M.; Clavier, H.; Mauduit, M.; Alexakis, A. *J. Am. Chem. Soc.* **2006**, *128*, 8416–8417. (b) Germain, N.; Magrez, M.; Kehrli, S.; Mauduit, M.; Alexakis, A. *Eur. J. Org.*

promoting EAS reactions with alkyl Grignard or zinc reagents. In 2007, we introduced a new type of NHC ligand bearing a sulfonate group (Scheme 1.1), which has demonstrated exceptional reactivity and selectivity for EAS reactions and ECA reactions.

1.2. Catalytic Enantioselective Allylic Substitutions

1.2.1 Catalytic Enantioselective Allylic Substitutions with Zn- and Al-Based Reagents

In 2007, we explored EAS reactions utilizing our sulfonate-based NHC ligands to achieve high efficiency in EAS reactions with alkyl nucleophiles. We highlighted the unique reactivity of our sulfonate-based NHC using the performance of our phenoxide-based NHC ligands as a benchmark.¹⁰ As shown in Scheme 1.1a, when we employed diethylzinc as the nucleophile, product **1.2** was generated in high efficiency, high S_N2' selectivity and high enantioselectivity for both phenoxide- and sulfonate-based NHC ligands.¹¹ However, a drastic increase in reactivity was observed utilizing sulfonate-base NHC ligand **1.5** compared with phenoxide-based ligand **1.4** when we turned to a much underexplored class of substrates for Cu-catalyzed EAS reactions: a trisubstituted allylic phosphate bearing a β-alkyl substituent, **1.6**. As shown in Scheme 1.1b, Me₃Al, a more reactive nucleophile, was then examined in Cu-catalyzed EAS reactions. (Preliminary studies showed that no conversion of substrate **1.6** was observed with dimethylzinc under

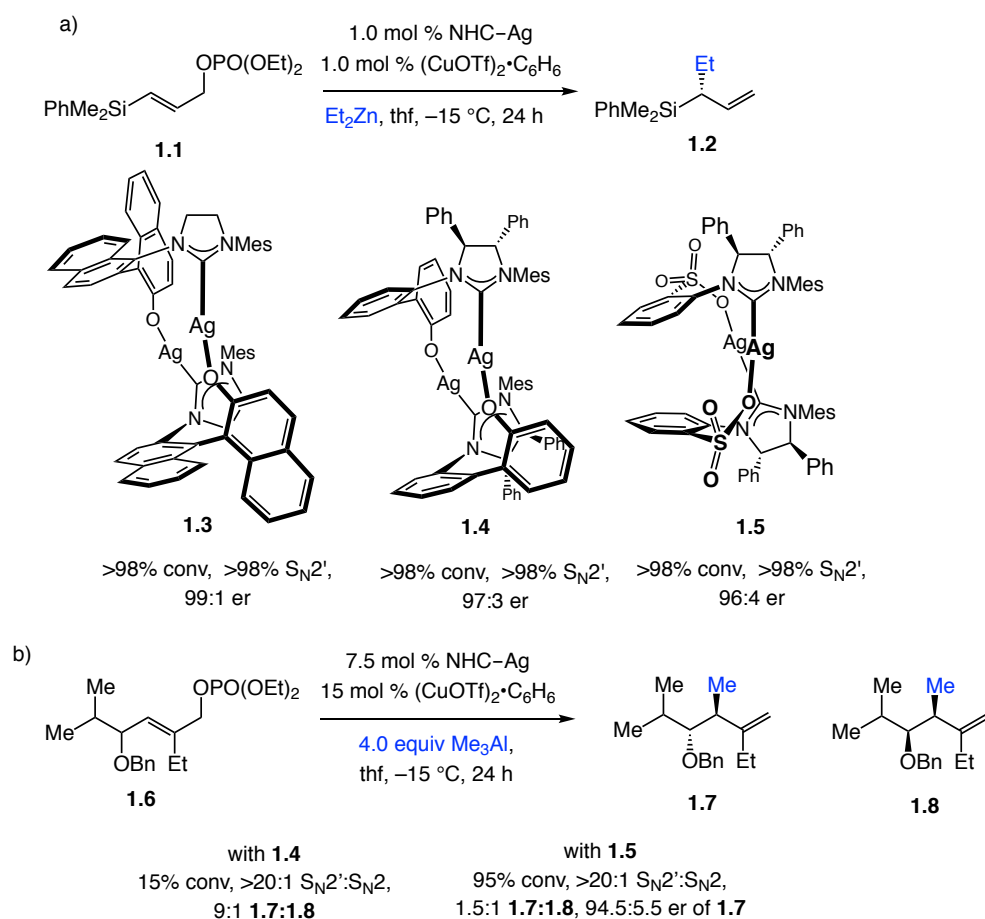
Chem. 2012, 5301–5306. (c) Magrez, M.; Le Guen, Y.; Baslé, O.; Crévisy, C.; Mauduit, M. *Chem. Eur. J.* **2013**, 19, 1199–1203.

(10) Kacprzyński, M. A.; May, T. L.; Kazane, S. A.; Hoveyda, A. H. *Angew. Chem., Int. Ed.* **2007**, 46, 4554–4558.

(11) NHC–Ag complexes were employed in the reaction instead of their corresponding imidazolium salts due to inefficient formation of NHC–Cu catalyst with the use of alkyl Zn reagents. The deprotonation of imidazolium salt with organozinc and organoaluminum reagents is not efficient for the formation of NHC–Cu complexes.

the previously reported catalytic system.¹²⁾ We found that NHC–Cu complexes derived from phenoxide ligand **1.4** delivered the desired product **1.7** in only 15% conversion with a 9:1 ratio of **1.7**:**1.8**. The low conversion suggests a possible match/mismatch scenario between the stereogenic centers on the substrate and chiral catalyst. However, sulfonate NHC **1.5** promoted the generation of **1.7** more efficiently: 95% conversion of **1.1** to **1.7** was observed with >20:1 S_N2': S_N2 selectivity, with a 1.5:1 ratio of **1.7**:**1.8** and 94.5:5.5 er of **1.7**.

Scheme 1.1 Cu-Catalyzed EAS reactions with Organozinc and Organoaluminum Reagent

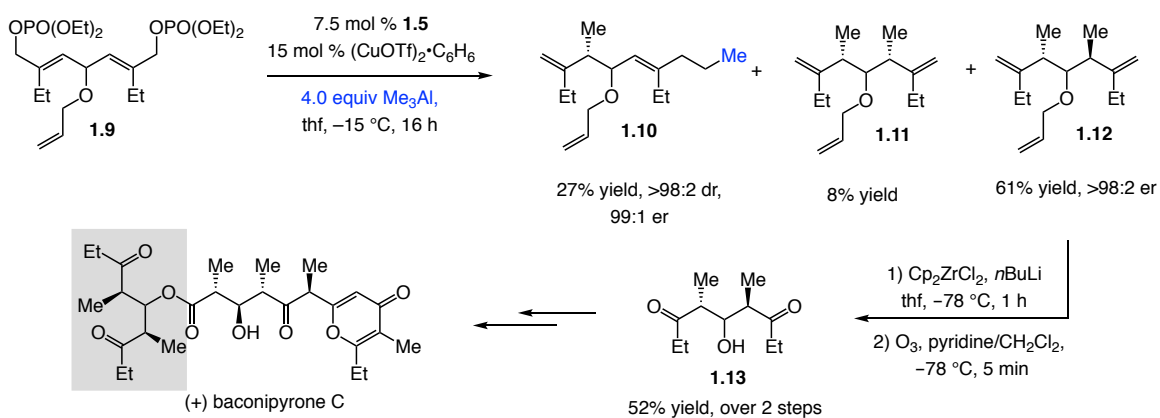


As shown in Scheme 1.2, when we applied these EAS reaction conditions en route to the synthesis of baconipyronone C, we found that NHC–Ag complex **1.5** delivers

(12) Gillingham, D. G.; Hoveyda, A. H. *Angew. Chem., Int. Ed.* **2007**, *46*, 3860–3864.

the desired methyl addition product **1.12** in 61% yield and >98:2 er. The stereoselective synthesis of **1.12** was followed by deprotection and oxidative cleavage of the double bond to generate **1.13**, which can be further elaborated to the natural product baconipyrrone C. The application demonstrated the utility of the EAS method. Sulfonate-based NHC ligands promoted the EAS reactions with a sterically-demanding electrophiles, enabling the formation of two stereogenic center in one step.

Scheme 1.2. Cu-Catalyzed EAS reactions with Trimethylaluminum and Application to the Synthesis of Baconipyrrone C



The majority of previous reports deal primarily with alkyl, and to a lesser extent aryl, metal reagent, as nucleophiles. EAS reactions with alkenyl nucleophiles are far less prevalent.

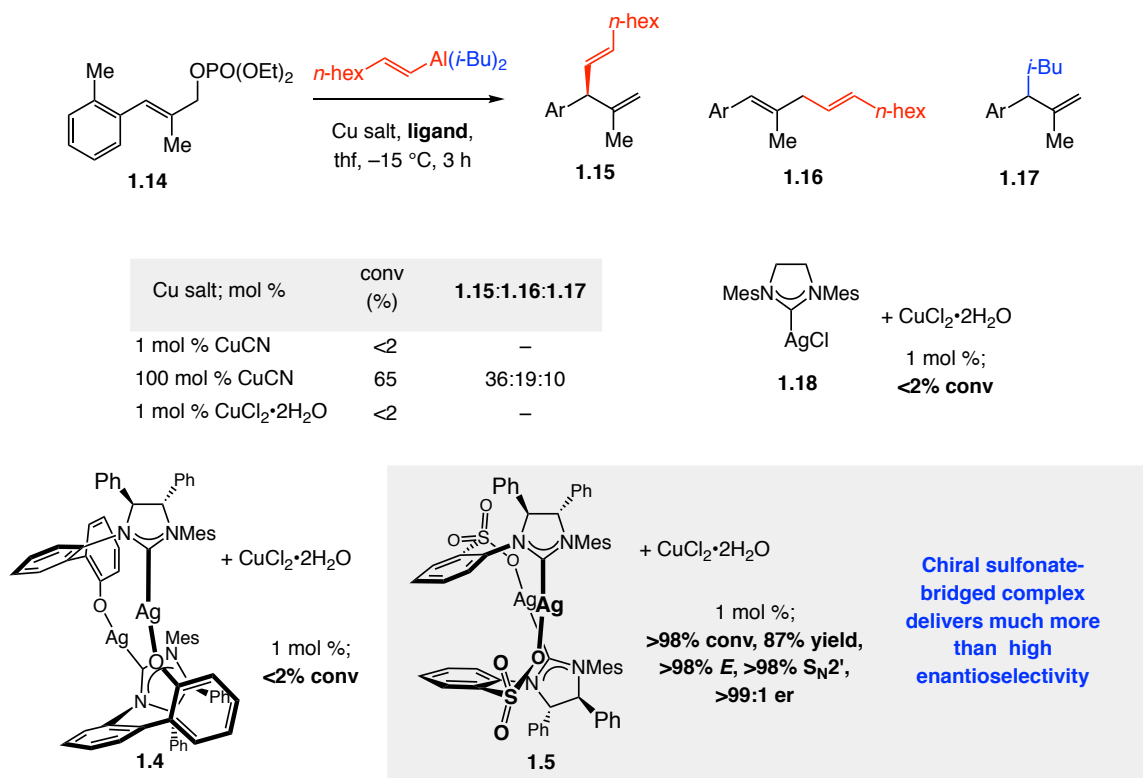
Our group started to explore alkenyl aluminum reagents as nucleophiles due to their ease of accessibility and functional group tolerance (compared to organolithium¹³ and Grignard reagents). In 2009, we reported the formation of tertiary stereogenic centers through the addition of *E*-alkenyl aluminum reagent to trisubstituted allylic.¹⁴ As shown in Scheme 1.3, neither the use of different copper salts or varying the amount of the copper salt lead to the efficient formation of desired product. Moreover, the use of

(13) Teichert, J. F.; Feringa, B. L. *Angew. Chem., Int. Ed.* **2010**, *49*, 2486–2528.

(14) Lee, Y.; Akiyama, K.; Gillingham, D. G.; Brown, M. K.; Hoveyda, A. H. *J. Am. Chem. Soc.* **2008**, *130*, 446–447.

NHC–Cu complex derived from copper salt and either NHC–Ag complex **1.18** or **1.4** led to <2% detection of the desired product. Only when the reaction was performed in the presence of a sulfonate-containing NHC–Cu complex, generated *in situ* from NHC–Ag complex **1.5** and $\text{CuCl}_2 \cdot 2\text{H}_2\text{O}$, was **1.15** obtained in over 87% yield with >98% $\text{S}_{\text{N}}2'$ selectivity and >99:1 enantiomeric ratio. This case exhibited the uniquely high reactivity of sulfonate-containing NHCs in promoting the formation of the desired branched product in enantioselective allylic substitutions.

Scheme 1.3. Initial Investigation of EAS Reactions with Alkenylaluminum Reagent



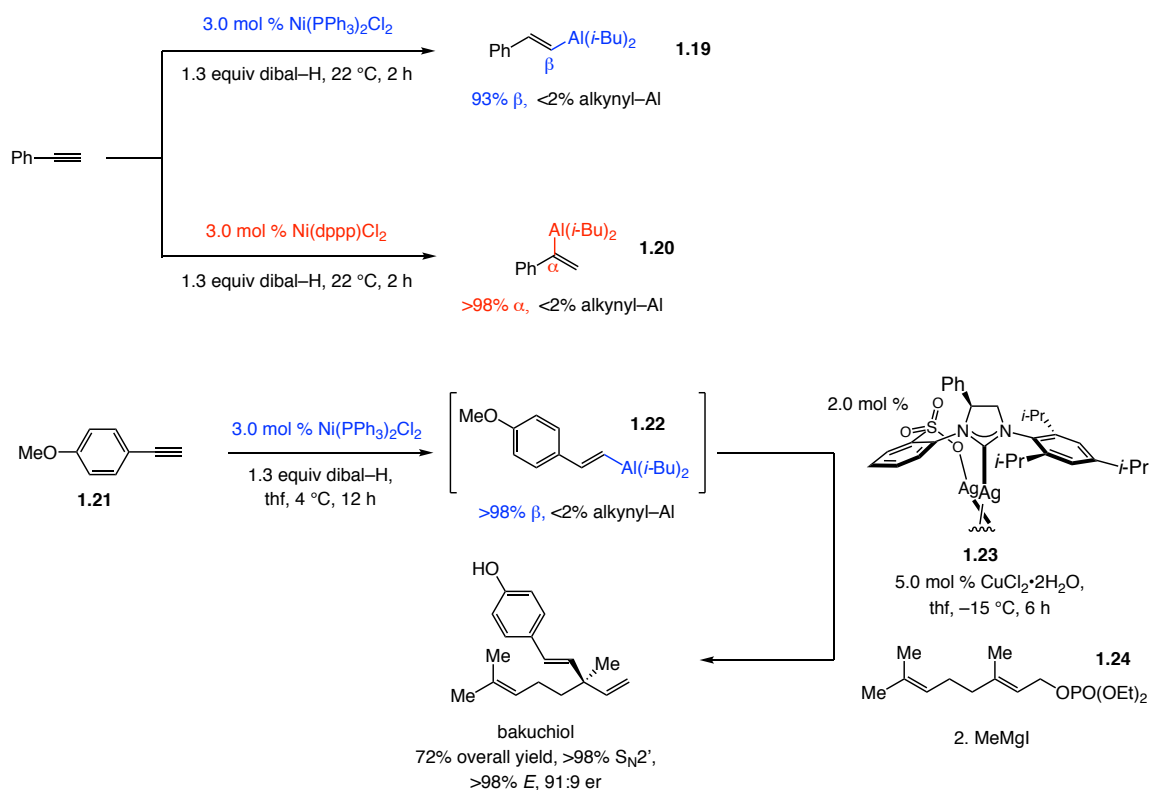
Alkyl-substituted alkenylaluminums can be prepared by reaction of alkynes with dibal-H^{15} and used in EAS reactions directly. However, the generation of aryl-substituted reagents suffer from competitive alkyne deprotonation, affording significant amounts of

(15) For a review on hydroaluminations of alkynes and alkenes, see: Eisch, J. J. In *Comprehensive Organic Synthesis*; Trost, B. M., Fleming, I., Schreiber, S. L., Eds.; Pergamon, Oxford, 1991; Vol. 8, pp 733.

the corresponding alkynylaluminums; the alkynyl metal reagent may lead to the formation of the undesired alkynyl addition product in EAS reactions. To address this issue, our group developed a Ni-catalyzed method to promote the stereoselective synthesis of aryl-substituted alkenylaluminum reagents.¹⁶ As shown in Scheme 1.4, with 3.0 mol % of monodentate Ni(PPh₃)₂Cl₂ and dibal-H, phenylacetylene undergoes hydroalumination in two hours at 22 °C with 93:7 β:α selectivity, and no detectable amount of the corresponding alkynylaluminum reagent is formed. **1.19** can then be used directly in allylic substitution reactions to generate skipped diene products with high efficiency, site-, and enantioselectivity. Switching to a bidentate nickel catalyst, Ni(dppp)Cl₂, the α-isomer **1.20** can be formed with complete site selectivity (>98:2 α:β). The utility of the method was illustrated in the synthesis of bakuchiol.¹⁷ Alkenylaluminum **1.22** was afforded under the reported conditions and employed in an EAS reactions with geraniol derived allylic phosphate **1.24** to generate a quaternary carbon stereogenic center, catalyzed by NHC-Cu complex derived from NHC-Ag complex **1.23** containing an ortho-substituted N-aryl group. After demethylation, the EAS product furnished bakuchiol.

(16) Gao, F.; Hoveyda, A. H. *J. Am. Chem. Soc.* **2010**, *132*, 10961–10963.

(17) Gao, F.; McGrath, K. P.; Lee, Y.; Hoveyda, A. H. *J. Am. Chem. Soc.* **2010**, *132*, 14315–14320.

Scheme 1.4. EAS Reaction to Generate A Quaternary Stereogenic Center and Synthesis of Bakuchiol

At this stage, we turned to X-ray crystallography in an effort to elucidate the unique behavior of the sulfonate-containing NHC–Cu complex. However, the X-ray crystal structure of the sulfonate-based NHC–Cu(I) complex could not be obtained, instead crystallographic analysis was carried out using Zn and Al-based analogs **1.25** and **1.26** (Figure 1.1).¹⁸ Unexpectedly, in both complexes, NHC serves as a bidentate ligand in which the sulfonate coordinates to the metal center, and the sulfonate group and adjacent phenyl group on the backbone are in a syn orientation. It appears that chelation of the sulfonate with the Zn center in **1.25** causes tilting of the N-aryl unit (C_{carbene}–N–C–C dihedral angle = 49.5°) such that the ortho unit of the same substituent

(18) Lee, Y.; Li, B.; Hoveyda, A. H. *J. Am. Chem. Soc.* **2009**, *131*, 11625–11633.

(H₁ in **1.25**, Scheme 2) and the backbone of the N-heterocyclic carbene (H₂ in **1.25**) are brought into close proximity, which is supported by the NOE studies.

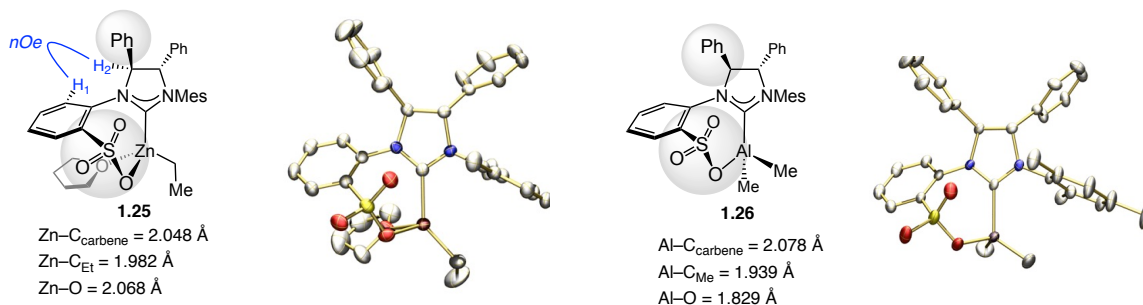


Figure 1.1. X-ray Crystallography Data of NHC-Zn and NHC-Al Complexes

A model shown in Figure 1.2 was proposed based on the X-ray crystallography data.¹⁷ Chelation of the cationic aluminum species ($\text{Al}(i\text{-Bu})_2^+$) counter to the equatorial oxygen of the sulfonate and phosphate of the substrate serves to increase the electrophilicity of the phosphate and facilitate substrate binding to allow for maximum orbital overlap. However, in the minor mode of addition, copper coordinates to the opposite face of the olefin, engendering steric repulsion between the large aryl ring of the substrate (R_L) and the ortho substituent ($i\text{-Pr}$ group) on the N-aryl group. As a result, the aluminum chelation is absent in this pathway which leads to a less organized transition state, due to geometric constraints.

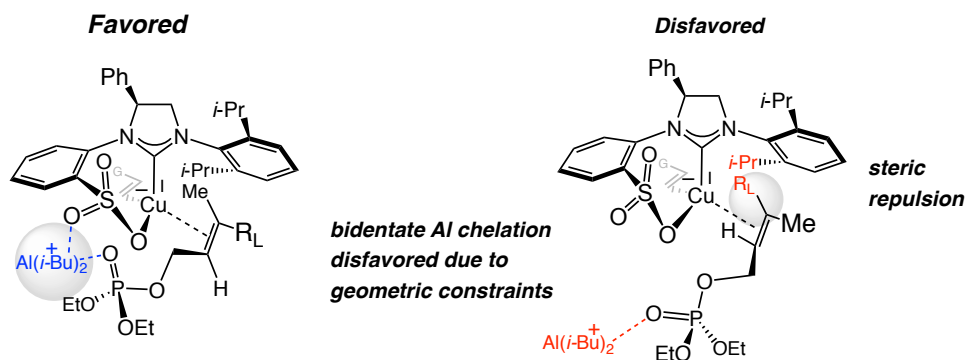


Figure 1.2. Proposed Stereochemical Model before 2015 (R_L , large substituent)

1.2.2 Catalytic Enantioselective Allylic Substitutions with Boron-Based Reagents

Despite the advances provided by the EAS methods developed in our laboratory, there are still fundamental limitations employing organoaluminum reagents: 1) EAS reactions involving this class of nucleophiles normally require cryogenic temperatures, limiting the industrial utility of current methods; 2) the reagent must be generated *in situ* and is not stable to prolonged storage; 3) alkenylaluminums are not compatible with several functional groups, such as carboxylic aldehydes and esters.

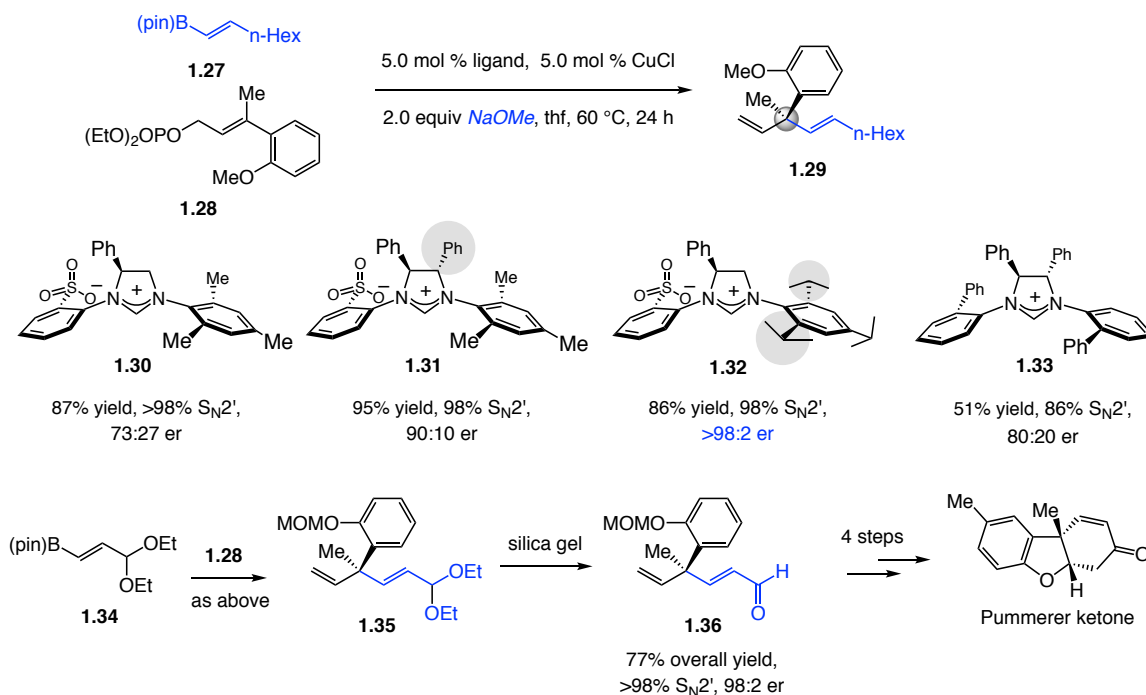
To remedy these limitations, we decided to employ alkenyl boron-based reagents in catalytic EAS reactions. However, this design raised a few questions. One issue relates to the relatively low reactivity of organoborons. For example, organoaluminum as nucleophiles allows EAS reactions to be performed at lower temperatures, leading to an improvement of enantioselectivity. However, reactions utilizing organoboron might require high temperature to achieve efficient formation of the products. The second problem is that the alkenyl-Cu species might not be efficiently generated with a substantially less nucleophilic organoboron.

We surmised the presence of a metal alkoxide, such as NaOMe¹⁹, should allow efficient formation of NHC-Cu-allene via alkenylboron. We found that imidazolium salts can be deprotonated in the presence of NaOMe and thus can be employed to generate the corresponding sulfonate NHC-Cu complex *in situ*. 5.0 mol % of sulfonate-containing NHC-Cu catalyst derived from **1.30** promotes the formation of a quaternary carbon stereogenic center, affording skipped diene **1.29** in 87% yield, over 98% site-

(19) Ohishi, T.; Nishiura, M.; Hou, Z. *Angew. Chem., Int. Ed.* **2008**, *47*, 5792–5795.

selectivity with 73:27 er at 60 °C for 24 h.²⁰ We found that incorporation of another phenyl substituent on the NHC backbone as in **1.31**, caused the N-aryl ring to rotate away from the proximal phenyl group to avoid the steric interaction between the phenyl group and the ortho substituent. This conformational change of NHC ligand improved the enantioselectivity of product to 90:10 er as in **1.31**. EAS reactions furnished the desired product in 86% yield, 98% S_N2' selectivity with >98% enantioselectivity when increasing the size of the ortho substituent on the N-aryl ring of NHC ligand from Me to *i*-Pr group as in **1.32**. Of note, EAS reactions catalyzed by NHC–Cu complexes derived from non-sulfonate-based NHCs also favored the formation of branched product, despite with lower site- and enantioselectivities (Scheme 1.5, **1.33**). The utility of this method is illustrated through the synthesis of Pummerer ketone utilizing organoboron reagent **1.34**. The corresponding organoaluminum reagent is not easily accessible, thus highlighting the robustness of this class of nucleophiles.

(20) Gao, F.; Carr, J. L.; Hoveyda, A. H. *Angew. Chem. Int. Ed.* **2012**, *51*, 6613–6617.

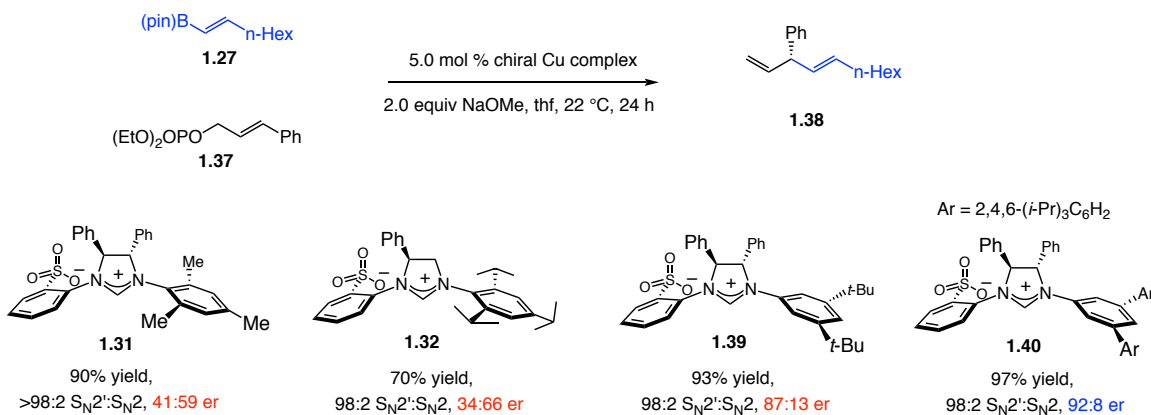
Scheme 1.5. Generation of Quaternary Carbon Stereogenic Centers with Alkenylboron Reagents

As shown above, the degree of enantioselectivity can be tuned by changing the substitution pattern of the backbone or increasing the size of the ortho substituent. However, this strategy did not apply to all the cases. For example, when we sought to establish EAS reactions utilizing disubstituted allylic phosphates in order to generate tertiary carbon stereogenic centers²¹ with alkenylboron reagents, NHC ligands with ortho substitution pattern no longer delivered the product in high enantioselectivity. As shown in Scheme 1.6, reactions delivered skipped diene **1.38** with less than 70% enantioselectivity in the presence of ortho-substituted NHC–Cu complex derived from the **1.31** or **1.32**. However, **1.38** was furnished with an increase in enantioselectivity by employing a new class of sulfonate-based NHC ligand with meta-substitution pattern on the N-aryl group (91:9 vs. 34:66 er, **1.39** vs. **1.32**). The NHC–Cu complex derived from sulfonate-containing imidazolium salt **1.40** with meta-substitution delivered the highest

(21) Gao, F.; Carr, J. L.; Hoveyda, A. H. *J. Am. Chem. Soc.* **2014**, *136*, 2149–2161.

enantioselectivity. Of note, the meta-substituted NHC ligands (Scheme 1.6, **1.39** and **1.40**) promoted the generation of the (*R*)-enantiomer as the major product, whereas the reaction catalyzed by NHC ligands with 2,6-substitution afforded the (*S*)-enantiomer (see **1.31**, **1.32**).

Scheme 1.6. Generation of Tertiary Carbon Stereogenic Centers with an Alkenylboron Reagent

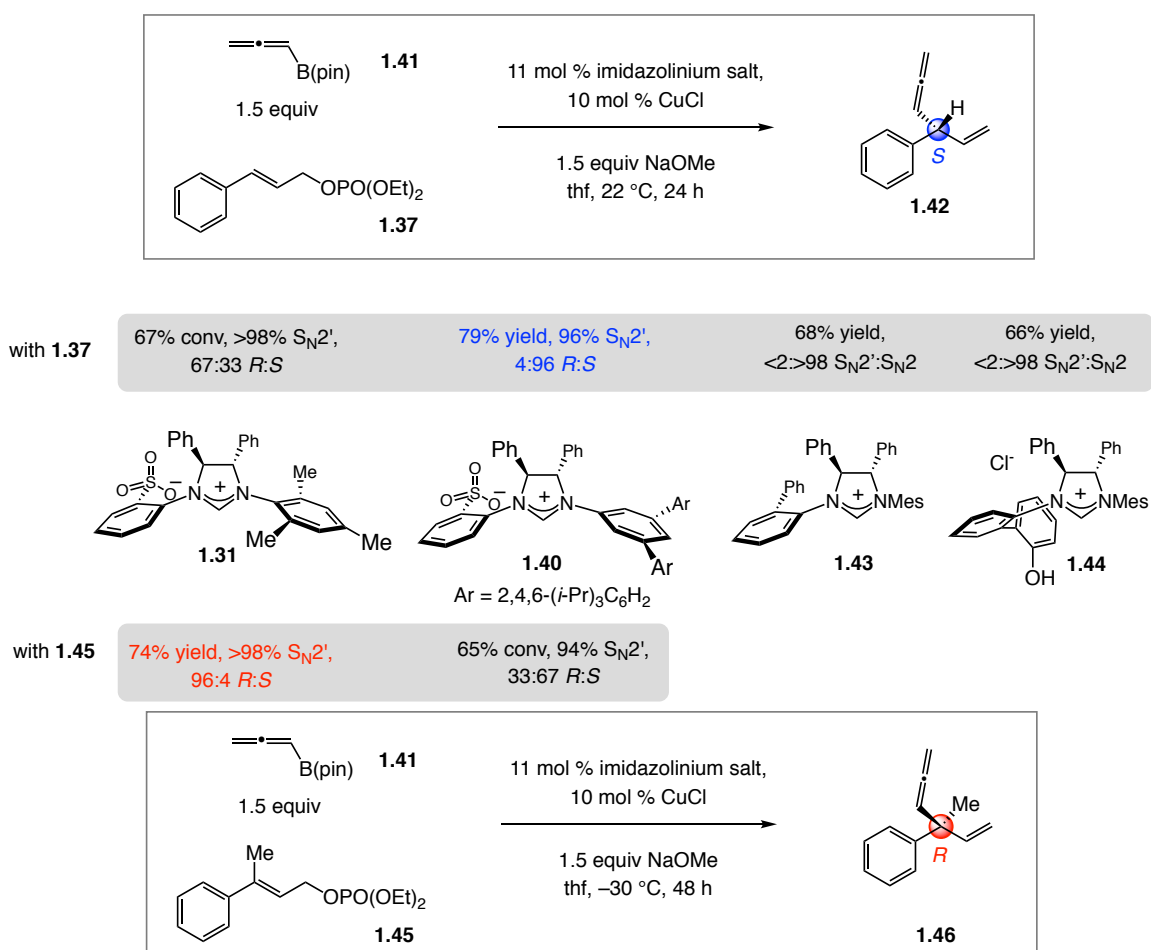


Both meta- and ortho-substituted NHC ligands were explored in EAS reactions with allenyl boron reagent **1.41**.²² A similar phenomenon was also observed; as shown in Scheme 1.7, the (*S*)-branched products (4:96 *R*:*S* and 33:67 *R*:*S*, **1.42** and **1.46**) were obtained utilizing meta-substituted NHC ligand **1.40** while ortho-substituted NHC **1.31** favored the formation of the opposite enantiomer (96:4 *R*:*S* and 67:33 *R*:*S*, **1.42** and **1.46**). Moreover, while the meta-substituted NHC ligand **1.40** was the optimal ligand for EAS reactions with 1,2-disubstituted allylic phosphate **1.36** (79% yield, 96% S_N2' , 4:96 *R*:*S*), reactions catalyzed by the NHC with ortho-substitution **1.31** afforded desired product **1.46** with quaternary carbon stereogenic centers from trisubstituted substrates with high enantioselectivity (96:4 *R*:*S*). Unlike when an alkenylboron reagent was used as the nucleophile, only NHC–Cu complexes derived from sulfonate-containing

(22) Jung, B.; Hoveyda, A. H. *J. Am. Chem. Soc.* **2012**, *134*, 1490–1493.

imidazolium salts lead to the dominant formation of branched product (S_N2' selectivity); non-sulfonate-containing NHC ligands favors the generation of the linear product ($<2>98 S_N2:S_N2'$, with **1.43**, **1.44**). We believe that the highly efficient background reaction catalyzed by free CuCl leads to dominant formation of undesired linear products (S_N2 selectivity). Only the sulfonate-based NHC–Cu complex can catalyze the S_N2' reaction to outcompete the undesired background reaction.

Scheme 1.7. Generation of Tertiary and Quaternary Carbon Stereogenic Centers with an Allenylboron Reagent

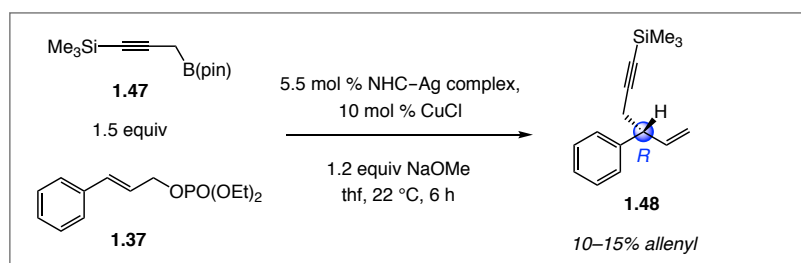


In 2015, we published the catalytic EAS reactions with di- and trisubstituted allylic phosphates using propargyl boron reagent **1.47** (Scheme 1.8).²³ Again, only

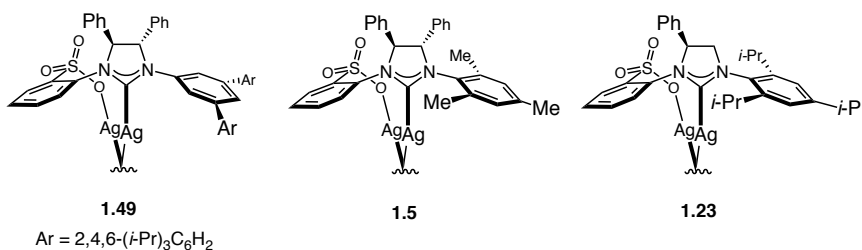
(23) Shi, Y.; Jung, B.; Torker, S.; Hoveyda, A. H. *J. Am. Chem. Soc.* **2015**, *137*, 8948–8964.

sulfonate-based NHCs promoted formation of the desired branched product **1.48** in the presence of an appropriate NHC–Ag complex, with meta-substituted NHC–Ag complex **1.49** proving to be optimal (75% yield, 97% S_N2' , 97:3 $R:S$). However, unlike cases utilizing alkenyl and allenyl boron-based nucleophiles, the optimal ligand to facilitate formation of product **1.50** with a quaternary carbon stereogenic center utilizing propargyl boron **1.47** is the NHC derived from **1.49** with meta-substitution (84% yield, 94% S_N2' , 92:8 $R:S$), instead of ortho-substituted NHC–Ag complexes.

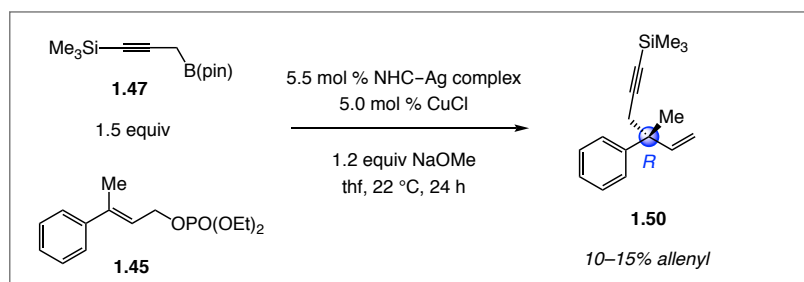
Scheme 1.8. Generation of Tertiary and Quaternary Carbon Stereogenic Centers with a Propargyl Boron Reagent



with 1.37	75% yield, 97% S_N2' , 97:3 $R:S$	74% yield, >98% S_N2' , 31:69 $R:S$	74% yield, >98% S_N2' , 69:31 $R:S$
------------------	--	--	--



with 1.45	84% yield, 94% S_N2' , 92:8 $R:S$	31% yield, 85% S_N2' , 32:68 $R:S$
------------------	--	---



1.2.3 Mechanistic Studies Assisted by DFT Calculations

At this point, we wanted to elucidate the reaction mechanism. Was the model we proposed valid, in which sulfonate NHCs chelated to the copper and delivered the S_N2' product? Why in some cases did sulfonate-based NHCs bearing meta substituents outperform those with ortho substituents? Could we develop a set of guidelines to follow in order to choose the proper NHC ligand for a certain substrate and nucleophile combination? We envisioned that with the assistance of computational analysis, we might shed mechanistic insight onto the the transformation and allow the opportunity for rational design of catalysts.

1.2.3.1 Elucidation of the Coordination Sphere of the Sulfonate-Based NHC–Cu Complexes

First, the ground states of sulfonate-bearing NHC–Cu complexes were analyzed in order to evaluate our previous hypothesis (as in **1.54**) which sulfonate group chelated to Cu center. As shown in Figure 1.3, the free energy of NHC–Cu complex **1.51** was 7.7 kcal/mol, in which NHC served as a bidentate ligand with the anionic sulfonate syn to the proximal phenyl group on the NHC backbone. When NHC served as a bidentate ligand in which the sulfonate group was in anti orientation with the phenyl group (see **1.52**), the relative energy dropped to 6.1 kcal/mol. The monodentate NHC–Cu complex **1.53** in which the sulfonate group situated anti to the proximal phenyl group was the lowest energy ground state. Unexpectedly, DFT calculations²⁴ indicated that it was unlikely that sulfonate-containing NHC ligands served as bidentate ligands for Cu, as proposed in our previous model **1.54**. Thus a new model **1.55** was proposed, in which the sulfonate group sat anti to the phenyl group and coordinated to the sodium cation instead of the copper. In

(24) See Chapter 2, 2.5 Experimentals.

this new model, the sodium cation bridged between the sulfonate and the substrate phosphate unit.

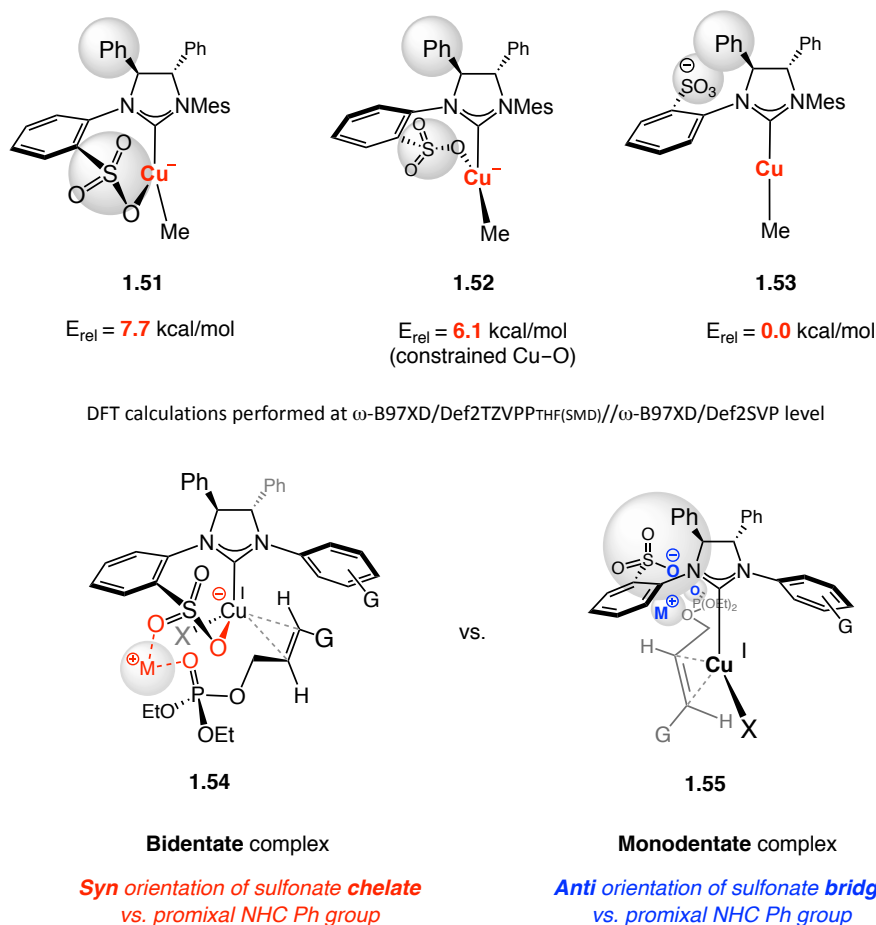
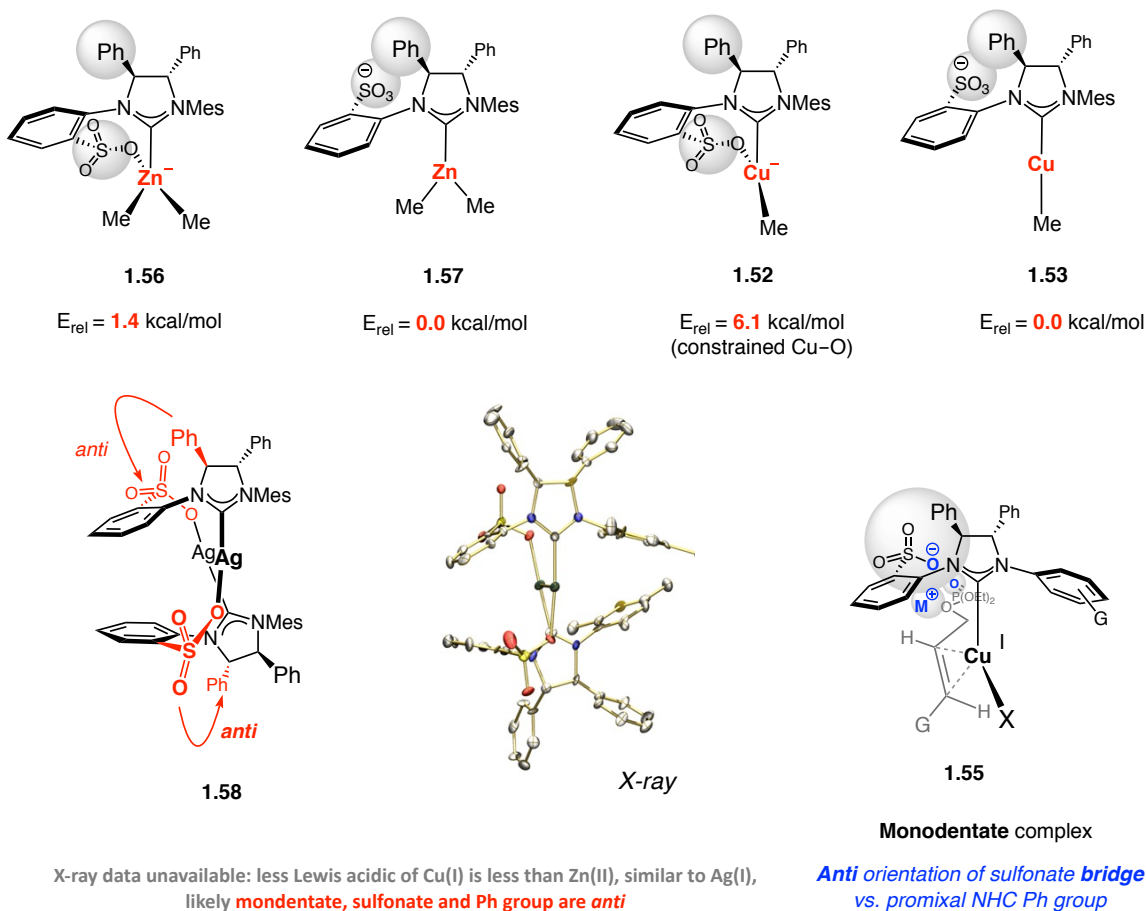


Figure 1.3. DFT Calculations for Three NHC-Cu Conformers and Two Possible Hypothesis

As shown in Figure 1.4, the sulfonate chelation to metal made NHC-Zn complex **1.56** slightly higher (1.4 kcal/mol) in energy than **1.57**, while for their copper counterparts, **1.52** was much more unstable than **1.53** (6.1 kcal/mol of free energy difference). The much larger energy gap of two NHC-Zn complexes **1.56** and **1.57** compared with NHC-Cu **1.52** and **1.53** could be explained by the significantly greater Lewis acidity of Zn(II) vs. Cu(I). It also might account for different favorable coordination profiles for their sulfonate NHC-metal complexes. As we found, in

NHC–Ag complex **1.58**, the sulfonate group also adopted an anti orientation with the proximal phenyl group on the NHC backbone without chelating to the metal center. This X-ray data²⁵ also indicates that the sulfonate-based NHC ligands are more likely to serve as a monodentate ligand for copper with the sulfonate group sitting anti to the adjacent phenyl substituent on the catalyst backbone as shown in **1.55**, due to the similar Lewis acidity of Cu(I) and Ag(I).



supported by DFT calculations at ω -B97XD/Def2TZVPP_{THF(SMD)}// ω -B97XD/Def2SVP level

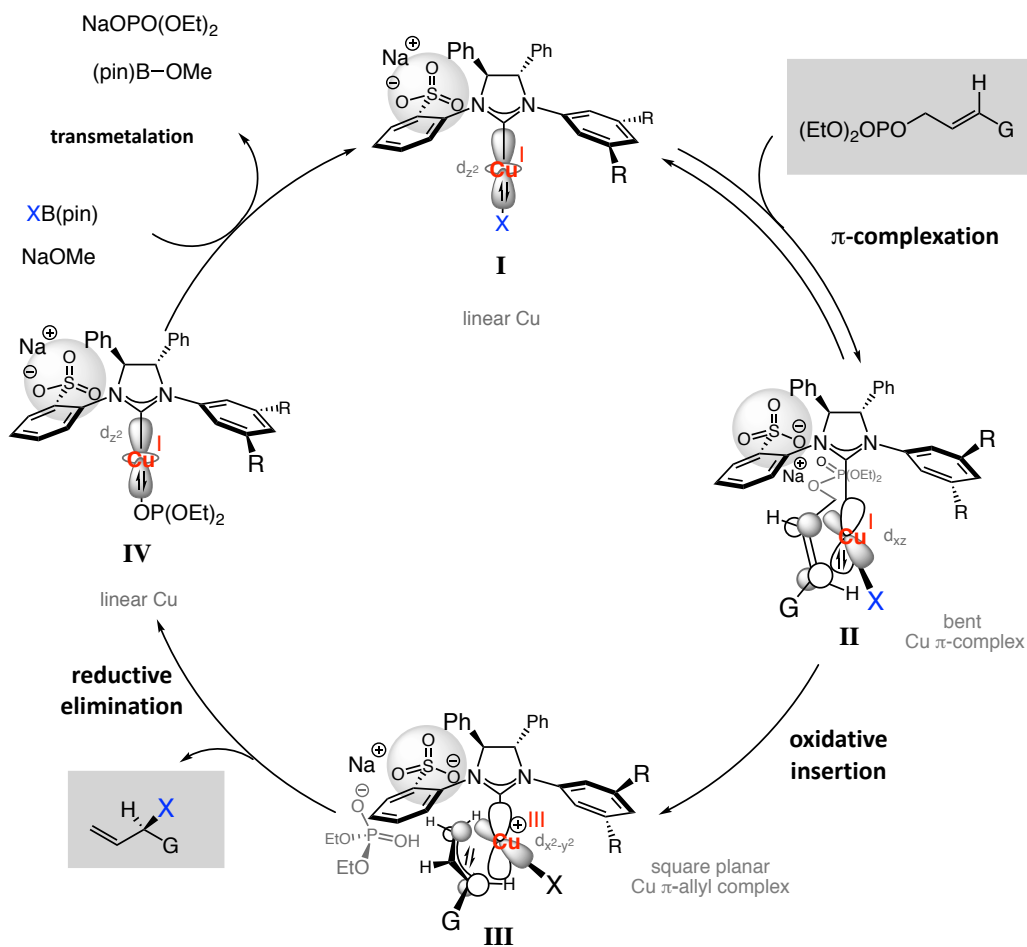
Figure 1.4. DFT Calculations of Mono- and Bidentate-NHC–Zn and NHC–Cu Conformers and X-ray of an NHC–Ag complex

We are fully aware that the energy profiles of the ground states do not have any implication on the energies of the transition states. All possible transition states were

(25) Brown, M. K.; May, T. L.; Baxter, C. A.; Hoveyda, A. H. *Angew Chem. Int. Ed.* **2008**, *46*, 1097–1100.

taken into consideration. As shown in Scheme 1.9, when computed in solution, the results indicate that it is more plausible that sulfonate-containing NHC–Cu species catalyze the reaction through a monodentate coordination structure. In other words, linear Cu(I) species **I** can form bent Cu(I) complex **II**, which can then undergo an oxidative addition to form **III**, which is consistent with the free energy profile for the group state of NHC–Cu complexes. A new stereochemical model **II** was proposed based on DFT calculations. The sulfonate group was oriented anti to the proximal phenyl group on the backbone. In this conformer, the nucleophilic group L on the copper was disfavored from being positioned on the back of the copper center due to steric congestion. Since L occupied the front binding site, the substrate could only approach the copper center from the rear. In order to minimize the lone pair repulsion between the sulfonate and phosphate groups, the sodium cation served to bridge between the two and minimize the transition state energy by reducing charge repulsion as well as stabilize the developing negative charge on the phosphate group. During oxidative insertion, as shown from **II** to **III**, the formation of the incipient Cu–C bond and the rupture of the C–O bond occurred anti to one another instead of syn, as we had previously recently proposed for NHC–Cu catalyzed EAS reactions with B(pin)-substituted allyl nucleophiles in 2014.²⁶

(26) Meng, F.; McGrath, K. P.; Hoveyda, A. H. *Nature* **2014**, *513*, 367–374.

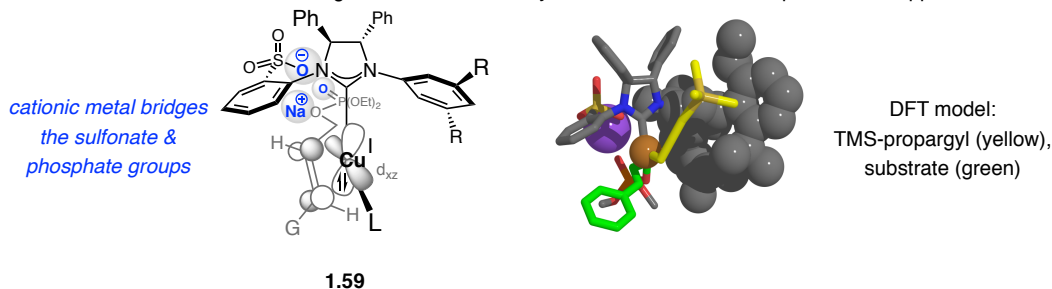
Scheme 1.9. DFT Calculations Support the Monodentate NHC–Cu Species

As shown in **1.59** (Scheme 1.10), it was evident that the cation played a crucial role in obtaining high S_N2' selectivity, because it promotes efficient substrate binding through a second point of contact.²⁴ To challenge this model, different cation metal species and allylic electrophiles with different leaving groups were examined under the EAS reaction conditions. When decreasing the Lewis acidity of the counter ion, less undesired linear (S_N2) product was generated (NaOMe vs. KOMe , 97:3 vs. 85:15 S_N2' : S_N2 selectivity). Changing the leaving group to planar carbonate and acetate, which might be too rigid to participate the cation bridge, also led to much lower yield of the

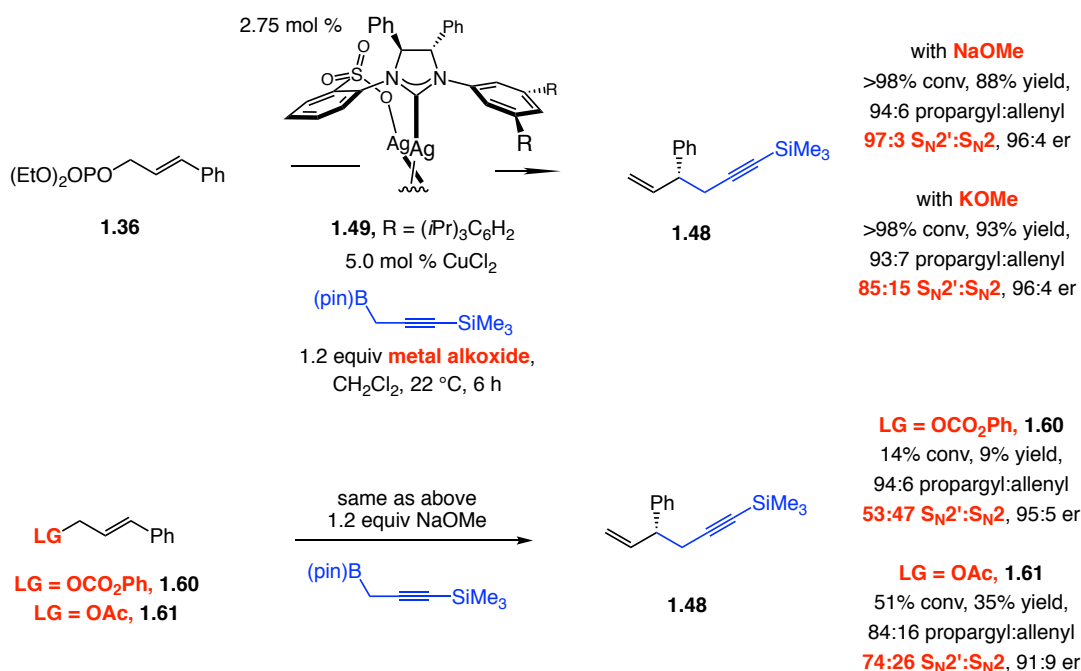
S_N2' addition product with a drastic decrease of branched selectivity (see **1.60**, **1.61**).

These findings also support the plausibility of the current model.

Scheme 1.10. The Existence of the Cation Bridge of Sulfonate NHC by DFT Calculations and Experimental Support



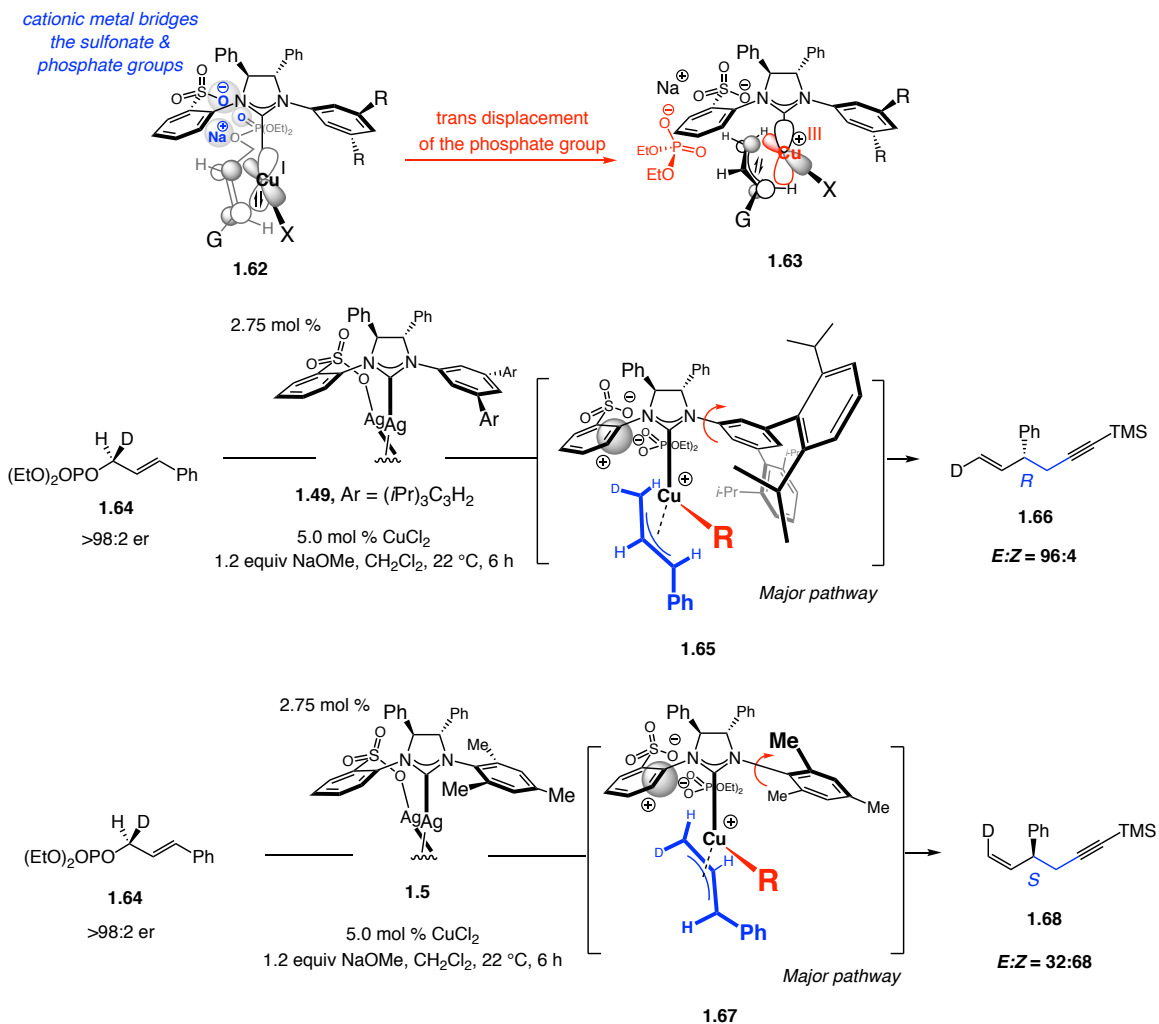
Experimental support for the **coordinating/directing function** of the cationic metal:



As shown in Scheme 1.11, DFT calculation supported during oxidation insertion, from **1.62** to **1.63**, the formation of the incipient Cu–C bond and the rupture of the C–O bond occurred anti to one another. We also performed deuterium-labeled experiments to further challenge our model with sulfonate-containing NHC ligands with meta-substitution and ortho-substitution derived from **1.49** and **1.5**. EAS reactions with the enantiomerically-enriched allylic phosphate **1.64** in the presence of **1.49** leads to a 96:4

E:Z mixture of (*R*)-**1.66** through Cu-(III) intermediate **1.65** while the reaction catalyzed by NHC–Cu generated from **1.5** affords a 32:68 *E:Z* mixture of (*S*)-**1.68** through Cu-(III) intermediate **1.67**, consistent with the enantiomeric ratio gained through the usage of a non-deuterated substrate. (cf. 97:3 er with **1.49** and 31:69 er with **1.5** in Scheme 1.8).

Scheme 1.11. ²D-labeled Experiments Support Trans Displacement of Leaving Group



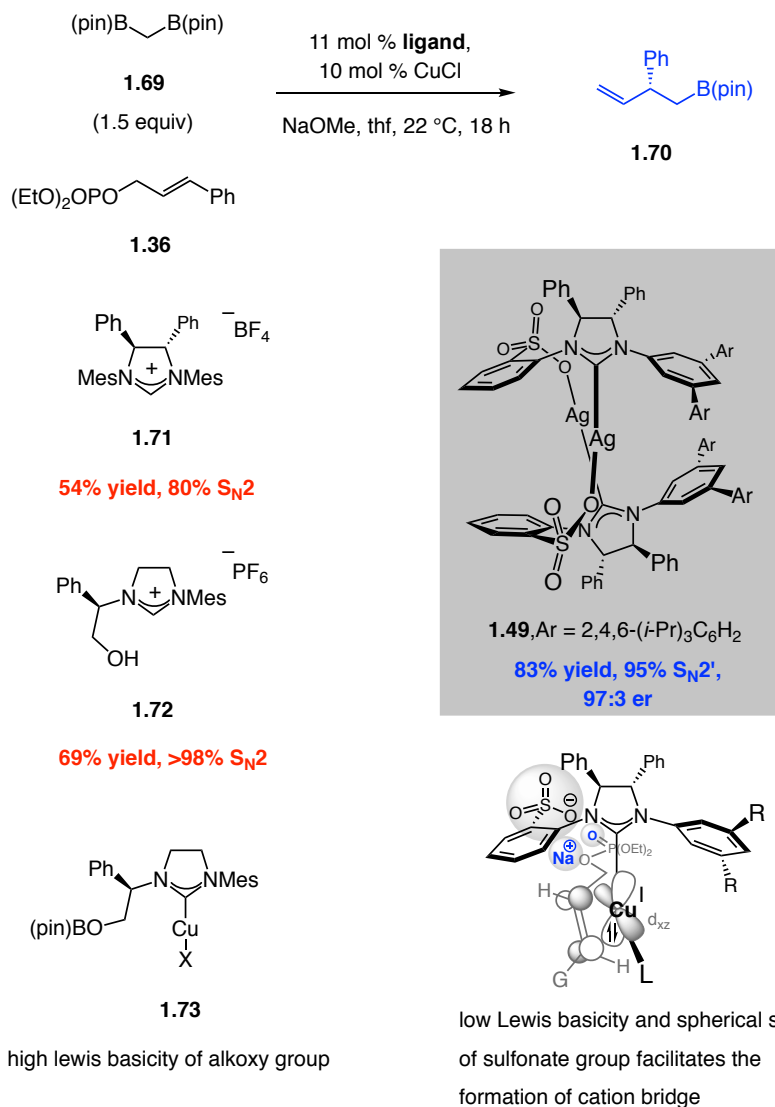
The sulfonate NHC afforded unique reactivity in a series of EAS reactions with a series of boron-based nucleophiles when compared to other NHC ligands without an anionic anchoring group, such as **1.71**, or NHC ligands with a hydroxyl group as an anchoring group, like **1.72**. As shown in Scheme 1.12, to promote the generation of

branched EAS product **1.70** containing an alkyl B(pin) group,²⁷ we examined the EAS reaction with methylenediboron reagent **1.69**. In this case, the sulfonate group is crucial for high S_N2' selectivity since **1.71** and **1.72** mainly deliver the linear S_N2 product.

From previous studies, the sulfonate group had been shown to engage in a secondary binding interaction with the substrate, which is believed to promote S_N2' reactivity. The relatively low Lewis acidity and spherical or symmetrical structure of a sulfonate group contributed to its unique reactivity. The greater Lewis basicity of the alkoxy group in **1.72** might prevent efficient formation of a bridging interaction since B(pin) group could compete with the sodium cation to form a B–O bond (see **1.73**). The symmetrical geometry of the sulfonate group was crucial to the transition state since another oxygen could readily participate in the formation of the cation bridge if the interaction was disrupted.

(27) Shi, Y.; Hoveyda, A. H. *Angew. Chem. Int. Ed.* **2016**, *55*, 3455–3458.

Scheme 1.12. Unique High S_N2' Selectivity and Enantioselectivity Delivered by Sulfonate NHC

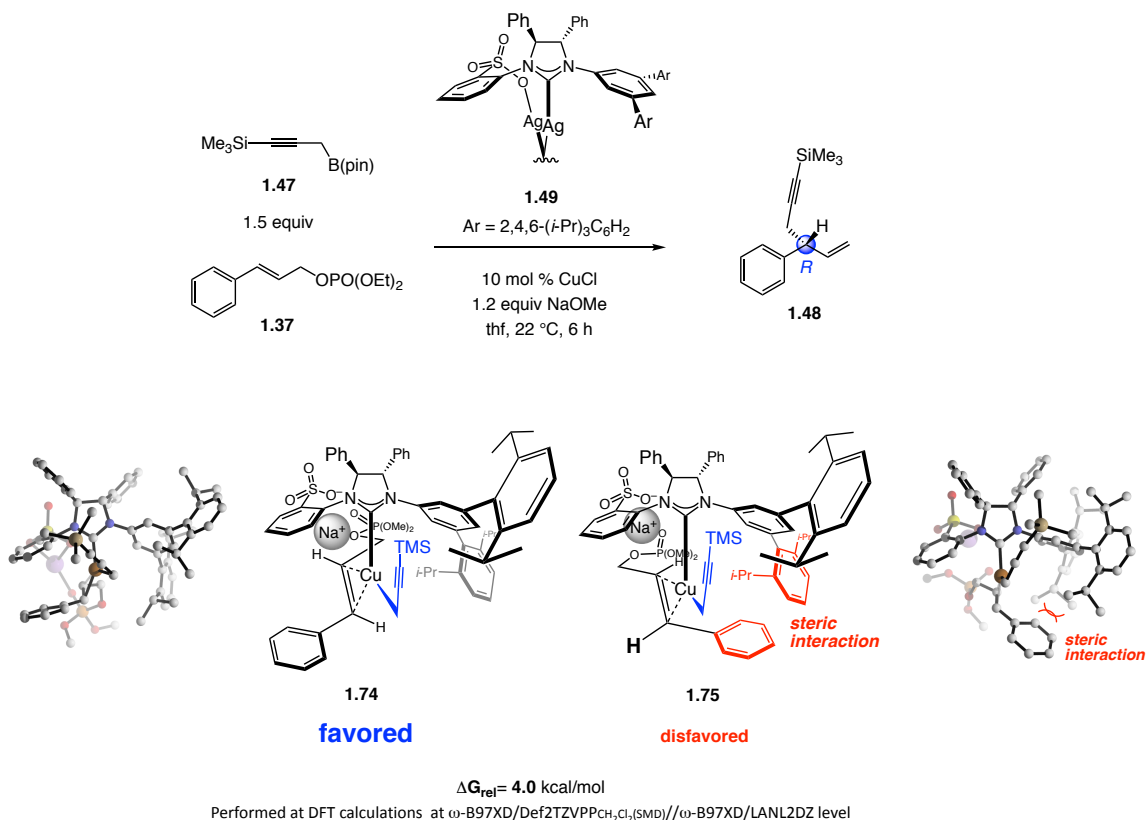


1.2.3.2 Stereochemical Models for EAS Reactions Promoted by Sulfonate-Containing NHC Ligands with Ortho and Meta Substitution Patterns

We sought to determine why sulfonate-based NHC ligands bearing meta- and ortho-substitution pattern yielded opposite enantiomers of product. We started by exploring the stereochemical model for EAS reactions employing a NHC–Cu complex with meta-substitution. In both the major and minor pathways, the sodium cation served

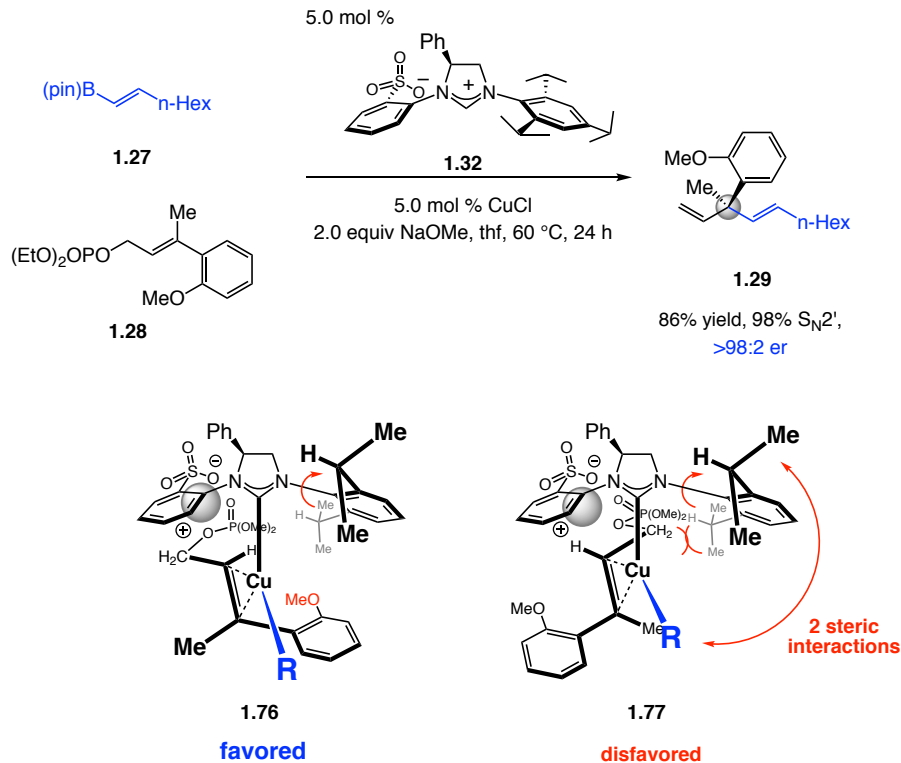
as a secondary binding site between the substrate and the copper catalyst. Additionally, in both pathways, disubstituted allylic phosphate **1.37** approached the copper center from the bottom and the rear of the complex, with its large phenyl group pointing to the left (**1.74**) or right (**1.75**). In the latter mode of binding, the transition state was higher in energy due to the strong steric repulsion between the bulky triisopropylphenyl (Trip) group on the meta position, while this destabilizing interaction was absent in the model for the major mode of addition. This rationale was supported when a decrease in the er was affected by reducing the size of the meta-substituent (compare 83:17 er with **1.40**, 92:8 er with **1.39**, Scheme 1.6).

Scheme 1.13. Stereochemical Model for EAS Reactions with a Propargyl B(pin) Reagent to Generate Tertiary Stereogenic Centers



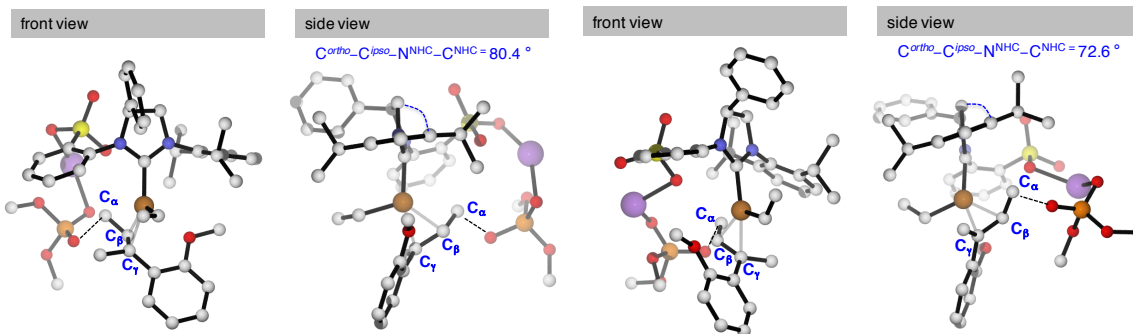
In order to gain more insight into the reaction profile of NHC ligands with an ortho-substituted N-aryl group, we examined the stereochemical model for EAS with

trisubstituted allylic phosphates and alkenyl boron reagents (Scheme 1.14). Similar to the case with the formation of tertiary stereogenic centers, the sodium cation bridge was also found to engage in both the major and minor mode of addition for the generation of the S_N2' product bearing a quaternary stereogenic center. However, in transition state **1.76** leading to the major enantiomer, the large *o*-OMe-phenyl group (compared to the Me group) on the substrate was pointing to the right while in the transition state **1.77** (accounting for the formation of the minor enantiomer), the *o*-OMe-phenyl was oriented to the left. Thus, the opposite enantiomer of product was obtained with the use of NHC–Cu complex derived from **1.32** (Scheme 1.5) in comparison to EAS reactions employing a meta-substituted NHC ligand as delineated in Scheme 1.5. The minor mode of addition **1.77** suffered from the steric interaction between the *i*-Pr group on the 6-position and the methylene group on the phosphate. However, the steric strain could not be alleviated by rotating the N-aryl ring to the front because of steric congestion caused by the proximal alkenyl nucleophile R to the *i*-Pr group on the 2-position. Thus the 2.2 kcal/mol free energy difference led to the higher *er* observed in Scheme 1.5.

Scheme 1.14. Stereochemical Model for EAS Reactions with Alkenyl B(pin) Reagents to Generate Quaternary Stereogenic Centers

$$\Delta G_{\text{rel}} = 2.2 \text{ kcal/mol}$$

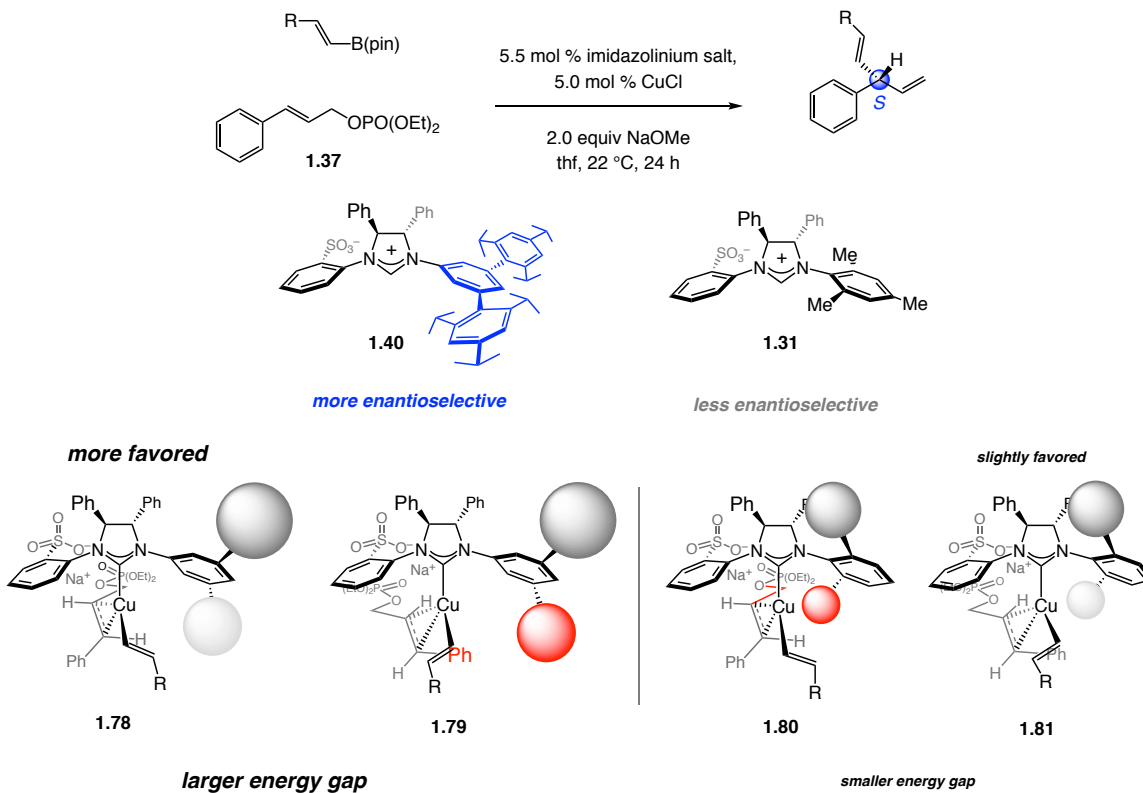
Performed at DFT calculations at $\omega\text{-B97XD/Def2TZVP}_{\text{THF}}(\text{SMD})//\omega\text{-B97XD/LANL2DZ}$ level



With the stereochemical models in hand, we tried to develop a method to inform proper selection of NHC ligands for each transformation. In most cases, in order to achieve high enantioselectivity, EAS reactions required the use of an NHC ligand with meta-substitution to generate tertiary carbon stereogenic centers; while quaternary stereogenic centers required an NHC–Cu complex with ortho substitution. However, this

guideline did not apply to the case of EAS methods with propargyl boron reagent **1.47**. To furnish quaternary stereogenic centers with trisubstituted substrates with high enantioselectivity, meta-substituted NHC ligand required to be used in combination with propargyl B(pin) reagent **1.47**.

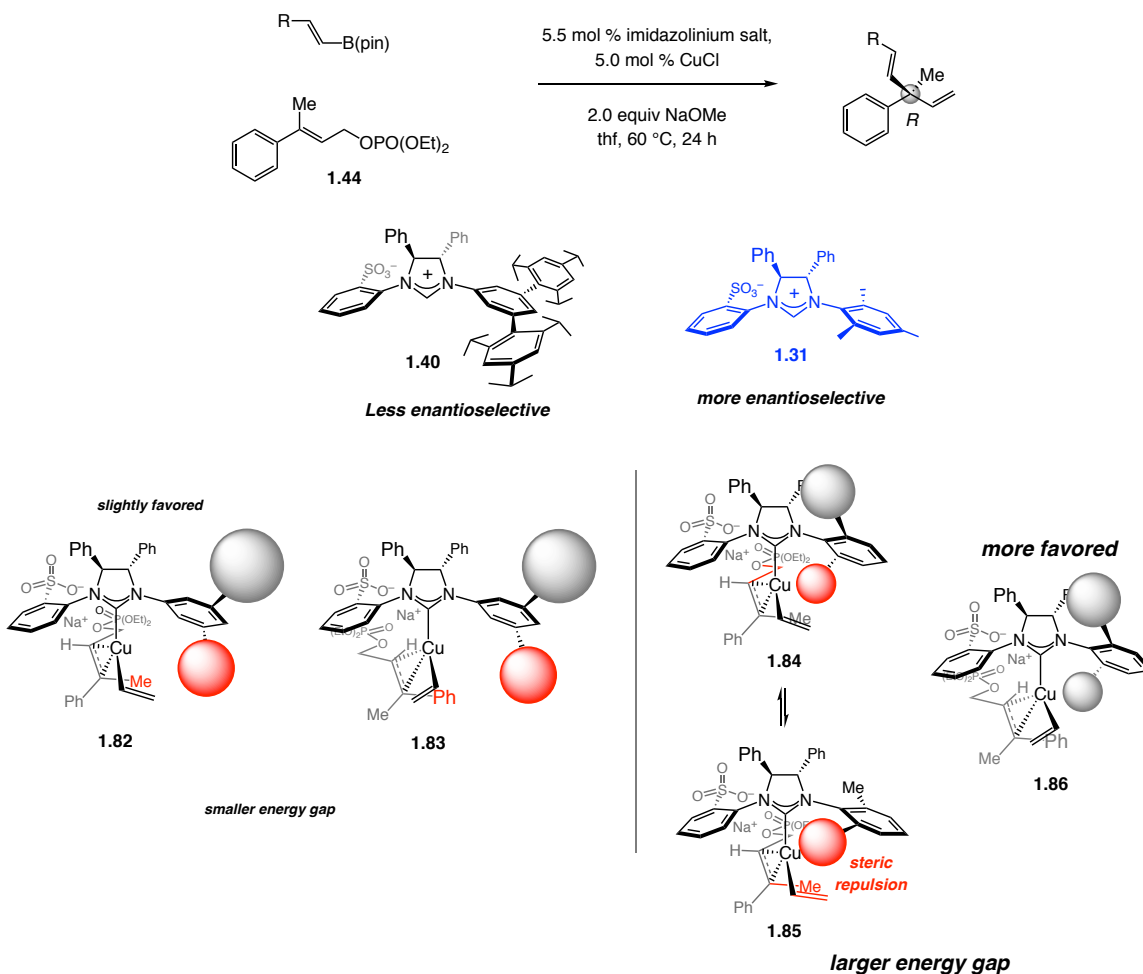
EAS with 1,2-disubstituted allylic phosphates and alkenyl boron reagents was studied as a starting point to understand the use of meta-substituted NHC ligand for the construction of tertiary stereogenic center. A simplified stereochemical model was proposed to explain higher enantiomeric ratios obtained with ligand **1.40** versus **1.31** (Scheme 1.15). As been explained above, the bulky Trip group on the meta position is crucial to obtain the high energy gap between the two possible modes of addition, thus contributing to the high *er* observed in EAS reactions to generate tertiary carbon stereogenic centers. However, when the ortho-substituted **1.31** was used in alkenyl additions to disubstituted substrate **1.37**, the previously favored mode of addition is destabilized due to the introduction of the steric interaction between the ortho substituent on the 6 position and the methylene group attached to the phosphate in **1.80**. However, due to the absence of the methyl group on the allylic phosphate, the energy difference between **1.80** and **1.81** was not large enough to induce high enantioselectivity with the combination of the ortho-substituted ligand and the disubstituted substrate. Thus in this case, EAS reactions catalyzed by ligand **1.39** with meta-substitution afforded the product in high *er*.

Scheme 1.15. Comparison of Stereochemical Models of Ortho- and Meta-N-Aryl NHCs with Disubstituted Substrates

To explain why an ortho-substituted NHC ligand was optimal for the construction of quaternary carbon stereogenic centers in EAS reactions, we applied the simplified model to the trisubstituted substrates as shown in Scheme 1.16. In this case, the optimal ligand was no longer the meta-substituted NHC (**1.40**) due to the undesirable interaction between the additional methyl group on the substrate and 5-substituent on the catalyst in the major pathway (**1.82**), which afforded to a smaller energy gap difference (compared to the transition state **1.83** in the minor pathway). However, when employing the ortho-substituted ligand, the steric interaction between the methyl group with the alkenyl nucleophile in **1.85** caused the N-aryl ring to rotate to the rear to yield the other conformer **1.84**. Thus, this mode of addition (**1.84**) suffered even more severe steric repulsion between the other ortho-substituent and the methylene group on the allylic

phosphate. In other words, the ortho-substituted NHC ligand is necessary for the formation of product with quaternary stereogenic centers in high enantioselectivity.

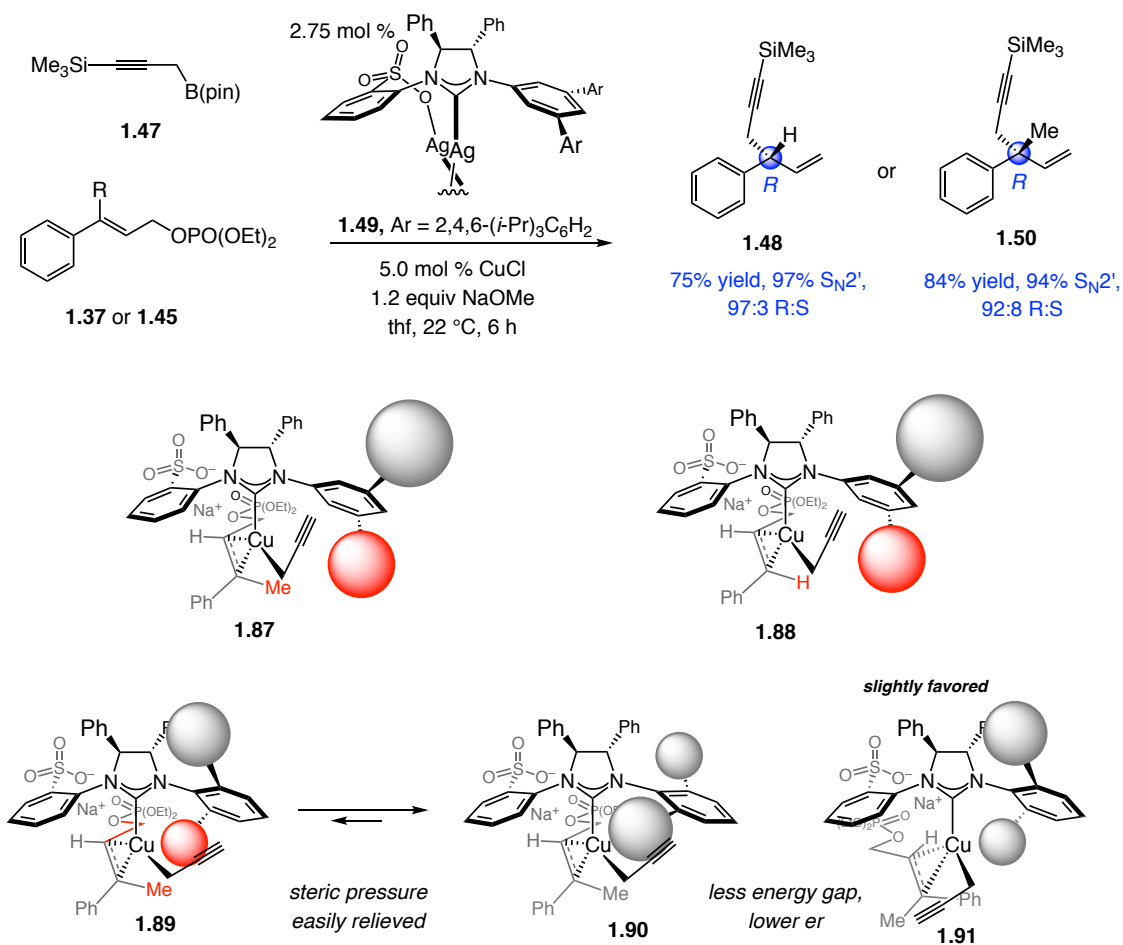
Scheme 1.16. Comparison of Stereochemical Models of Ortho- and Meta-Substituted N-Aryl NHCs with Trisubstituted Substrates



It was surprising to find that in the case of propargyl additions to trisubstituted allylic phosphates, the optimal ligand was the meta-substituted ligand **1.49** (Scheme 1.17), which delivered lower enantioselectivity in most cases. 92:8 er was obtained in the formation of product **1.50** with a quaternary stereogenic center albeit with slightly lower er versus the formation of tertiary stereogenic centers as in **1.48**. The major mode of addition **1.87** is energetically favored over the minor mode of addition **1.88** due to the absence of the steric repulsion between the phenyl group and the substituent on the 5-

position on N-aryl ring. However, in this case, the optimal ligand is no longer ortho-substituted ligand **1.5**. Our rationale for the lower enantiomeric ratio obtained with **1.5** is that the linear propargyl nucleophile is less sterically demanding (compared to the bulky alkenyl group), which reduces the steric strain in the front right quadrant of transition state **1.90**. Due to the flexibility of the methylene group of the propargyl moiety, the ortho-substituent on the NHC is well accommodated when conformer **1.89** rotates to form **1.90**. Thus, the energy of the transition state in the minor pathway (**1.90**) is not destabilized enough compared with **1.91**, the transition state leading to the major enantiomer, to afford high enantioselectivity. In this way, the ortho-substituent can no longer deliver the highest enantioselectivity.

Scheme 1.17. Comparison of Stereochemical Models of Ortho- and Meta-N-Aryl NHC in EAS Reactions with a Propargylboron Reagent



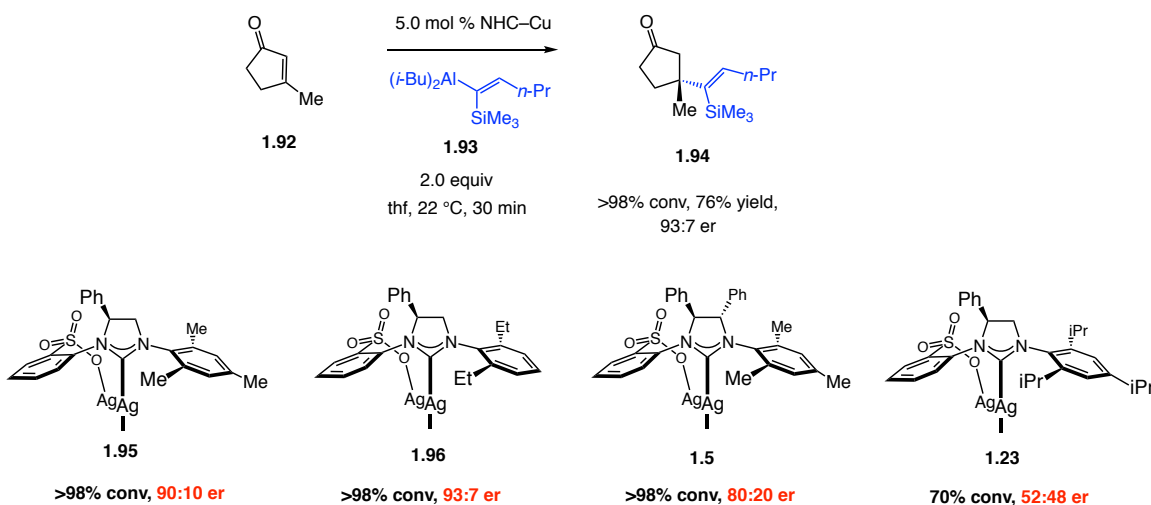
1.3. Catalytic Enantioselective Conjugate Additions

Since DFT calculations can provide detailed mechanistic insight when used in combination with laboratory experiments, we attempted to gain a more complete understanding of the stereochemical model for sulfonate-based NHC–Cu-catalyzed enantioselective conjugate addition (ECA).

1.3.1 Stereochemical Model for Cyclic Enones

In 2008, our group reported the enantioselective conjugate addition of α -silyl alkenylaluminum reagent **1.93** to cyclic enones.²⁸ As shown in Scheme 1.17, **1.94** was obtained in 76% yield with 93:7 er catalyzed by an NHC–Cu complex derived from **1.96**. Decreasing the size of the ortho substituent to methyl groups on the N-aryl ring led to 90:10 er (**1.95**), while increasing the size of the ortho substituent to isopropyl (see **1.23**) completely eroded the enantioselectivity. Incorporation of additional phenyl group on the backbone of the NHC also had a detrimental effect on enantioselectivity (**1.5**).

Scheme 1.18. Stereochemical Model for Conjugate Additions to Cyclic Enones



The stereochemical model in this reaction was also generated through DFT calculations. As shown in Figure 1.5, the sulfonate group again served as a secondary binding site for the substrate. This aluminum bridge through the sulfonate group on the NHC accounted for the high reactivity and enantioselectivity obtained in ECA reactions promoted by this type of ligand. The interaction between the aluminum species and the sulfonate group was covalent bond instead of an electrostatic interaction. Since cyclic enones, such as **1.92**, were more rigid substrates as compared to allylic phosphates, the

(28) May, T. L.; Dabrowski, J. A.; Hoveyda, A. H. *J. Am. Chem. Soc.* **2011**, *133*, 736–739.

secondary binding greatly limited the possible modes of approach for the substrate. In both modes of addition, the enone and the alkenyl group were situated in different quadrants, with the large silyl group on the nucleophile pointing away from the enone (see **1.97** and **1.98**).

It was surprising to find that, in the major pathway, the cyclic enone sits beneath the ortho-substituted N-aryl ring, while in the minor pathway, the substrate accommodates the empty space under the sulfonate-bearing N-aryl group. Initially, it seemed counterintuitive that the substrate would prefer to stay under the more sterically hindered N-aryl ring in the major pathway **1.97**. However, we now believe that three factors contribute to the large energetic difference between the major and minor pathway. As shown in Figure 1.5, in the major pathway, the sulfonate N-aryl ring is oriented towards the rear of the complex in a configuration that favors formation of the aluminum bridge with the enone. This causes the aromatic ring to point away from the large silyl group. In the minor pathway, the sulfonate rotates upwards to accommodate the Al bridge. This rotation of the sulfonate phenyl ring causes the large silyl group to relocate to the right of the complex, where it suffers from steric repulsion with ortho-substituted N-aryl ring. Thus, it led to large energy gap between **1.97** and **1.98**.

The Al–O(sulfonate) bond and the two Al–Me bonds are pointing out of the plane of the page. The other sulfonate oxygen (O_1) can donate its lone pair of electrons to the σ^* Al–O(enone) to stabilize the transition state structure in the major pathway. Of note, this stabilizing interaction is absent due to the orientation of O_1 in the minor pathway **1.98**. Another factor leading to the energetic difference between the major/minor pathways comes from the steric interaction between the Me group on the aluminum

bridge with the enone α -position C_1 . From Scheme 1.5, we can tell that there is a big steric effect depending on the orientation of the Al–Me group with enone C_3 ; the A(1,3) interaction between the two groups raises the free energy in **1.98**.

The above model is in good agreement with the ligand screening data, which shows that increasing the size of the ortho substituent from Me to Et (Scheme 1.18, **1.95** and **1.96**) contributes to an increased energetic difference. This is the result of a more severe interaction between the silyl moiety with the ortho substituent in the minor pathway **1.98**. However, increasing the size of the ortho substituent destabilizes the major transition state when an isopropyl group is installed.

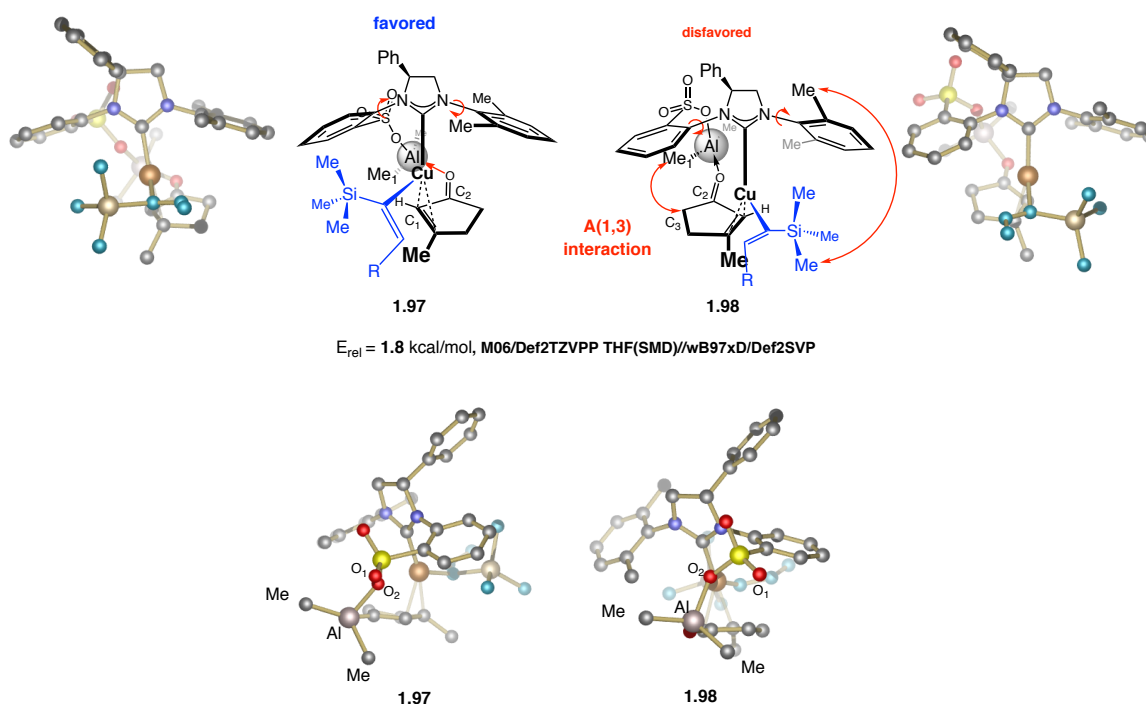


Figure 1.5. Stereochemical Model for Conjugate Additions to Cyclic Enones

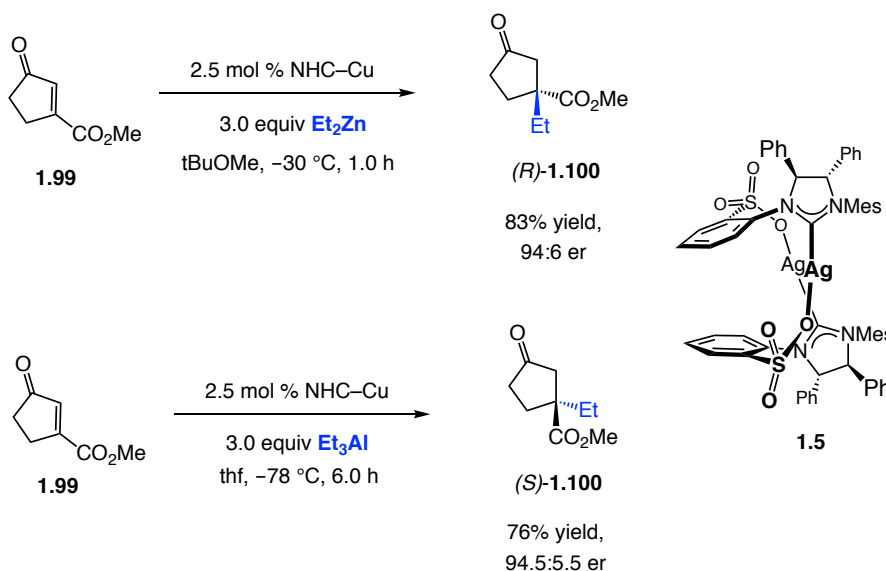
In the case of ECA reactions with organoaluminum reagents, the character of the metal cation bridge possesses covalent bonding character. As has been shown in the scheme above, the covalent nature of the secondary binding site leads to a more rigid

transition state. Thus, better differentiation between the two modes of addition affords the high enantioselectivity.

1.3.2 The Bridging Metal Species is Important

As shown in Scheme 1.19, ECA reactions to a β -ester cyclic enone **1.99** catalyzed by NHC–Cu complex derived from **1.5** employing diethylzinc to afford product (*R*)-**1.100** in 83% yield and 94:6 er.²⁹ To our surprise, when switching the reagent to triethylaluminum,³⁰ the other enantiomer (*S*)-**1.100** was obtained in 76% yield and 94.5:5.5 er. The complete reversal of enantioselectivity was observed when different organometallic metal reagents were used.

Scheme 1.19. Complete Reversal of Enantioselectivity Employing ECA with Organozinc and Organoaluminum Reagents



As shown in Figure 1.6, when the reaction was carried out with triethylaluminum, DFT calculations show that the major and minor pathway **1.101** and **1.102** share a similar scenario as those in Figure 1.6. **1.102** suffers from the steric interaction between the alkyl

(29) Brown, M. K.; May, T. L.; Baxter, C. A.; Hoveyda, A. H. *Angew. Chem., Int. Ed.* **2007**, *46*, 1097–1100.

(30) May, T. L.; Brown, M. K.; Hoveyda, A. H. *Angew. Chem., Int. Ed.* **2008**, *47*, 7358–7362.

substituent on Al and the enone backbone. Thus, the enone prefers to approach the Cu center from the rear of the complex shown in **1.102**. However, when the bridging species is alkylzinc, the Zn bridge adopts a trigonal planar coordination sphere instead of the tetrahedral coordination sphere of the Al bridge due to the relatively low Lewis acidity of the zinc. (Organozinc species do not usually adopt a tetrahedral coordination sphere with one solvent molecule occupying the last coordination site, especially in *t*BuOMe). Thus, when enone **1.99** adopts a similar pathway as it does in **1.101**, the Zn bridge suffers from the steric interaction between the phenyl group on the NHC backbone and the ortho substituent on the N-aryl ring of the NHC. This mode of addition **1.104** is no longer favored due to the absence of A(1,3) interaction in the major pathway **1.103**. Thus in this case, the ECA reaction prefers to form the C–C bond as in mode **1.103** with the lower energy barrier.

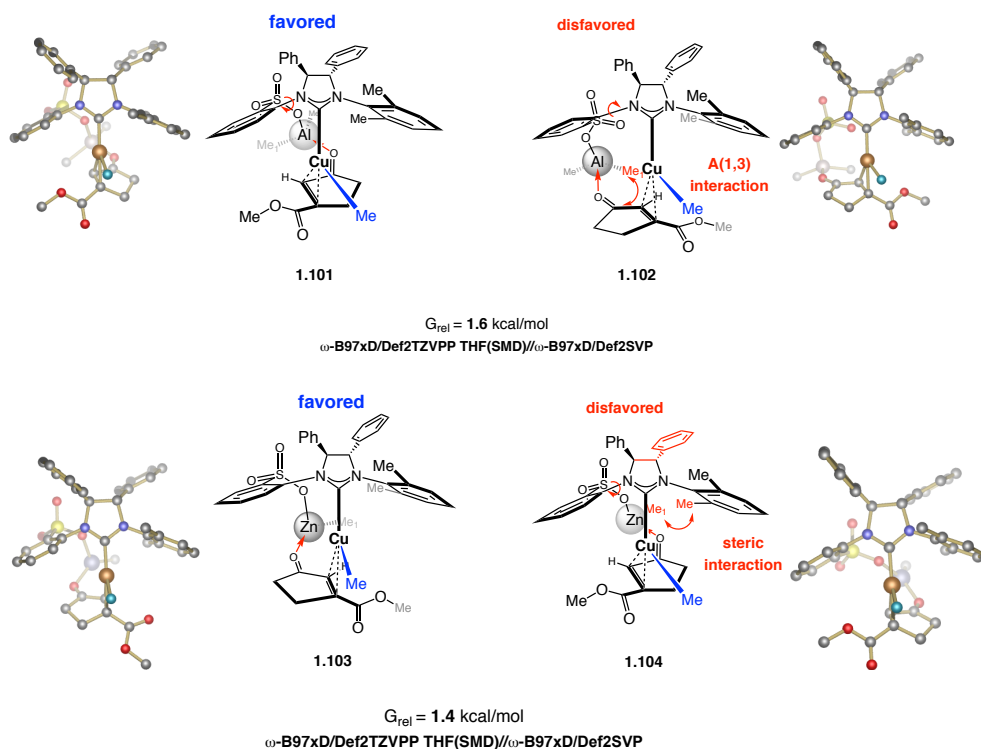


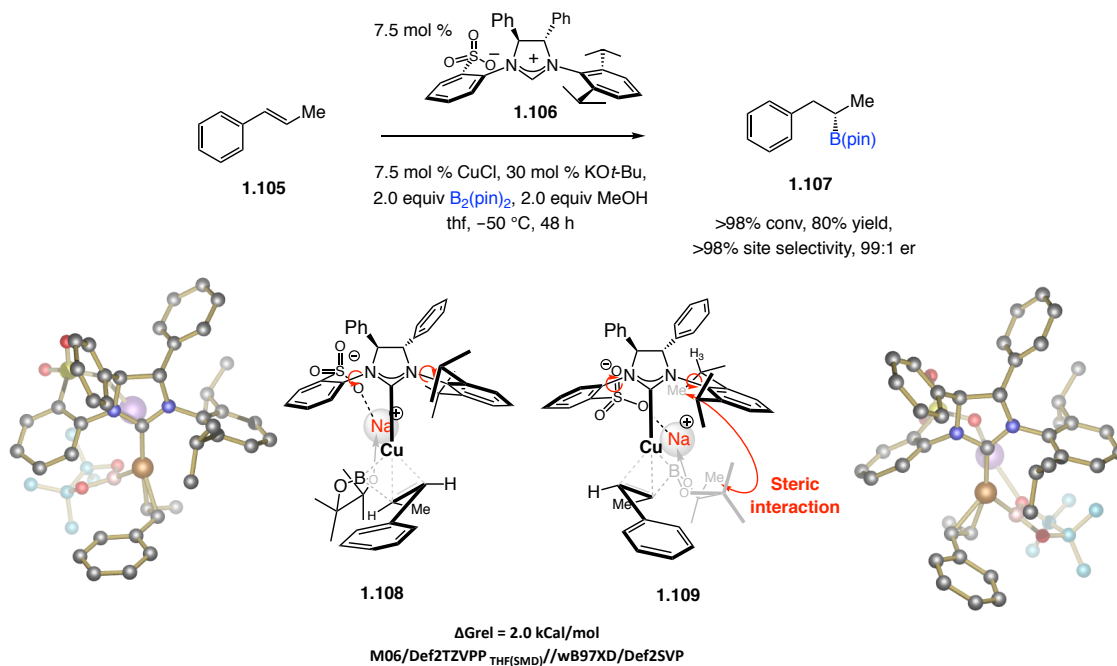
Figure 1.6. The Crucial Role of Bridging Metal Species

1.4. Catalytic Enantioselective Cu–B Additions

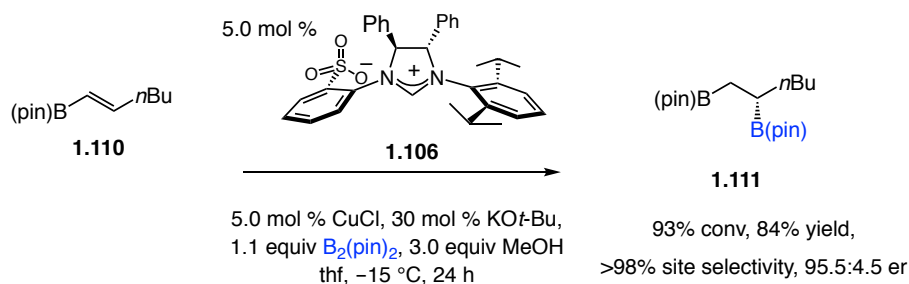
Our group has also explored enantioselective Cu–B additions to activated olefins employing sulfonate-bearing NHC ligands. In these cases, sulfonate NHC ligands afford uniquely high enantioselectivity. Unlike NHC–Cu catalyzed EAS and ECA reactions involving the use of activated olefins with a Lewis basic binding site, the substrates in Cu–B additions generally do not contain an additional Lewis basic binding site. Therefore, the stereochemical model involving a cation bridge between the substrate and the sulfonate is no longer relevant. DFT calculations is required to elucidate the role of sulfonate-based NHC in Cu–B addition reactions.

As shown in Scheme 1.20, ligand **1.106** led to secondary alkyl B(pin) **1.107** in 80% yield, with over 98:2 site-selectivity and 99:1 er.³¹ A stereochemical model was proposed to explain the high enantioselectivity. In this case, the sodium cation no longer bridges the catalyst and the substrate, instead it coordinates to the sulfonate group and the B(pin) nucleophile on the copper center. This facilitates the generation of a bent Cu(I) structure, which is crucial for the binding of the olefin. Generally, this geometric contortion causes the energy of the Cu(I) complex to increase by 20 kcal/mol, but is compensated in this case by the formation of Cu– π -complex. In the major mode of addition, **1.108**, the B(pin) group can be easily accommodated in the rear empty space. However, in the minor pathway **1.109**, the phenyl group on the substrate is situated to avoid repulsive steric interactions with the ortho substituent on the N-aryl ring. This leaves the B(pin) moiety beneath the large isopropyl group in the back. This destabilizing interaction leads to a large energetic difference, generating the high enantioselectivity.

(31) Lee, Y.; Hoveyda, A. H. *J. Am. Chem. Soc.* **2009**, *131*, 3160–3161.

Scheme 1.20. Stereochemical Model for Cu–B Addition Reactions

In 2011, we reported a method involving Cu–B addition to E-alkenyl B(pin) **1.110** to generate 1,2-vincinal diboron product **1.111** as shown in Scheme 1.21.³² In this case the substrate contains another B(pin) to serve as a secondary binding site with the sodium. However, it was interesting to find out that only the B(pin) moiety derived from B₂(pin)₂ participates in the cationic bridge, rather than the B(pin) group on the substrate.

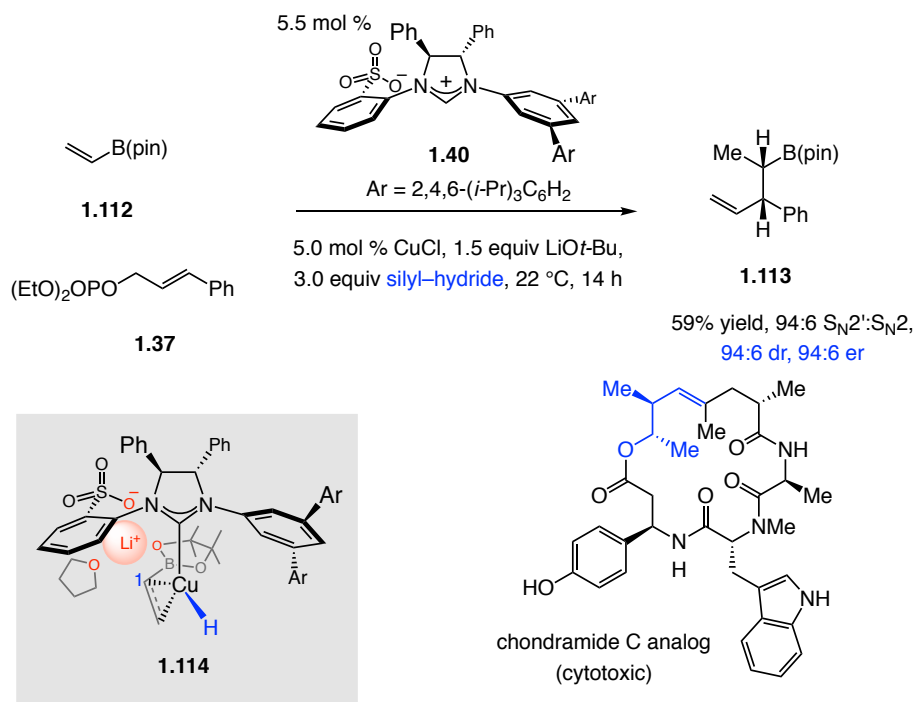
Scheme 1.21. Cu–B Addition to Alkenyl B(pin)

1.5. Catalytic Enantioselective Multicomponent Reactions

(32) Lee, Y.; Jang, H.; Hoveyda, A. H. *J. Am. Chem. Soc.* **2009**, *131*, 18234–18235.

As more stereochemical models have been constructed through the help of DFT calculations, sulfonate NHC ligands have shown to be exceptionally effective in promoting reactions other than EAS and ECA reactions. Recently, multicomponent reaction protocols involving Cu–H addition followed by allylic substitution have been developed in our group. In 2016, we showed that **1.113** was obtained from Cu–H addition to be followed by trapping with allylic phosphate **1.37**.³³ Product containing two contiguous stereogenic centers was obtained in 59% yield, 94:6 dr with 94:6 er. In this case, the Li cation served as the bridging species in the stereochemical model, as in **1.114**. The application to the formal synthesis of chondramide C analog has also demonstrated of the utility of this method.

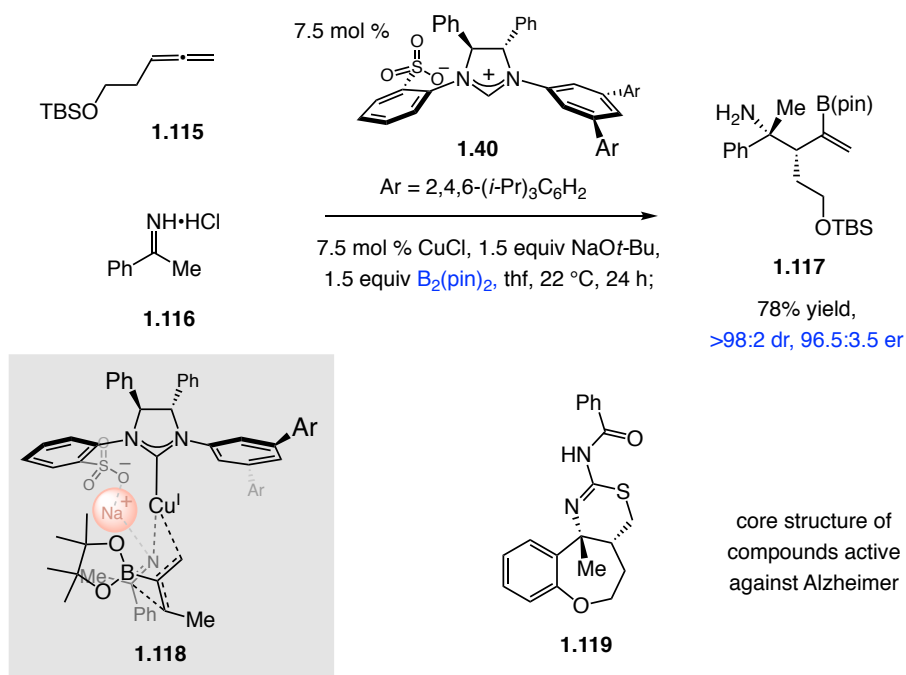
Scheme 1.22. Multicomponent Reaction with Cu–B Species



(33) Lee, J.; Sebastian, T.; Hoveyda, A. H. *Angew. Chem., Int. Ed.* **2017**, *56*, 821–826.

In 2017, our group published another multicomponent reaction to generate α -tertiary amines containing an alkenyl-B(pin) motif (Scheme 1.23).³⁴ The existence of the cationic bridge was confirmed by DFT calculations as shown in **1.118**. The products are derived from ketimines, such as **1.116**, yielding unprotected amines, such as **1.117**, which was directly transformed with without cumbersome or low yielding deprotection strategies. The utility of this method had been demonstrated through the application to the synthesis of compound biologically active **1.119**.

Scheme 1.23. Multicomponent Reaction with Cu-H Species



1.6. Conclusions

The sulfonate-bearing NHC promotes enantioselective Cu-catalyzed transformations of a broad scope of nucleophiles and electrophiles. Mechanistic investigations assisted by DFT calculations point to the existence of secondary binding between the substrate and the catalyst. Thus, the sulfonate bridge helps to form a well-

(34) Jang, H.; Romiti, F.; Sebastian, T.; Hoveyda, A. H. *Nat. Chem.* **2017**, *AOP*.

organized transition state, leading to high enantioselectivity in the Cu-catalyzed reactions. Sulfonate-bearing NHC ligands with different substitution patterns promote EAS reactions with complementary reactivity and enantioselectivity. The modularity of the sulfonate NHC scaffold plays a pivotal role in the process to reach beyond the limitation of the EAS reactions.

Chapter Two

NHC–Cu-Catalyzed Enantioselective Allylic Substitutions with a Silyl-protected Propargyl Boron Reagent to Generate Tertiary and Quaternary Carbon Stereogenic Centers

2.1. Introduction

Catalytic enantioselective allylic substitution (EAS) reactions¹ are among the most versatile classes of transformations in organic chemistry. Such processes deliver enantiomerically enriched products bearing a stereogenic center adjacent to a functionalizable alkene from readily accessible allylic electrophiles. Despite significant progress made in the past two decades, the majority of the studies in this area focused on the additions of an alkyl group through Cu-catalysis with the choice of proper nucleophilic “hard” alkyl metal reagent (Figure 2.1).²

(1) For reviews on allylic substitution reactions catalyzed by other transition metals and with “soft” nucleophiles, see: (a) Trost, B. M.; Lee, C. In *Catalytic Asymmetric Synthesis*; Ojijima, I., Ed.; Wiley-VCH:Weinheim, Germany, 2000; Chapter 8E. (b) Trost, B. M.; Crawley, M. L. *Chem. Rev.* **2003**, *103*, 2921–2944. (c) Stanley, L. M.; Hartwig, J. F. *Acc. Chem. Res.* **2010**, *43*, 1461–1475. (d) Trost, B. M. *Org. Process Res. Dev.* **2012**, *16*, 185–194. (e) Tosatti, P.; Nelson, A.; Marsden, S. P. *Org. Biomol. Chem.* **2012**, *10*, 3147–3163.

(2) References for the Pie-Chart of Catalytic Enantioselective Allylic Substitutions generating a tertiary stereogenic center involving a “hard” nucleophile: *Alkyl Additions*: see reviews: (a) Hoveyda, A. H.; Hird, A. W.; Kacprzynski, M. A. *Chem. Commun.* **2004**, 1779–1785. (b) Yorimitsu, H.; Oshima, K. *Angew. Chem., Int. Ed.*, **2005**, *44*, 4435–4439. (c) Kar, A.; Argade, N. P. *Synthesis*, **2005**, 2995–3022. (d) Alexakis, A.; Malan, C.; Lea, L.; Tissot-Croset, K.; Polet, D.; Falciola, C. *Chimia*, **2006**, *60*, 124–130. (e) Falciola, C. A.; Alexakis, A. *Eur. J. Org. Chem.* **2008**, *22*, 3765–3780. (f) Yokobori, U.; Ohmiya, H.; Sawamura, M.

Organometallics, **2012**, *31*, 7909–7913. *Aryl/Heteroaryl Additions*: (aa) Jackowski, O.; Alexakis, A. *Angew. Chem. Int. Ed.* **2010**, *49*, 3346–3350. (ab) Falciola, C. A.; Alexakis, A. *Chem. Eur. J.* **2008**, *14*, 10615–10627. (ac) Polet, D.; Rathgeb, X.; Falciola, C. A.; Langlois, J.-B.; Hajjaji, S. E.; Alexakis, A. *Chem. Eur. J.* **2009**, *15*, 1205–1216. (ad) Selim, K. B.; Matsumoto, Y.; Yamada, K.; Tomioka, K. *Angew. Chem. Int. Ed.* **2009**, *48*, 8733–8735. (ae) Millet, R.; Bernardez, T.; Palais, L.; Alexakis, A. *Tetrahedron Lett.* **2009**, *50*, 3474–3477. (af) Selim, K. B.; Yamada, K.; Tomioka, K. *Chem. Commun.* **2008**, 5140–5142. (ag) Alexakis, A.; Hajjaji, S. E.; Polet, D.; Rathgeb, X. *Org. Lett.* **2007**, *9*, 3393–3395. (ah) Selim, K. B.; Nakanishi, H.; Matsumoto, Y.; Yamamoto, Y.; Yamada, K.; Tomioka, K. *J. Org. Chem.* **2011**, *76*, 1398–1408. (ai) Pérez, M.; Fañanás-Mastral, M.; Bos, P. H.; Rudolph, A.; Harutyunyan, S. R.; Feringa, B. L. *Nat. Chem.* **2011**, *3*, 377–381. *Alkenyl Additions*: (ba) Gao, F.; Carr, J. L.; Hoveyda, A. H. *Angew. Chem. Int. Ed.*, **2012**, *51*, 6613–6617. (bb) Shintani, R.; Takatsu, K.; Takeda, M.; Hayashi, T. *Angew. Chem. Int. Ed.*, **2011**, *50*, 8656–8659. (bc) Lee, Y.; Akiyama, K.; Gillingham, D. G.; Brown, K. M.; Hoveyda, A. H. *J. Am. Chem. Soc.* **2008**, *130*, 446–447. (bd) Hamilton, J. Y.; Sarlah, D.; Carreira, E. M. *J. Am. Chem. Soc.* **2013**, *135*, 994–997. (be) Gao, F.; Hoveyda, A. H. *J. Am. Chem. Soc.* **2010**, *132*, 10961–10963. (bf) Akiyama, K.; Gao, F.; Hoveyda, A. H. *Angew. Chem. Int. Ed.* **2010**, *49*, 419–423. *Alkynyl Additions*: (ca) Harada, A.; Makida, Y.; Sato, T.; Ohmiya, H.; Sawamura, M. *J. Am. Chem. Soc.* **2014**, *136*, 13932–13939. (cb) Dabrowski, J. A.; Haeffner, F.; Hoveyda, A. H. *Angew. Chem. Int. Ed.* **2013**, *52*, 7694–7699. (cc) Hamilton, J. Y.; Sarlah, D.; Carreira, E. M. *Angew. Chem. Int. Ed.* **2013**, *52*, 7532–7535. *Allenyl Additions*: (da) Jung, B.; Hoveyda, A. H. *J. Am. Chem. Soc.* **2012**, *134*, 1490–1493. *Allyl Additions*: (ea) Le, H.; Kyne, R. E.; Brozek, L. A.; Morken, J. P. *Org. Lett.* **2013**, *15*, 1432–1435. (eb) Zhang, P.; Morken, J. P. *J. Am. Chem. Soc.* **2009**, *131*, 12550–12551. (ec) Ardolino, M. J.; Morken, J. P. *J. Am. Chem. Soc.* **2014**, *136*, 7092–7100. (ed) Hamilton, J. Y.; Sarlah, D.; Carreira, E. M. *J. Am. Chem. Soc.* **2014**, *136*, 3006–3009. (ee) Hornillos, V.; Pérez, M.; Fañanás-Mastral, M.; Feringa, B. L. *J. Am. Chem. Soc.* **2013**, *135*, 2140–2143. (ef) Brozek, L. A.; Ardolino, M. J.; Morken, J. P. *J. Am. Chem. Soc.* **2011**, *133*, 16778–16781. (eg) Hamilton, J. Y.; Hauser, N.; Sarlah, D.; M. Carreira, E. M. *Angew. Chem. Int. Ed.* **2014**, *53*, 10759–10762. (eh) Zhang, P.; Brozek, L. A.; Morken, J. P. *J. Am. Chem. Soc.* **2010**, *132*, 10686–10688. (ei) Meng, F.; McGrath, K. P.; Hoveyda, A. H. *Nature* **2014**, *513*, 367–374. *Boryl Additions*: (fa) Ito, H.; Ito, S.; Sasaki, Y.; Matsuura, K.; Sawamura, M. *J. Am. Chem. Soc.* **2007**, *129*, 14856–14857. (fb) A. Guzman-Martinez, A.; Hoveyda, A. H. *J. Am. Chem. Soc.*, **2010**, *132*, 10634–10637. (fc) Park, J. K.; Lackey, H. H.; Ondrusek, B. A.; McQuade, D. T. *J. Am. Chem. Soc.* **2011**, *133*, 2410–2413. Yamamoto, E.; Takenouchi, Y.; Ozaki, T.; Miya, T.; Ito, H. *J. Am. Chem. Soc.* **2014**, *136*, 16515–16521. (fd) Park, J. K.; McQuade, D. T. *Synthesis* **2012**, *44*, 1485–1490. (fe) Ito, H.; Okura, T.; Kou Matsuura, K.; Sawamura, M. *Angew. Chem. Int. Ed.*, **2010**, *49*, 560–563. *Silyl Additions*: (ga) Delvos, L. B.; Vyas, D. J.; Oestreich, M. *Angew. Chem. Int. Ed.*, **2013**, *52*, 4650–4653. (gb) Takeda, M.; Shintani, R.; Hayashi, T. *J. Org. Chem.* **2013**, *78*, 5007–5017. Catalytic EAS reactions generating a quaternary carbon stereogenic center involving a “hard” nucleophile: *Alkyl Additions*: (ha) Luchaco-Cullis, C. A.; Mizutani, H.; Murphy, K. E.; Hoveyda, A. H. *Angew. Chem., Int. Ed.*, **2001**, *40*, 1456–1460. (hb) Kacprzynski, M. A.; Hoveyda, A. H. *J. Am. Chem. Soc.* **2004**, *126*, 10676–10681. (hc) Lee, Y.; Hoveyda, A. H. *J. Am. Chem. Soc.*, **2006**, *128*, 15604–15605. (hd) Lee, Y.; Li, B.; Hoveyda, A. H. *J. Am. Chem. Soc.*, **2009**, *131*, 11625–11633. (he) Grassi, D.; Li, H.; Alexakis, A. *Chem. Comm.* **2012**, *48*, 11404–11406. (hf) Fañanás-Mastral, M.; Pérez, M.; Bos, P. H.; Rudolph, A.; Harutyunyan, S. R.; Feringa, B. L. *Angew. Chem. Int. Ed.* **2012**, *51*, 1922–1925. (hg) Jackowski, O.; Alexakis, A. *Angew. Chem. Int. Ed.* **2010**, *49*, 3346–3350. (hh) Magrez, M.; Le Guen, Y.; Baslé, O.; Crvisy, C.; Mauduit, M. *Chem. Eur. J.* **2013**, *19*, 1199–1203. (hi) Larsen, A. O.; Leu, W.; Oberhuber, C. N.; Campbell, J. E.; Hoveyda, A. H. *J. Am. Chem. Soc.* **2004**, *126*, 11130–11131. (hj) J. J. Van Veldhuizen, J. E. Campbell, R. E. Giudici, R. E.; Hoveyda, A. H. *J. Am. Chem. Soc.*, **2005**, *127*, 6877–6882. (hk) M. A. Kacprzynski, M. A.; May, T. L.; Kazane; S. A.; Hoveyda, A. H. *Angew. Chem., Int. Ed.*, **2007**, *46*, 4554–4558. (hl) Falciola, C. A.; Alexakis, A. *Chem. Eur. J.* **2008**, *14*, 10615–10627. (hm) Grassi, D.; Alexakis, A. *Angew. Chem. Int. Ed.* **2013**, *52*, 13642–13646. (hn) Hojoh, K.; Shido, Y.; Ohmiya, H.; Sawamura, M. *Angew. Chem. Int. Ed.* **2014**, *53*, 4954–4958. *Aryl/Heteroaryl Additions*: (ia) Gao, F.; McGrath, K. P.; Y. Lee, Y.; Hoveyda, A. H. *J. Am. Chem. Soc.*, **2010**, *132*, 14315–14320. (ib) Kacprzynski, M. A.; May, T. L.; Kazane, S. A.; Hoveyda, A. H. *Angew. Chem. Int. Ed.* **2007**, *46*, 4554–4558. (ic) Takeda, M.; Takatsu, K.; Shintani, R.; Hayashi, T. *J. Org. Chem.* **2014**, *79*, 2354–2367. *Alkenyl Additions*: (ja) Gao, F.; McGrath, K. P.; Lee, Y.; Hoveyda, A. H. *J. Am. Chem. Soc.* **2010**, *132*, 14315–14320. (jb) Gao, F.; Carr, J. L.; Hoveyda, A. H. *Angew. Chem. Int. Ed.* **2012**, *51*, 6613–6617. *Alkynyl Additions*: (ka) Dabrowski, J. A.; Gao, F.; Hoveyda, A. H. *J. Am. Chem. Soc.* **2011**, *133*, 4778–4781. *Allenyl Additions*:

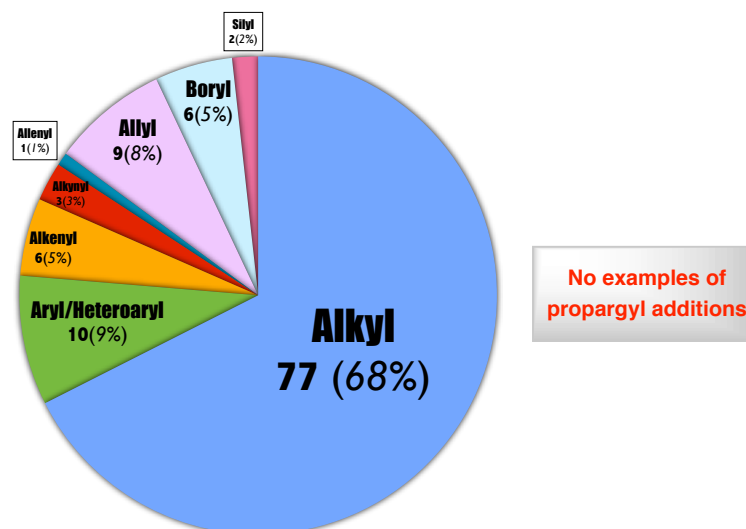
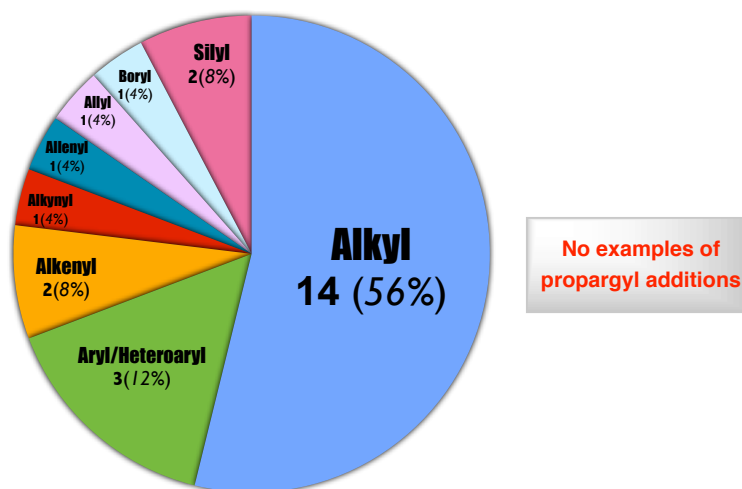
a) Distribution of catalytic EAS reactions generating a *tertiary* stereogenic centerb) Distribution of catalytic EAS reactions generating a *quaternary* stereogenic center

Figure 2.1. Moieties Introduced by Catalytic EAS Reactions (2015)

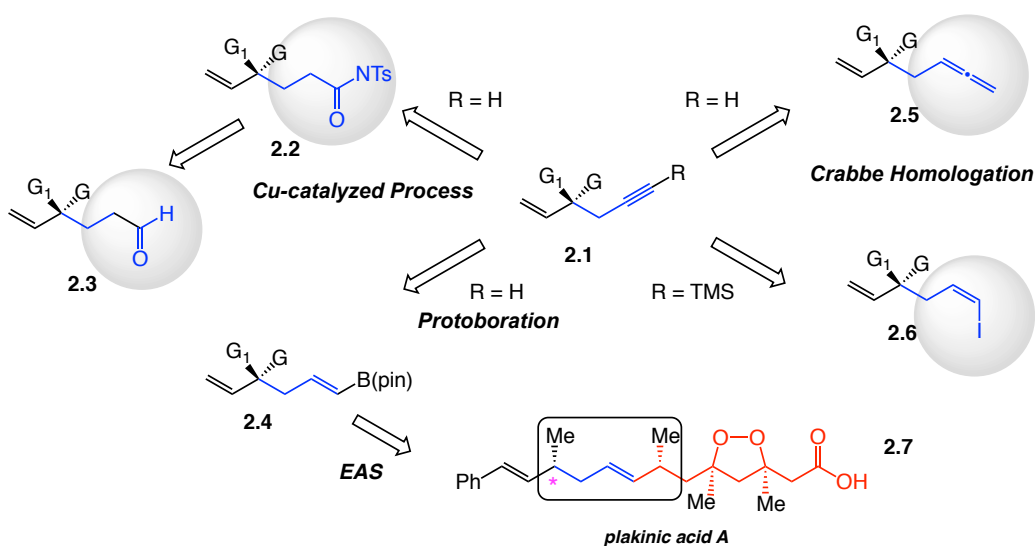
Alkynes are of high value in synthetic chemistry.³ Not only are alkynes often found embedded in the structures of natural products, they are also useful for installation of multiple functional groups. Efficient protocols for the preparation of enantiomerically enriched alkyne-substituted molecules is of substantial synthetic value as precursors to

(la) Jung, B.; Hoveyda, A. H. *J. Am. Chem. Soc.* **2012**, *134*, 1490–1493. *Allyl Additions*: (ma) Zhang, P.; Le, H.; Kyne, R. E.; Morcken, J. P. *J. Am. Chem. Soc.* **2011**, *133*, 9716–9719. *Boryl Additions*: (na) Guzman-Martinez, A.; Hoveyda, A. H. *J. Am. Chem. Soc.* **2010**, *132*, 10634–10637. *Silyl Additions*: (oa) Takeda, M.; Shintani, R.; Hayashi, T. *J. Org. Chem.* **2013**, *78*, 5007–5017. (ob) Delvos, L. B.; Hensel, A.; Oestreich, M. *Synthesis* **2014**, *46*, 2957–2964.

(3) *Modern Acetylene Chemistry*; Stang, P. J., Diederich, F., Eds; VCH: Weinheim, 1995.

alkyl, alkenyl, allenyl and carbonyl adducts as shown in Scheme 2.1.⁴ We envisioned that the development of an EAS reaction to incorporate a stereogenic center bearing a propargyl group could be of synthetic utility and streamline the synthesis of natural products, such as plakinic acid A, from the enantiomerically-enriched alkyne product **2.1**. However, Cu-catalyzed enantioselective propargyl additions to allylic phosphates had not been previously reported.

Scheme 2.1. Utility of Propargyl Addition Product and Its Application to Natural Product Synthesis

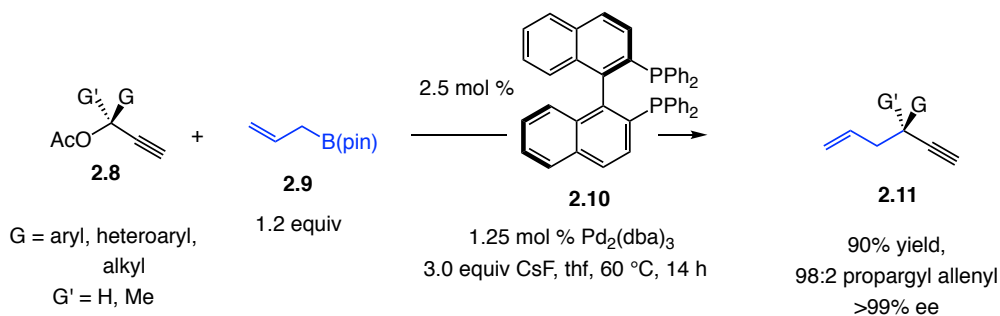


2.2. Background

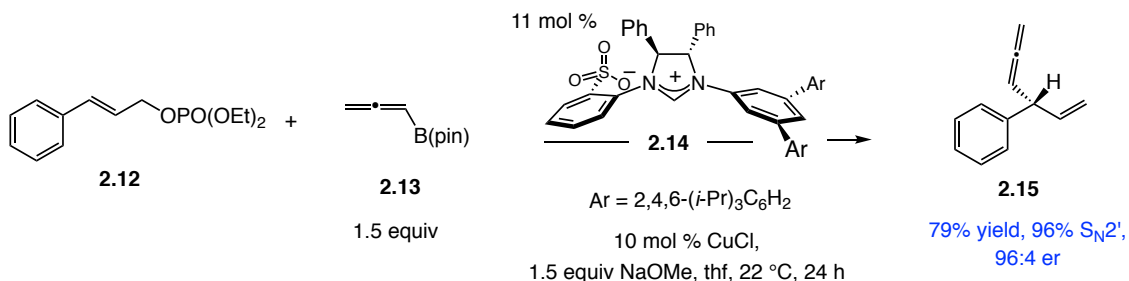
In 2012, the Morken group delineated the protocol for Pd-catalyzed diastereoselective allylations of enantiomerically-enriched propargyl acetates. 1, 5-Enynes, such as **2.11**, were generated in up to 90% yield and 98:2 propargyl/allenyl selectivity and >99% ee.⁵ Alkyl, aryl and heteroaryl substrates with a tertiary or quaternary substituted stereogenic center are all suitable for the transformation.

(4) For transformations of alkynes into various functional groups, see: (a) R. C. Larock, *Comprehensive Organic Transformations*; VCH: New York, NY, 1999. (b) Yu, S.; Ma, S. *Chem. Commun.* **2011**, 47, 5384–5418.

(5) Ardolino, M. J.; Morken, J. P. *J. Am. Chem. Soc.* **2012**, 134, 8770–8773.

Scheme 2.2. Diastereoselective Allylation of Enantiomerically-Enriched Propargyl Acetates

Boron-based reagents⁶ have only recently been introduced as partners in Cu-catalyzed EAS reactions, offering a more practical, tolerant and mild alternative to the traditional organometallic reagents. In 2012, our group disclosed a Cu-catalyzed allenyl addition reaction to allylic phosphates with commercially available allenyl B(pin) **2.13**.⁷ Installation of the stereogenic center can be achieved by employing a NHC–Cu catalyst derived from CuCl and imidazolium salt **2.14**.

Scheme 2.3. Cu-Catalyzed EAS Reaction with An Allenylboron Reagent

2.3. Catalytic Enantioselective Allylic Substitutions with a Silyl-Protected Propargyl Boron Reagent

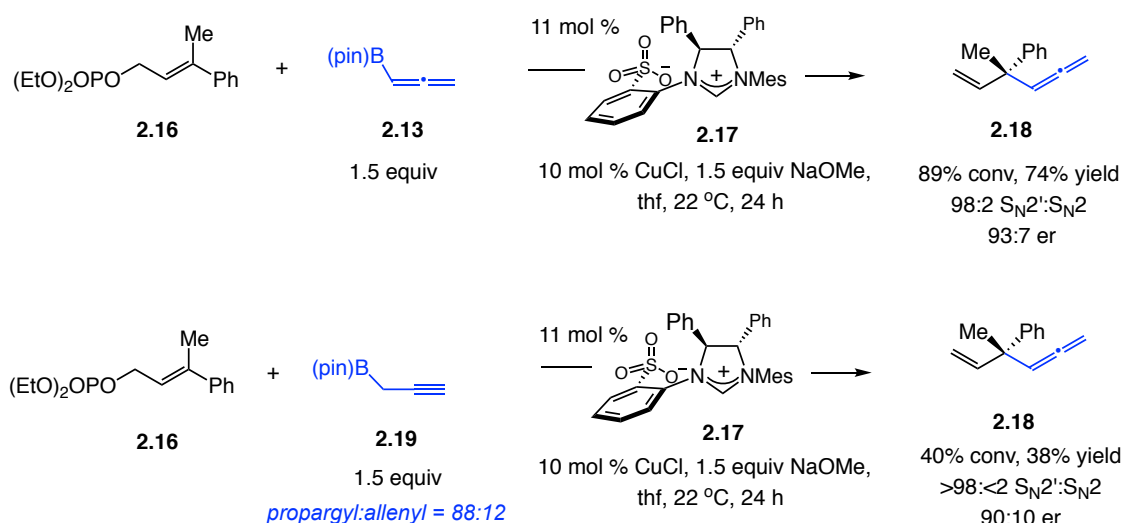
2.3.1 An Easily Accessible Propargyl Pinacolboron Reagent

(6) Cu-catalyzed EAS with *aryl* boron nucleophiles: (a) see ref 3bb, 3ic; with *alkenyl* boron nucleophiles: (b) see 3ba. (c) Gao, F.; Carr, J. L.; Hoveyda, A. H. *J. Am. Chem. Soc.* **2014**, *136*, 2149–2161; with *alkyl* boron nucleophiles: (d) Shido, Y.; Yoshida, M.; Tanabe, M.; Ohmiya, H.; Sawamura, M. *J. Am. Chem. Soc.* **2012**, *134*, 18573–18576; with *alkenyl* boron nucleophiles: (e) Jung, B.; Hoveyda, A. H. *J. Am. Chem. Soc.* **2012**, *134*, 1490–1493; with *allyl* boron nucleophiles: (f) Yasuda, Y.; Ohmiya, H.; Sawamura, M. *Angew. Chem. Int. Ed.*, **2016**, *55*, 10816–10820.

(7) see reference 6e.

We tried to develop a protocol for Cu-catalyzed enantioselective propargyl additions to allylic phosphates with an unprotected propargyl B(pin) reagent **2.19**⁸, but only the allenyl addition product **2.18** was obtained in 38% yield and 90:10 er using previously reported conditions.⁹ This showed that 1) π -allyl isomerization between the allenyl–Cu and propargyl–Cu species readily interconverted following transmetalation and 2) the more reactive allenyl–Cu species¹⁰ undergoes transformation to afford EAS products.

Scheme 2.4. Cu-Catalyzed EAS Reaction with an Unprotected Propargylboron Reagent



2.3.2 Synthesis of Propargyl-Substituted Tertiary Carbon Stereogenic Centers:

Additions to Allylic Phosphates that Contain a Disubstituted Alkene

We envisioned that a TMS-protected propargyl B(pin) **2.20** may enable selective addition of the propargyl group by disfavoring allenyl addition through steric control. As shown in Table 2.1, we found that when **2.20** was utilized under the reaction conditions,

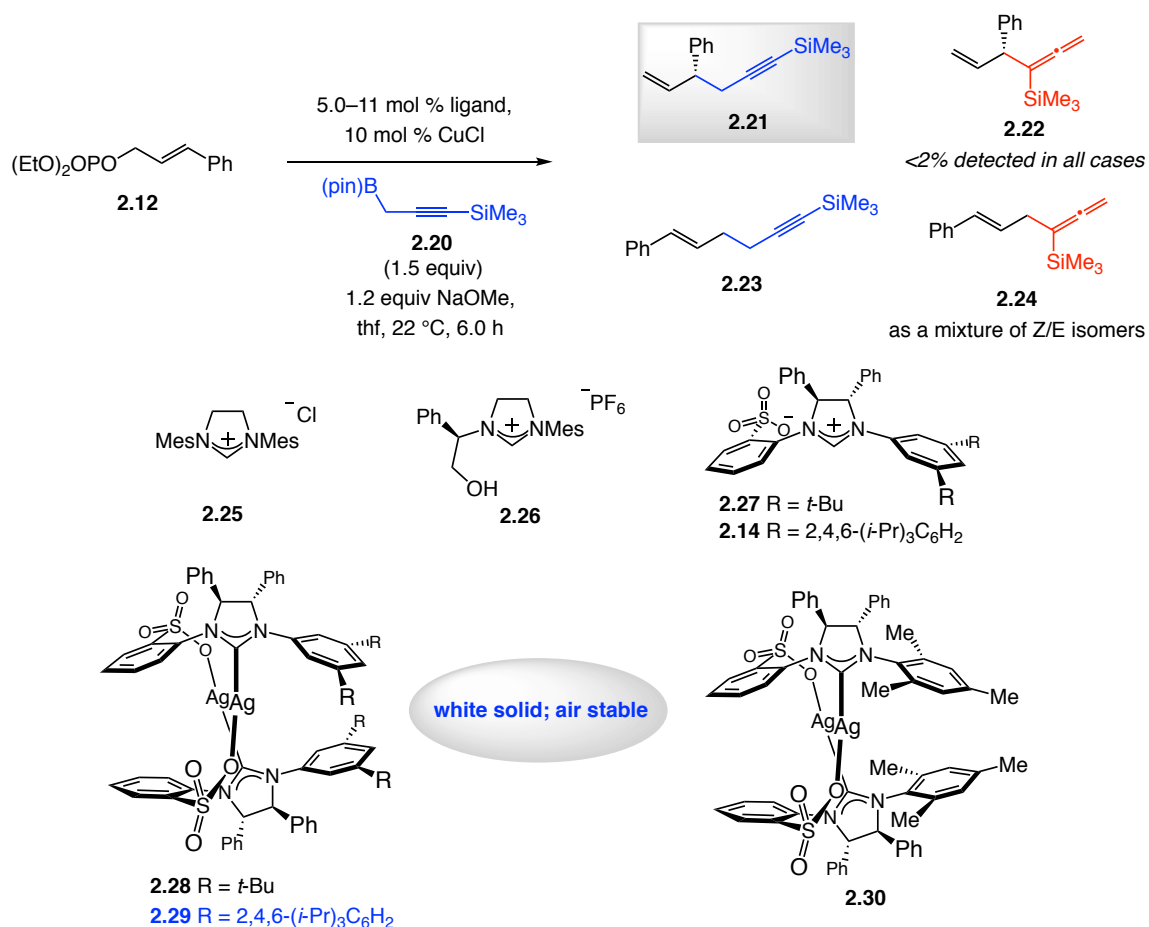
(8) Fandrick, D. R.; Saha, J.; Fandrick, K. R.; Sanyal, S.; Ogikubo, J.; Lee, H.; Roschangar, F.; Song, J. J.; Senanayake, C. H. *Org. Lett.* **2011**, *13*, 5616–5619.

(9) Shi, Y.; Jung, B.; Torker, S.; Hoveyda, A. H. *J. Am. Chem. Soc.* **2015**, *137*, 8948–8964.

(10) Mszar, N. W.; Haeffner, F.; Hoveyda, A. H. *J. Am. Chem. Soc.* **2014**, *136*, 3362–3365.

propargyl addition outcompete allenyl addition even in the absence of any ligands (entry 1), albeit in S_N2 selective fashion. To access the more valuable branched product **2.21**, NHC ligands were examined under the reaction conditions. NHC–Cu complexes derived from both **2.25** and **2.26** led to the generation of undesired linear propargyl product **2.23** (entry 2 and 3). Only when sulfonate-bearing NHC–Cu catalysts were employed, could the branched product **2.21** be generated with high S_N2' selectivity. EAS reaction promoted by the NHC–Cu complex derived from **2.27** bearing a meta-substituted N-aryl group delivered **2.21** in 68% yield, 95:5 S_N2' : S_N2 ratio and 90:10 enantioselectivity (entry 4). Increasing the size of the meta-substituent of the NHC ligand to a triisopropyl group improved the enantioselectivity to 97:3 er (entry 5). However, poor regioselectivities were observed when imidazolium salts were used to generate the NHC–Cu complexes: unbound organocopper species readily facilitated an efficient background reaction, yielded undesired linear product. Thus, when the corresponding Ag complexes **2.28** and **2.29** were examined in the reaction, **2.21** was obtained with high regio- and enantioselectivity (entries 6 and 7).¹¹ We found that with the use of NHC derived from Ag complex **2.30**, **2.21** was generated in much lower enantioselectivity (31:69 er), and favoring formation of the opposite enantiomer (entry 8).

(11) The formation of NHC–Cu complex is facilitated employing NHC–Ag and CuCl since the formation of AgCl precipitate from the solution, driving the complexation reaction to completion.

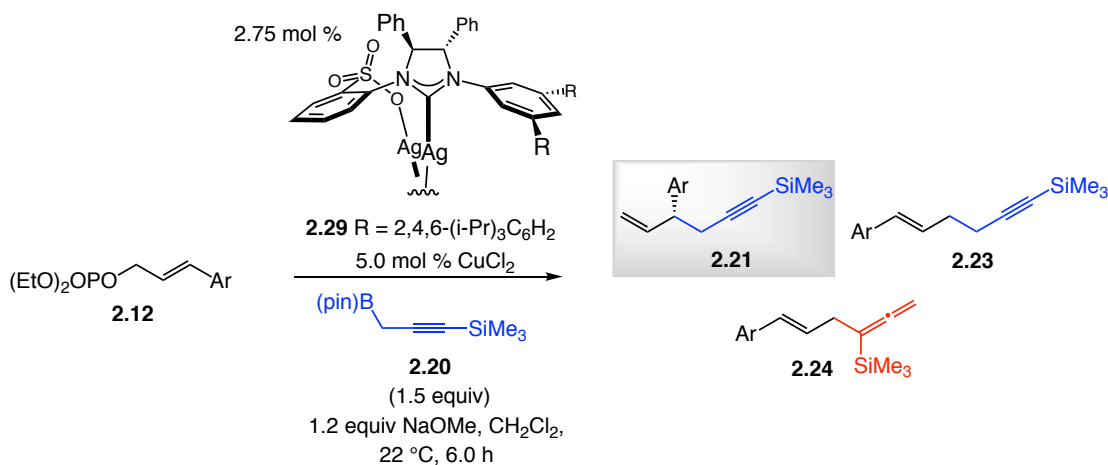
Table 2.1. Formation of Tertiary Carbon Centers: Examination of Different Types of NHC–Cu Complexes^a

entry	ligand/complex	conv (%) ^b yield (%) ^c	S _N 2':S _N 2 ^b (2.21 : 2.23)	(2.21 + 2.23): 2.24 ^b	er ^d
1	none	86; 67	6:94	86:14	na
2	2.25 ^e	>98; 77	5:95	88:12	na
3	2.26	86; 71	16:84	87:13	nd
4	2.27	92; 68	95:5	84:16	90:10
5	2.14	>98; 75	91:9	89:11	97:3
6	2.28	>98; 70	96:4	84:16	91:9
7	2.29	>98; 75	97:3	89:11	97:3
8	2.30	>98; 74	>98:<2	87:13	31:69

^a Reactions performed under N₂ atm. ^b Conversion (allylic phosphate consumption) and group (propargyl/allenyl addition) selectivities (±2%) were determined by analysis of 400 MHz ¹H NMR spectra of product mixtures prior to purification. Site selectivities were determined by analysis of 400 MHz ¹H NMR spectra of purified material. ^c Yield (±5%) of propargyl addition products after silica gel chromatography (includes inseparable linear isomer **2.23** but no allenyl compounds). ^d Enantioselectivity (±1%) determined by GC analysis. See the Supporting Information for experimental and analytical details. ^e Preformed NHC–Cu complex was used; see the Supporting Information for details. Mes, 2,4,6-(Me)₃C₆H₂; na, not applicable; nd, not determined.

As shown in Table 2.2, propargyl additions to allylic phosphates **2.12a–l** afforded enynes **2.21a–l** in >98% conversion, 75–89% yield, 87%–98% S_N2' selectivity, and

95:5–98:2 er using 5.0 mol % of the NHC–Cu complex derived from 2.75 mol % **2.29** and 5.0 mol % CuCl. Notably, reactions are performed at ambient temperature in CH₂Cl₂ and are generally complete in 6 h to provide both aryl- and alkyl-substituted propargyl addition products in high efficiency, site-selectivity and stereoselectivity. Allylic phosphates with an electron-donating group or halogen are compatible under the reaction conditions (cf. **2.12b-d**, **2.12f**, and **2.12g**). Electron-deficient allylic phosphates **2.12h** and **2.12i** proceeded with diminished site-selectivities (93:7 and 87:13 S_N2': S_N2 ratio). Sterically hindered substrates **2.12d-e** and **2.12i** are suitable substrates, affording propargyl addition products in high yields with good regio- and enantioselectivity. In all cases, allenyl addition product **2.24** was generated as the minor byproduct in 4–10% yield, but is readily separable.

Table 2.2. EAS Reactions with Aryl-Substituted Substrates^a

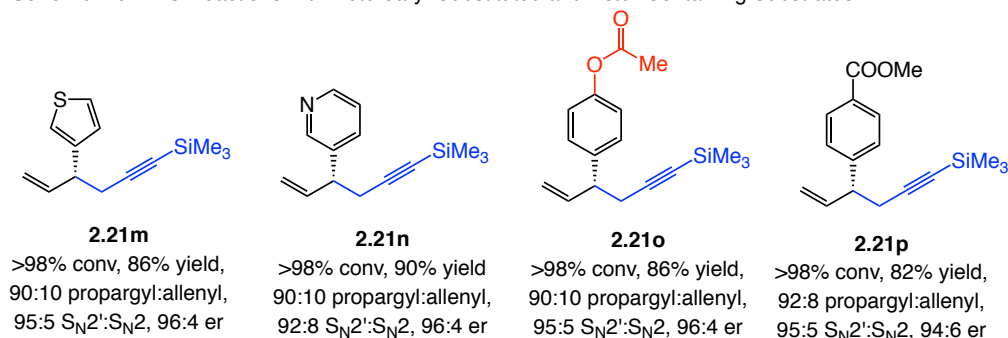
entry	substrate (Ar)	conv (%), ^b yield (%) ^c	S _N 2':S _N 2 ^b (2.21:2.23)	(2.21+2.23):2.24 ^b	er ^d
1	2.12a (Ph)	>98; 75	97:3	91:9	97:3
2	2.12b (<i>o</i> -FC ₆ H ₄)	>98; 82	96:4	92:8	97:3
3	2.12c (<i>o</i> -BrC ₆ H ₄)	>98; 80	97:3	95:5	97:3
4	2.12d (<i>o</i> -OMeC ₆ H ₄)	>98; 81	98:2	94:6	96:4
5	2.12e (<i>o</i> -MeC ₆ H ₄)	>98; 89	97:3	92:8	96:4
6	2.12f (<i>m</i> -BrC ₆ H ₄)	>98; 85	98:2	93:7	98:2
7	2.12g (<i>m</i> -MeC ₆ H ₄)	>98; 76	98:2	92:8	98:2
8	2.12h (<i>m</i> -CF ₃ C ₆ H ₄)	>98; 79	93:7	89:11	98:2
9	2.12i (2-naphthyl)	>98; 81	96:4	96:4	97:3
10	2.12j (<i>p</i> -ClC ₆ H ₄)	>98; 80	96:4	92:8	97:3
11	2.12k (<i>p</i> -ClC ₆ H ₄)	>98; 83	97:3	93:7	97:3
12	2.12l (<i>p</i> -ClC ₆ H ₄)	>98; 83	87:13	90:10	95:5

^{a-d} same as Table 2.1

1,5-Enynes possessing a heteroaromatic moiety were synthesized efficiently as shown in Scheme 2.5. Thienyl-substituted **2.21m** was isolated in 86% yield (pure propargyl product) through a reaction that proceeds with 95% site selectivity and 96:4 er. Addition to a pyridyl substrate took place without any adverse effect by the Lewis basic nitrogen site on the activity of the Cu complex. Enyne **2.21n** was isolated in 90% yield, 92% site selectivity, and 96:4 er. Ester-containing substrates **2.21o-p** were also compatible under the reaction conditions. The efficient formation of 1,5-enyne **2.21o** in

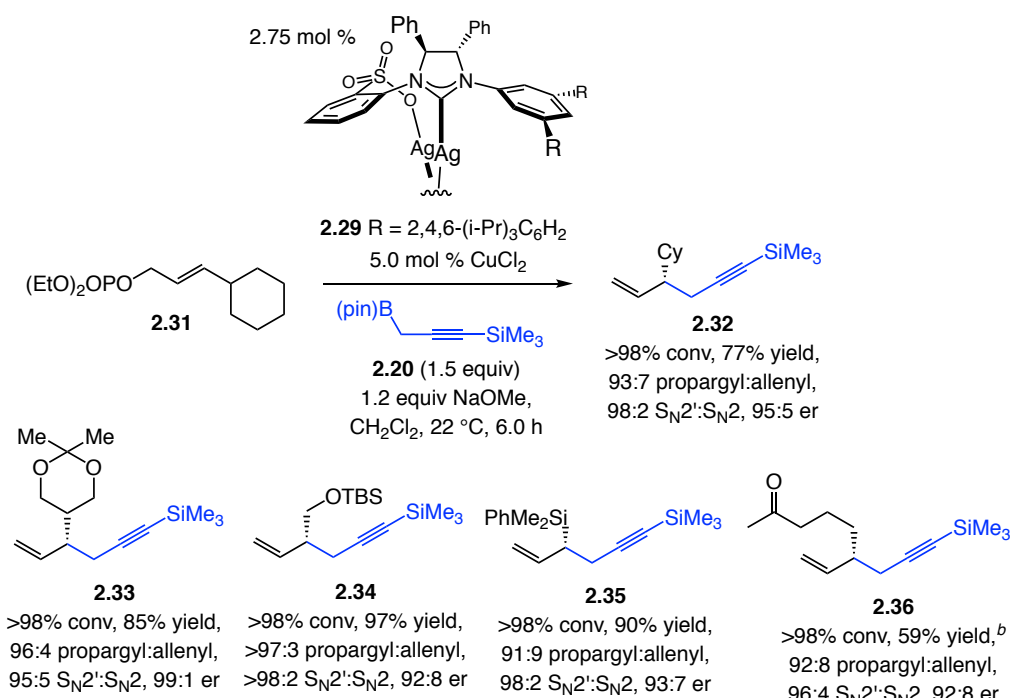
96:4 er, demonstrated the robustness and chemoselectivity of the developed method even in the presence of comparatively electrophilic moieties such as an acylated phenol.

Scheme 2.5. EAS Reactions with Heteroaryl-Substituted and Ester-Containing Substrates^a



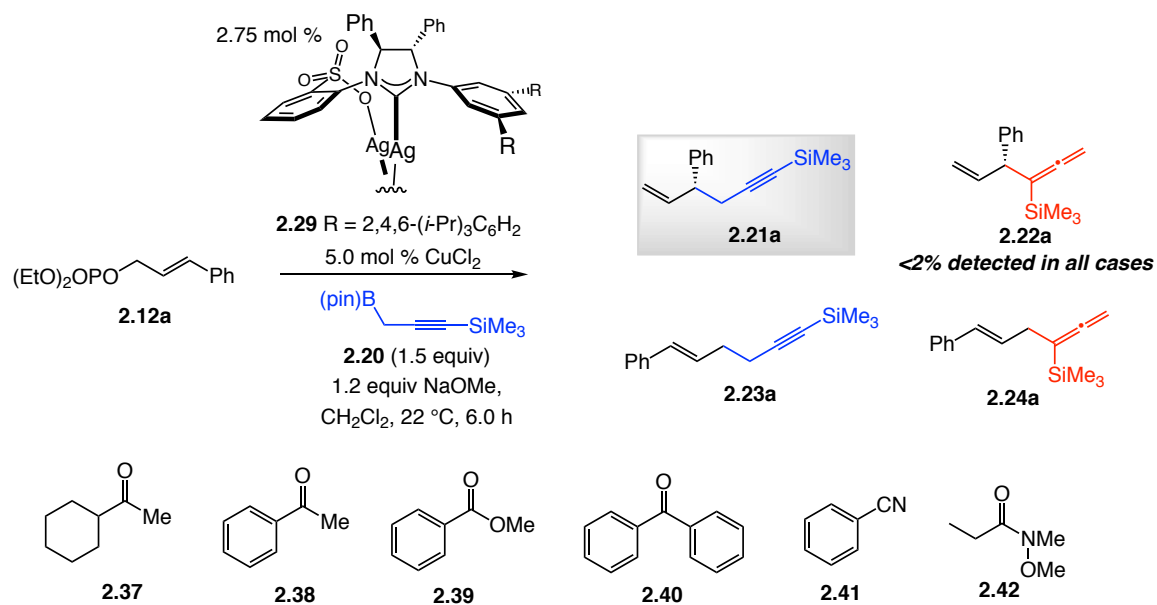
^a Reactions performed under N₂ atm.

Propargyl additions to alkyl-substituted allylic phosphates proceeded efficiently, affording branched products in up to 90% yield, 96:4 propargyl/allenyl, >98:2 S_N2':S_N2 selectivity and 99:1 er (Scheme 2.6). Synthesis of allylsilane **2.35** in 90% yield, 91:9 propargyl/allenyl, 98:2 branched/linear selectivity, and 93:7 er shows that alkenylsilanes are suitable substrates as well. Moreover, preparation of methyl ketone **2.36** in 59% yield, 92:8 propargyl/allenyl, 96:4 branched/linear selectivity and 92:8 er in 2.0 h (vs 6.0 h) further underscores tolerance of the catalytic protocol towards electrophilic/enolizable units.

Scheme 2.6. EAS Reactions with Alkyl-Substituted Substrates^a

^aReactions conditions and methods of product analysis identical to those indicated in Table 2.1. Yields ($\pm 5\%$) are the lowest obtained after a minimum of three runs and are of propargyl addition products (branched and linear). See the Supporting Information for all experimental and analytical details. ^bReaction time was 2.0 h.

To gain additional insight into the functional group tolerance of the method, we performed studies with the external additives as summarized in Table 2.3. We found that alkyl ketone **2.37** (entry 1), aryl ester **2.39** (entry 3), phenyl cyanide **2.41** (entry 5) and Weinreb amide **2.42** (entry 6) were tolerated under the EAS conditions reasonably well (74% to >98% unreacted electrophilic additive). However, the more electrophilic ketones, such as acetophenone **2.38** (entry 3) and benzophenone **2.40** (entry 5), were not inert. Allylation of the carbonyl group occurred competitively in these cases. In all cases, **2.23a** was generated with the same selectivity levels as in trials not employing of an additive (cf. entry 1, Table 2.2).

Table 2.3. Exploration of Functional Group Tolerance of Propargyl EAS Reaction

entry	additive	conv (%); yield (%)	S _N 2':S _N 2 (2.19a : 2.21a)	(2.19a + 2.21a : 2.22a)	recovery of additive 2.37 – 2.42 ^a
1	2.37	>98; 79	97:3	89:11	>98
2	2.38	89; 38	97:3	88:12	25 ^b
3	2.39	>98; 75	97:3	90:10	>98
4	2.40	79; 48	97:3	89:11	41 ^b
5	3.41	95; 76	96:4	89:11	74
6	2.42	92; 76	96:4	89:11	90

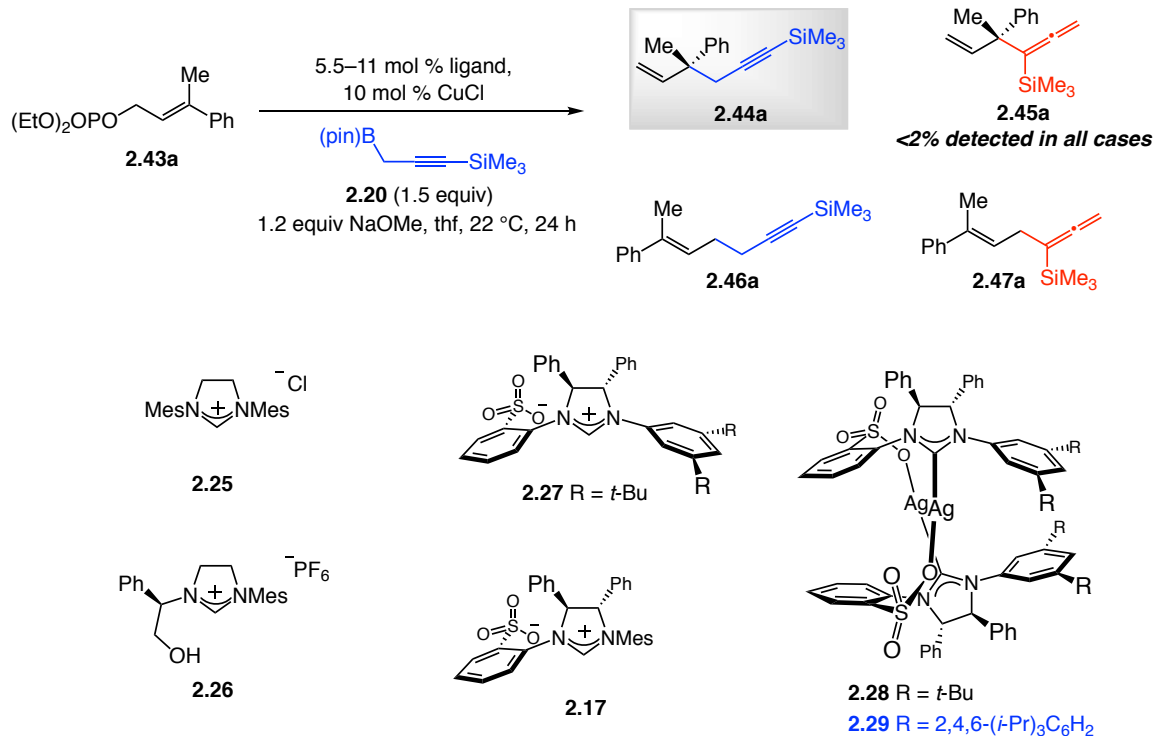
^a based on internal standard. ^b allyl addition to carbonyl group was observed as byproduct

2.3.3 Synthesis of Propargyl-Substituted Quaternary Carbon Stereogenic

Centers: Additions to Allylic Phosphates that Contain a Trisubstituted Alkene

We then investigated the EAS process for the formation of all-carbon quaternary stereogenic centers using trisubstituted allylic phosphates. Preliminary catalyst screening (Table 2.4) revealed that the use of sulfonate-based NHC–Cu complexes was crucial to obtain the desired branched selectivity (compare entries 5–7 vs 1–3). Compared to the case of disubstituted alkenes in EAS reactions (cf. Tables 2.1), the complex derived from **2.27** delivered **2.44a** yielded poor regioselectivity (39:61 S_N2':S_N2 vs 95:5 in the case of disubstituted allylic phosphate **2.12a**). It indicated that the background reaction affording

linear S_N2 product outcompeted the desired EAS reaction. When the NHC–Cu complex derived from imidazolium salt **2.17** with an ortho-substituted N-aryl group was employed (entry 5), the opposite enantiomer was again generated predominantly (32:68 er); as described in Chapter 1, this observation offered considerable insight into the mechanism of the EAS promoted by sulfonate NHC–Cu complexes. The same selectivity reversal was observed in related EAS reactions with an allenyl B(pin) **2.13**⁷ with an even greater level of reversal (12:88 er). Unlike transformations with an allenyl–B(pin), EAS using the complex derived from **2.29**, afforded **2.44a** in 92:8 er (entry 7, Table 2.4) as compared to 67:33 er (94:6 S_N2' : S_N2). These findings highlighted the mechanistic distinction between the transformations involving the allenyl B(pin) **2.13** and propargyl B(pin) **2.20**.

Table 2.4. Formation of Quaternary Carbon Centers: Examination of Different Types of NHC–Cu Complexes^a

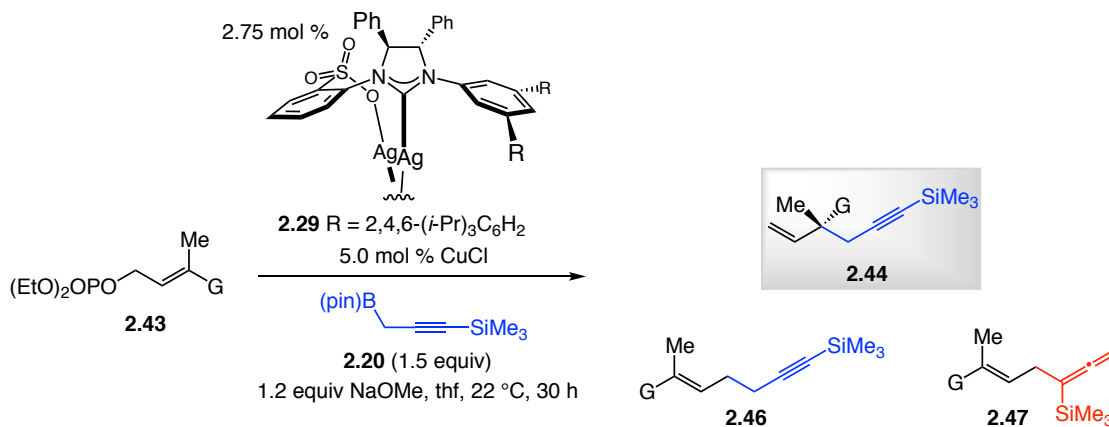
entry	ligand/complex; mol % catalyst	conv (%), ^b yield (%) ^c	S _N 2':S _N 2 ^b (2.44a:2.46a)	(2.44a+2.45a):2.47a ^b	er ^d
1	none; 10	45; 35	<2:98	82:18	na
2	2.25; 10	49; 47	<2:98	92:8	na
3	2.26; 10	57; 50	3:97	91:9	nd
4	2.27; 10	93; 83	39:61	89:11	86:14
5	2.17; 10	48; 31	85:15	85:15	32:68
6	2.28; 5.0	>98; 82	91:9	92:8	87:13
7	2.29; 5.0	>98; 84	94:6	88:12	92:8

^{a-d} same as Table 2.1

Transformations with trisubstituted allylic phosphates proceeded to $\geq 95\%$ conversion after 30 h at room temperature in thf in the presence of 5.0 mol % of catalyst derived from **2.29** (Table 2.5). Propargyl addition products were isolated in 78–95% yield after purification; the 9–11% of the allenyl byproduct (**2.47a**) formed was completely separable by silica gel chromatography. Site selectivity was comparable to that obtained with disubstituted allylic phosphates (cf. Table 2.2), but er values were

somewhat lower (83:17–94:6 er vs. 92:8–>99:1 er). The most challenging case, shown in entry 2 of Table 2.5, employed an ortho-substituted aryl group. In this case, the less hindered NHC–Cu complex derived from **2.28** proved to be the most effective. With the optimal ligand **2.29**, there was 75% conversion, and a 60:40 ratio of branched/linear products was generated (vs 98% conversion and 94% S_N2' selectivity) for **2.43b**. Aliphatic trisubstituted allylic phosphates were also effective, yielding **2.44e** in 78% yield, >98:2 S_N2' : S_N2 , and 94:6 er.

Table 2.5. Enantioselective Synthesis of Enynes with a Quaternary Carbon^a



entry	substrate (G)	conv (%); ^b yield (%) ^c	S_N2' : S_N2 ^b (2.44 : 2.46)	(2.44 + 2.46): 2.47 ^b	er ^d
1	2.43a (Ph)	>98; 81	94:6	89:11	91:9
2	2.43b (<i>o</i> -MeOC ₆ H ₅) ^e	98; 95	94:6	91:9	83:17
3	2.43c (<i>m</i> -BrC ₆ H ₅)	95; 93	>98:2	89:11	92:8
4	2.43d (<i>p</i> -ClC ₆ H ₅)	>98; 91	96:4	90:10	93:7
5	2.43e (Cy)	>98; 78	>98:2	90:10	94:6

^{a-d} same as Table 2.1. ^eThe complex derived from **2.28** was used; see text for details. See the Supporting Information for all experimental and analytical details.

The slower rates of EAS reactions that afford all-carbon quaternary stereogenic centers versus those that involve 1,2-disubstituted alkenes, render the corresponding conditions with reduced chemoselectivity in the presence of other electrophilic functional groups than was formerly illustrated (cf. Table 2.3). We found that carboxylic ester **2.39** (1.0 equiv) were recovered in >98% yield with minimal influence on the efficiency of the

EAS reaction to afford **2.44a** (81% yield, 94% S_N2', 89:11 propargyl:allenyl, 91:9 er). In contrast, when methyl ketones **2.37** and **2.38** were added to the mixture, **2.44a** was obtained in 67% and 29% yield, respectively, and the carbonyl additive were recovered in 30% and 15% yield, respectively.

2.3.4 Mechanistic Studies

The free energy surface of a truncated model system corresponding to the EAS reaction that affords **2.21a** (cf. entry 1, Table 2.2), obtained through DFT calculations at the ω B97xD/Def2TZVPP_{DCM(SMD)}// ω B97xD/LANL2DZ level, is exhibited in Figure 2.2. The low-energy transition state TS_{iso} (11.3 kcal/mol) for interconversion of the linear Cu(I)-propargyl (**A**) and the related allenyl species (**B**) indicates a Curtin-Hammett kinetic profile, consistent with complex **B** being 0.9 kcal/mol more stable than complex **A** and the fact that none of the chiral S_N2' addition products were generated through intermediacy of **B** (i.e., <2% formed in the studies summarized in Table 2.2). The significance of the large trimethylsilyl group in providing sufficient quantities of complex **A** has been previously reported and is consistent with the EAS reaction with Scheme 2.4; reaction with the propargyl B(pin)/allenyl B(pin) reagent mixture (**2.19**, 88:12) that lacks the silyl unit is less efficient and produces the allenyl product **2.18** exclusively, engenders repulsive steric interaction with the large N-aryl moiety of the Cu complex. As already mentioned, because of the size and mobility of the system it would be difficult to reach a reliable conclusion based on DFT calculations as to whether the oxidative addition or the reductive elimination step is turnover-limiting. Additionally, complications due to conformational complexity are exacerbated by the loosely associated NaOPO(OMe)₂ salt (cf. PA_A→Prod_A, Figure 2.2). Nonetheless, our investigations indicate that the pathways

leading to allenyl addition are energetically disfavored.

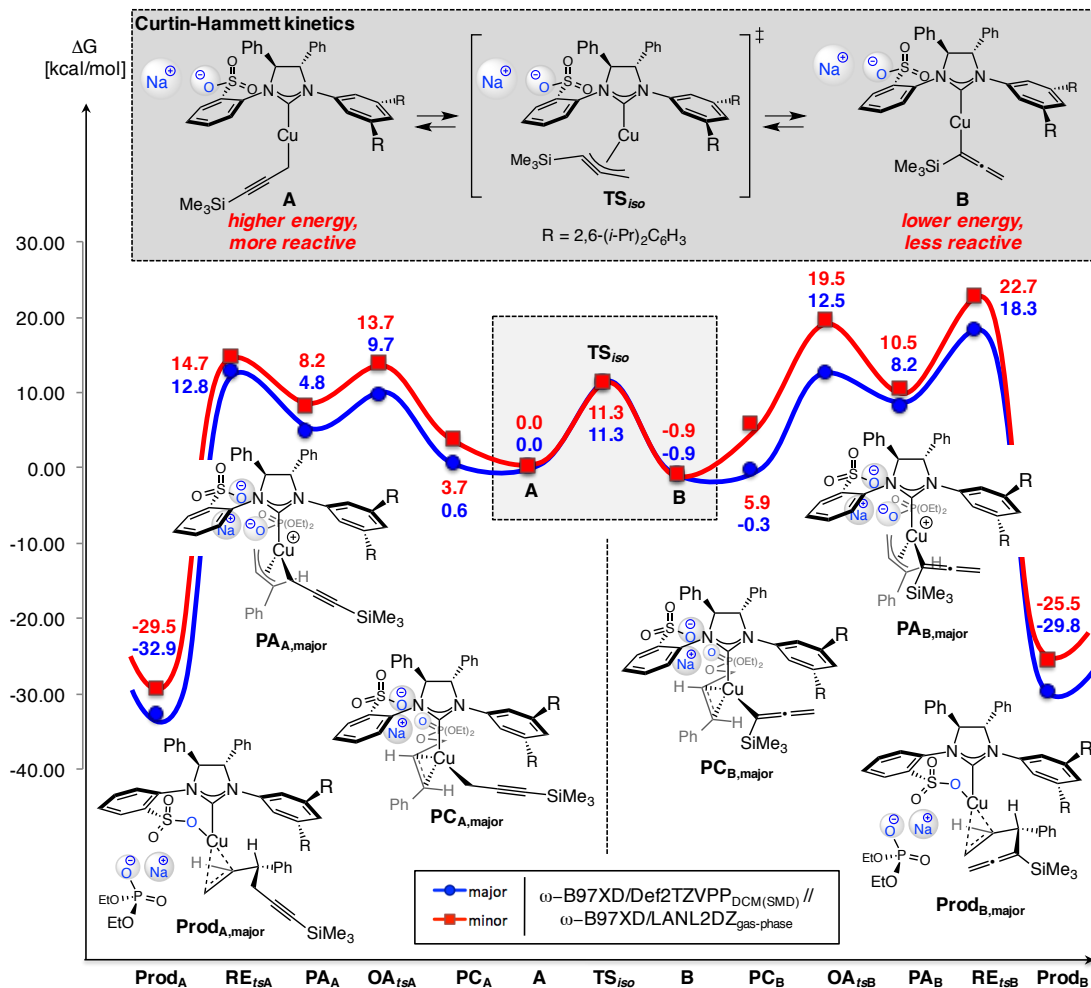


Figure 2.2. Energy profile regarding the origin of high site and group transfer selectivity (high S_N2' : S_N2 and propargyl/allenyl addition) derived from DFT calculations. Abbreviations: RE, reductive elimination; TS, transition state; OA, oxidative addition; PA, π -allyl; PC, π -complex.

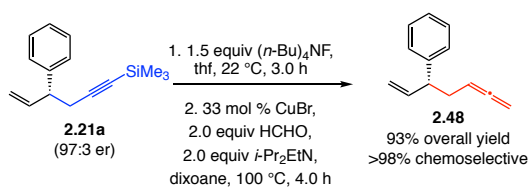
2.3.5 Functionalizations and Application to the Synthesis of Plakinic Acid A

We were able to demonstrate the utility of our method by generating homoallenyl compounds, as represented by **2.48** in Scheme 2.7a. Treating **2.21a** with $(n-Bu)_4NF$ and then 33 mol % CuBr, 2.0 equiv of para-formaldehyde, and 2.0 equiv of $(i-Pr)_2NH$ at 100 °C for 4.0 h furnished the product in 93% yield in one-pot without erosion of enantiomeric purity and with complete chemoselectivity (<2% reaction at the alkene site).

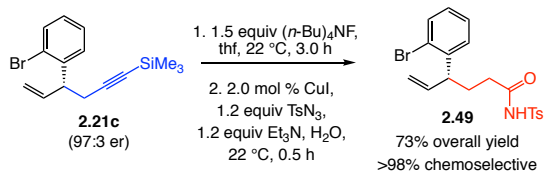
The difficulties associated with converting the product of an allyl–allyl coupling process to the corresponding homoallenyl compounds, and the increasing number of catalytic stereoselective transformations that involve monosubstituted allenes renders this functionalization especially striking. Another notable Cu-catalyzed process converts the EAS products with exclusive chemoselectivity (>98% reaction at the alkyne unit) to enantiomerically enriched tosylamides such as **2.49** (Scheme 2.7b). Such electronically activated functional units, accessible in a single step only from an alkyne unit (unlike an olefin), are readily amenable to further modification. The silyl alkyne group may be converted to the corresponding *Z*-alkenyl silane (see **2.50**) by treatment with dibal–H at 55 °C for 2.0 h (Scheme 2.7c). Consistent with the cases above, chemoselectivity was complete (<2% by 400 MHz ¹H NMR). Subsequent treatment with *N*-iodosuccinimide, 30 mol % Ag₂CO₃, and hexafluoroisopropyl alcohol for 10 min at 0 °C led to the formation of the desired *Z*-alkenyl iodide **2.51**, with ~10% loss in alkene stereoisomeric purity. This latter sequence demonstrates that the silyl unit of the propargyl–B(pin) reagent **2.20** can impart attractive characteristics to the catalytic approach that extend far beyond serving as a protecting group.

Scheme 2.7. Representative Functionalizations of EAS Products by Reactions that are Particularly Facile with Alkyne Units^a

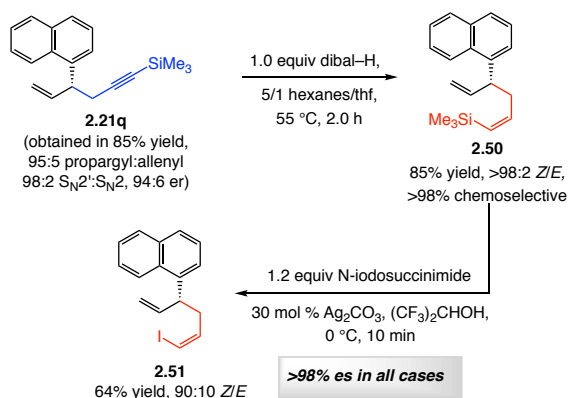
a) Conversion to a homoallenyl containing compound:



b) Conversion to a 3-amido-propyl containing compound:

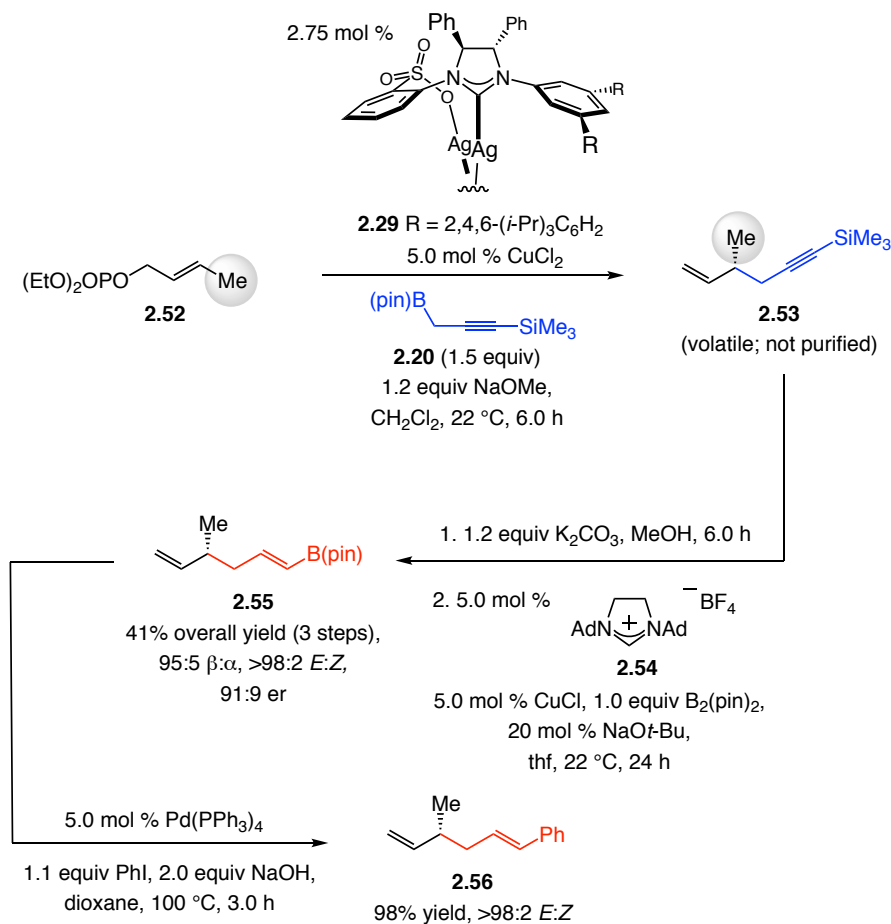


c) Conversion to *Z*-1-silyl-allyl and *Z*-1-iodo-allyl containing compounds:



^aYields (±5%) are the lowest obtained after a minimum of three runs and are for propargyl addition products after silica gel chromatography (includes inseparable linear isomers but no allenyl compounds). See the Supporting Information for details. es = enantiospecificity (product enantiomeric excess/substrate enantiomeric excess) by 100.

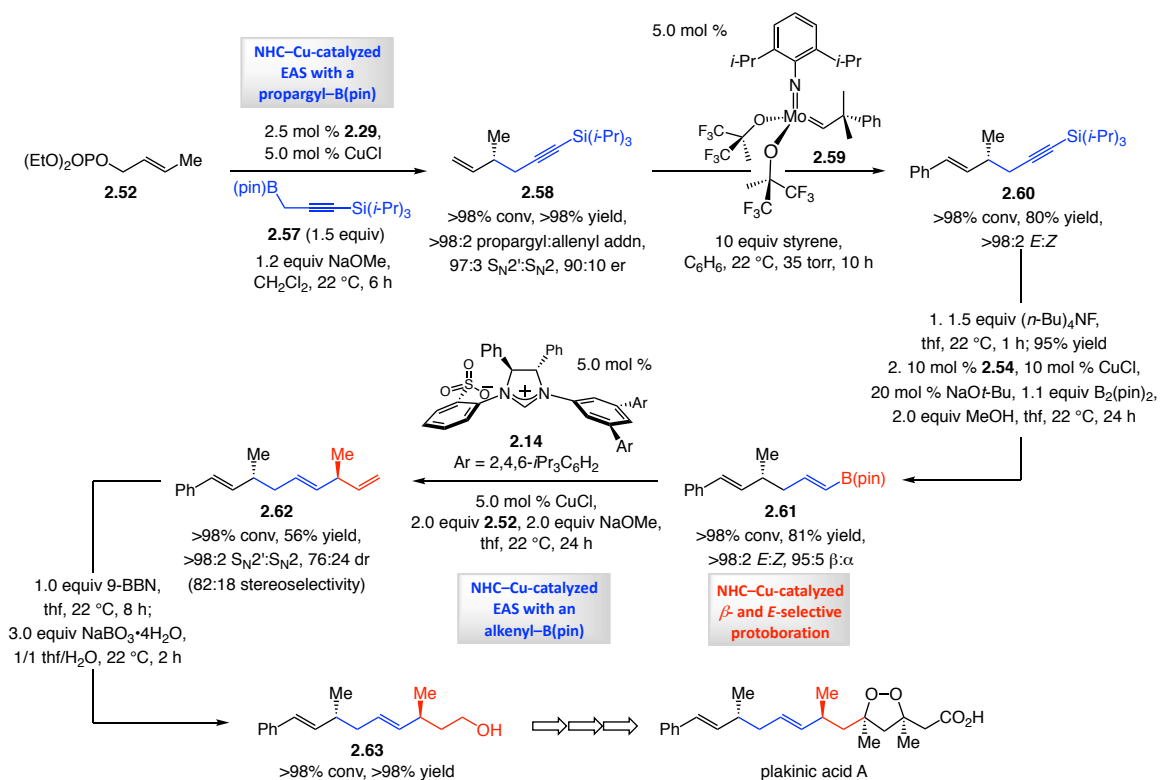
As shown in Scheme 2.8, exposure of **2.52** to NHC–Cu-catalyzed EAS conditions resulted in complete consumption and formation of trimethylsilyl-substituted **2.53**, which is volatile and cannot be easily isolated in high yield. Accordingly, we treated the unpurified mixture containing **2.53** to mildly basic methanol to remove the silyl unit, followed by NHC–Cu-catalyzed protoboryl addition of the resulting terminal alkyne to furnish β -alkenyl B(pin) **2.55** in 41% overall yield over 3 steps with 95% β selectivity, >98% E selectivity, and 91:9 er. β -substituted styrene **2.56** was prepared in 98% yield by means of phosphine–Pd-catalyzed cross-coupling with iodobenzene. Alkenylboron derivatives such as **2.55** may not be accessed with the same ease and efficiency through the use of dienyl products obtained from EAS reactions that incorporate an allyl moiety, since differentiation of two alkene units would be less straightforward than that of an alkyne and an olefin [e.g., by site- and stereoselective cross-metathesis with vinyl–B(pin)]. This is particularly the case with a relatively diminutive methyl group at the allylic site.

Scheme 2.8. EAS with a Key Substrate and Conversion to 1,5-Dienes

1.2.2 Application to the Synthesis of Plakinic Acid A

We envisioned that if we could transform the alkyne to an alkenyl B(pin), the product could be used in another EAS reaction to facilitate formation of another stereogenic center with a 1,5-relationship. To demonstrate the feasibility of this protocol further and highlight its complementary relationship with other catalytic and stereoselective processes, we undertook a diastereo- and enantioselective synthesis of the acyclic segment of antifungal natural product plakinic acid A (Scheme 2.9). The route commenced with NHC–Cu-catalyzed EAS involving methyl-substituted allylic phosphate **2.52** and tri(isopropylsilyl)-substituted propargyl–B(pin) reagent **2.57**. Enyne **2.58** was isolated in quantitative yield with complete control of group selectivity (<2%

allenyl product) in 97:3 S_N2' : S_N2 selectivity and in 90:10 er. Cross-metathesis with styrene in the presence of 5.0 mol % of a molybdenum alkylidene **2.59** delivered enyne **2.60** in 80% yield with retention of isomeric purity of the olefin (>98:2 *E/Z*) and, importantly, without reaction at the alkynylsilane site (<2% enyne cross-metathesis). The next objective was to transform the acetylene moiety into an alkenylboron unit to be utilized in an NHC–Cu-catalyzed EAS that would generate the other methyl-substituted stereogenic center. Removal of the silyl group followed by site- and stereoselective NHC–Cu-catalyzed protoboryl addition to the resulting terminal alkyne, which proceeded with >98% chemoselectivity (<2% reactions at the styrenyl group), afforded *E*- β -alkenyl B(pin) intermediate **2.61** in 81% yield, >98:2 *E/Z* and 95:5 β : α selectivity. Treatment of **2.61** with 5.0 mol % enantiomerically pure imidazolium salt **2.26**, 5.0 mol % CuCl, and 2.0 equiv of allylic phosphate **2.52** generated triene **2.62** in 56% yield, with complete branched selectivity (>98% S_N2') and in 76:24 diastereomeric ratio (dr; 82:18 selectivity).^{6c} Site-selective hydroboration of the monosubstituted alkene afforded primary alcohol **2.63** in >98% yield (Scheme 2.9).

Scheme 2.9. Application to Stereoselective Synthesis of the Diene Fragment of Plakinic Acid A

2.4 Development of New Sulfonate-Containing NHC Ligands Assisted by DFT

Calculations—A New NHC Ligand Bearing a 2,5-Disubstituted *N*-Aryl Group

Despite developing a model to explain the role of the sulfonate group and the substitution pattern on the NHC–Cu complexes with the aid of DFT calculations,¹² there were cases that showed the limitations of our current ligand system: as shown in Scheme 2.9, EAS reaction with allylic phosphate **2.52** in combination with relatively large alkenyl B(pin) reagent **2.61** led to only moderate stereoselectivity (82:18) promoted by an NHC–Cu complex derived from **2.14**. Therefore, we applied the insight we obtained from mechanistic studies to rationally design new NHC ligands to achieve high selectivity. We settled on a new type of sulfonate-containing NHC ligand with 2,5-

(12) see Chapter 1.

disubstituted N-aryl ring that allowed for new protocols to streamline synthesis of several natural products and pharmaceuticals.

2.4.1 Development of a New NHC Ligand with a 2,5-Substitution Pattern for EAS Reactions Employing 1,2-Disubstituted Allylic Phosphates

Our goal was to develop a new ligand to improve the selectivity of the second EAS step towards plakinic acid A. With our previously proposed stereochemical model, we proceeded to search for the reason behind lower enantioselectivity when the nucleophile was switched from propargyl to alkenyl. As shown in Figure 2.3, in transition state **2.65** leading to the minor enantiomer, there existed a strong steric repulsion between the large triisopropylphenyl group on the catalyst and the phenyl group on the substrate; while this penalizing interaction was absent in transition state **2.64** (leading to the major enantiomer). The large energy gap between the two modes of additions (4.0 kcal/mol) contributed to the high enantioselectivity observed with the NHC–Cu complex bearing 3,5-substitution. In both transition states, the propargyl nucleophile is pointing towards the top; this is due to the linear geometry of the propargyl group and flexibility of the C(sp³)-hybridized methylene unit. However, as shown by the transition states leading to the major and minor enantiomers of **2.66** and **2.67** in Figure 2.4, incorporation of the alkenyl group induces a penalizing interaction with the methyl group of the substrate, which raises the energy of the major pathway, consequently lowering the energy difference between **2.66** and **2.67** (Figure 2.4), leading to lower enantioselectivity. This destabilizing interaction is due to the increased size of the nucleophile and the rigidity of the sp² hybridized alkenyl group.

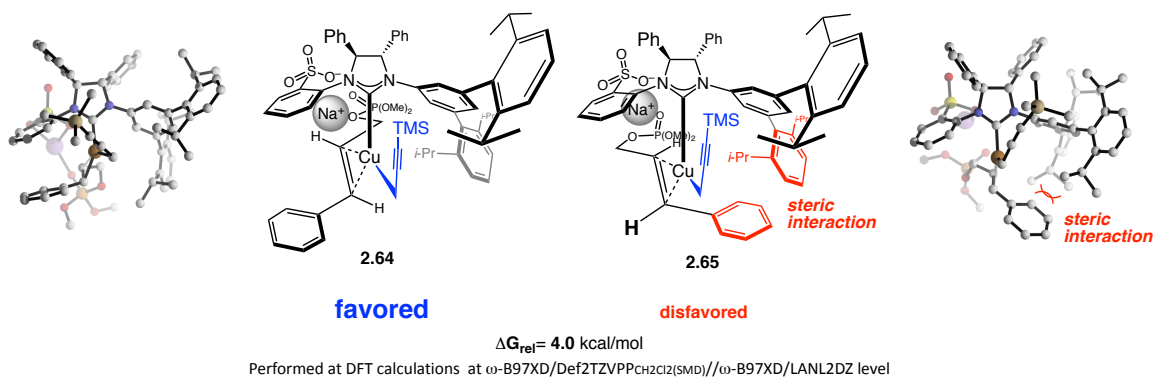


Figure 2.3. Stereochemical Model for the EAS Reactions with a Propargyl B(pin) Reagent

We postulated that removing the 3-substituent on the N-aryl group and incorporating a substituent at the 2-position as shown in Figure 2.4, the possible transition states leading to the major and minor enantiomer (**2.69** and **2.70**) could be better differentiated. We hypothesized that in the case of the minor pathway, the rigidity of the alkenyl group might lead to the rotation of the N-aryl ring to the back right quadrant which would induce a steric clash between the substituent on the 5-position with the methyl allylic phosphate, raising the energy of this pathway. Thus, the NHC–Cu complex derived from a imidazolium salt **2.68** might induce higher enantioselectivity. The development of this new type of NHC with a 2,5-disubstituted N-aryl group proved to be critical for the synthesis of plakinic acid A.

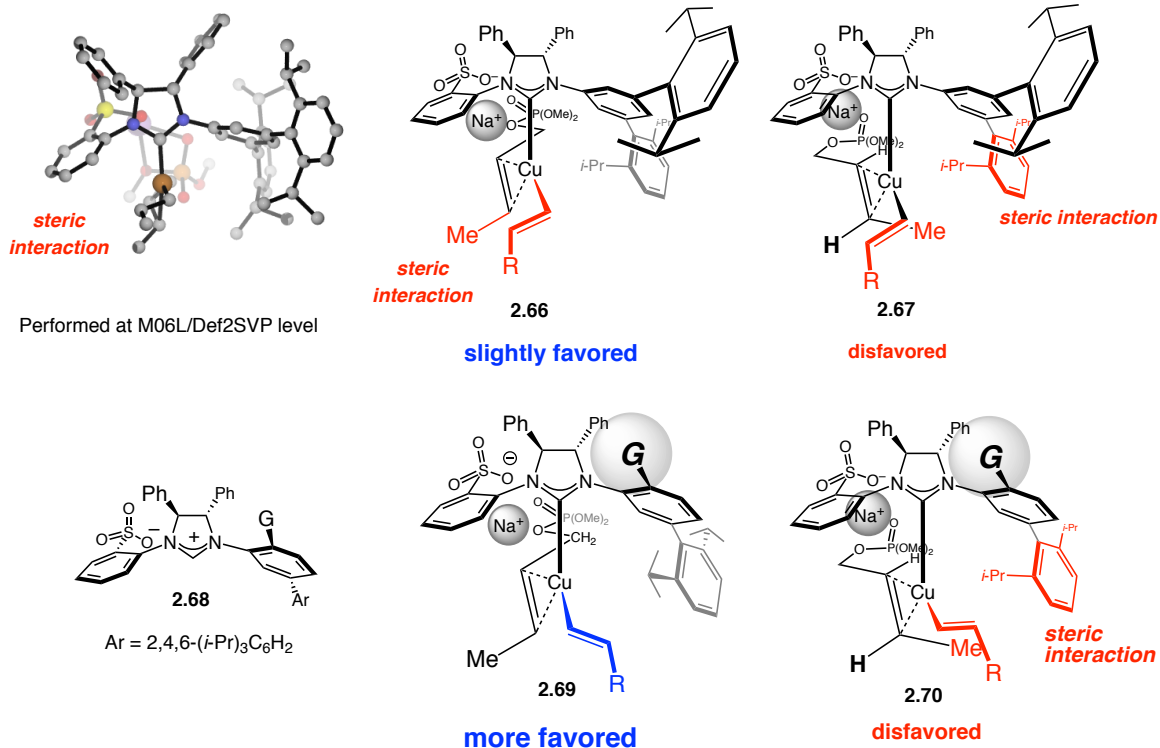
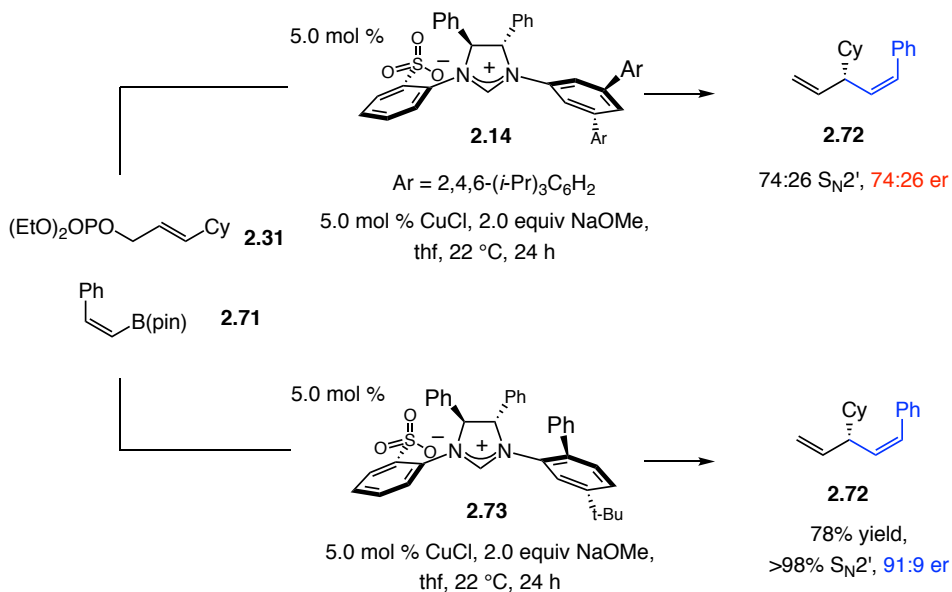


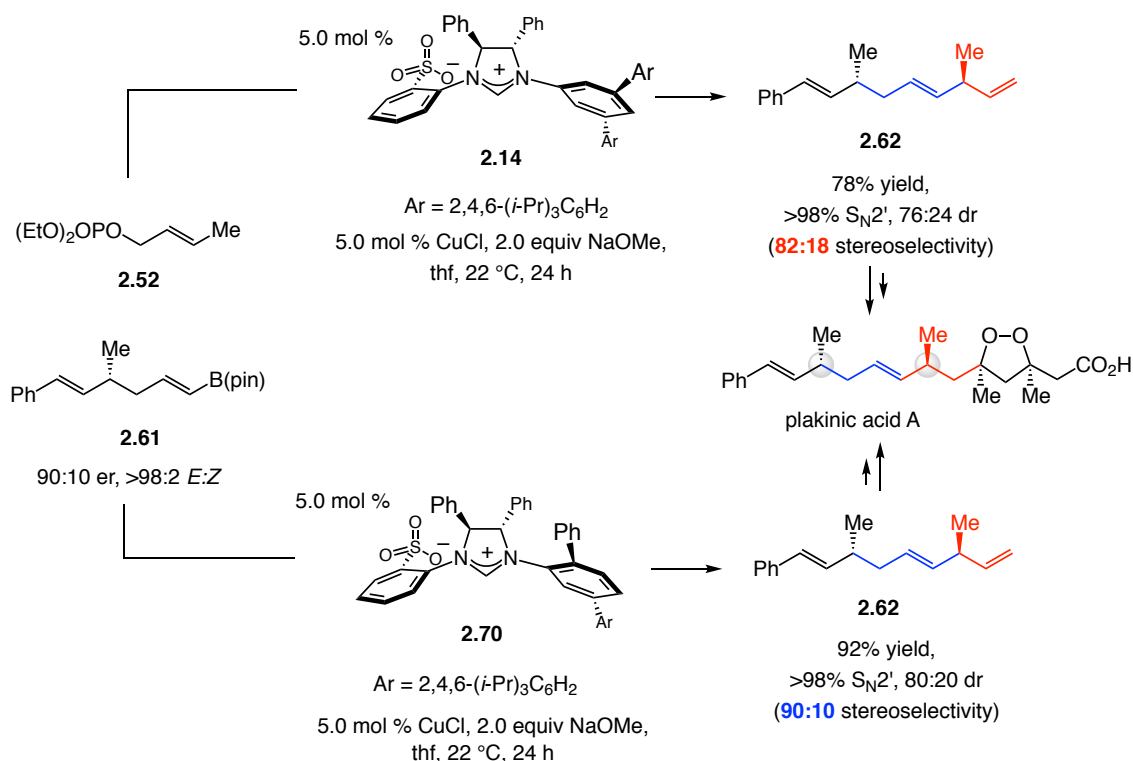
Figure 2.4. Hypothesis for an NHC Ligand with a 2,5-Disubstituted N-Aryl Group to Improve Enantioselectivity

Our hypothesis was also supported by the EAS method of alkenyl B(pin) additions to disubstituted allylic phosphates published in 2014 (Scheme 2.10),^{6c} NHC–Cu complex derived from **2.71** promoted the formation of alkenyl addition product **2.72** with >98% S_N2' selectivity and 91:9 er, while only 82:12 enantioselectivity was obtained by the use of NHC–Cu complex derived from **2.14**. The improvement of diastereoselectivity yielded the conclusion that an NHC with a 2,5-disubstituted N-aryl group provided optimal result as compared to an NHC with a 3,5-disubstituted N-aryl ring, when a large alkenyl nucleophile is utilized in EAS reactions with a disubstituted allylic phosphate.

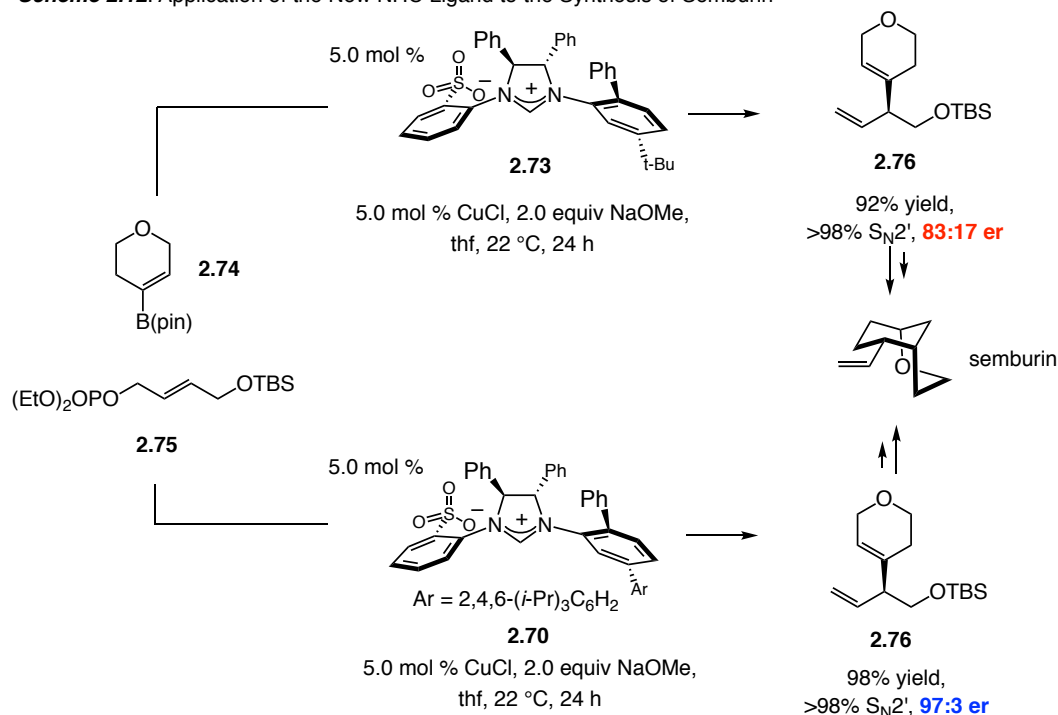
Scheme 2.10. EAS with an Alkenyl B(pin) Reagent catalyzed by an NHC–Cu complex derived from a imidazolium salt with a 2,5-disubstituted N-aryl group



From the previous case, we envisioned that triene **2.62** could be synthesized in higher diastereoselectivity assisted by an NHC ligand with an even larger substitution on the 5-position (larger than *t*-butyl group in **2.73**). Thus imidazolium salt **2.70** with 2,5-disubstitution bearing a 5-triisopropylphenyl group was synthesized and examined in the EAS reaction for the synthesis of plakinic acid A. To our delight, this new ligand yielded improved selectivity for the formation of triene **2.62** as shown in Scheme 2.11. The facial selectivity was improved from 82:18 to 90:10, which further supports our hypothesis as delineated in Figure 2.4.

Scheme 2.11. Introduction of a New Sulfonate-containing NHC Ligand with 2,5-Disubstitution

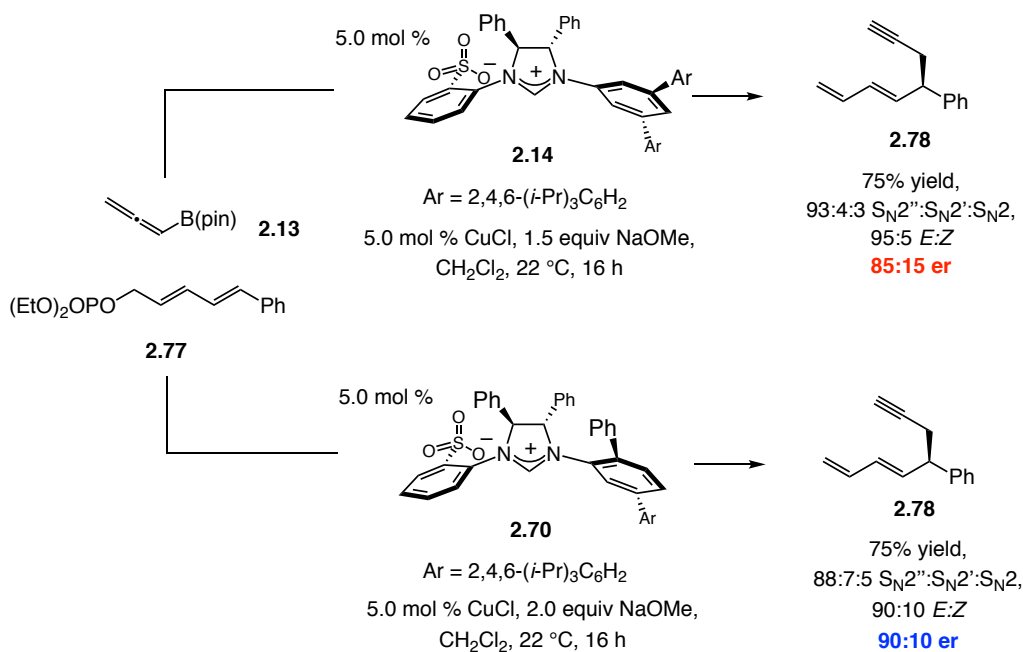
The utility of this new ligand was also showcased in the synthesis of semburin. As shown in Scheme 2.12,^{6c} cyclic alkenyl boron **2.74** was utilized in EAS reaction with allylic phosphate **2.75** to incorporate a pyran group at the stereogenic center. The EAS product **2.76** can be further elaborated to semburin. The low enantioselectivity (83:17 er) was observed in EAS reactions requiring the addition of a large alkenyl nucleophile. The EAS reaction catalyzed by NHC-Cu complex derived from the newly-synthesized imidazolium salt **2.70** furnished skipped diene **2.76** in higher enantioselectivity (97:3 er).

Scheme 2.12. Application of the New NHC Ligand to the Synthesis of Semburin

2.4.2 Application of the New NHC Ligand with 2,5-Substitution for Enantioselective S_N2'' Addition to Alkenyl-Substituted Allylic Phosphates

Recently, we disclosed an enantioselective S_N2'' addition of alkenyl B(pin) **2.13** to alkenyl allylic phosphates such as **2.77**, furnishing the propargyl addition product **2.78** bearing a tertiary carbon stereogenic center adjacent to a diene as shown in Scheme 2.13.¹³ Ligand screening showed that sulfonate-containing NHC–Cu complex derived from **2.14** with a 2,5-substitution pattern promoted the generation of **2.78** in 90:10 er. Again, the sulfonate NHC ligand with a meta substitution pattern delivered the product in a less stereoselective fashion (85:15 er). Of note, the of sulfonate-bearing NHC is crucial for the observed high enantioselectivity; the S_N2'' addition reaction catalyzed by non-sulfonate-containing NHC ligands or phosphine ligands led to the formation of racemic **2.78**.

(13) Unpublished data.

Scheme 2.13. Enantioselective S_N2'' Reaction Promoted by an NHC Ligand with 2,5-Disubstitution

DFT calculations not only provided insight into the mechanism of the S_N2'' additions, but informed design of this new NHC ligand as well. In this case, the cationic sodium bridge also plays an important role in the transition states leading to both the major and minor enantiomers as shown in Figure 2.5. The sulfonate group served as the secondary binding site of the substrate-catalyst complex, rendering a well-defined transition state leading to the S_N2'' addition. The allenyl-Cu species bound to the double bond of **2.77** close to the leaving group and then the Cu- π complex underwent a 3,3'-elimination followed by the cleavage of the C-O bond between the carbon and phosphate. As depicted in Figure 2.5, in order for the 3,3'-elimination to occur in the minor pathway, the allenyl group had to rotate to the right to approach the C1 position of the distal olefin on the allylic phosphate. Thus, it would induce a steric strain between the allenyl moiety and the substituent on the 2-position of N-aryl group. However, the N-aryl ring could not rotate to the back to alleviate the strain due to the steric pressure between

the triisopropylphenyl group on the 5-position on the N-aryl ring and the alkenyl substituent on the electrophile. From the model, we could see that the sulfonate group and the 2,5-substitution on the NHC ligand were essential for this S_N2'' reaction to occur in a stereoselective fashion.

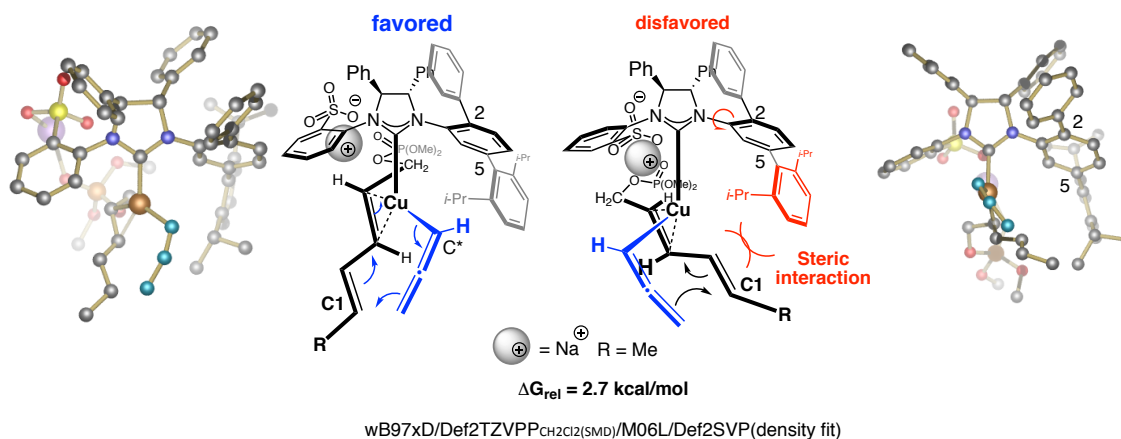


Figure 2.5. Stereochemical Model for the New NHC ligand with 2,5-Substitution in Enantioselective S_N2'' reaction

2.5 Conclusions

We have developed a method for the allylic substitution of TMS-substituted propargyl B(pin) to a variety of di- and trisubstituted allylic phosphates to generate tertiary and quaternary carbon centers. Reactions are catalyzed by an NHC–Cu complex derived from a sulfonate-containing NHC–Ag complex with a 3,5-disubstituted N-aryl group. 1,5-Enynes can be isolated in 75–90% yield, 87:13 to >98:2 S_{N2}' : S_{N2} (branched/linear) selectivity and 83:17–99:1 enantiomeric ratio. Products can be elaborated to rapidly form allenyl, *Z*-alkenyl iodide, and alkenyl B(pin) containing compounds that are of high synthetic value. An application of the current method has been shown in the formal synthesis of plakinic acid A. DFT calculations provided a stereochemical model accounting for the high levels of enantioselectivity observed, and

based on that, informed design of a new imidazolium salt with a 2,5-substituted N-aryl ring.

2.6 Experimentals

General. Infrared (IR) spectra were recorded on a Bruker FT-IR Alpha (ATR mode) spectrophotometer, λ_{\max} in cm^{-1} . Bands are characterized as broad (br), strong (s), medium (m), and weak (w). ^1H NMR spectra were recorded on a Varian Unity INOVA 400 (400 MHz) or Varian Unity INOVA 500 (500 MHz) spectrometer. Chemical shifts are reported in ppm from tetramethylsilane with the solvent resonance as the internal standard (CDCl_3 : δ 7.26 ppm). Data are reported as follows: chemical shift, integration, multiplicity (s = singlet, d = doublet, t = triplet, q = quartet, br = broad, m = multiplet), and coupling constant (Hz). ^{13}C NMR spectra were recorded on a Varian Unity INOVA 400 (100 MHz) spectrometer with complete proton decoupling. Chemical shifts are reported in ppm from tetramethylsilane with the solvent resonance as the internal standard (CDCl_3 : δ 77.16 ppm). High-resolution mass spectrometry was performed on a JEOL AccuTOF DART (positive mode) at the Mass Spectrometry Facility, Boston College. Enantiomer ratios were determined by GC analysis (Alltech Associated Chiraldex B-DM (30 m x 0.25 mm), Chiraldex G-TA (30 m x 0.25 mm), and Betadex 120 column (30 m x 0.25 mm)), or HPLC analysis (Chiral Technologies Chiralpak AZ-H (4.6 x 250 mm), Chiralcel OD-H (4.6 x 250 mm) and Chiralcel OJ-H (4.6 x 250 mm) in comparison with authentic racemic materials. Specific rotations were measured on an ATAGO[®] AP-300 Automatic Polarimeter or a Rudolph Research Analytical Autopol IV Polarimeter. Melting points were measured on a Thomas Hoover capillary melting point apparatus and are uncorrected.

Unless otherwise noted, all reactions were carried out with distilled and degassed solvents under an atmosphere of dry N₂ in oven- (135 °C) or flame-dried glassware with standard dry box or vacuum-line techniques. Solvents were purified under a positive pressure of dry argon by a modified Innovative Technologies purification system: toluene, benzene and hexanes were purified through a copper oxide and alumina column; CH₂Cl₂ and Et₂O were purged with Ar and purified by passage through two alumina columns. Tetrahydrofuran (Aldrich Chemical Co.) was purified by distillation from sodium benzophenone ketyl immediately prior to use unless otherwise specified. All work-up and purification procedures were carried out with reagent grade solvents (purchased from Fisher Scientific, Inc.) in air.

Reagents

***N*-benzyl-*N,N*-diethylethanaminium dichloroiodate** was prepared according to a previously reported procedure.¹⁴

Bis(pinacolato)diboron (B₂(pin)₂) was purchased from Frontier Scientific, Inc. and recrystallized from pentane.

1,3-Bis(1-adamantyl)imidazolinium tetrafluoroborate was purchased from Aldrich and used as received.

1,3-Bis(2,4,6-trimethylphenyl)imidazolinium chloride (SIMes) was purchased from Aldrich and used as received.

(*E*)-4-[(*tert*-Butyldimethylsilyloxy)but-2-en-1-yl] diethyl phosphate (substrate for 14)¹⁵

1-Bromo-4-nitrobenzene was purchased from Aldrich and used as received.

Calcium (II) carbonate (CaCO₃) was purchased from Strem and used as received.

Copper (I) bromide (CuBr) was purchased from Strem and used as received.

Copper (I) chloride (CuCl) was purchased from Strem and used as received.

Copper (II) chloride (CuCl₂) was purchased as CuCl₂•2H₂O from Aldrich and dried over P₂O₅ under vacuum at 80 °C overnight.

(14) Kosynkin, D. V.; Tour, J. M. *Org. Lett.* **2001**, 3, 991–992.

(15) Delvos, L. B.; Vyas, D. J.; Oestreich, M. *Angew. Chem., Int. Ed.* **2013**, 52, 4650–4653.

Copper (I) iodide was purchased from Strem and used as received.

(E)-Diethyl 3-(3-bromophenyl)but-2-enyl phosphate (2.43c)¹⁶

(E)-Diethyl 3-(2-bromophenyl)prop-2-enyl phosphate (2.12c)¹⁷

(E)-Diethyl 3-(3-bromophenyl)prop-2-enyl phosphate (2.12f)¹⁸

(E)-Diethyl 3-(4-chlorophenyl)but-2-enyl phosphate (2.43d)¹⁹

(E)-Diethyl 3-(4-chlorophenyl)prop-2-enyl phosphate (2.12j)¹⁸

(E)-Diethyl 3-cyclohexylbut-2-enyl phosphate (2.43e)¹⁹

(E)-Diethyl 3-cyclohexylprop-2-enyl phosphate (2.32)¹⁸

(E)-Diethyl 3-(2-fluorophenyl)prop-2-enyl phosphate (2.12b)¹⁷

(E)-Diethyl 3-(2-methoxyphenyl)but-2-enyl phosphate (2.43b)¹⁶

(E)-Diethyl 3-(2-methoxyphenyl)prop-2-enyl phosphate (2.12d)¹⁸

(E)-Diethyl 3-(2-methylphenyl)prop-2-enyl phosphate (2.12e)¹⁸

(E)-Diethyl 3-(3-methylphenyl)prop-2-enyl phosphate (2.12g)¹⁷

(E)-Diethyl 3-(4-methylphenyl)prop-2-enyl phosphate (2.12k)¹⁸

(E)-Diethyl 3-(2-naphthyl)prop-2-enyl phosphate (2.12i)²⁰

(E)-Diethyl 3-(4-nitrophenyl)prop-2-enyl phosphate (2.12l)²¹

(E)-Diethyl 3-phenylbut-2-enyl phosphate (2.43a)²⁰

(E)-Diethyl 3-phenylprop-2-enyl phosphate (2.12a)¹⁶

(E)-Diethyl 3-(3-trifluoromethylphenyl)prop-2-enyl phosphate (2.12h)¹⁷

Diisobutylaluminum hydride (dibal-H) was purchased neat from Aldrich and used as received.

Diisopropyl amine was purchased from Aldrich and used as received.

Dimethylmethylenediammonium iodide (Eschenmoser's salt) was purchased from Aldrich and used as received.

(E)-3-[Dimethyl(phenyl)silyl]prop-2-enyl diethyl phosphate (substrate for **2.35**)²⁰

(-)-(S,S)-Diphenylethylenediamine (99% purity) was purchased from Ivy Chemical Company and used as received.

Glacial acetic acid was purchased from Aldrich and used as received.

Hexafluoro-2-propanol (HFIP) was purchased from Aldrich and used as received.

(16) Gao, F.; McGrath, K. P.; Lee, Y.; Hoveyda, A. H. *J. Am. Chem. Soc.* **2010**, *132*, 14315–14320.

(17) Jung, B.; Hoveyda, A. H. *J. Am. Chem. Soc.* **2012**, *134*, 1490–1493.

(18) Akiyama, K.; Gao, F.; Hoveyda, A. H. *Angew. Chem., Int. Ed.* **2010**, *49*, 419–423.

(19) Dabrowski, J. A.; Gao, F.; Hoveyda, A. H. *J. Am. Chem. Soc.* **2011**, *133*, 4778–4781.

(20) Kacprzynski, M. A.; Hoveyda, A. H. *J. Am. Chem. Soc.* **2004**, *126*, 10676–10681.

(21) Luchaco-Cullis, C. A.; Mizutani, H.; Murphy, K. E.; Hoveyda, A. H. *Angew. Chem., Int. Ed. Engl.* **2001**, *40*, 1456–1460.

Imidazolinium salts 2.26, 2.27 and 2.14 were prepared previously reported methods according to previously reported procedures.²²

Isoamyl nitrite was purchased from TCI America and used as received.

Isobutyl 2-bromobenzenesulfonate was prepared according to a previously reported procedure.²³

Methanol was purchased from Acros and purified by distillation from Na (Aldrich) prior to use.

4-Methylbenzenesulfonyl azide was prepared according to a previously reported procedure.²⁴

NHC–Ag complex 2.28 and 2.29 were prepared according to a previously reported procedure.²⁵

N-Iodosuccinimide (NIS) was purchased from Aldrich and re-crystallized under 1,4-dioxane/ CCl_4 at 4 °C without light.

Paraformaldehyde was purchased from Aldrich and used as received.

Palladium (II) acetate ($\text{Pd}(\text{OAc})_2$) was purchased from Strem and used as received.

Silver carbonate was purchased from Aldrich and used as received.

Sodium borohydride (NaBH_4) was purchased from Aldrich and used as received.

Sodium *t*-butoxide (NaOt-Bu) was purchased from Strem and used as received.

Sodium perborate tetrahydrate ($\text{NaBO}_3 \cdot 4\text{H}_2\text{O}$) was purchased from Aldrich and used as received.

Sodium methoxide (NaOMe) was purchased from Strem and used as received.

Tetrabutylammonium fluoride (TBAF) was purchased as a 1.0 M solution in thf from Fisher and used as received.

Tetrakis(triphenylphosphine)palladium was purchased from Strem and used as received.

Tin (II) chloride (SnCl_2) was purchased from Aldrich and used as received.

(2,4,6-Triisopropylphenyl)boronic acid was purchased from Combi-blocks and used as received.

3-(Trimethylsilyl)-2-propyn-1-ylboronic acid pinacol ester (2.57) was prepared according to a previously reported procedure.²⁶

(22) (a) Van Veldhuizen, J. J.; Campbell, J. E.; Guidici, R. E.; Hoveyda, A. H. *J. Am. Chem. Soc.* **2005**, *127*, 6877–6882. (b) Lee, K.-S.; Hoveyda, A. H. *J. Org. Chem.* **2009**, *74*, 4455–4462.

(23) Brown, M. K.; May, T. L.; Baxter, C. A.; Hoveyda, A. H. *Angew. Chem., Int. Ed.* **2007**, *46*, 1097–1100.

(24) Serwinski, P. R.; Esat, B.; Lahti, P. M.; Liao, Y.; Walton, R.; Lan, J. *J. Org. Chem.* **2004**, *69*, 5247–5260.

(25) May, T. L.; Brown, M. K.; Hoveyda, A. H. *Angew. Chem., Int. Ed.* **2008**, *47*, 7358–7362.

(26) Fandrick, D. R.; Reeves, J. T.; Song J. J. International Patent WO 2010/141328 A2.

Triethylamine (Et₃N) was purchased from Fisher Scientific, Inc. and distilled over CaH₂ prior to use.

Synthesis

Characterization Data for Previously Unreported Allylic Phosphates

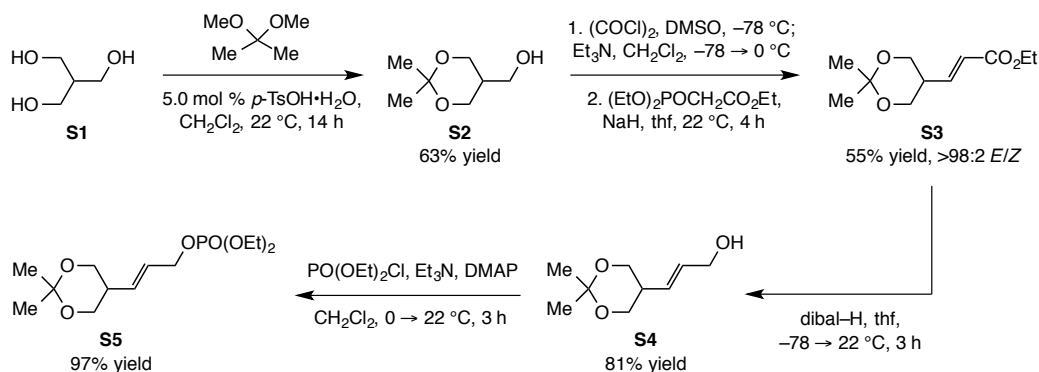
(*E*)-Diethyl (3-(thiophen-3-yl)allyl) phosphate (**2.12m**)

2.12m was synthesized according to a previously reported procedure.¹⁷ **IR (neat):** 3455(br,w), 3087 (w), 2983 (w), 2934 (w), 2908 (w), 1657 (w), 1444 (w), 1393 (w), 1370 (w), 1261 (s), 1164 (w), 1101 (w), 1007 (s), 964 (s), 859 (m), 824 (m), 772 (s), 627 (w), 549 (w) cm⁻¹; **¹H NMR (CDCl₃, 400 MHz):** δ 7.28–7.26(1H, m), 7.21–7.20 (2H, m), 6.68 (1H, d, *J* = 16.0 Hz), 6.15 (1H, dt, *J* = 16.0, 6.4 Hz), 4.65 (2H, t, *J* = 7.6 Hz), 4.16–4.08 (4H, m), 1.33 (6H, t, *J* = 6.8 Hz); **¹³C NMR (CDCl₃, 100 MHz):** δ 138.8, 128.3, 126.4, 125.1, 123.5 (d, *J*_{CP} = 6.8 Hz), 123.4, 67.8 (d, *J*_{CP} = 5.3 Hz), 63.8 (d, *J*_{CP} = 6.1 Hz), 16.1 (d, *J*_{CP} = 6.9 Hz). **HRMS (ESI⁺):** Calcd for C₁₁H₁₈O₄PS [M+H]⁺: 277.0663; Found: 277.0657.

(*E*)-Diethyl (3-(pyridin-3-yl)allyl) phosphate (**2.12n**)

2.12n was synthesized according to a previously reported procedure.¹⁷ **IR (neat):** 3474(br,w), 2984 (w), 2933 (w), 1648 (w), 1587 (w), 1570 (w), 179 (w), 1260 (m), 1165 (w), 1097 (w), 1011 (s), 966 (s), 883 (w), 824 (m), 795 (m), 747 (w), 708 (m), 555 (w) cm⁻¹; **¹H NMR (CDCl₃, 400 MHz):** δ 8.62 (1H, d, *J* = 2.4 Hz), 8.51 (1H, d, *J* = 4.8 Hz), 7.16 (1H, dt, *J* = 8.0, 1.6 Hz), 7.29–7.26 (1H, m), 6.69 (1H, d, *J* = 15.6 Hz), 3.84 (1H, dt, *J* = 15.6, 6.0 Hz), 4.73 (1H, dd, *J* = 6.0, 1.6 Hz), 4.71 (1H, dd, *J* = 6.0, 1.6 Hz), 4.19–4.12 (4H, m), 1.36 (6H, t, *J* = 7.2 Hz); **¹³C NMR (CDCl₃, 100 MHz):** δ 149.3, 148.6, 133.2, 131.8, 129.9, 126.2, 126.1, 123.6, 67.4 (d, *J*_{CP} = 5.3 Hz), 64.0 (d, *J*_{CP} = 6.1 Hz), 16.2 (d, *J*_{CP} = 6.1 Hz). **HRMS (ESI⁺):** Calcd for C₁₂H₁₈NO₄P [M+H]⁺: 272.1052; Found: 272.1053.

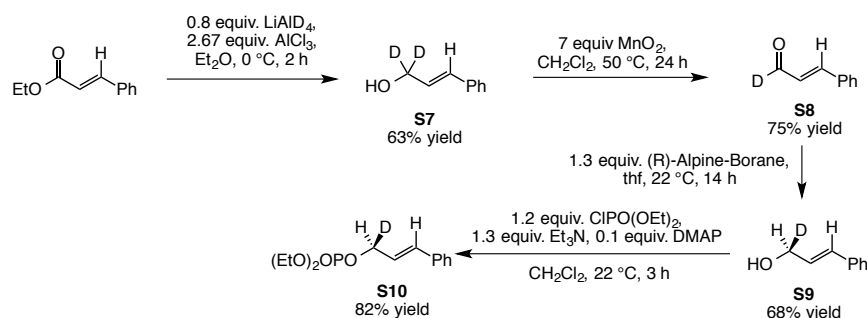
Scheme S1. Preparation of an Allylic Phosphate



(*E*)-Diethyl 3-(2,2-dimethyl-[1,3]dioxin-5-yl)prop-2-enyl phosphate (S5, substrate for **2.33**)

IR (neat): 3487 (br,w), 2988 (w), 2923 (w), 2857 (w), 1479 (w), 1455 (w), 1371 (w), 1273 (m), 1196 (m), 1161 (m), 1022 (s), 972 (s), 940 (s), 831 (m), 802 (m), 754 (w), 702 (w), 518 (m) cm^{-1} ; **^1H NMR (CDCl₃, 400 MHz):** δ 5.75–5.62 (2H, m), 4.49 (1H, d, $J = 8$ Hz), 4.48 (1H, d, $J = 8$ Hz), 4.15–4.07 (4H, m), 3.87 (1H, d, $J = 4.4$ Hz), 3.84 (1H, d, $J = 4.4$ Hz), 3.73 (1H, d, $J = 9.6$ Hz), 3.70 (1H, d, $J = 9.6$ Hz), 2.62–2.53 (1H, m), 1.44 (3H, d, $J = 0.8$ Hz), 1.41 (3H, d, $J = 0.8$ Hz), 1.34 (3H, t, $J = 7.2$ Hz), 1.33 (3H, t, $J = 7.2$ Hz); **^{13}C NMR (CDCl₃, 100 MHz):** δ 131.5, 127.4 (d, $J_{\text{CP}} = 6.7$ Hz), 97.8, 77.3, 67.5 (d, $J_{\text{CP}} = 5.2$ Hz), 64.0, 63.9 (d, $J_{\text{CP}} = 6.0$ Hz), 37.8, 27.5, 20.5, 16.3 (d, $J_{\text{CP}} = 6.7$ Hz); **HRMS (ESI⁺):** Calcd for C₁₃H₂₆O₆P₁ [M+H]⁺: 309.1467; Found: 309.1472.

Scheme S2. Preparation of Allylic Phosphate **S10**



(*S,E*)-Diethyl (3-phenylallyl-1-*d*) phosphate (S10, cf. **1.64** in Chapter 1)

IR (neat): 3408 (br, w), 2983 (w), 2909 (w), 1449 (w), 1393 (w), 1369 (w), 1261 (m), 1020 (s), 966 (s), 863 (m), 747 (m), 693 (m), 552 (w) cm^{-1} ; **^1H NMR (CDCl₃, 500 MHz):** δ 7.39 (2H, d = 9.0 Hz), 7.34–7.31 (2H, m), 7.28–7.25 (1H, m), 6.68 (1H, d = 16.5 Hz), 6.30 (1H, dd, $J = 16.0, 6.5$ Hz), 4.68 (1H, t, $J = 6.5$ Hz), 4.16–4.10 (4H, m), 1.34 (1H, t, $J = 6.5$ Hz); **^{13}C NMR (CDCl₃, 100 MHz):** δ 136.2, 134.1, 128.8, 128.7, 128.3, 126.8, 123.7 (d, $J_{\text{CP}} = 6.8$ Hz), 67.7 (dt, $J_{\text{CP}(d)} = 4.5$ Hz, $J_{\text{CD}(t)} = 22.0$ Hz), 63.9 (d, $J_{\text{CP}} = 6.1$ Hz), 16.3 (d, $J_{\text{CP}} = 6.9$ Hz); **HRMS (ESI⁺):** Calcd for C₁₃H₁₉DO₄P [M+H]⁺: 272.1162; Found: 272.1159. Specific rotation: $[\alpha]_{\text{D}}^{20.0}$ 0.0 (c 1.17, CHCl₃) for an enantiomerically enriched sample of >98:2 er.

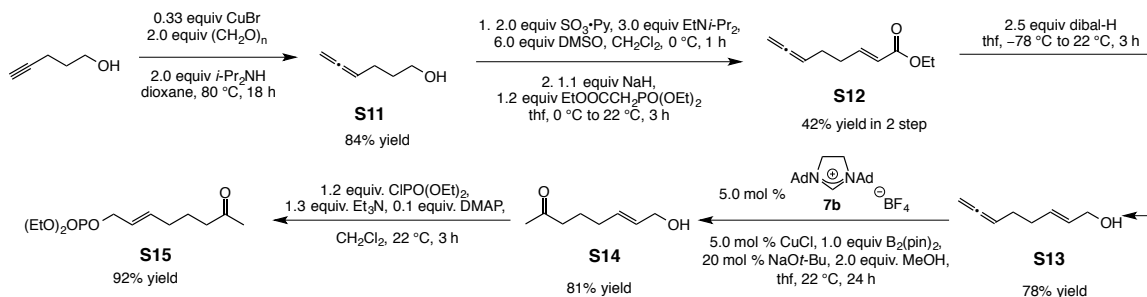
Enantiomeric purity was determined by ^1H NMR, ^{19}F NMR analysis of the Mosher's ester for S9.

(*S,E*)-3-Phenylallyl-1-*d* (*R*)-3,3,3-trifluoro-2-methoxy-2-phenylpropanoate (*R*-MTPA for S9)

IR (neat): 2952 (w), 2849 (w), 1745 (s), 1495 (w), 1451 (w), 1269 (s), 1241 (s), 1167 (s), 1122 (s), 1081 (m), 1022 (m), 995 (m), 966 (s), 765 (w), 716 (s), 693 (m), 644 (w) cm^{-1} ; **^1H NMR (CDCl₃, 400 MHz):** δ 7.54 (d, $J = 7.0$ Hz), 7.40–7.33 (7H, m), 7.32–7.26 (1H, m), 6.69 (1H, d, $J = 15.5$ Hz), 6.28 (1H, d, $J = 15.5, 6.5$ Hz), 4.96 (1H, d, $J = 6.5$ Hz),

3.58 (3H, d, s); ^{13}C NMR (CDCl_3 , 100 MHz): δ 166.5, 136.0, 132.4, 129.8, 128.8, 128.6, 128.5, 127.4, 126.9, 123.4 (q, $J_{\text{CF}} = 286.6$ Hz), 84.8 (q, $J_{\text{CF}} = 27.3$ Hz), 66.6 (t, $J_{\text{CD}} = 22.7$ Hz), 55.7; ^{19}F NMR (CDCl_3): δ 81.1. HRMS (ESI^+): Calcd for $\text{C}_{19}\text{H}_{17}\text{DF}_3\text{O}_3$ [$\text{M}+\text{H}$] $^+$: 352.1271; Found: 352.1284. Specific rotation: $[\alpha]_{\text{D}}^{20.0} -51.7$ (c 0.58, CHCl_3) for an enantiomerically enriched sample of >98:2 dr.

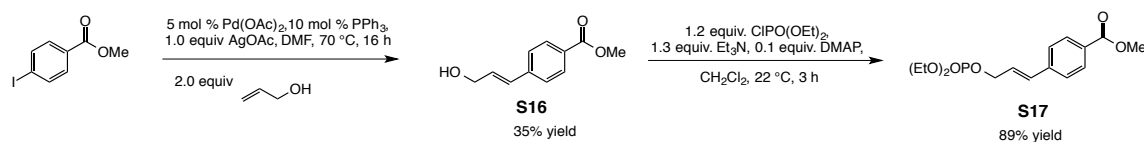
Scheme S3. Preparation of Allylic Phosphate S15



(*E*)-Diethyl (7-oxooct-2-en-1-yl) phosphate (S15)

IR (neat): 3495 (br, w), 2985 (w), 2937 (w), 1713 (m), 1444 (w), 1368 (w), 1262 (m), 1163 (m), 1093 (w), 1003 (s), 968 (s), 844 (m), 801 (m), 744 (w), 517 (m), 402 (w) cm^{-1} ;
 ^1H NMR (CDCl_3 , 400 MHz): δ 5.78–5.70 (1H, m), δ 5.63–5.56 (1H, m), 4.45 (2H, t, $J = 7.6$ Hz), 4.13–4.05 (4H, m), 2.42 (2H, t, $J = 7.8$ Hz), 2.11 (3H, s), 2.05 (2H, q, $J = 7.2$ Hz), 1.66 (2H, q, $J = 7.2$ Hz), 1.31 (6H, t, $J = 8.0$ Hz); ^{13}C NMR (CDCl_3 , 100 MHz): δ 208.7, 135.3, 125.4 (d, $J_{\text{CP}} = 6.8$ Hz), 67.9 (d, $J_{\text{CP}} = 5.3$ Hz), 63.7 (d, $J_{\text{CP}} = 6.1$ Hz), 42.9, 31.5, 30.1, 22.8, 16.2 (d, $J_{\text{CP}} = 6.8$ Hz); HRMS (ESI^+): Calcd for $\text{C}_{12}\text{H}_{23}\text{O}_5\text{PNa}$ [$\text{M}+\text{Na}$] $^+$: 301.1181; Found: 301.1181.

Scheme S4. Preparation of Allylic Phosphate S17



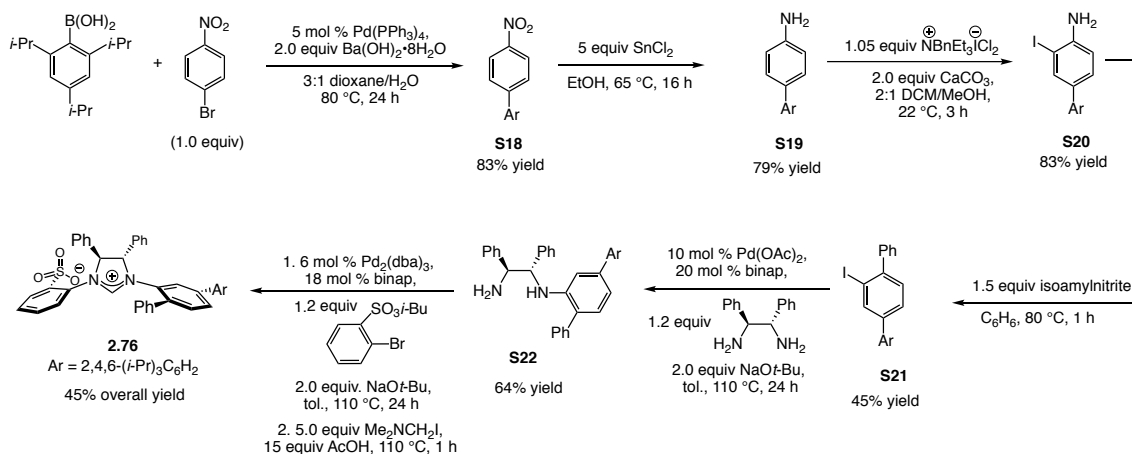
Methyl (*E*)-4-(3-((diethoxyphosphoryl)oxy)prop-1-en-1-yl)benzoate (S17)

IR (neat): 2984 (w), 2954 (w), 1717 (s), 1607 (w), 1436 (w), 1269 (s), 1179 (m), 1107 (m), 1010 (s), 958 (s), 863 (m), 837 (m), 804 (m), 753 (m), 509 (w), 476 (w) cm^{-1} ;
 ^1H NMR (CDCl_3 , 400 MHz): δ 7.99 (2H, d, $J = 8.4$ Hz), 7.44 (2H, d, $J = 8.8$ Hz), 6.72 (1H, d, $J = 16.0$ Hz), 6.41 (1H, dt, $J = 16.0, 6.0$ Hz), 4.72 (2H, t, $J = 6.0$ Hz), 4.18–4.12 (4H, d, $J = 6.8$ Hz), 3.91 (3H, s), 1.35 (6H, t, $J = 6.8$ Hz); ^{13}C NMR (CDCl_3 , 100 MHz): δ 166.9, 140.6, 132.5, 130.1, 129.7, 126.6, 126.5 (d, $J_{\text{CP}} = 6.8$ Hz), 67.6 (d, $J_{\text{CP}} = 5.3$ Hz), 64.0 (d, $J_{\text{CP}} = 5.3$ Hz), 52.6, 16.3 (d, $J_{\text{CP}} = 6.8$ Hz); HRMS (ESI^+): Calcd for $\text{C}_{15}\text{H}_{22}\text{O}_6\text{P}$ [$\text{M}+\text{H}$] $^+$: 329.1154; Found: 329.1169.

Characterization Data for the Propargyl B(pin) Reagent

Triisopropyl(3-(4,4,5,5-tetramethyl-1,3,2-dioxaborolan-2-yl)prop-1-yn-1-yl)silane (**2.59**)

This compound was prepared previously reported methods⁴: **IR (neat)**: 2942 (m), 2892 (w), 2865 (m), 2167 (w), 1494 (w), 1381 (m), 1342 (s), 1184 (w), 1143 (m), 1031 (w), 994 (w), 967 (w), 882 (m), 845 (w), 859 (m), 675 (m) cm^{-1} ; **¹H NMR (CDCl₃, 400 MHz)**: δ 1.87 (2H, s) 1.26 (12H, s), 1.08–1.02 (21H, m); **¹³C NMR (CDCl₃, 100 MHz)**: δ 104.9, 84.1, 79.1, 24.9, 18.8, 11.5, -7.7. **HRMS (ESI⁺)**: Calcd for C₁₈H₃₆BO₂Si [M+H]⁺: 323.2578; Found: 323.2566.

Preparation of Imidazolium Salt **2.70****Scheme S5. Synthesis of Imidazolium Salt 2.76**

2,4,6-Triisopropyl-4'-nitro-1,1'-biphenyl (S18)

In a nitrogen-filled glove-box, to a solution of Pd(PPh₃)₄ (163 mg, 0.141 mmol) in 1,4-dioxane (12 mL) was added 1-bromo-4-nitrobenzene (570 mg, 2.82 mmol), an aqueous solution of Ba(OH)₂·8H₂O (1.78 g, 5.64 mmol) and (2,4,6-triisopropylphenyl)boronic acid (700 mg, 2.82 mmol). The mixture was allowed to warm to at 80 °C for 24 h under nitrogen atmosphere. The solvents were removed *in vacuo*, and the resulting brown solid residue was dissolved in CH₂Cl₂ and was washed with a 1N solution of HCl (10 mL). The aqueous layer was washed with CH₂Cl₂ (3 x 12 mL) and the combined organic layers were washed with brine (10 mL), water (10 mL), dried over MgSO₄, filtered and concentrated *in vacuo*. The yellow solid residue was purified by silica gel chromatography (100% hexanes, R_f = 0.65) to afford 761 mg (2.34 mmol, 83% yield) of **S18** as pale yellow solid. Mp = 213–215 °C. **IR (neat)**: 2956 (m), 2926 (m), 2867 (m), 1592 (m), 1567 (w), 1509 (s), 1459 (m), 1382 (w), 1362 (w), 1342 (s), 1282 (m), 1170

(w), 1099 (m), 1071 (m), 1057 (m), 1005 (m), 966 (m), 945 (s), 881 (s), 761 (m), 707 (s), 487 (m) cm^{-1} ; $^1\text{H NMR}$ (CDCl_3 , 400 MHz): δ 8.28 (2H, app. d, $J = 8.8$ Hz), 7.37 (2H, app. d, $J = 8.8$ Hz), 7.08 (2H, s), 2.98–2.91 (1H, m), 2.51–2.41 (2H, m), 1.31 (6H, d, $J = 7.2$ Hz), 1.08 (12H, d, $J = 7.2$ Hz); $^{13}\text{C NMR}$ (CDCl_3 , 100 MHz): δ 149.2, 148.8, 147.0, 146.1, 134.9, 130.9, 123.4, 121.0, 34.5, 30.6, 24.2. **HRMS** (ESI^+): Calcd for $\text{C}_{21}\text{H}_{28}\text{NO}_2$ $[\text{M}+\text{H}]^+$: 326.2120; Found: 326.2135.

2',4',6'-Triisopropyl-(1,1'-biphenyl)-4-amine (S19)

A 100-mL round bottom flask was charged with **S18** (325 mg, 1.00 mmol), SnCl_2 (948 mg, 5.00 mmol), and ethanol (20.0 mL). The round bottom flask was fitted with a reflux condenser, and the mixture was allowed to warm to 65 °C with stirring. The resulting homogeneous solution was kept at 65 °C for 15 h before careful addition of a saturated solution of NaHCO_3 . The aqueous layer was washed with EtOAc (3 x 100 mL). The organic layers were combined, dried over MgSO_4 , and the volatiles were removed *in vacuo*. The white oil residue was purified by silica gel chromatography (2:1 hexanes/EtOAc, R_f 0.80) to afford **S19** as off-white solid (285 mg, 0.771 mmol, 79% yield). $\text{Mp} = 149\text{--}150$ °C. **IR** (neat): 3439 (w), 3359 (w), 2957 (s), 2925 (m), 2863(m), 1619 (s), 1607 (s), 1565 (w), 1519 (s), 1459 (s), 1430 (w), 1380 (m), 1360 (m), 1336 (w), 1316 (m), 1273 (s), 1247(w), 1236(w), 1178(m), 1168 (w), 1125(w), 1099(m), 1069 (m), 1056 (m), 1002(w), 958 (w), 939 (w), 921 (w), 879(s), 835 (s), 815 (m), 782(m), 741 (m), 685 (w), 653 (s), 623 (m), 582 (m), 554 (s), 540 (s), 508 (s), 492(s) (s), 2927 (m), 2868 (m), 1606 (w), 1567 (w), 1401 (m), 1382 (m), 1361 (m), 1317 (w), 939 (s), 762 (s), 748 (m), 650 (m) cm^{-1} ; $^1\text{H NMR}$ (CDCl_3 , 400 MHz): δ 7.03 (2H, s), 6.95 (2H, d, $J = 8.4$ Hz), 6.72 (2H, d, $J = 8.4$ Hz), 3.68 (2H, s), 2.96–2.89 (1H, m), 2.74–2.68 (2H, m), 1.30 (6H, d, $J = 7.2$ Hz), 1.07 (12H, d, $J = 7.2$ Hz); $^{13}\text{C NMR}$ (CDCl_3 , 100 MHz): δ 147.6, 147.2, 144.7, 137.3, 131.1, 130.7, 120.5, 114.9, 34.4, 30.3, 24.4, 24.2. **HRMS** (ESI^+): Calcd for $\text{C}_{21}\text{H}_{30}\text{N}$ $[\text{M}+\text{H}]^+$: 296.2378; Found: 296.2367.

3-Iodo-2',4',6'-triisopropyl-(1,1'-biphenyl)-4-amine (S20)

Aniline **S19** (134 mg, 0.45 mmol) was dissolved in CH_2Cl_2 (5 mL) and MeOH (2.5 mL). To this solution were added benzyltriethylammonium dichloroiodate (184 mg, 0.47 mmol) and CaCO_3 (100 mg, 1.0 mmol). The suspension was allowed to stir at 22 °C for 1 h. The reaction mixture was filtered through a bed of celite and was concentrated *in vacuo* to approximately 1/3 volume. The red residue was washed with 5% NaHSO_3 solution (1 ml), saturated NaHCO_3 solution (1 ml), water (1 ml), and brine (1 ml). The organic layer was dried over MgSO_4 , filtered, and concentrated to afford red solid. Purification by silica gel chromatography (85:15 hexanes/EtOAc, R_f 0.40) furnished **S20** (157 mg, 83% yield) as orange solid. $\text{Mp} = 210\text{--}212$ °C. **IR** (neat): 3464 (w), 3369 (w), 2955 (m), 2922 (w), 2864 (w), 1610 (m), 1500 (m), 1459 (w), 1429 (w), 1381 (w), 1360 (m), 1337 (w), 1315

(w), 1301 (w), 1291 (w), 1264 (w), 1243 (w), 1156 (w), 1069 (w), 1010 (w), 881 (m), 830 (w), 740 (w), 693 (w), 663 (w) cm^{-1} ; $^1\text{H NMR (CDCl}_3, 400 \text{ MHz)}$: δ 7.50 (1H, d, $J = 2.0$ Hz), 7.04 (2H, s), 6.97 (1H, dd, $J = 8.0, 2.0$ Hz), 6.79 (1H, d, $J = 8.0$ Hz), 4.12 (2H, s), 2.97–2.90 (1H, m), 2.73–2.67 (2H, m), 1.31 (6H, d, $J = 6.8$ Hz), 1.11 (6H, d, $J = 6.4$ Hz), 1.09 (6H, d, $J = 6.8$ Hz); $^{13}\text{C NMR (CDCl}_3, 100 \text{ MHz)}$: δ 148.1, 147.2, 145.2, 139.8, 135.7, 132.7, 130.9, 120.6, 114.3, 84.1, 34.4, 30.4, 24.4, 24.3, 24.2. **HRMS (ESI⁺)**: Calcd for $\text{C}_{21}\text{H}_{29}\text{IN [M+H]}^+$: 422.1345; Found: 422.1327.

3'-Iodo-2,4,6-triisopropyl-1,1':4',1''-terphenyl (S21)

To a solution of aniline **S20** (421 mg, 1.0 mmol) in benzene (4 ml) was added 200 μl of isoamyl nitrite (176 mg, 1.5 mmol). The mixture was allowed to heat at 80 °C for 1 h. After cooling to 22 °C, the solution was concentrated *in vacuo* and purified by silica gel chromatography (100% hexanes, R_f 0.70) to afford 217 mg (0.45 mmol, 45% yield) of **S21** as white solid. Mp = 135–137 °C. **IR (neat)**: 3058 (w), 3025 (w), 2959 (s), 2868 (m), 2926 (m), 2867 (m), 1607 (w), 1567 (w), 1526 (w), 1462 (m), 1443 (w), 1382 (w), 1364 (w), 1338 (w), 1102 (w), 1065 (w), 1031 (w), 1004 (w), 877 (w), 840 (w), 817 (w), 763 (m), 735 (w), 700 (m), 682 (w), 660 (w), 648 (w) cm^{-1} ; $^1\text{H NMR (CDCl}_3, 400 \text{ MHz)}$: δ 7.81 (1H, d, $J = 1.6$ Hz), 7.47–7.45 (4H, m), 7.45–7.40 (1H, m), 7.32 (1H, d, $J = 7.6$ Hz), 7.21 (1H, dd, $J = 8.0, 1.6$ Hz), 7.07 (2H, s), 2.98–2.91 (1H, m), 2.70–2.63 (2H, m), 1.31 (6H, d, $J = 6.8$ Hz), 1.15 (6H, d, $J = 6.4$ Hz), 1.11 (6H, d, $J = 7.2$ Hz); $^{13}\text{C NMR (CDCl}_3, 100 \text{ MHz)}$: δ 148.5, 146.7, 144.7, 144.1, 141.8, 140.7, 135.2, 129.8, 129.6, 129.5, 128.1, 127.7, 120.8, 98.2, 34.5, 30.5, 24.5, 24.3, 24.2. **HRMS (ESI⁺)**: Calcd for $\text{C}_{27}\text{H}_{32}\text{I [M+H]}^+$: 483.1549; Found: 483.1544.

(1*S*,2*S*)-1,2-Diphenyl-*N*¹-(2'',4'',6''-triisopropyl-[1,1':4',1''-terphenyl]-2'-yl)ethane-1,2-diamine (S22)

(–)-(*S,S*)-1,2-Diphenylethylenediamine (254 mg, 1.2 mmol), aryl iodide **S21** (482 mg, 1.0 mmol), Pd(OAc)_2 (22.4 mg, 0.10 mmol), *rac*-BINAP (125 mg, 0.20 mmol) and NaOt-Bu (192 mg, 2.0 mmol) were weighed out into a flame-dried 100-mL two-neck round-bottom flask under a N_2 atmosphere in a glove box. The flask was equipped with a reflux condenser and removed from the glove box. Toluene (20 mL) was added through syringe and the resulting mixture was allowed to stir at 110 °C for 24 h. The mixture was allowed to cool to 22 °C and the volatiles were removed *in vacuo* affording deep red oil, which was dissolved in toluene and purified by silica gel chromatography (5:1 hexanes/EtOAc, R_f 0.20) to afford 362 mg (0.64 mmol, 64% yield) of **S22** as orange oil. **IR (neat)**: 3402 (w), 3059 (w), 3026 (w), 2958 (m), 2925 (w), 2866 (w), 1607 (m), 1556 (m), 1517 (m), 1491 (m), 1453 (m), 1414 (m), 1381 (w), 1361 (w), 1319 (w), 1302 (w), 1272 (w), 1227 (w), 1169 (w), 1129 (w), 1099 (w), 1070 (w), 1029 (w), 1008 (w), 994 (w), 944 (w), 909 (s), 876 (m), 858 813 768 (m), 732 (s), 701 (s), 650 (w), 573 (w), 510 (w), 426 (w) cm^{-1} ;

¹H NMR (CDCl₃, 400 MHz): δ 7.58–7.57 (4H, m), 7.49–7.46 (1H, m), 7.30–7.25 (5H, m), 7.24–7.21 (5H, m), 7.07 (1H, d, *J* = 8.0 Hz), 7.03 (1H, d, *J* = 1.6 Hz), 6.94 (1H, d, *J* = 2.0 Hz), 6.46 (1H, dd, *J* = 8.0, 2.0 Hz), 6.11 (1H, d, *J* = 1.6 Hz), 5.43 (1H, d, *J* = 7.6 Hz), 4.55 (1H, dd, *J* = 7.6, 4.0 Hz), 4.33 (1H, d, *J* = 3.6 Hz), 2.97–2.90 (1H, m), 2.77–2.70 (1H, m), 2.42–2.35 (1H, m), 1.32–1.30 (8H, m), 1.12 (6H, dd, *J* = 6.8, 4.8 Hz), 0.96 (3H, d, *J* = 6.8 Hz), 0.56 (3H, d, *J* = 7.2 Hz; **¹³C NMR (CDCl₃, 100 MHz):** δ 147.2, 146.6, 146.4, 143.2, 142.7, 140.8, 140.7, 139.8, 137.6, 129.7, 129.3, 128.7, 128.4, 128.1, 127.2, 127.0, 126.8, 125.9, 120.3, 120.2, 118.4, 113.3, 63.1, 60.7, 34.2, 30.0, 29.8, 24.6, 24.3, 24.1, 24.0, 23.9. **HRMS (ESI⁺):** Calcd for C₄₁H₄₇N₂ [M+H]⁺: 567.3739; Found: 567.3743. Specific rotation: [α]_D^{23.1} –51.0 (*c* 0.98, CHCl₃).

Imidazolium salt **2.70**

Diamine **S22** (1.19 g, 2.1 mmol), Pd₂(dba)₃ (115 mg, 0.13 mmol), *rac*-BINAP (235 mg, 0.38 mmol) and NaOt-Bu (404 mg, 4.2 mmol) were weighed out into a flame-dried 100-mL two-neck round-bottom flask under a N₂ atmosphere in a glove box. The flask was equipped with a reflux condenser and removed from the glove box. A solution of *iso*-butyl-2-bromobenzenesulfonate (739 mg, 2.5 mmol) in toluene (40 mL) was added through syringe and the resulting mixture was allowed to stir at 110 °C for 24 h. The mixture was allowed to cool to 22 °C and the volatiles were removed *in vacuo* affording dark red oil. The oil was dissolved in toluene, loaded on top of a column containing silica gel, and purified by silica gel chromatography (9:1 hexanes/Et₂O, R_f 0.18) to afford brown liquid, which was transferred into a screw cap vial (2 x 8 cm), which was sealed with a septum and purged with N₂. Acetic acid (1.80 mL, 31.5 mmol) followed by Eschenmoser's salt (1.94 g, 10.5 mmol) was added to the mixture. The vial was sealed with a screw cap and allowed to stir at 110 °C (the mixture becomes dark brown-homogeneous solution). After 1 h, the mixture was allowed to cool to 22 °C and diluted with CH₂Cl₂ (10 mL) and water (10 mL). The solution was neutralized by the slow addition of a saturated aqueous K₂CO₃ solution until gas evolution ceased. The aqueous layer was washed with CH₂Cl₂ (4 x 30 mL) and the combined organic layers were dried over MgSO₄, filtered and concentrated *in vacuo*, which was purified by silica gel chromatography (3:1 hexanes/EtOAc to 5:1 CH₂Cl₂/Acetone, R_f 0.30 in 3:1 hexanes/EtOAc) to afford 692 mg (0.95 mmol, 45% overall yield) of **2.70** as pale yellow solid (Note: This material was obtained in pale yellow powder form by trituration from CH₂Cl₂/hexanes bilayer). Mp = >300 °C. **IR (neat):** 3060 (w), 2960 (m), 2927 (w), 2868 (w), 1623 (m), 1587 (w), 1552 (w), 1493 (w), 1458 (w), 1399 (w), 1383 (w), 1362 (w), 1277 (w), 1222 (m), 1140 (w), 1091 (w), 1057 (w), 1022 (w), 1009 (w), 877 (w), 843 (w), 753 (w), 719 (w), 701 (w), 666 (w), 612 (w), 564 (w), 539(w); **¹H NMR (CDCl₃, 400 MHz):** δ 9.13 (1H, s), 8.25 (1H, dd, *J* = 7.8, 1.2 Hz), 7.72–7.68 (3H, m), 7.63–7.59 (1H, m), 7.54–7.52 (2H, m), 7.40–7.34 (3H, m), 7.32–7.28 (4H, m), 7.26–7.20 (3H, m), 7.21 (1H, dd, *J* = 8.0, 1.6 Hz), 7.06–7.01 (5H, m), 6.43 (1H, dd, *J* = 8.1, 1.2 Hz), 5.93 (1H, d,

$J = 11.2$ Hz), 4.79 (1H, d, $J = 11.2$ Hz), 2.97–2.90 (1H, m), 2.53–2.46 (1H, m), 2.15–2.08 (1H, m), 1.32 (6H, d, $J = 6.4$ Hz), 1.15 (3H, d, $J = 6.8$ Hz), 1.07 (3H, d, $J = 6.8$ Hz), 1.06 (3H, d, $J = 7.2$ Hz), 0.93 (3H, d, $J = 6.8$ Hz); ^{13}C NMR (CDCl_3 , 100 MHz): δ 158.4, 148.8, 146.3, 146.1, 143.8, 143.0, 138.3, 135.7, 135.0, 134.4, 133.1, 132.0, 131.6, 130.9, 130.7, 130.4, 130.2, 130.0, 129.9, 129.8, 129.6, 129.4, 129.3, 129.2, 129.0, 128.8, 127.4, 121.0, 120.9, 75.1, 34.5, 30.7, 20.2, 24.6, 24.4, 24.3, 24.2. HRMS (ESI): Calcd for $\text{C}_{48}\text{H}_{49}\text{N}_2\text{O}_3\text{S}$ $[\text{M}+\text{H}]^+$: 733.3464; Found: 733.3470. Specific rotation: $[\alpha]_{\text{D}}^{22.4} +89.2$ (c 0.56, CHCl_3).

NHC–Cu Catalyzed Enantioselective Propargyl Addition to Disubstituted Allylic Phosphates

Representative Procedure

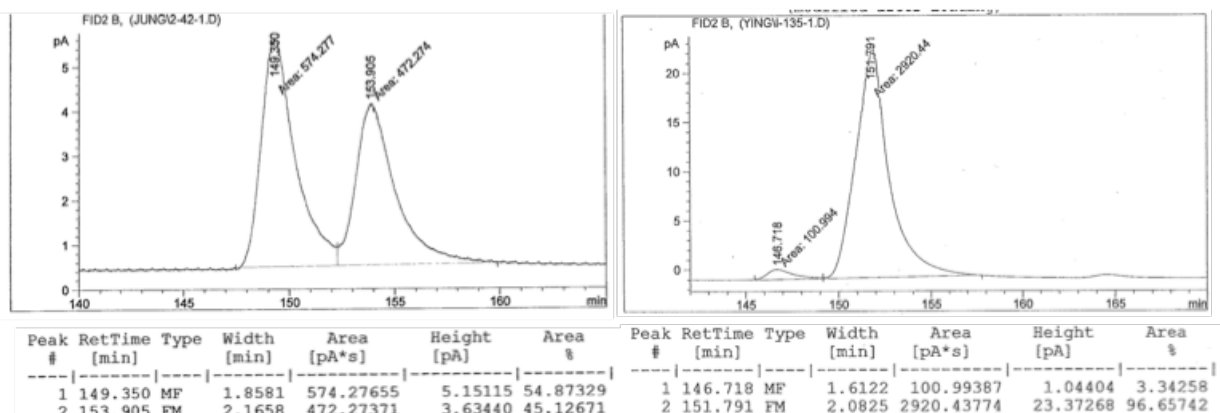
An oven-dried 1-dram vial equipped with a stir bar was charged with imidazolium salt **2.29** (4.8 mg, 5.0 μmol), NaOMe (6.5 mg, 150 μmol), and CuCl_2 (0.67 mg, 5.0 μmol) in a nitrogen-filled glove box. The vial was sealed with a cap (phenolic open top cap with a red PFTE/white silicon septum) and electrical tape, and removed from the glove box. CH_2Cl_2 (0.80 mL) was added and the mixture was allowed to stir for 1 h under N_2 at 22 $^\circ\text{C}$ (the mixture became bright-yellow solution). The solution of allylic phosphate **2.12a** (28 mg, 0.10 mmol) and propargyl–B(pin) reagent **2.20** (40 μL , 0.15 mmol) in thf (2 mL) was added to the mixture slowly through a syringe. The resulting mixture was allowed to stir at 22 $^\circ\text{C}$ for 6 h. The mixture was passed through a short plug of silica gel (4 cm x 1 cm) and eluted with Et_2O . The organic layer was concentrated *in vacuo*, resulting in a yellow oily residue, which was purified by silica gel chromatography (50:1 hexanes/ Et_2O , R_f 0.53) to afford 17.1 mg of the desired product **2.21a** and $\text{S}_{\text{N}}2$ product (97:3 $\text{S}_{\text{N}}2'/\text{S}_{\text{N}}2$) as colorless oil (0.075 mmol, 75% yield).

Characterization Data for Enynes with a Tertiary Carbon Stereogenic Center

(*R*)-Trimethyl(4-phenylhex-5-en-1-yn-1-yl)silane (**2.21a**)

IR (neat): 3084 (w), 3030 (w), 2959 (w), 2901 (w), 2177 (w), 1638 (w), 1602 (w), 1494 (w), 1453 (w), 1412 (w), 1249 (m), 917 (w), 837 (s), 757 (s), 697 (s), 640 (m) cm^{-1} ; ^1H NMR (CDCl_3 , 400 MHz): δ 7.33–7.28 (2H, m), 7.24–7.20 (3H, m), 6.07 (1H, ddd, $J = 17.2, 10.0, 6.8$ Hz), 5.15–5.08 (2H, m), 3.52 (1H, app. q, $J = 7.2$ Hz), 2.67–2.55 (2H, m), 0.11 (9H, s); ^{13}C NMR (CDCl_3 , 100 MHz): δ 142.8, 140.1, 128.5, 127.9, 126.8, 115.5, 105.5, 86.7, 48.6, 26.9, 0.2. HRMS (ESI $^+$): Calcd for $\text{C}_{15}\text{H}_{20}\text{Si}$ $[\text{M}+\text{H}]^+$: 229.1413; Found: 229.1404. Specific rotation: $[\alpha]_{\text{D}}^{25.2} +0.83$ (c 1.33, CHCl_3) for an enantiomerically enriched sample of 97:3 er.

Enantiomeric purity was determined by GC analysis in comparison with authentic racemic material; CD-GTA column, 75 $^\circ\text{C}$, 15 psi.

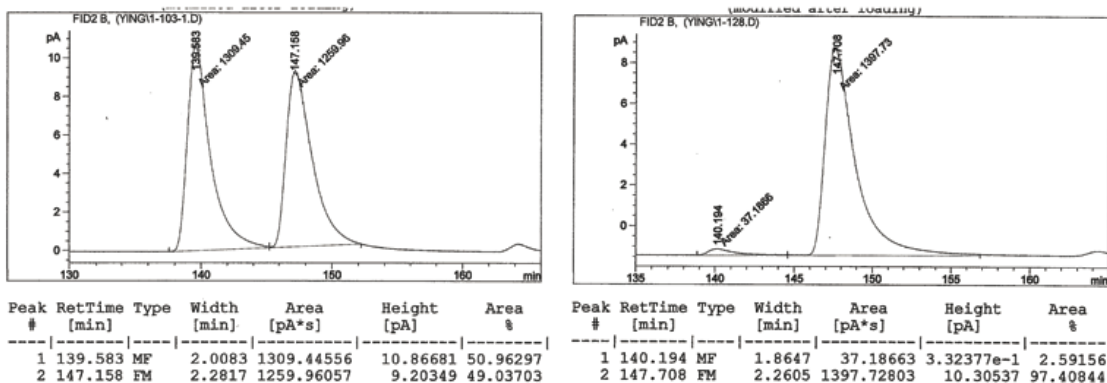


Retention Time	Area	Area%	Retention Time	Area	Area%
149.350	574.27655	54.873	146.718	100.99387	3.343
153.905	472.27371	45.127	151.791	2920.43774	96.657

(*R*)-(4-(2-Fluorophenyl)hex-5-en-1-yn-1-yl)trimethylsilane (**2.21b**)

IR (neat): 2959 (w), 2177 (w), 1490 (m), 1456 (w), 1249 (m), 1230 (m), 1036 (w), 993 (w), 920 (w), 838 (s), 752 (s), 698 (w), 667 (w), 642 (w), 554 (w) cm^{-1} ; **^1H NMR (CDCl_3 , 400 MHz):** δ 7.26-7.18 (2H, m), 7.09 (1H, td, $J = 7.6, 1.2$ Hz), 7.02 (1H, ddd, $J = 9.6, 7.6, 1.2$ Hz), 6.09 (1H, dddd, $J = 17.2, 10.4, 6.8, 1.2$ Hz), 5.16-5.09 (2H, m), 3.87 (1H, q, $J = 7.6$ Hz), 2.69-2.58 (2H, m), 0.09 (9H, s); **^{13}C NMR (CDCl_3 , 100 MHz):** δ 160.8 (d, $J_{\text{CF}} = 244.1$ Hz), 138.7, 129.3 (d, $J_{\text{CF}} = 5.3$ Hz), 128.3 (d, $J_{\text{CF}} = 8.4$ Hz), 124.1 (d, $J_{\text{CF}} = 3.1$ Hz), 116.0, 115.6 (d, $J_{\text{CF}} = 22.4$ Hz), 105.0, 86.7, 42.0, 25.7, 0.3, 0.1. **HRMS (ESI $^+$):** Calcd for $\text{C}_{15}\text{H}_{20}\text{FSi}$ [$\text{M}+\text{H}$] $^+$: 247.1317; Found: 247.1318. Specific rotation: $[\alpha]_{\text{D}}^{20.0} -1.01$ (c 2.26, CHCl_3) for an enantiomerically enriched sample of 97:3 er.

Enantiomeric purity was determined by GC analysis in comparison with authentic racemic material; CD-GTA column, 75 °C, 15 psi.

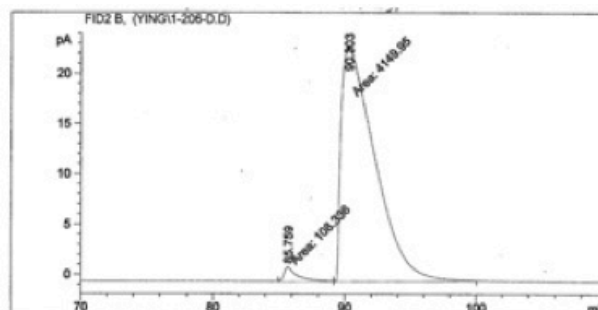
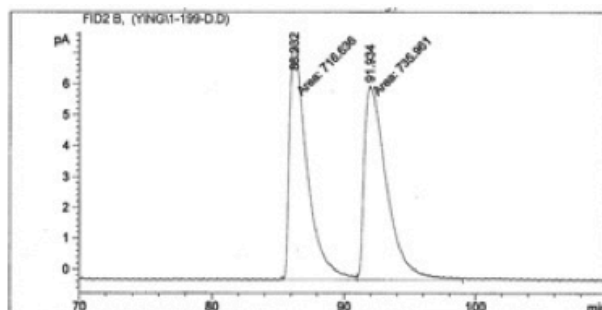


Retention Time	Area	Area%	Retention Time	Area	Area%
139.583	1309.44556	50.96297	140.194	37.18663	2.59156
147.708	1259.96057	49.03703	147.708	1397.72803	97.40844

(R)-(4-(2-Bromophenyl)hex-5-en-1-yn-1-yl)trimethylsilane (**2.21c**)

IR (neat): 3061 (w), 2959 (w), 2900 (w), 2175 (w), 1639 (m), 1468 (w), 1436 (w), 1382 (w), 1331 (w), 1248 (m), 1217 (w), 1143 (w), 1116 (w), 1041 (w), 1023 (m), 963 (w), 919 (w), 837 (s), 750 (s), 697 (m), 670 (w), 641 (m) cm^{-1} ; **$^1\text{H NMR}$ (CDCl_3 , 400 MHz):** δ 7.56–7.55 (1H, m), 7.29–7.25 (2H, m), 7.10–7.07 (1H, m), 6.06 (1H, ddd, $J = 17.2$, 10.4, 6.8 Hz), 5.20–5.13 (2H, m), 4.12 (1H, q, $J = 6.8$ Hz), 2.64 (2H, d, $J = 6.8$ Hz), 0.10 (9H, s); **$^{13}\text{C NMR}$ (CDCl_3 , 100 MHz):** δ 141.7, 138.6, 133.0, 129.1, 128.2, 127.5, 124.9, 116.2, 104.6, 87.0, 46.4, 25.6, 0.1. **HRMS (ESI^+):** Calcd for $\text{C}_{15}\text{H}_{20}\text{BrSi}$ $[\text{M}+\text{H}]^+$: 307.0518; Found: 307.0509. Specific rotation: $[\alpha]_{\text{D}}^{22.1} -25.2$ (c 2.51, CHCl_3) for an enantiomerically enriched sample of 97:3 er.

Enantiomeric purity was determined by GC analysis in comparison with authentic racemic material of terminal alkyne obtained after removal of the silyl group with K_2CO_3 in MeOH; CD-GTA column, 90 °C, 15 psi.



Peak #	RetTime [min]	Type	Width [min]	Area [pA*s]	Height [pA]	Area %
1	86.232	MF	1.5668	716.63605	7.62305	49.33481
2	91.934	FM	1.9527	735.96112	6.28153	50.66519

Peak #	RetTime [min]	Type	Width [min]	Area [pA*s]	Height [pA]	Area %
1	85.759	MF	1.2341	108.33573	1.46313	2.54412
2	90.303	FM	2.9400	4149.95020	23.52615	97.45588

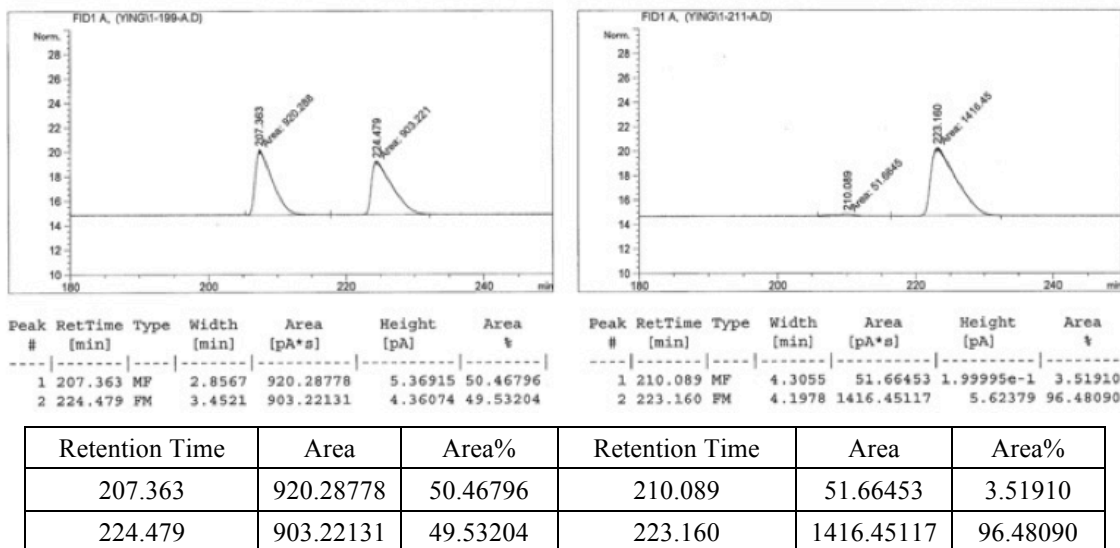
Retention Time	Area	Area%	Retention Time	Area	Area%
86.232	716.63605	49.33481	85.759	108.33573	2.54412
91.934	735.96112	50.66519	90.303	4149.95020	97.45588

(R)-(4-(2-Methoxyphenyl)hex-5-en-1-yn-1-yl)trimethylsilane (**2.21d**)

IR (neat): 3078 (w), 2958 (w), 2901 (w), 2836 (w), 2175 (w), 1638 (w), 1599 (w), 1586 (w), 1491 (m), 1463 (w), 1438 (w), 1289 (w), 1243 (s), 1185 (w), 1162 (w), 1109 (w), 1051 (w), 1031 (m), 994 (w), 915 (w), 837 (s), 786 (w), 749 (s), 697 (m), 671 (w), 643 (m) cm^{-1} ; **$^1\text{H NMR}$ (CDCl_3 , 400 MHz):** δ 7.26–7.16 (2H, m), 6.91 (1H, t, $J = 6.0$ Hz), 6.86 (1H, d, $J = 6.4$ Hz), 6.13 (1H, ddd, $J = 13.6$, 8.0, 5.6 Hz), 5.13–5.09 (2H, m), 3.96

(1H, q, $J = 5.6$ Hz), 3.83 (3H, s), 2.61 (2H, app. d, $J = 5.6$ Hz), 0.10 (9H, s); ^{13}C NMR (CDCl_3 , 100 MHz): δ 157.0, 139.5, 131.2, 128.6, 127.7, 120.6, 115.3, 101.7, 106.1, 86.1, 55.5, 42.0, 25.5, 0.3, 0.2. HRMS (ESI $^+$): Calcd for $\text{C}_{16}\text{H}_{23}\text{OSi}$ $[\text{M}+\text{H}]^+$: 259.1518; Found: 259.1521. Specific rotation: $[\alpha]_{\text{D}}^{21.9} -30.0$ (c 1.50, CHCl_3) for an enantiomerically enriched sample of 96:4 er.

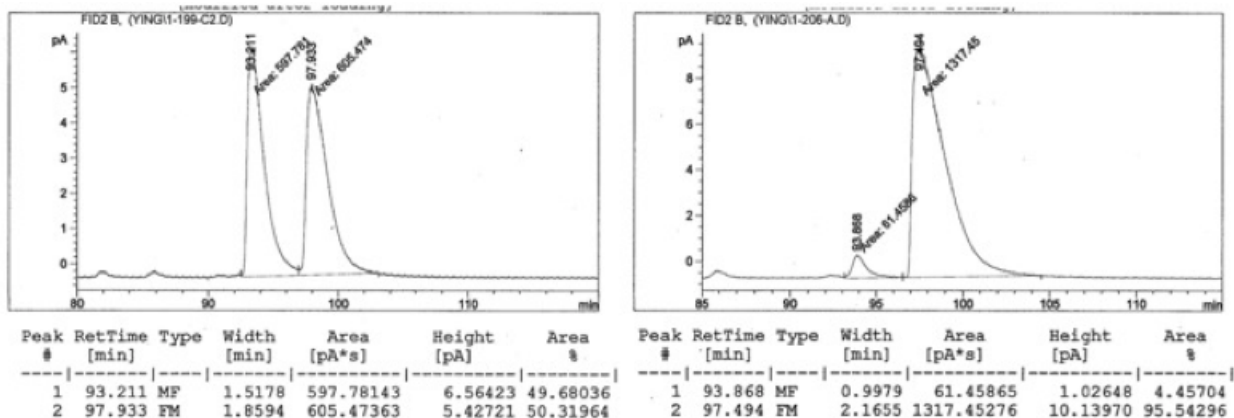
Enantiomeric purity was determined by GC analysis in comparison with authentic racemic material of terminal alkyne obtained after removal of the silyl group with K_2CO_3 in MeOH; CDB-DM column, 70 °C, 20 psi.



(R)-Trimethyl(4-(*o*-tolyl)hex-5-en-1-yn-1-yl)silane (2.21e)

IR (neat): 3020 (w), 2958 (w), 2176 (w), 1637 (w), 1603 (w), 1490 (w), 1461 (w), 1409 (w), 1380 (s), 1248 (m), 1037(w), 997 (w), 964 (w), 915 (w), 837 (s), 756 (s), 726 (m), 697 (w), 642 (m), 578 (w) cm^{-1} ; ^1H NMR (CDCl_3 , 400 MHz): δ 7.19–7.10 (4H, m), 6.03 (1H, ddd, $J = 17.2, 10.4, 6.8$ Hz), 5.12 (1H, app. dt, $J = 10.4, 1.2$ Hz), 5.09 (1H, app. dt, $J = 17.2, 1.6$ Hz), 3.83–3.77 (1H, m), 2.68–2.55 (2H, m), 2.37 (3H, s), 0.11 (9H, s); ^{13}C NMR (CDCl_3 , 100 MHz): δ 140.9, 139.9, 136.1, 130.5, 126.7, 126.5, 126.2, 115.3, 105.6, 86.3, 43.9, 26.1, 19.8, 0.2. HRMS (ESI $^+$): Calcd for $\text{C}_{16}\text{H}_{23}\text{Si}$ $[\text{M}+\text{H}]^+$: 243.1569; Found: 243.1577. Specific rotation: $[\alpha]_{\text{D}}^{23.0} -20.4$ (c 2.16, CHCl_3) for an enantiomerically enriched sample of 96:4 er.

Enantiomeric purity was determined by GC analysis in comparison with authentic racemic material of terminal alkyne obtained after removal of the silyl group with K_2CO_3 in MeOH; CD-GTA column, 65°C, 20 psi.

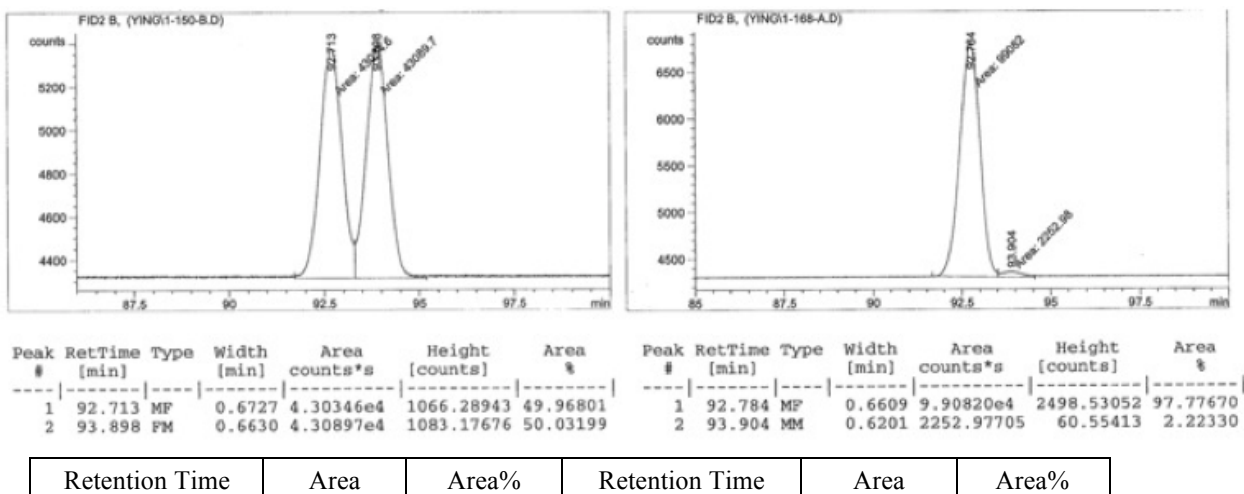


Retention Time	Area	Area%	Retention Time	Area	Area%
93.211	597.78143	49.68036	93.868	61.45865	4.45704
97.933	605.47363	50.31964	97.494	1317.45276	95.54296

(*R*)-4-(3-Bromophenyl)hex-5-en-1-yn-1-yl)trimethylsilane (**2.21f**)

IR (neat): 3082 (w), 2959 (w), 2900 (w), 2176 (w), 1639 (w), 1593 (w), 1567 (w), 1474 (w), 1425 (w), 1249 (m), 1073 (w), 1042 (w), 997 (w), 920 (w), 838 (s), 644 (m), 779 (m), 758 (m), 695 (m) 642 (m) cm^{-1} ; **^1H NMR (CDCl_3 , 400 MHz):** δ 7.40–7.39 (1H, m), 7.36 (1H, app. dt, $J = 5.6, 1.6$ Hz), 7.19–7.15 (2H, m), 6.03 (1H, ddd, $J = 17.2, 10.4, 7.2$ Hz), 5.16 (1H, app. dt, $J = 10.4, 1.2$ Hz), 5.12 (1H, app. dt, $J = 17.2, 1.2$ Hz), 3.49 (1H, q, $J = 7.2$ Hz), 2.62 (1H, dd, $J = 17.2, 7.2$ Hz), 2.55 (1H, dd, $J = 17.2, 7.2$ Hz), 0.11 (9H, s); **^{13}C NMR (CDCl_3 , 100 MHz):** δ 145.1, 139.3, 131.2, 130.0, 129.9, 126.6, 122.5, 115.7, 116.0, 104.7, 87.3, 48.1, 26.8, 0.1. HRMS (ESI^+): Calcd for $\text{C}_{15}\text{H}_{20}\text{BrSi}$ $[\text{M}+\text{H}]^+$: 307.0518; Found: 307.0513. Specific rotation: $[\alpha]_{\text{D}}^{22.0} +6.22$ (c 2.41, CHCl_3) for an enantiomerically enriched sample of 98:2 er.

Enantiomeric purity was determined by GC analysis in comparison with authentic racemic material; β -dex column, 140 $^\circ\text{C}$, 15 psi.

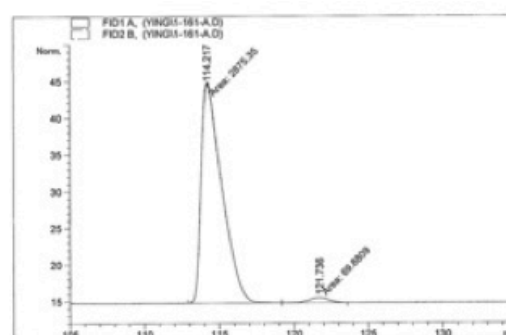
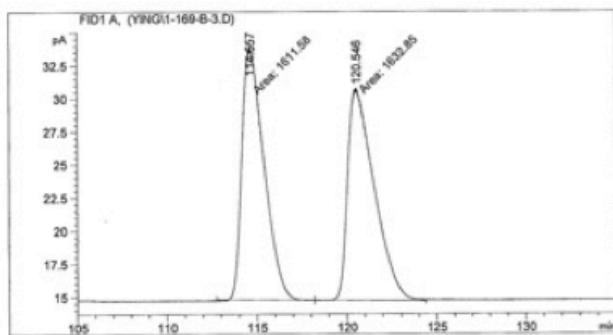


92.713	43034.6	49.96801	92.784	99082.0	97.77670
993.898	43089.7	50.03199	93.904	2252.97705	2.22330

(*R*)-Trimethyl(4-(*m*-tolyl)hex-5-en-1-yn-1-yl)silane (**2.21g**)

IR (neat): 2959 (w), 2901 (m), 2176 (w), 1638 (w), 1606 (w), 1589 (w), 1489 (w), 1413 (w), 1249 (m), 1094 (w), 1041 (w), 915 (w), 838 (s), 783 (m), 758 (s), 701 (m), 675 (w), 643 (w), 439 (w) cm^{-1} ; **$^1\text{H NMR}$ (CDCl_3 , 400 MHz):** δ 7.20 (1H, t, $J = 7.2$ Hz), 7.05–7.02 (3H, m), 6.07 (1H, ddd, $J = 17.2, 10.0, 7.2$ Hz), 5.14–5.09 (2H, m), 3.49 (1H, app. q, $J = 7.2$ Hz), 2.65–2.55 (2H, m), 2.34 (3H, s), 0.12 (9H, s); **$^{13}\text{C NMR}$ (CDCl_3 , 100 MHz):** δ 142.8, 140.1, 138.0, 128.6, 128.4, 127.5, 124.8, 115.3, 105.6, 86.6, 48.6, 26.9, 21.6, 0.2. **HRMS (ESI $^+$):** Calcd for $\text{C}_{16}\text{H}_{23}\text{Si}$ $[\text{M}+\text{H}]^+$: 243.1569; Found: 243.1578. Specific rotation: $[\alpha]_{\text{D}}^{21} +3.53$ (c 4.13, CHCl_3) for an enantiomerically enriched sample of 98:2 er.

Enantiomeric purity was determined by GC analysis in comparison with authentic racemic material; CDB-DM column, 95 °C, 20 psi.



Peak #	RetTime [min]	Type	Width [min]	Area [pA*s]	Height [pA]	Area %
1	114.657	MF	1.3937	1611.58154	19.27285	49.67230
2	120.546	FM	1.6962	1632.84521	16.04439	50.32770

Peak #	RetTime [min]	Type	Width [min]	Area [pA*s]	Height [pA]	Area %
1	114.217	MF	1.5883	2875.35107	30.17236	97.62732
2	121.736	FM	1.5972	69.88090	7.29215e-1	2.37268

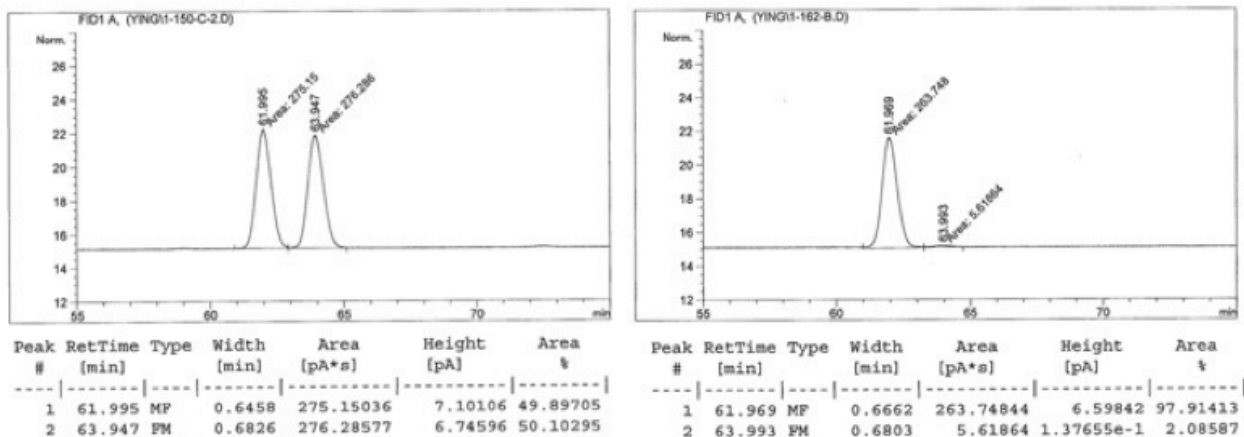
Retention Time	Area	Area%	Retention Time	Area	Area%
114.657	1611.58154	49.67230	114.217	2875.35107	97.627332
120.546	1632.84521	50.32770	121.736	69.88090	2.37268

(*R*)-Trimethyl(4-(3-(trifluoromethyl)phenyl)hex-5-en-1-yn-1-yl)silane (**2.21h**)

IR (neat): 2961 (w), 2177 (w), 1728 (w), 1640 (w), 1596 (w), 1491 (w), 1448 (w), 1326 (s), 1250 (m), 1163 (s), 1125 (s), 1096 (w), 1073 (s), 1043 (w), 1002 (w), 963 (w), 920 (w), 895 (w), 839 (s), 800 (s), 759 (s), 701 (s), 653 (w), 638 (w), 456 (w) cm^{-1} ; **$^1\text{H NMR}$ (CDCl_3 , 400 MHz):** δ 7.52–7.49 (2H, m), 7.45–7.42 (2H, m), 6.06 (1H, ddd, $J = 17.2, 10.4, 6.0$ Hz), 5.18 (1H, app. dt, $J = 10.4, 1.2$ Hz), 5.13 (1H, app. dt, $J = 17.2, 1.2$ Hz), 3.59 (1H, q, $J = 6.8$ Hz), 2.70–2.56 (2H, m), 0.9 (9H, s); **$^{13}\text{C NMR}$ (CDCl_3 , 100 MHz):** δ 143.6, 139.2, 131.4, 130.7 (q, $J_{\text{CF}} = 31.8$ Hz), 128.9, 124.9 (q, $J_{\text{CF}} = 3.8$ Hz), 124.7 (q, $J_{\text{CF}} = 3.8$ Hz), 124.4 (q, $J_{\text{CF}} = 270.9$ Hz), 116.2, 104.4, 87.5, 48.2, 26.8, 0.0. **HRMS**

(ESI⁺): Calcd for C₁₆H₂₀F₃Si [M+H]⁺: 297.1286; Found: 297.1296. Specific rotation: $[\alpha]_D^{22.5} +6.33$ (*c* 2.40, CHCl₃) for an enantiomerically enriched sample of 98:2 er.

Enantiomeric purity was determined by GC analysis in comparison with authentic racemic material; CDB-DM column, 100 °C, 15 psi.

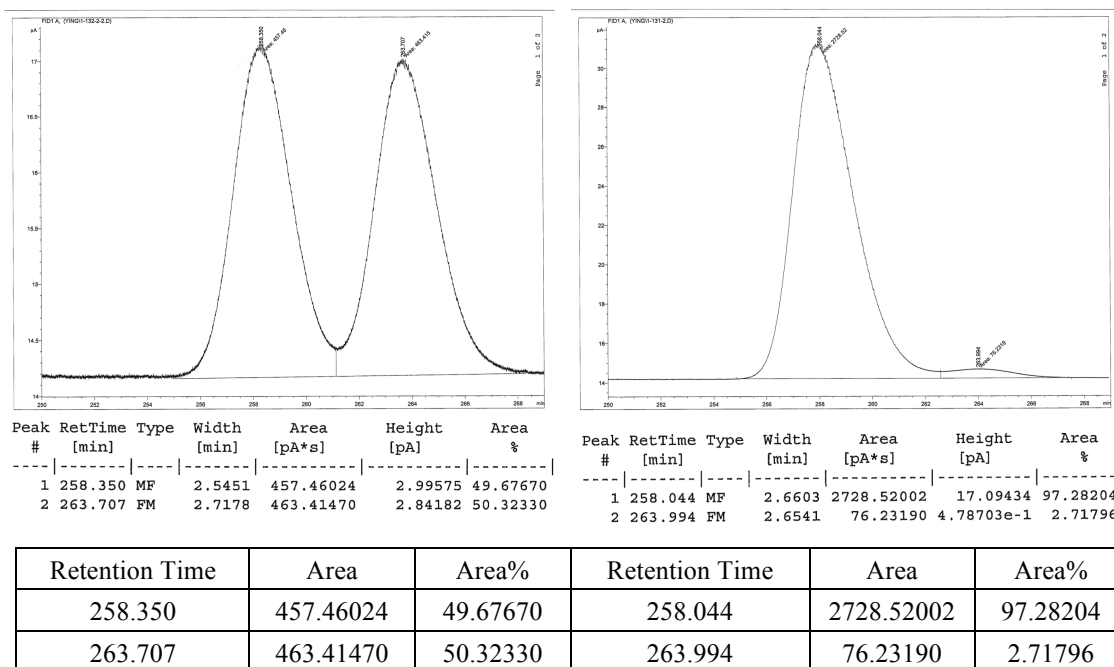


Retention Time	Area	Area%	Retention Time	Area	Area%
61.995	275.15036	49.89705	61.969	263.74844	97.91413
63.947	276.28577	50.10295	63.993	5.61864	2.08587

(*R*)-Trimethyl(4-(naphthalen-2-yl)hex-5-en-1-yn-1-yl)silane (**2.21i**)

IR (neat): 3056 (w), 2958 (w), 2900 (w), 2175 (w), 1634 (w), 1600 (w), 1508 (w), 1413 (w), 1368 (w), 1248 (m), 1042 (w), 1018 (w), 991 (w), 962 (w), 917 (w), 888 (w), 838 (s), 815 (s), 758 (s), 744 (s), 698 (w), 642 (m), 580 (s), 475 (w) cm⁻¹; **¹H NMR (CDCl₃, 400 MHz):** δ 7.83–7.79 (3H, m), 7.69 (1H, s), 7.49–7.43 (2H, m), 7.38 (1H, d, *J* = 8.8 Hz), 6.18 (1H, ddd, *J* = 17.2, 10.4, 7.2 Hz), 5.21–5.14 (2H, m), 3.71 (1H, q, *J* = 7.6 Hz), 2.78–2.66 (2H, m), 0.11 (9H, s); **¹³C NMR (CDCl₃, 100 MHz):** δ 140.3, 140.0, 133.3, 132.6, 128.1, 127.9, 127.7, 126.42, 126.37, 126.1, 125.6, 115.7, 105.4, 86.9, 48.6, 26.7, 0.2. **HRMS (ESI⁺):** Calcd for C₁₉H₂₃Si [M+H]⁺: 279.1569; Found: 279.1568. Specific rotation: $[\alpha]_D^{22.0} -1.78$ (*c* 6.76, CHCl₃) for an enantiomerically enriched sample of 97:3 er.

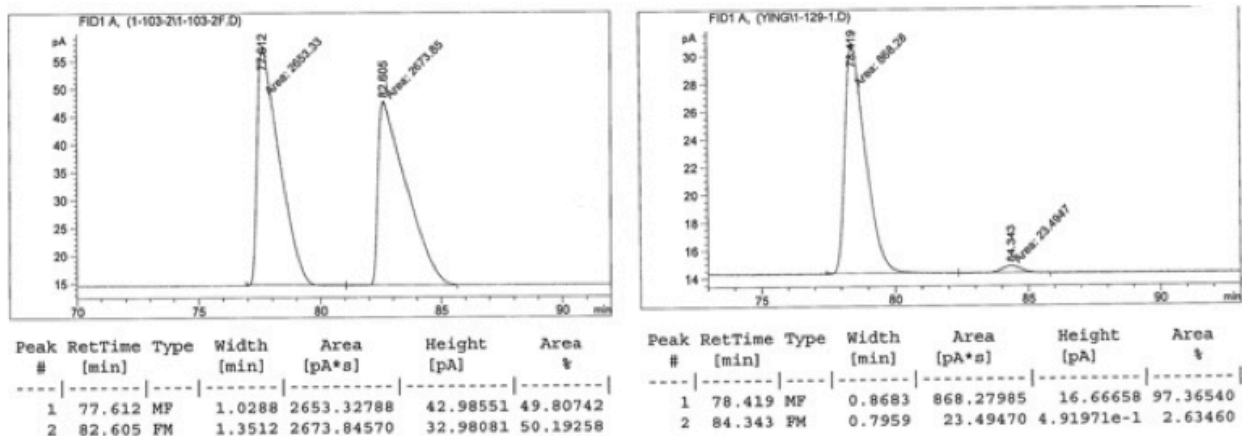
Enantiomeric purity was determined by GC analysis in comparison with authentic racemic material; CDB-DM column, 130 °C, 15 psi.



(R)-(4-(4-Chlorophenyl)hex-5-en-1-yn-1-yl)trimethylsilane (**2.21j**)

IR (neat): 2959 (w), 2176 (w), 1491 (w), 1407 (w), 1249 (m), 1092 (w), 1043 (w), 1015 (w), 919 (w), 838 (s), 780 (w), 758 (s), 722 (w), 698 (w), 637 (w), 578 (w), 540 (w) cm^{-1} ;
 ^1H NMR (CDCl_3 , 400 MHz): δ 7.28–7.24 (2H, m), 7.16–7.13 (2H, m), 6.01 (1H, ddd, $J = 17.2, 10.4, 6.8$ Hz), 5.13 (1H, app. d, $J = 10.4$ Hz), 5.07 (1H, app. d, $J = 17.2$ Hz), 3.48 (1H, q, $J = 7.2$ Hz), 2.60 (1H, dd, $J = 16.8, 7.2$ Hz), 2.53 (1H, dd, $J = 16.8, 7.2$ Hz), 2.47 (3H, s), 0.09 (9H, s);
 ^{13}C NMR (CDCl_3 , 100 MHz): δ 141.2, 139.6, 132.5, 129.3, 128.6, 115.8, 104.9, 87.1, 47.8, 26.8, 0.1. **HRMS (ESI $^+$):** Calcd for $\text{C}_{15}\text{H}_{20}\text{ClSi}$ $[\text{M}+\text{H}]^+$: 263.1023; Found: 263.1015. Specific rotation: $[\alpha]_{\text{D}}^{21.7} +8.1$ (c 7.04, CHCl_3) for an enantiomerically enriched sample of 97:3 er.

Enantiomeric purity was determined by GC analysis in comparison with authentic racemic material; CDB-DM column, 120 °C, 15 psi.

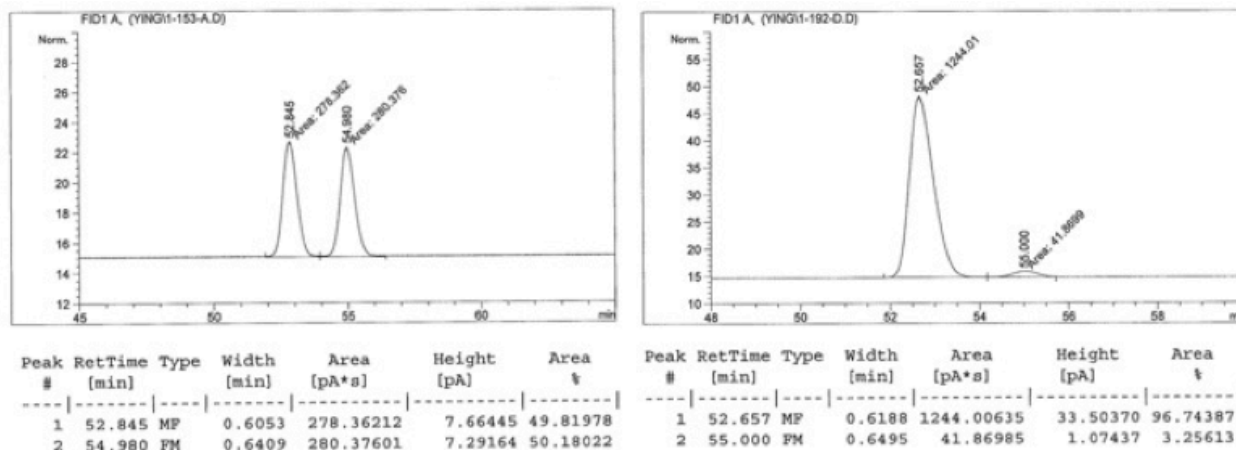


Retention Time	Area	Area%	Retention Time	Area	Area%
77.612	2653.32788	49.80742	78.419	868.27985	97.36540
82.605	2673.84570	50.19258	84.343	23.49470	2.63460

(R)-Trimethyl(4-(*p*-tolyl)hex-5-en-1-yn-1-yl)silane (**2.21k**)

IR (neat): 2959 (w), 2922 (w), 2176 (w), 1638 (w), 1513 (w), 1411 (w), 1248 (m), 1111 (w), 1042 (w), 1020 (w), 996 (w), 965 (w), 915 (w), 838 (s), 814 (s), 758 (s), 720 (w), 698 (w), 640 (m), 581 (w), 551 (w) cm^{-1} ; **^1H NMR (CDCl_3 , 400 MHz):** δ 7.12–7.11 (4H, m), 6.06 (1H, ddd, $J = 17.2, 10.4, 7.2$ Hz), 5.12 (1H, d, $J = 10.4$ Hz), 5.09 (1H, d, $J = 17.2$ Hz), 3.49 (1H, q, $J = 7.2$ Hz), 2.61 (1H, dd, $J = 16.8, 7.2$ Hz), 2.56 (1H, dd, $J = 16.8, 7.2$ Hz), 0.12 (9H, s); **^{13}C NMR (CDCl_3 , 100 MHz):** δ 140.2, 139.9, 136.3, 129.2, 127.7, 115.3, 105.6, 86.6, 48.2, 27.0, 21.2, 0.2. **HRMS (ESI $^+$):** Calcd for $\text{C}_{16}\text{H}_{23}\text{Si}$ $[\text{M}+\text{H}]^+$: 243.1569; Found: 243.1569. Specific rotation: $[\alpha]_{\text{D}}^{21.5} +1.6$ (c 6.33, CHCl_3) for an enantiomerically enriched sample of 97:3 er.

Enantiomeric purity was determined by GC analysis in comparison with authentic racemic material; CDB-DM column, 110 $^\circ\text{C}$, 20 psi.



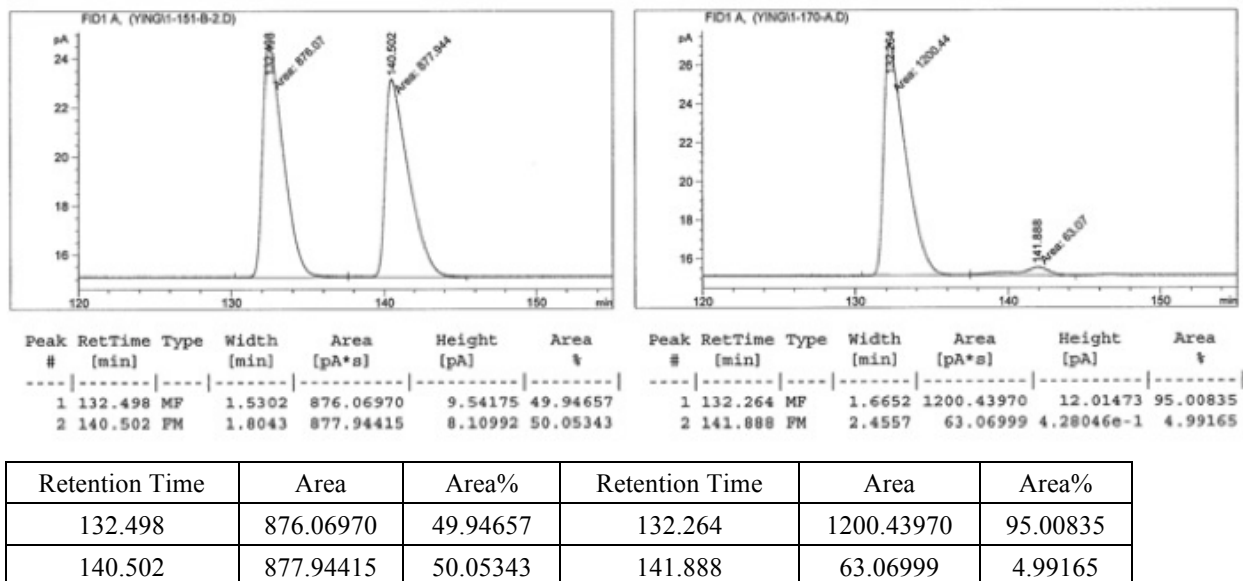
Retention Time	Area	Area%	Retention Time	Area	Area%
52.845	278.36212	49.81978	52.657	1244.00635	96.74387
54.980	280.37601	50.18022	55.000	41.86985	3.25613

(R)-Trimethyl(4-(4-nitrophenyl)hex-5-en-1-yn-1-yl)silane (**2.21l**)

IR (neat): 3081 (w), 2959 (w), 2901 (w), 2176 (w), 1928 (w), 1639 (w), 1598 (s), 1519 (s), 1411 (w), 1343 (s), 913 (m), 1249 (m), 1182 (w), 1041 (w), 1015 (w), 922 (w), 838 (s), 758 (m), 700 (m), 642 (m) 576 (w), 531 (w) cm^{-1} ; **^1H NMR (CDCl_3 , 500 MHz):** δ 8.17 (2H, app. d, $J = 9.0$ Hz), 7.41 (2H, app. d, $J = 9.0$ Hz), 6.04 (1H, ddd, $J = 17.0, 10.0, 6.5$ Hz), 5.21 (1H, app. d, $J = 10.0$ Hz), 5.13 (1H, app. d, $J = 17.0$ Hz), 4.76 (1H, q, $J = 7.0$ Hz), 2.68 (1H, dd, $J = 16.5, 6.5$ Hz), 2.60 (1H, dd, $J = 16.5, 6.5$ Hz), 0.08 (9H, s); **^{13}C NMR (CDCl_3 , 100 MHz):** δ 150.2, 147.0, 138.6, 128.9, 126.7, 123.7, 116.8, 103.9, 87.8,

48.2, 26.5, 0.2. **HRMS (ESI⁺)**: Calcd for C₁₅H₂₀NO₂Si [M+H]⁺: 274.1263; Found: 274.1267. Specific rotation: [α]_D^{23.2} +13.0 (*c* 3.70, CHCl₃) for an enantiomerically enriched sample of 95:5 er.

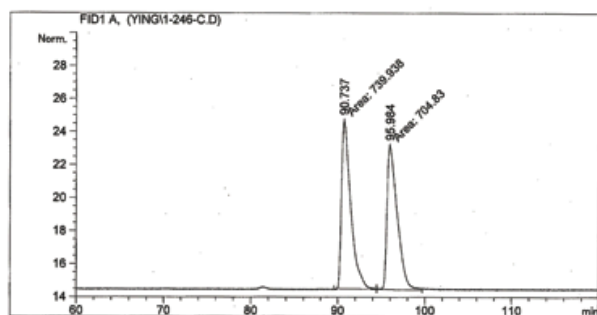
Enantiomeric purity was determined by GC analysis in comparison with authentic racemic material; CDB-DM column, 140 °C, 15 psi.



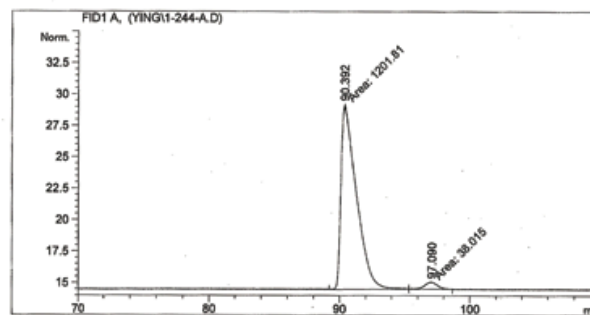
(*R*)-Trimethyl(4-(thiophen-3-yl)hex-5-en-1-yn-1-yl)silane (**2.21m**)

IR (neat): 3081 (w), 2959 (w), 2901 (w), 2176 (w), 1639 (w), 1530 (w), 1411 (w), 1329 (w), 1249 (m), 1153 (w), 1082 (w), 1042 (w), 1016 (w), 963 (w), 918 (w), 837 (s), 779 (s), 758 (s), 698 (w), 639 (m), 536 (w), 469 (w) cm⁻¹; **¹H NMR (CDCl₃, 400 MHz)**: δ 7.26 (1H, dd, *J* = 4.8, 1.2 Hz), 7.06–7.04 (1H, m), 7.00 (1H, dd, *J* = 4.8, 1.2 Hz), 6.02 (1H, ddd, *J* = 17.6, 10.0, 7.2 Hz), 5.14–5.08 (2H, m), 3.63 (1H, q, *J* = 7.2 Hz), 2.62 (1H, dd, *J* = 17.2, 6.8 Hz), 2.57 (1H, dd, *J* = 17.2, 7.2 Hz), 0.13 (9H, s); **¹³C NMR (CDCl₃, 100 MHz)**: δ 143.4, 139.7, 127.4, 125.4, 120.7, 115.6, 105.3, 86.8, 44.2, 26.8, 0.2. **HRMS (ESI⁺)**: Calcd for C₁₃H₁₉SSi [M+H]⁺: 235.0977; Found: 235.0982. Specific rotation: [α]_D^{23.7} -27.1 (*c* 1.75, CHCl₃) for an enantiomerically enriched sample of 97:3 er.

Enantiomeric purity was determined by GC analysis in comparison with authentic racemic material; CDB-DM column, 100 °C, 15 psi.



Peak #	RetTime [min]	Type	Width [min]	Area [pA*s]	Height [pA]	Area %
1	90.737	MF	1.1945	739.93762	10.32426	51.21501
2	95.984	FM	1.3311	704.82959	8.82507	48.78499



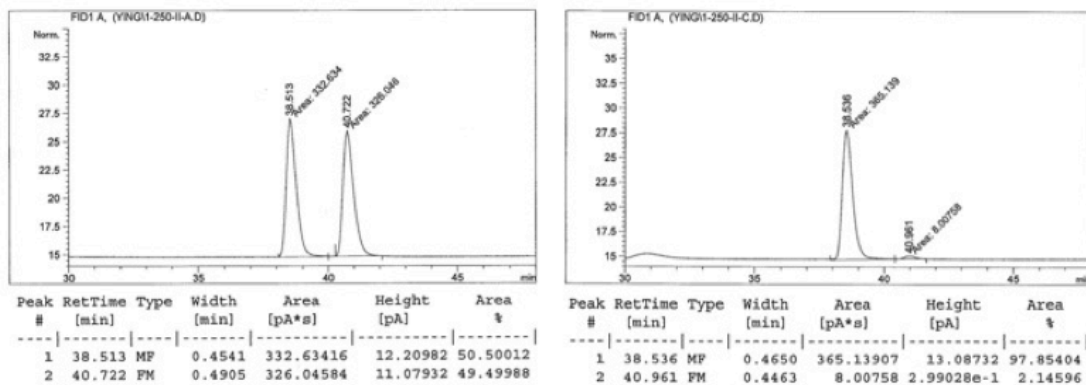
Peak #	RetTime [min]	Type	Width [min]	Area [pA*s]	Height [pA]	Area %
1	90.392	MF	1.3581	1201.81348	14.74862	96.93385
2	97.090	FM	1.1225	38.01496	5.64460e-1	3.06615

Retention Time	Area	Area%	Retention Time	Area	Area%
90.737	739.93762	51.21501	90.392	1201.81348	96.93385
95.984	704.82959	48.78499	97.090	38.01496	3.06615

(R)-3-(6-(Trimethylsilyl)hex-1-en-5-yn-3-yl)pyridine (**2.21a**)

IR (neat): 2976 (w), 2176 (w), 1577 (w), 1518 (w), 1474 (m), 1456 (m), 1428 (w), 1371 (w), 1335 (w), 1249 (m), 1218 (w), 1148 (m), 1105 (w), 1043 (w), 1029 (w), 1008 (w), 984 (w), 951 (w), 923 (w), 839 (s), 759 (m), 713 (m), 699 (m), 676 (m), 642 (w), 578 (w), 519 (w), 495 (w) cm^{-1} ; **^1H NMR (CDCl_3 , 400 MHz):** δ 8.49–8.47 (2H, m), 7.55 (1H, dt, $J = 8.0, 2.0$ Hz), 7.26–7.22 (1H, m), 6.05 (1H, ddd, $J = 17.2, 10.0, 6.4$ Hz), 5.18 (1H, dt, $J = 10.4, 1.2$ Hz), 5.11 (1H, dt, $J = 17.2, 1.2$ Hz), 3.55 (1H, q, $J = 6.8$ Hz), 2.66 (1H, dd, $J = 16.8, 6.8$ Hz), 2.58 (1H, dd, $J = 16.8, 7.6$ Hz), 0.08 (9H, s); **^{13}C NMR (CDCl_3 , 100 MHz):** δ 149.7, 148.2, 138.9, 138.0, 135.3, 123.3, 116.3, 104.3, 87.6, 45.9, 26.6, 0.1; **HRMS (ESI^+):** Calcd for $\text{C}_{14}\text{H}_{20}\text{NSi}$ $[\text{M}+\text{H}]^+$: 230.1365; Found: 230.1374; specific rotation: $[\alpha]_{\text{D}}^{23.8} +13.9$ (c 2.31, CHCl_3) for an enantiomerically enriched sample of 98:2 er.

Enantiomeric purity was determined by GC analysis in comparison with authentic racemic material; CDB-DM column, 120 °C, 20 psi.

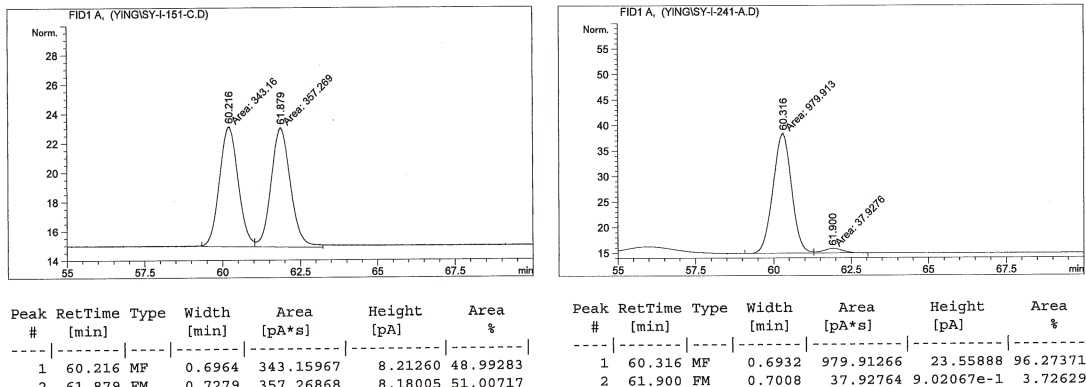


Retention Time	Area	Area%	Retention Time	Area	Area%
38.513	332.63416	50.50012	38.536	365.13907	97.85404
40.722	326.04584	49.49988	40.961	8.00758	2.14596

(R)-4-(6-(Trimethylsilyl)hex-1-en-5-yn-3-yl)phenyl acetate (**2.21o**)

IR (neat): 2959 (w), 2924 (w), 2175 (w), 1763 (m), 1506 (m), 1369 (w), 1249 (m), 1195 (s), 1166 (m), 1042 (w), 1017 (m), 910 (m), 838 (s), 759 (m), 697 (w), 683 (w), 643 (w) cm^{-1} ; **$^1\text{H NMR}$ (CDCl_3 , 500 MHz):** δ 7.23 (2H, d, $J = 8.4$ Hz), 7.02 (2H, d, $J = 8.4$ Hz), 6.04 (1H, ddd, $J = 17.2, 10.0, 7.2$ Hz), 5.14–5.08 (2H, m), 3.52 (1H, q, $J = 7.2$ Hz), 2.62 (1H, dd, $J = 16.8, 7.2$ Hz), 2.56 (1H, dd, $J = 16.8, 7.2$ Hz), 0.11 (9H, s); **$^{13}\text{C NMR}$ (CDCl_3 , 100 MHz):** δ 169.7, 149.4, 140.3, 139.8, 128.9, 121.5, 115.6, 105.2, 87.0, 47.9, 26.9, 21.3, 0.2. **HRMS (ESI $^+$):** Calcd for $\text{C}_{17}\text{H}_{23}\text{O}_2\text{Si}$ $[\text{M}+\text{H}]^+$: 287.1467; Found: 287.1459. Specific rotation: $[\alpha]_{\text{D}}^{20.0} = 8.9$ (c 2.24, CHCl_3) for an enantiomerically enriched sample of 95:5 er.

Enantiomeric purity was determined by GC analysis in comparison with authentic racemic material; CDB-DM column, 140 °C, 20 psi.

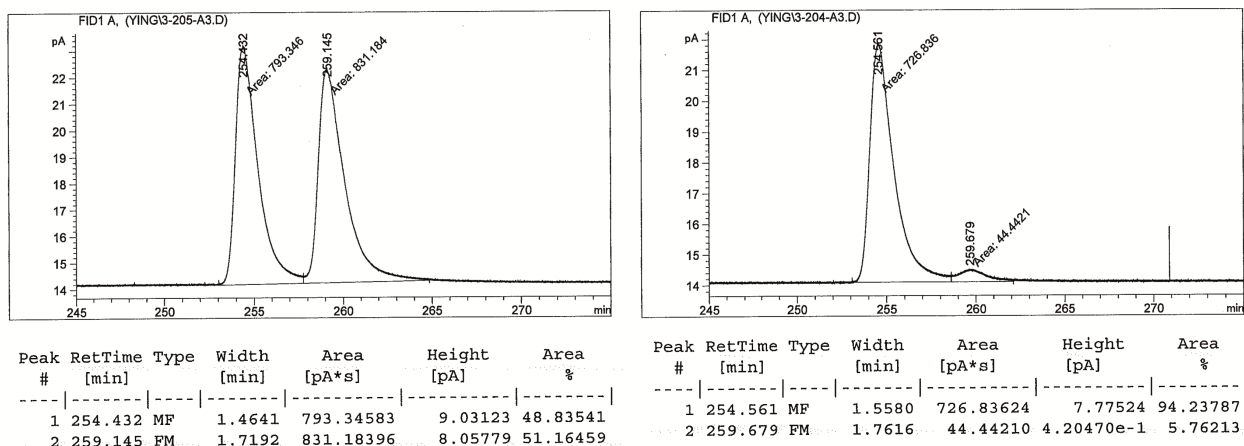


Retention Time	Area	Area%	Retention Time	Area	Area%
60.216	343.15967	48.992	60.316	979.913	96.273
61.879	357.26868	51.007	61.900	37.928	3.726

Methyl (*R*)-4-(6-(trimethylsilyl)hex-1-en-5-yn-3-yl)benzoate (**2.21p**)

IR (neat): 2955 (w), 2901 (w), 2176 (w), 1722 (s), 1639 (w), 1435 (m), 1275 (s), 1248 (s), 1180 (m), 1106 (m), 837 (s), 758 (s), 708 (m), 640 (m) cm^{-1} ; **^1H NMR (CDCl_3 , 600 MHz):** δ 7.98 (2H, d, $J = 8.4$ Hz), 7.30 (1H, d, $J = 8.4$ Hz), 6.05 (1H, ddd, $J = 15.0, 9.0, 6.6$ Hz) 5.17–5.09 (2H, m), 3.91 (3H, s), 3.58 (1H, q, $J = 7.2$ Hz), 2.67–2.57 (2H, m), 0.09 (9H, s); **^{13}C NMR (CDCl_3 , 100 MHz):** δ 167.2, 148.0, 139.3, 129.8, 128.7, 128.0, 116.1, 104.7, 87.2, 52.2, 48.5, 26.6, 0.1. **HRMS (ESI^+):** Calcd for $\text{C}_{17}\text{H}_{23}\text{O}_2\text{Si}$ $[\text{M}+\text{H}]^+$: 287.1467; Found: 287.1453. Specific rotation: $[\alpha]_{\text{D}}^{20.0}$ 3.9 (c 1.13, CHCl_3) for an enantiomerically enriched sample of 94:6 er.

Enantiomeric purity was determined by GC analysis in comparison with authentic racemic material; CDB-DM column, 120 °C, 200 min, 120 °C to 140 °C for 1 °C/min, 140 °C, 15 psi.

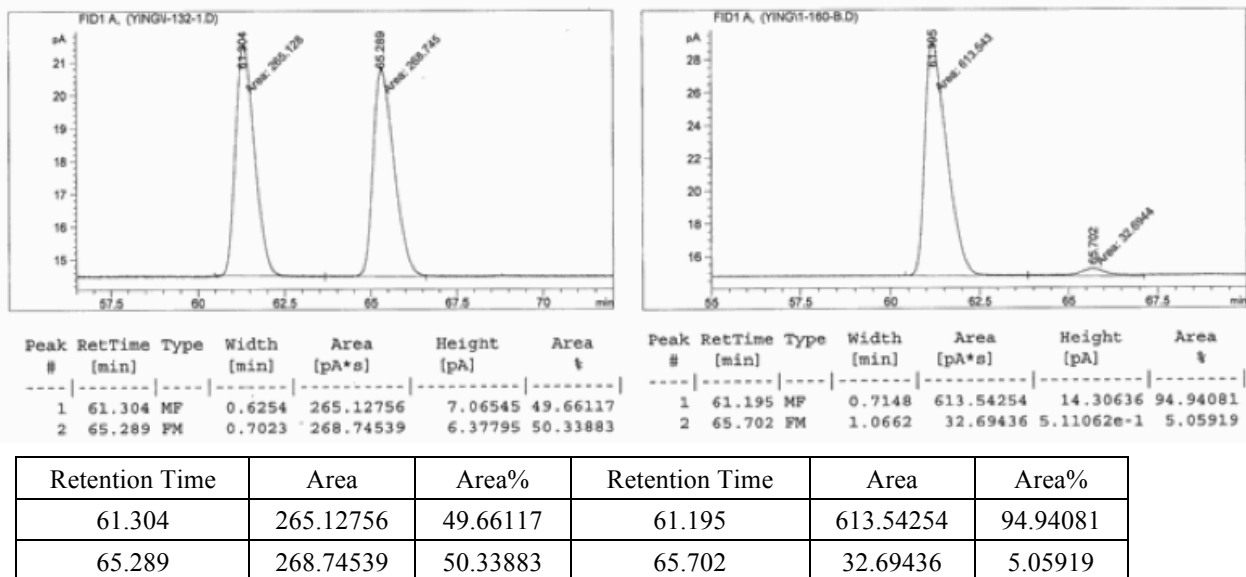


Retention Time	Area	Area%	Retention Time	Area	Area%
254.432	793.34583	48.83541	254.561	726.83624	94.23787
259.145	831.18396	51.16459	259.679	44.44210	5.76213

(R)-(4-Cyclohexylhex-5-en-1-yn-1-yl)trimethylsilane (**2.32**)

IR (neat): 3076 (w), 2922 (m), 2852 (m), 2175 (m), 1639 (w), 1449 (w), 1248 (s), 1042 (w), 999 (w), 965 (w), 913 (m), 885 (w), 837 (s), 758 (s), 697 (m), 644 (m), 579 (w), 487 (w), 433 (w) cm^{-1} ; **^1H NMR (CDCl_3 , 400 MHz):** δ 5.68 (1H, dt, $J = 17.2, 5.6$ Hz), 5.03 (1H, app. d, $J = 10.8$ Hz), 4.99 (1H, app. d, $J = 17.6$ Hz), 2.33 (1H, dd, $J = 16.8, 6.0$ Hz), 2.27 (1H, dd, $J = 16.8, 6.8$ Hz), 2.04–1.97 (1H, m), 1.74–1.63 (5H, m), 1.47–1.38 (1H, m), 1.29–1.05 (3H, m), 1.03–0.84 (2H, m), 0.14 (9H, s); **^{13}C NMR (CDCl_3 , 100 MHz):** δ 139.9, 115.7, 106.3, 85.9, 48.8, 40.2, 31.1, 29.7, 26.7, 26.6, 23.2, 0.3. **HRMS (ESI^+):** Calcd for $\text{C}_{12}\text{H}_{13}$ $[\text{M}+\text{H}]^+$: 235.1882; Found: 235.1882. Specific rotation: $[\alpha]_{\text{D}}^{23.8}$ +6.4 (c 1.86, CHCl_3) for an enantiomerically enriched sample of 95:5 er.

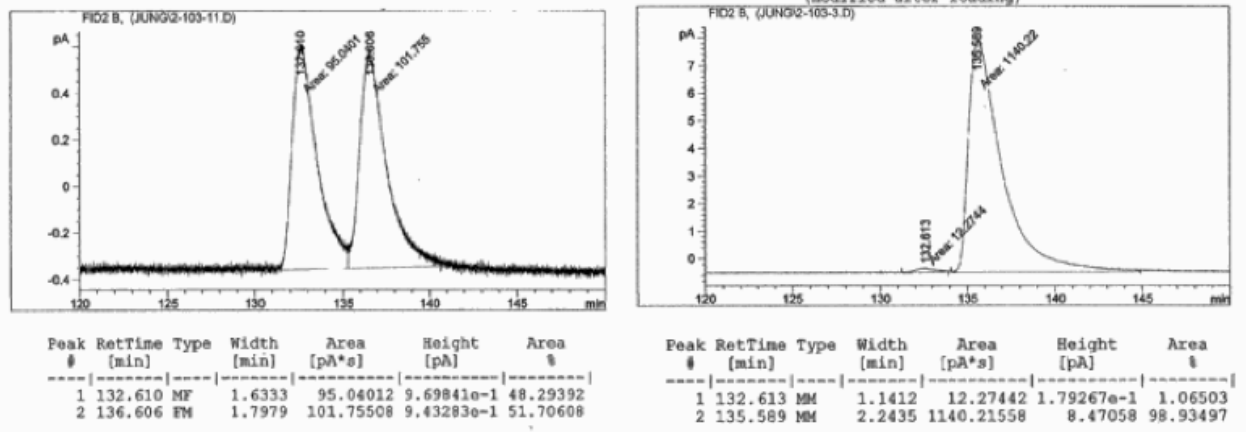
Enantiomeric purity was determined by GC analysis in comparison with authentic racemic material; CDB-DM column, 100 °C, 15 psi.



(*R*)-4-(2,2-Dimethyl-[1,3]dioxin-5-yl)-1-trimethylsilyl-hex-5-en-1-yne (**2.33**)

IR (neat): 3078 (w), 2991 (m), 2959 (m), 2866 (m), 2174 (m), 1640 (w), 1454 (w), 1420 (w), 1369 (m), 1331 (w), 1248 (s), 1196 (s), 1133 (m), 1067 (m), 1034 (m), 996 (m), 966 (m), 918 (m), 834 (s), 758 (s), 731 (m), 698 (m), 639 (m), 519 (m) cm^{-1} ; **$^1\text{H NMR}$ (CDCl_3 , 400 MHz):** δ 5.69 (1H, ddd, $J = 18.2, 9.0, 8.8$ Hz), 5.09 (1H, dd, $J = 9.0, 1.6$ Hz), 5.07 (1H, dd, $J = 18.2, 1.6$ Hz), 3.93 (1H, ddd, $J = 11.4, 4.6, 1.6$ Hz), 3.83 (1H, ddd, $J = 11.4, 4.6, 1.6$ Hz), 3.68 (1H, dd, $J = 26, 8.8$ Hz), 3.65 (1H, dd, $J = 26, 8.8$ Hz), 2.31 (1H, d, $J = 1.2$ Hz), 2.30 (1H, d, $J = 1.2$ Hz), 2.21–2.13 (1H, m), 1.92–1.89 (1H, m), 1.39 (6H, s), 0.13 (9H, s); **$^{13}\text{C NMR}$ (CDCl_3 , 100 MHz):** δ 138.2, 116.9, 104.1, 97.8, 87.0, 63.03, 63.00, 42.3, 35.9, 26.8, 23.2, 21.2, 0.2. **HRMS (ESI^+):** Calcd for $\text{C}_{15}\text{H}_{27}\text{O}_2\text{Si}_1$ [$\text{M}+\text{H}$] $^+$: 267.1780; Found: 267.1772. Specific rotation: $[\alpha]_{\text{D}}^{21.0} -27.3$ (c 2.92, CHCl_3) for an enantiomerically enriched sample of 99:1 er.

Enantiomeric purity was determined by GC analysis in comparison with authentic racemic material; CD-GTA column, 90 °C, 15 psi.

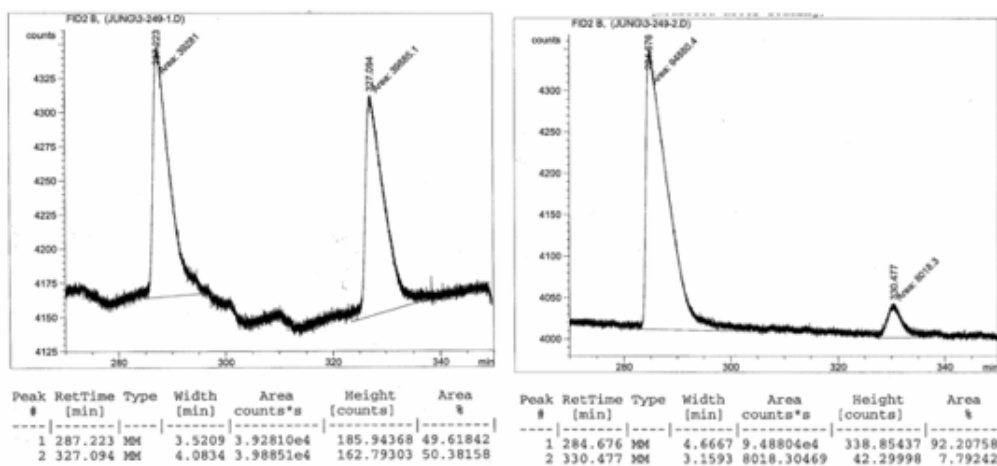


Retention Time	Area	Area%	Retention Time	Area	Area%
132.610	95.04	48.293	132.613	12.27	1.065
136.606	101.75	51.707	135.589	1140.2	98.935

(R)-4-(*tert*-Butyldimethylsilyloxymethyl)-1-trimethylsilyl-hex-5-en-1-yne (**2.34**)

IR (neat): 2956 (m), 2929 (m), 2899 (w), 2857 (m), 2175 (m), 1642 (w), 1471 (w), 1421 (w), 1387 (w), 1361 (w), 1336 (w), 1249 (s), 1102 (s), 1064 (w), 1031 (m), 1004 (w), 917 (w), 833 (s), 774 (s), 758 (s), 696 (m), 665 (m), 642 (m), 571 (w) cm^{-1} ; **^1H NMR (CDCl_3 , 400 MHz):** δ 5.82–5.74 (1H, m), 5.11 (1H, overlapped with other H), 5.07 (1H, overlapped with other H), 3.64–3.62 (2H, m), 2.42–2.32 (3H, m), 0.89 (9H, s), 0.14 (9H, s), 0.05 (6H, s); **^{13}C NMR (CDCl_3 , 100 MHz):** δ 138.3, 116.1, 105.5, 85.9, 64.8, 45.0, 26.0, 21.8, 18.4, 0.2, –5.2. **HRMS (ESI^+):** Calcd for $\text{C}_{16}\text{H}_{33}\text{O}_1\text{Si}_2$ $[\text{M}+\text{H}]^+$: 297.2069; Found: 297.2055. Specific rotation: $[\alpha]_{\text{D}}^{22.0} +3.17$ (c 3.15, CHCl_3) for an enantiomerically enriched sample of 92:8 er.

Enantiomeric purity was determined by GC analysis in comparison with authentic racemic material of primary alcohol obtained after removal of the silyl group; β -dex column, 50 °C, 15 psi).



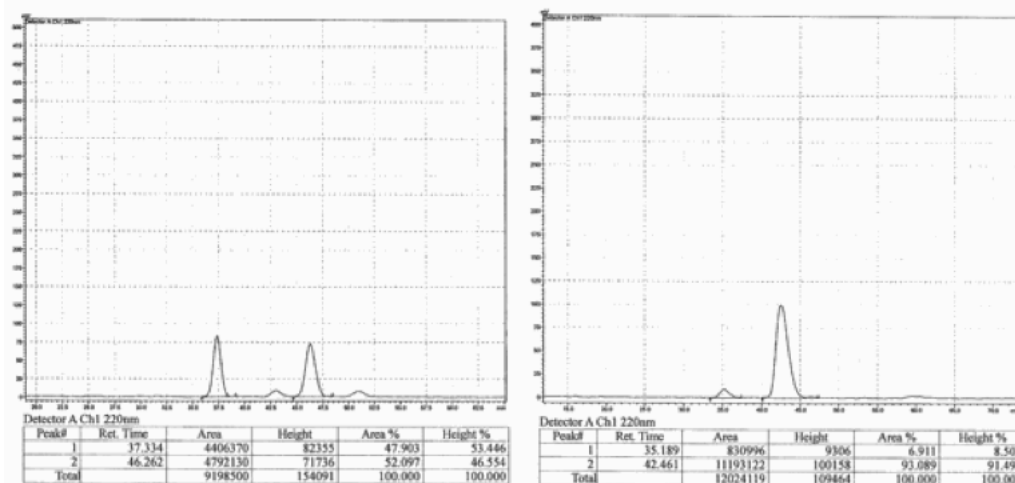
Retention Time	Area	Area%	Retention Time	Area	Area%
287.223	39281.0	49.618	284.676	94880.4	92.207
327.094	39885.1	50.382	330.477	8018.30469	7.793

(R)-(4-(Simethyl(phenyl)silyl)hex-5-en-1-yn-1-yl)trimethylsilane (**2.35**)

IR (neat): 3070 (w), 2958 (w), 2899 (w), 2173 (w), 1626 (w), 1487 (w), 1427 (w), 1411 (w), 1317 (w), 1248 (m), 1112 (m), 1040 (w), 998 (w), 942 (w), 899 (w), 836 (s), 813 (s), 778 (m), 758 (s), 723 (s), 697 (s), 642 (m), 548 (w), 469 (m) cm^{-1} ; **^1H NMR (CDCl_3 , 500 MHz):** δ 7.53–7.50 (2H, m), 7.37–7.34 (3H, m), 5.76 (1H, ddd, $J = 17.0, 10.5, 9.0$ Hz), 4.96 (1H, app. d, $J = 10.5$ Hz), 4.88 (1H, app. d, $J = 17.5$ Hz), 2.38 (1H, dd, $J = 17.0, 5.5$

Hz), 2.30 (1H, dd, $J = 17.5, 8.0$ Hz), 1.99–1.95 (1H, m), 0.35 (3H, s), 0.34 (3H, s), 0.13 (9H, s); ^{13}C NMR (CDCl_3 , 100 MHz): δ 138.2, 137.2, 134.2, 129.3, 127.9, 113.2, 107.2, 85.6, 33.5, 0.3, -4.1, -4.4. HRMS (ESI^+): Calcd for $\text{C}_{17}\text{H}_{27}\text{Si}_2$ $[\text{M}+\text{H}]^+$: 287.1651; Found: 287.1654. Specific rotation: $[\alpha]_{\text{D}}^{22.1} +18.3$ (c 2.49, CHCl_3) for an enantiomerically enriched sample of 93:7 er.

Enantiomeric purity was determined by GC analysis in comparison with authentic racemic material; column, 99:1 hexanes/ *i*PrOH, 1.0 mL/min, 220 nm.

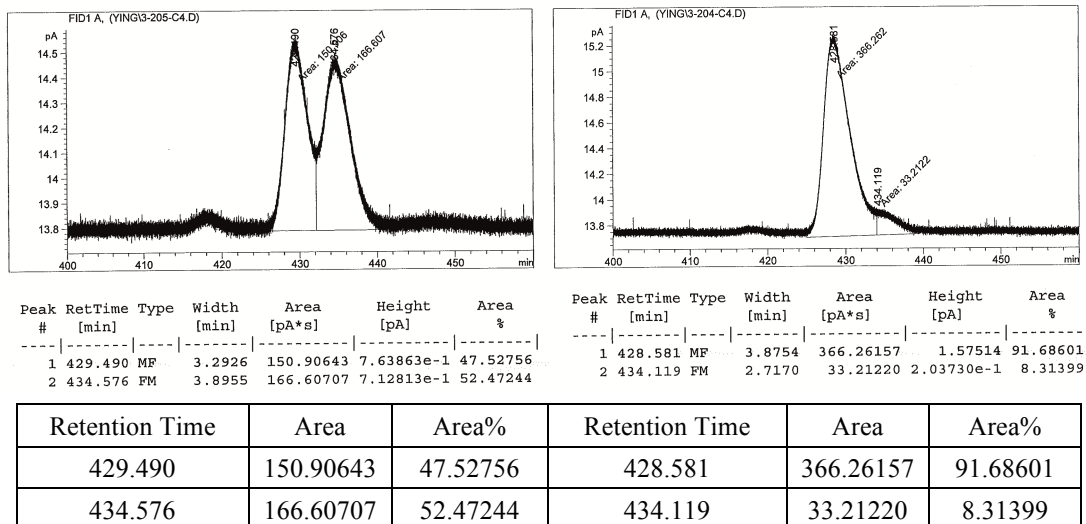


Retention Time	Area	Area%	Retention Time	Area	Area%
37.334	4406370	49.618	35.189	830996	6.911
46.262	4792130	50.382	42.463	11193122	93.089

(*R*)-9-(Trimethylsilyl)-6-vinylnon-8-yn-2-one (2.36)

IR (neat): 3025 (m), 2956 (s), 2927 (s), 2854 (s), 1603 (w), 1538 (w), 1496 (m), 1437 (s), 1267 (s), 1258 (s), 1134 (s), 1080 (w), 1031 (s), 975 (s), 880 (s), 811 (s), 766 (s), 736 (s), 698 (s) cm^{-1} ; ^1H NMR (CDCl_3 , 400 MHz): δ 5.69–5.60 (1H, m), 5.07–5.02 (2H, m), 2.44–2.40 (2H, m), 2.27–2.25 (2H, m), 2.23–2.19 (1H, m), 2.13 (3H, s), 1.66–1.48 (2H, m), 1.37–1.26 (2H, m), 0.14 (9H, s); ^{13}C NMR (CDCl_3 , 100 MHz): δ 209.0, 140.9, 115.5, 105.5, 86.2, 43.8, 42.8, 33.1, 30.0, 25.9, 21.5, 0.3. HRMS (ESI^+): Calcd for $\text{C}_{14}\text{H}_{25}\text{OSi}$ $[\text{M}+\text{H}]^+$: 237.1675; Found: 237.1673. Specific rotation: $[\alpha]_{\text{D}}^{20.0} 8.8$ (c 0.97, CHCl_3) for an enantiomerically enriched sample of 92:8 er.

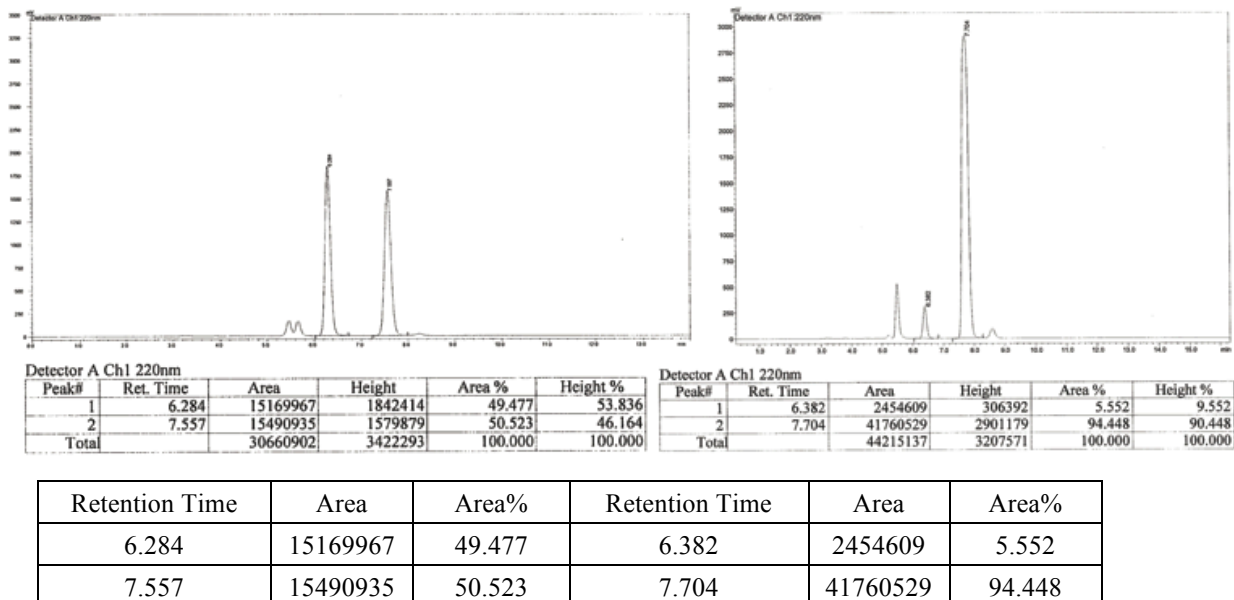
Enantiomeric purity was determined by GC analysis in comparison with authentic racemic material; CDB-DM column, 60°C, 90 min, 60 °C to 70 °C for 1°C/min, 70 °C, 90 min, 70 °C to 80 °C for 1°C/min, 15 psi.



(R)-trimethyl(4-(naphthalen-1-yl)hex-5-en-1-yn-1-yl)silane (**2.21q**)

IR (neat): 3049 (w), 2959 (w), 2924 (w), 2854 (w), 2175 (w), 1637 (w), 1598 (w), 1510 (w), 1396 (w), 1249 (m), 1166 (w), 1094 (w), 1022 (m), 917 (w), 840 (s), 796 (s), 776 (s), 759 (s), 731 (w), 698 (w), 650 (w), 637 (w), 551 (w), 509 (w), 477 (w), 441 (w), 423 (w) cm^{-1} ; **^1H NMR (CDCl_3 , 500 MHz):** δ 8.13 (1H, d, $J = 8.5$ Hz), 7.87 (1H, d, $J = 8.5$ Hz), 7.73 (1H, d, $J = 7.0$ Hz), 7.54–7.51(1H, m), 7.50–7.47 (1H, m), 7.47 (1H, d, $J = 7.5$ Hz) 7.40 (1H, dd, $J = 7.5, 1.5$ Hz), 6.22 (1H, ddd, $J = 17.0, 10.5, 6.5$ Hz), 5.21 (1H, app. d, $J = 10.5$ Hz), 5.18 (1H, app. d, $J = 17.5$ Hz), 4.41 (1H, q, $J = 7.0$ Hz), 2.81 (1H, dd, $J = 16.5, 7.0$ Hz), 2.78 (1H, dd, $J = 16.5, 6.5$ Hz), 0.08 (9H, s); **^{13}C NMR (CDCl_3 , 100 MHz):** δ 139.8, 138.8, 134.1, 131.7, 129.1, 127.4, 126.0, 125.6, 125.5, 124.6, 123.5, 115.9, 105.5, 86.8, 43.2, 26.3, 0.1. **HRMS (ESI $^+$):** Calcd for $\text{C}_{19}\text{H}_{23}\text{Si}$ $[\text{M}+\text{H}]^+$: 279.1569; Found: 279.1554. Specific rotation: $[\alpha]_{\text{D}}^{22.5} -14.2$ (c 1.14, CHCl_3) for an enantiomerically enriched sample of 94:6 er.

Enantiomeric purity was determined by HPLC analysis in comparison with authentic racemic material obtained from the derived alcohol, which was prepared through oxidative cleavage of the olefin then reduction of the derived aldehyde with NaBH_4 ; Chiralpak OD–H column, 99:1 hexanes/ *i*-PrOH, 1.0 mL/min, 220 nm.

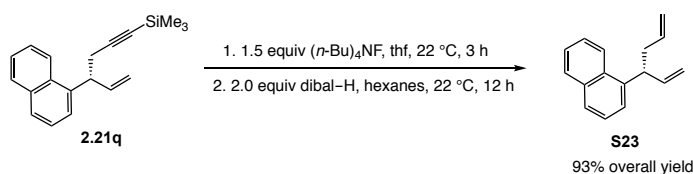


(*R,E*)-Trimethyl(4-phenylhex-5-en-1-yn-1-yl-6-*d*)silane (cf. **1.66** in Chapter 1)

IR (neat): 3030 (w), 2959 (w), 2176 (w), 1496 (w), 1248 (m), 1075 (w), 1039 (w), 837 (s), 758 (s), 697 (s), 654 (m), 645 (m) cm^{-1} ; **^1H NMR (CDCl_3 , 400 MHz):** δ 7.33 (1H, d, $J = 8.5$ Hz), 7.87 (1H, d, $J = 8.5$ Hz), 7.73 (1H, d, $J = 7.0$ Hz), 7.33–7.29 (2H, m), 7.24–7.20 (3H, m), 6.08 (1H, dd, $J = 17.2, 7.2$ Hz), 5.11 (3 mol % *Z*-diastereomer, 1H, dd, $J = 6.0, 1.6$ Hz), 5.09 (97 mol % *E*-diastereomer, 1H, dd, $J = 17.2, 1.6$ Hz), 3.53 (1H, qd, $J = 7.2, 1.2$ Hz), 2.67–2.53 (2H, m), 0.11 (9H, s); **^{13}C NMR (CDCl_3 , 100 MHz):** δ 142.8 (d, $J_{\text{CD}} = 1.5$ Hz), 128.5, 127.9, 126.8, 126.7, 115.2 (t, $J_{\text{CD}} = 24.4$ Hz), 105.5 (d, $J_{\text{CD}} = 1.5$ Hz), 86.7 (d, $J_{\text{CD}} = 1.5$ Hz), 48.6, 26.9, 0.2. **HRMS (ESI $^+$):** Calcd for $\text{C}_{15}\text{H}_{20}\text{DSi}$ [$\text{M}+\text{H}$] $^+$: 230.1475; Found: 230.1473. Specific rotation: $[\alpha]_{\text{D}}^{20.0}$ 0.76 (c 0.58, CHCl_3) for an enantiomerically enriched sample of 96:4 dr.

Proof of Stereochemistry for Products with a *Tertiary* Carbon Stereogenic Center

Scheme S6. Preparation of 1,5-Diene **S23**



An oven-dried vial (4 mL, 17 x 38 mm) equipped with a stir bar was charged with TMS-protected alkyne **2.21q** (28.0 mg, 100 μmol) and thf (1 mL). Tetrabutylammonium fluoride (0.15 mL of 1.0 M thf solution, 150 μmol) was added to the mixture and the mixture was allowed to stir at 22 $^\circ\text{C}$ for 3 h. The reaction was quenched upon the addition of a saturated solution of ammonium chloride (1 mL), washed with Et_2O (3 x 2

mL). The combined organic layers were filtered through a short plug of celite/MgSO₄ (4 cm x 1 cm) and eluted with Et₂O. The filtrate was concentrated *in vacuo* to provide a pale yellow oily residue, which was used for next step without further purification. An oven-dried vial (4 mL, 17 x 38 mm) equipped with a stir bar was charged with the terminal alkyne and hexanes (1 mL). Dibal-H (36 μ L, 200 μ mol) was added to the mixture through a syringe and the reaction mixture was allowed to stir at 22 °C for 12 h. The reaction was quenched upon the addition of a saturated solution of sodium potassium tartrate (0.5 mL) and stirred under N₂. After allowing the mixture to stir at 22 °C for an additional 2 h, the aqueous solution was washed with pentane (3 x 1 mL) and the combined organic layers were passed through a short plug of silica gel (3 cm x 1 cm) eluting with pentane. The organic layer was concentrated *in vacuo* and purified by silica gel chromatography (100% pentane, R_f 0.70) to afford 19.4 mg of the desired product **S23** as colorless oil (93 μ mol, 93% yield). Specific rotation: $[\alpha]_{\text{D}}^{22.0} -21.2$ (*c* 0.83, CHCl₃). Based on reported optical rotation value ($[\alpha]_{\text{D}}^{20} +26.6$ (*c* 0.89, CHCl₃), the absolute stereochemistry of the major enantiomer is assigned to be *R*.²⁷

NHC–Cu Catalyzed Enantioselective Propargyl Addition to Trisubstituted Allylic Phosphates

Representative Procedure

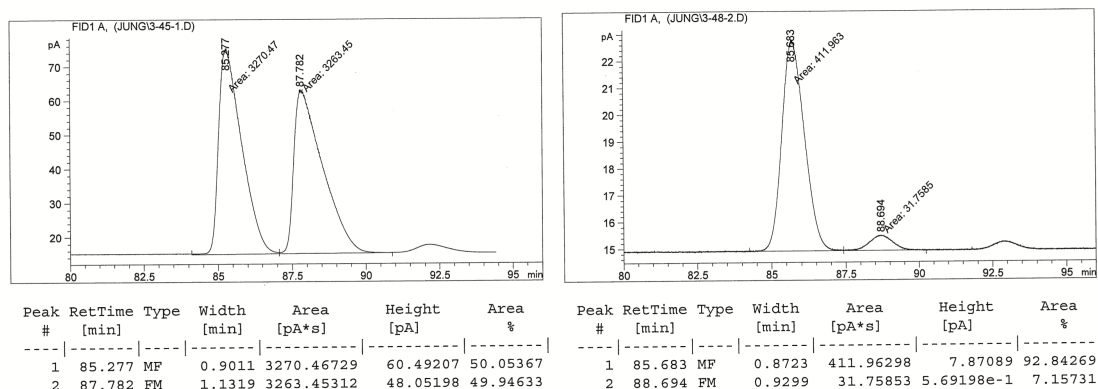
An oven-dried 2-dram vial equipped with a stir bar was charged with NHC–Ag complex **2.29** (24 mg, 12.5 μ mol), NaOMe (32 mg, 0.6 mmol), and CuCl (2.47 mg, 25 μ mol) in a nitrogen-filled glove box. The vial was sealed with a septum and electrical tape, and removed from the glove box. Thf (3 mL) was added and the mixture was allowed to stir for 1 h under N₂ at 22 °C (The mixture became bright-yellow solution). The solution of allylic phosphate **2.43a** (142 mg, 0.5 mmol) and propargyl–B(pin) reagent **2.20** (0.2 mL, 0.75 mmol) in thf (2 mL) was added to the mixture slowly through a platic syringe. The resulting mixture was allowed to stir at 22 °C for 30 h and quenched by passing through a short plug of silica gel (4 cm x 1 cm) and eluted with Et₂O. The organic layer was concentrated *in vacuo*, resulting in yellow oil, which was purified by silica gel chromatography (100% hexanes, R_f 0.32) to afford 97 mg of inseparable mixture of **2.44a** and S_N2 product (94:6 S_N2'/S_N2) as colorless oil (0.40 mmol, 81% yield).

(14) Zhang, P.; Brozek, L. A.; Morken, J. P. *J. Am. Chem. Soc.* **2010**, *132*, 10686–10688.

Characterization Data for Enynes with a *Quaternary* Carbon Stereogenic Center*(R)*-4-Methyl-4-phenyl-1-trimethylsilyl-hex-5-en-1-yne (**2.44a**)

IR (neat): 3085 (w), 3059 (w), 2960 (m), 2900 (w), 2175 (m), 1636 (w), 1600 (w), 1494 (w), 1445 (w), 1410 (w), 1372 (w), 1248 (s), 1075 (w), 1026 (m), 1000 (w), 915 (m), 837 (s), 758 (s), 696 (s), 646 (s), 595 (w), 555 (w) cm^{-1} ; **$^1\text{H NMR}$ (CDCl_3 , 400 MHz):** δ 7.37–7.34 (2H, m), 7.32–7.28 (2H, m), 7.23–7.18 (1H, m), 6.09 (1H, dd, $J = 17.6, 10.8$ Hz), 5.15 (1H, dd, $J = 10.8, 0.8$ Hz), 5.09 (1H, dd, $J = 17.6, 0.8$ Hz), 2.64 (1H, s), 2.63 (1H, s), 1.51 (3H, s), 0.09 (9H, s); **$^{13}\text{C NMR}$ (CDCl_3 , 100 MHz):** δ 146.0, 145.3, 128.1, 126.8, 126.3, 112.7, 104.9, 87.4, 44.4, 32.6, 25.3, 0.1. **HRMS (ESI^+):** Calcd for $\text{C}_{16}\text{H}_{23}\text{Si}_1$ $[\text{M}+\text{H}]^+$: 243.1569; Found: 243.1563. Specific rotation: $[\alpha]_{\text{D}}^{20.9} +10.0$ (c 1.56, CHCl_3) for an enantiomerically enriched sample of 93:7 er.

Enantiomeric purity was determined by GC analysis in comparison with authentic racemic material; CDB-DM column, 100 °C, 15 psi.

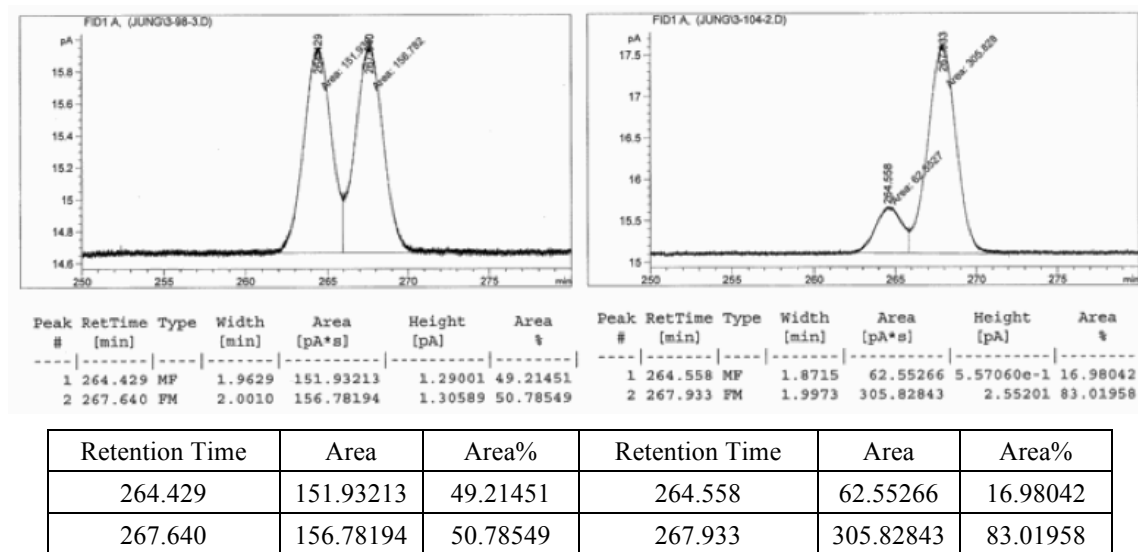


Retention Time	Area	Area%	Retention Time	Area	Area%
85.277	3270.46729	50.05367	85.683	411.96298	92.84269
87.782	3263.45312	49.94633	88.694	31.75853	7.15731

(R)-4-Methyl-4-(2-methoxyphenyl)-1-trimethylsilyl-hex-5-en-1-yne (**2.44b**)

IR (neat): 2958 (w), 2900 (m), 2834 (w), 2173 (m), 1635 (w), 1598 (w), 1580 (w), 1489 (m), 1462 (m), 1434 (m), 1409 (w), 1369 (w), 1286 (w), 1237 (s), 1179 (w), 1121 (w), 1071 (w), 1028 (s), 912 (m), 837 (s), 789 (m), 747 (s), 697 (m), 670 (m), 646 (s), 573 (w) cm^{-1} ; **$^1\text{H NMR}$ (CDCl_3 , 400 MHz):** δ 7.29 (1H, dd, $J = 7.6, 1.6$ Hz), 7.24–7.19 (1H, m), 6.91 (1H, dd, $J = 7.6, 1.6$ Hz), 6.87–6.86 (1H, m), 6.28 (1H, dd, $J = 17.4, 10.8$ Hz), 5.04 (1H, dd, $J = 10.8, 1.2$ Hz), 4.97 (1H, dd, $J = 17.4, 1.2$ Hz), 3.80 (3H, s), 2.86 (1H, s), 2.85 (1H, s), 1.55 (3H, s), 0.04 (9H, s); **$^{13}\text{C NMR}$ (CDCl_3 , 100 MHz):** δ 158.1, 145.4, 134.0, 128.3, 127.8, 120.3, 111.8, 111.7, 106.1, 86.5, 55.3, 44.1, 30.6, 24.4, 0.2. **HRMS (ESI^+):** Calcd for $\text{C}_{17}\text{H}_{25}\text{O}_1\text{Si}_1$ $[\text{M}+\text{H}]^+$: 273.1674; Found: 273.1684. Specific rotation: $[\alpha]_{\text{D}}^{20} +19.9$ (c 2.00, CHCl_3) for an enantiomerically enriched sample of 83:17 er.

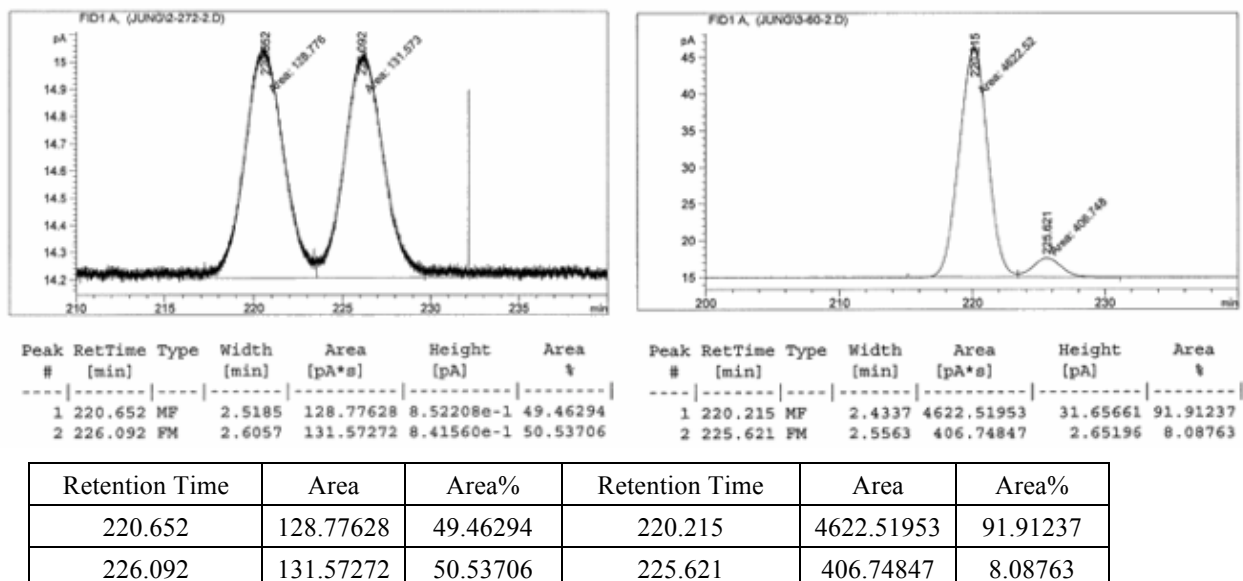
Enantiomeric purity was determined by GC analysis in comparison with authentic racemic material of the ketone derivative obtained through protoboration/oxidative work-up after removal of the silyl group; CDB-DM column, 90 °C, 60 min, then 0.05 °C /min to 100 °C, 15 psi.



(*R*)-4-Methyl-4-(3-bromophenyl)-1-trimethylsilyl-hex-5-en-1-yne (**2.44c**)

IR (neat): 3084 (w), 2960 (m), 2899 (w), 2175 (m), 1637 (w), 1592 (m), 1563 (m), 1475 (m), 1415 (m), 1372 (m), 1299 (w), 1248 (s), 1205 (w), 1068 (w), 1033 (m), 1015 (m), 996 (m), 918 (m), 837 (s), 781 (s), 758 (s), 696 (s), 646 (s) cm⁻¹; **¹H NMR (CDCl₃, 400 MHz):** δ 7.50 (1H, dd, *J* = 2.0, 2.0 Hz), 7.35–7.33 (1H, m), 7.29–7.26 (1H, m), 7.19–7.15 (1H, m), 6.04 (1H, dd, *J* = 17.6, 10.8 Hz), 5.18 (1H, dd, *J* = 10.8, 0.8 Hz), 5.10 (1H, dd, *J* = 17.6, 0.8 Hz), 2.59 (2H, s), 1.48 (3H, s), 0.09 (9H, s); **¹³C NMR (CDCl₃, 100 MHz):** δ 148.4, 144.6, 130.2, 129.6, 129.4, 125.6, 122.3, 113.3, 104.2, 87.9, 44.4, 32.6, 25.3, 0.1; **HRMS (ESI⁺):** Calcd for C₁₆H₂₂Br₁Si₁ [M+H]⁺: 321.0674; Found: 321.0680. Specific rotation: [α]_D^{21.3} +21.4 (*c* 1.40, CHCl₃) for an enantiomerically enriched sample of 92:8 er.

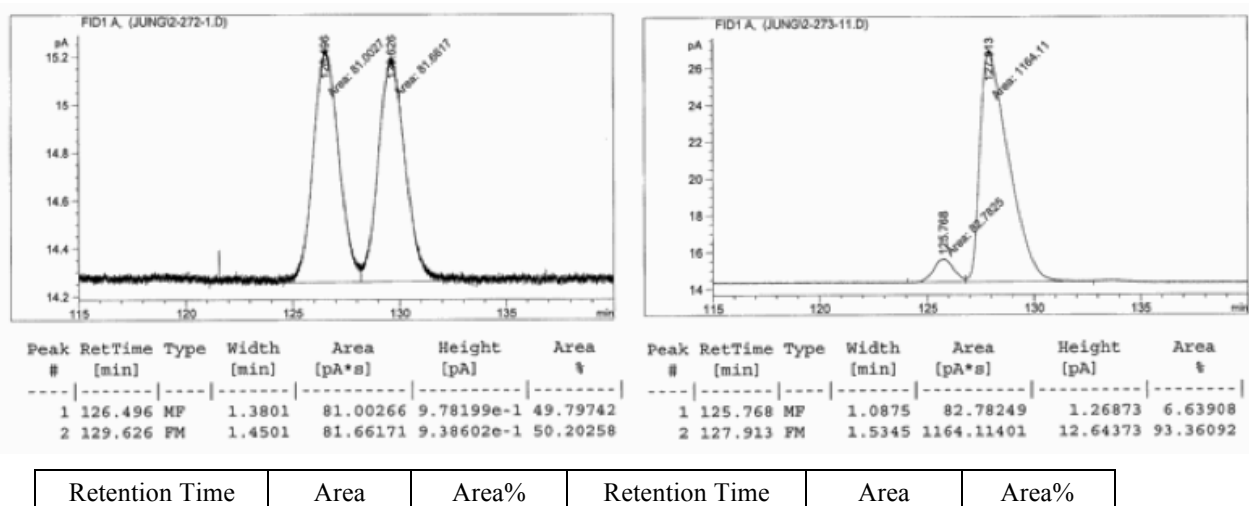
Enantiomeric purity was determined by GC analysis in comparison with authentic racemic material; CDB-DM column, 110 °C, 15 psi.



(R)-4-Methyl-4-(4-chlorophenyl)-1-trimethylsilyl-hex-5-en-1-yne (**2.44d**)

IR (neat): 3085 (w), 2961 (m), 2900 (w), 2176 (m), 1636 (w), 1596 (w), 1493 (m), 1460 (w), 1411 (w), 1372 (w), 1298 (w), 1248 (s), 1096 (m), 1033 (m), 1012 (s), 917 (m), 838 (s), 823 (s), 758 (s), 742 (m), 722 (m), 697 (m), 646 (m), 594 (w), 532 (m) cm^{-1} ; **^1H NMR (CDCl_3 , 400 MHz):** δ 7.28–7.26 (4H, m), 6.04 (1H, dd, $J = 17.2, 10.8$ Hz), 5.15 (1H, dd, $J = 10.8, 0.8$ Hz), 5.07 (1H, dd, $J = 17.2, 0.8$ Hz), 2.60 (1H, s), 2.59 (1H, s), 1.48 (3H, s), 0.08 (9H, s); **^{13}C NMR (CDCl_3 , 100 MHz):** δ 145.0, 144.5, 132.2, 128.4, 128.2, 113.1, 104.4, 87.8, 44.2, 32.7, 25.4, 0.1. **HRMS (ESI $^+$):** Calcd for $\text{C}_{16}\text{H}_{22}\text{Cl}_1\text{Si}_1$ $[\text{M}+\text{H}]^+$: 277.1179; Found: 277.1177. Specific Rotation: $[\alpha]_{\text{D}}^{21.2} +20.0$ (c 1.50, CHCl_3) for an enantiomerically enriched sample of 93:7 er.

Enantiomeric purity was determined by GC analysis in comparison with authentic racemic material; CDB-DM column, 115 °C, 15 psi.

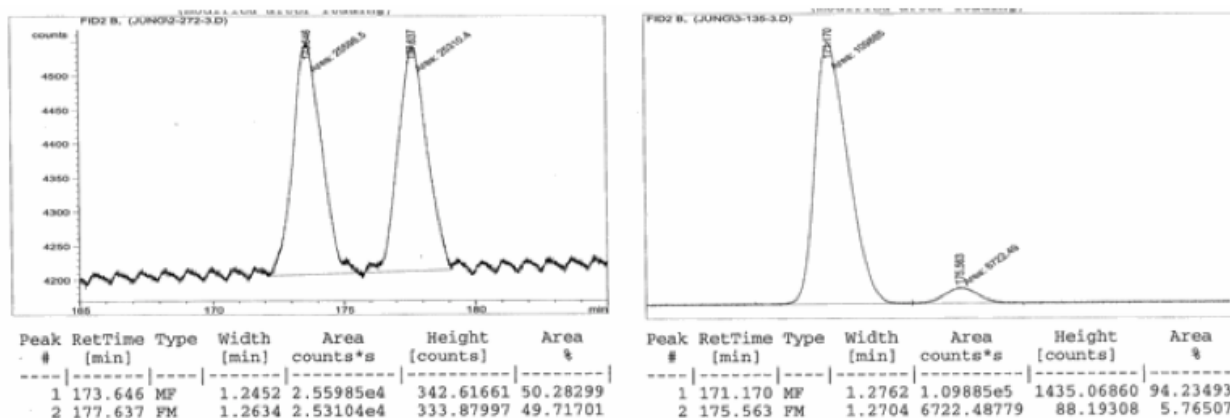


126.496	81.00266	49.79742	125.768	82.78249	6.63908
129.626	81.66171	50.20258	127.913	1164.11401	93.36092

(*R*)-4-Cyclohexyl-4-methyl-1-trimethylsilyl-hex-5-en-1-yne (**2.44e**)

IR (neat): 3082 (w), 2923 (m), 2852 (m), 2173 (m), 1636 (w), 1449 (m), 1414 (m), 1374 (w), 1294 (s), 1248 (w), 1131 (w), 1036 (m), 1004 (m), 911 (m), 890 (w), 837 (s), 758 (s), 698 (m), 646 (s) cm^{-1} ; **^1H NMR (CDCl_3 , 400 MHz):** δ 5.80 (1H, dd, $J = 17.6, 10.8$ Hz), 5.03 (1H, dd, $J = 10.8, 1.6$ Hz), 4.93 (1H, dd, $J = 17.6, 1.6$ Hz), 2.23 (1H, s), 2.22 (1H, s), 1.81-1.62 (6H, m), 1.42-1.37 (1H, m), 1.22-1.04 (2H, m), 1.00 (3H, s), 0.99-0.83 (2H, m), 0.14 (9H, s); **^{13}C NMR (CDCl_3 , 100 MHz):** δ 144.9, 112.5, 105.5, 86.6, 44.8, 42.3, 31.7, 30.3, 27.8, 27.3, 27.2, 26.7, 20.0, 0.3. **HRMS (ESI $^+$):** Calcd for $\text{C}_{16}\text{H}_{29}\text{Si}_1$ [$\text{M}+\text{H}$] $^+$: 249.2038; Found: 249.2045. Specific rotation: $[\alpha]_{\text{D}}^{21.6} +13.0$ (c 1.20, CHCl_3) for an enantiomerically enriched sample of 94:6 er.

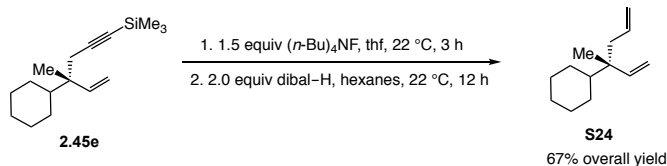
Enantiomeric purity was determined by GC analysis in comparison with authentic racemic material; β -dex column, 100 $^\circ\text{C}$, 15 psi.



Retention Time	Area	Area%	Retention Time	Area	Area%
173.646	25598.5	50.28299	171.170	10988.5	94.23493
177.637	25310.4	49.71701	175.563	6722.48779	5.76507

Proof of Stereochemistry for Products with a *Quaternary* Carbon Stereogenic Center

Scheme S7. Preparation of 1,5-Diene **S24**



An oven-dried vial (4 mL, 17 x 38 mm) equipped with a stir bar was charged with TMS-protected alkyne **2.44e** (19 mg, 76 μmol) and thf (1 mL). Tetrabutylammonium

fluoride (0.12 mL of 1.0 M thf solution, 0.12 mmol) was added to the mixture, which was allowed to stir at 22 °C for 3 h. The reaction was quenched upon the addition of a saturated solution of ammonium chloride (1 mL), washed with Et₂O (3 x 2 mL). The combined organic layers were filtered through a short plug of celite/MgSO₄ (4 cm x 1 cm) and eluted with Et₂O. The filtrate was concentrated *in vacuo* to provide yellow oily residue, which was used without purification. An oven-dried vial (4 mL, 17 x 38 mm) equipped with a stir bar was charged with the terminal alkyne and hexanes (1 mL). Dibal-H (27 μL, 150 μmol) was added to the mixture through the syringe and the reaction mixture was allowed to stir at 22 °C for 12 h. The reaction was quenched upon the addition of a saturated solution of sodium potassium tartrate (0.5 mL) and allowed to stir at 22 °C for an additional 2 h, the aqueous solution was washed with pentane (3 x 1 mL) and the combined organic layers were passed through a short plug of silica gel (3 cm x 1 cm) and eluted with pentane. The organic layer was concentrated *in vacuo*, resulting in colorless oil that was purified by silica gel chromatography (100% pentane, R_f = 0.82) to afford 9.3 mg of the desired product **S24** as colorless oil (52 μmol, 67% yield). Specific rotation: $[\alpha]_{\text{D}}^{22} +7.02$ (*c* 0.83, CHCl₃). Based on reported optical rotation value ($[\alpha]_{\text{D}}^{20} +6.85$ (*c* 0.96, CHCl₃)), the absolute stereochemistry of the major enantiomer is assigned to be *R* enantiomer.²⁸

Further Functionalization of Propargyl Addition Products (cf. Schemes 2.7–2.9)

(*S*)-5-Phenyl-1,2,6-heptatriene (2.48)

An oven-dried vial (4 mL, 17 x 38 mm) equipped with a stir bar was charged with TMS-protected alkyne **2.21a** (46 mg, 0.20 mmol) and thf (1 mL). Tetrabutylammonium fluoride (0.30 mL of 1.0 M thf solution, 0.30 mmol) was added to the mixture, which was allowed to stir at 22 °C for 3 h. The reaction was quenched upon the addition of a saturated solution of ammonium chloride (1 mL), washed with Et₂O (3 x 2 mL). The combined organic layers were filtered through a short plug of celite/MgSO₄ (4 cm x 1 cm) and eluted with Et₂O. The filtrate was concentrated *in vacuo* to provide pale yellow oil, which was used for next step without further purification. An oven-dried round bottom flask (5 mL) equipped with a reflux condenser and a magnetic stir bar was charged with the unpurified mixture, paraformaldehyde (12 mg, 0.40 mmol), CuBr (9.4 mg, 0.066 mmol), diisopropylamine (0.054 mL, 0.40 mmol) and 1,4-dioxane (1 mL) under N₂ atmosphere. The resulting mixture was allowed to stir at 100 °C for 4 h and the reaction was quenched by addition of a saturated aqueous solution of Na₂CO₃ (5 mL). The aqueous layer was washed with Et₂O (3 x 3 mL) and the combined organic layers were washed with brine (5 mL), dried over MgSO₄, filtered and concentrated *in vacuo*. The residue was purified by silica gel chromatography (100% hexanes, R_f 0.56) to afford the

(15) Zhang, P.; Le, H.; Kyne, R. E.; Morken, J. P. *J. Am. Chem. Soc.* **2011**, *133*, 9716–9719.

desired product **2.48** (31 mg, 0.186 mmol, 93% overall yield) as colorless oil. **(S)-5-Phenyl-1,2,6-heptatriene (2.48)**: IR (neat): 3081 (w), 3061 (w), 3027 (w), 2979 (w), 2912 (w), 1954 (m), 1636 (w), 1600 (w), 1492 (m), 1451 (m), 1414 (w), 1303 (w), 1241 (w), 1180 (w), 1075 (w), 1028 (m), 992 (w), 965 (w), 914 (s), 841 (s), 782 (w), 753 (s), 697 (s), 676 (m), 608 (w), 514 (m) cm^{-1} ; $^1\text{H NMR}$ (CDCl_3 , 400 MHz): δ 7.32–7.29 (2H, m), 7.22–7.19 (3H, m), 5.99 (1H, ddd, $J = 17.3, 10.2, 7.2$ Hz), 5.08 (1H, d, $J = 7.2$ Hz), 5.06 (1H, d, $J = 17.3$ Hz), 5.03 (1H, tt, $J = 14.4, 6.8$ Hz), 4.63–4.59 (2H, m), 3.39 (1H, td, $J = 7.4, 7.2$ Hz), 2.48–2.42 (2H, m); $^{13}\text{C NMR}$ (CDCl_3 , 100 MHz): δ 209.2, 143.6, 141.4, 128.5, 127.8, 126.5, 114.8, 88.0, 74.7, 49.7, 34.5. HRMS (ESI⁺): Calcd for $\text{C}_{13}\text{H}_{15}$ $[\text{M}+\text{H}]^+$: 171.1173; Found: 171.1175. Specific rotation: $[\alpha]_{\text{D}}^{22.8} +4.16$ (c 3.00, CHCl_3) for an enantiomerically enriched sample of 97:3 er.

N-[(*S*)-4-(2-Bromophenyl)-5-hexenoyl]-4-methylbenzenesulfonamide (**2.49**)

An oven-dried vial (4 mL, 17 x 38 mm) equipped with a stir bar was charged with TMS-protected alkyne **2.21c** (74 mg, 0.24 mmol) and thf (1 mL). Tetrabutylammonium fluoride (0.36 mL of 1.0 M thf solution, 0.36 mmol) was added to the mixture, which was allowed to stir at 22 °C for 3 h. The reaction was quenched upon the addition of a saturated solution of ammonium chloride (1 mL), washed with Et_2O (3 x 2 mL). The combined organic layers were filtered through a short plug of celite/ MgSO_4 (4 cm x 1 cm) and eluted with Et_2O . The filtrate was concentrated *in vacuo* to provide an oily residue that was purified by silica gel chromatography (100% pentane, R_f 0.77) to afford 57 mg of terminal alkyne as colorless oil (0.24 mmol, 98% yield). An opened vial (4 mL, 17 x 38 mm) equipped with a stir bar was charged with the terminal alkyne obtain from last step (50 mg, 0.21 mmol), CuI (0.8 mg, 4.2 μmol), TsN_3 (49 mg, 0.25 mmol) and H_2O (0.5 mL). Et_3N (35 μL , 0.25 mmol) was slowly added to the mixture through syringe and the reaction mixture was allowed to stir at 22 °C for 30 min in air. The mixture was diluted with CH_2Cl_2 (2 mL) and the reaction was quenched upon the addition of a saturated solution of ammonium chloride (1 mL). The aqueous solution was washed with CH_2Cl_2 (3 x 1 mL) and the combined organic layers were passed through a short plug of silica gel (3 cm x 1 cm) and eluted with CH_2Cl_2 . The organic layer was concentrated *in vacuo*, resulting in yellow oil that was purified by silica gel chromatography (30:1 $\text{EtOAc}/\text{CH}_2\text{Cl}_2$, R_f 0.27) to afford 66 mg of the desired product **2.49** as yellow oil (0.156 mmol, 74% yield). **(S)-4-(2-Bromophenyl)hex-5-en-1-yne**: IR (neat): 3299 (m), 3081 (w), 3008 (w), 2981 (w), 2913 (w), 2119 (w), 1637 (w), 1589 (w), 1566 (w), 1468 (s), 1437 (m), 1415 (m), 1276 (w), 1243 (w), 1161 (w), 1119 (w), 1021 (s), 994 (m), 919 (s), 861 (w), 822 (w), 779 (w), 750 (s), 734 (s), 724 (s), 630 (s), 546 (w), 513 (w), 447 (m) cm^{-1} ; $^1\text{H NMR}$ (CDCl_3 , 400 MHz): δ 7.56–7.54 (1H, m), 7.29–7.23 (2H, m), 7.10–7.06 (1H, m), 6.03 (1H, ddd, $J = 17.2, 10.6, 6.8$ Hz), 5.19 (1H, dd, $J = 10.6, 1.6$ Hz), 5.16 (1H, dd, $J = 17.2, 1.6$ Hz), 4.10 (1H, td, $J = 8.0, 6.8$ Hz), 2.62–2.60 (2H, m), 1.9 (1H, t, $J = 2.8$ Hz); $^{13}\text{C NMR}$ (CDCl_3 , 100 MHz): δ 141.5, 138.4, 133.1, 128.8, 128.3, 127.6, 124.8,

116.4, 82.0, 70.1, 46.3, 24.0. **HRMS (ESI⁺)**: Calcd for C₁₂H₁₂Br₁ [M+H]⁺: 235.0122; Found: 235.0117. Specific rotation: [α]_D^{21.7} -4.99 (*c* 5.00, CHCl₃) for an enantiomerically enriched sample of 97:3 er.

***N*-[(*S*)-4-(2-Bromophenyl)-5-hexenoyl]-4-methylbenzenesulfonamide (2.49):** **IR (neat)**: 3243 (br), 3064 (w), 2925 (w), 1697 (m), 1636 (w), 1596 (w), 1468 (m), 1435 (s), 1339 (s), 1307 (m), 1292 (m), 1265 (m), 1215 (m), 1188 (m), 1168 (s), 1140 (s), 1117 (s), 1084 (s), 1045 (m), 1020 (s), 995 (m), 920 (m), 853 (s), 813 (s), 750 (m), 703 (s), 660 (s), 545 (s), 482 (m) cm⁻¹; **¹H NMR (CDCl₃, 400 MHz)**: δ 7.91 (2H, d, *J* = 8.4 Hz), 7.51 (1H, d, *J* = 8.0 Hz), 7.36 (2H, s), 7.32 (2H, d, *J* = 8.4 Hz), 7.25–7.22 (1H, m), 7.13 (1H, d, *J* = 8.0 Hz), 7.07–7.03 (1H, m), 5.82 (1H, ddd, *J* = 17.2, 10.4, 7.2 Hz), 5.07 (1H, d, *J* = 10.4 Hz), 5.05 (1H, d, *J* = 17.2 Hz), 3.67 (1H, td, *J* = 7.6, 7.2 Hz), 2.44 (3H, s), 2.30–2.22 (1H, m), 2.20–2.12 (1H, m), 2.09–2.00 (1H, m), 1.96–1.87 (1H, m); **¹³C NMR (CDCl₃, 100 MHz)**: δ 170.0, 145.3, 141.9, 139.5, 133.1, 129.7, 128.6, 128.5, 128.4, 128.2, 128.0, 124.8, 116.0, 46.7, 34.0, 29.0, 21.8. **HRMS (ESI⁺)**: Calcd for C₁₉H₂₁Br₁N₁O₂S₁ [M+H]⁺: 422.0425; Found: 422.0408. Specific rotation: [α]_D^{21.6} +7.50 (*c* 6.00, CHCl₃) for an enantiomerically enriched sample of 97:3 er.

(*R,Z*)-Trimethyl(4-(naphthalen-1-yl)hexa-1,5-dien-1-yl)silane (2.50)

A 50-mL flask equipped with a stir bar was charged with enyne **2.21q** (278 mg, 1.0 mmol), hexanes (10 mL) and thf (2.0 mL). Dibal-H (360 μL, 2.0 mmol) was added to the solution through the syringe and the mixture was allowed to stir at 55 °C for 2 h. The reaction was quenched upon the addition of a saturated solution of sodium potassium tartrate (5 mL) and allowed to stir at 22 °C for an additional 2 h, and then washed with Et₂O (3 x 10 mL). The combined organic layers were dried over MgSO₄, filtered, concentrated *in vacuo*, resulting in colorless oil that was purified by silica gel chromatography (100% pentane, R_f 0.65) to afford 238 mg of the desired product **2.50** as colorless oil. **(*R,Z*)-Trimethyl(4-(naphthalen-1-yl)hexa-1,5-dien-1-yl)silane (2.50)**: **IR (neat)**: 3048 (w), 2954 (w), 2897 (w), 1636 (w), 1601 (w), 1510 (w), 1396 (w), 1247 (s), 1167 (w), 992 (w), 915 (w), 856 (s), 836 (s), 796 (s), 777 (s), 764 (m), 731 (w), 690 (w), 560 (w), 518 (w), 422 (w) cm⁻¹; **¹H NMR (CDCl₃, 400 MHz)**: δ 8.13 (1H, d, *J* = 8.0 Hz), 7.89–7.86 (1H, m), 7.75 (1H, d, *J* = 7.6 Hz), 7.54–7.45 (3H, m), 7.41 (1H, dd, *J* = 7.2, 1.2 Hz), 6.33 (1H, dt, *J* = 14.0, 7.2 Hz), 6.12 (1H, ddd, *J* = 17.2, 10.0, 6.8 Hz), 5.55 (1H, dt, *J* = 14.0, 1.6 Hz), 5.12 (1H, app.d, *J* = 9.6 Hz), 5.10 (1H, app.d, *J* = 17.2 Hz), 4.23 (1H, q, *J* = 7.2 Hz), 2.79–2.74 (2H, m), 0.12 (9H, s); **¹³C NMR (CDCl₃, 100 MHz)**: δ 146.7, 141.3, 139.8, 134.2, 131.8, 130.6, 129.1, 127.1, 125.9, 125.6, 125.5, 124.4, 123.6, 115.2, 44.5, 38.7, 0.3. **HRMS (ESI⁺)**: Calcd for C₁₉H₂₄Si [M+H]⁺: 281.1726; Found: 281.1732. Specific rotation: [α]_D^{20.8} -45.1 (*c* 1.77, CHCl₃) for an enantiomerically enriched sample of 94:6 er.

(*R,Z*)-1-(6-Iodohexa-1,5-dien-3-yl)naphthalene (2.51)

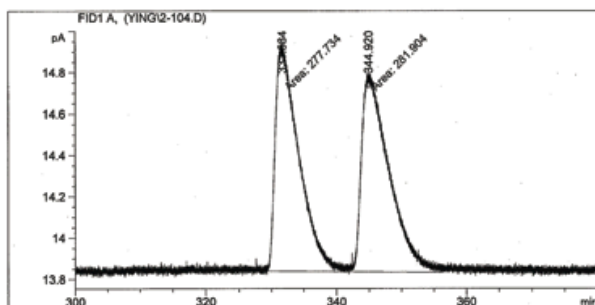
An oven-dried vial (4 mL, 17 x 38 mm) equipped with a stir bar was charged with alkenyl silane **2.52** (28 mg, 0.10 mmol), Ag₂CO₃ (8.3 mg, 30 μmol) and (CF₃)₂CHOH (1.0 mL). The suspension was allowed to cool to 0 °C. N-iodosuccinimide (27 mg, 0.12 mmol) was added to the mixture, which was allowed to stir at 0 °C for 10 min. The reaction was quenched upon the addition of a saturated solution of NaHSO₃ (0.5 mL). The aqueous solution was washed with Et₂O (3 x 1 mL) and the combined organic layers were passed through a short plug of silica gel and eluted with Et₂O. The organic layer was concentrated *in vacuo*, and the yellow oil was purified by silica gel chromatography (100% pentane, R_f0.50) to afford 21.4 mg of the desired product **2.51** (0.064 mmol, 64% yield) as colorless oil. **(*R,Z*)-1-(6-Iodohexa-1,5-dien-3-yl)naphthalene (2.51): IR (neat):** 3047 (w), 3002 (w), 2921 (w), 1636 (w), 1597 (w), 1510 (w), 1435 (w), 1412 (w), 1395 (w), 1284 (m), 1263 (m), 1193 (w), 1167 (w), 1102 (w), 993 (w), 949 (w), 917 (m), 858 (w), 837 (w), 797 (m), 777 (s), 751 (w), 734 (w), 691 (w), 647 (w), 560 (w), 477 (w), 427 (w); **¹H NMR (CDCl₃, 400 MHz):** δ 8.14 (1H, d, *J* = 8.4 Hz), 7.89–7.87 (1H, m), 7.76 (1H, d, *J* = 8.4 Hz), 7.56–7.42 (4H, m), 6.26–6.19 (2H, m), 6.14 (1H, ddd, *J* = 17.2, 10.4, 6.8 Hz), 5.18–5.12 (2H, m), 4.34 (1H, q, *J* = 7.2 Hz), 2.77 (2H, app. t, *J* = 6.8 Hz); **¹³C NMR (CDCl₃, 100 MHz):** δ 140.7, 139.6, 139.0, 134.2, 131.7, 129.1, 127.3, 126.1, 125.6, 124.5, 123.5, 115.6, 83.8, 43.0, 40.1. **HRMS (ESI⁺):** Calcd for C₁₆H₁₆I [M+H]⁺: 335.0297; Found: 335.0291. Specific rotation: [α]_D^{23.1} –68.7 (*c* 1.60, CHCl₃) for an enantiomerically enriched sample of 94:6 er.

4,4,5,5-Tetramethyl-1-(4-methylhexa-1,5-dienyl)-1,3,2-dioxaborolane (2.53)

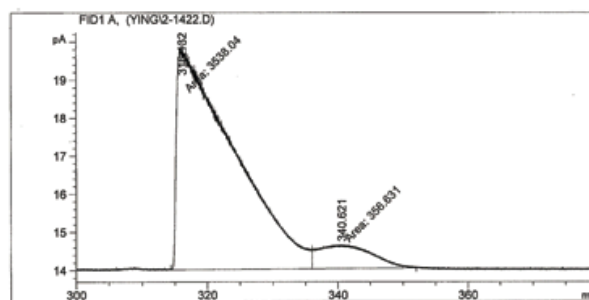
An oven-dried 1-dram vial equipped with a stir bar was charged with NHC–Ag complex **2.29** (14.5 mg, 7.5 μmol), NaOMe (19.4 mg, 0.36 mmol), and CuCl (1.47 mg, 15 μmol) in a nitrogen-filled glove box. The vial was sealed with a cap (phenolic open top cap with a red PTFE/white silicon septum) and electrical tape, and removed from the glove box. CH₂Cl₂ (2 mL) was added and the mixture was allowed to stir for 1 h under N₂ at 22 °C (The solution became bright-yellow). The solution of allylic phosphate **2.52** (62 mg, 0.3 mmol) and propargyl–B(pin) reagent **2.20** (0.12 mL, 0.45 mmol) in CH₂Cl₂ (1 mL) was added to the mixture slowly through syringe. The resulting mixture was allowed to stir at 22 °C for 6 h after which the reaction was quenched by passing it through a short plug of silica gel (4 cm x 1 cm) and eluted with Et₂O. The organic layer was concentrated *in vacuo* and the unpurified residue was used without further purification. An oven-dried 1-dram vial equipped with a stir bar was charged with the unpurified mixture, K₂CO₃ (12.4 mg, 0.09 mmol) and MeOH (0.93 mL, 18 mmol) in a nitrogen-filled glove box. The vial was sealed with a cap and the mixture was allowed to stir at 22 °C for 6 h in a nitrogen-filled glove box. To another oven-dried 1-dram vial

equipped with a stir bar, imidazolium salt **2.54** (7.0 mg, 16.5 μmol), CuCl (1.48 mg, 15 μmol) and NaOt-Bu (5.8 mg, 60 μmol) were added in a nitrogen-filled glove box. Thf (1.5 mL) was added and the solution was allowed to stir for at 22 °C for 1 h under N₂ atmosphere. B₂(pin)₂ (76 mg, 0.3 mmol) was added to the mixture, which was allowed to stir for an additional 30 min. A solution of the terminal alkyne in MeOH was added to the mixture by syringe and the mixture was allowed to stir for 24 h at 22 °C. The reaction was quenched by passing through a short plug of silica gel (4 cm x 1 cm) and eluted with Et₂O. The organic layer was concentrated *in vacuo* and purified by silica gel chromatography (20:1 hexanes/Et₂O, R_f 0.51) to afford 27.8 mg of alkenylboron **2.55** (95:5 β/α) as colorless oil (0.13 mmol, 41% overall yield). **(S)-4,4,5,5-Tetramethyl-1-(4-methylhexa-1,5-dienyl)-1,3,2-dioxaborolane (2.55)**: IR (neat): 3079 (w), 2977 (m), 2928 (w), 1637 (s), 1457 (w), 1396 (m), 1359 (s), 1317 (s), 1265 (w), 1236 (w), 1214 (w), 1143 (s), 1113 (w), 994 (m), 969 (m), 909 (m), 882 (w), 849 (m), 737 (w), 674 (w), 637 (w), 577 (w) cm⁻¹; ¹H NMR (CDCl₃, 400 MHz): δ 6.58 (1H, dt, *J* = 18.0, 6.8 Hz), 5.76 (1H, ddd, *J* = 17.2, 10.4, 6.8 Hz), 5.43 (1H, dt, *J* = 18.0, 1.2 Hz), 4.97 (1H, dt, *J* = 17.2, 1.6 Hz), 4.93 (1H, dt, *J* = 10.4, 1.6 Hz), 2.30–2.19 (2H, m), 2.14–2.08 (1H, m), 1.25 (12H, s), 1.00 (3H, d, *J* = 6.8 Hz); ¹³C NMR (CDCl₃, 100 MHz): δ 152.7, 144.0, 120.2, 112.7, 83.1, 43.2, 36.8, 24.8, 19.6; HRMS (ESI⁺): Calcd for C₁₃H₂₄B₁O₂ [M+H]⁺: 223.1869; Found: 223.1861. Specific rotation: $[\alpha]_D^{20}$ +9.9 (*c* 2.00, CHCl₃) for an enantiomerically enriched sample of 91:9 er.

Enantiomeric purity was determined by GC analysis in comparison with authentic racemic material by converting **2.53** to the desilylation product of **2.60** through formation of the dicobalt complex with Co₂(CO)₈, cross-metathesis with styrene, decomplexation/deprotection; CDB-DM column, 70 °C, 15 psi.



Peak #	RetTime [min]	Type	Width [min]	Area [pA*s]	Height [pA]	Area %
1	331.684	MF	4.1710	277.73416	1.10979	49.62742
2	344.920	FM	4.8426	281.90439	9.70232e-1	50.37258



Peak #	RetTime [min]	Type	Width [min]	Area [pA*s]	Height [pA]	Area %
1	316.132	MF	9.9250	3538.04248	5.94128	90.84312
2	340.621	FM	9.5122	356.63058	6.24866e-1	9.15688

Retention Time	Area	Area%	Retention Time	Area	Area%
331.684	277.73416	49.62742	316.132	3538.04248	90.84312
344.920	281.90439	50.37258	340.621	356.63058	9.15688

(S)-4-Methyl-1-phenylhexa-1,5-diene (2.56)

An oven-dried 4-dram vial equipped with a stir bar was charged with Pd(PPh₃)₄ (16 mg, 0.014 mmol) and 1,4-dioxane (0.5 mL) under N₂ atmosphere. A solution of the substrate **2.55** (60 mg, 0.27 mmol) and iodobenzene (33 μL, 0.297 mmol) in 1,4-dioxane (0.5 mL) was added to the mixture and 10% NaOH aqueous solution (0.22 mL, 0.54 mmol) was added. The resulting mixture was allowed to stir for at 100 °C for 3 h and then cooled to 22 °C, which was quenched by the addition of water (1 mL) and the aqueous phase was washed with Et₂O (3 x 4 mL). The combined organic layers were dried over MgSO₄, concentrated *in vacuo* and purified by silica gel chromatography (100% hexanes, R_f 0.45) to afford 45.6 mg of the compound **2.56** as colorless oil (0.26 mmol, 98% yield). **(S)-4-Methyl-1-phenylhexa-1,5-diene (2.56): IR (neat):** 1640 (w), 1600 (w), 992 (m), 960 (s), 908 (w) cm⁻¹; **¹H NMR (CDCl₃, 400 MHz):** δ 7.35–7.33 (2H, m), 7.29 (2H, t, *J* = 7.2 Hz), 7.19 (1H, tt, *J* = 7.2, 1.2 Hz), 7.32–7.29 (2H, m), 7.25–7.23 (3H, m), 6.38 (1H, d, *J* = 16.4 Hz), 6.20 (1H, dt, *J* = 16.4, 6.8 Hz), 5.81 (1H, ddd, *J* = 17.2, 10.4, 6.8 Hz), 5.01 (1H, dt, *J* = 17.2, 1.2 Hz), 4.96 (1H, dt, *J* = 10.4, 1.2 Hz), 2.33–2.27 (2H, m), 2.23–2.15 (1H, m), 1.05 (1H, d, *J* = 6.8 Hz); **¹³C NMR (CDCl₃, 100 MHz):** δ 144.1, 137.9, 131.2, 129.1, 128.6, 127.0, 126.1, 112.9, 40.3, 37.9, 19.6. **HRMS (ESI⁺):** Calcd for C₁₃H₁₇ [M+H]⁺: 173.1330; Found: 173.1325. Specific rotation: [α]_D^{21.4} –10.6 (*c* 1.03, CHCl₃).

Formal Synthesis of Plakinic Acid A (cf. Scheme 2.9)**(R)-Triisopropyl(4-methylhex-5-en-1-yn-1-yl)silane (2.58)**

A 100-mL oven-dried vial equipped with a stir bar was charged with imidazolium salt **2.29** (43 mg, 50 μmol), NaOMe (65 mg, 1.20 mmol), and CuCl (5.0 mg, 50 μmol) in a nitrogen-filled glove box. The vial was sealed with a septum and electrical tape, and removed from the glove box. CH₂Cl₂ (8.0 mL) was added and the solution was allowed to stir for 1 h under N₂ at 22 °C. The solution became bright yellow. Propargyl–B(pin) reagent **2.57** (483 mg, 0.15 mmol) and allylic phosphate **2.52** (208 mg, 1.0 mmol) was in CH₂Cl₂ (2.0 mL) was transferred to the mixture through a syringe and the resulting solution was allowed to stir at 22 °C for 6 h. The mixture was passed through a short plug of silica gel and eluted with Et₂O. The organic layer was concentrated *in vacuo*, affording yellow oil that was purified by silica gel chromatography (100% hexanes, R_f 0.80) to afford 248 mg of **2.58** (97:3 S_N2'/S_N2) as pale yellow oil (0.99 mmol, 99% yield). **(R)-Triisopropyl(4-methylhex-5-en-1-yn-1-yl)silane (2.58): IR (neat):** 2958 (m), 2942 (s), 2892 (m), 2865 (s), 2173 (m), 1462 (m), 1073 (w), 1028 (w), 994 (m), 915 (s), 882 (s), 674 (s), 660 (s), 632 (s), 456 (w) cm⁻¹; **¹H NMR (CDCl₃, 400 MHz):** δ 5.84 (1H, ddd, *J* = 17.2, 10.0, 6.8 Hz), 5.04 (1H, dt, *J* = 17.2, 1.6 Hz), 4.97 (1H, dt, *J* = 10.4, 1.2 Hz), 2.42–2.36 (1H, m), 2.34–2.20 (2H, m), 1.19 (3H, d, *J* = 6.8 Hz), 1.07–0.98 (21H, m); **¹³C NMR (CDCl₃, 100 MHz):** δ 142.9, 113.4, 107.3,

81.6, 37.2, 27.4, 19.2, 18.8, 11.5. **HRMS (ESI⁺)**: Calcd for C₁₆H₃₁Si [M+H]⁺: 251.2195; Found: 251.2196. Specific rotation: $[\alpha]_{\text{D}}^{21.7} -3.81$ (*c* 2.62, CHCl₃) for an enantiomerically enriched sample of 90:10 er.

(*R,E*)-Triisopropyl(4-methyl-6-phenylhex-5-en-1-yn-1-yl)silane (2.60)

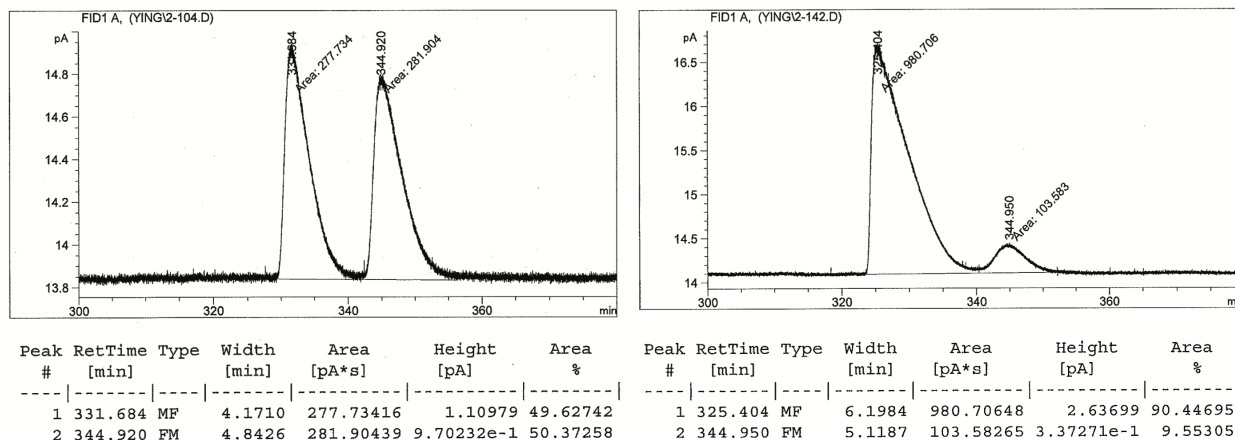
In a nitrogen-filled glove box, a 250 mL flask with a stir bar was charged with enyne **2.60** (613 mg, 2.45 mmol) and styrene (2.55 g, 24.5 mmol). A solution of Mo complex **2.59** (0.1 M in benzene, 1.22 mL, 0.122 mmol, 5.0 mol %) was introduced and the mixture was allowed to stir at 22 °C for 3 h under 35 torr. After 10 h, the solution was exposed to air and moved out of the glove box, and concentrated *in vacuo*. The resulting green oil was passed through a short plug of activated charcoal and eluted with pentane to remove stilbene. The organic layer was concentrated and purified by silica gel chromatography (100% hexanes, R_f = 0.35) to afford **2.60** (>98:2 E/Z) as colorless oil (643 mg, 80% yield). **(*R,E*)-Triisopropyl(4-methyl-6-phenylhex-5-en-1-yn-1-yl)silane (2.60)**: IR (neat): 3026 (w), 2957 (s), 2941 (s), 2864 (s), 2171 (m), 1492 (w), 1461 (m), 1427 (w), 1381 (w), 1329 (w), 1242 (w), 1072 (w), 1028 (m), 995 (m), 963 (s), 938 (w), 919 (w), 882 (s), 745 (s), 692 (s), 664 (s), 612 (s), 520 (m), 455 (m), 416 (m) cm⁻¹; **¹H NMR (CDCl₃, 400 MHz)**: δ 7.35 (2H, d, *J* = 7.6 Hz), 7.29 (2H, t, *J* = 7.6 Hz), 7.20 (1H, t, *J* = 7.2 Hz), 6.45 (1H, d, *J* = 16.0 Hz), 6.22 (1H, dd, *J* = 16.0, 7.2 Hz), 2.61–2.54 (1H, m), 2.42–2.32 (2H, m), 1.22 (3H, d, *J* = 6.8 Hz), 1.12–1.01 (21H, m); **¹³C NMR (CDCl₃, 100 MHz)**: δ 137.7, 134.8, 128.9, 128.6, 127.1, 126.2, 107.1, 81.9, 36.7, 27.8, 19.8, 18.8, 11.4. **HRMS (ESI⁺)**: Calcd for C₂₂H₃₅Si [M+H]⁺: 327.2508; Found: 327.2498. Specific rotation: $[\alpha]_{\text{D}}^{22.1} -16.6$ (*c* 1.85, CHCl₃) for an enantiomerically enriched sample of 90:10 er.

(*R,E*)-(3-Methylhex-1-en-5-yn-1-yl)benzene

To a solution of enyne **2.60** (327 mg, 1.0 mmol) in thf (10 ml) was added tbaF (1.5 mL of 1.0 M thf solution, 1.5 mmol) at 22 °C. The resulting solution was allowed to stir at 22 °C for 1.5 h. Then the reaction was quenched by addition of an aqueous saturated solution of NH₄Cl (10 ml). The resulting solution was washed with Et₂O (10 ml), and the combined organic layers was concentrated *in vacuo* to afford a pale yellow oily residue, which was purified by silica gel chromatography (50:1 hexanes/Et₂O, R_f 0.30) to deliver the desired a terminal alkyne as colorless oil (162 mg, 0.95 mmol, 95% yield). **(*R,E*)-(3-Methylhex-1-en-5-yn-1-yl)benzene**: IR (neat): 3301 (m), 3026 (w), 2961 (m), 2924 (m), 1493 (m), 1449 (m), 1429 (w), 1071 (w), 1029 (w), 965 (s), 747 (s), 693 (s), 634 (s), 515 (w) cm⁻¹; **¹H NMR (CDCl₃, 400 MHz)**: δ 7.39–7.36 (2H, m), 7.33–7.29 (2H, m), 7.24–7.19 (1H, m), 6.43 (1H, d, *J* = 16.4 Hz), 6.22 (1H, dd, *J* = 16.4, 7.2 Hz), 2.58 (1H, q, *J* = 7.2 Hz), 2.34 (1H, ddd, *J* = 16.8, 7.2, 2.4 Hz), 2.27 (1H, ddd, *J* = 16.8, 7.2, 2.4 Hz), 2.01 (1H, t, *J* = 2.4 Hz), 1.22 (3H, d, *J* = 6.4 Hz); **¹³C NMR (CDCl₃, 100 MHz)**: δ 137.6,

134.4, 129.1, 128.6, 127.3, 126.3, 82.9, 69.8, 36.3, 26.3, 19.7. **HRMS (ESI⁺)**: Calcd for C₁₃H₁₅ [M+H]⁺: 171.1174; Found: 171.1175. Specific rotation: [α]_D^{20.9} -29.9 (*c* 1.56, CHCl₃) for an enantiomerically enriched sample of 90:10 er.

Enantiomeric purity was determined by GC analysis in comparison with authentic racemic material; CDB-DM column, 70 °C, 15 psi.



Retention Time	Area	Area%	Retention Time	Area	Area%
331.684	277.73416	49.62742	316.132	3538.04248	90.44695
344.920	281.90439	50.37258	340.621	356.63058	9.55305

4,4,5,5-Tetramethyl-2-((*R*,1*E*,5*E*)-4-methyl-6-phenylhexa-1,5-dien-1-yl)-1,3,2-dioxaborolane (**2.61**)

In a nitrogen-filled glove box, an oven-dried flask equipped with a stir bar was charged with imidazolium salt **2.54** (37.5 mg, 0.10 mmol, 10.0 mol %), CuCl (10 mg, 0.10 mmol, 10.0 mol%), NaOt-Bu (19 mg, 0.2 mmol, 20 mol %) and thf (3.0 mL). The vessel was sealed with a septum and the solution was allowed to stir at 22 °C for 1 h. Bis(pinacolato)diboron (279 mg, 1.1 mmol, 1.1 equiv) was added to the solution, causing it to turn dark brown immediately. The vial was re-sealed and removed from the glove box. The mixture was allowed to stir at 22 °C for 30 min under an atmosphere of N₂. The terminal alkyne obtained from last step (170 mg, 1.0 mmol, 1.0 equiv) and MeOH (82 μL, 2.0 mmol, 2.0 equiv) were added by syringe. The resulting solution was allowed to stir at 22 °C for 24 hours before the reaction was quenched by passing the mixture through a short plug of celite and silica gel and eluted with Et₂O (3 × 20 mL). The filtrate was concentrated *in vacuo* to provide yellow oil, which was purified by silica gel chromatography (10:1 hexanes/Et₂O, R_f 0.45) to afford alkenyl-B(pin) **2.61** 255 mg as colorless oil (81% yield). **4,4,5,5-Tetramethyl-2-((*R*,1*E*,5*E*)-4-methyl-6-phenylhexa-1,5-dien-1-yl)-1,3,2-dioxaborolane (**2.61**): IR (neat): 3025 (w), 2976 (m), 2927 (w), 1637 (s), 1599 (w), 1493 (w), 1449 (w), 1396 (m), 1359 (s), 1318 (s), 1269 (m), 1231 (m), 1214 (m), 1164 (m), 1142 (s), 1112 (w), 1072 (w), 995 (m), 966 (s), 909 (w), 882 (w),**

848 (s), 786 (w), 746 (s), 693 (s), 648 (w), 578 (w) cm^{-1} ; $^1\text{H NMR}$ (CDCl_3 , 400 MHz): δ 7.35–7.33 (2H, m), 7.31–7.26 (2H, m), 7.21–7.17 (1H, m), 6.62 (1H, dt, $J = 17.6, 7.2$ Hz), 6.36 (1H, d, $J = 16.0$ Hz), 6.15 (1H, dd, $J = 16.0, 7.2$ Hz), 5.47 (1H, app. d, $J = 17.6$ Hz), 2.50–2.43 (1H, m), 2.37–2.30 (1H, m), 2.24–2.17 (1H, m), 1.26 (1H, d, $J = 9.2$ Hz), 1.11 (1H, d, $J = 6.8$ Hz); $^{13}\text{C NMR}$ (CDCl_3 , 100 MHz): δ 152.5, 137.9, 136.1, 128.6, 128.3, 127.0, 126.2, 83.2, 69.8, 43.6, 36.4, 24.9, 20.2. **HRMS** (ESI^+): Calcd for $\text{C}_{19}\text{H}_{28}\text{BO}_2$ $[\text{M}+\text{H}]^+$: 316.2448; Found: 316.2436. Specific rotation: $[\alpha]_{\text{D}}^{21.4} -44.2$ (c 1.13, CHCl_3) for an enantiomerically enriched sample of 90:10 er.

((1*E*,3*R*,5*E*,7*S*)-3,7-Dimethylnona-1,5,8-trien-1-yl)benzene (**2.62**)

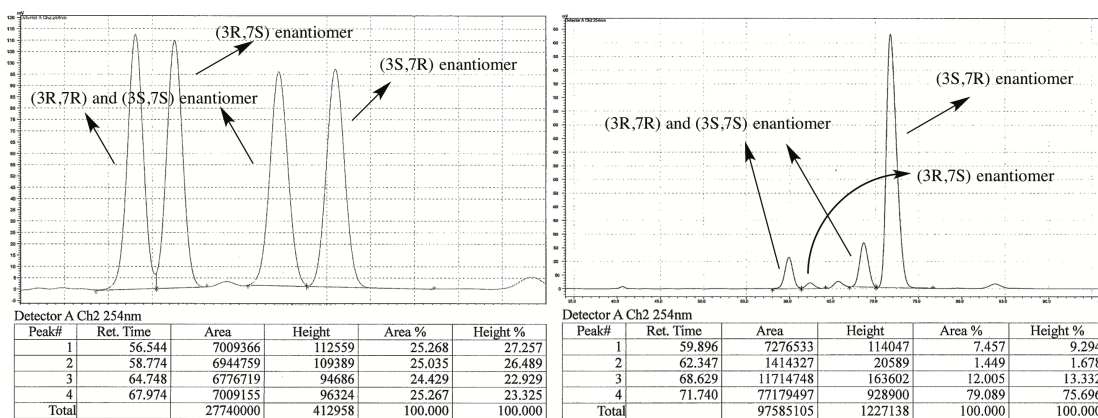
An oven-dried 1-dram vial equipped with a stir bar was charged with imidazolium salt **2.70** (37 mg, 50 μmol), NaOMe (81 mg, 1.5 mmol), and CuCl (25 mg, 250 μmol) in a nitrogenfilled glove box. The vial was sealed with septum and electrical tape, and removed from the glove box. Thf (8.0 mL) was added and the mixture was allowed to stir for 1 h under N_2 at 22 $^\circ\text{C}$. The mixture turned bright yellow. Alkenyl-B(pin) **2.61** (315 mg, 1.0 mmol) was added to the solution, which was allowed to stir for an additional 20 min. Allylic phosphate **2.52** (208 mg, 0.10 mmol) was weighed into another oven-dried vial and degassed *in vacuo*. The substrate **2.61** in thf (2.0 mL) was transferred to the mixture with syringe and the resulting solution was allowed to stir for 24 h at 22 $^\circ\text{C}$. The mixture was passed through a short plug of silica gel and eluted with Et_2O . The organic layer was concentrated *in vacuo*, resulting in yellow oil, which was purified by silica gel chromatography (100% hexanes, R_f 0.40) to afford 208 mg of **2.62** product as colorless oil (0.92 mmol, 92% yield of a mixture of 80:20 anti:syn diastereomer). ((1*E*,3*R*,5*E*,7*S*)-3,7-Dimethylnona-1,5,8-trien-1-yl)benzene (**2.62**): **IR** (**neat**): 3081 (w), 3060 (w), 3025 (w), 2962 (w), 2925 (w), 2869 (w), 1636 (w), 1599 (w), 1493 (w), 1450 (w), 1413 (w), 1371 (w), 1071 (w), 1028 (w), 992 (w), 965 (m), 911 (m), 746 (m), 692 (m) cm^{-1} ; $^1\text{H NMR}$ (CDCl_3 , 400 MHz): δ 7.38–7.35 (2H, m), 7.33–7.28 (2H, m), 7.23–7.19 (1H, m), 6.36 (1H, d, $J = 16.0$ Hz), 6.16 (1H, dd, $J = 16.0, 7.2$ Hz), 5.81 (1H, dddd, $J = 17.2, 10.4, 6.4, 2.0$ Hz), 5.45–5.42 (2H, m), 5.03–4.92 (2H, m), 2.87–2.83 (1H, m), 2.42–2.35 (1H, m), 2.20–2.14 (1H, m), 2.12–2.05 (1H, m), 1.10 (3H, d, $J = 6.4$ Hz), 1.09 (3H, d, $J = 6.4$ Hz); $^{13}\text{C NMR}$ (CDCl_3 , 100 MHz): δ 143.4, 138.1, 136.5, 135.9, 128.6, 128.2, 127.3, 126.9, 126.1, 40.5, 40.3, 37.4, 30.5, 20.2, 20.0. **HRMS** (ESI^+): Calcd for $\text{C}_{17}\text{H}_{23}$ $[\text{M}+\text{H}]^+$: 227.1800; Found: 227.1789. Specific rotation: $[\alpha]_{\text{D}}^{23.1} -142.7$ (c 0.21, CHCl_3) for an enantiomerically enriched sample of 98:2 er.

(3*S*,4*E*,7*R*,8*E*)-3,7-Dimethyl-9-phenylnona-4,8-dien-1-ol (**2.63**)

To an oven-dried 1-dram vial equipped with a stir bar was added was added 9-BBN dimer (20.0 mg, 0.084 mmol) and thf (0.5 mL) under nitrogen. The solution was allowed to cool to 0 $^\circ\text{C}$ and was added slowly a solution of triene **2.62** (18.4 mg, 0.084

mmol) in thf (0.5 mL). The solution was then allowed to warm to 22 °C and stirred for 8 h. Then 1 mL of water and sodium perborate tetrahydrate (129 mg, 0.25 mmol) were added slowly. The resulting white suspension was allowed to stir for 2 h, after which Et₂O (1 mL) was added to the mixture. The layers were separated, the aqueous phase was washed with Et₂O (3 x 1mL), and the combined organic layers were dried over MgSO₄, filtered and concentrated *in vacuo*, resulting in yellow oil that was purified by silica gel chromatography (2:1 hexanes/EtOAc, R_f 0.57) to afford 20.3 mg of the desired product **2.63** as colorless oil (0.075 mmol, 98% yield of a mixture of 80:20 anti:syn diastereomer). **(3S,4E,7R,8E)-3,7-Dimethyl-9-phenylnona-4,8-dien-1-ol (2.63)**: IR (neat): 3352 (br), 3025 (w), 2957 (m), 2925 (m), 2869 (m), 1649 (w), 1598 (w), 1493 (w), 1450 (m), 1373 (m), 1259 (w), 1216 (w), 1050 (m), 1028 (m), 964 (s), 911 (w), 848 (w), 745 (s), 692 (s), 667 (w), 601 (w), 522 (w), 403 (w) cm⁻¹; ¹H NMR (CDCl₃, 400 MHz): δ 7.36–7.34 (2H, m), 7.34–7.28 (2H, m), 7.21–7.17 (1H, m), 6.34 (1H, d, *J* = 16.4 Hz), 6.13 (1H, dd, *J* = 16.4, 7.8 Hz), 5.46–5.38 (1H, m), 5.35–5.27 (1H, m), 3.63 (2H, dt, *J* = 6.4, 1.2 Hz), 2.40–2.33 (1H, m), 2.29–2.22 (1H, m), 2.17–2.03 (2H, m), 1.62–1.44 (2H, m), 1.08 (3H, d, *J* = 6.8 Hz), 0.99 (3H, d, *J* = 6.8 Hz); ¹³C NMR (CDCl₃, 100 MHz): δ 138.0, 137.7, 136.4, 128.6, 128.3, 127.2, 127.0, 126.1, 61.1, 40.2, 39.9, 37.4, 34.1, 21.4, 20.0. HRMS (ESI⁺): Calcd for C₁₇H₂₃O [M+H]⁺: 243.1758; Found: 243.1749. Specific rotation: [α]_D^{23.6} –37.3 (*c* 1.61, CHCl₃) for an enantiomerically enriched sample of 98:2 er.

Enantiomeric purity was determined by HPLC analysis in comparison with authentic racemic material; Chiralpak AZ–H column, 99.5:0.5 hexanes/ *i*PrOH, 0.3 mL/min, 254 nm.



Retention Time	Area	Area%	Retention Time	Area	Area%
56.544	7009166	25.268	59.896	7276533	7.457
58.774	6944759	25.035	62.347	1414327	1.449
64.748	6776719	24.429	68.629	11714748	12.005
67.974	7009155	25.267	71.740	77179497	79.089

The Influence of the Alkyne Substituents on the Efficiency of Cross-metathesis Reactions

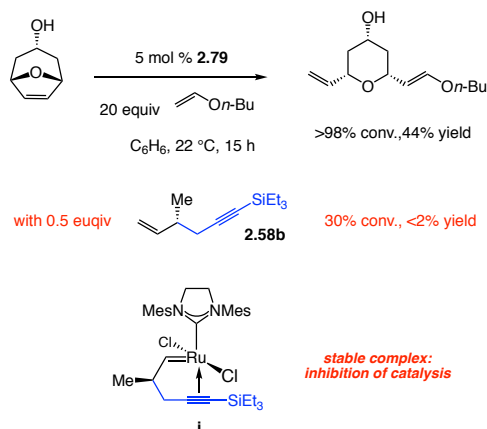
For the catalytic CM stage in the above sequence, use of the more sterically hindered silyl unit [$(i\text{-Pr})_3\text{Si}$ in **2.58** vs Me_3Si] was based on two reasons: ease of product isolation, as the smaller silyl unit renders the EAS product inconveniently volatile, and the facility of the subsequent catalytic CM step. The latter issue revealed to us a number of unappreciated factors regarding this important class of CM reactions.

We first evaluated the feasibility of using triethylsilyl-substituted enyne **2.58b**, since it is generated with similar efficiency and selectivity as **2.58**, while being sufficiently non-volatile so that it can be purified and isolated with relative ease. Still, as illustrated in Scheme S8a, CM of **2.58b** with styrene under the same conditions as used for **2.58** led to only 5–10% conv. Moreover, use of Ru-based carbene **2.79**²⁹ as catalyst precursor resulted in relatively facile substrate consumption but yielded an assortment of products among which only the identity of 1,3-diene **2.80** could be established (18%); in all likelihood, **2.80** is formed from reaction with ethylene generated from homocoupling of styrene or **2.58b**.³⁰ Further optimization revealed that, at best, with 2.0 equiv styrene at 60 °C (open vessel), **2.60b** may be obtained in 32% yield after 3.0 h (84% conv). Control experiments indicated that low efficiency of the aforementioned CM process is probably due to catalyst deactivation caused by the alkyne unit;³¹ this hypothesis is supported by the substantially higher efficiency observed with **2.58** wherein the acetylene group is shielded by a sterically more demanding silyl moiety.

(29) Garber, S. B.; Kingsbury, J. S.; Gray, B. L.; Hoveyda, A. H. *J. Am. Chem. Soc.* **2000**, *122*, 8168–8179.

(30) For a review on catalytic enyne metathesis reactions, see: Diver, S. T.; Giessert, A. J. *Chem. Rev.* **2004**, *104*, 1317–1382.

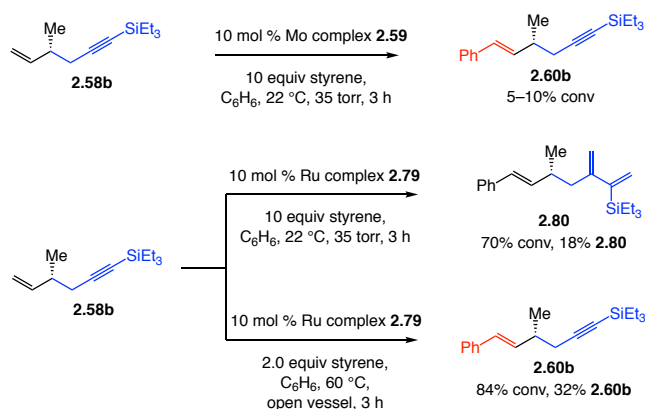
(31) When 0.5 equiv **2.58b** is introduced in a reaction where substrate consumption is observed within h (>98% conv, significant amount of cyclic alkene oligomerization), the reaction becomes significantly more sluggish and none of the product from ring-opening/cross-metathesis process, which occurs slower than oxabicyclic olefin oligomerization, is formed. Intermediacy of **i**, leading to sequestration of the Ru complex offers a plausible rationale for the observed reactivity trends.



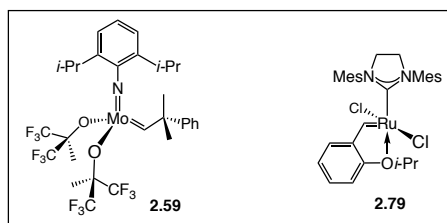
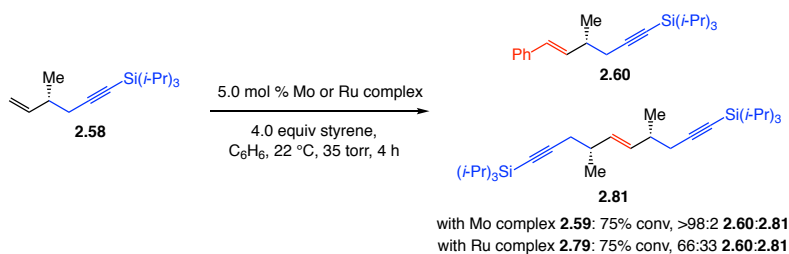
While alkylidene **2.59** and carbene **2.79** can be used for CM of **2.58** and styrene, the former Mo complex is preferable because a significant amount of homocoupling byproduct remains in the mixture when the Ru carbene is employed (Scheme S5b). This is likely because the more active **2.59** is able to react with the relatively hindered internal alkene of **2.81** to re-generate **2.58** and its corresponding Mo alkylidene, which can then undergo transformation with styrene to generate **2.60**.³² The above findings reveal a critical attribute of the catalytic EAS reaction: synthesis and structural modification of enantiomerically enriched 1,5-enynes seem to pose complications that do not apply to the products derived from addition of other C-based moieties. Such distinction originates from the strong propensity of alkynyl units to associate with transition metal salts, giving rise to catalyst inhibition.

Scheme S8. Representative Data for Catalytic Cross-Metathesis of Enynes with Styrene

a. Preliminary studies with (triethyl)silyl-substituted alkene **2.58b**:



b. Preliminary studies with (tri-*iso*-propyl)silyl-substituted alkene **2.58**:



(32) For studies regarding the ability of Mo complex **2.59** to reverse a homocoupling reaction involving two terminal alkenes, see: Xu, Z.; Johannes, C. W.; Houry, A. F.; La, D. S.; Cogan, D. A.; Hofilena, G. E.; Hoveyda, A. H. *J. Am. Chem. Soc.* **1997**, *119*, 10302–10316.

Density Functional Theory (DFT) calculations

DFT³³ computations were performed with the Gaussian 09 suite of programs³⁴ employing the dispersion corrected ω B97XD functional.^{35,36} The LANL2DZ basis set was used for geometry optimizations and evaluation of thermal corrections to the Gibbs free energy at standard conditions (298.15 K, 1 atm). The nature of all stationary points was checked through vibrational analysis. Several of the located transition states have been verified through IRC calculations employing the L(ocal) Q(uadratic) A(approximation) method.³⁷ The geometries for model System 1 (SYS1, cf. Scheme S9 below) have further been re-optimized with the larger Def2SVP³⁸ basis set. Single point electronic energy (ΔE_{sp}) calculations applying functionals ω B97XD and M06³⁹ in solution (tetrahydrofuran and dichloromethane) with the SMD solvation model⁴⁰ were performed on the gas phase geometries obtained with LANL2DZ or Def2SVP and the larger Def2TZVPP³⁸ basis set. The single point electronic energies (ΔE_{sp}) at the Def2TZVPP level were corrected by addition of thermal corrections to the Gibbs free energy (ΔG_{corr}) obtained at the corresponding LANL2DZ or Def2SVP level. Tables of electronic and free energies with

(33) For a recent review on the application of DFT to complexes containing transition metals, see: Cramer, C. J.; Truhlar, D. G. *Phys. Chem. Chem. Phys.* **2009**, *11*, 10757.

(34) Frisch, M. J.; Trucks, G. W.; Schlegel, H. B.; Scuseria, G. E.; Robb, M. A.; Cheeseman, J. R.; Scalmani, G.; Barone, V.; Mennucci, B.; Petersson, G. A.; Nakatsuji, H.; Caricato, M.; Li, X.; Hratchian, H. P.; Izmaylov, A. F.; Bloino, J.; Zheng, G.; Sonnenberg, J. L.; Hada, M.; Ehara, M.; Toyota, K.; Fukuda, R.; Hasegawa, J.; Ishida, M.; Nakajima, T.; Honda, Y.; Kitao, O.; Nakai, H.; Vreven, T.; Montgomery, Jr., J. A.; Peralta, J. E.; Ogliaro, F.; Bearpark, M.; Heyd, J. J.; Brothers, E.; Kudin, K. N.; Staroverov, V. N.; Kobayashi, R.; Normand, J.; Raghavachari, K.; Rendell, A.; Burant, J. C.; Iyengar, S. S.; Tomasi, J.; Cossi, M.; Rega, N.; Millam, J. M.; Klene, M.; Knox, J. E.; Cross, J. B.; Bakken, V.; Adamo, C.; Jaramillo, J.; Gomperts, R.; Stratmann, R. E.; Yazyev, O.; Austin, A. J.; Cammi, R.; Pomelli, C.; Ochterski, J. W.; Martin, R. L.; Morokuma, K.; Zakrzewski, V. G.; Voth, G. A.; Salvador, P.; Dannenberg, J. J.; Dapprich, S.; Daniels, A. D.; Farkas, Ö.; Foresman, J. B.; Ortiz, J. V.; Cioslowski, J.; Fox, D. J. *Gaussian 09, Revision D.01*, Gaussian, Inc., Wallingford CT, 2009.

(35) Chai, J.-D.; Head-Gordon, M. *Phys. Chem. Chem. Phys.*, **2008**, *10*, 6615.

(36) For supporting mechanistic studies suggesting the use of dispersion corrected density functionals, see: (a) Torker, S.; Merki, D.; Chen, P. *J. Am. Chem. Soc.* **2008**, *130*, 4808. (b) Zhao, Y.; Truhlar, D. G. *Org. Lett.* **2007**, *9*, 1967. (c) Minenkov, Y.; Occhipinti, G.; Singstad, A.; Jensen, V. R. *Dalton Trans.* **2012**, *41*, 5526.

(37) (a) Page, M.; McIver Jr., J. W. *J. Chem. Phys.* **1988**, *88*, 922–935. (b) Page, M.; Doubleday Jr., C.; McIver Jr., J. W. *J. Chem. Phys.* **1990**, *93*, 5634–5642.

(38) Weigend, F.; Ahlrichs, R. *Phys. Chem. Chem. Phys.* **2005**, *7*, 3297–3305.

(39) Zhao, Y.; Truhlar, D. G. *Acc. Chem. Res.* **2008**, *41*, 157.

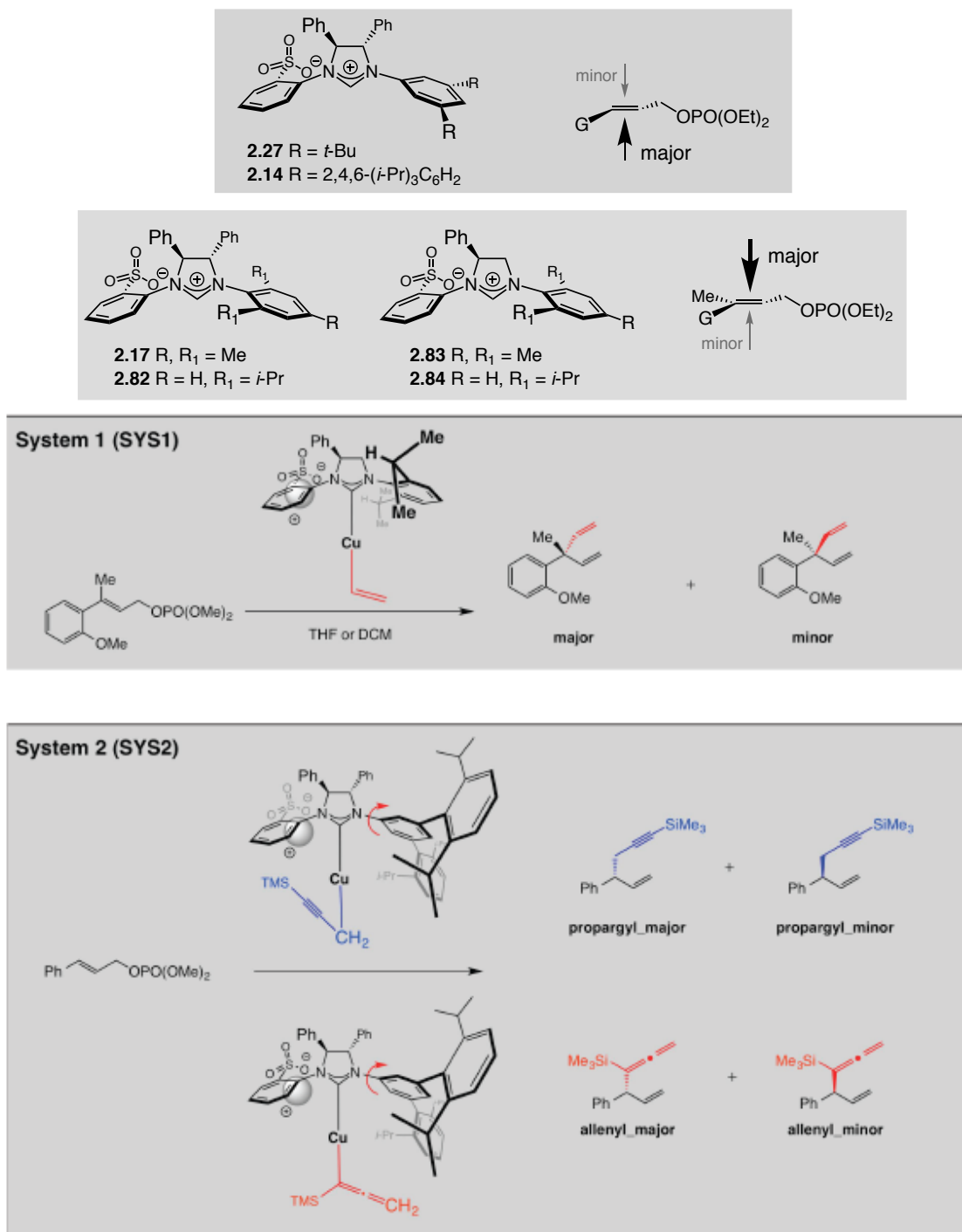
(40) Marenich, A. V.; Cramer, C. J.; Truhlar, D. G. *J. Phys. Chem. B*, **2009**, *113*, 6378–6396.

functionals ω b97XD and M06 after geometry optimization and single point energy calculation and the geometries obtained with ω B97XD/ LANL2DZ or Def2SVP.

Model systems under investigation

We have chosen vinyl addition to substrate **2.44b** (cf. Table 2.5 in manuscript) with ligand **2.82** to derive the general stereochemical model for EAS reactions promoted by sulfonate-based NHC–Cu complexes containing 2,6-disubstituted aryl rings [System 1 (SYS1) in Scheme S9].⁴¹ Likewise, propargyl and allenyl addition in presence of **2.29**, containing a 3,5-disubstituted aryl ring, to generate products with a reversal in enantioselectivity was modeled as shown in [System 2 (SYS2) in Scheme S9]. Based on the assumption that the entire ligand structure would be crucial for enantioselectivity, removal of para-substituents and exchange of ethyl for methyl groups on the phosphate were the only truncations performed. In the following sections, the structures in the pathways leading to the major and minor enantiomers are denoted “**major**” and “**minor**”, extended by the identity of the transferred nucleophile (e.g. **propargyl_major** vs **allenyl_major**).

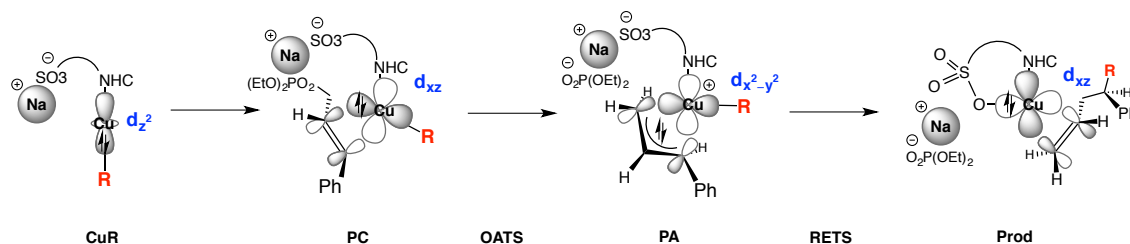
(41) For the corresponding experimental data, see: Gao, F.; Carr, J. L.; Hoveyda, A. H. *Angew. Chem., Int. Ed.* **2012**, *51*, 6613–6617.



Scheme S9. Model systems studied computationally for EAS reactions promoted by sulfonate NHC-Cu complexes.

Nomenclature

In addition to the **major** and **minor** nomenclature (cf. Scheme S9) we denoted the type of intermediate and transition state as following (Scheme S10): **CuR** stands for the linear Cu(I) species, wherein R can be vinyl (**Cu_vinyl**), propargyl (**Cu-propargyl** = **A** in Figure 2 in manuscript) or allenyl (**Cu_allenyl** = **B** in Figure 2 manuscript). **PC** is used for π -complexes, **OATS** for transition states leading to oxidative addition to generate **PA** (i.e. the π -allyl complex). Through the transition state for reductive elimination (**RETS**) π -complexes between the product and Cu(I) are generated (**Prod**). Furthermore, **TS_iso** (= **TS_{iso}** in manuscript) is used for isomerization between **Cu_propargyl** (= **A** in manuscript) and **Cu_allenyl** (= **B** in manuscript) in System 2 (cf. Figure 2 in manuscript). As mentioned below, in certain pathways, no π -allyl intermediate (**PA**) and hence reductive elimination transition state (**RETS**) could be located.



Scheme S10. Reaction sequence for EAS reactions promoted by sulfonate NHC–Cu complexes.

The role of the sulfonate group

Initially we investigated the strength of the $\text{SO}_3\text{--Cu}$ interaction (Figures S1–S3). Calculations in gas phase predict a minimum for structure **1.51** (cf. Figure 1.3 in Chapter 1) with a Cu–O distance of 2.49 Å (Figure S1). This structure is 7.7 kcal/mol higher in energy than **1.53**; in the latter the sulfonate is *anti* to the phenyl ring on the backbone with a Cu–O distance of 4.44 Å. Geometry **1.52**, wherein the Cu–O distance has been constrained to 2.30 Å, is not a minimum and 6.1 kcal/mol higher in energy than **1.53**.

Comparison of **1.57** and **1.56** with the corresponding structures of the (NHC– SO_3)–Zn– Me_2 anion (Figure S2) reveals that sulfonate dissociation from **Zn1** ($E_{\text{rel}} = 0.0$ kcal/mol) is only weakly exothermic with $\omega\text{-B97XD/Def2SVP}$ in gas phase to yield **Zn2** (–0.7 kcal/mol) via transition state **Zn12** and slightly more exothermic with the Def2TZVPP basis set in THF (–3.3 kcal/mol). Part of the calculated exothermicity originates from release of steric repulsion due to rotation of the Me_2Zn fragment from **Zn1** to **Zn2**. Constraining the Me–Zn–C–N angle to 32.3, 27.3, 22.3 and 17.3 ° (cf. **Zn3**) as opposed to 102.3 ° in **Zn2** partly corrects for the strain release so that sulfonate dissociation from **Zn1** becomes less exothermic (–2.4, –2.1, –1.8 and –1.4 kcal/mol,

respectively with ω -B97XD/Def2TZVPP in THF). This trend illustrates the significantly greater Lewis acidity of Zn(II) vs Cu(I).

The propensity of the sulfonate group to stabilize Cu(III) intermediates has been evaluated by comparison of free energies of η^1 - and η^3 -allyl species relative to **Cu_propargyl** (= **A**). While calculations in gas phase with the small LANL2DZ basis set show that η^1 -allyl structures are favored due to minimal charge separation, there is a preference for η^3 -allyl species in solution (THF) and/or with the larger basis set (Figure S3).

Sulfonate binding 1 – *syn* vs *anti* orientation in (NHC-SO₃)–Cu–Me anion (cf. Scheme 1.3 in Chapter 1)

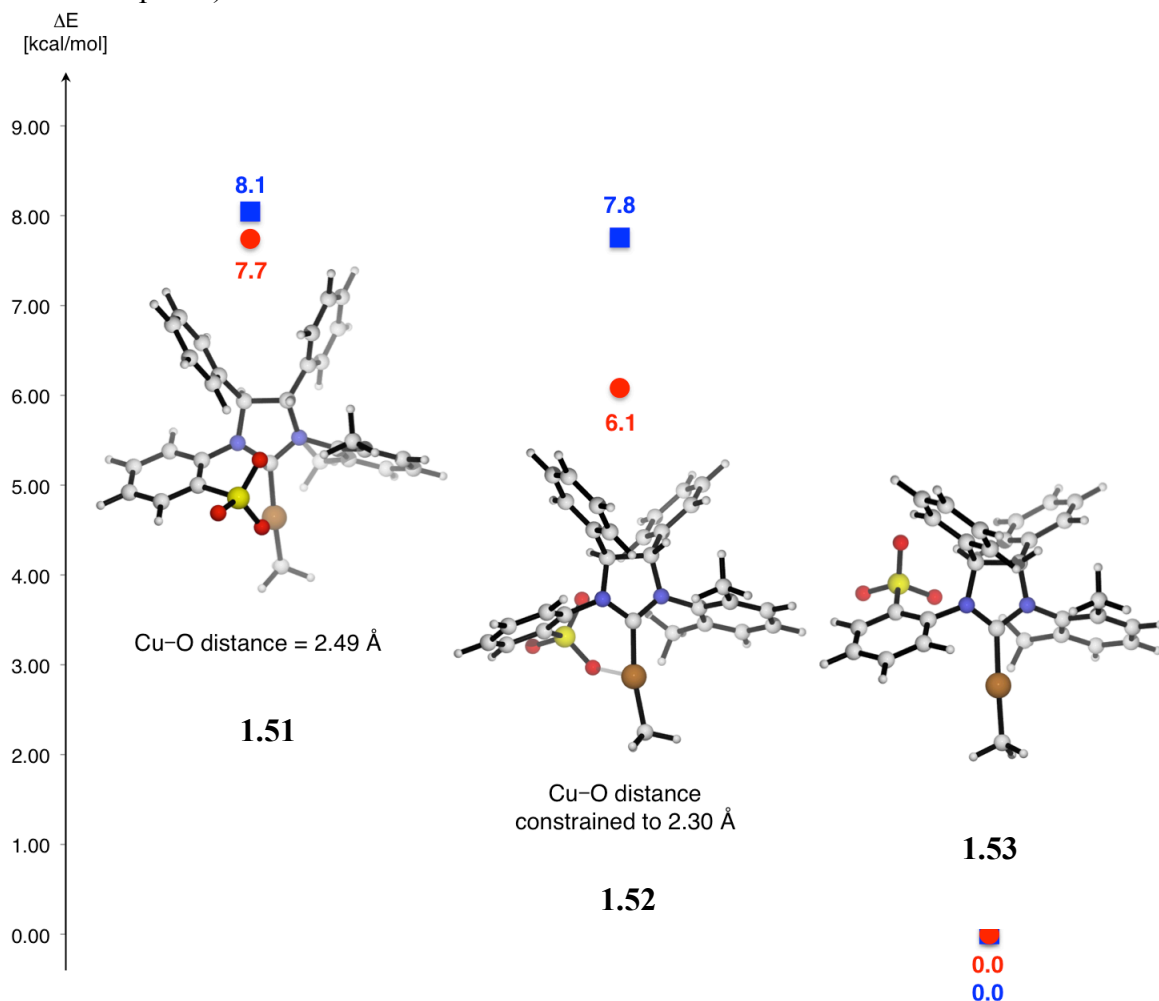


Figure S1. Comparison of SO₃-binding in anionic NHC–Cu–Me complexes [electronic energy in kcal/mol with ω B97XD/Def2SVP (blue squares) and ω -B97XD/Def2TZVPP_{THF(SMD)}/ ω -B97XD/Def2SVP_{gas-phase} (red circles)].}

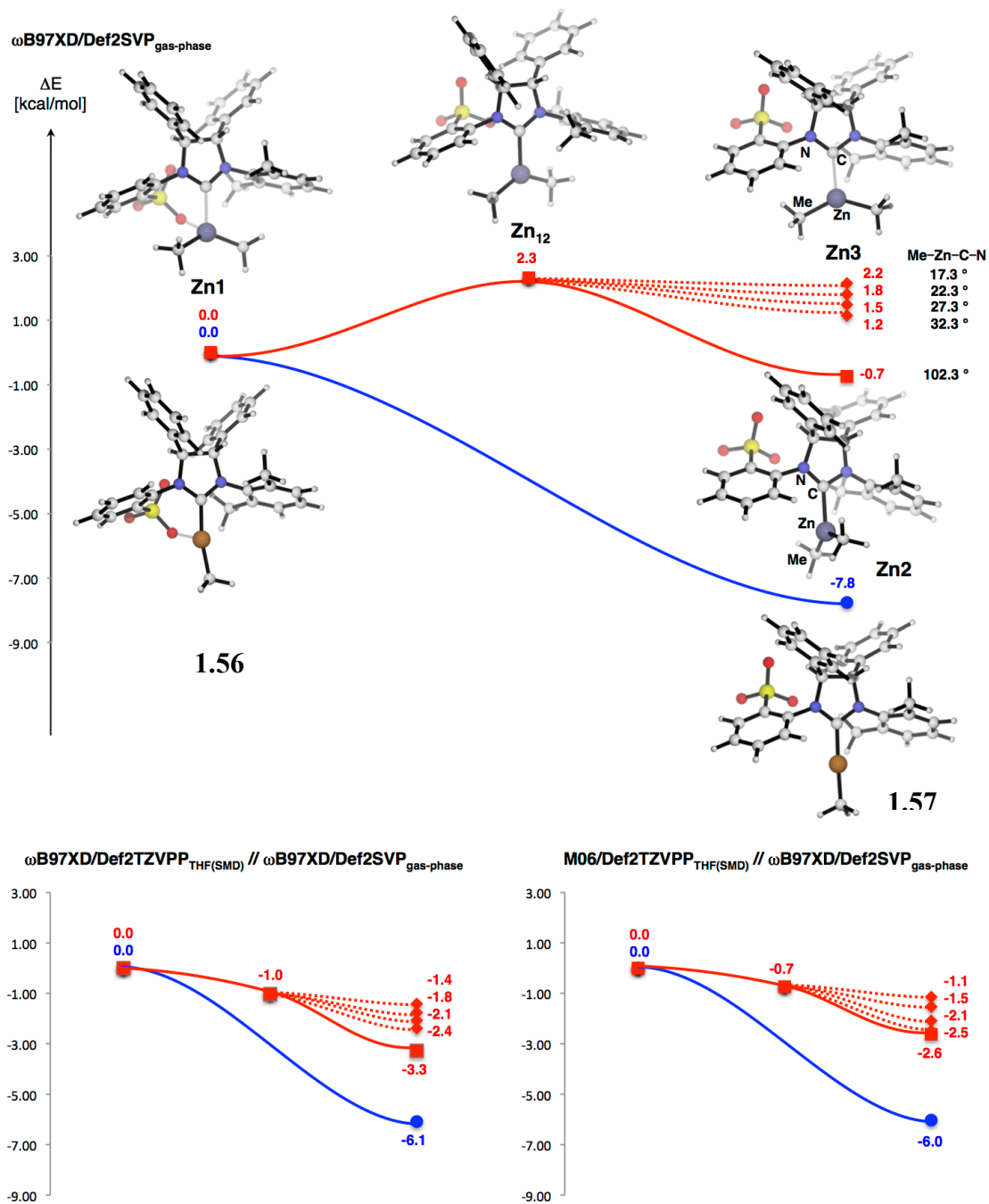
Sulfonate binding 2 – (NHC-SO₃)-Cu-Me anion vs (NHC-SO₃)-Zn-Me₂ anion

Figure S2. Comparison of SO₃-binding in NHC-Cu-Me and NHC-Zn-Me₂ anions (electronic energy in kcal/mol at various levels of theory after optimization with ω B97XD/Def2SVP in gas-phase). For geometries see SI in Reference 8.

Sulfonate binding 3 – η^1 vs η^3 -allyl species (cf. Scheme 1.9 in Chapter 1)

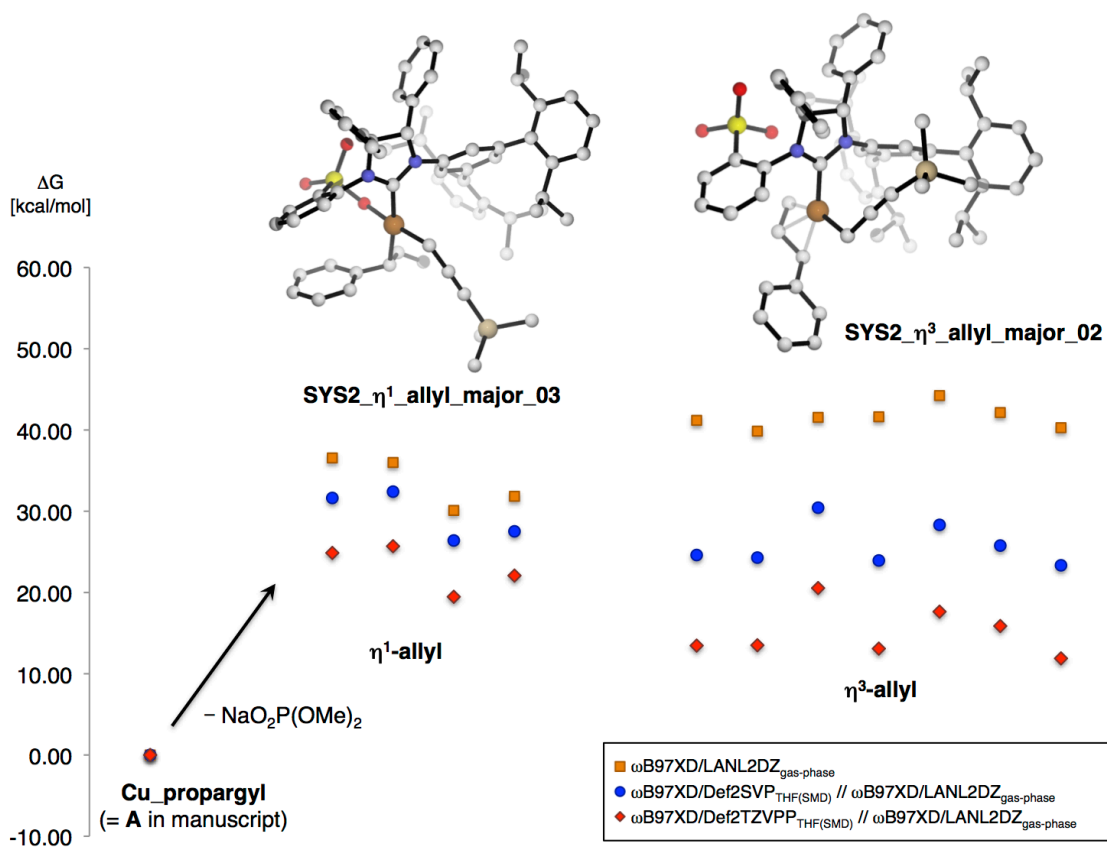


Figure S3. Comparison of SO_3 -binding in square planar Cu(III) intermediates as a function of basis set and solvation (THF); two representative structures are shown (for geometries see reference 8).

Pathways investigated for system 1 (SYS1)

In order to further test the most favorable orientation of the sulfonate group (*syn* or *anti* to the phenyl ring on the NHC backbone), the following pathways have been calculated for System 1 (SYS1, Figure S4).

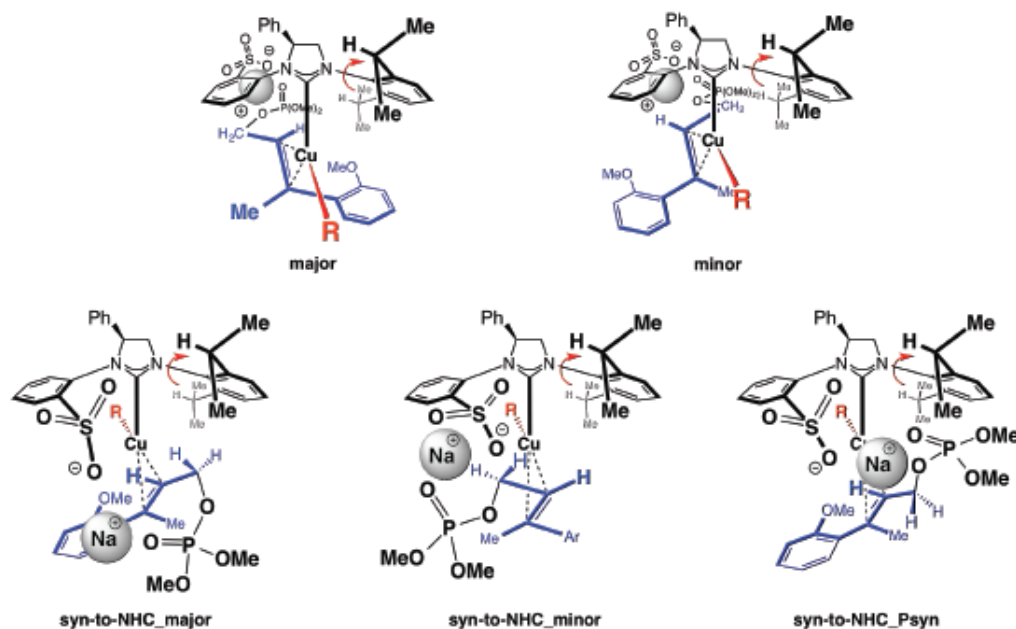


Figure S4. Investigated reaction pathways for system 1 (SYS1).

In pathways **major** and **minor** the sulfonate anion is situated *anti* to the phenyl ring on the NHC backbone, so that the nucleophilic group **R** (i.e. vinyl) is in the front. Alternatively, in pathways **syn-to-NHC_major** and **syn-to-NHC_minor** the sulfonate is on the same side as the backbone phenyl ring. In these cases, a bridging interaction between the sulfonate and the phosphate through the sodium cation is only possible if the **R** group is in the rear. Furthermore, we investigated the possibility when the phosphate anion is displaced on the same side as the Cu center during oxidative addition (**syn-to-NHC_Psyn**).

The energies (at the ω -B97XD or M06/Def2TZVPP_{DCM}(DCM)// ω -B97XD/LANL2DZ level) for several investigated rotamers (i.e. different orientation of the *ortho*-OMe-phenyl ring on the substrate or the vinyl group **R**) for each of the above mentioned intermediates and pathways are shown in Figure S5. For the corresponding geometries. For pathways **syn-to-NHC_major**, **syn-to-NHC_minor** and **syn-to-NHC_Psyn** no PA intermediate could be located, resulting in direct collapse of the OATS structure to the product complex (**Prod**).

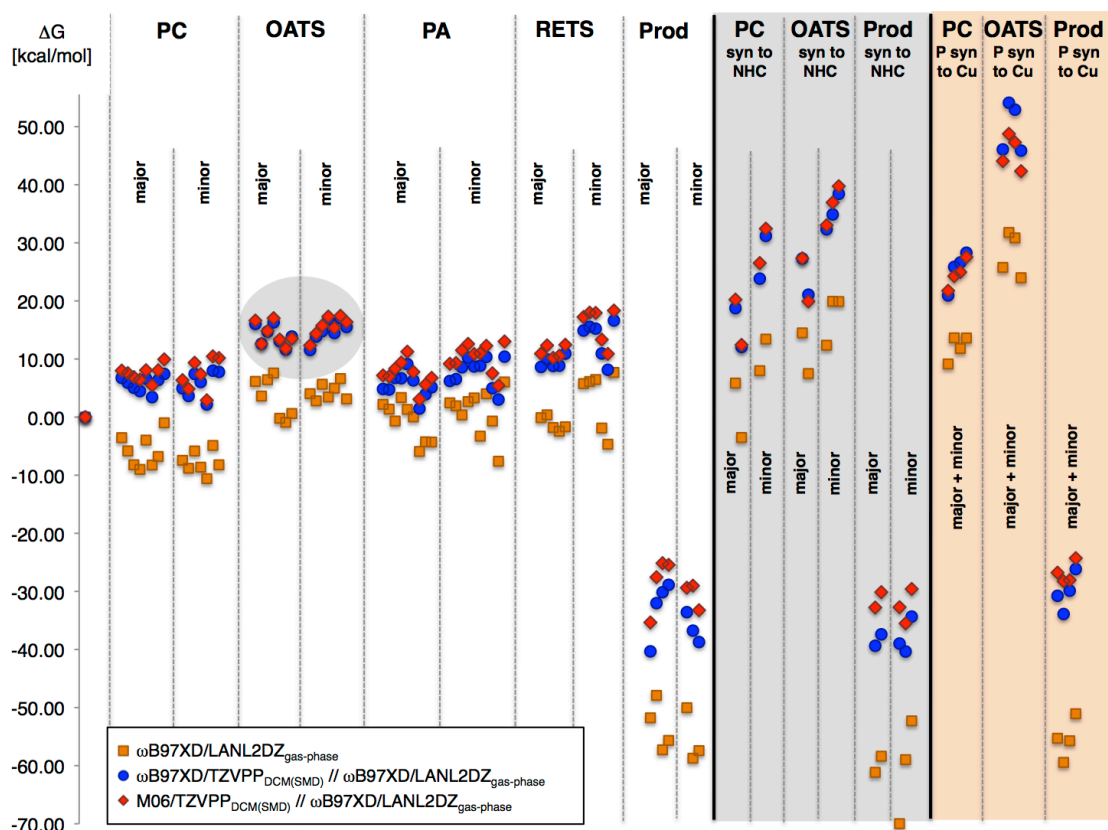


Figure S5. Computed free energies for several conformers of the pathways shown in Figure S4 with different levels of theory after geometry optimization with ω B97XD/LANL2DZ.

The energy span between the investigated conformers for **OATS_major** and **OATS_minor** (highlighted with round grey background in Figure S5) amounts to 5–10 kcal/mol, which underscores the difficulty associated with accurate determination of reaction pathways leading to major and minor enantiomers on the order of 2–3 kcal/mol for systems of such size and complexity. Nonetheless, pathways **syn-to-NHC_major**, **syn-to-NHC_minor** and **syn-to-NHC_Psyn** can be excluded since the energy difference relative to structures **OATS_major** and **OATS_minor** exceeds the “noise level” (5–10 kcal/mol). Plots of the free energy surfaces of the lowest energy conformers with different density functionals (ω B97XD and M06) and solvents (THF and DCM) predict similar energies for the pathways leading to major and minor enantiomers (Figure S6). For example, the energy difference between **SYS1_OATS_major** (11.8 kcal/mol) and **SYS1_OATS_minor** (12.3 kcal/mol) at the M06/Def2TZVPP_{DCM(SMD)}// ω -B97XD/LANL2DZ_{gas-phase} level of theory amounts to only 0.5 kcal/mol.

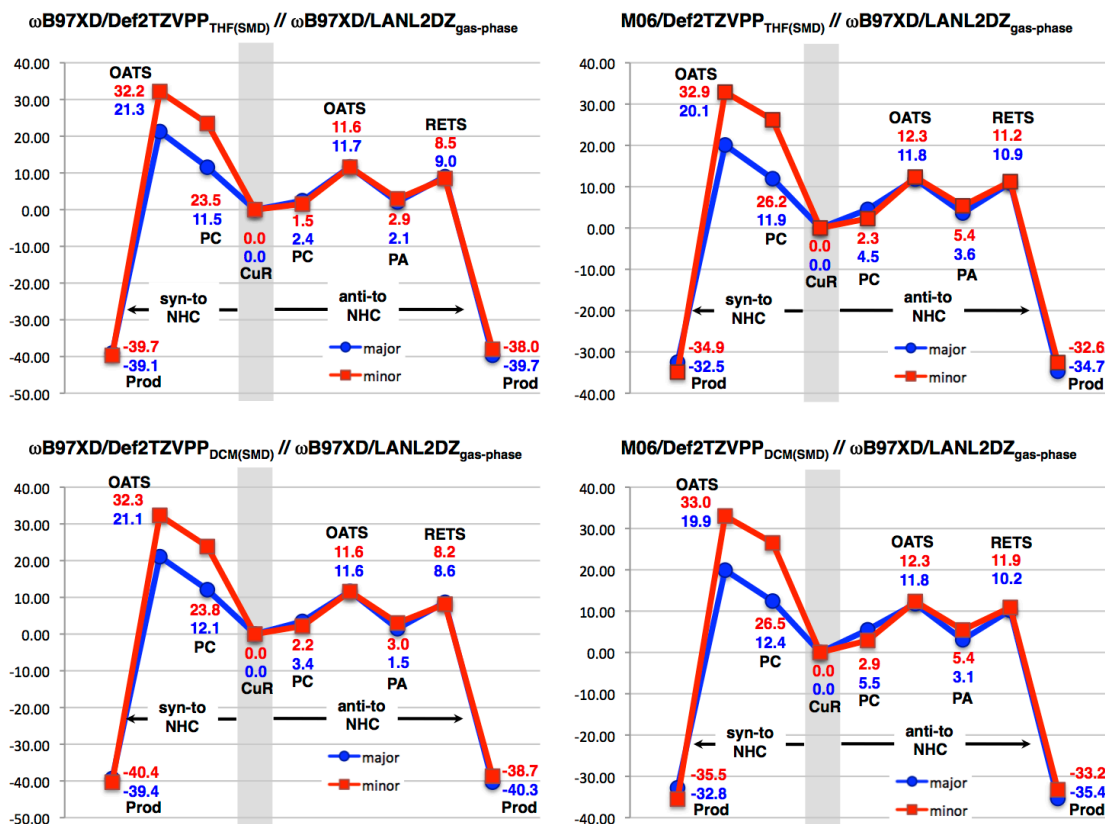


Figure S6. Computed free energies for the most stable conformers of the pathways shown in Figure S4 (except for **syn-to-NHC_Psyn**) with different density functionals (ω B97XD and M06) and solvents (THF and DCM) after geometry optimization with ω B97XD/LANL2DZ_{gas-phase}.

We have re-optimized the structures (cf. Figure S5) with the slightly larger Def2SVP basis set. Through this a larger energy difference between **OATS_{major}** and **OATS_{minor}**, in favor of the former, is predicted (highlighted with round grey background in Figure S7). For example, the energy difference between **SYS1_OATS_{major}** (16.9 kcal/mol) and **SYS1_OATS_{minor}** (20.2 kcal/mol) at the M06/Def2TZVPP_{DCM(SMD)}// ω -B97XD/Def2SVP_{gas-phase} level of theory amounts to 3.3 kcal/mol (Figure S8). Due to the considerable uncertainty of the obtained energy values (cf. Figures S5 and S7) it is not possible at this point to make a conclusive statement on basis of the calculations regarding the rate-limiting barrier (**OATS** vs **RETS**). This is furthermore complicated due to the significant increase in conformational complexity of the latter (i.e. **RETS**) as a result of the loosely associated sodium phosphate salt (cf. **PA** → **Prod** in Scheme S10).

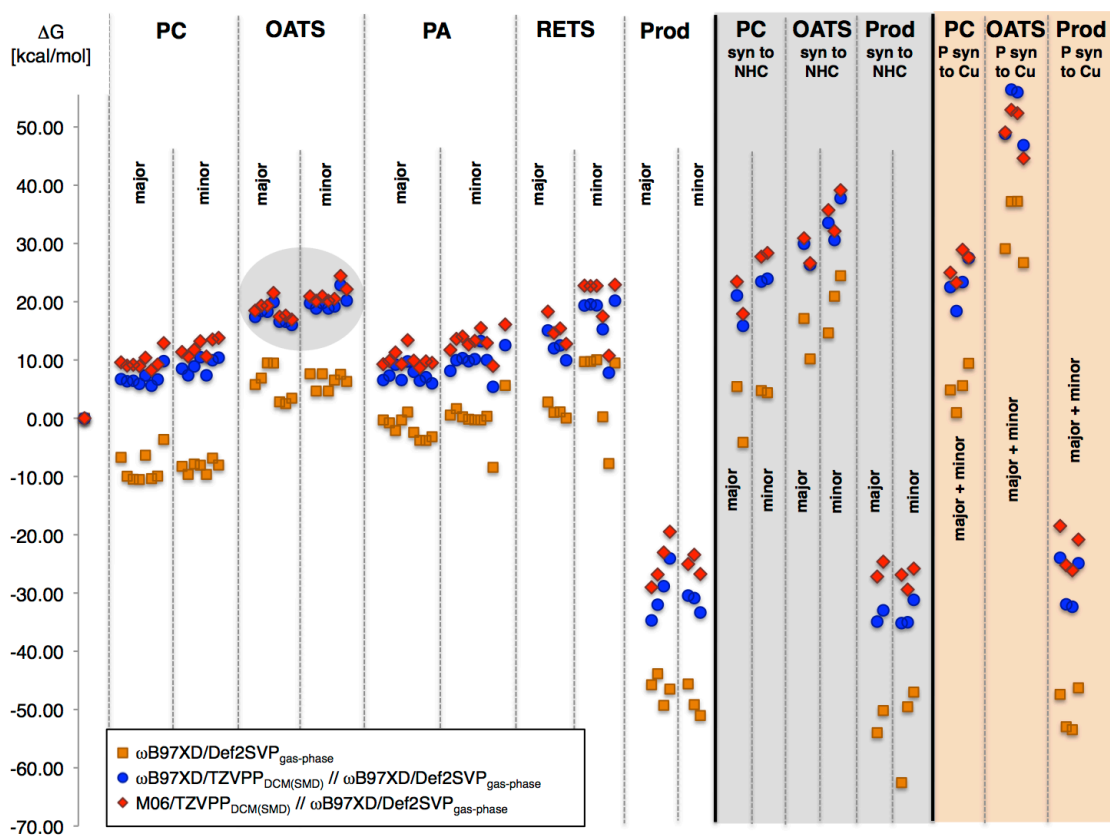


Figure S7. Computed free energies for several conformers of the pathways shown in Figure S4 with different levels of theory after geometry optimization with ω B97XD/Def2SVP.

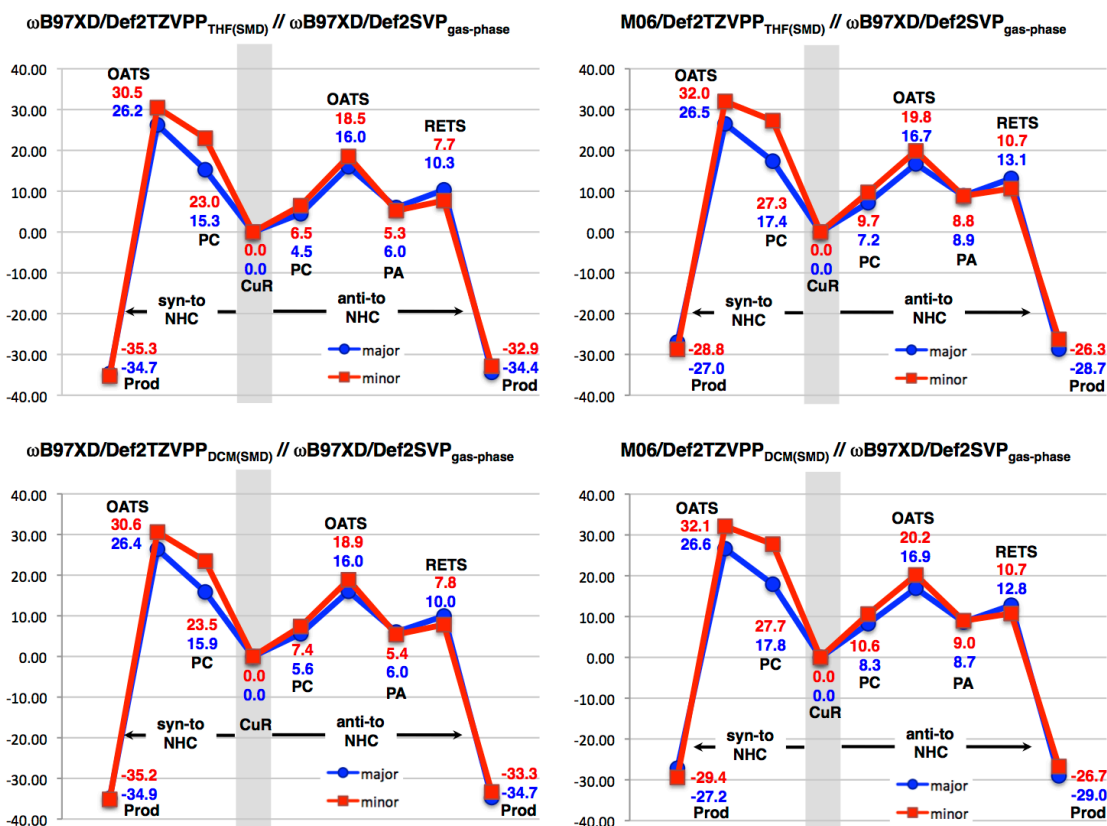


Figure S8. Computed free energies for the most stable conformers of the pathways shown in Figure S4 (except for **syn-to-NHC_Psyn**) with different density functionals (ω B97XD and M06) and solvents (THF and DCM) after geometry optimization with ω B97XD/Def2SVP_{gas-phase}.

Despite the above-mentioned difficulties, commonly occurring structural features in the various conformers of **PC/OATS_{major}** and **PC/OATS_{minor}** provide a hint regarding the stereo-controlling role of the sulfonate-based NHC ligand. $\text{Cu}(d_{xz}) \rightarrow \text{olefin}(\pi^*)$ donation rigidifies the allylic substrate, and as a consequence, the α -carbon atom (C_α) points towards the back isopropyl group of the 2,6-diisopropylphenyl ring in **PC_{minor}** (cf. Figure S9). This results in a tilt of the 2,6-diisopropylphenyl ring relative to the central 5-membered NHC ring (cf. side view in Figure S9). Therefore, the dihedral angle $C^{\text{ortho}}-C^{\text{ipso}}-\text{N}^{\text{NHC}}-C^{\text{NHC}}$ in **PC_{minor}** (70.9°) is significantly smaller than in **PC_{major}** (96.4°). Although the π -allyl framework has to rotate during transformation to generate π -allyl complex **PA** (cf. Scheme S10), which places the α -carbon further away from the *ortho*-isopropyl group, the above-mentioned steric interaction is still considerably large in **OATS_{minor}** (cf. $C^{\text{ortho}}-C^{\text{ipso}}-\text{N}^{\text{NHC}}-C^{\text{NHC}} = 72.6^\circ$ in Figure S10). In contrast, such unfavorable proximity between the α -carbon atom and the back isopropyl group is avoided in **OATS_{major}** (cf. $C^{\text{ortho}}-C^{\text{ipso}}-\text{N}^{\text{NHC}}-C^{\text{NHC}} = 80.4^\circ$).

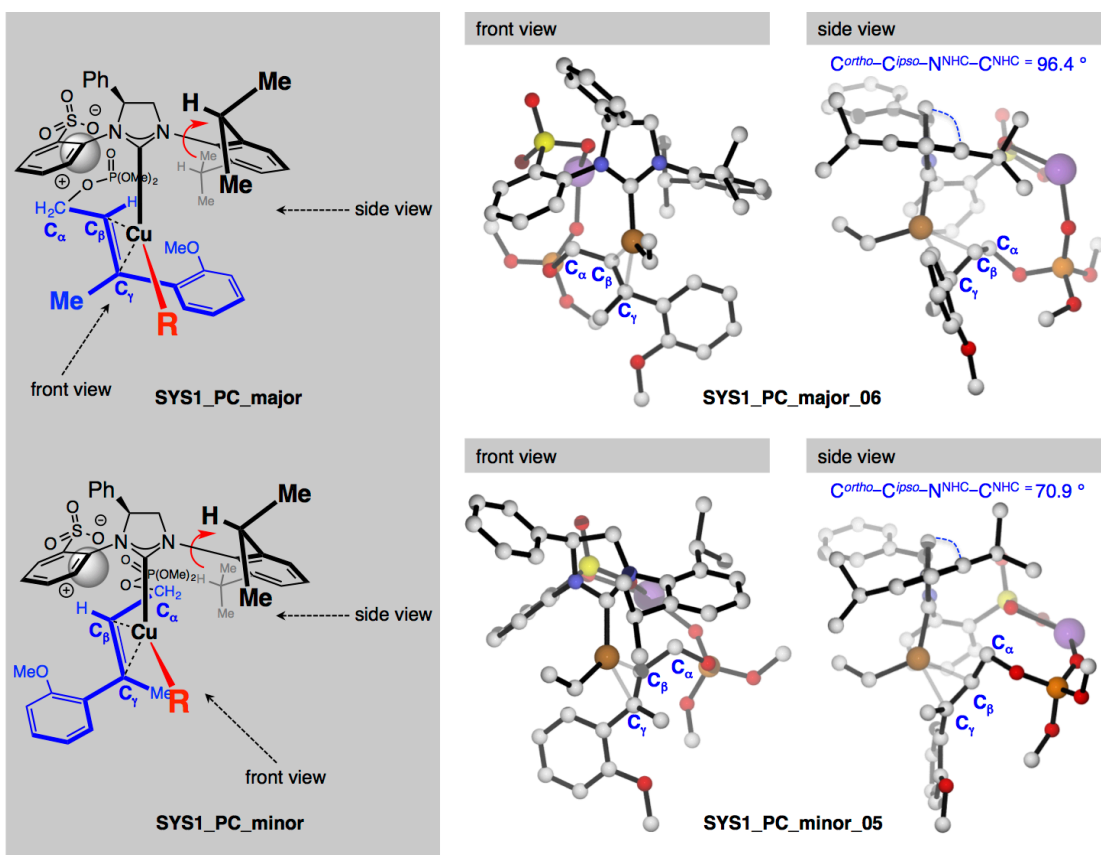


Figure S9. Comparison of computed structures for **SYS1_PC_major** and **SYS1_PC_minor** obtained at the ω B97XD/LANL2DZ level of theory.

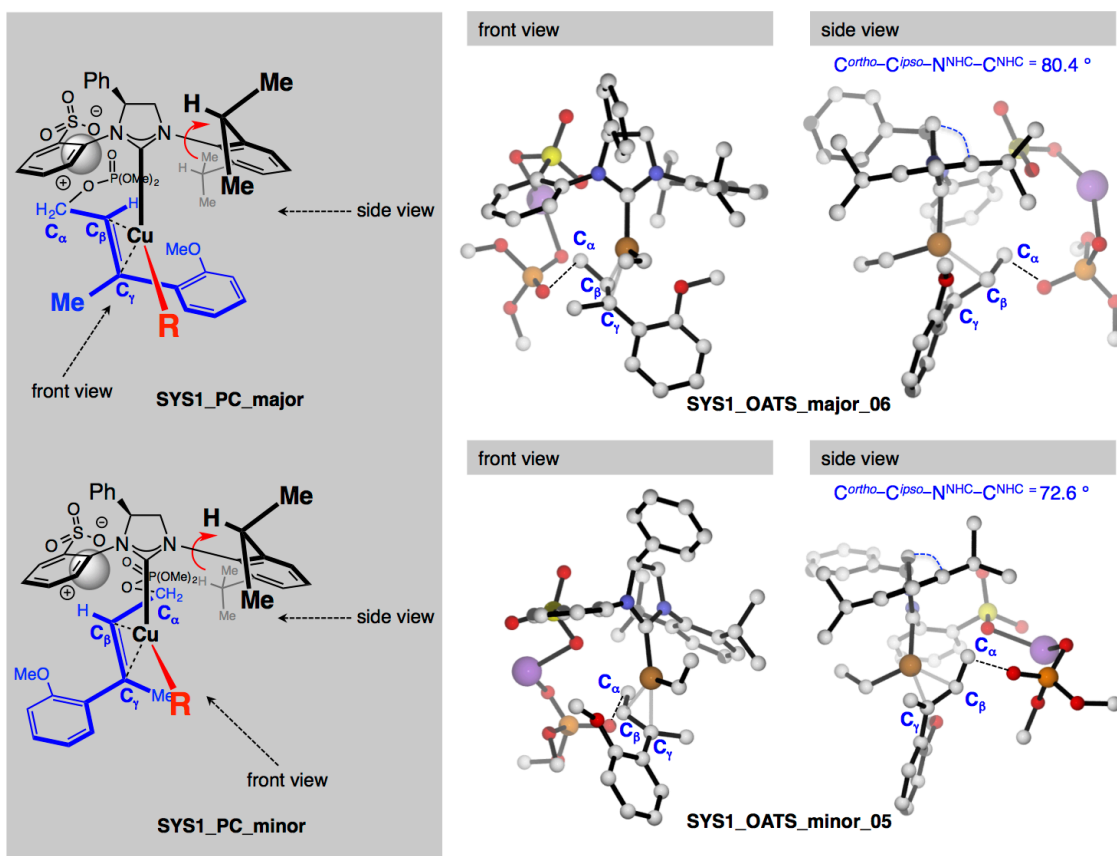
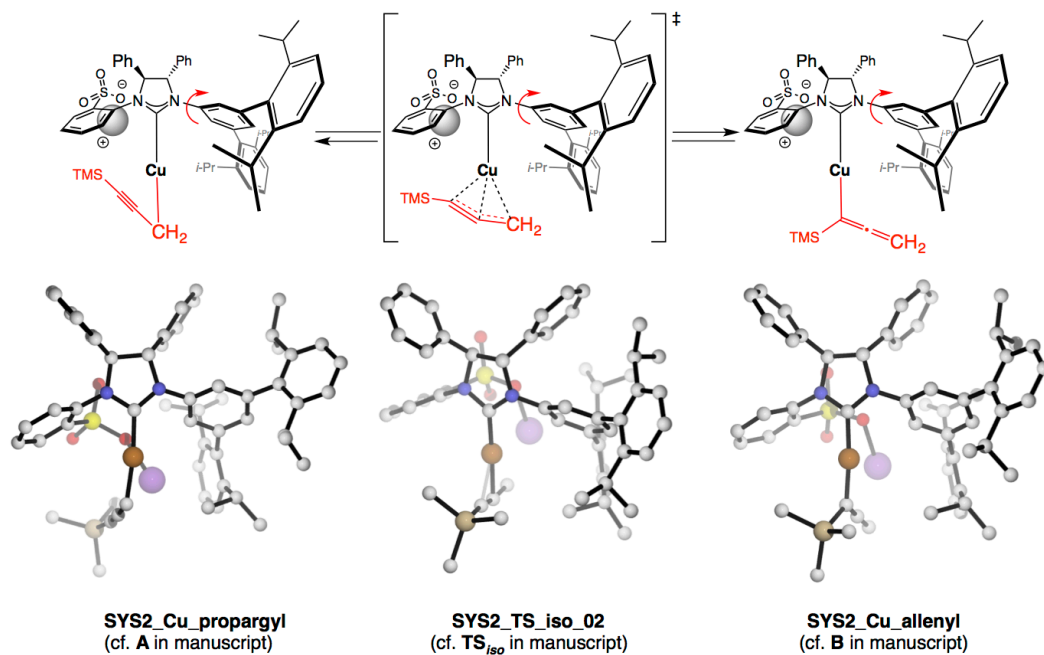


Figure S10. Comparison of computed structures for **SYS1_OATS_major** and **SYS1_OATS_minor** obtained at the ω B97XD/LANL2DZ level of theory in comparison with ChemDraw drawings of **SYS1_PC_major** and **SYS1_PC_minor**.

Pathways investigated for system 2 (SYS2)

Having derived the most favorable orientation of the sulfonate group in system 1 (*anti* to phenyl ring on the NHC backbone), we tested the validity of the stereochemical model for system 2 (SYS2), for which we have investigated the 4 pathways shown in Figure S11. The pathways for propargyl addition (**propargyl_major** and **propargyl_minor**) and allenyl addition (**allenyl_major** and **allenyl_minor**) are connected through low-lying transition state **TS_iso** (Figure S12). The corresponding relative free energies for **Cu_propargyl** (= **A** in manuscript), **TS_iso** (= **TS_{iso}** in manuscript) and **Cu_allenyl** (= **B** in manuscript) at the M06/Def2TZVPP_{DCM(SMD)} // ω B97XD/LANL2DZ_{gas-phase} level of theory are 0.0, 10.5 and -1.9 kcal/mol, respectively (see Figures S12, below).

Figure S11. Investigated reaction pathways for system 2 (SYS2).**Figure S12.** Computed structures for **SYS2_Cu_propargyl** (= **A** in manuscript), **TS_iso** (= **TS_{iso}** in manuscript) and **SYS2_Cu_allenyl** (= **B** in manuscript) obtained at the ω B97XD/LANL2DZ level of theory.

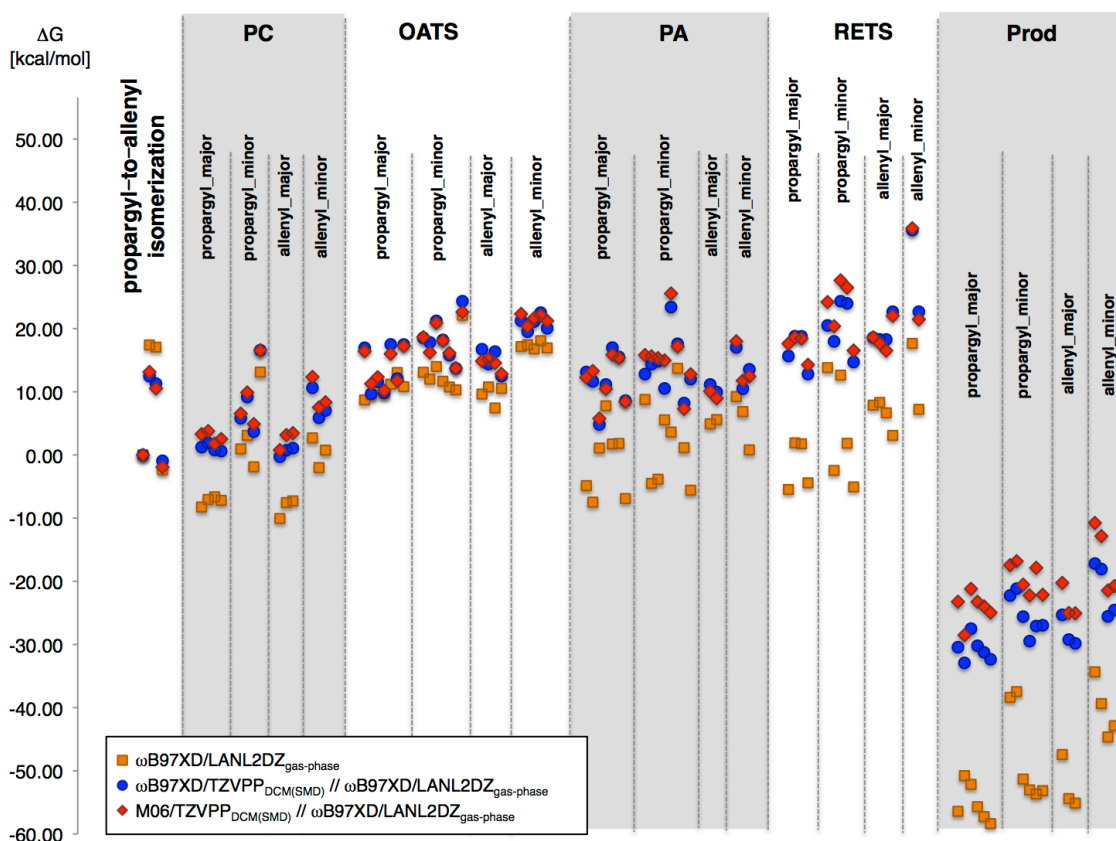


Figure S13. Computed free energies for several conformers of the pathways shown in Figure S4 with different levels of theory after geometry optimization with ω B97XD/LANL2DZ.

As is the case in system 1 (SYS1), the energy difference between the various conformers exceeds the 2–3 kcal/mol relevant for stereodifferentiation (Figure S13). Although comparison of the lowest energy conformers predicts the proper order between **OATS_propargyl_major** (=OAts_{A,major} in manuscript) and **OATS_propargyl_minor** (=OAts_{A,minor} in manuscript), in agreement with the experimental results, **OATS_allenyl_major** (=OAts_{B,major} in manuscript), the product of which is not observed experimentally, lies below the transition state leading to the minor enantiomer (**OATS_propargyl_minor**). For example, the corresponding free energies for **OATS_propargyl_major** (= OAts_{A,major}), **OATS_propargyl_minor** (= OAts_{A,minor}), **OATS_allenyl_major** (= OAts_{B,major}) and **OATS_allenyl_minor** (= OAts_{B,minor}) at the M06/Def2TZVPP_{DCM(SMD)}// ω -B97XD/LANL2DZ_{gas-phase} level of theory are 10.2, 13.7, 12.8 and 20.4 kcal/mol, respectively (Figure S14).

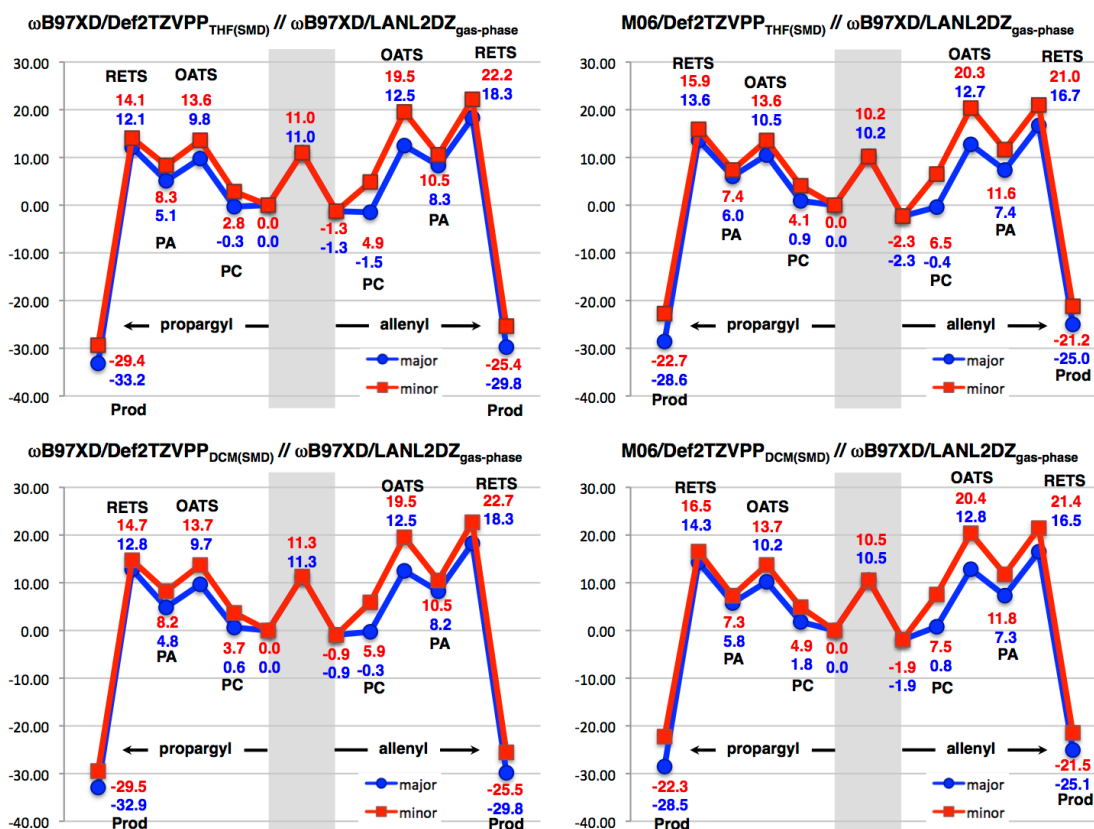


Figure S14. Computed free energies for the most stable conformers of the pathways shown in Figure S11 with different density functionals (ω B97XD and M06) and solvents (THF and DCM) after geometry optimization with ω B97XD/LANL2DZ_{gas-phase} (cf. Figure 2 in manuscript).

Structural comparison of **PC_propargyl_major** (= PC_{A,major} in manuscript) and **PC_propargyl_minor** (= PC_{A,minor} in manuscript) provides a reasonable rationale for the experimentally observed reversal in enantioselectivity between systems 1 and 2 (Figure S15). Due to the absence of *ortho* substituents on the 3,5-disubstituted aryl ring on the NHC there is no severe penalty for placing the α -carbon atom on the allyl phosphate to the right side (**PC_propargyl_major**). In contrast, the further extending phenyl group on the allyl phosphate comes into close proximity with the isopropyl groups on the 3,5-diaryl substituted phenyl ring in **PC_propargyl_minor**. Similar interactions are seen in the corresponding transition states for oxidative addition (**OATS**).

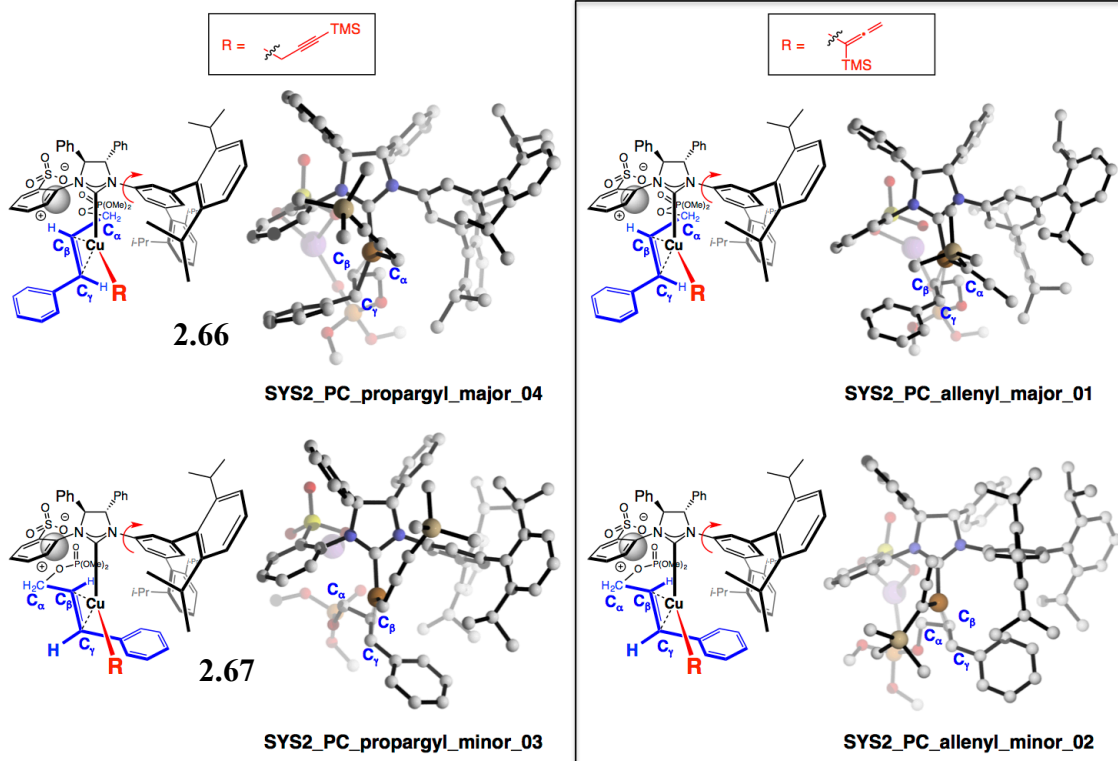
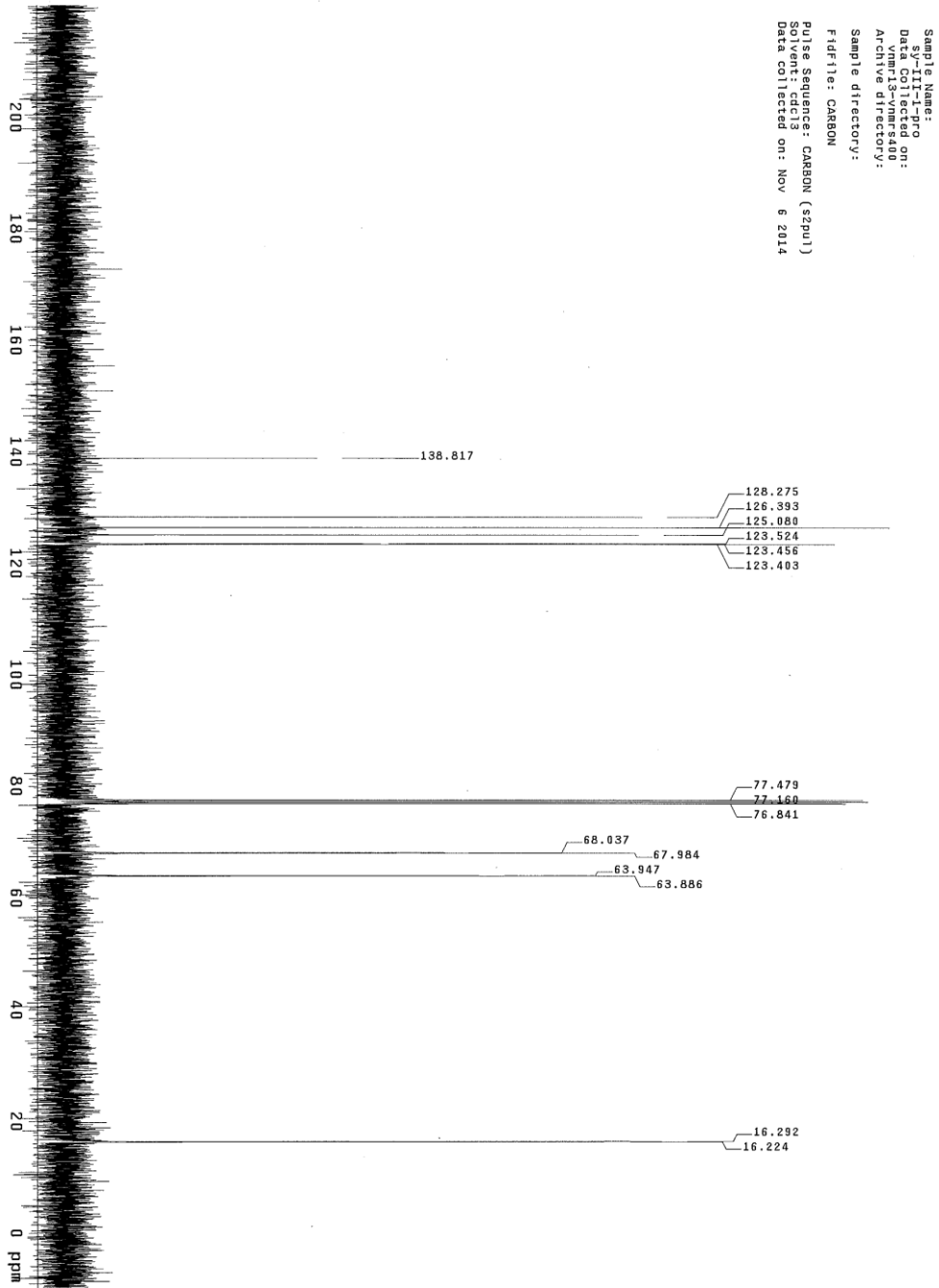
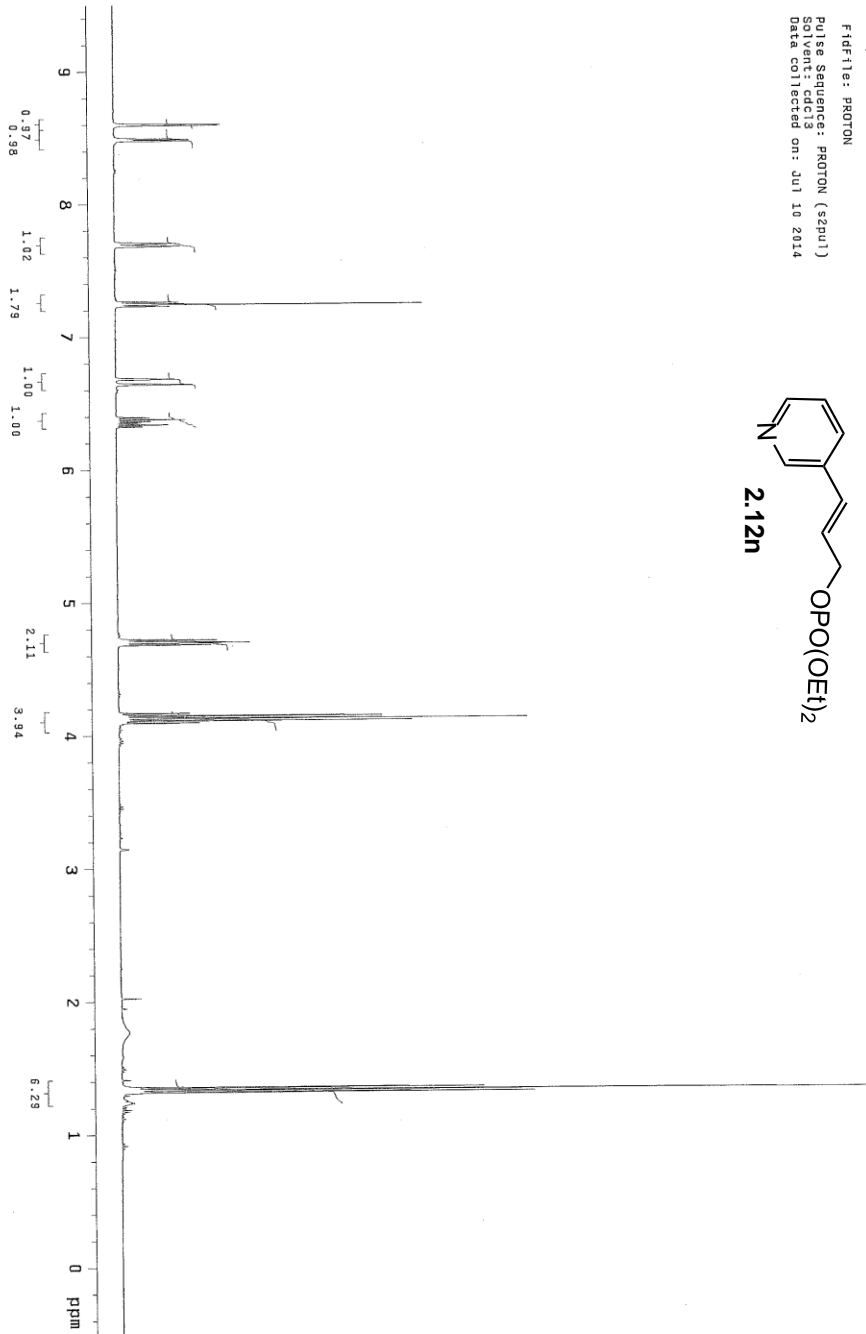
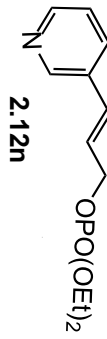
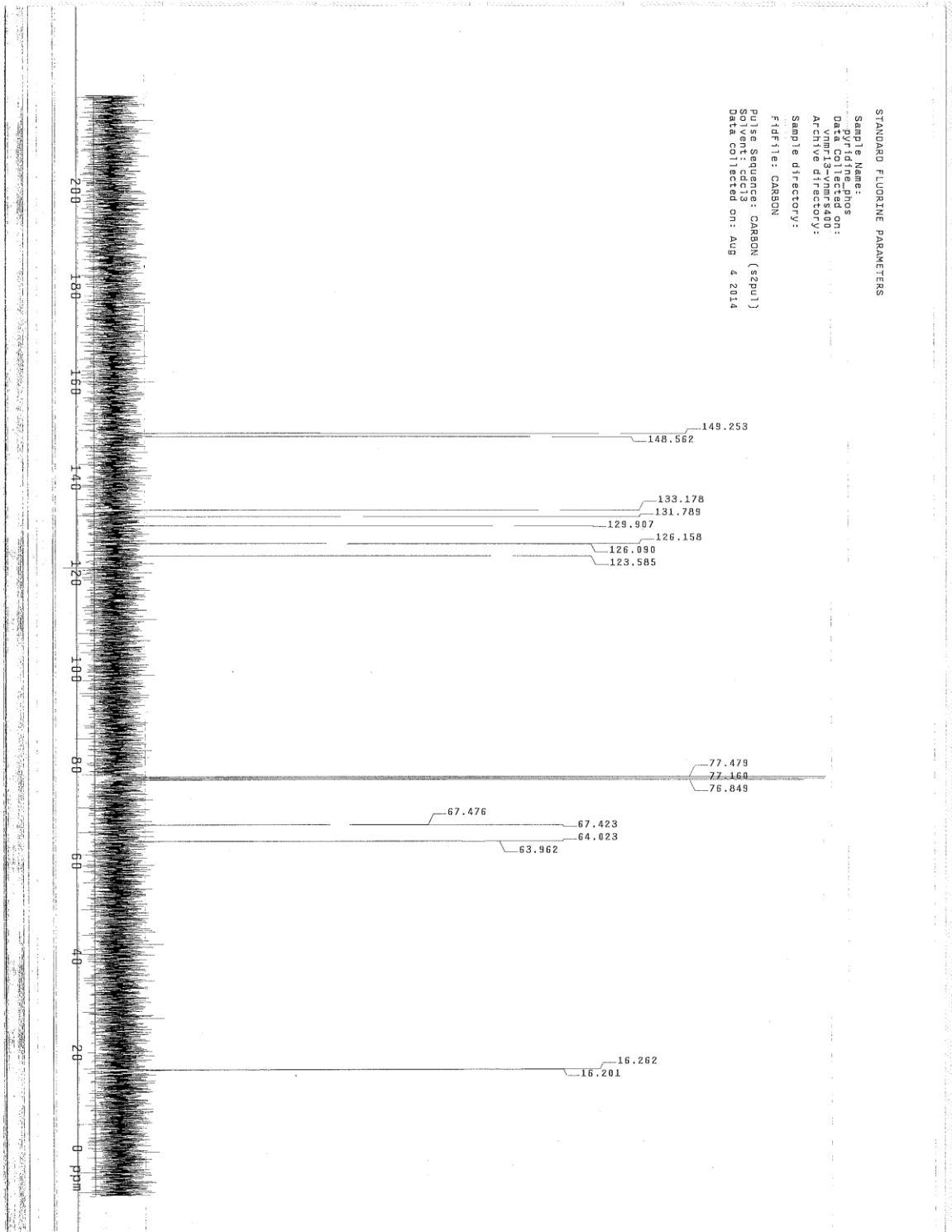


Figure S15. Comparison of computed structures for **SYS2_PC_propargyl_major**, **SYS2_PC_propargyl_minor**, **SYS2_PC_allenyl_major** and **SYS2_PC_allenyl_minor** obtained at the ω B97XD/LANL2DZ level of theory.

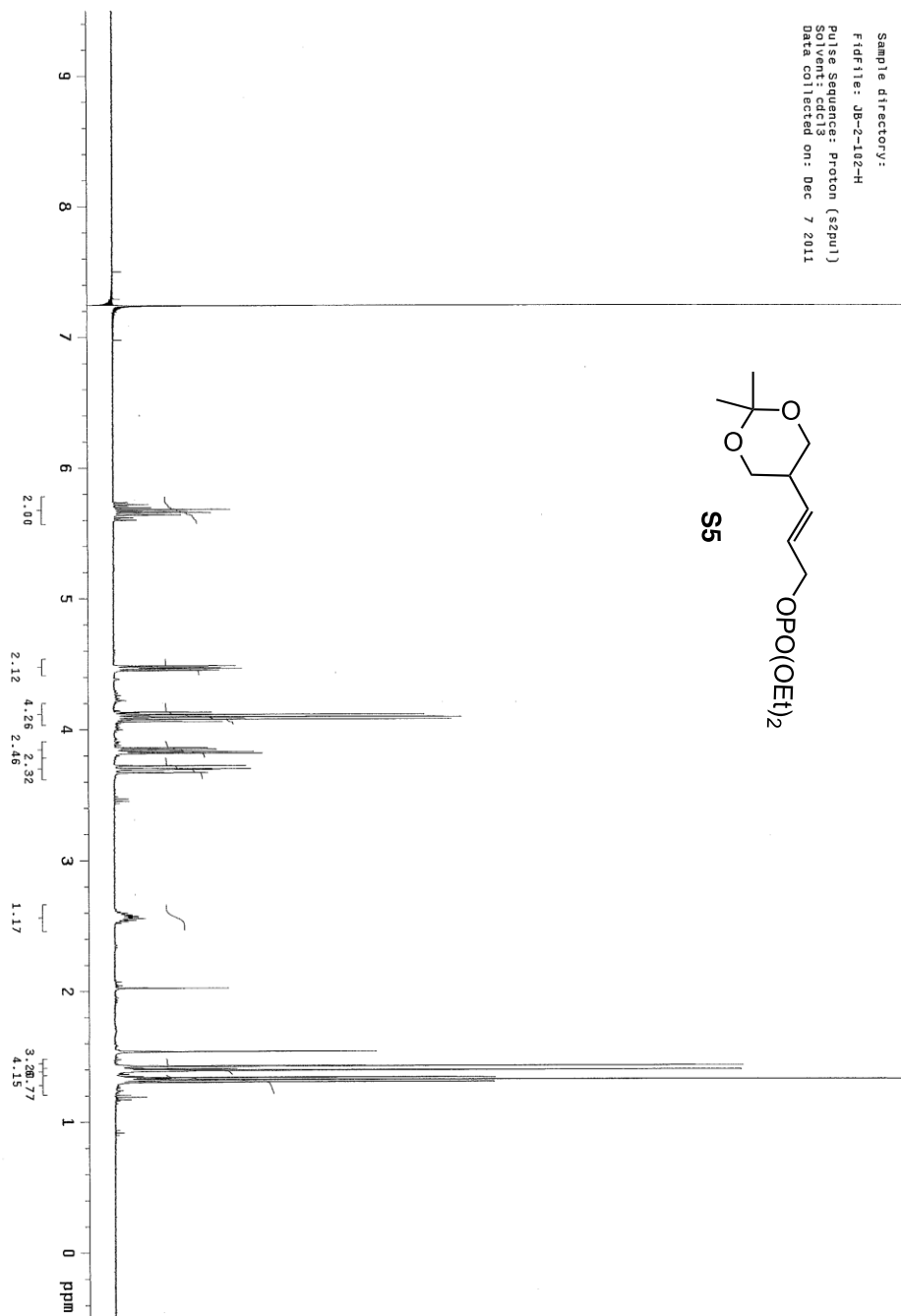


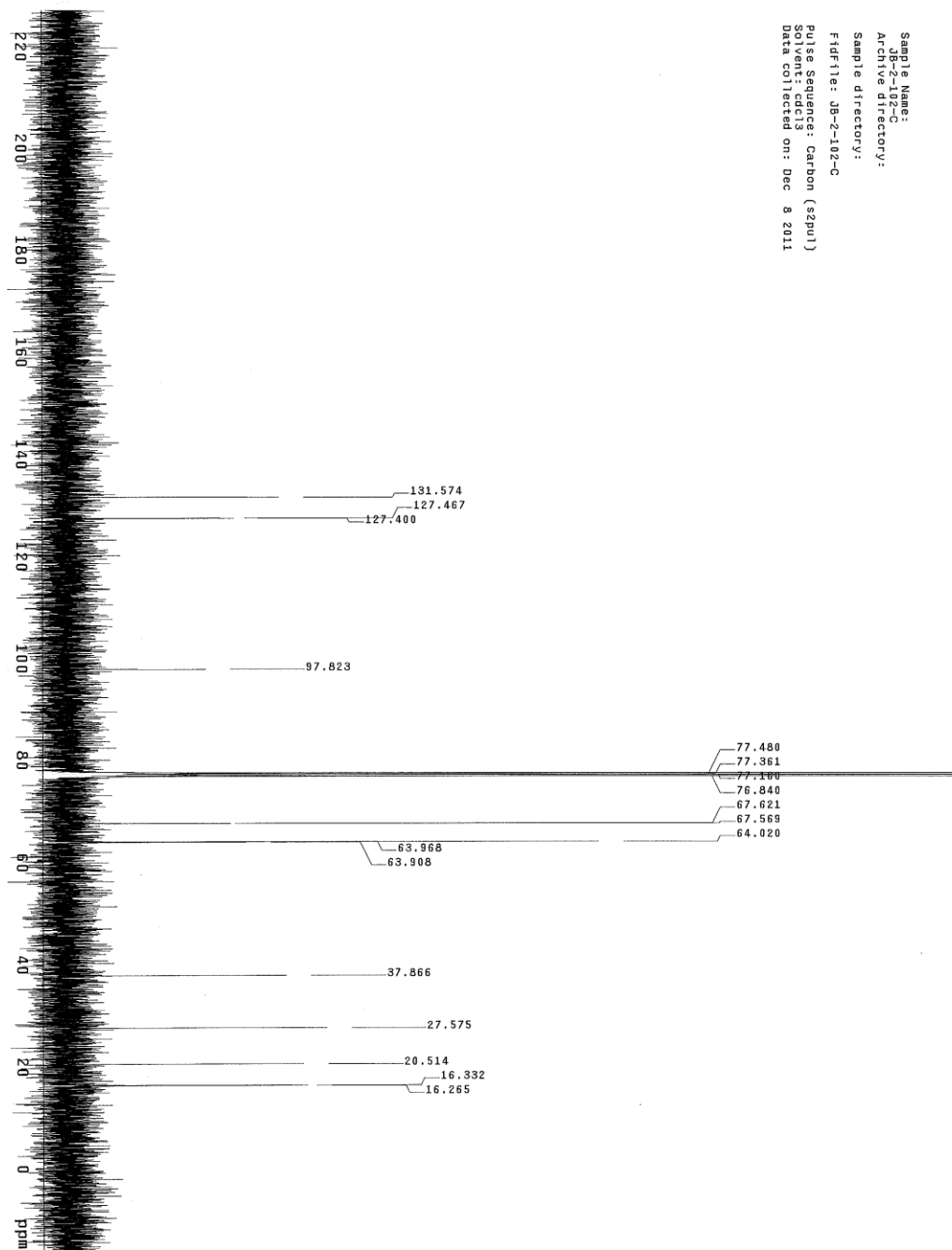
Sample Name: pyr-1d1he-ai1y1c-phos-Hao
Data: 13-00065400
Sample: 13-00065400
Archive directory:
Sample directory:
Fidfile: PROTON
Pulse Sequence: PROTON (zgpg3)
Solvent: cdcl3
Data collected on: Jul 10 2014



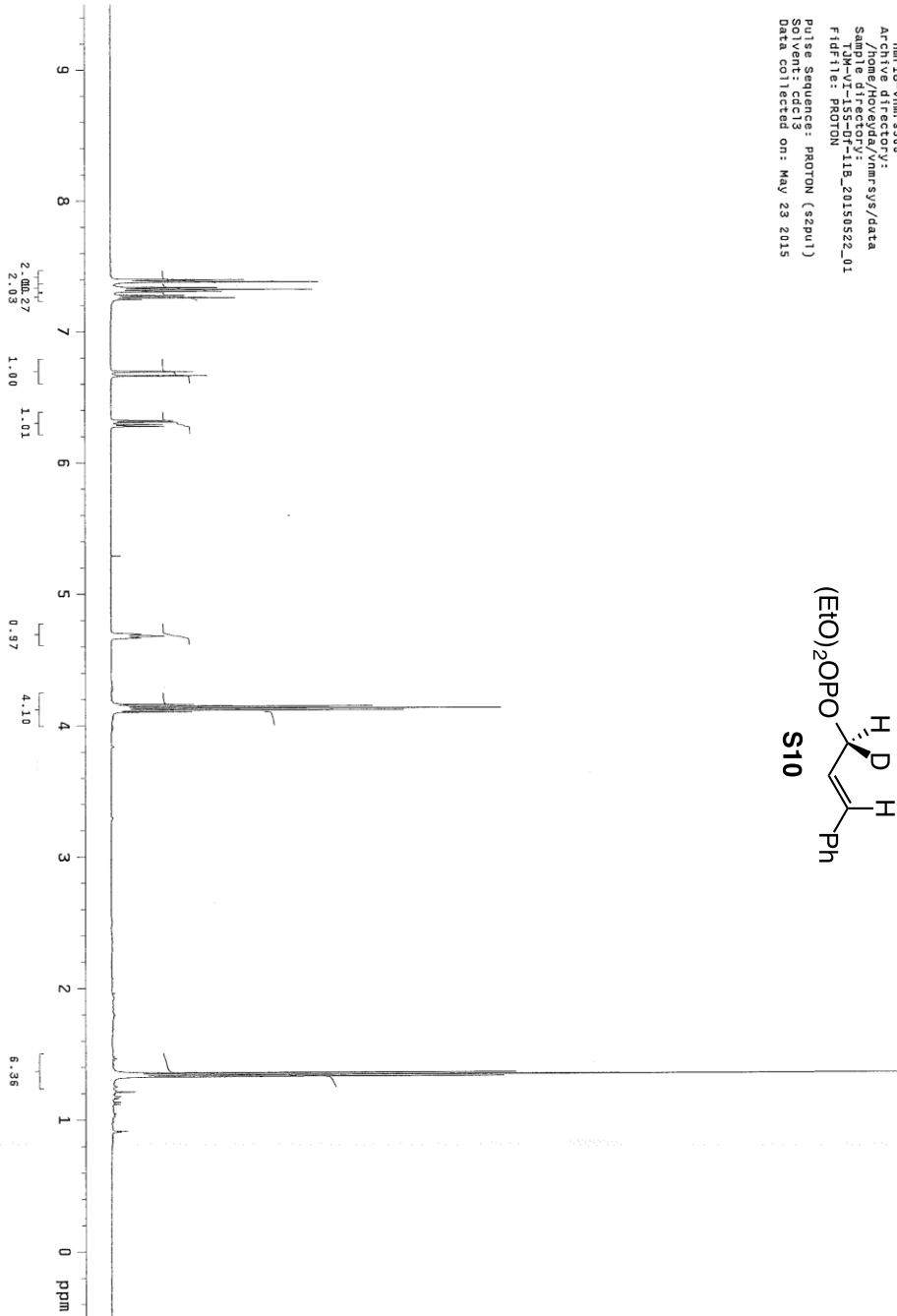
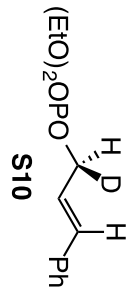


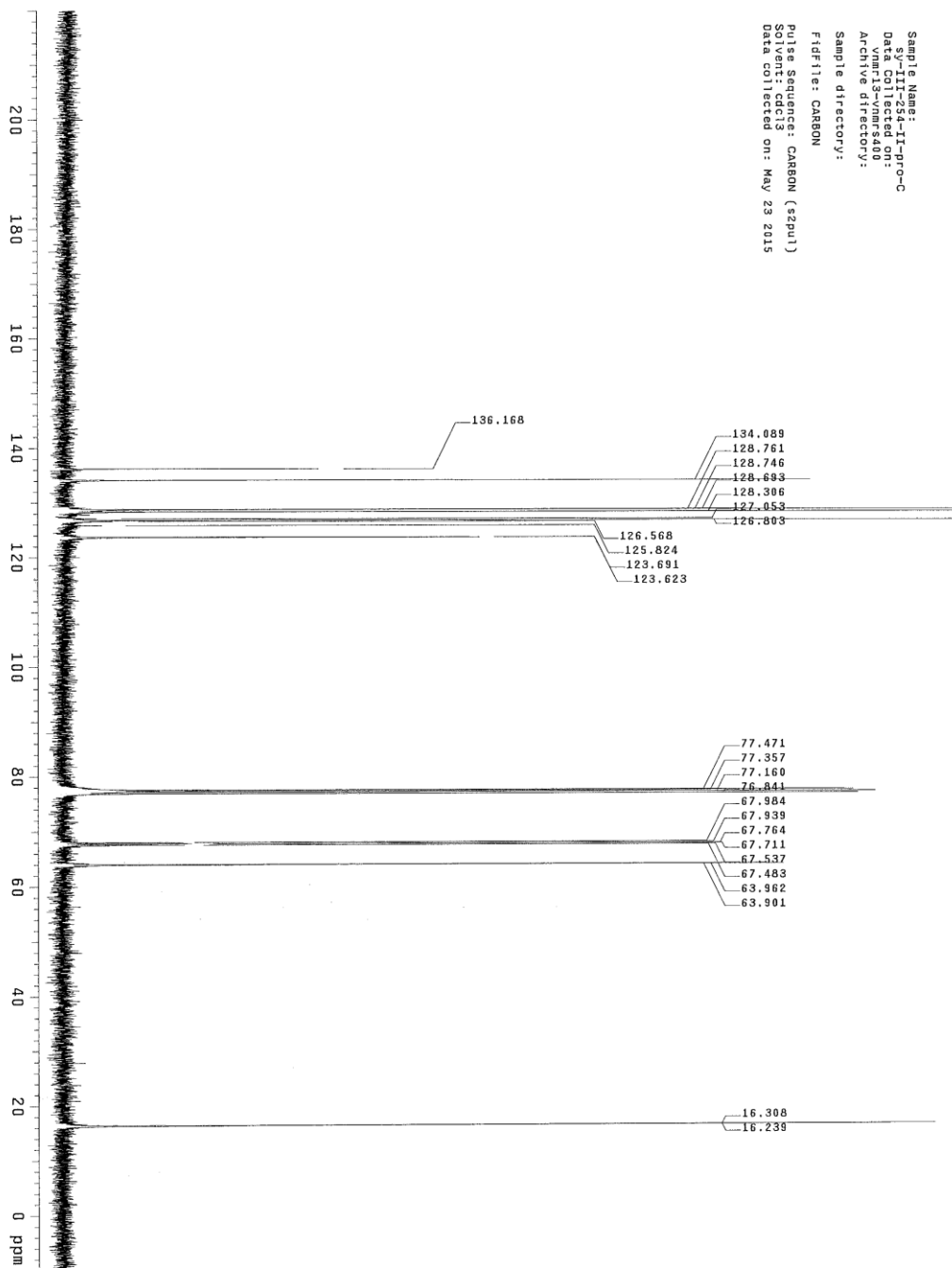
Sample Name: JB-2-102
Archive directory:
Sample directory:
FIDFile: JB-2-102-H
Pulse Sequence: Proton (szpu1)
Solvent: cdcl3
Data collected on: Dec 7 2011





TJM-VI-155-0f-11B
 Sample Name: sy-III-234-1f-pro
 Data Collection: /home/Hoveyda/Vmr/sys/data
 Archive directory: /home/Hoveyda/Vmr/sys/data
 Sample directory: /home/Hoveyda/Vmr/sys/data
 Date: 11-18-2015 02:01
 F1: PROTON
 Pulse Sequence: PROTON (szpu1)
 Solvent: cdc13
 Data collected on: May 23 2015





STANDARD FLUORINE PARAMETERS

Sample Name:

sy-III-248-III-pro

Data collected on:

Archive directory:

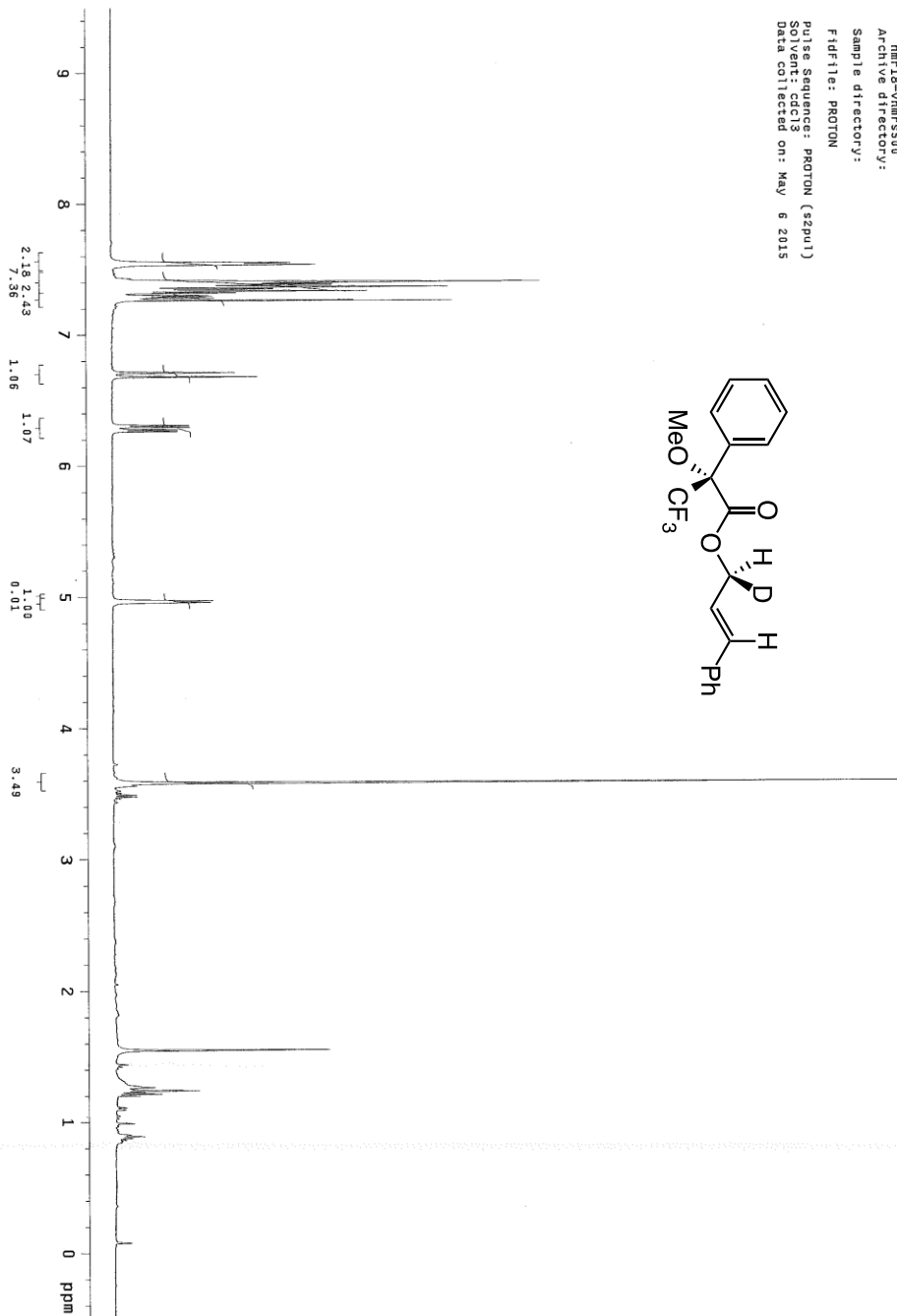
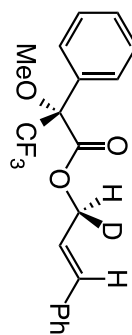
Sample directory:

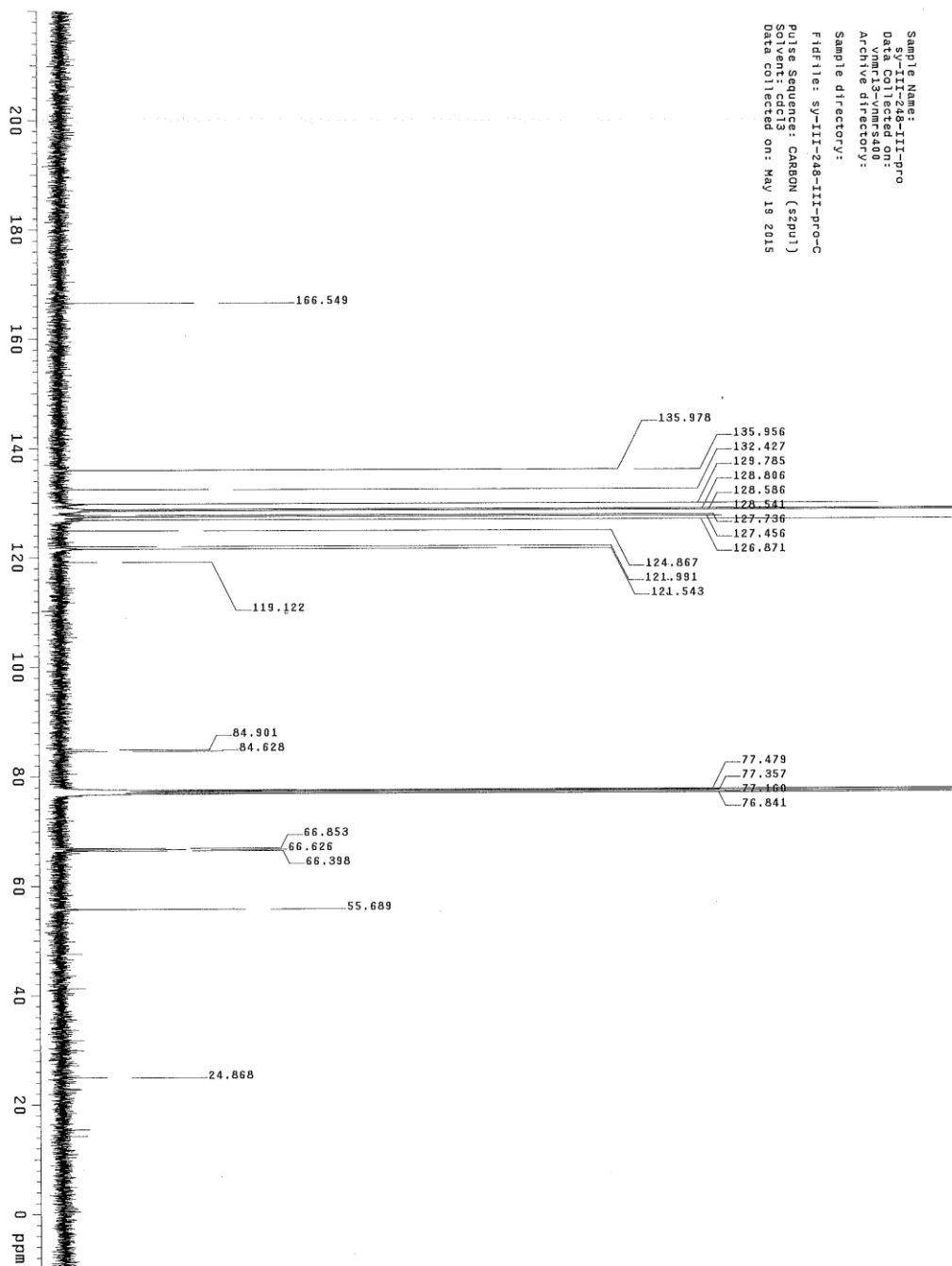
Fidfile: PROTON

Pulse Sequence: PROTON (szpu1)

Solvent: CDCl3

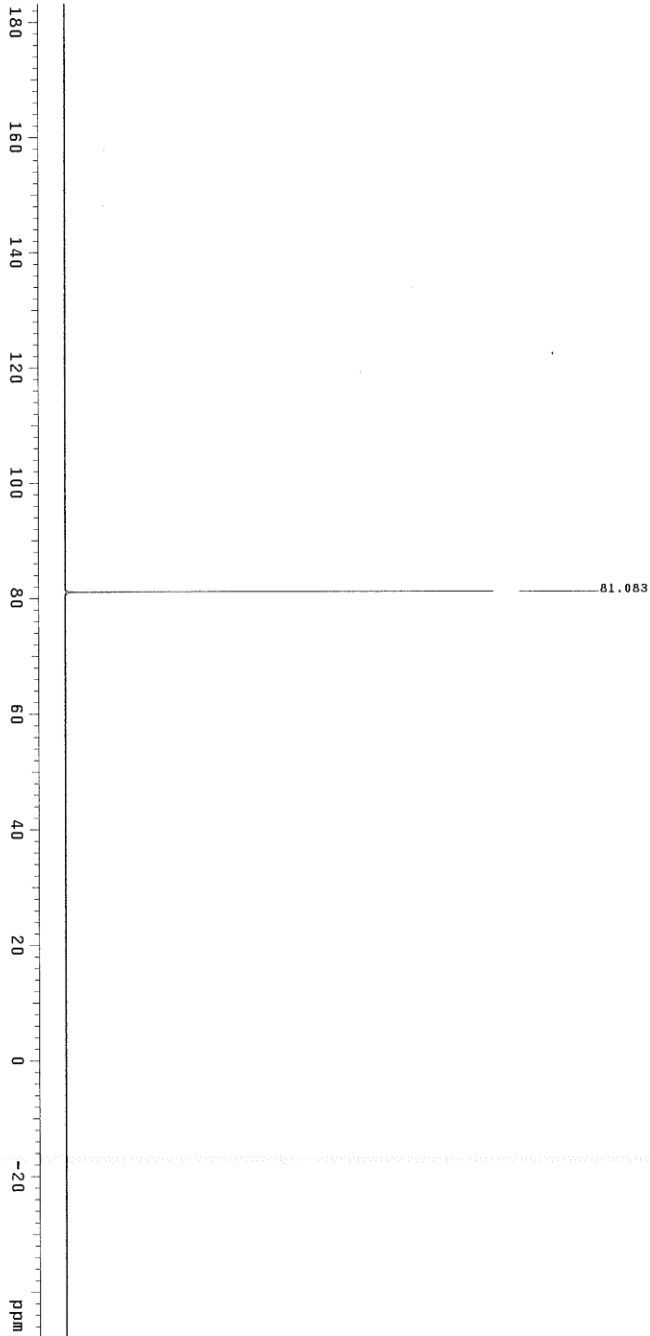
Data collected on: May 6 2015



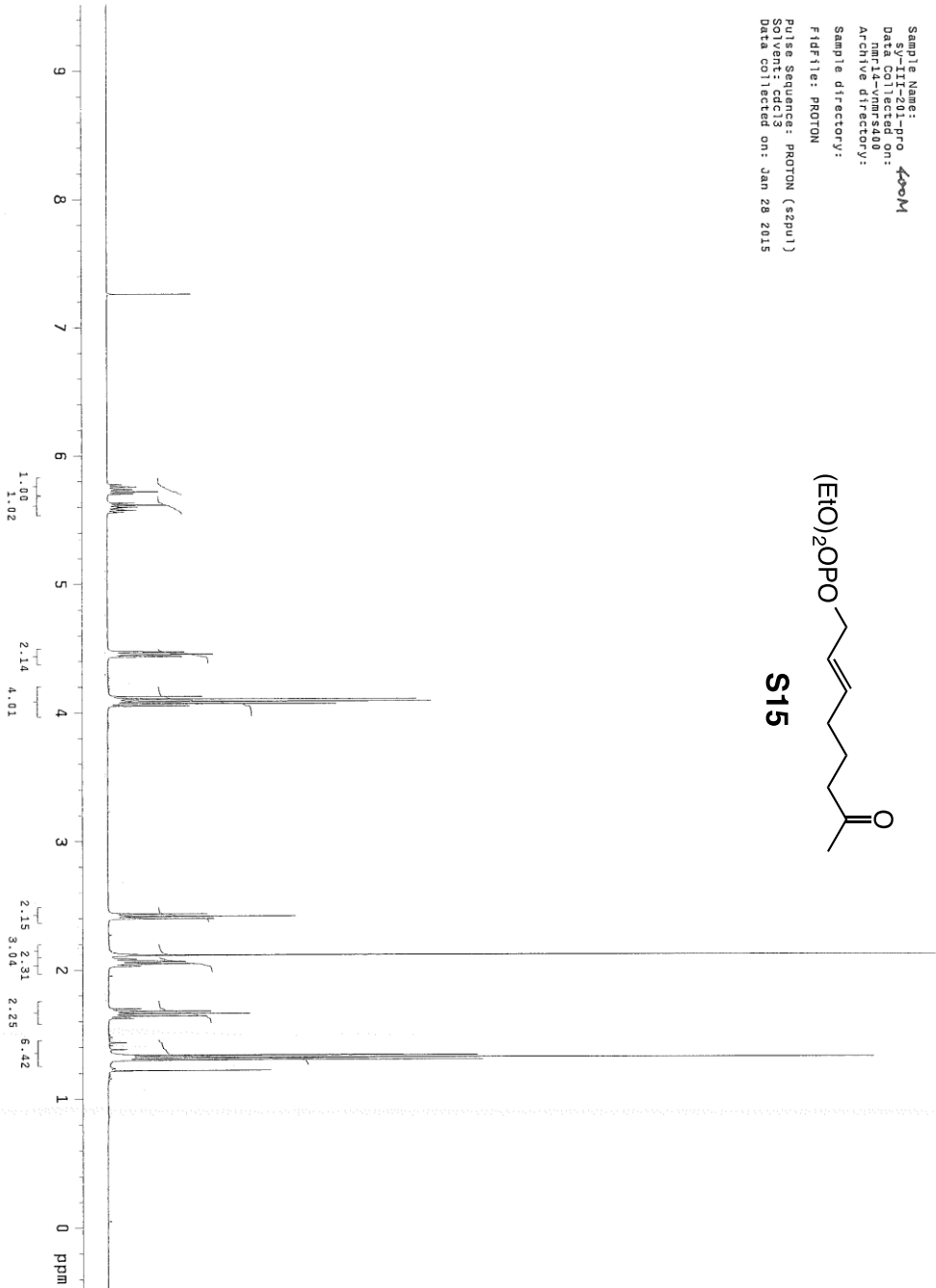
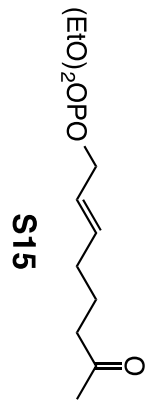


STANDARD FLUORINE PARAMETERS

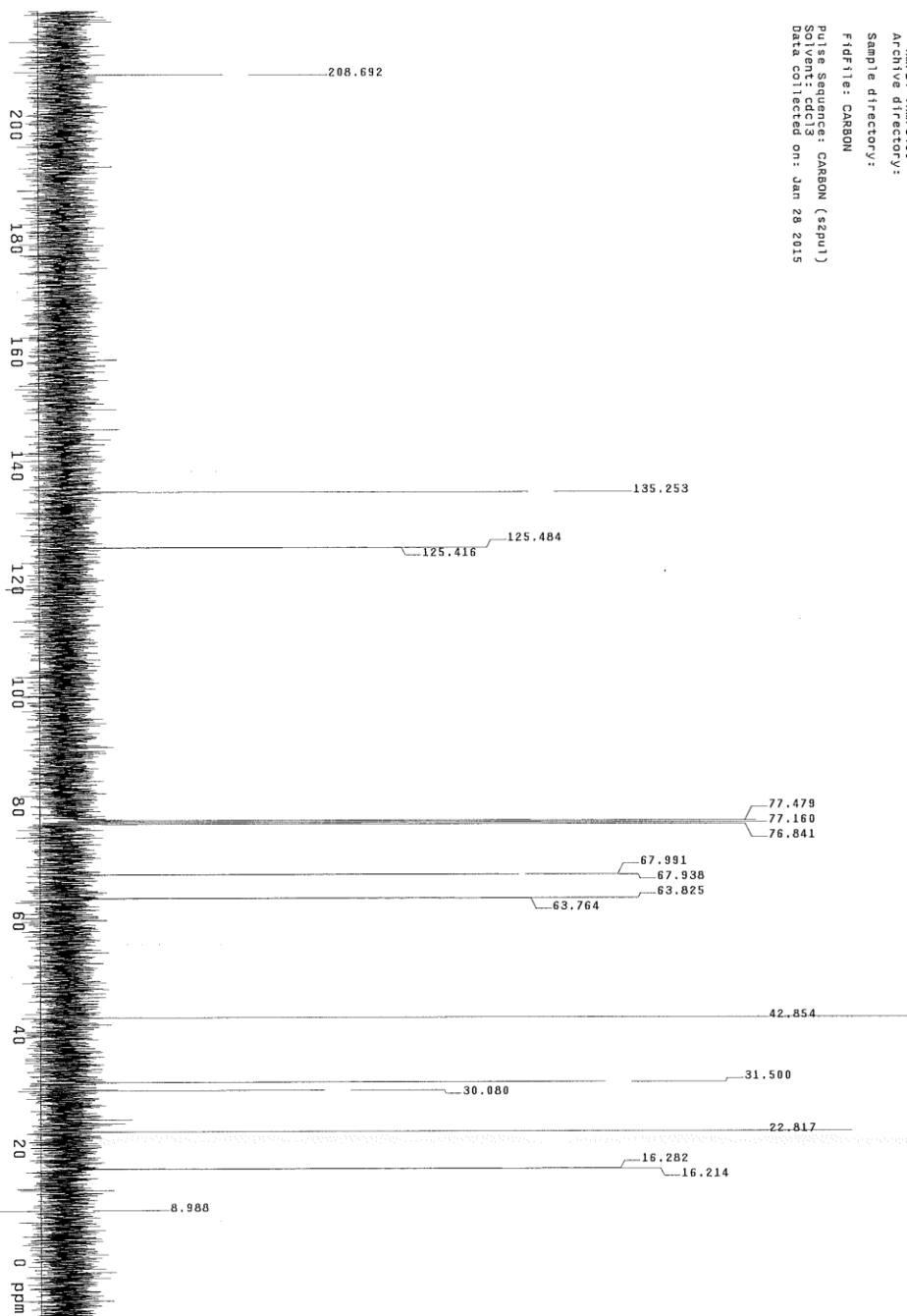
Sample Name: SY-II-248-II-F
Data Collected on:
Sample directory:
Sample directory:
Fidfile: FLUORINE
Pulse Sequence: FLUORINE (zgpg1)
Solvent: cdc13
Data collected on: May 6 2015



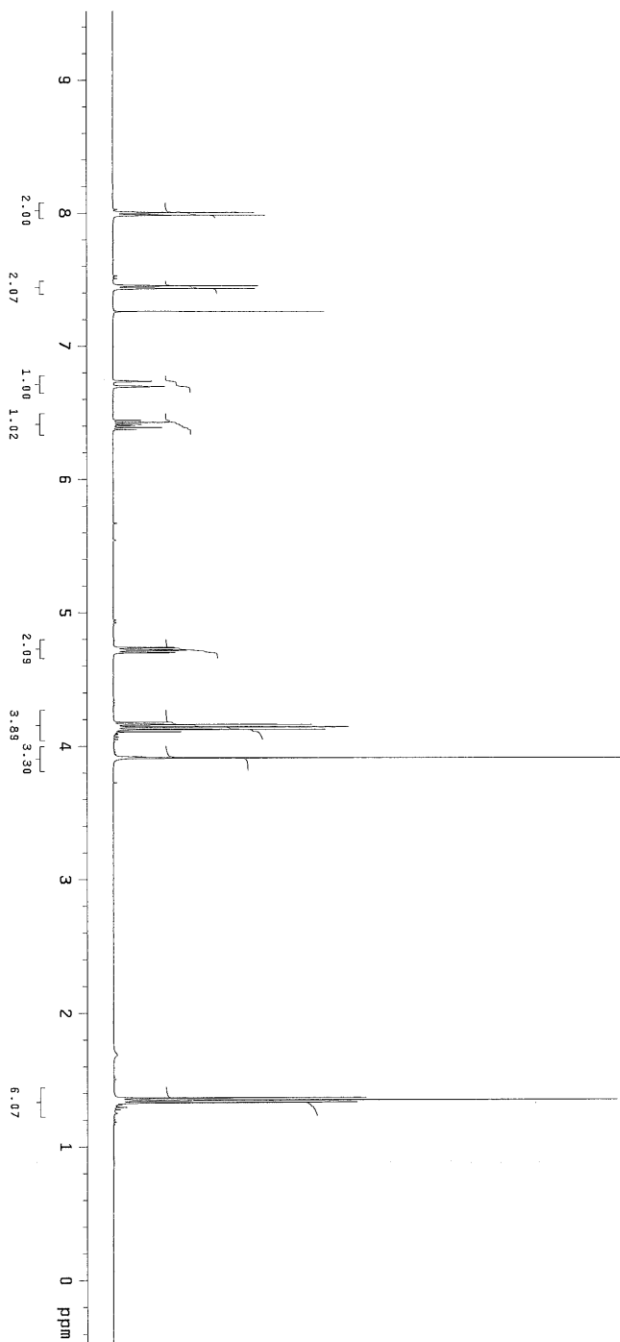
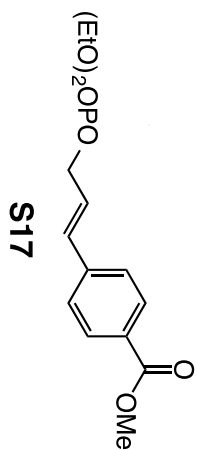
Sample Name: sy-111-201-pro 400M
Data Collected on: 1/28/15
Pulse Sequence: zgpg30
Archive directory: /data/111-201-pro
Sample directory: /data/111-201-pro
Fidfile: PROTON
Pulse Sequence: PROTON (zgpg30)
Solvent: cdcl3
Data collected on: Jan 28 2015



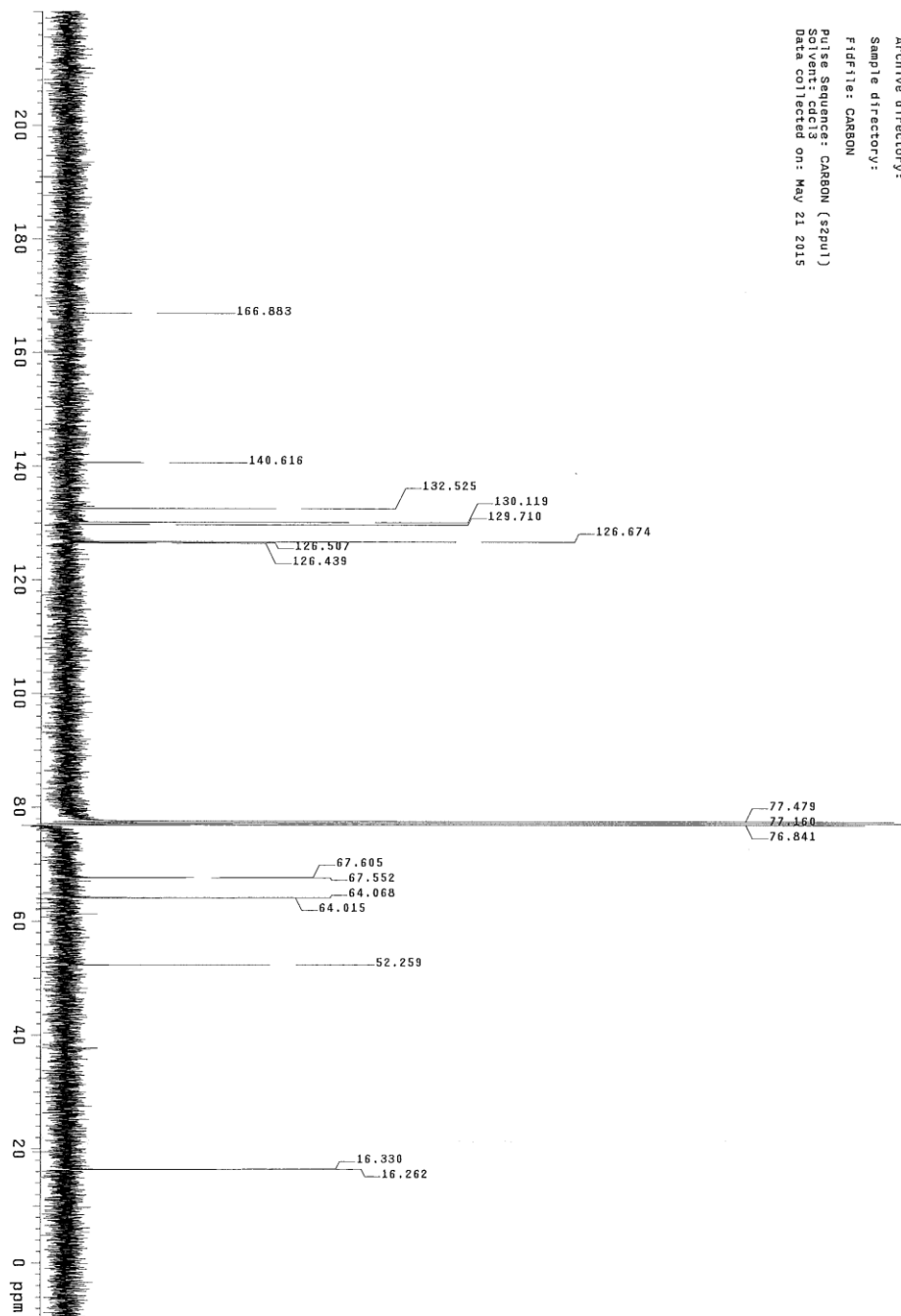
Sample Name: sy-11-201-pro
Data Collected on: 11/11/2014
Archive directory: /data/11/11/2014/sy-11-201-pro
Sample directory: /data/11/11/2014/sy-11-201-pro
FIDFile: CARBON
Pulse Sequence: CARBON (szpu1)
Solvent: cdcl3
Data collected on: Jan 29 2015



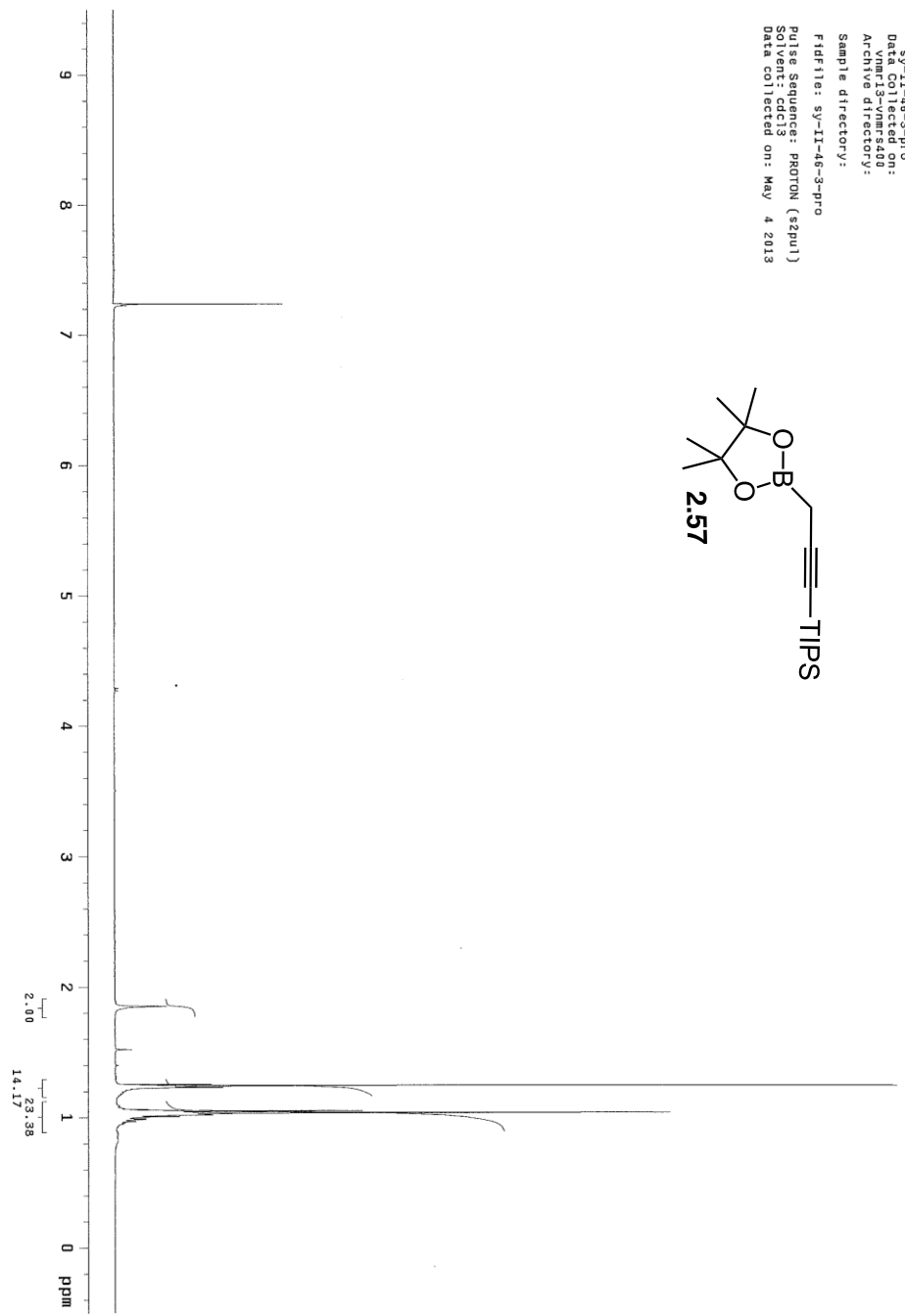
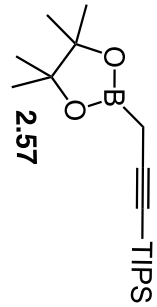
Sample Name: sy-111-191-g-pro
 Date Acquired: 05/21/2015
 Name of the Operator: JRM
 Archive directory:
 Sample directory:
 F1 file: PROTON
 Pulse Sequence: PROTON (s2pu1)
 Solvent: cdcl3
 Data collected on: May 21 2015

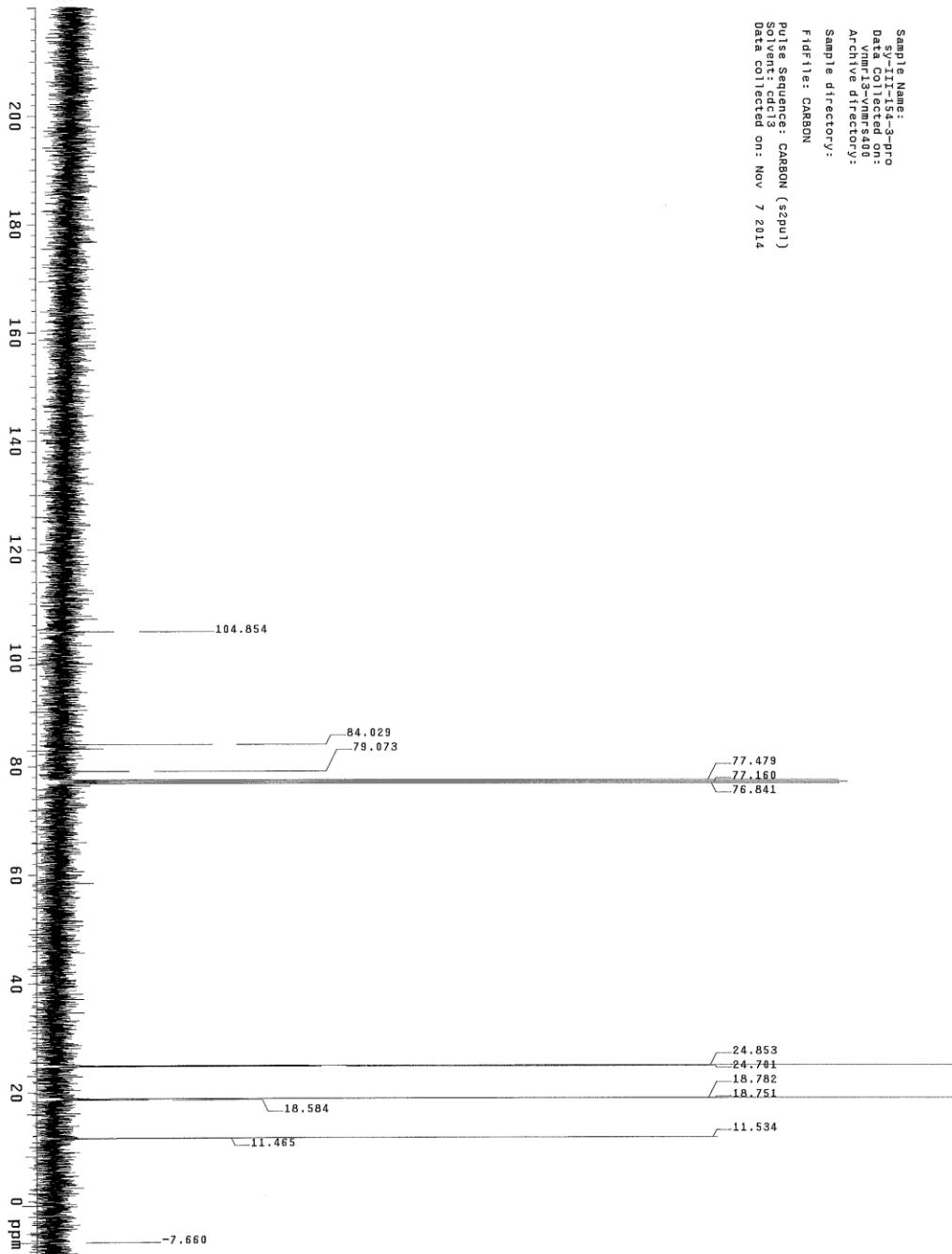


Sample Name: 57-011-31-01-pro
Date Collected: 5/21/2015
Vnmr13-vmr9400
Archive directory:
Sample directory:
FidFile: CARBON
Pulse Sequence: CARBON (zgpg1)
Solvent: cdcl3
Data collected on: May 21 2015

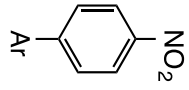


T0W-IV-207-sm-f2
phenothiazine
Sample Name:
Data Collected on:
vnmr13-vnmr5400
Archive directory:
Sample directory:
Fidfile: sy-II-46-3-pro
Pulse Sequence: PROTON (szpu1)
Solvent: CDCl3
Data collected on: May 4 2013

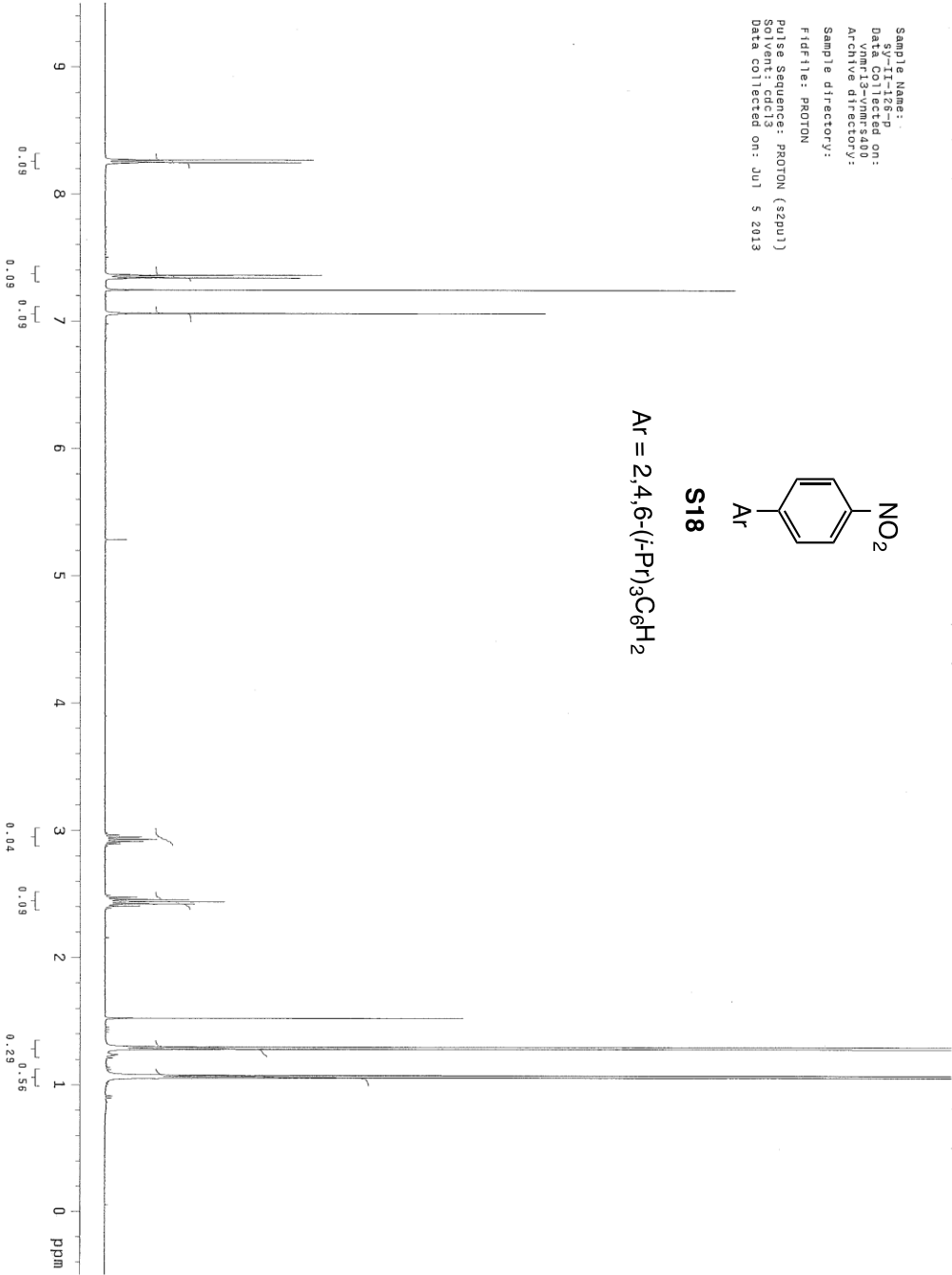
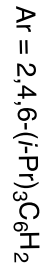


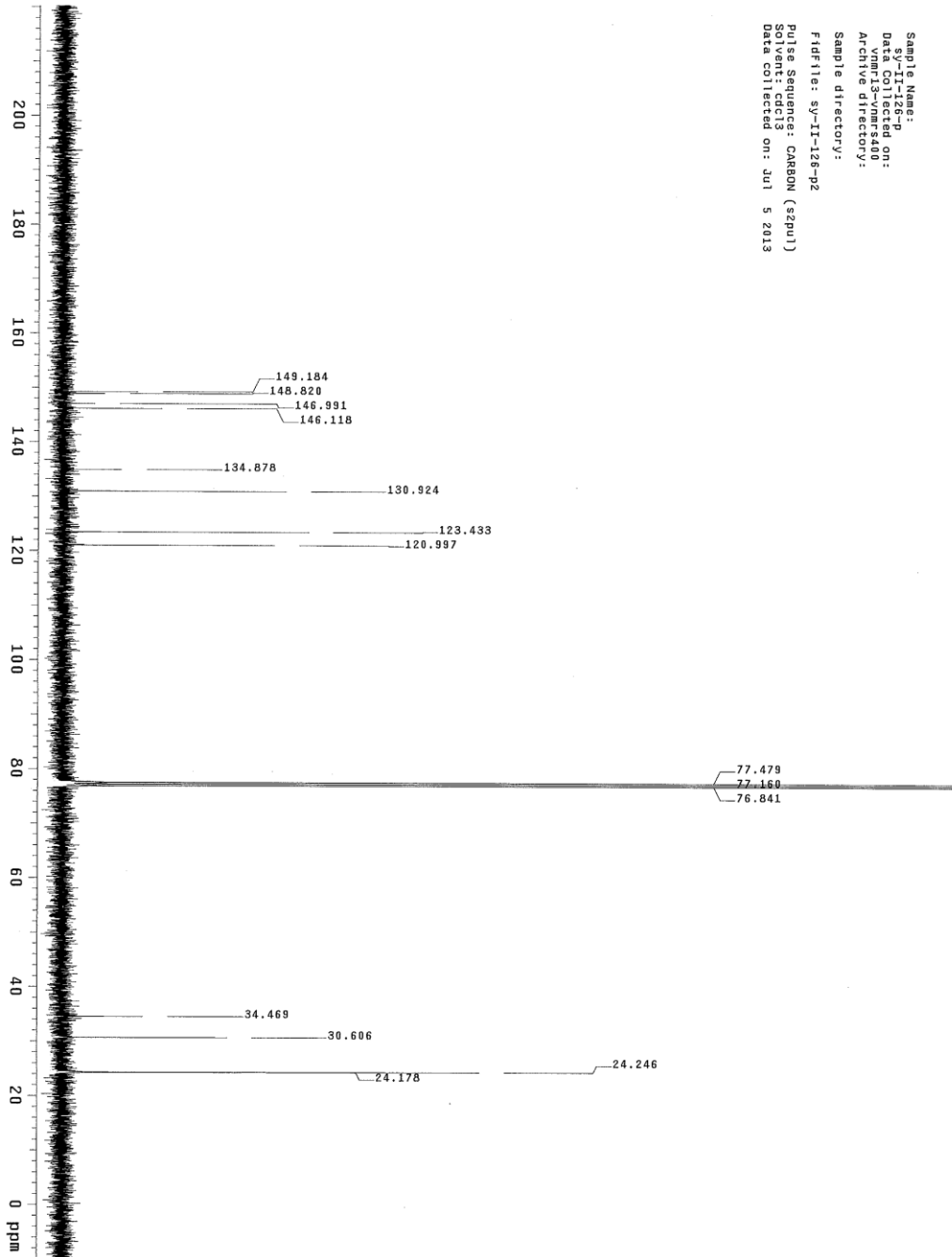


Sample Name: S18
Data Collected on: 5/13/2013
Vmr: 13-nmr5400
Archive directory:
Sample directory:
Fid file: PROTON
Pulse sequence: PROTON (szpu1)
S18
Data collected on: Jul 5 2013



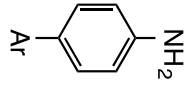
S18



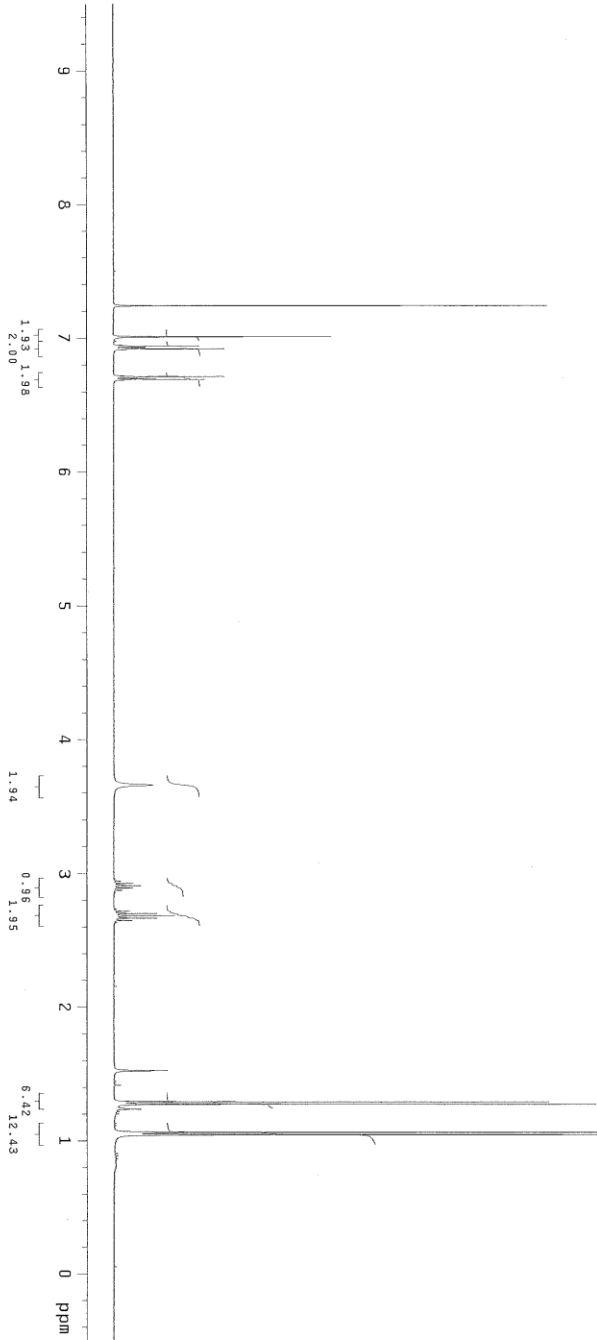


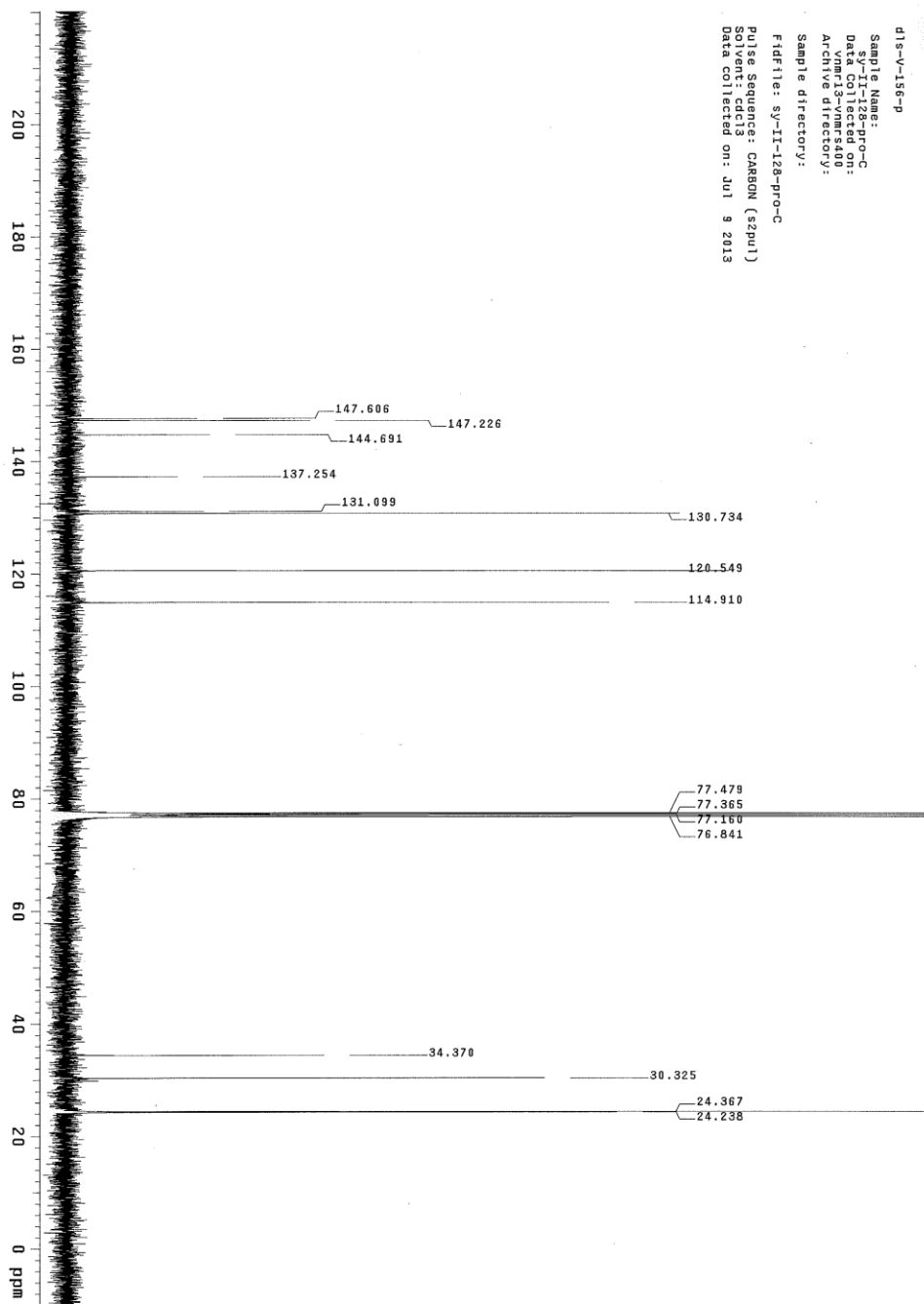
Sample Name: sy-II-126-p
Data Collected on: vnmr13-vnmr440
Archive directory: Sample directory:
Fidfile: sy-II-126-p2
Pulse Sequence: CARBON (cpul)
Solvent: cdcl3
Data collected on: Jul 5 2013

Sample Name: sy-11-128-pro
Da: 2011-11-28 10:00
Xmmp13-vnmr5400
Archive directory:
Sample directory:
Fidfile: PROTON
Pulse Sequence: PROTON (szpuj)
Solvent: cdcl3
Date Collected on: Jul 9 2013

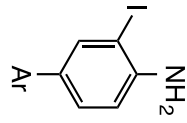


S19
Ar = 2,4,6-(*i*-Pr)₃C₆H₂



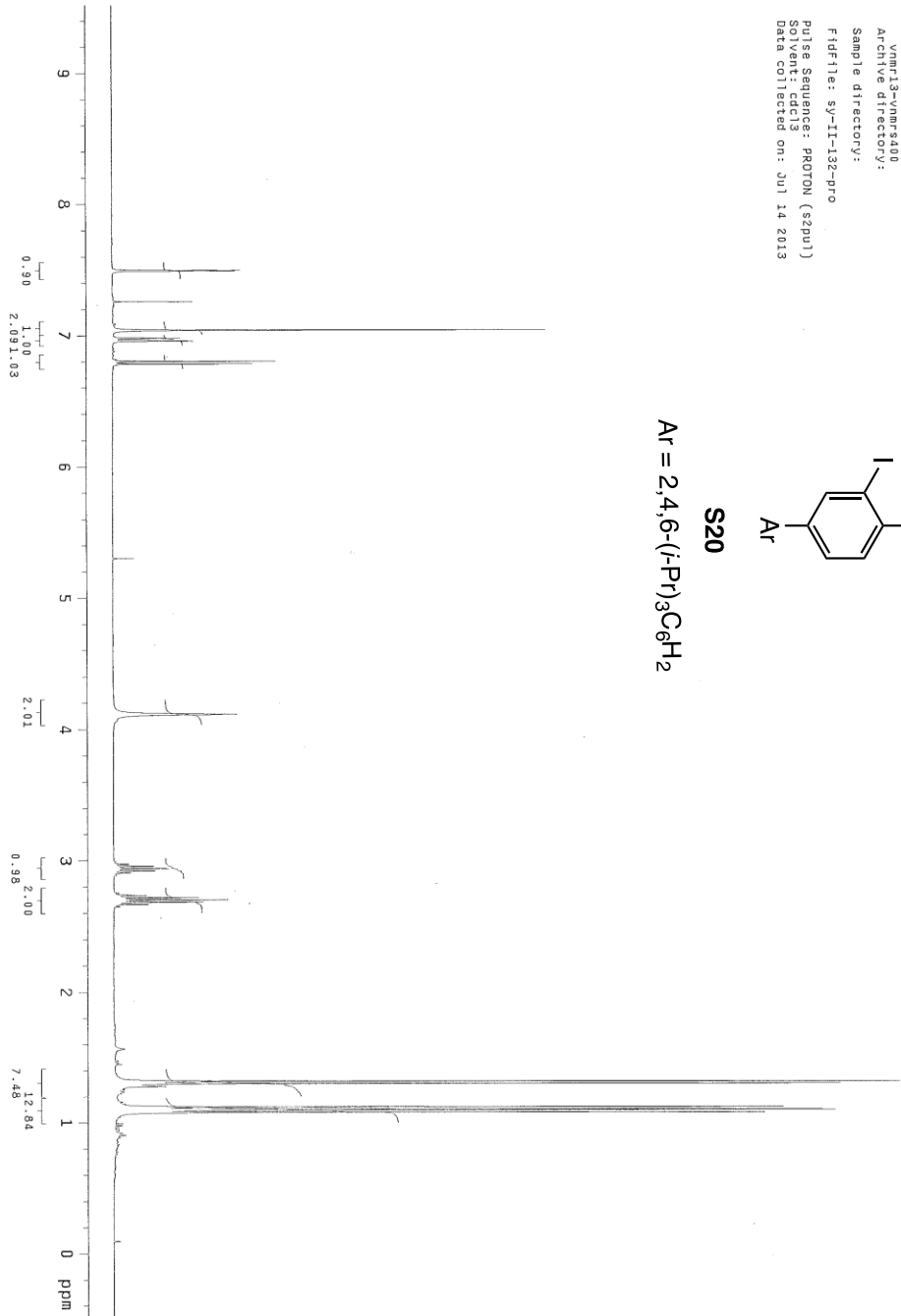


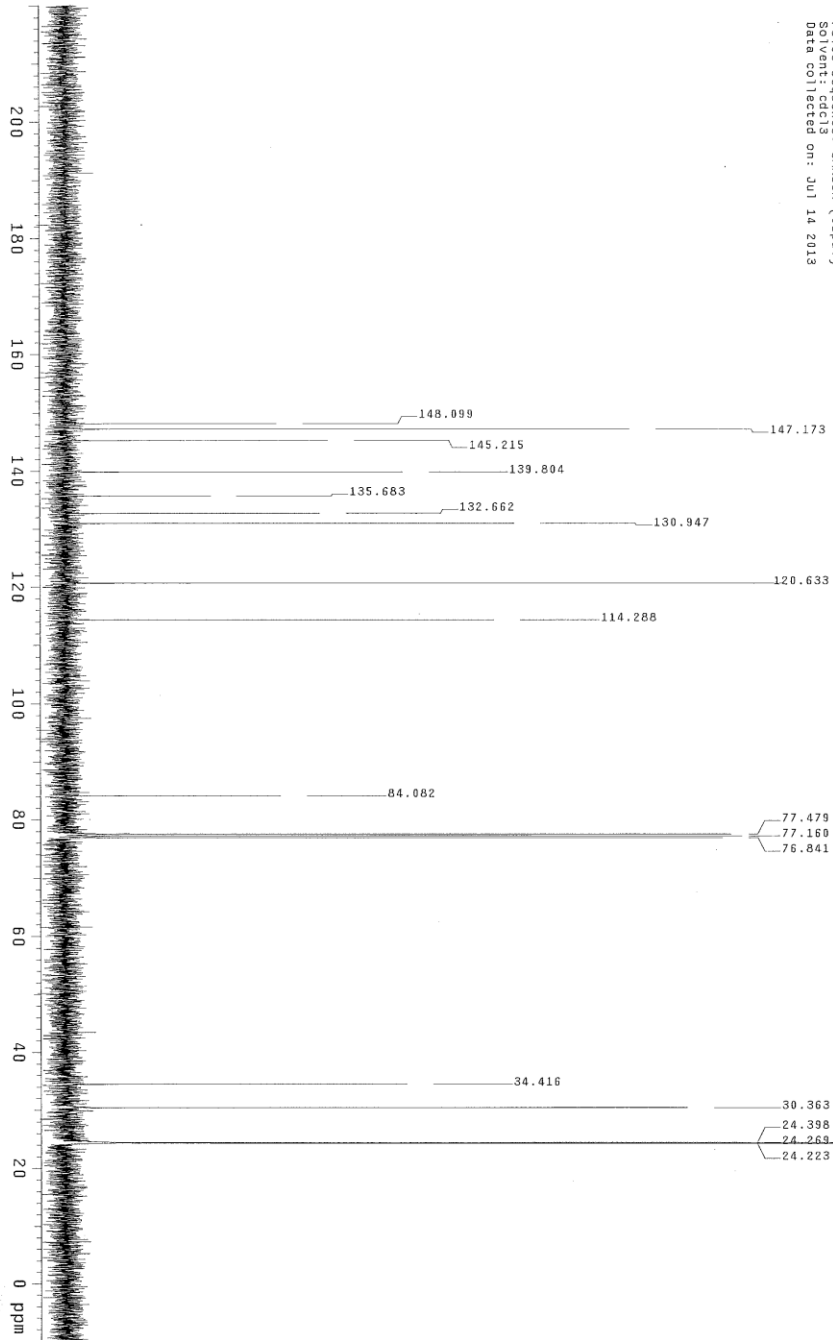
Sample Name: sy-II-132-pro
Data Dir: collected
Archive directory:
Sample directory:
Fidfile: sy-II-132-pro
Pulse Sequence: PROTON (szpu1)
Solvent: cdcl3
Data collected on: Jul 14 2013



S20

Ar = 2,4,6-(*i*-Pr)₃C₆H₂

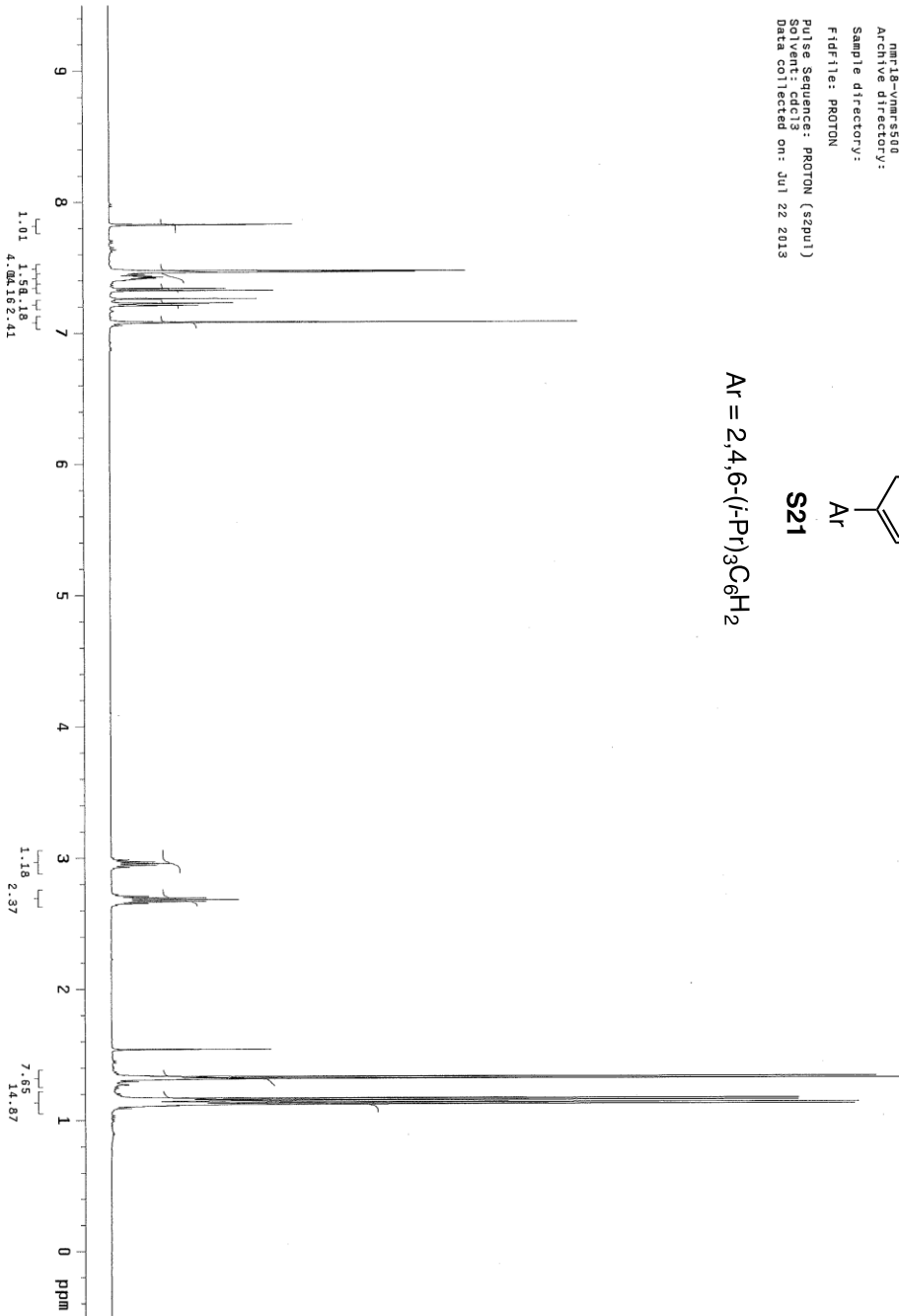
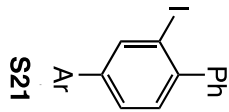


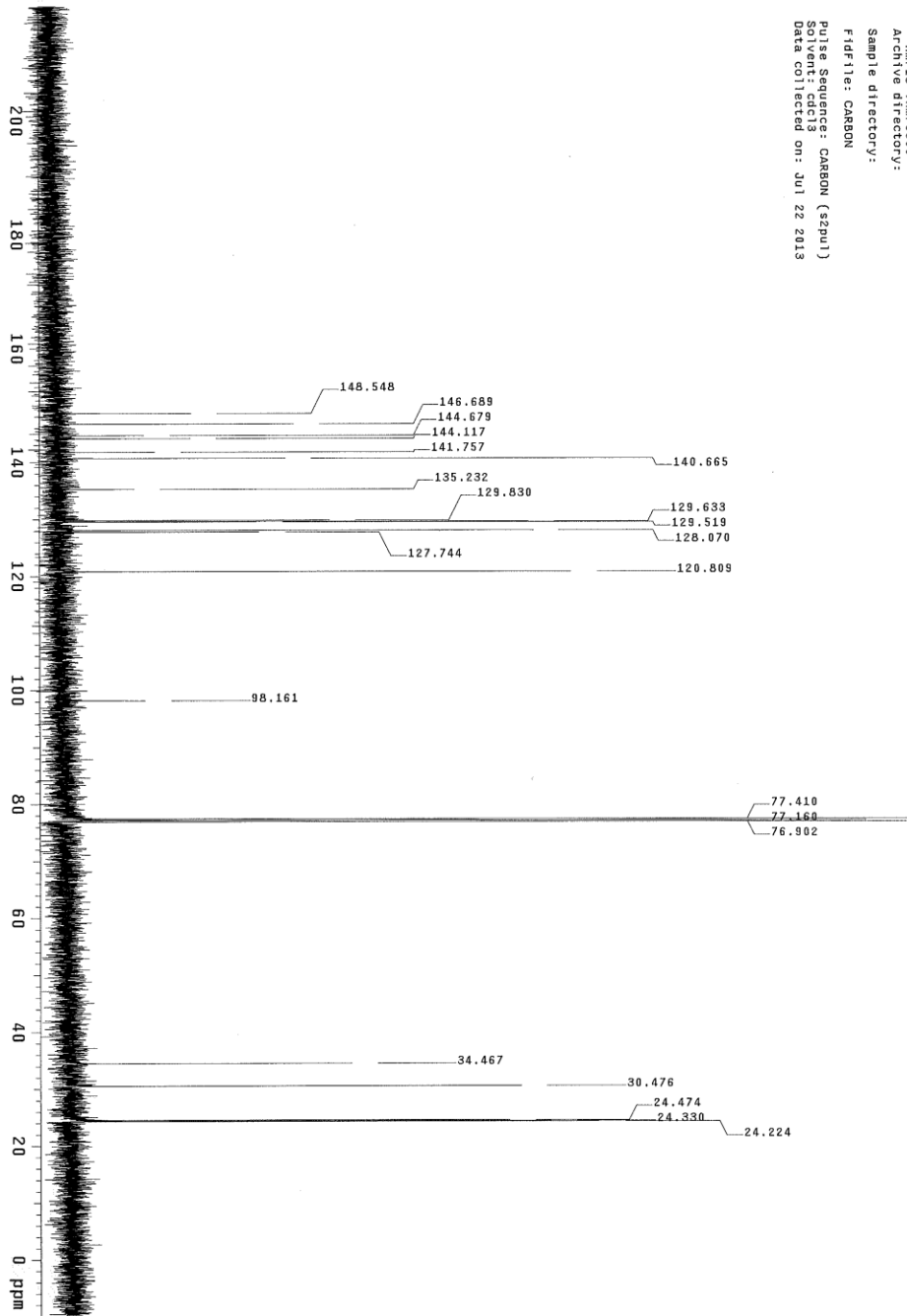


Sample Name: sy-11-132-pro-c
Data Collected: 001
Sample ID: 11-132-pro-c
Archive directory:
Sample directory:
FID File: CARBON
Pulse Sequence: CARBON (szpu1)
Solvent: cdc13
Data Collected on: Jul 14 2013

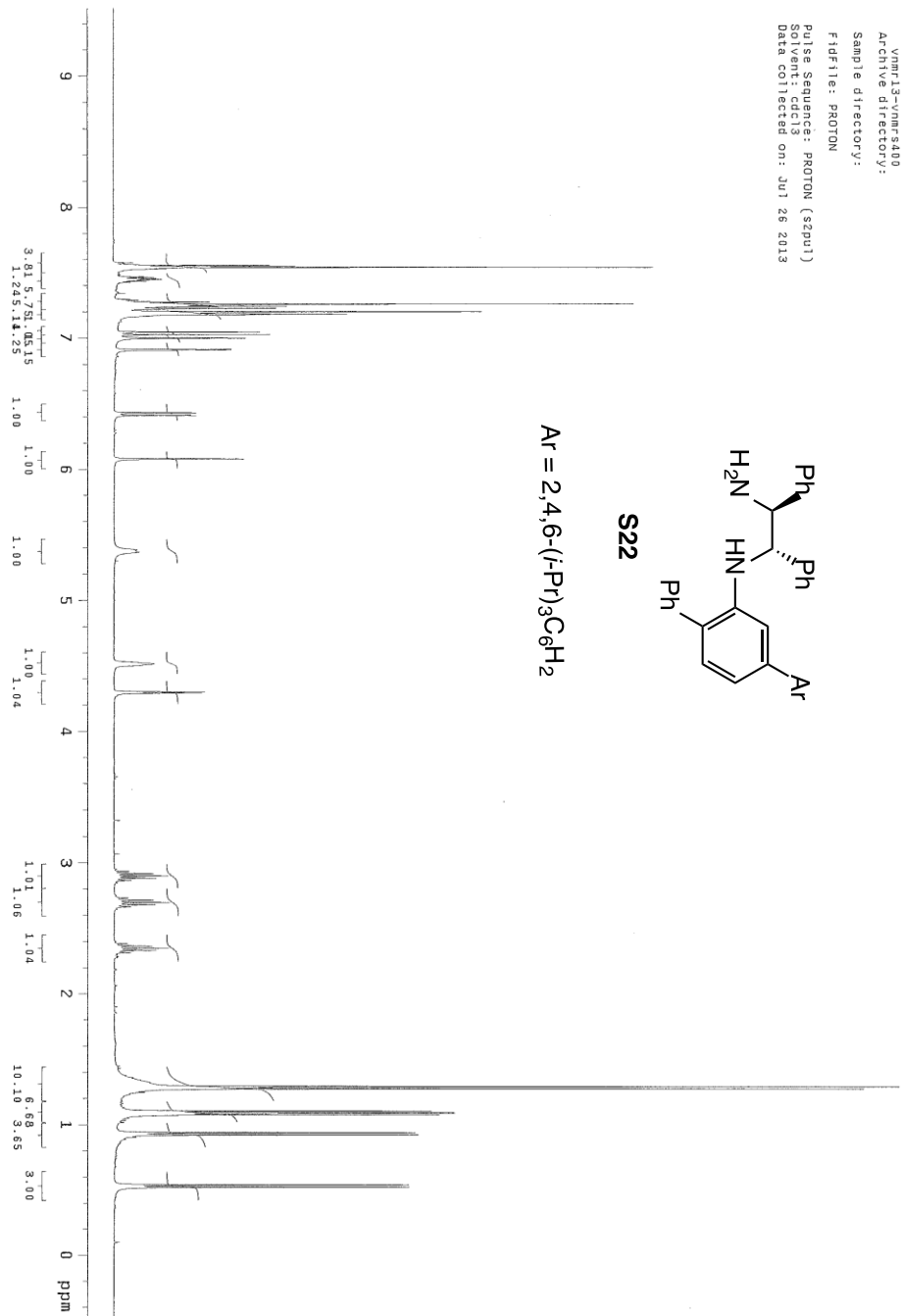
LKA-I-214-CP-F
Sample Name: 8Y-12-134-11-2
Date: 08/18/2013
Operator: vmmr500
Archive directory:
Sample directory:
Fidfile: PROTON
Pulse Sequence: PROTON (szpu1)
Solvent: CDCl3
Data collected on: Jul 22 2013

Ar = 2,4,6-(*i*-Pr)₃C₆H₂

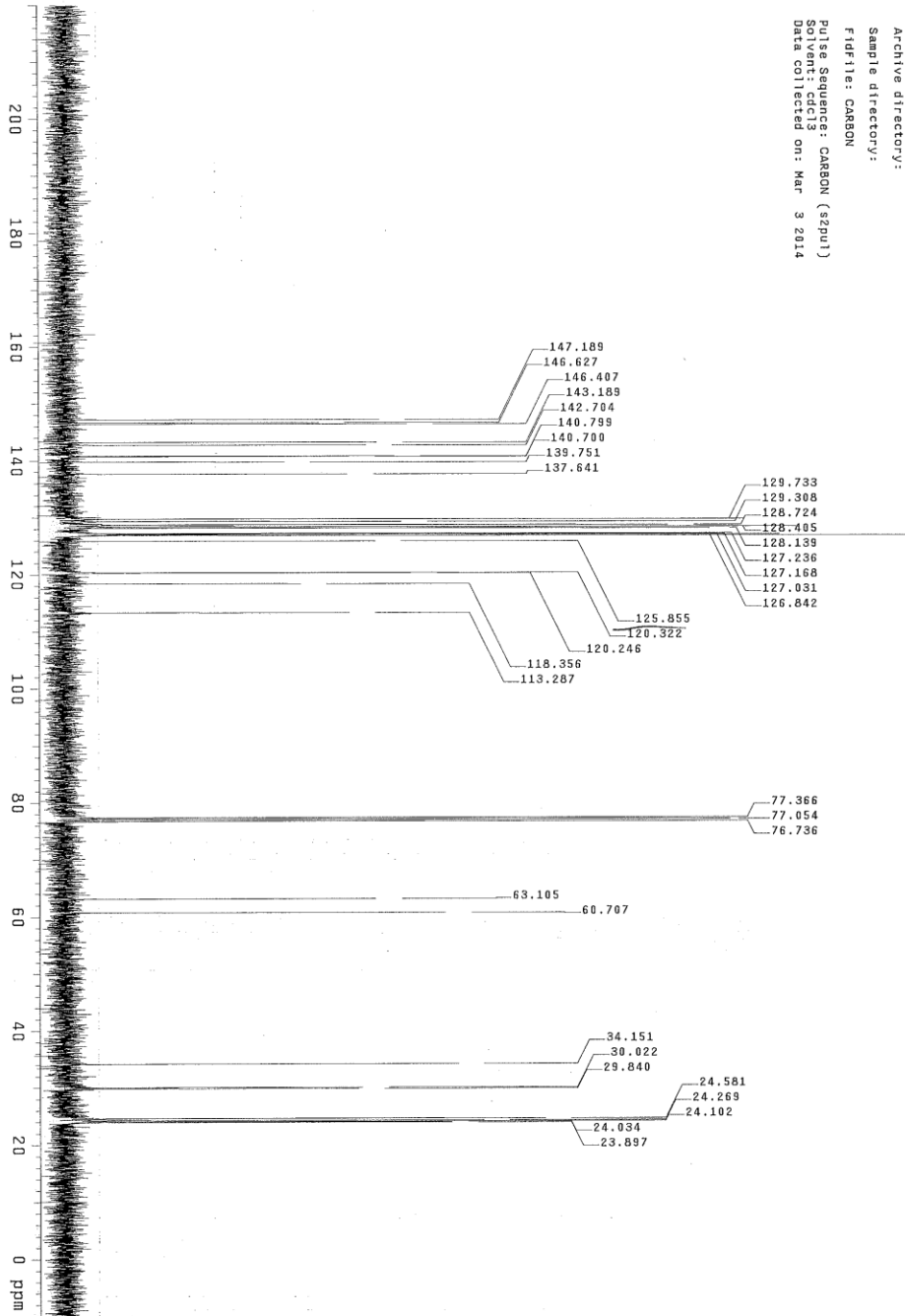




Probe tuning parameter
Sample Name:
Data collected on:
Date: 08-18-2013 09:00
Archive directory:
Sample directory:
FID file: CARBON
Pulse Sequence: CARBON (szpu)
Data collected on: Jul 22 2013

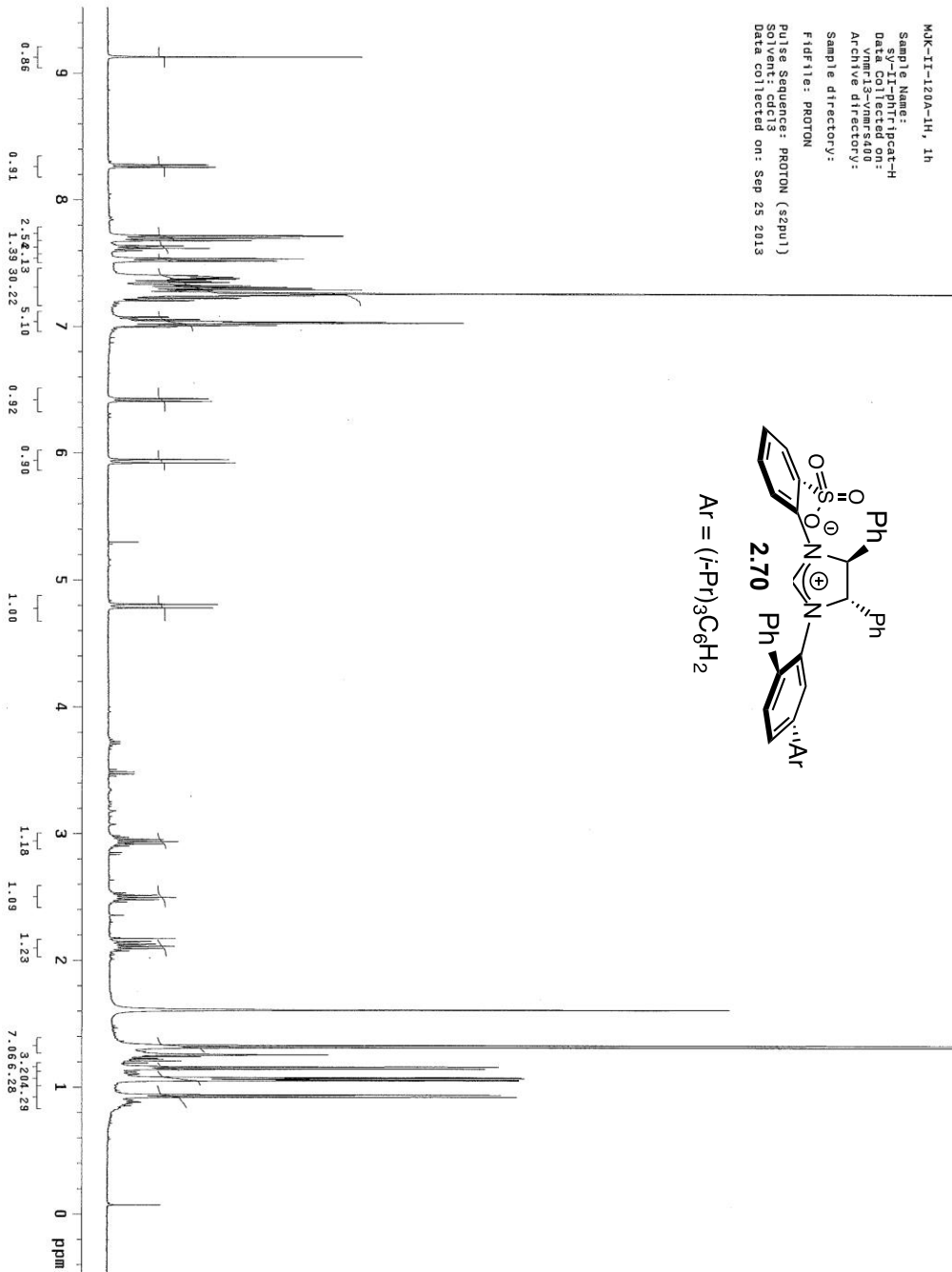
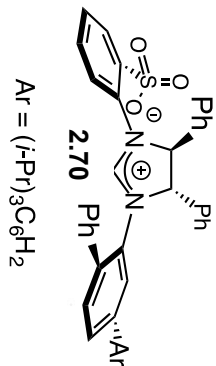


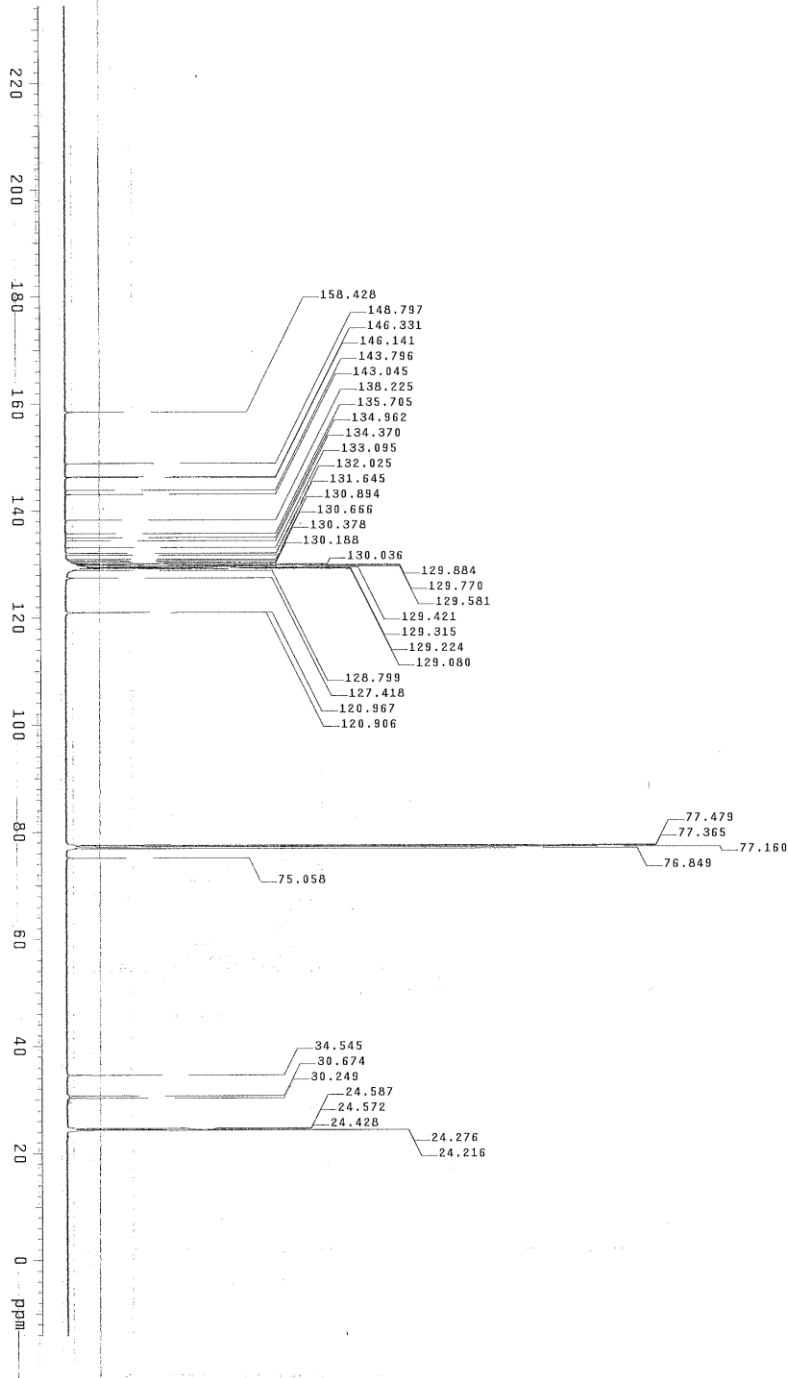
Sample Name: S22
 Date: 2013-07-26
 Sample Directory: /home/...
 FID File: PROTON
 Pulse Sequence: PROTON (sequl)
 Solvent: cdcl3
 Data collected on: Jul 26 2013



TJM-V-117-Ac2
Sample Name:
Sample ID:
Data Collected on:
Vnmr13-vnmr-s400
Archive directory:
Sample directory:
F1 file: CARBON
Pulse Sequence: CARBON (s2pu1)
SO PROPT
Data collected on: Mar 3 2014

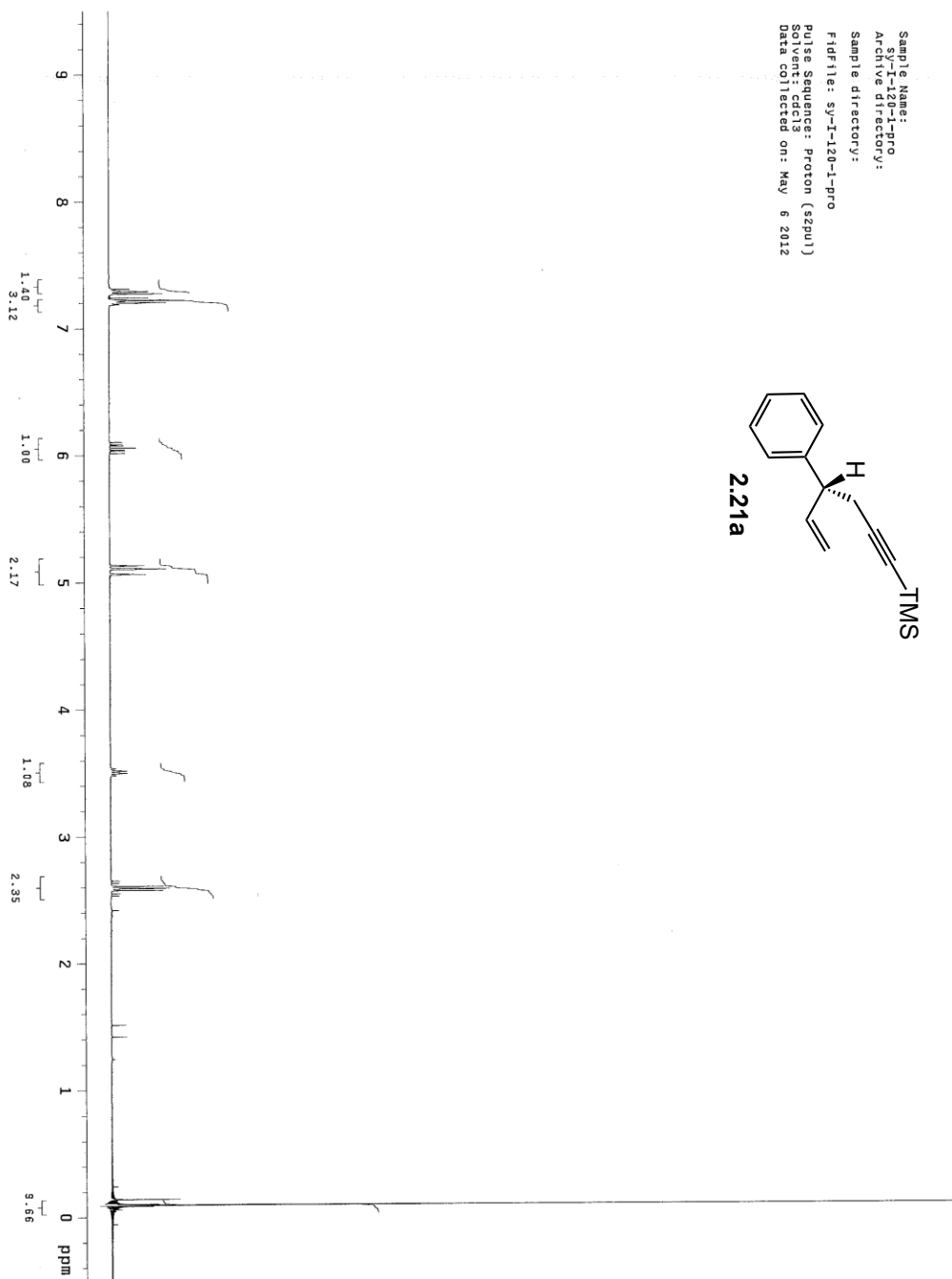
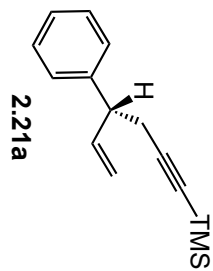
MJK-11-120A-1H, 1h
 Sample Name:
 Exp: 11-120A-1H
 Data Collected on:
 vnmr13-vnmr400
 Archive directory:
 Sample directory:
 F1F11e: PROTON
 Pulse Sequence: PROTON (zgpg3)
 Solvent: cdcl3
 Data collected on: Sep 25 2013

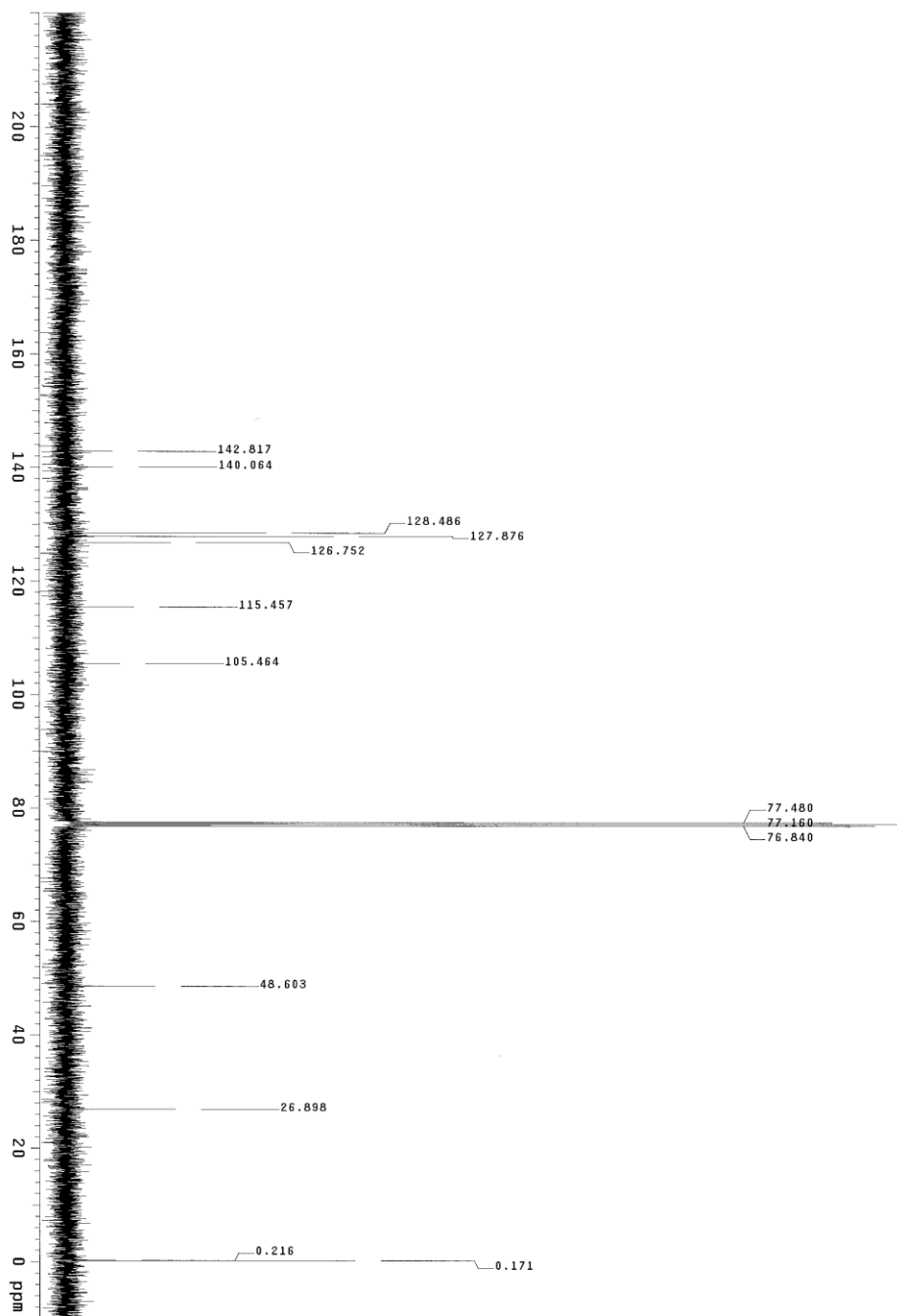




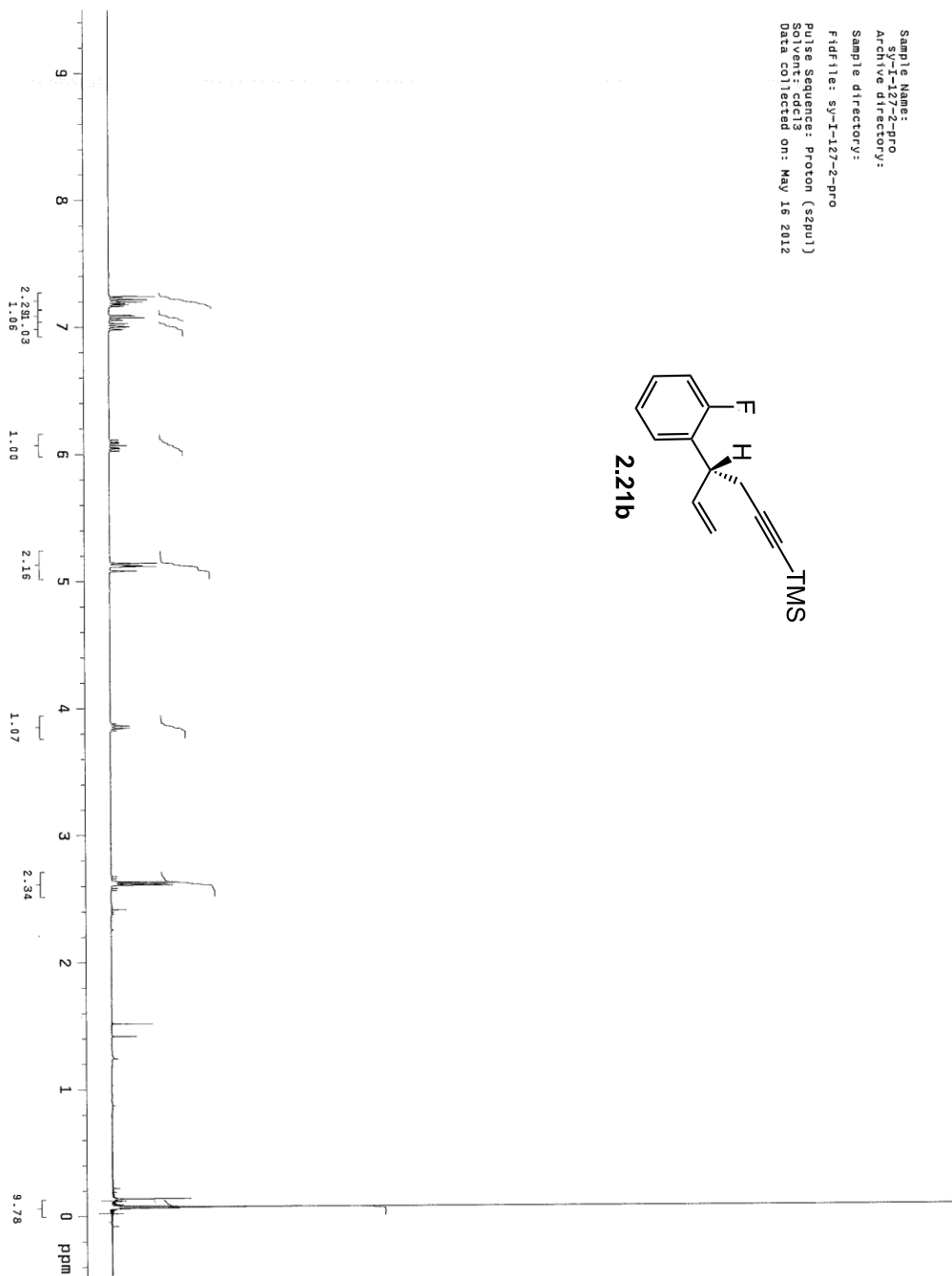
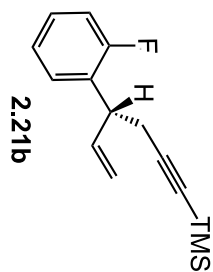
FV-I-046-c
Sample Name: I-046-c
Data Collected on: vnmr13-vnmr13400
Archive directory:
Sample directory:
FID file: CARBON
Pulse Sequence: CARBON (szpu1)
Scan delay: 0.000
Data collected on: Mar 10 2014

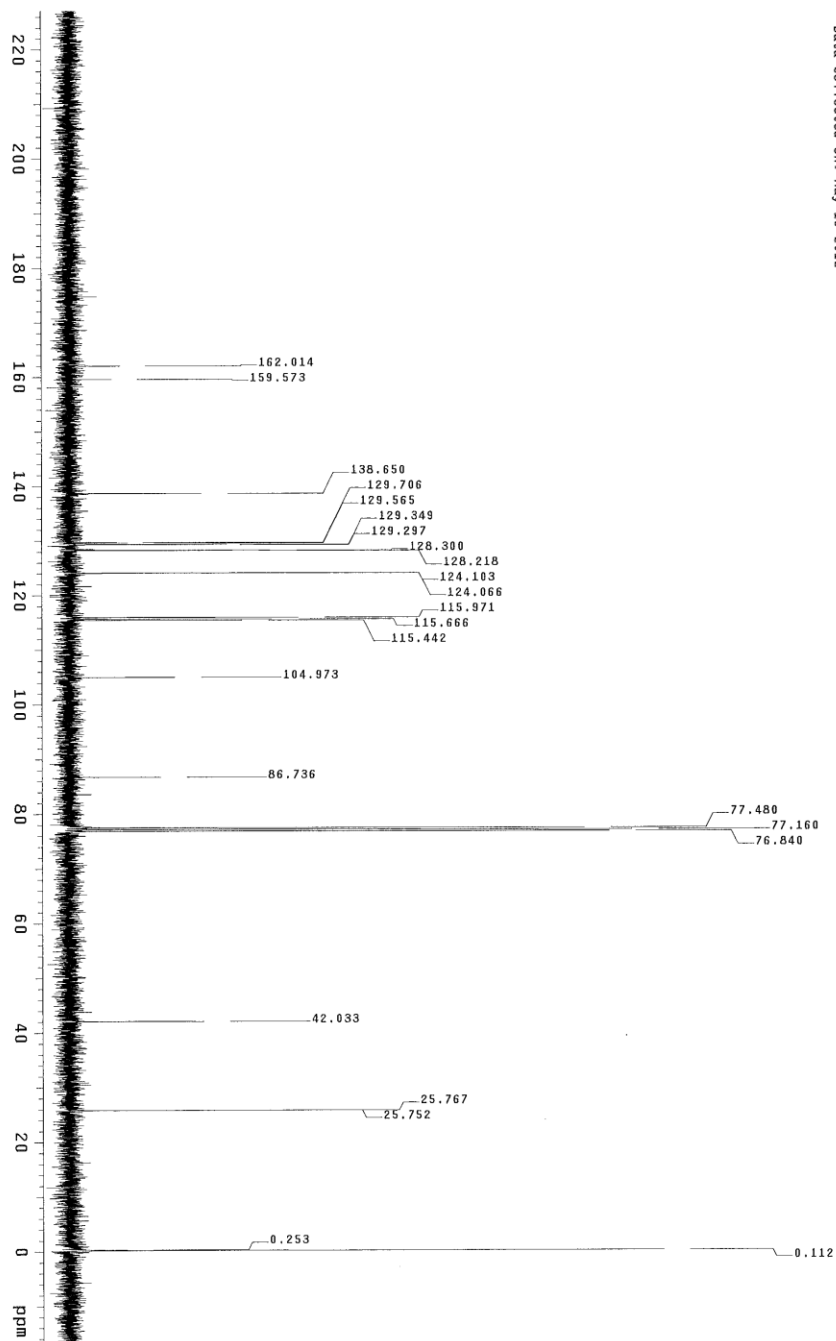
Sample Name: 2.21a
Sample ID: 2.21a-pro
Archive directory:
Sample directory:
Fid file: sj-1-120-1-pro
Pulse Sequence: Proton (szpu1)
Solvent: cdcl3
Data collected on: May 6 2012





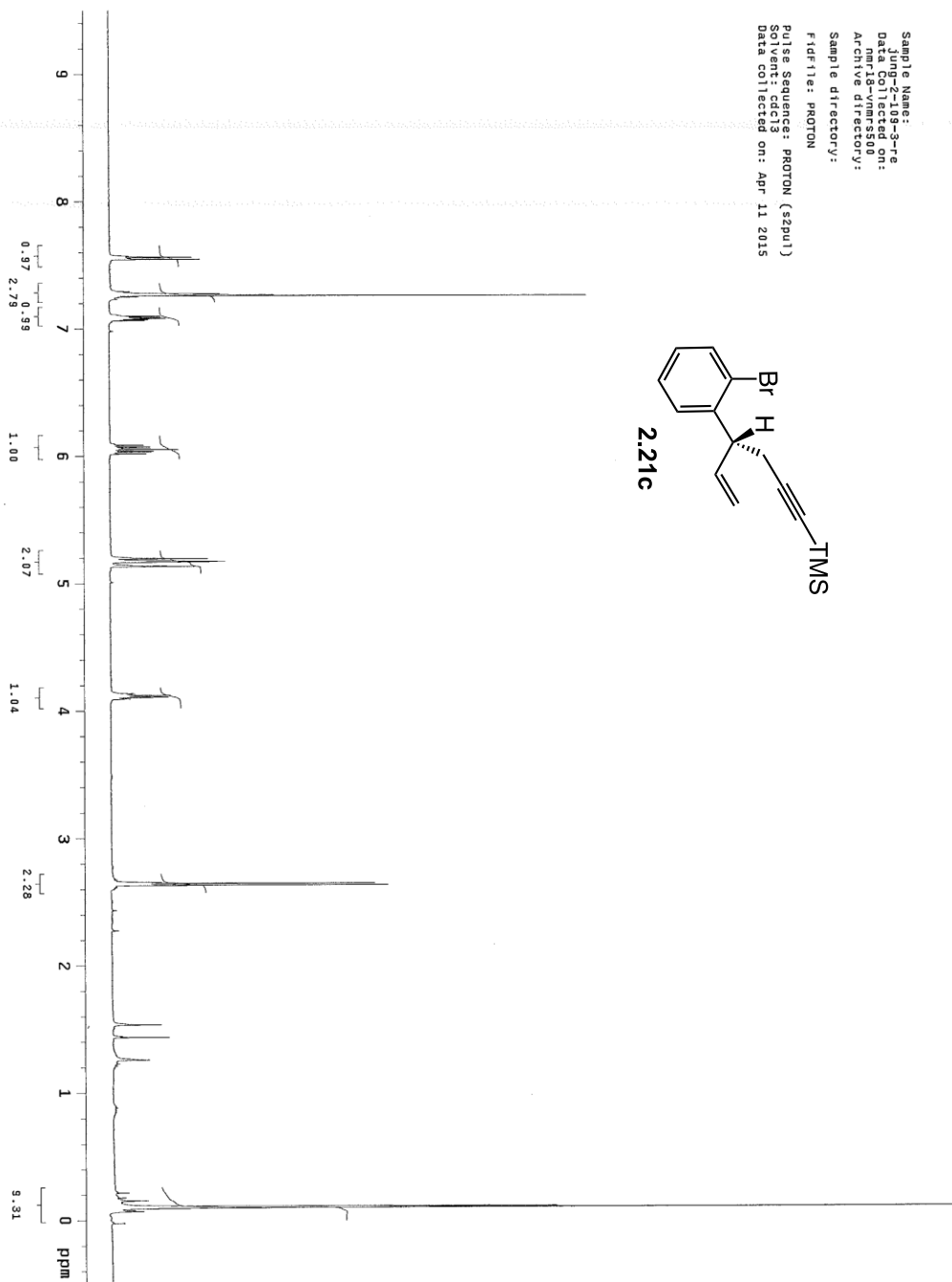
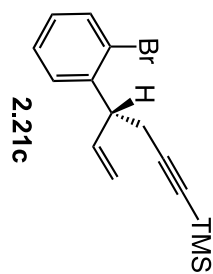
Sample Name: 2-21b
Archive directory:
Sample directory:
Fidfiles: sj-1127-2-pro
Pulse Sequence: Proton (zgpg3)
Solvent: cdcl3
Data collected on: May 16 2012



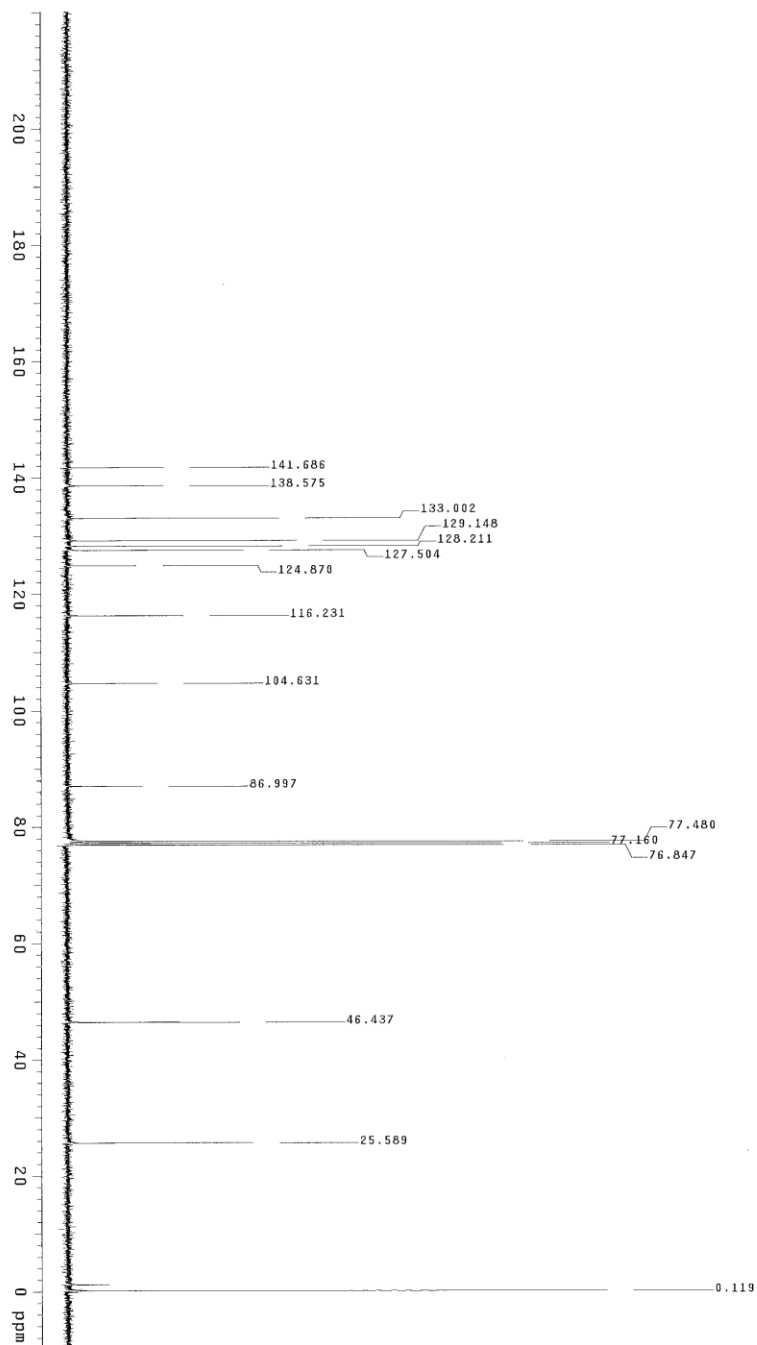


Sample Name: sy-I-128-pro-C
Archive directory:
Sample directory:
Fidfile: sy-I-128-pro
Pulse Sequence: Carbon (szpu1)
Solvent: CDCl3
Data collected on: May 16 2012

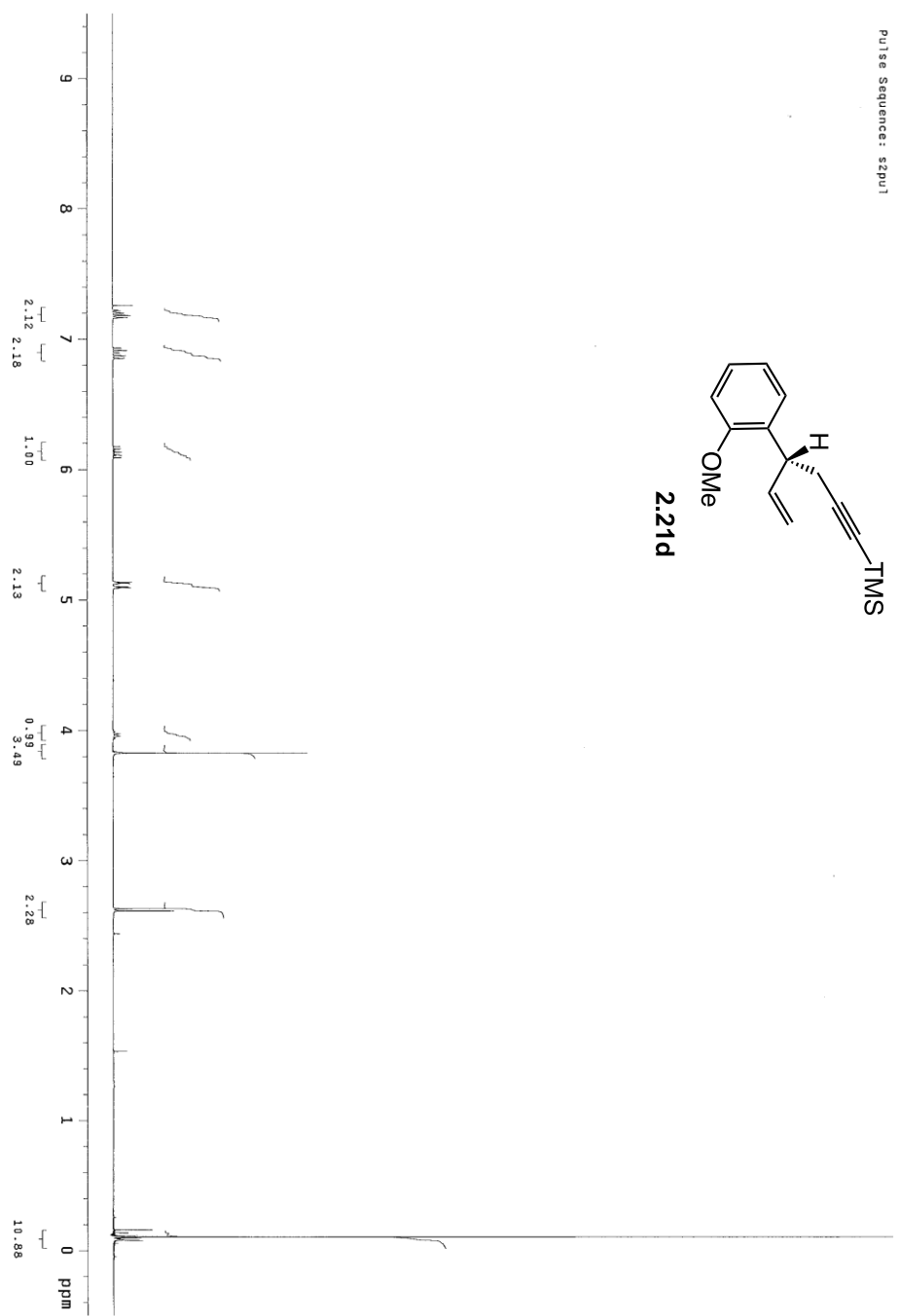
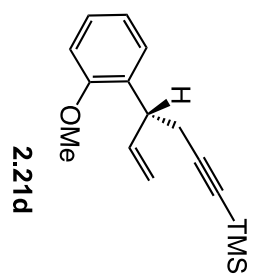
Sample Name: 4106-2106-3-rf
Data Collected on: nmr18-ymr5500
Archive directory:
Sample directory:
Fid file: PROTON
Pulse Sequence: PROTON (s2pu1)
Solvent: cdcl3
Data collected on: Apr 11 2015

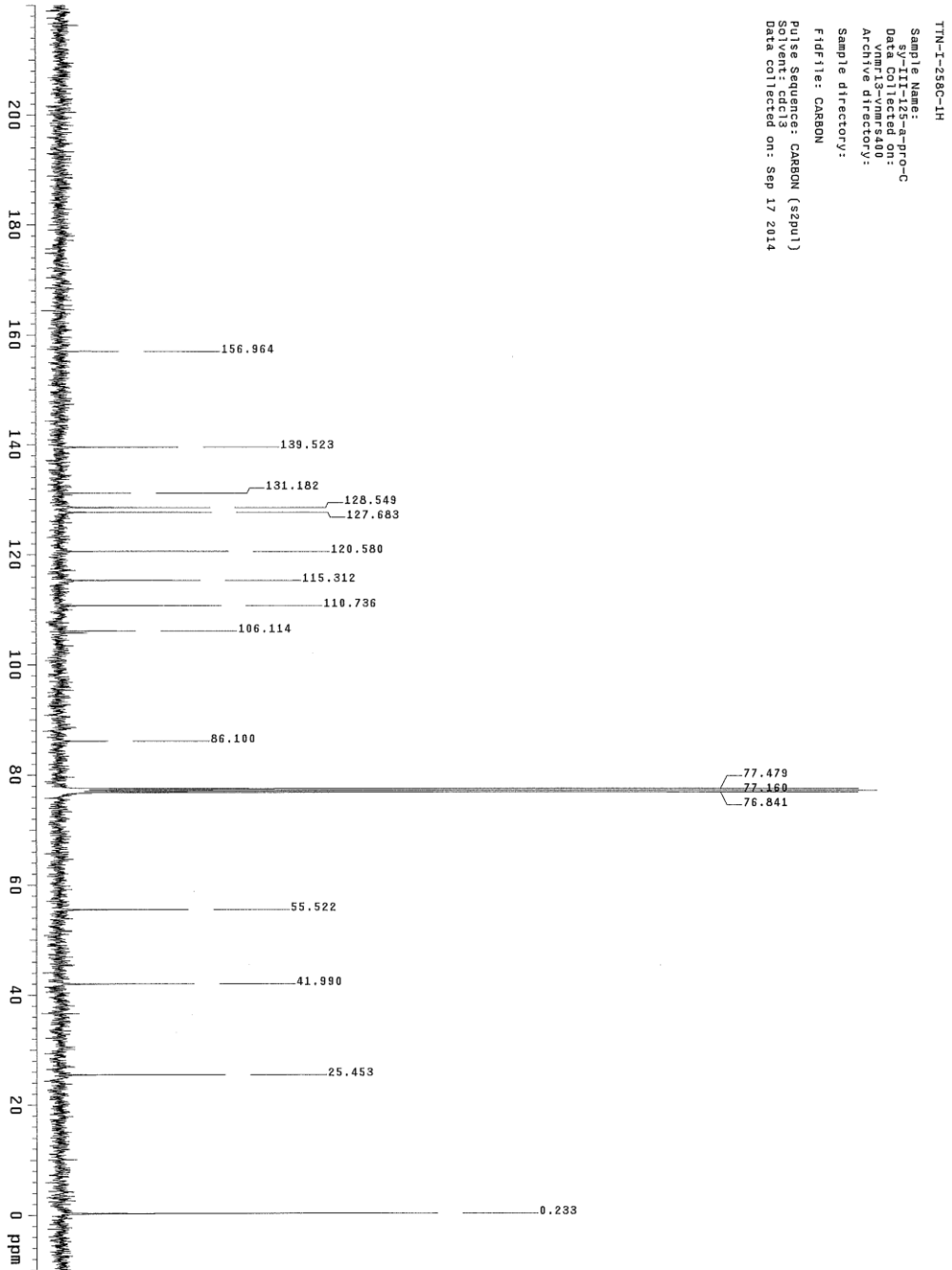


Sample: sy-1-1s9-b-pro
File: exp
Pulse Sequence: zgpu1

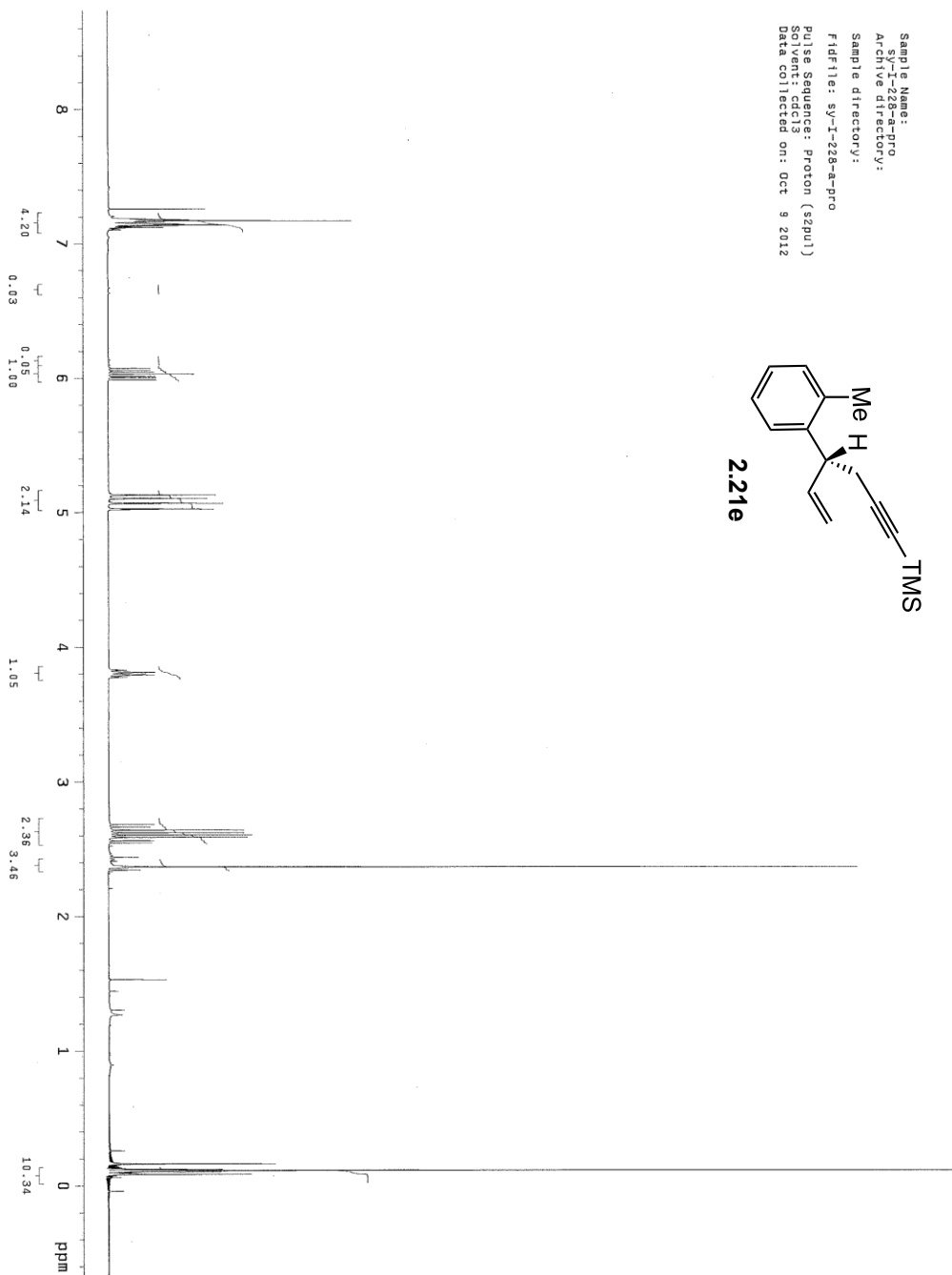
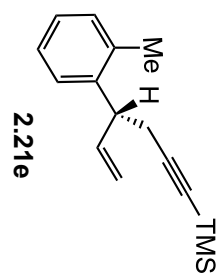


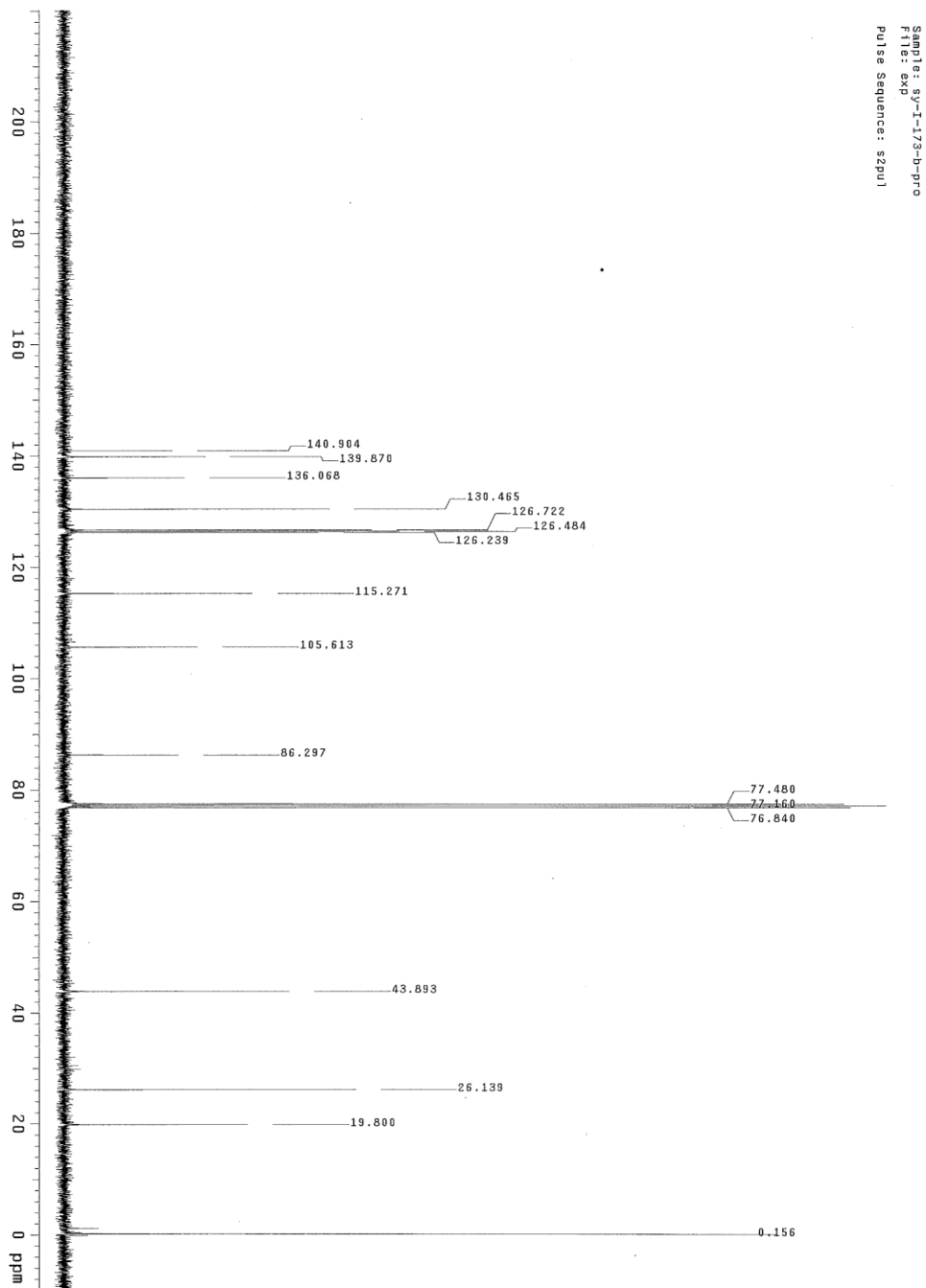
Sample: sy-I-228-b-pro
File: exp
Pulse Sequence: szpu1



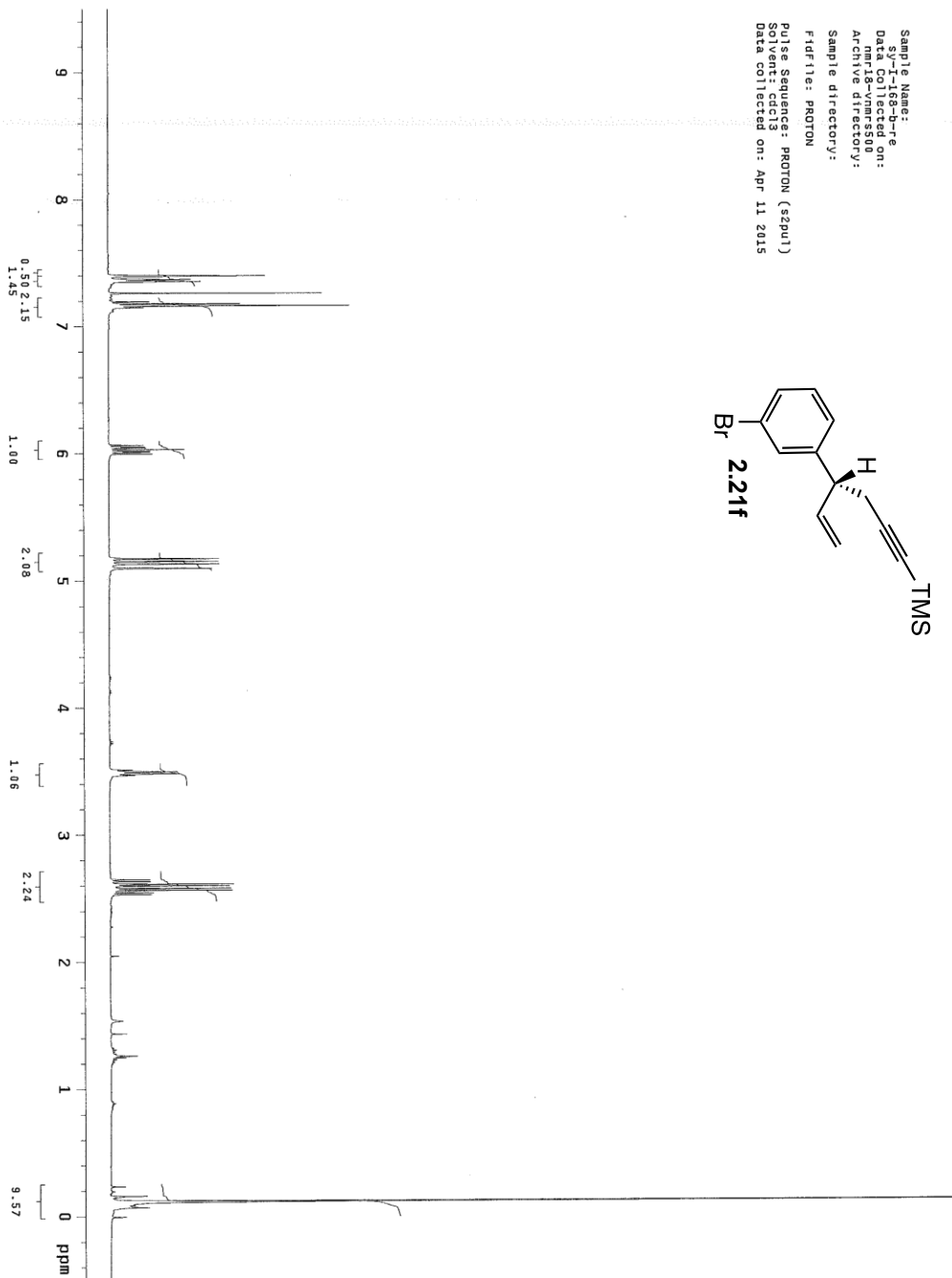
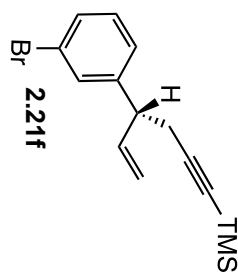


Sample Name: 2.21e-2012
Archive directory:
Sample directory:
Fidfile: sv-T-228-a-pro
Pulse Sequence: Proton (szpu1)
Solvent: cdcl3
Data collected on: Oct 9 2012

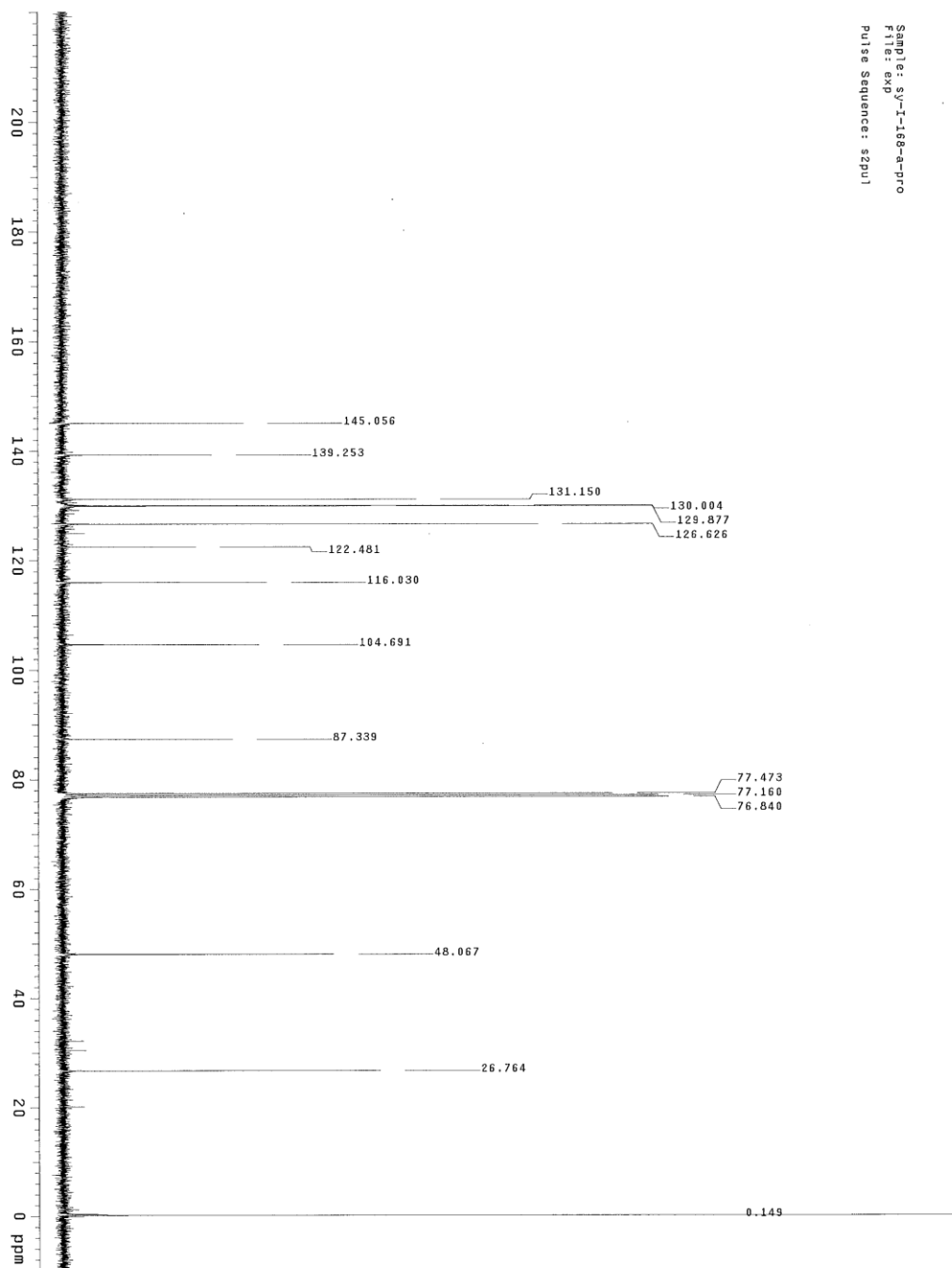




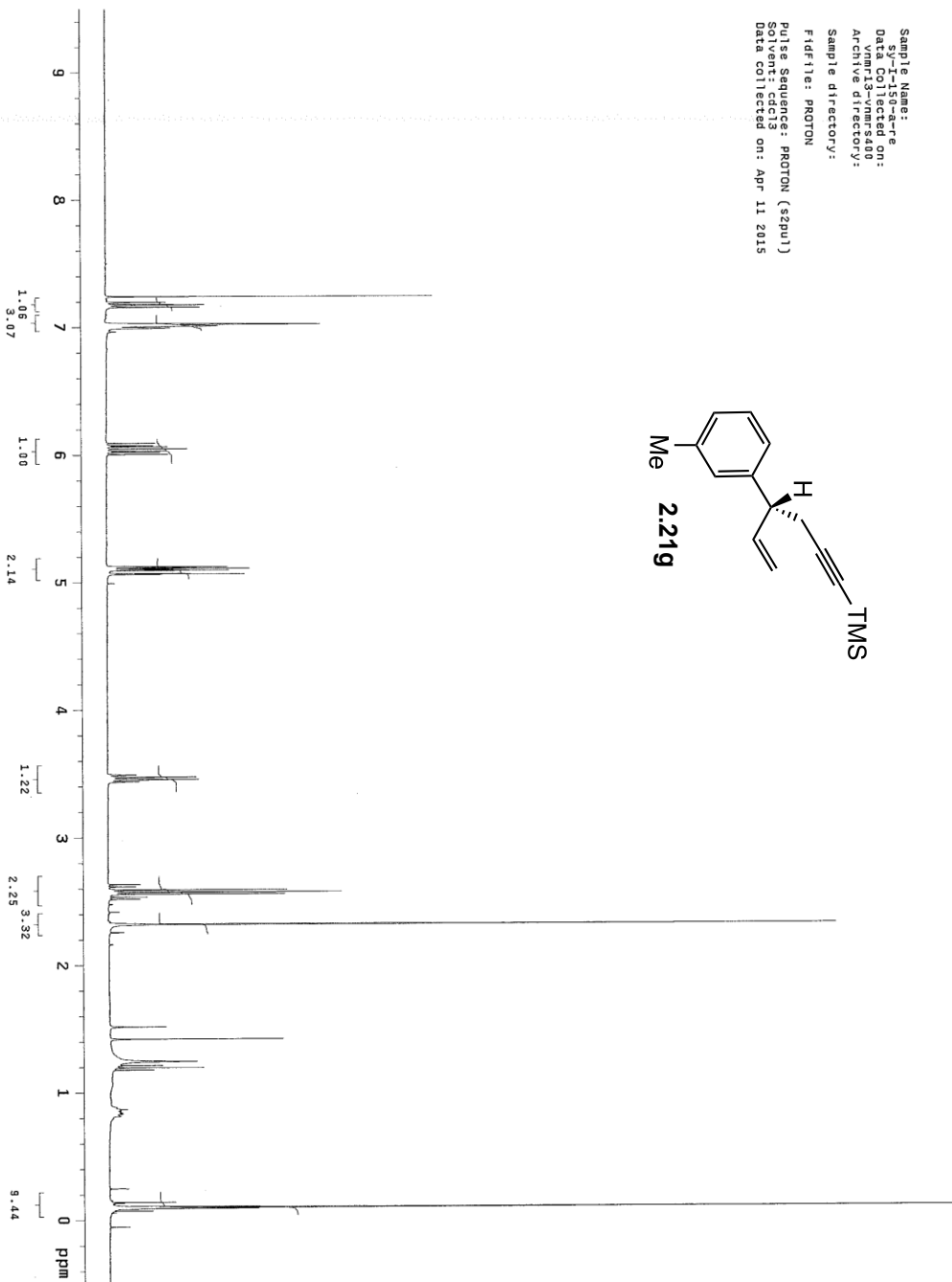
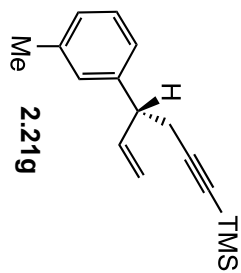
Sample Name: 165b-re
 Data collected on: mm18-vnmr500
 Archive directory:
 Sample directory:
 F1dfile: PROTON
 Pulse Sequence: PROTON (s2pu1)
 Solvent: cdcl3
 Data collected on: Apr 11 2015

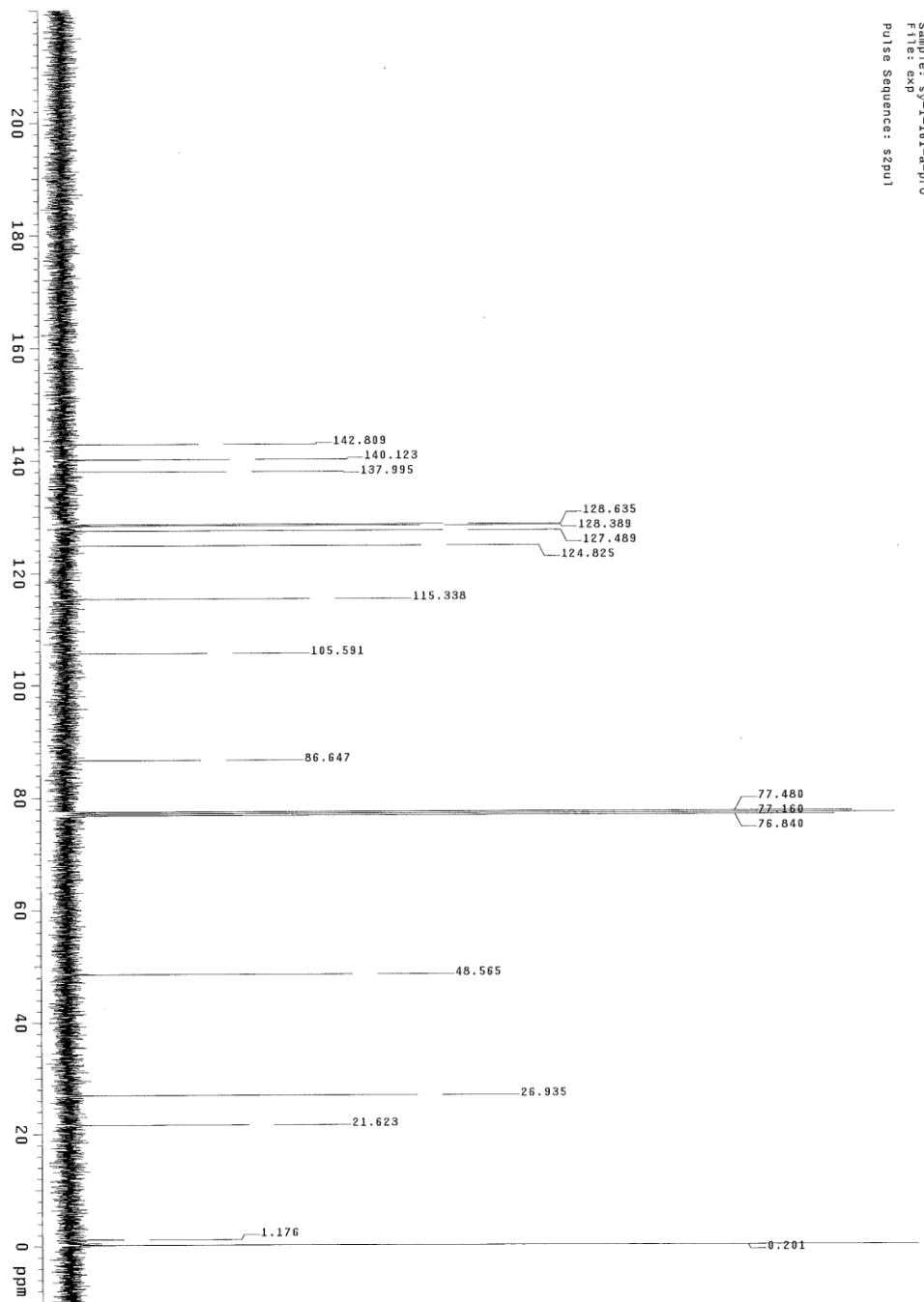


Sample: SY-I-168-a-pro
File: exp
Pulse Sequence: szpu1

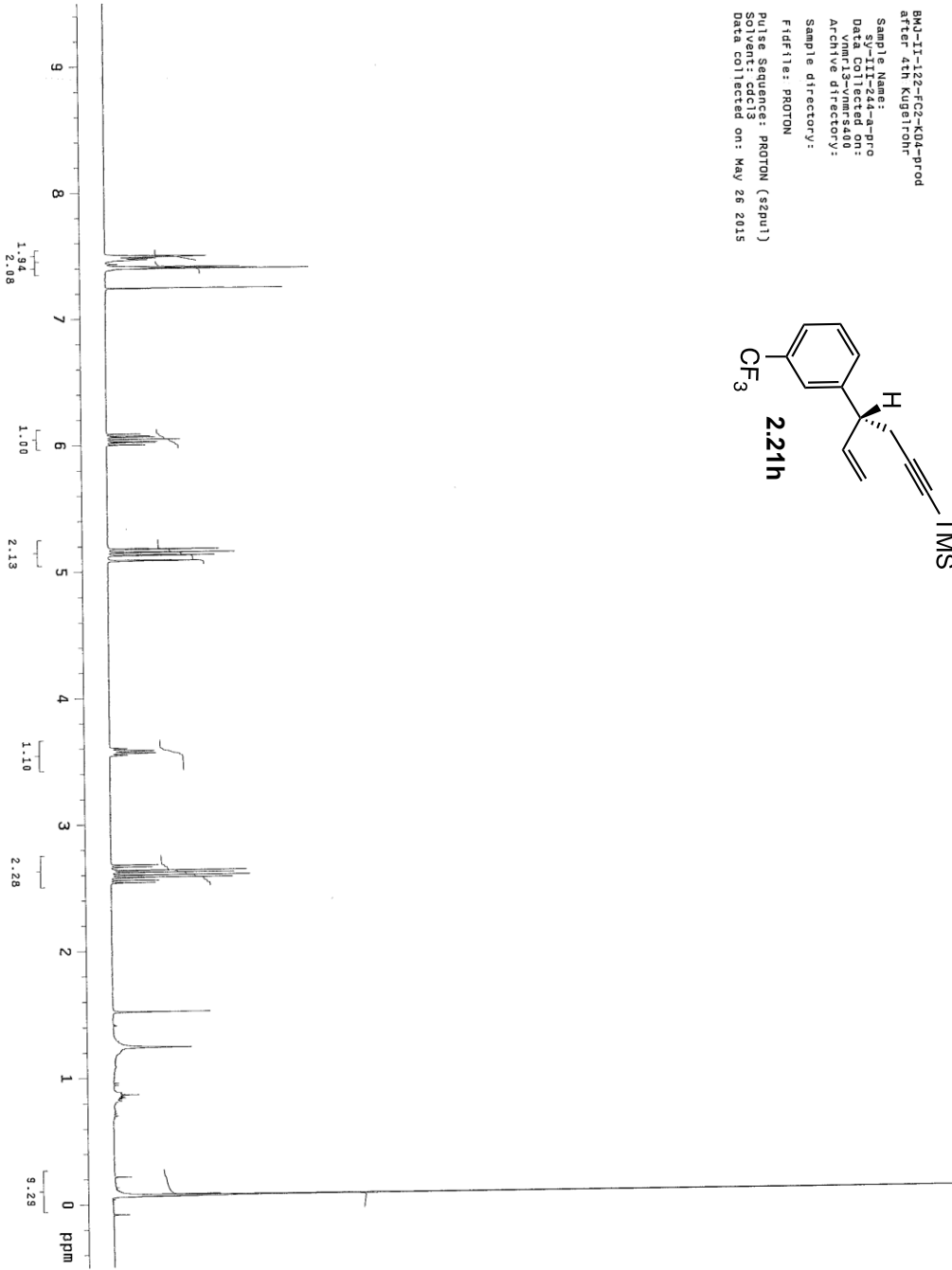
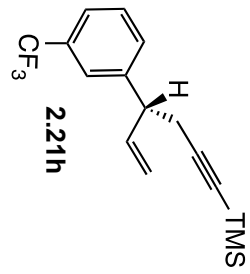


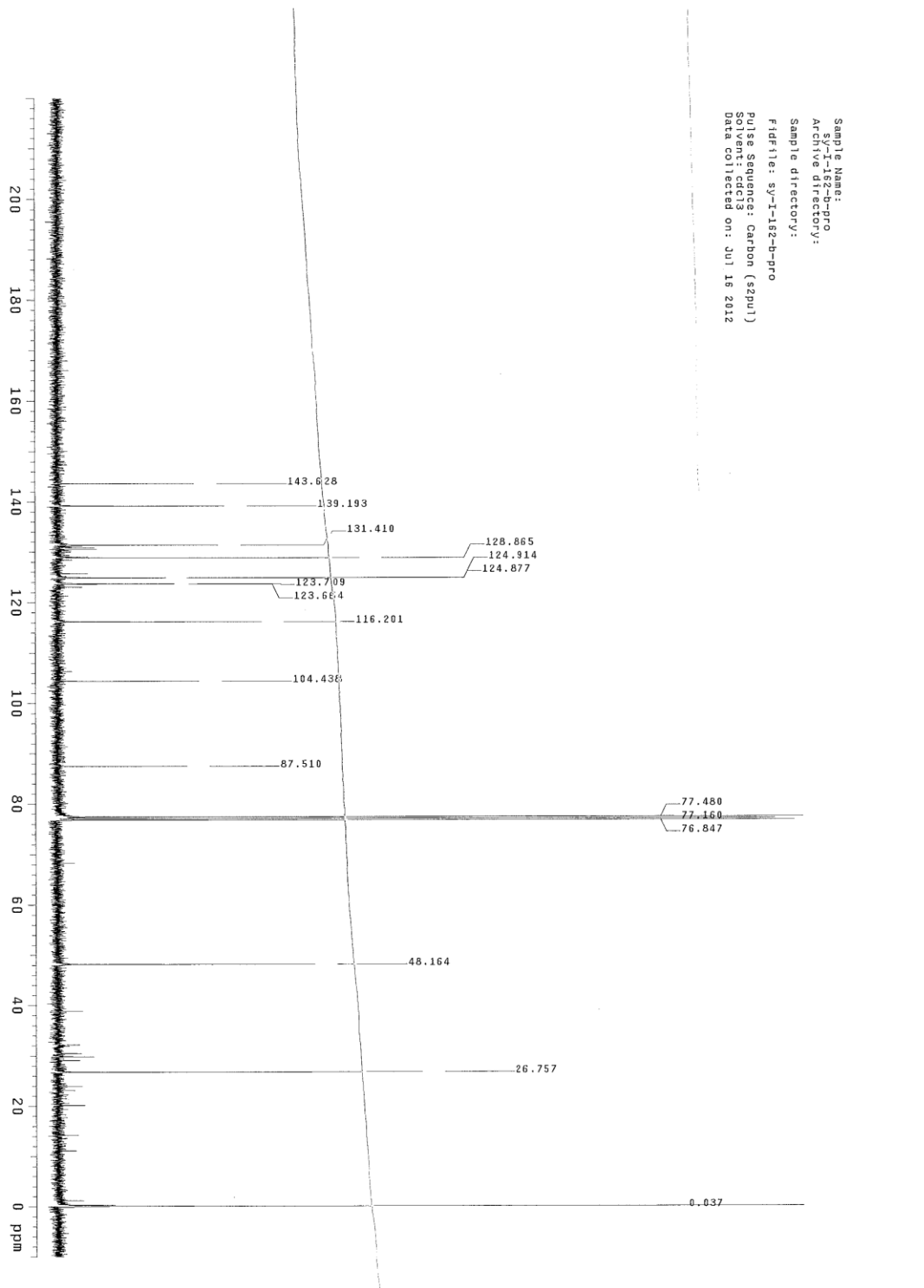
Sample Name: 2.219
 Sample ID: 2.219
 Data Collected on: vnmr13-vnmr-s400
 Archive directory:
 Sample directory:
 F1dfile: PROTON
 Pulse Sequence: PROTON (zgpg3)
 Solvent: cdcl3
 Data collected on: Apr 11 2015



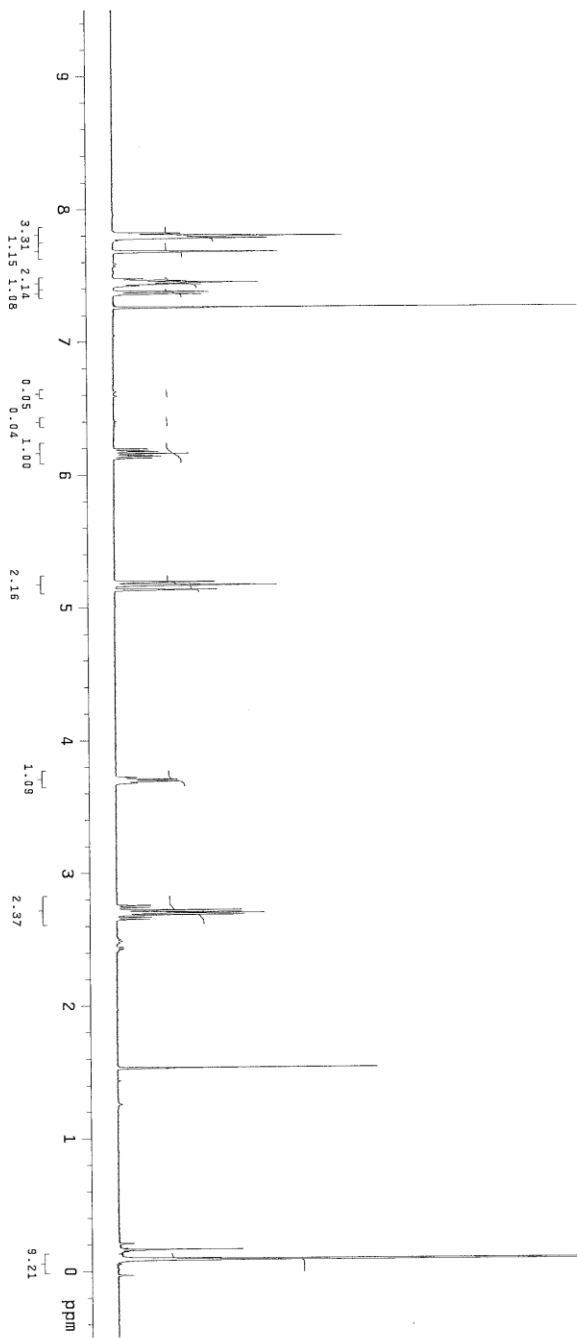
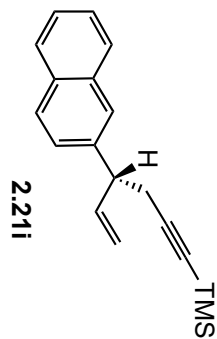


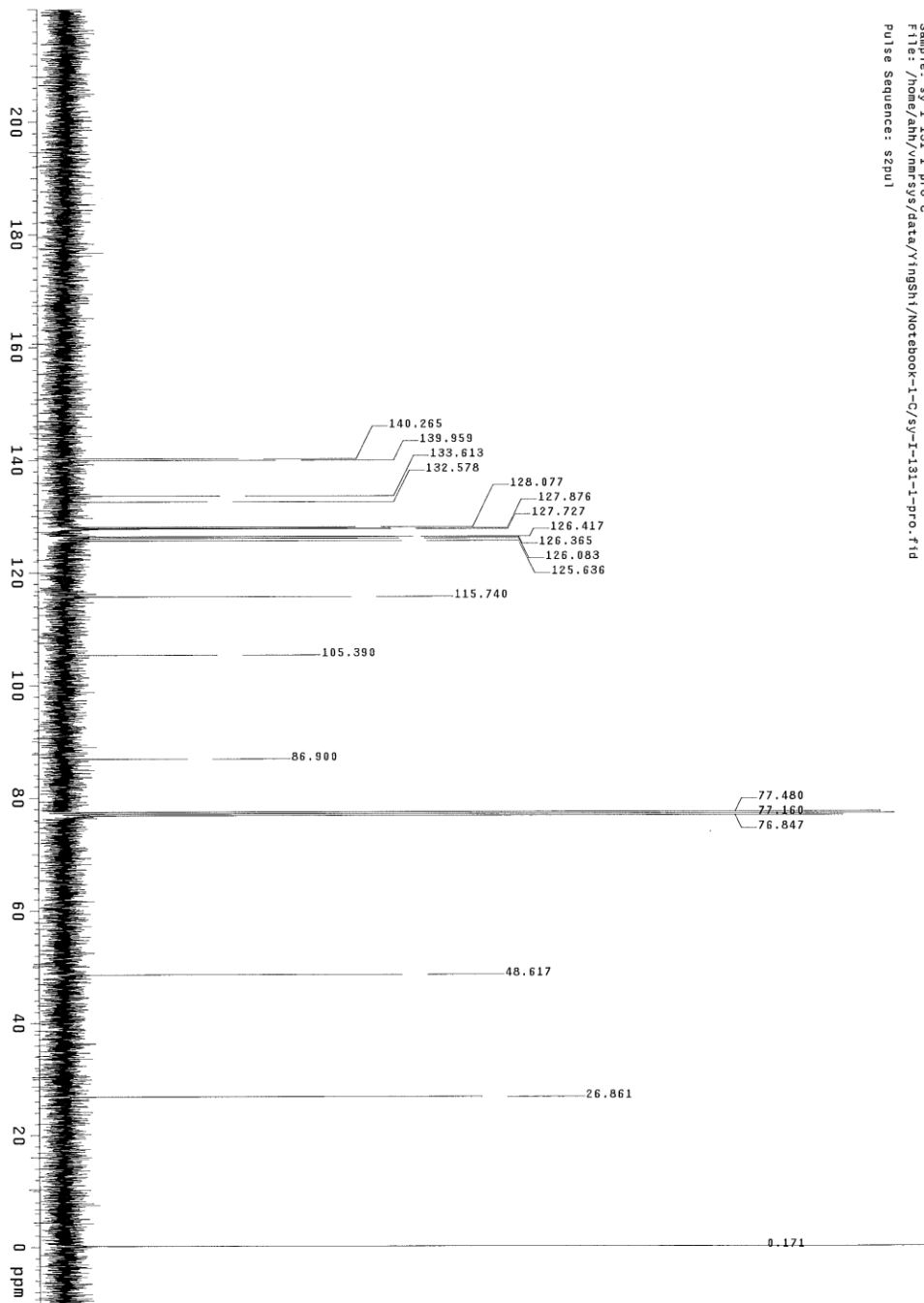
BMJ-II-122-FC2-K04-prod
after 4th Kugelrohr
Sample Name:
SP-II-244-a-pro
Data collected on:
Vnmr13-vnmr5400
Archive directory:
Sample directory:
Fidfile: PROTON
Pulse Sequence: PROTON (zgpg1)
Solvent: cdcl3
Data collected on: May 26 2015



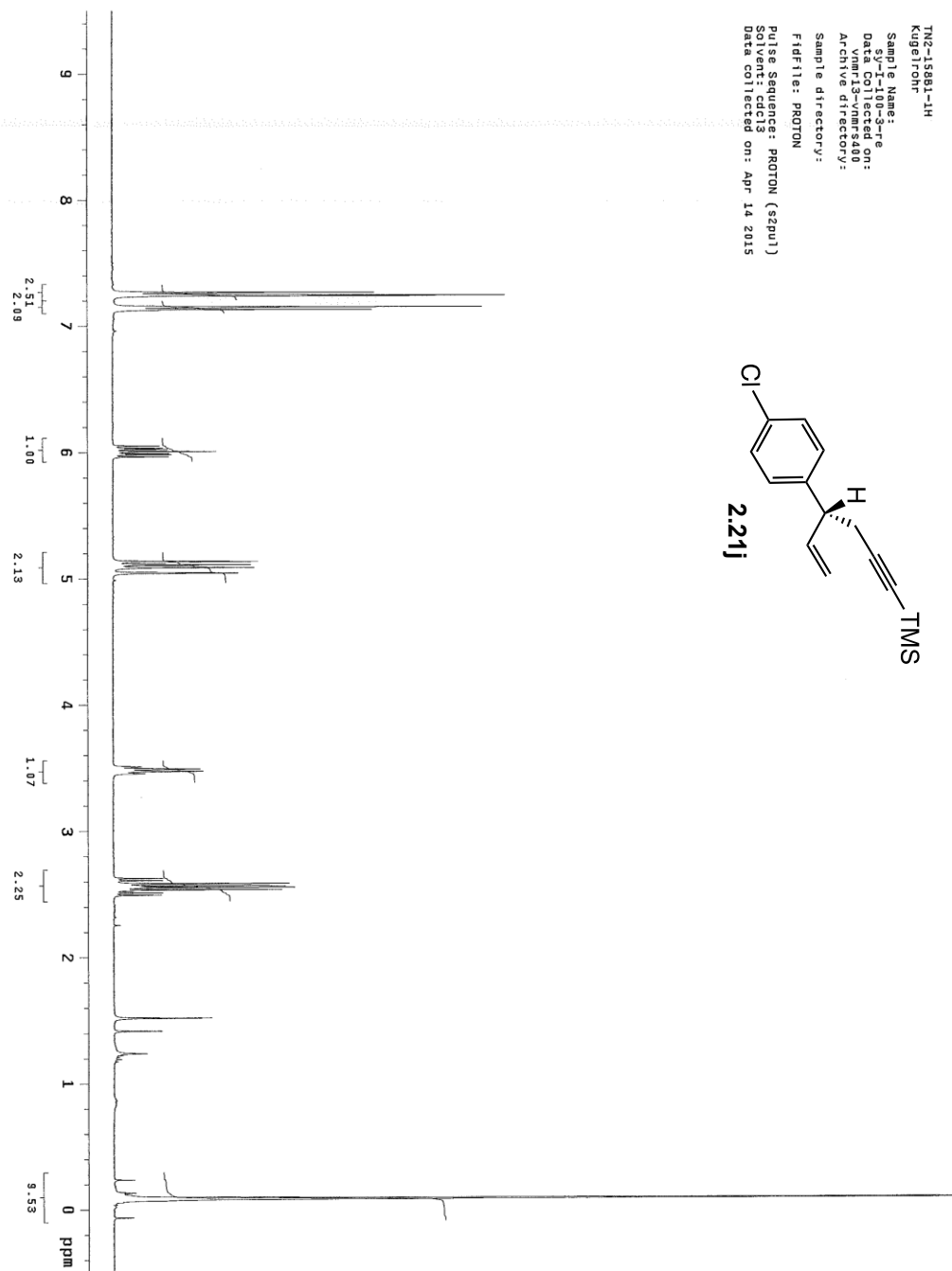
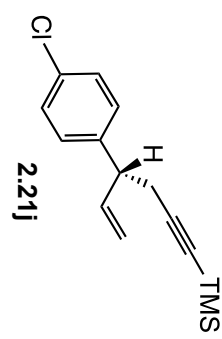


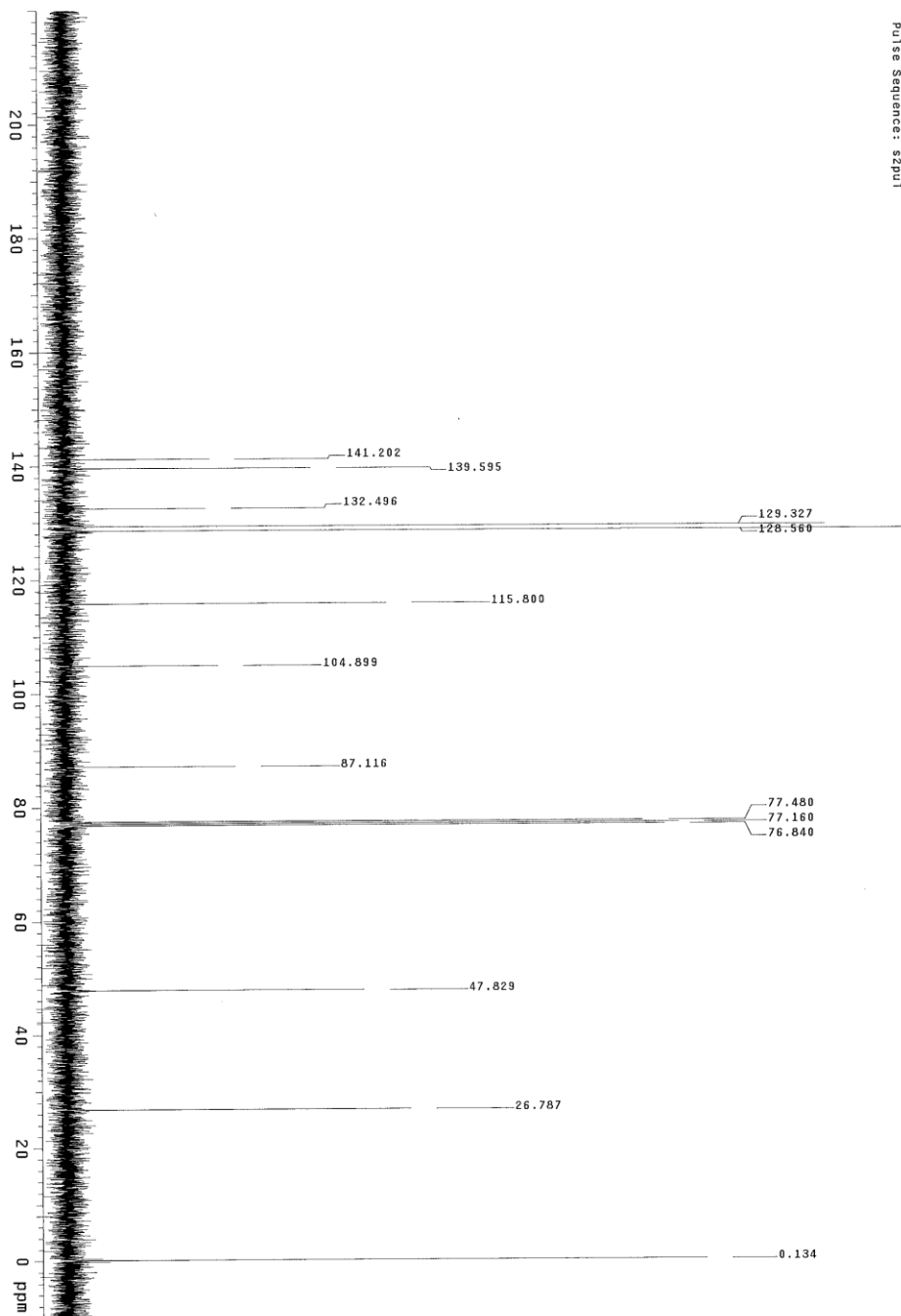
Sample Name: sy-1-132-2-pro
 Archive directory:
 Sample directory:
 Fidfile: sy-1-132-2-pro
 Pulse Sequence: Proton (szpu1)
 Solvent: cdcl3
 Data collected on: Jun 5 2012



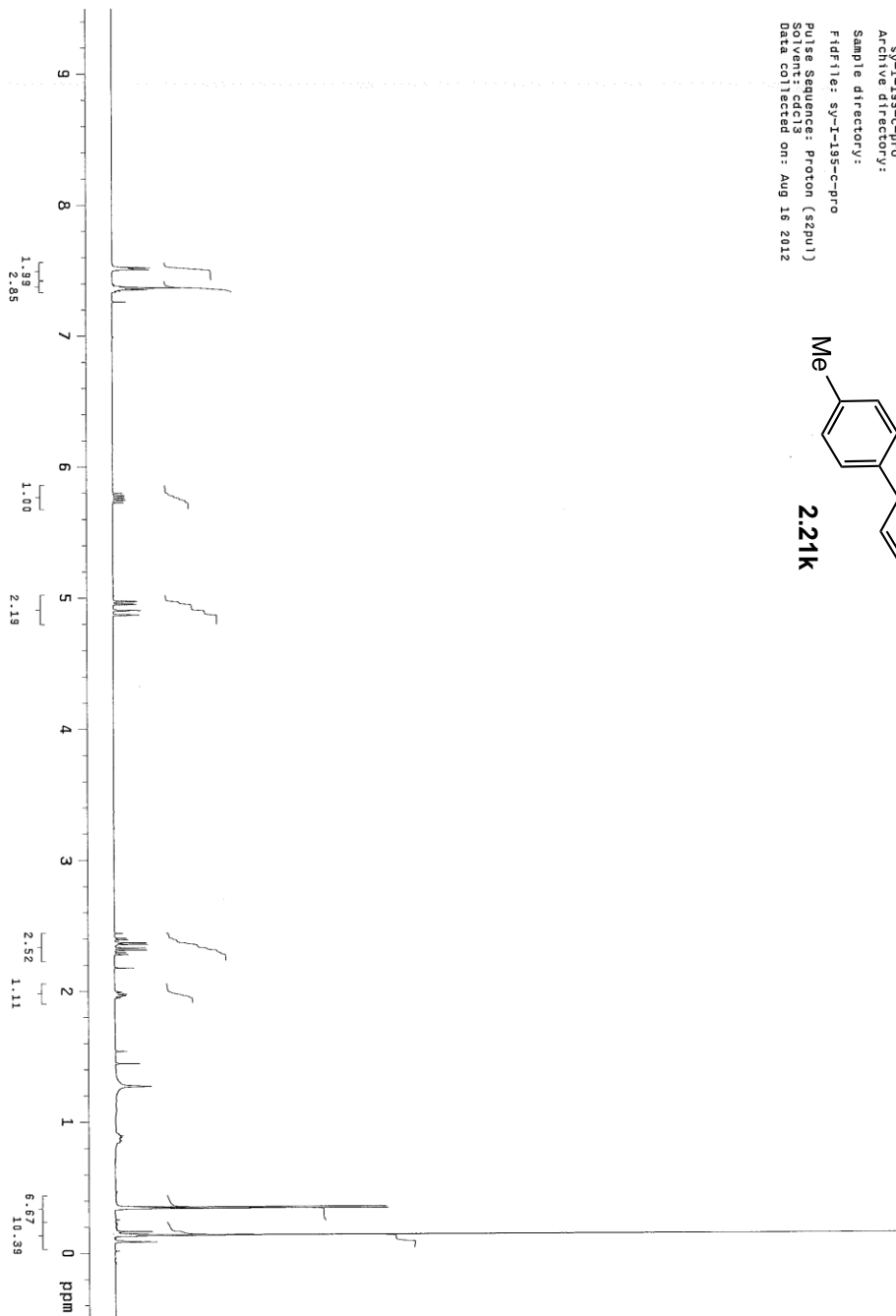
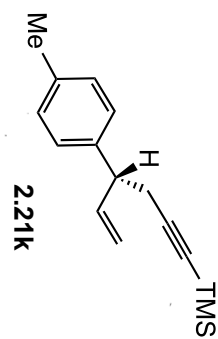


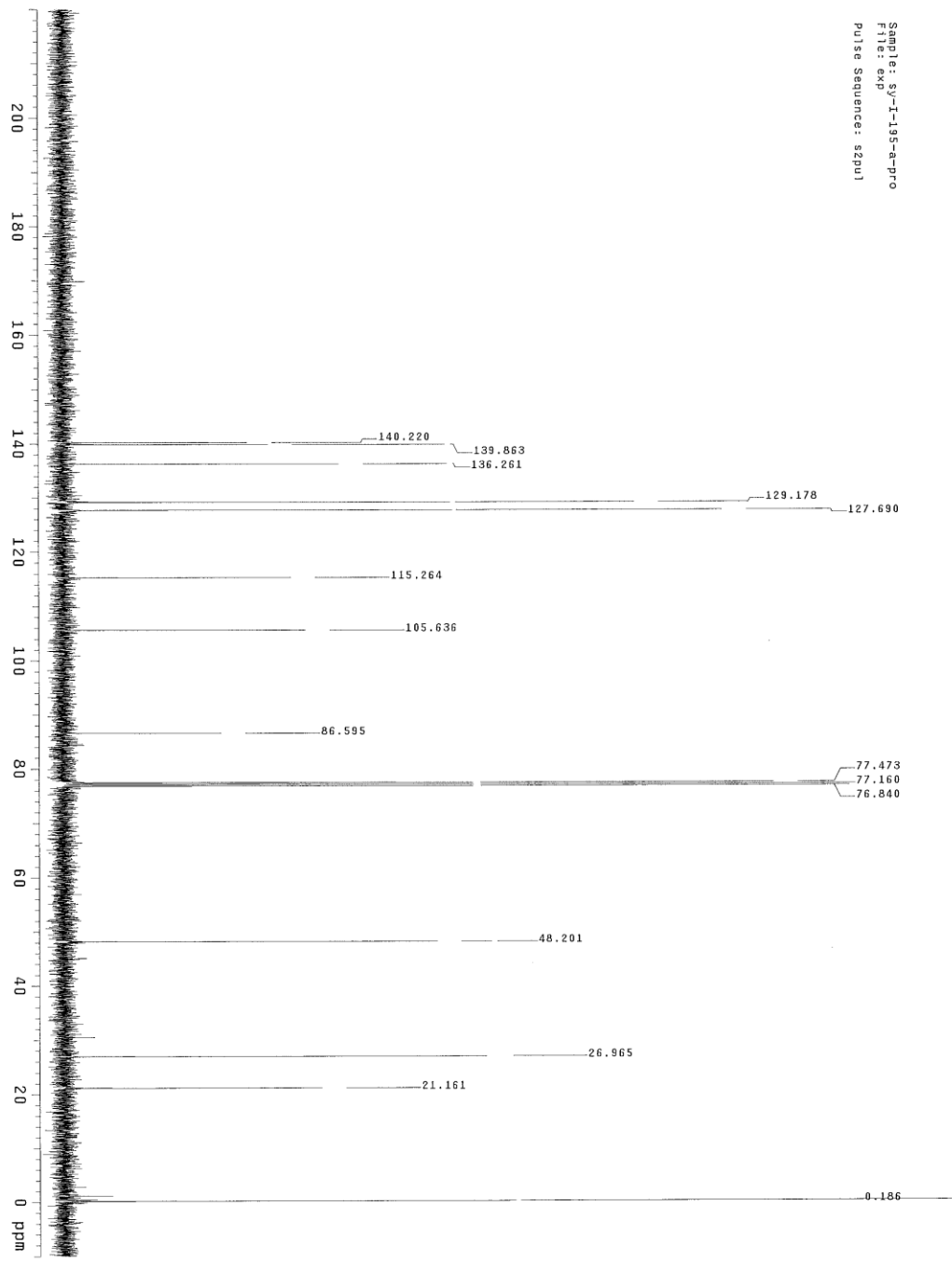
TN2-15281-1H
 Kugelrohr
 Sample Name:
 sy-I-100-3-re
 Data Collected on:
 Vnmr13-vnmr5400
 Archive directory:
 Sample directory:
 F1dfile: PROTON
 Pulse Sequence: PROTON (szpu1)
 Solvent: cdcl3
 Data collected on: Apr 14 2015





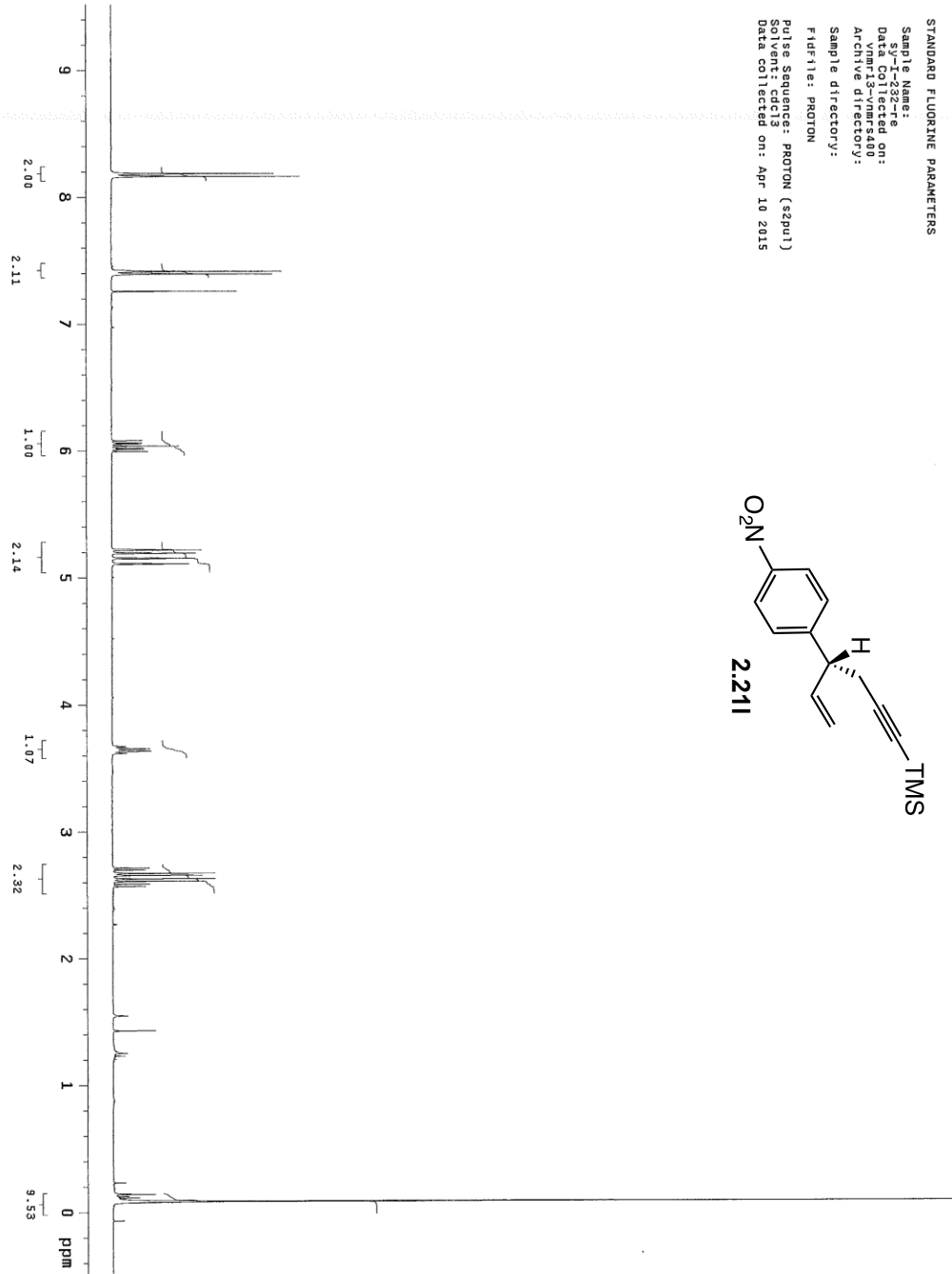
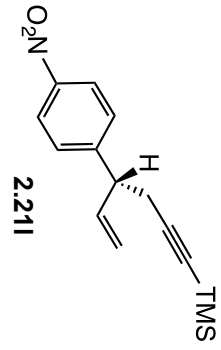
TJM-IV-018-c
 Sample Name: sy-I-195-c-pro
 Archive directory:
 Sample directory:
 FIDFile: sy-I-195-c-pro
 Pulse Sequence: Proton (zgpg3)
 Solvent: cdcl3
 Data collected on: Aug 18 2012

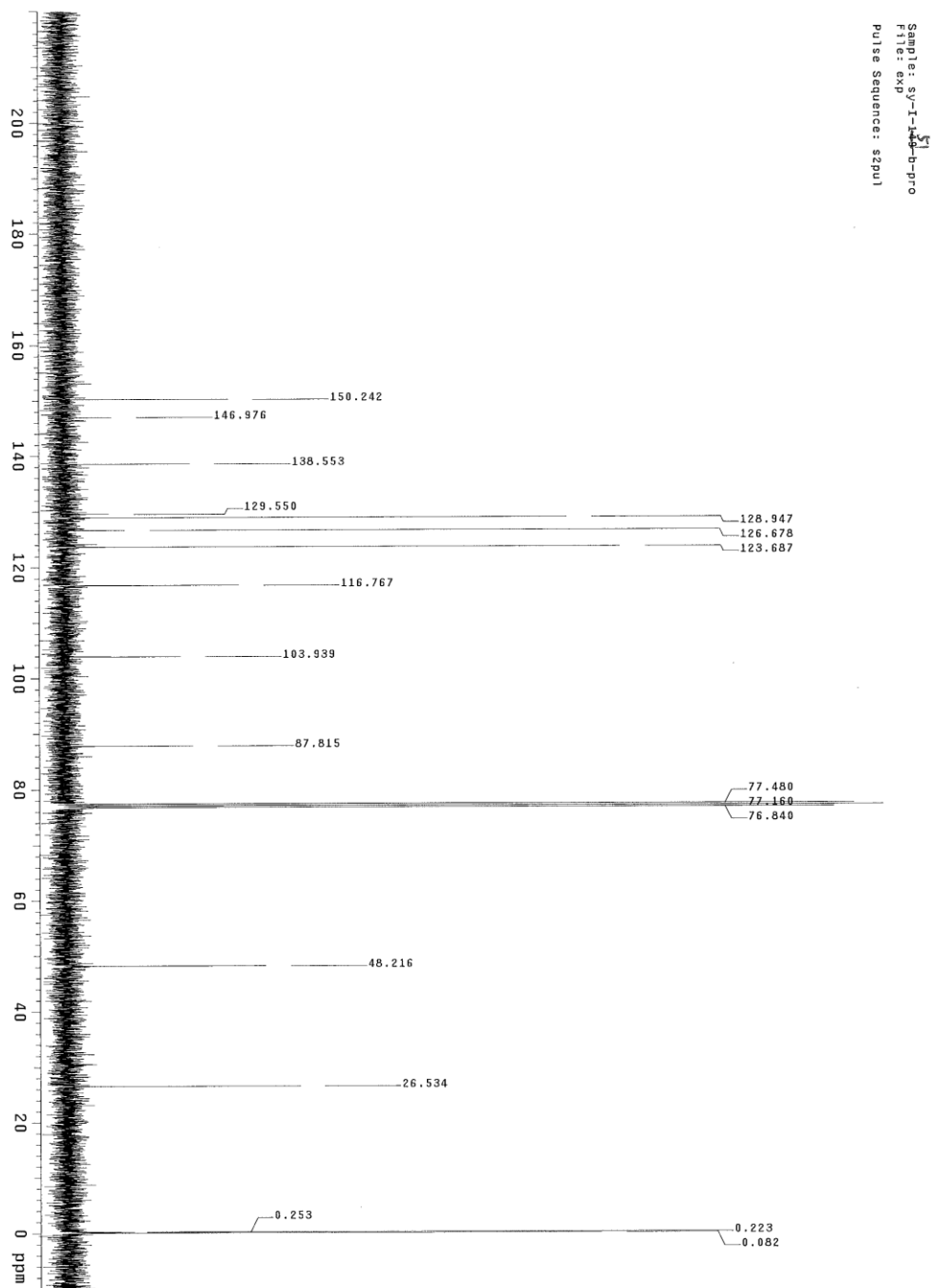




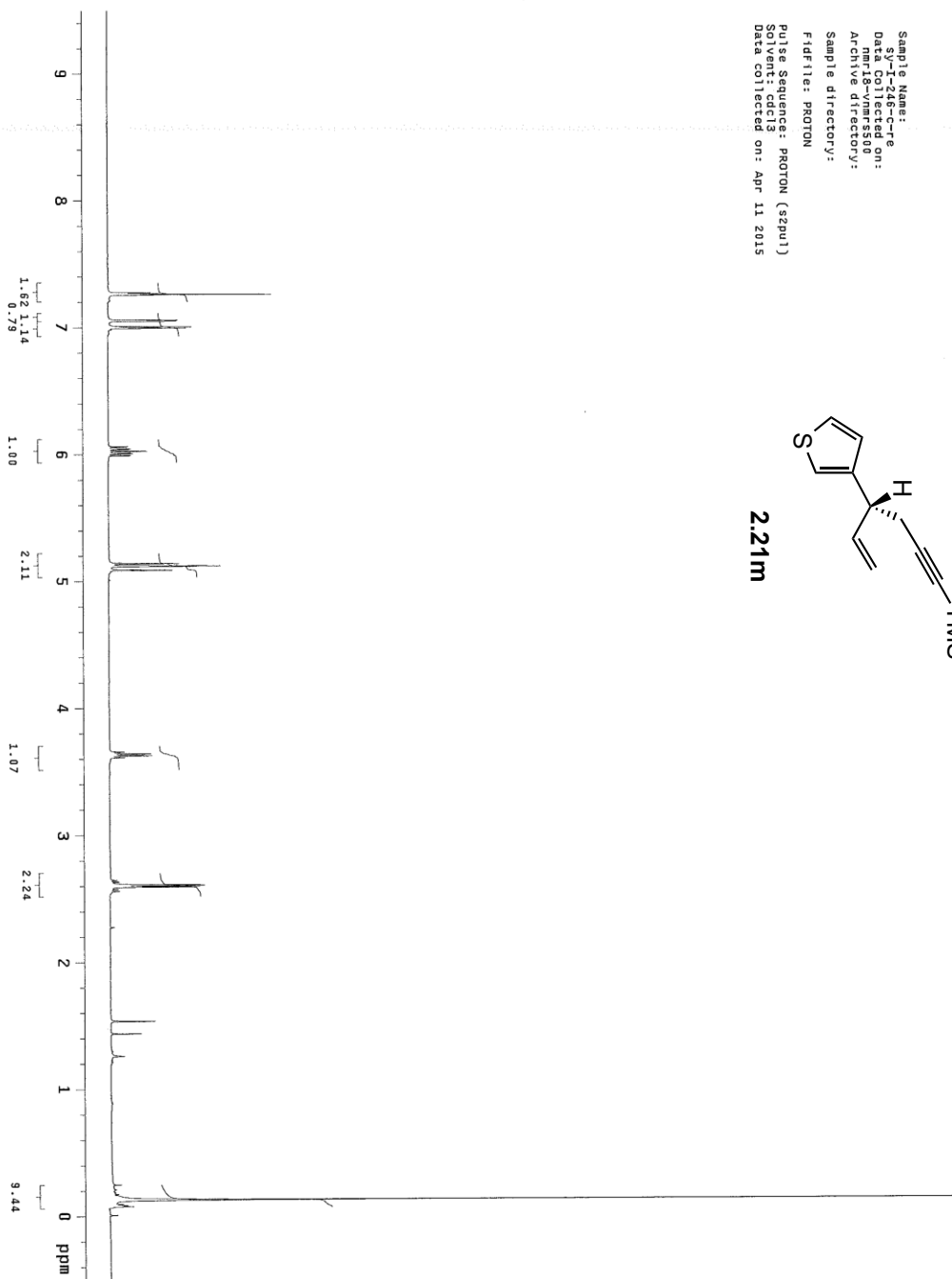
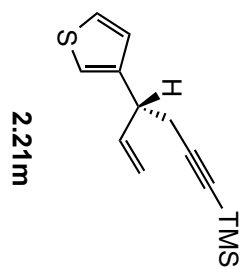
STANDARD FLUORINE PARAMETERS

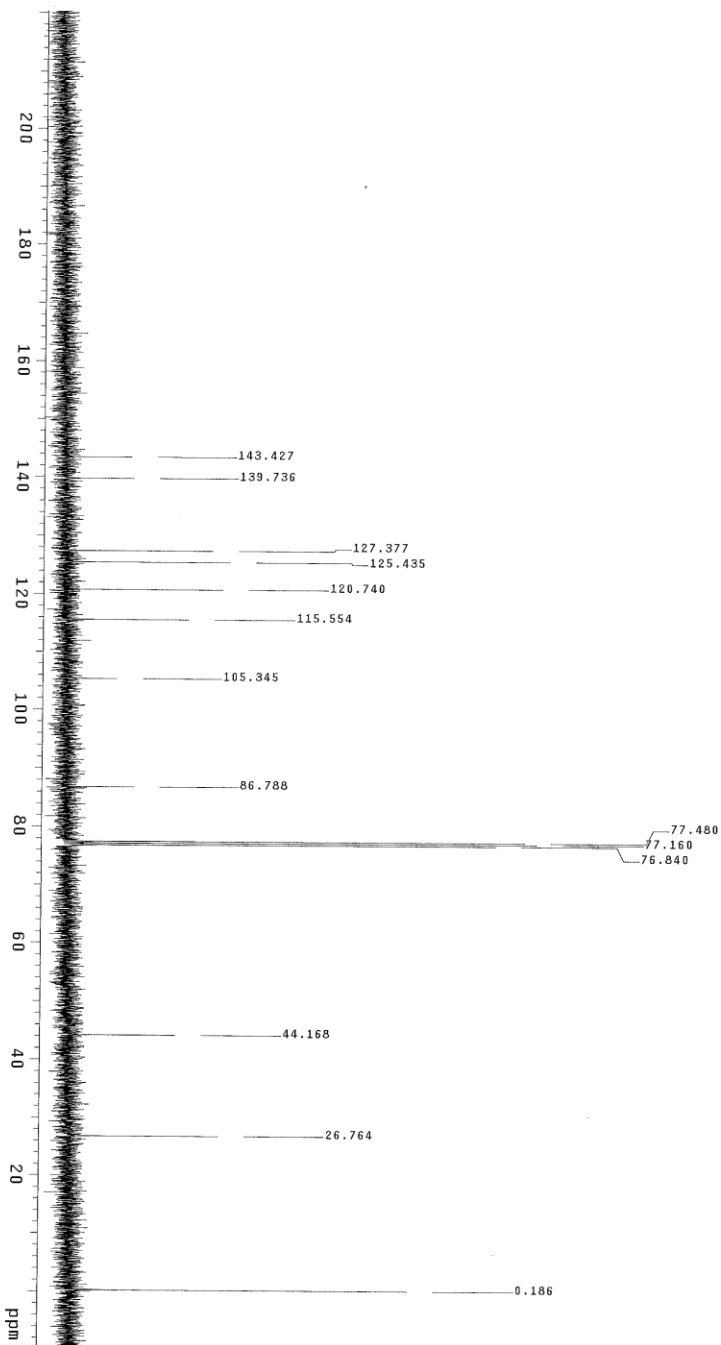
Sample Name:
 Data Collected on:
 vnmr13-vnmr-s400
 Archive directory:
 Sample directory:
 F1 file: PROTON
 Pulse Sequence: PROTON (zgpg3)
 Solvent: cdcl3
 Data collected on: Apr 10 2015





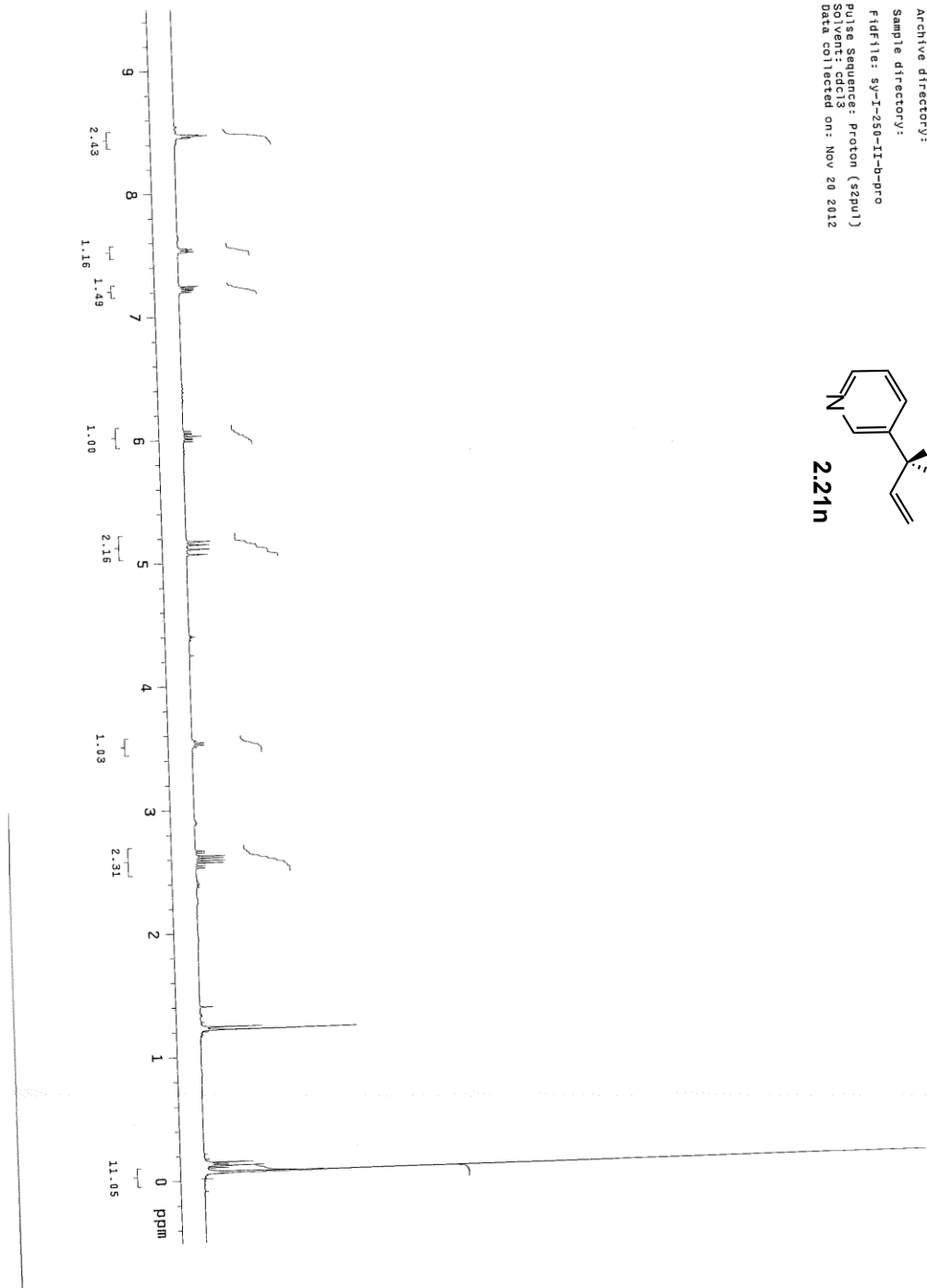
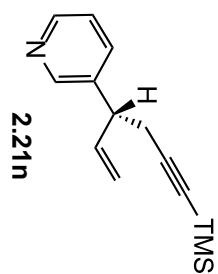
Sample Name:
 Data Collected on:
 nmr18-vnmr-5500
 Archive directory:
 Sample directory:
 F1:
 Pulse Sequence: PROTON (zgpg30)
 Solvent: cdcl3
 Data collected on: Apr 11 2015

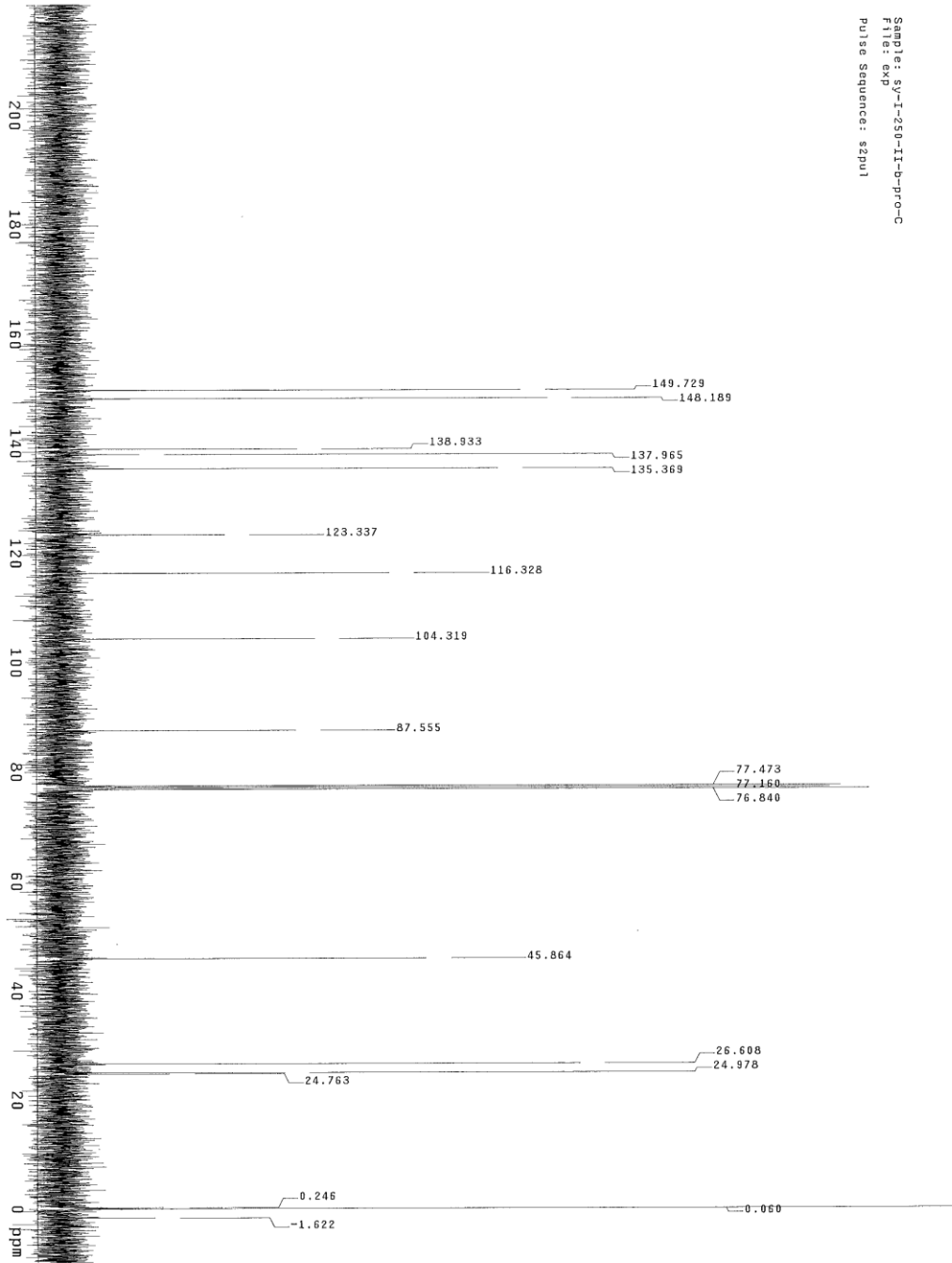


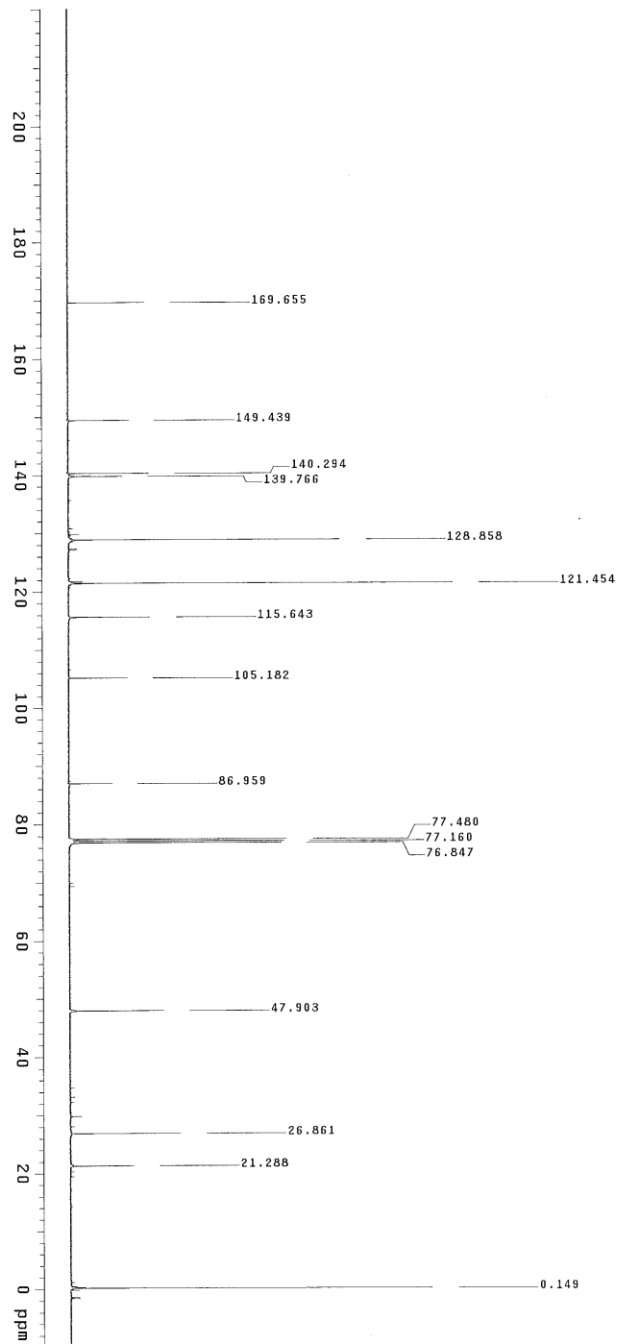


Sample: sy-I-244-a-pro
File: /home/ahh/vmr/svs/data/YingShi/Notebook-1-C/sy-I-244-a-pro.fid
Pulse Sequence: szpu1

Sample Name: sy-I-250-I-b-pro
 Sample directory: sy-I-250-I-b-pro
 Sample directory: sy-I-250-I-b-pro
 Pulse Sequence: Proton (zgpg3)
 Solvent: cdcl3
 Data collected on: Nov 20 2012

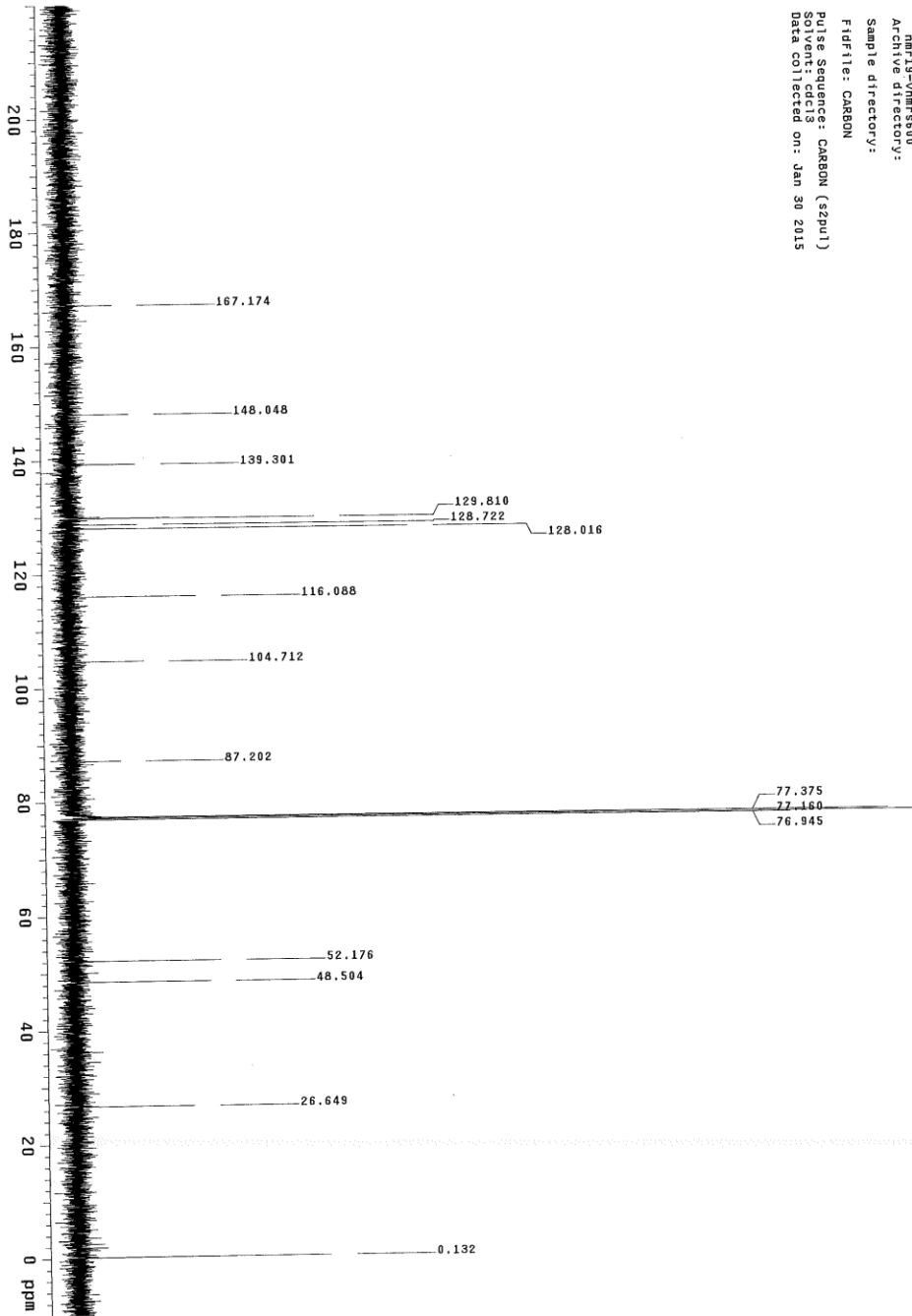




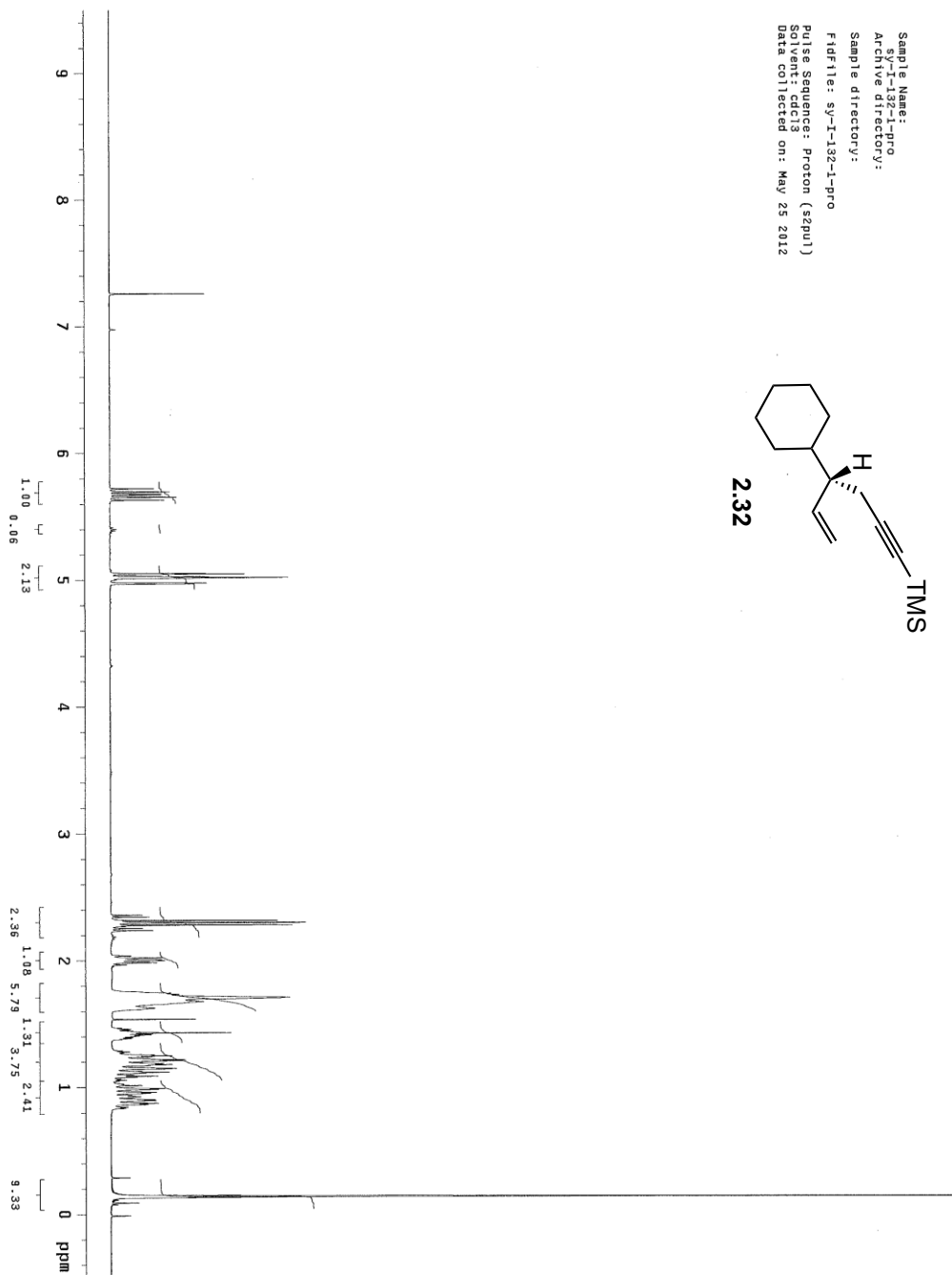
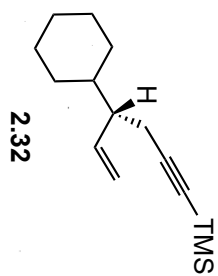


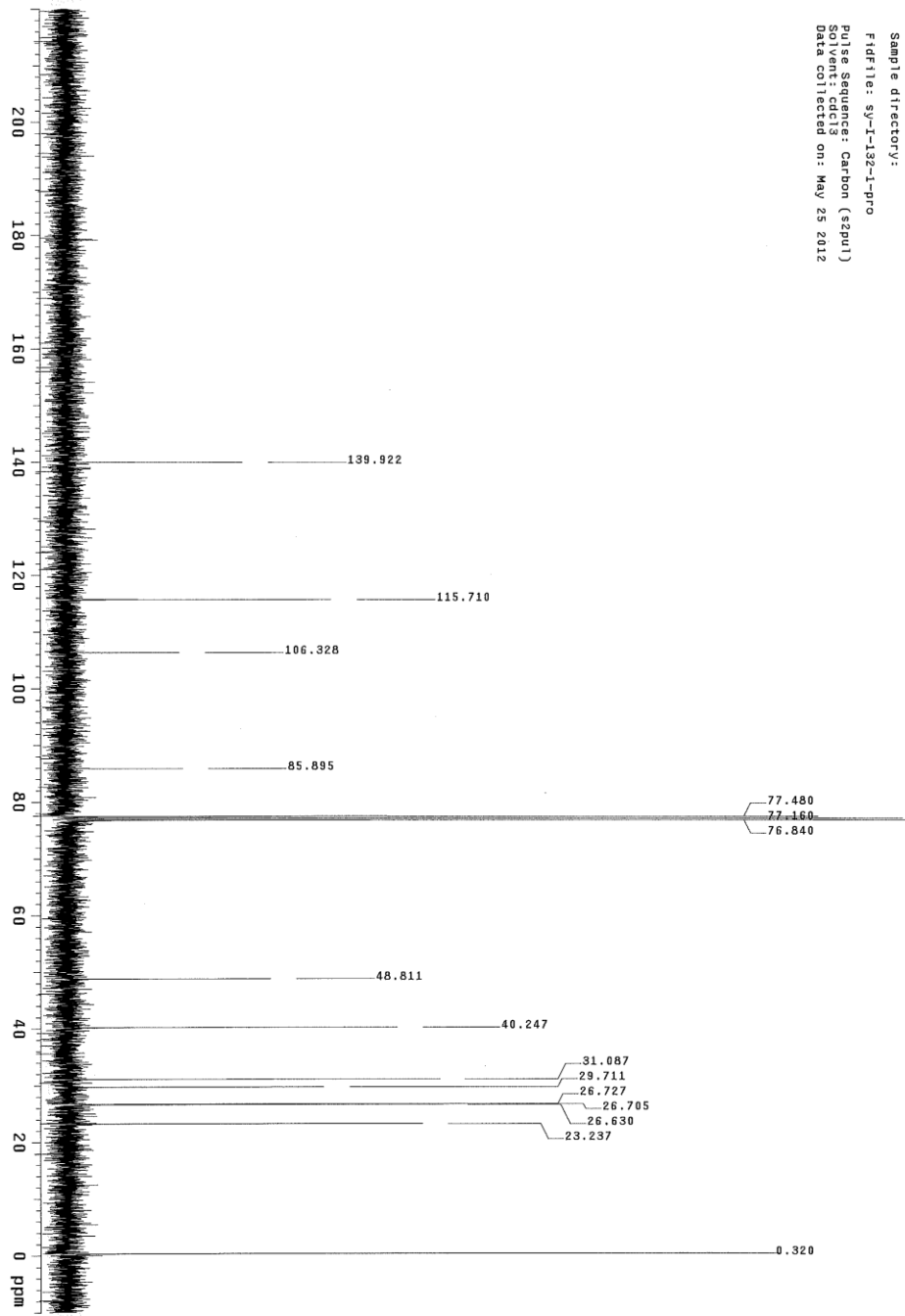
Sample: sv-I-241-b-pro-C
File: /home/ath/vmr/sys/data/Ingsht/Notebook--1-C/sv-I-241-b-pro.fid
Pulse Sequence: s2pul1

Sample Name: nm-19-vmars00
Date Collected on: nm-19-vmars00
Archive directory:
Sample directory:
FileType: CARBON
Pulse Sequence: CARBON (spul)
Acquisition Date: 20150130
Data collected on: Jan 30 2015



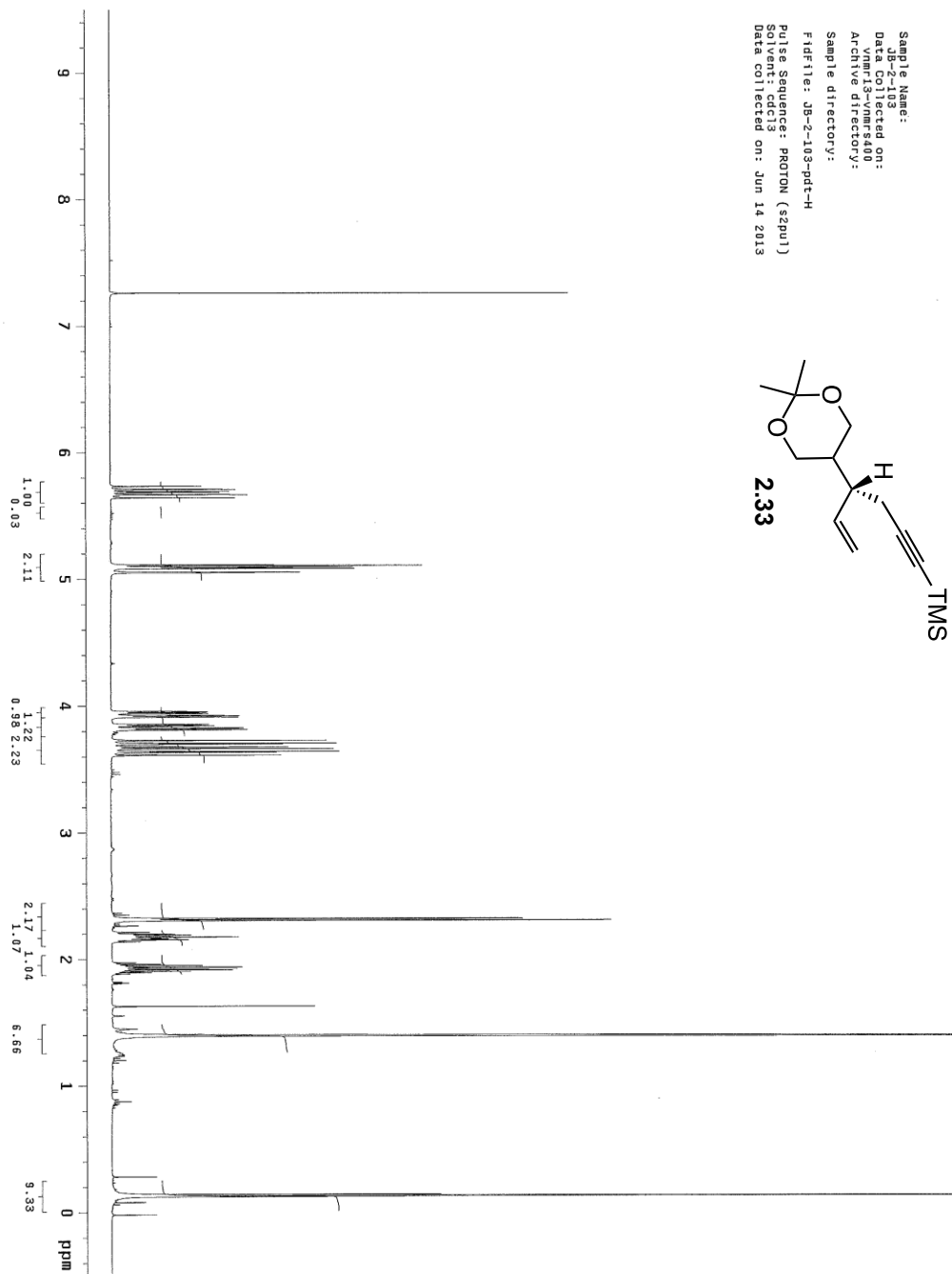
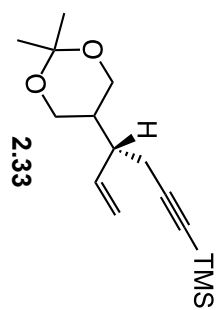
Sample Name: sy-1-132-1-pro
 Archive directory:
 Sample directory:
 FIDFile: sy-1-132-1-pro
 Pulse Sequence: Proton (s2pu1)
 Solvent: cdcl3
 Data collected on: May 25 2012

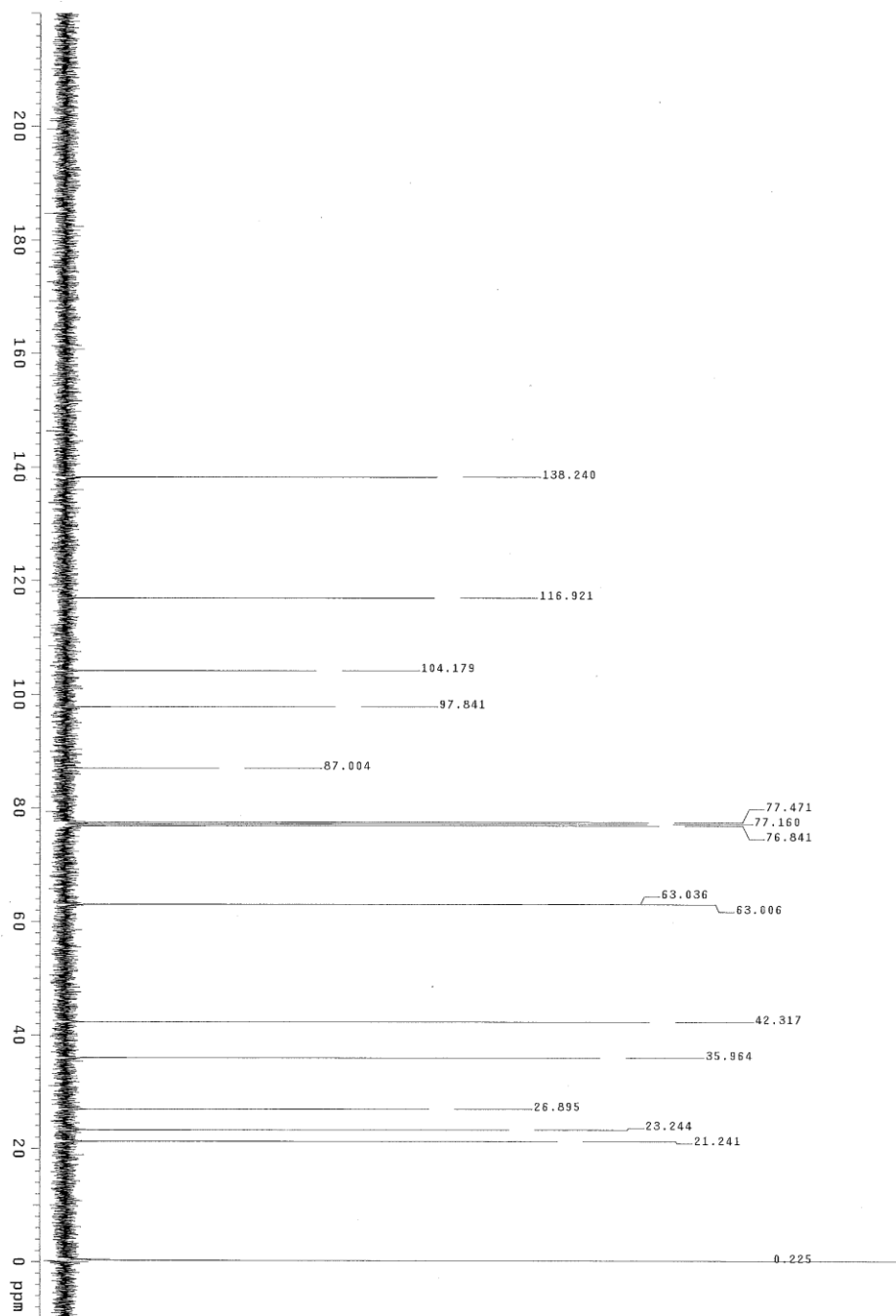




Sample Name: sy-1-132-1-pro
Archive directory: Sample directory:
Fidfile: sy-1-132-1-pro
Pulse Sequence: Carbon (zgpg1)
Solvent: cdcl3
Data collected on: May 25 2012

Sample Name: JB-2-103
 Data collected on: 06/13/13
 Vnmr13-vnmr3400
 Archive directory:
 Sample directory:
 F1df11e: JB-2-103-pdt-H
 Pulse Sequence: PROTON (szpu1)
 Solvent: cdcl3
 Data collected on: Jun 14 2013

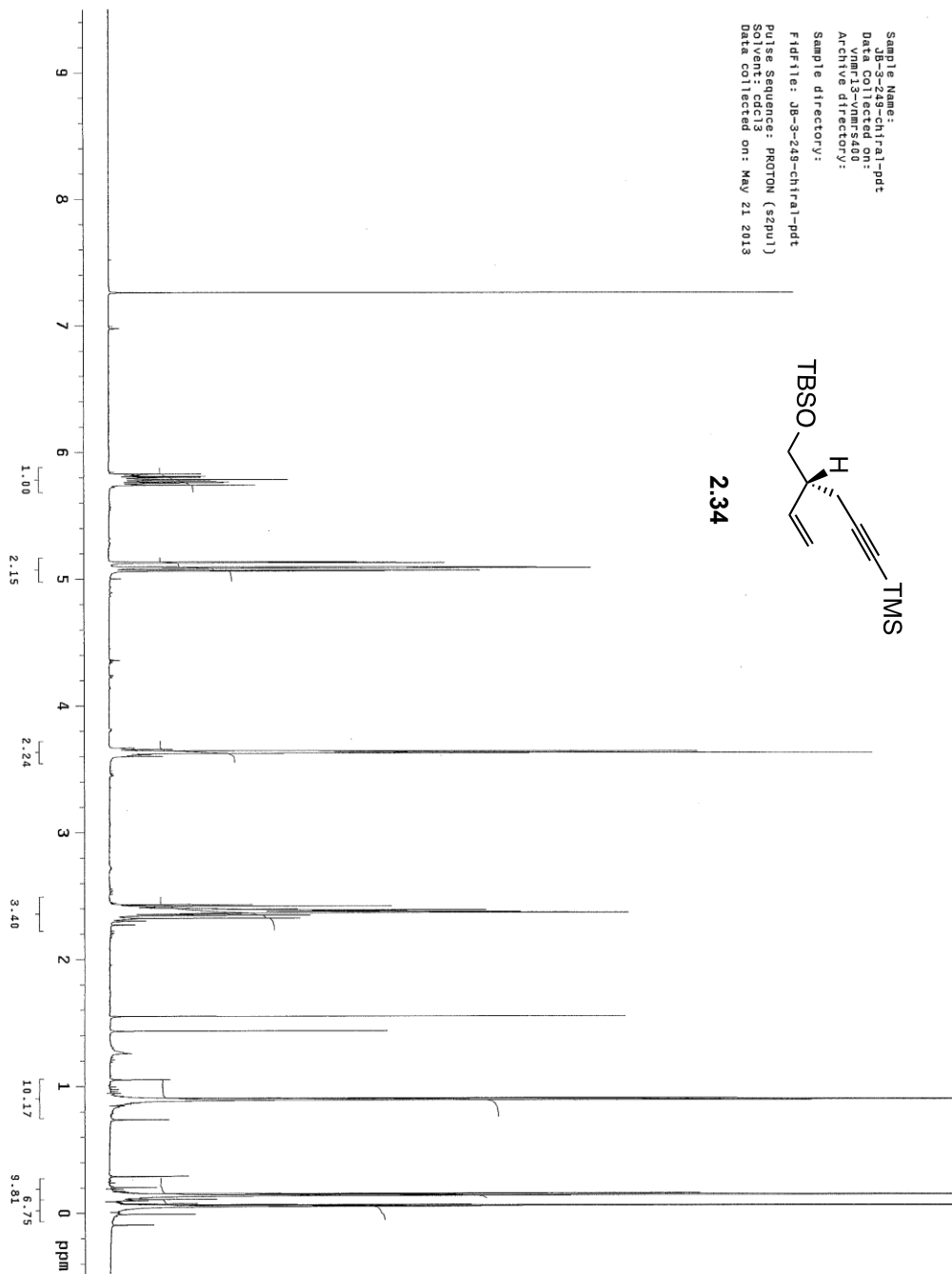


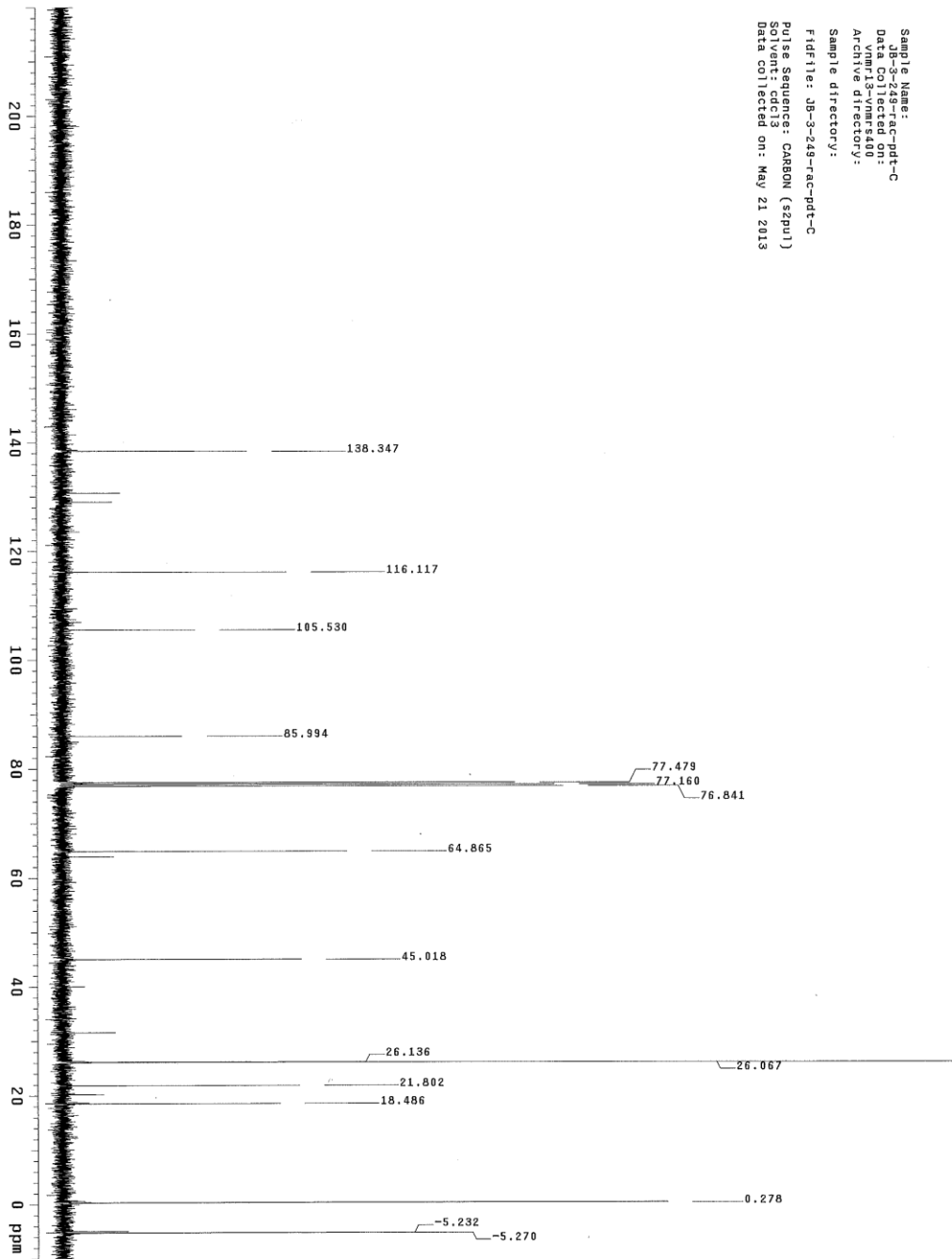


Sample Name: j8-3-249-1
 Date Collected on: 05/21/2013
 Vnmr13-vnmr9480
 Archive directory:
 Sample directory:
 F1df11e: j8-3-249-chiral-pdt
 Pulse Sequence: PROTON (zgpg3)
 Solvent: CDCl3
 Data collected on: May 21 2013



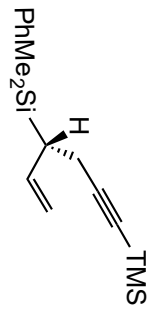
2.34



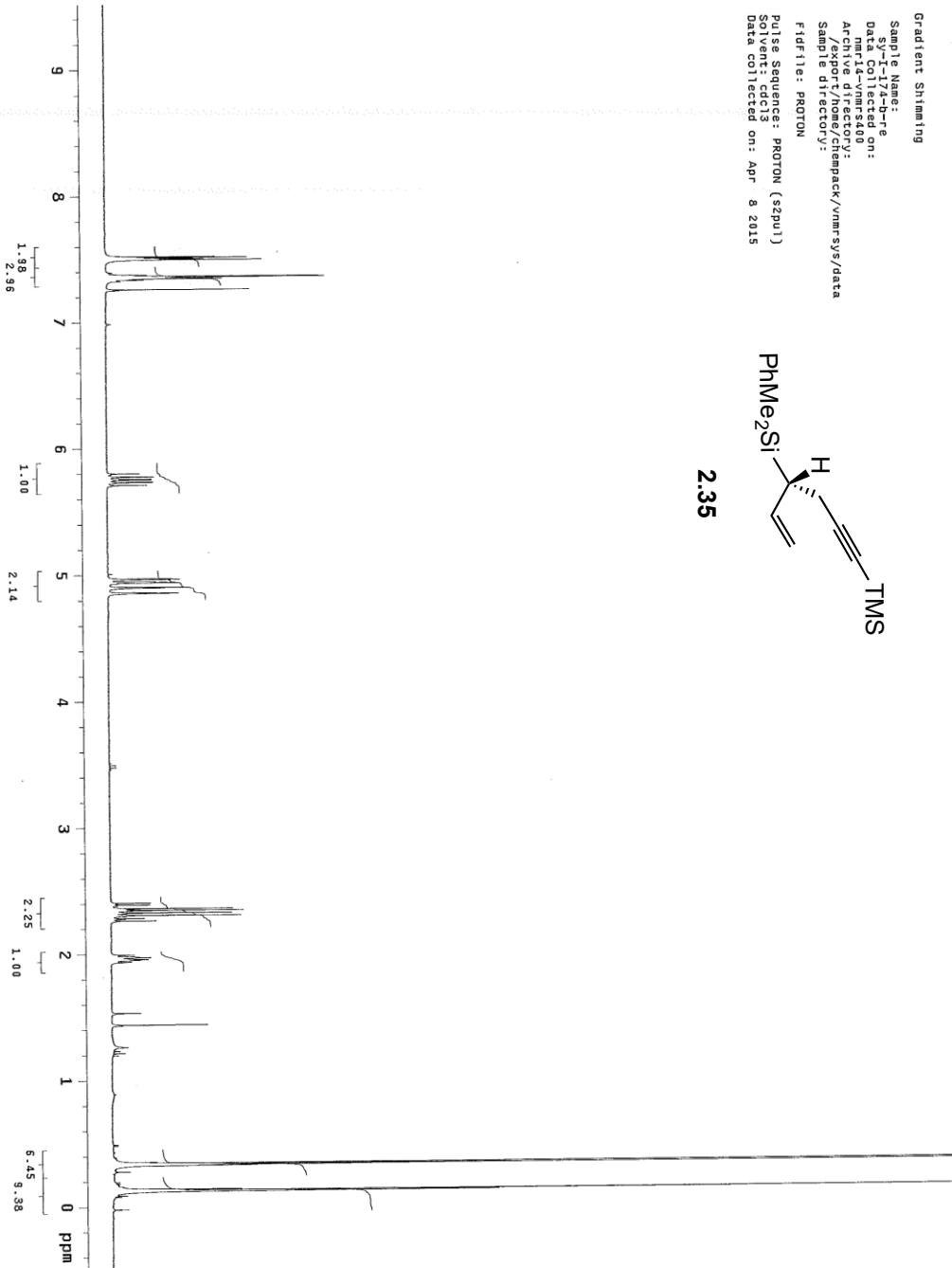


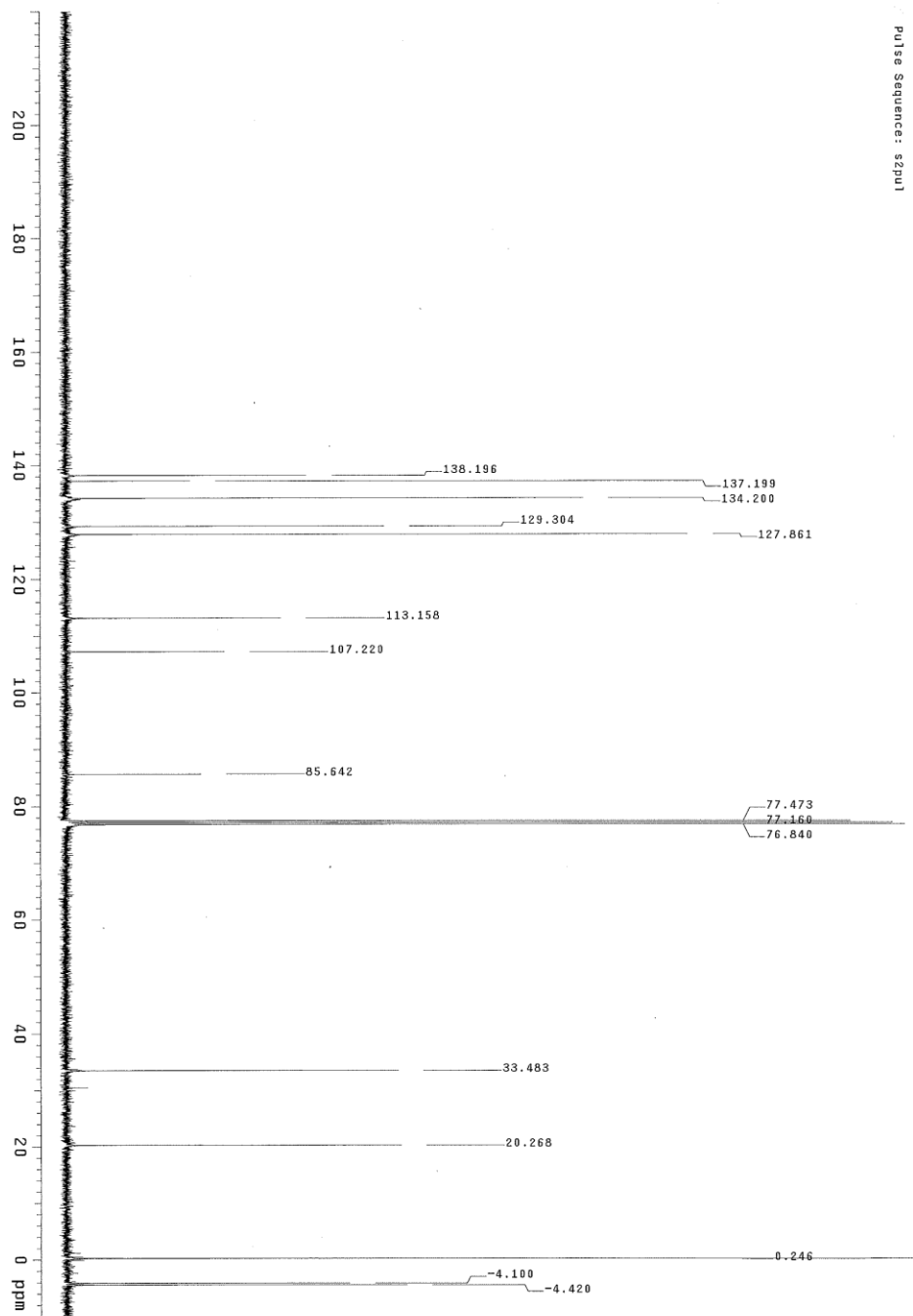
Sample Name: JB-3-249-rec-pdt-C
Date: 2013-05-21 14:40:00
Vnmr13-vmr3480
Archive directory:
Sample directory:
Fidfile: JB-3-249-rec-pdt-C
Pulse Sequence: CARBON (szpu)
Solvent: cdcl3
Data collected on: May 21 2013

Gradient Shimming
Sample Name:
Data Collected on:
Archive directory:
Sample directory:
Fidfile: PROTON
Pulse Sequence: PROTON (szpu1)
Solvent: cdcl3
Data collected on: Apr 8 2015



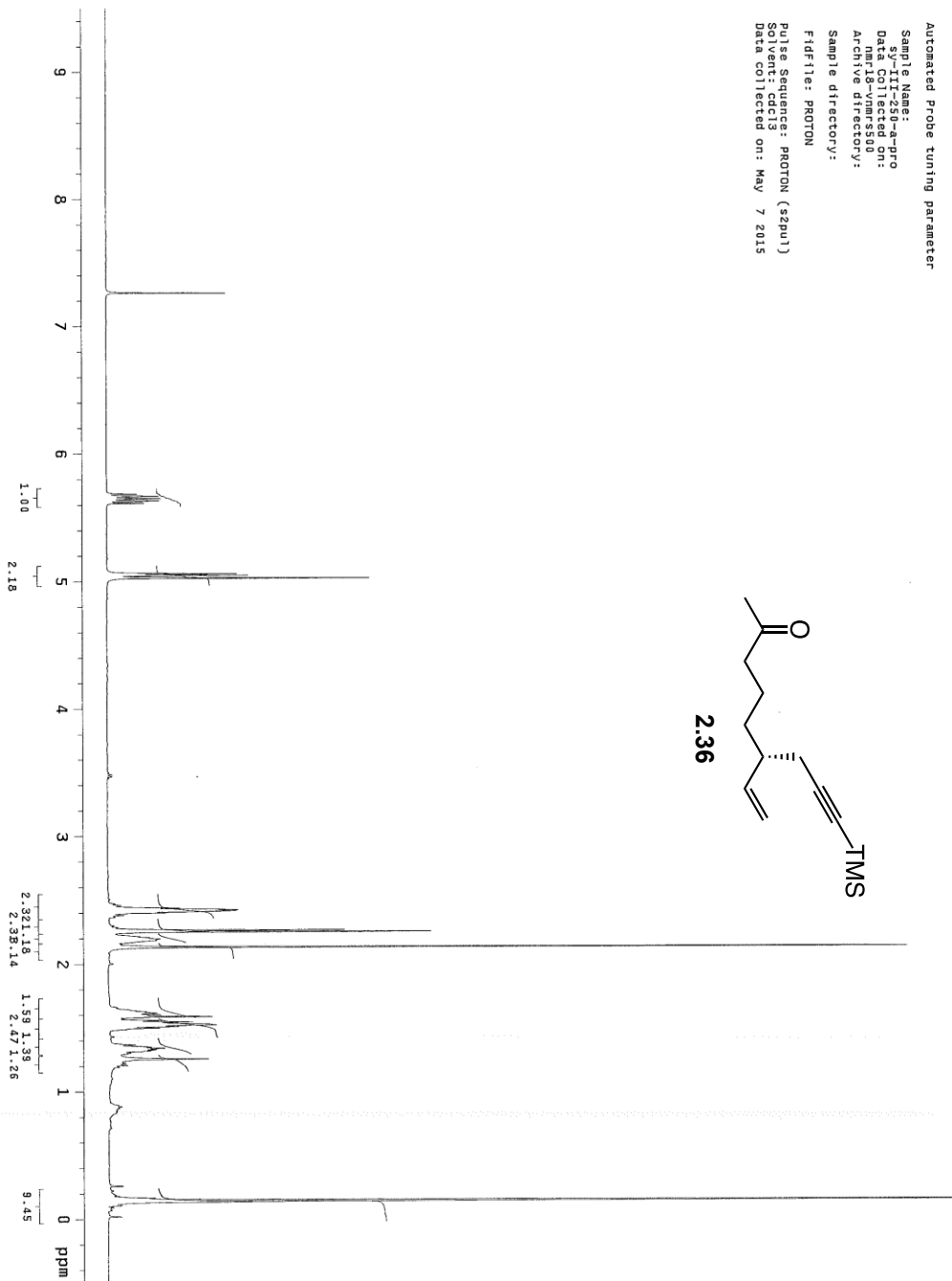
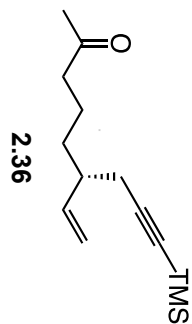
2.35

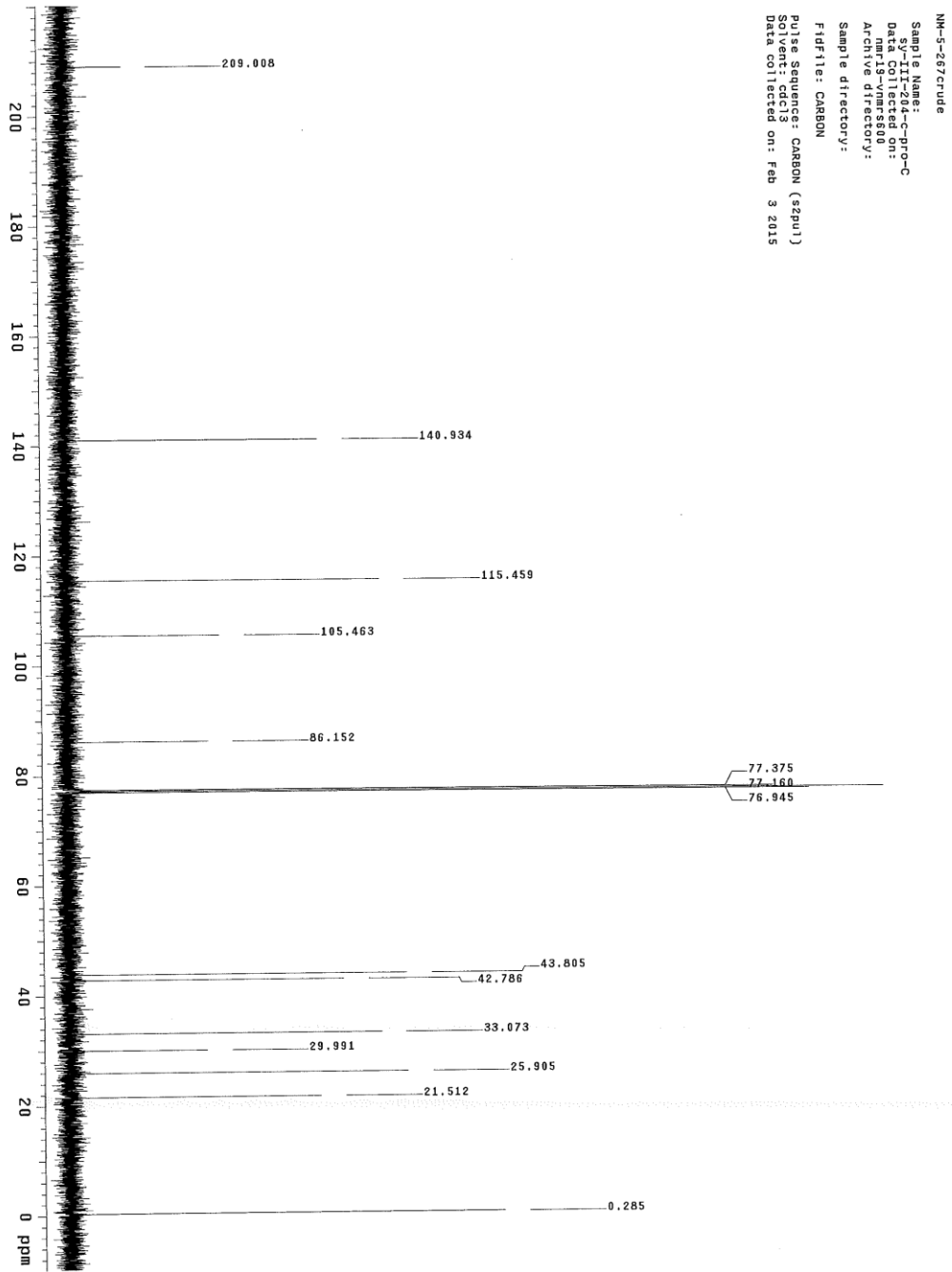




Sample: sy-1-174-b-*ms*
Filter: exp
Pulse Sequence: szpu1

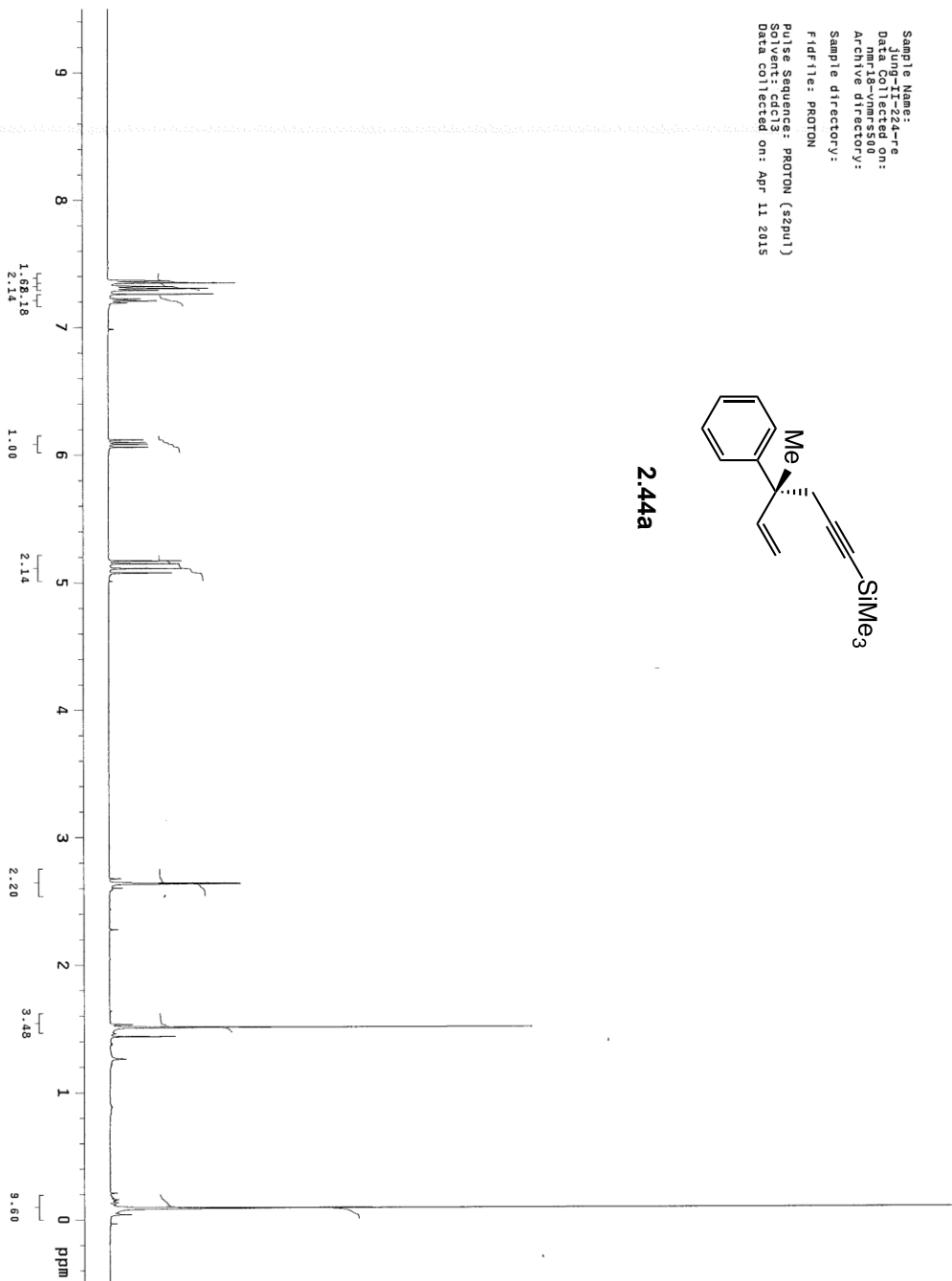
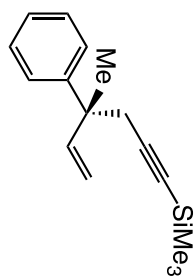
Automated Probe tuning parameter
 Sample Name: s2y-11-230-a4-pro
 Data File: s2y-11-230-a4-pro
 Name: vnmrs500
 Archive directory:
 Sample directory:
 F1df file: PROTON
 Pulse Sequence: PROTON (s2pu1)
 Solvent: cdc13
 Data collected on: May 7 2015

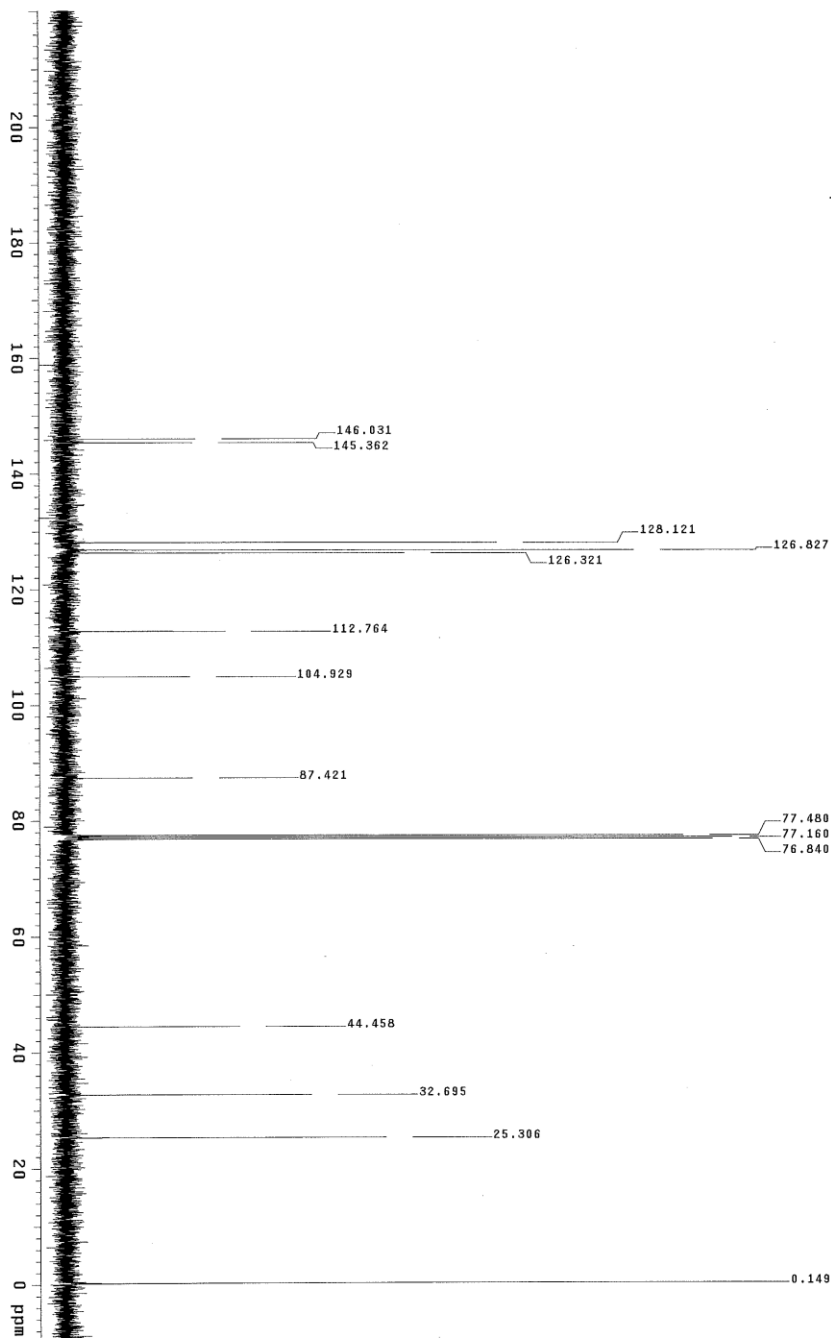




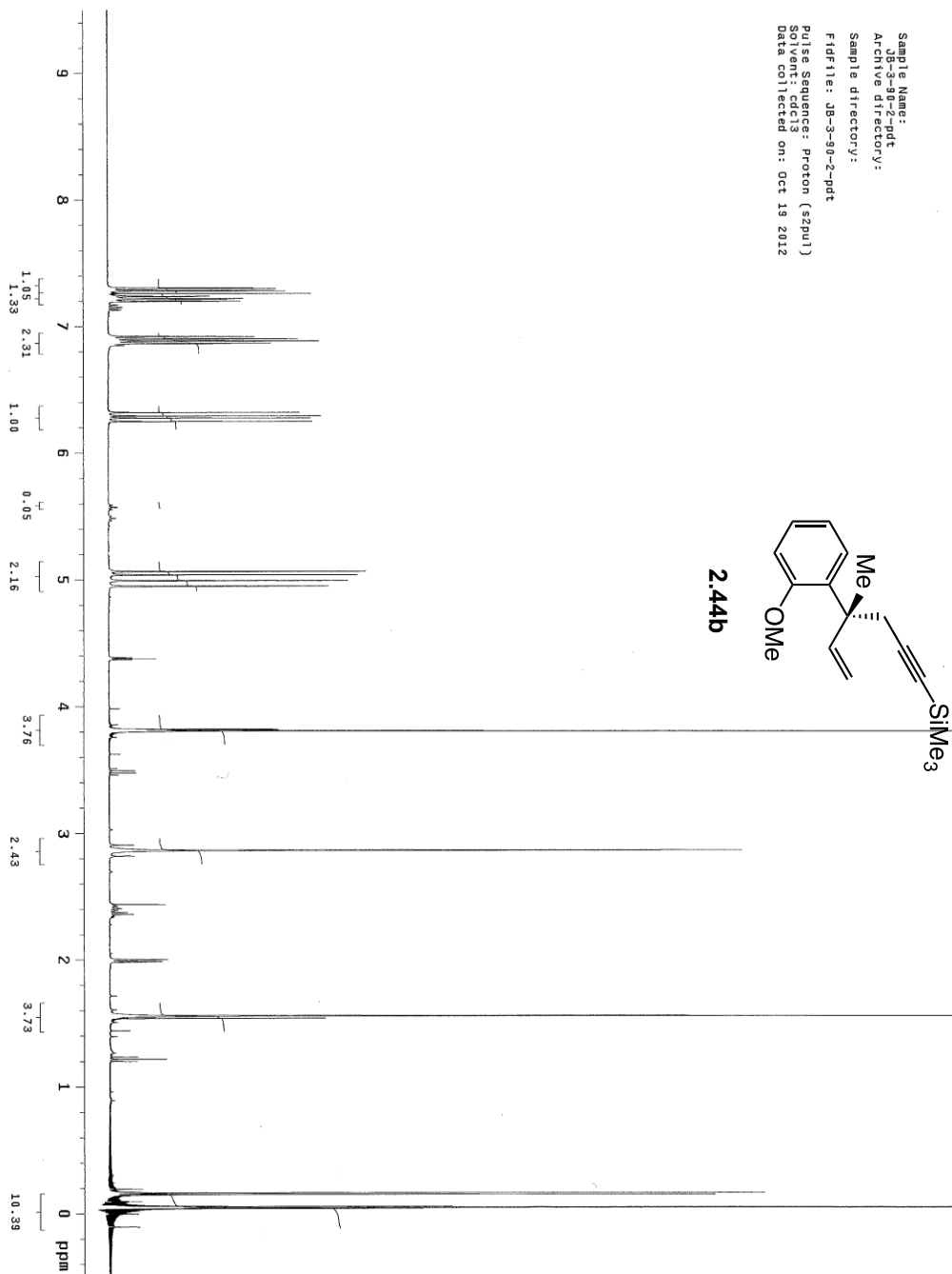
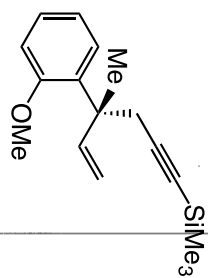
NM-5-267crude
Sample Name: sy-III-204-C-pro-C
Data Collected on: mmrj3-vnmr800
Archive directory:
Sample directory:
FIDFile: CARBON
Pulse Sequence: CARBON (zpu1)
Solvent: cdcl3
Data collected on: Feb 3 2015

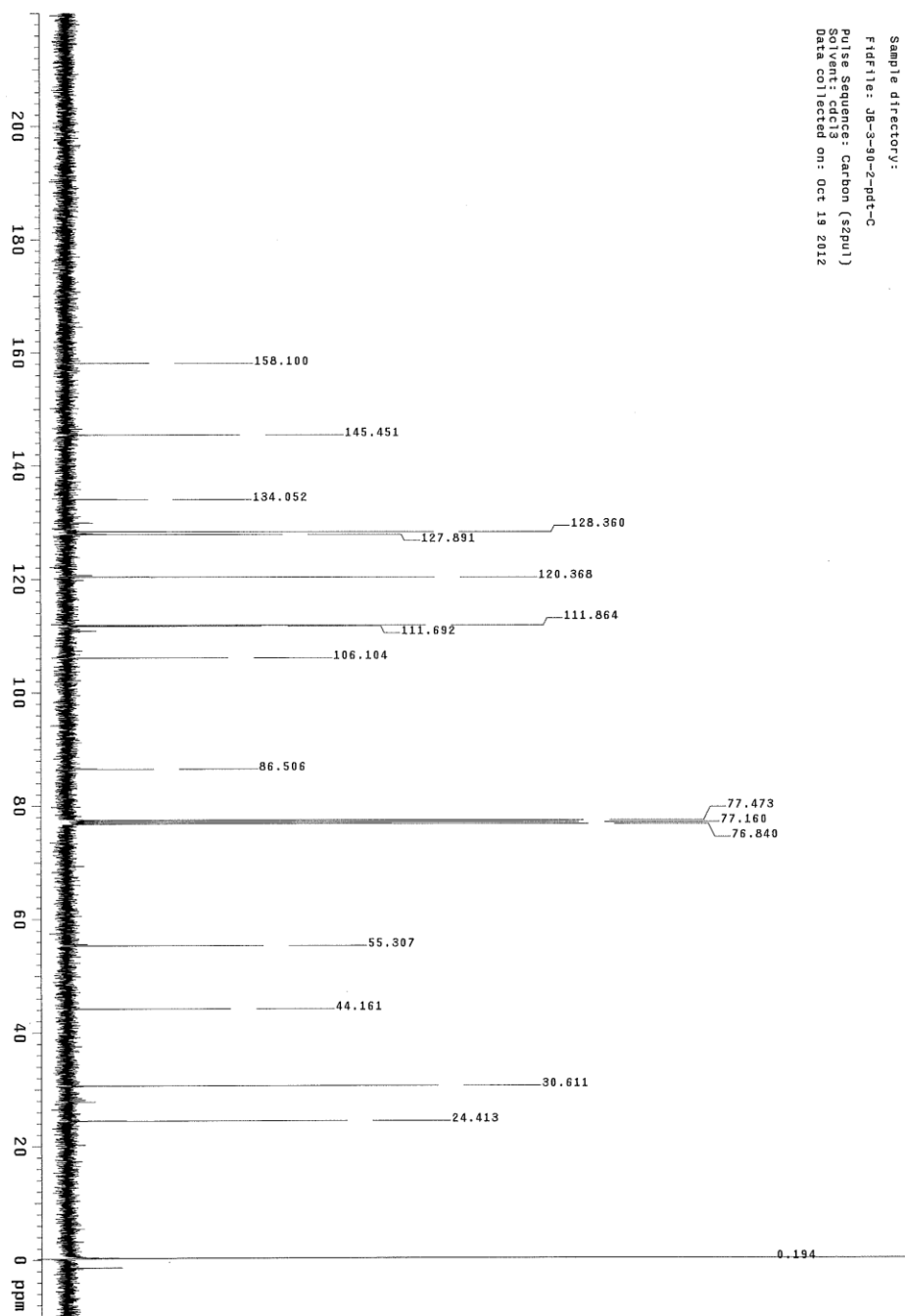
Sample Name: **nmr24-re**
 Date Collected on: **mr18-vnm-5500**
 Archive directory:
 Sample directory:
 F1 file: **PROTON**
 Pulse Sequence: **PROTON (zgpg1)**
 Solvent: **cdcl3**
 Data collected on: **Apr 11 2015**





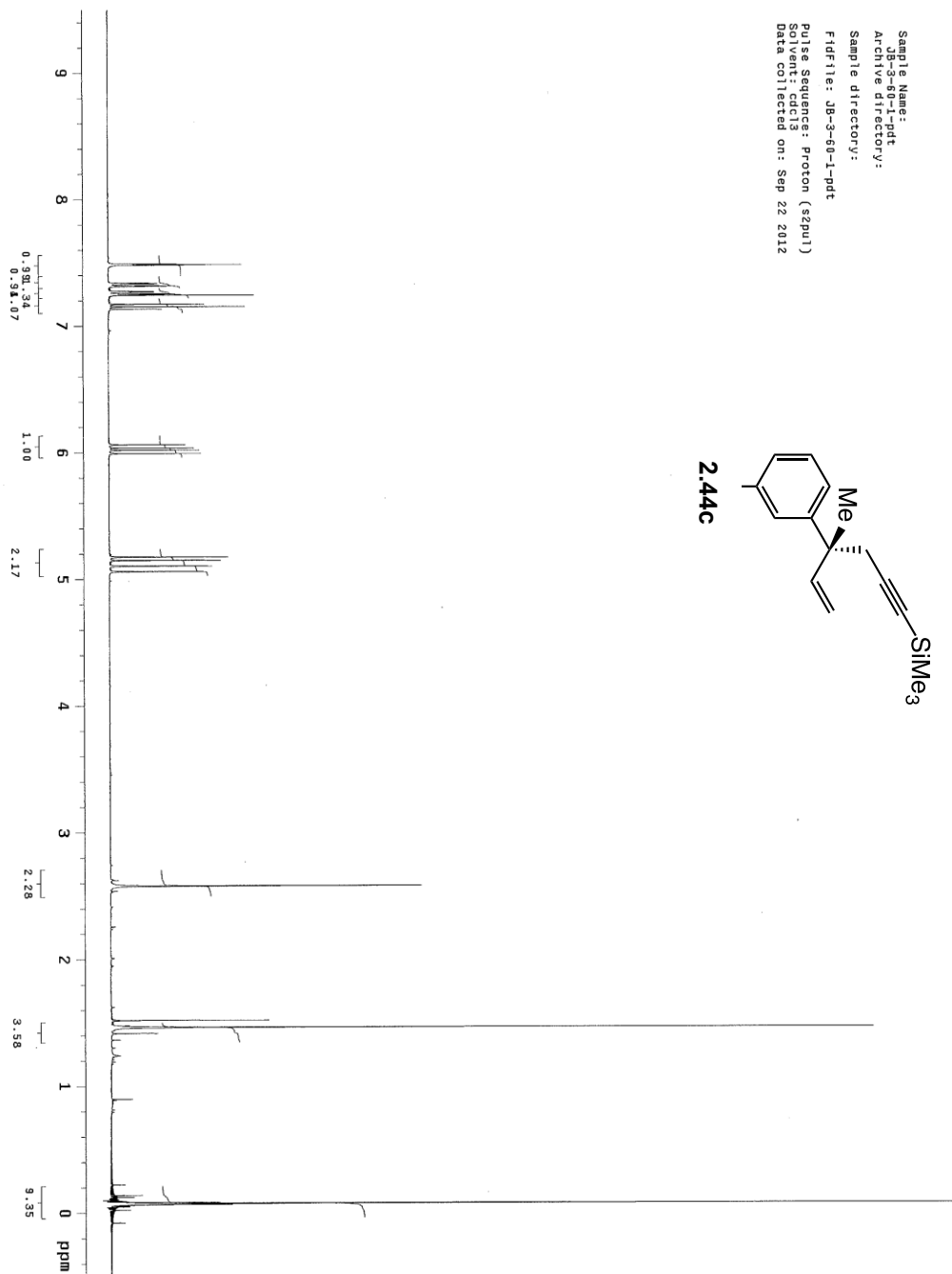
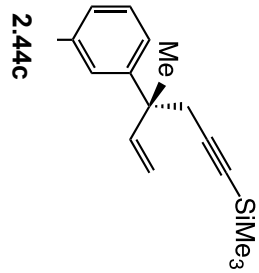
Sample Name: JB-3-90-2-pdt
 Archive directory:
 Sample directory:
 FID: JB-3-90-2-pdt
 Pulse Sequence: proton (szpu1)
 Solvent: cdcl3
 Data collected on: Oct 19 2012

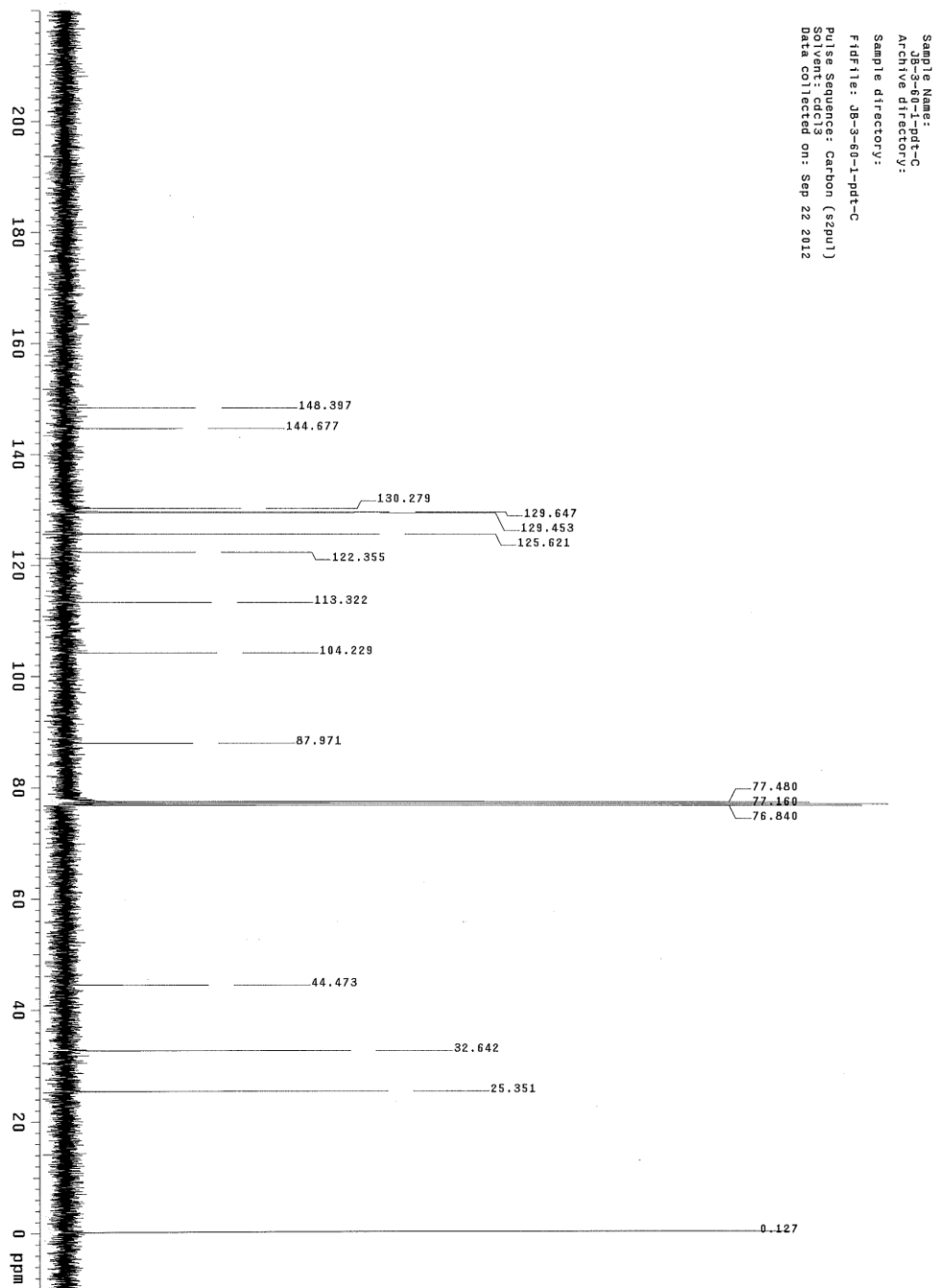




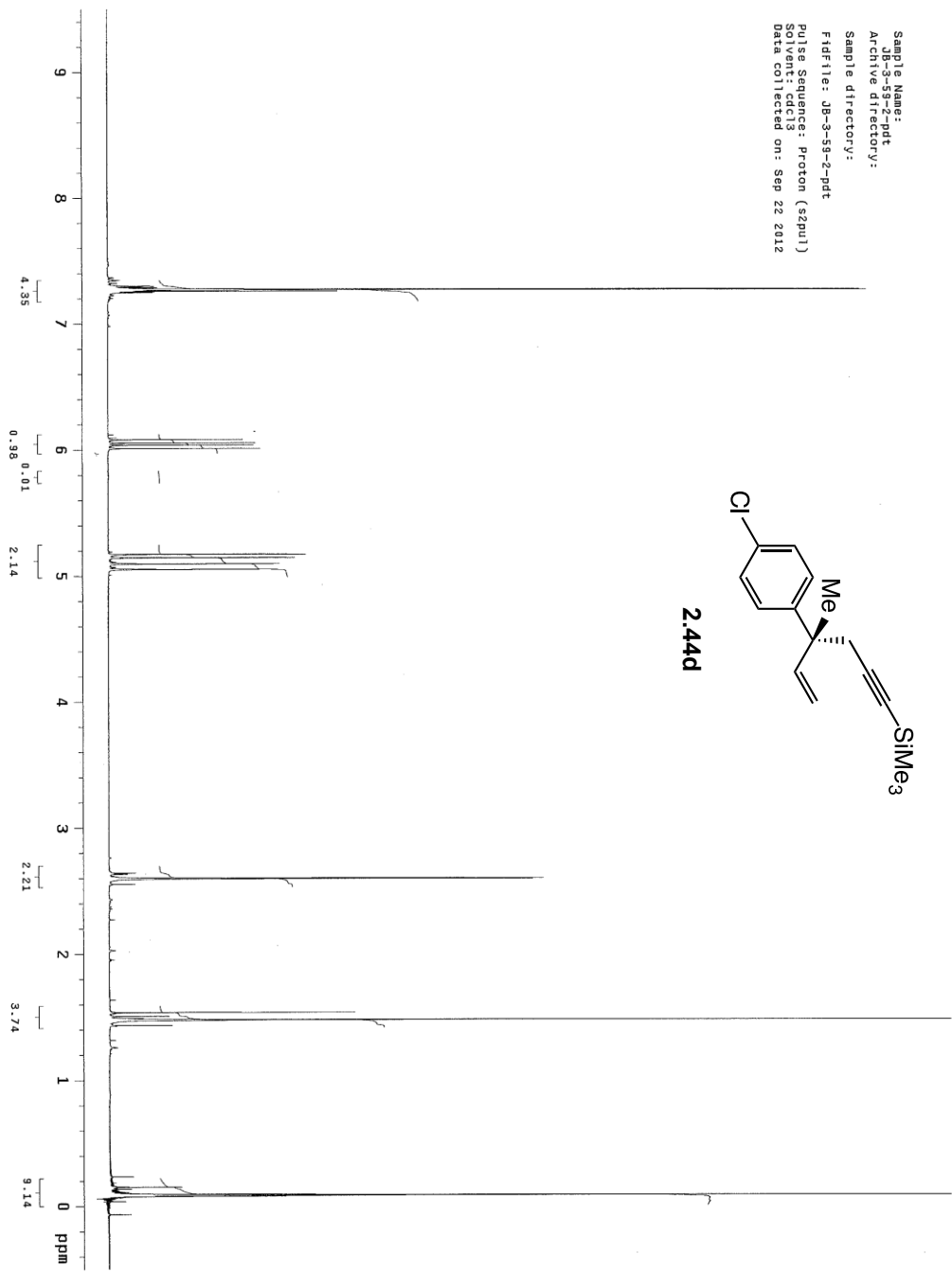
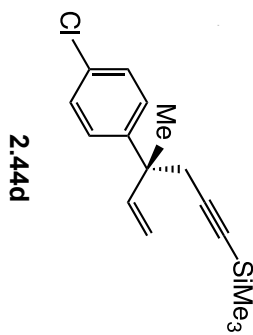
Sample Name: JB-3-90-2-pdt-C
Archive directory: JB-3-90-2-pdt-C
Sample directory: JB-3-90-2-pdt-C
Fidfile: JB-3-90-2-pdt-C
Pulse Sequence: Carbon (szpu1)
Solvent: cdcl3
Data collected on: Oct 19 2012

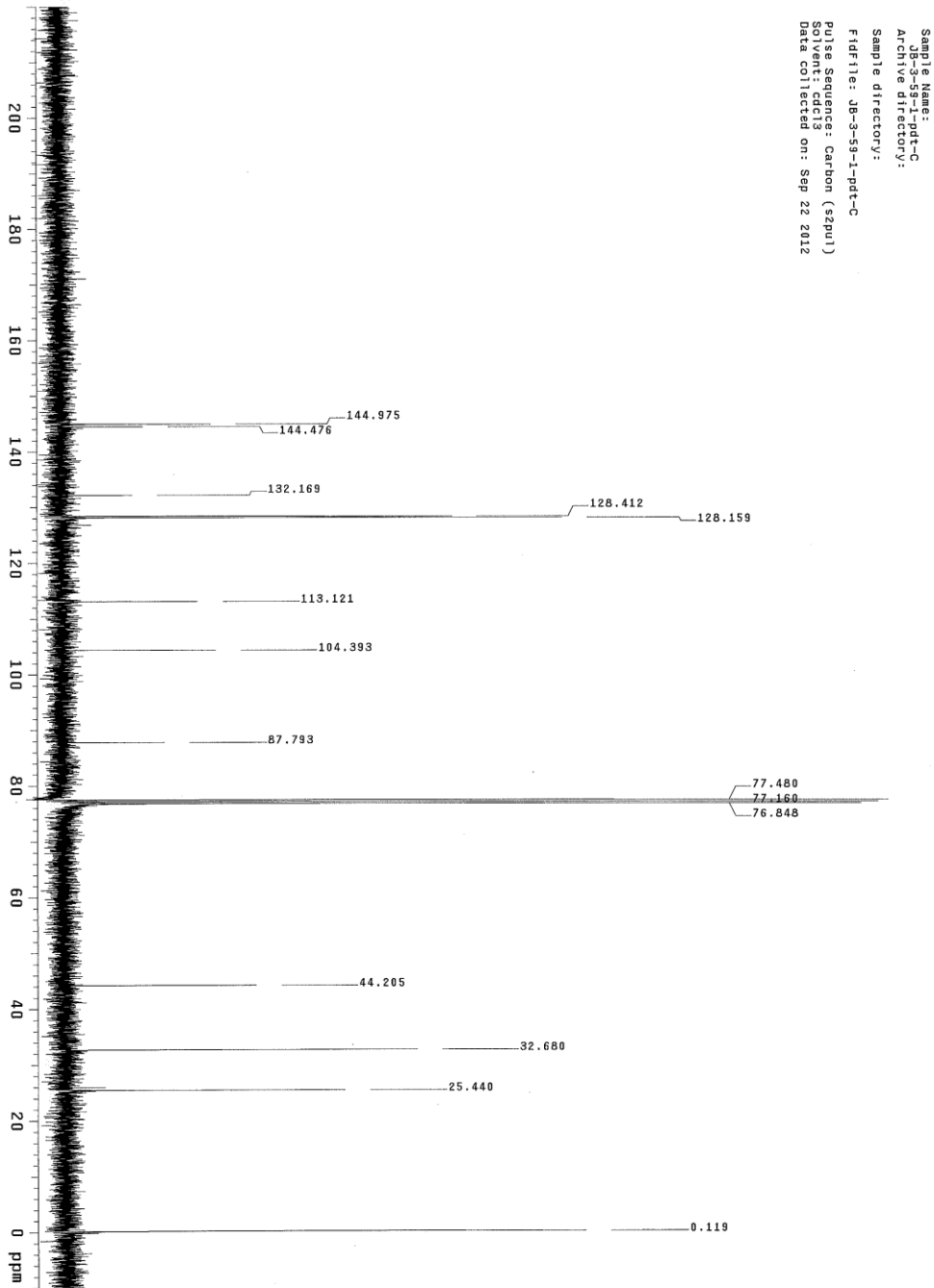
Sample Name: JB-3-60-1-pdt
 Archive directory:
 Sample directory:
 FIDfile: JB-3-60-1-pdt
 Pulse Sequence: Proton (szpu1)
 Solvent: cdcl3
 Data collected on: Sep 22 2012



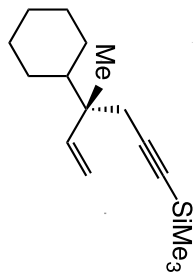


Sample Name: JB-3-59-2-pdt
 Archive directory:
 Sample directory:
 F1d11e: JB-3-59-2-pdt
 Pulse Sequence: Proton (zgpg3)
 Solvent: cdcl3
 Data collected on: Sep 22 2012

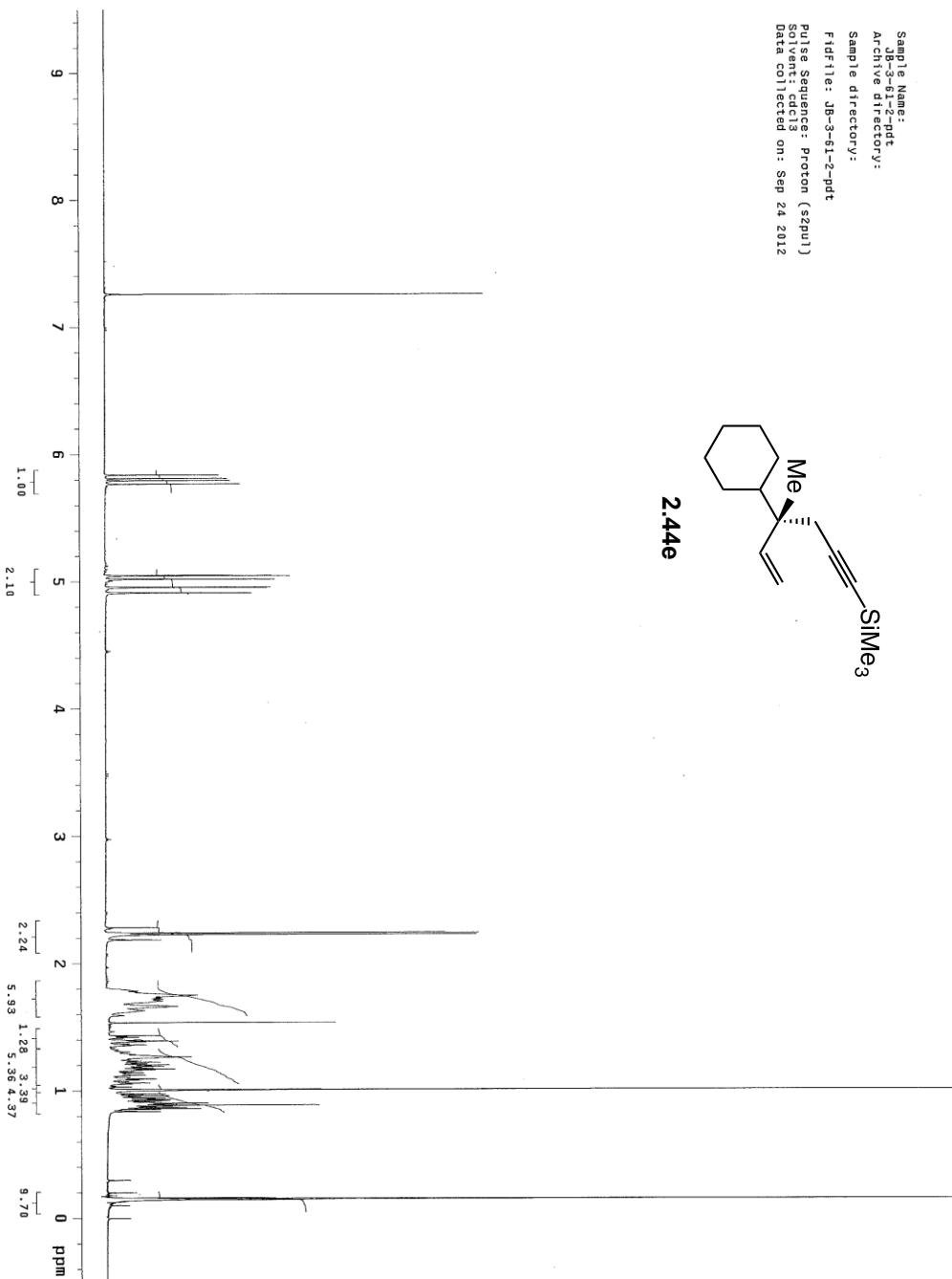


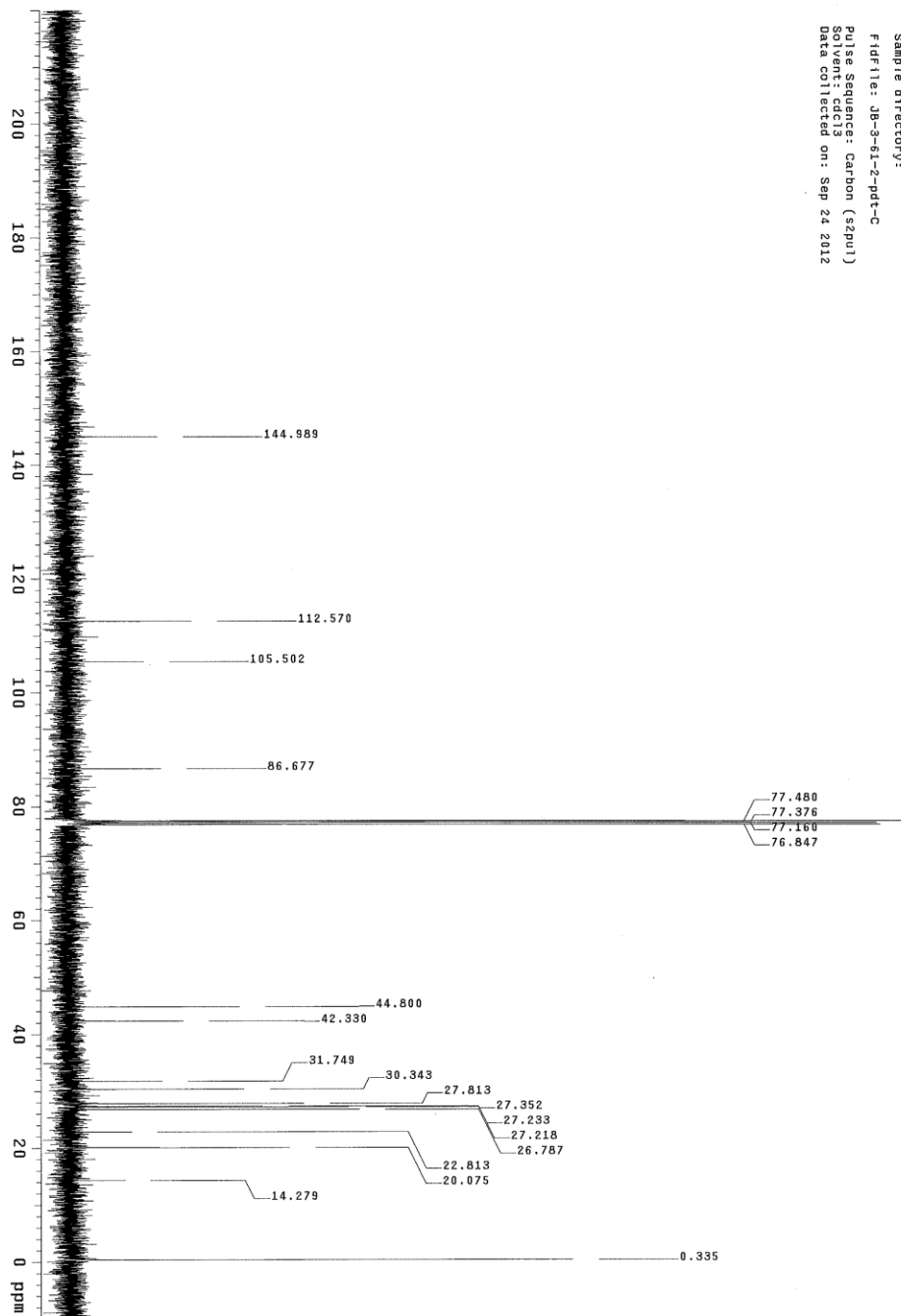


Sample Name: JB-3-61-2-pdt
 Archive directory:
 Sample directory:
 F1df-file: JB-3-61-2-pdt
 Pulse Sequence: Proton (szpu1)
 Solvent: cdcl3
 Data collected on: Sep 24 2012



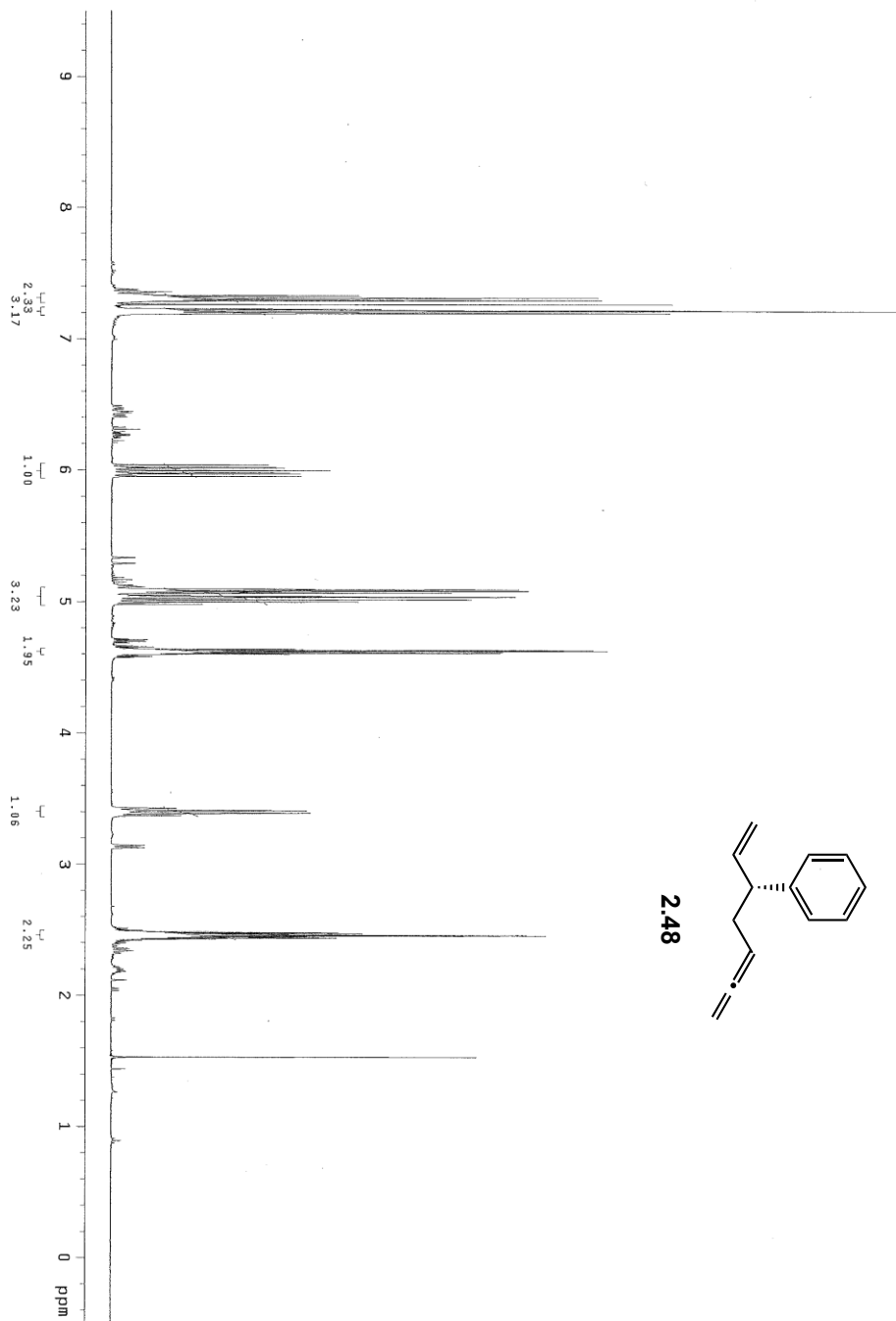
2.44e

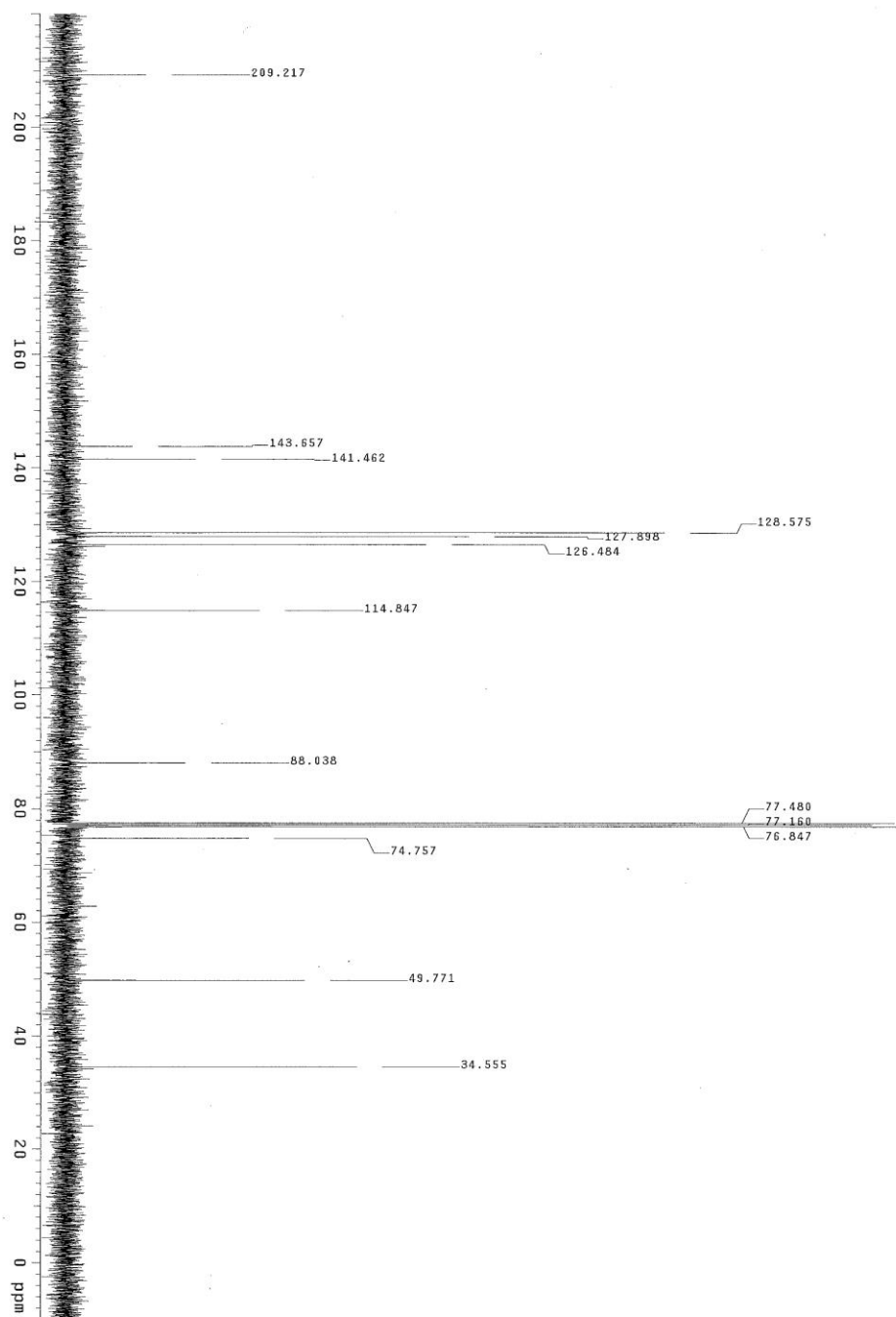


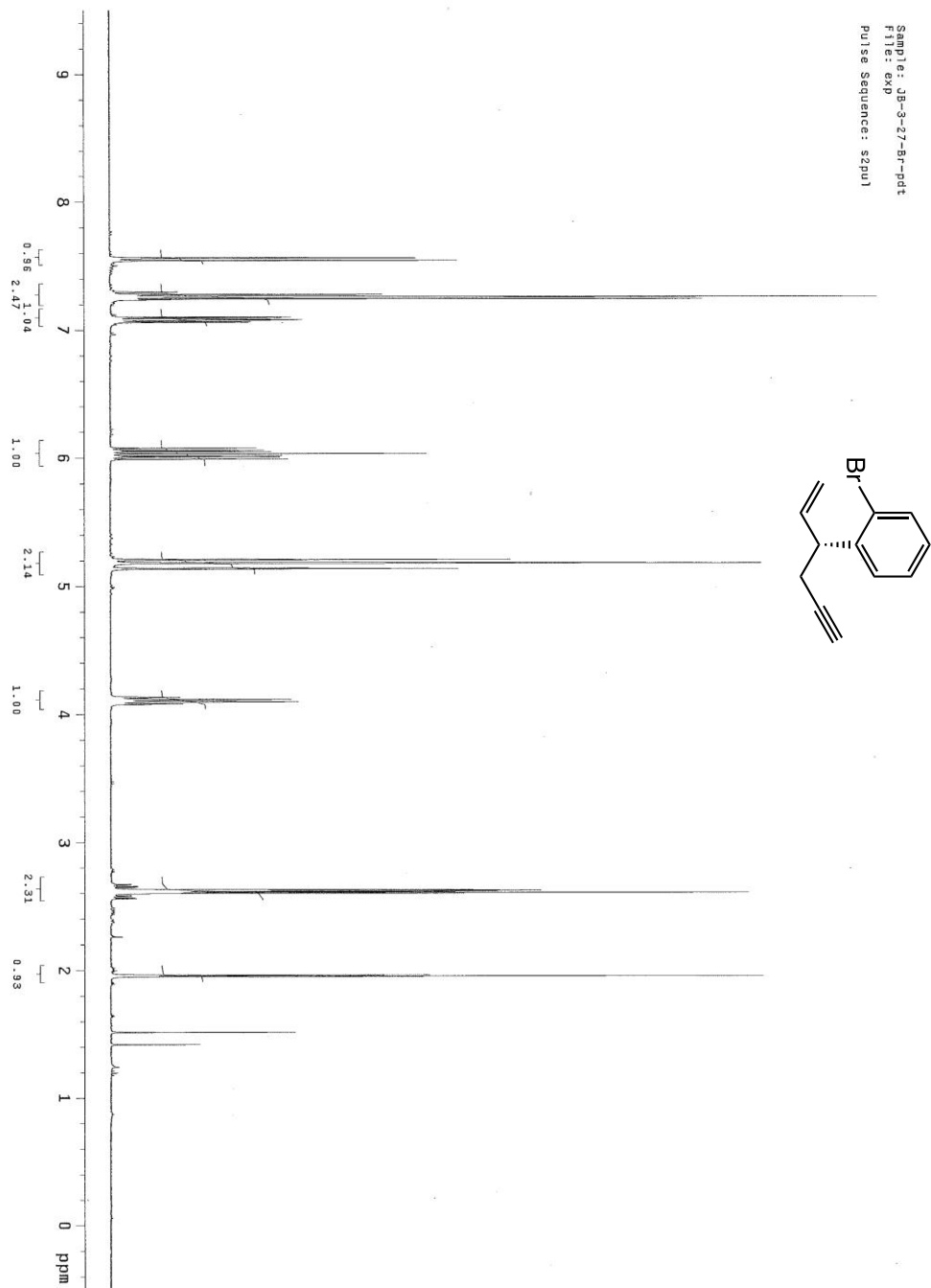


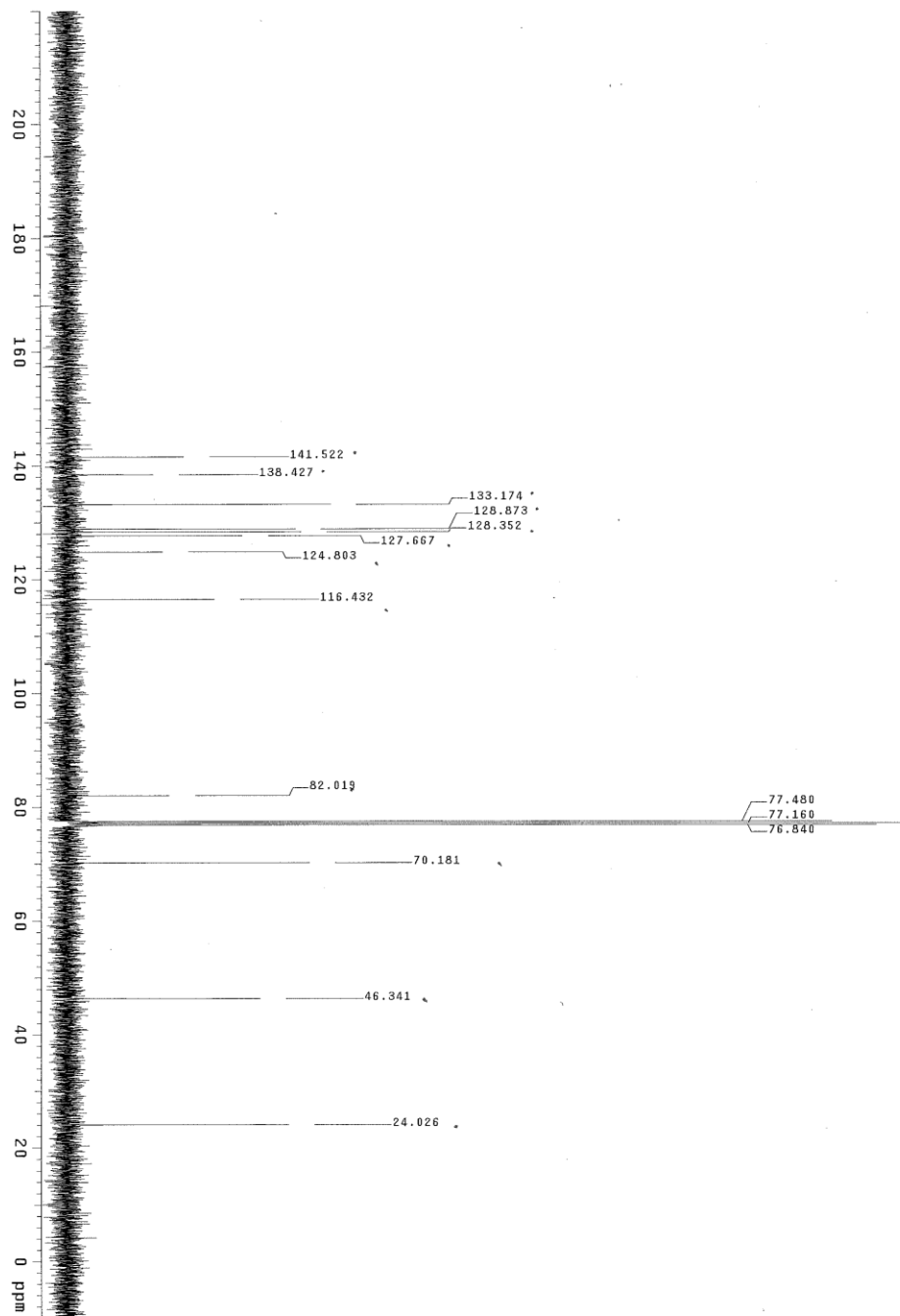
Sample Name: JB-3-61-2-pdt-C
Archive directory: JB-3-61-2-pdt-C
Sample directory: JB-3-61-2-pdt-C
FIDFile: JB-3-61-2-pdt-C
Pulse Sequence: Carbon (s2pu1)
Solvent: cdcl3
Data collected on: Sep 24 2012

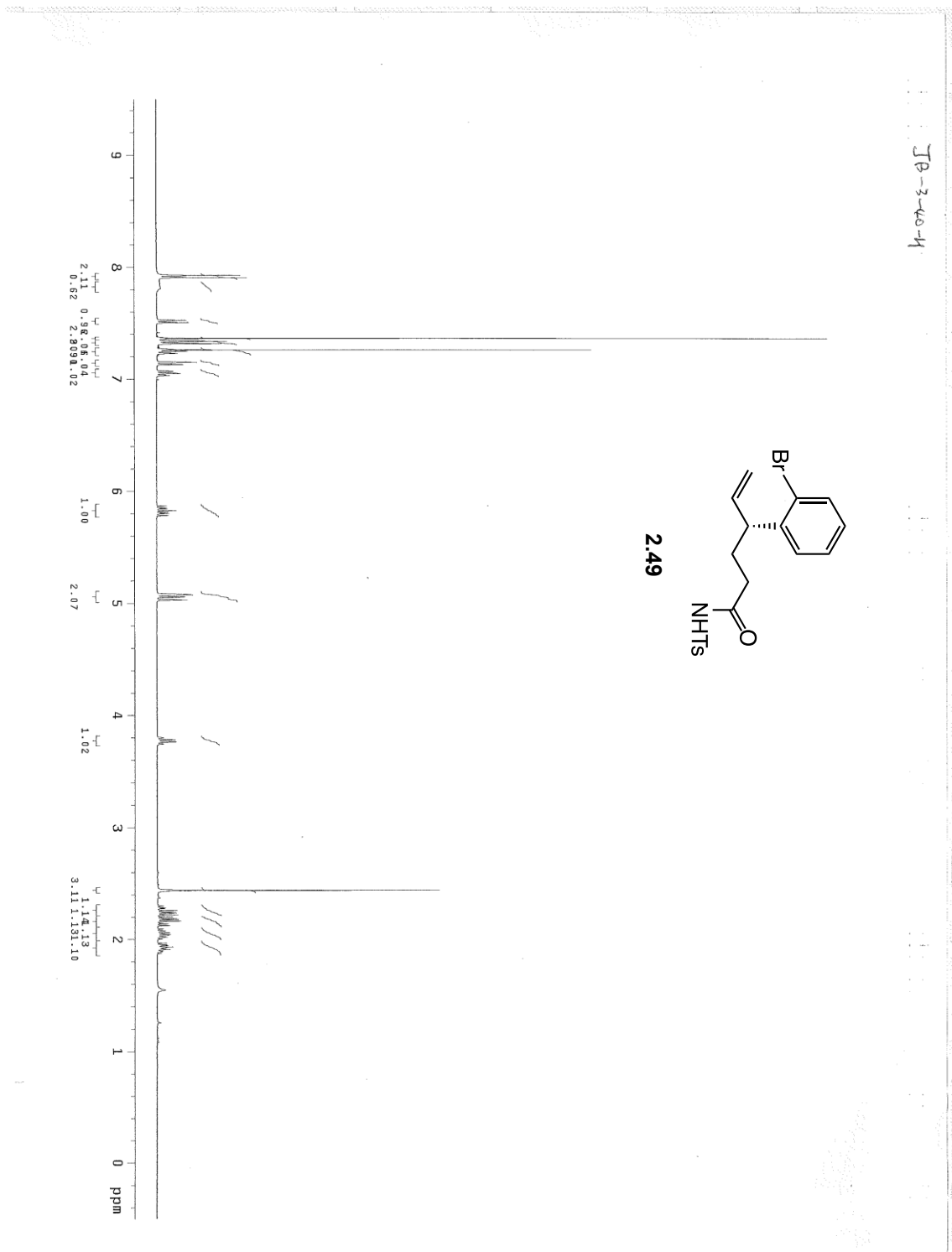
JB-3-47-14

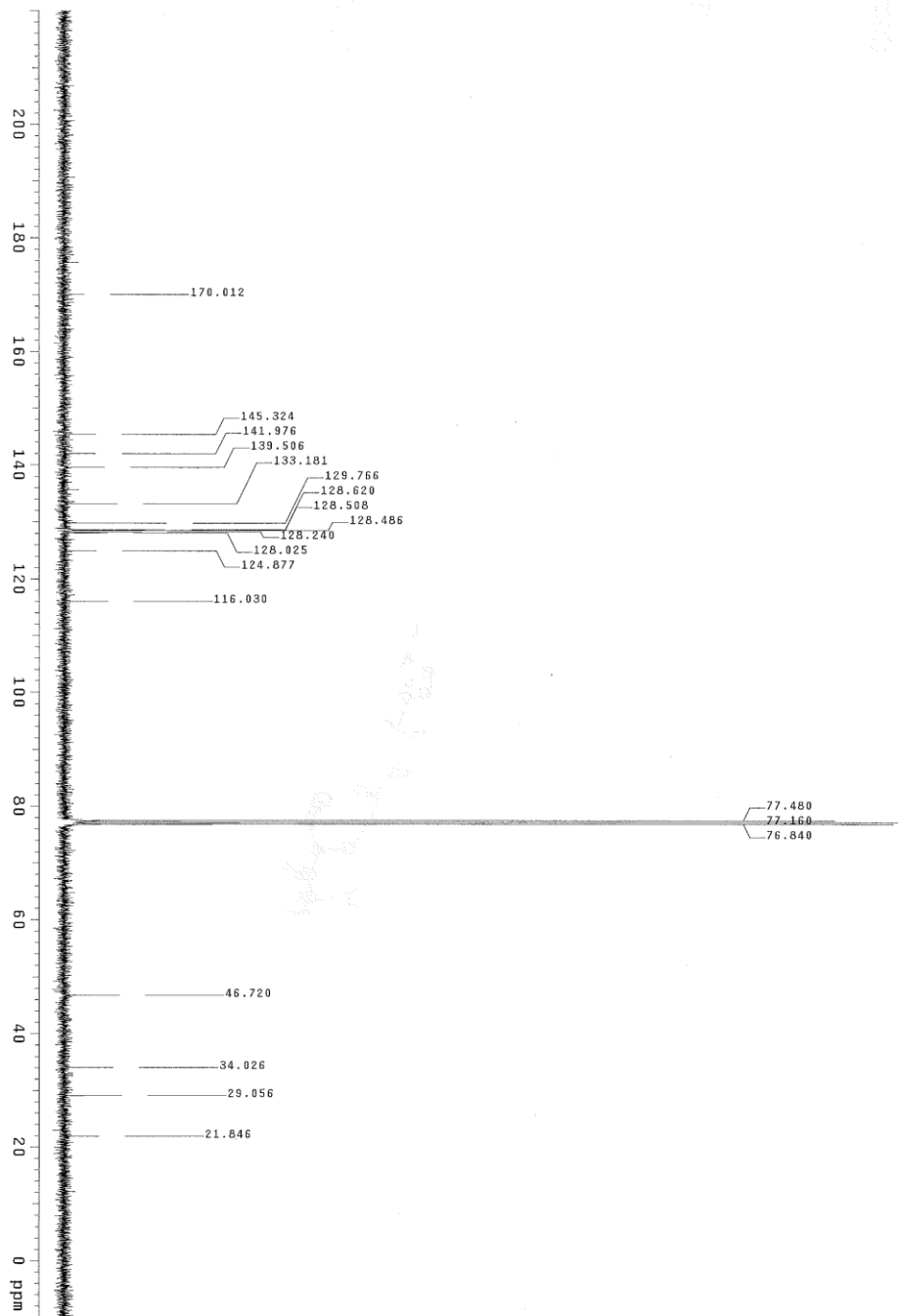


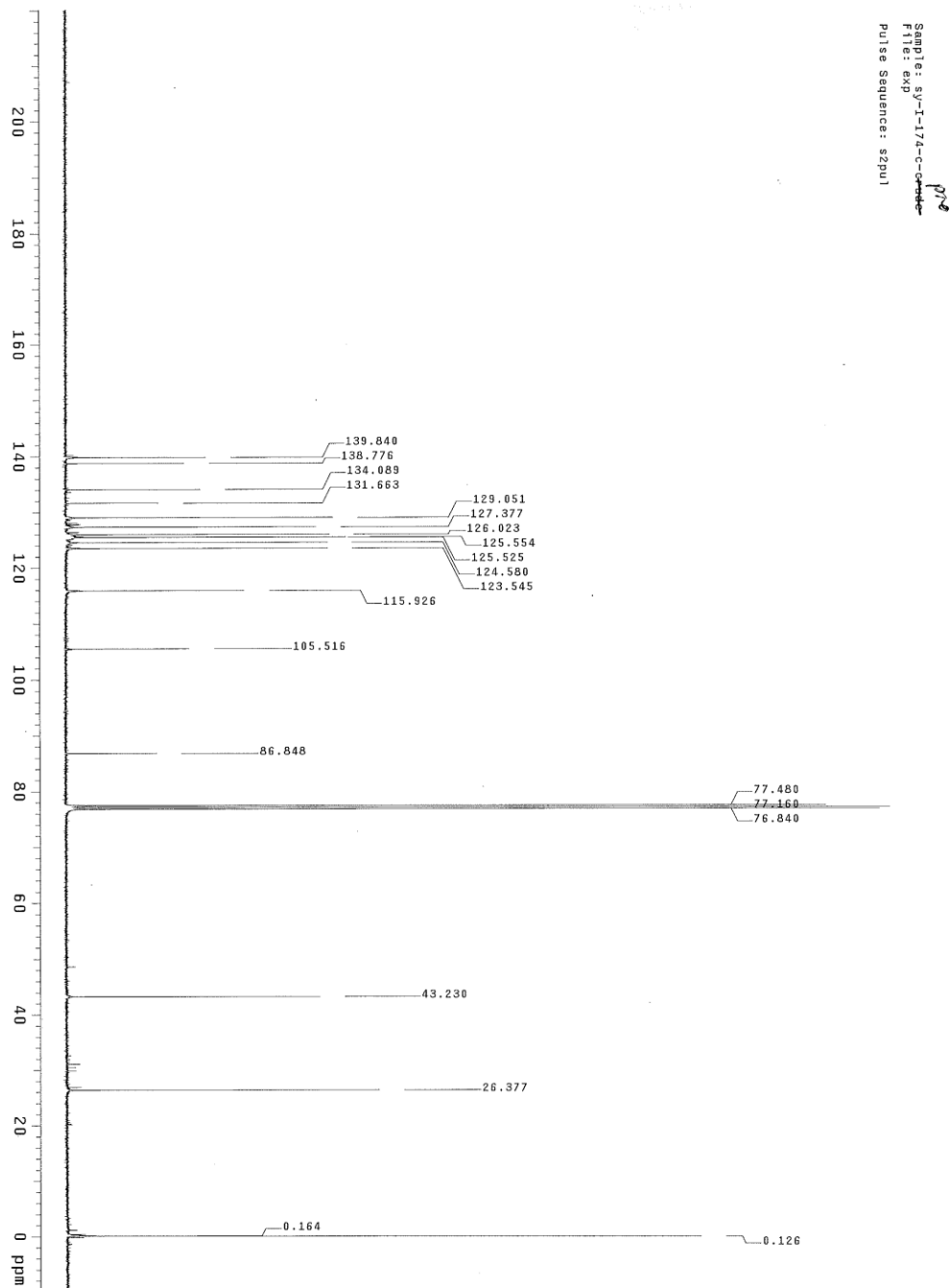






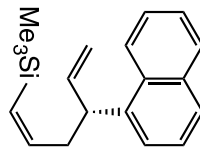




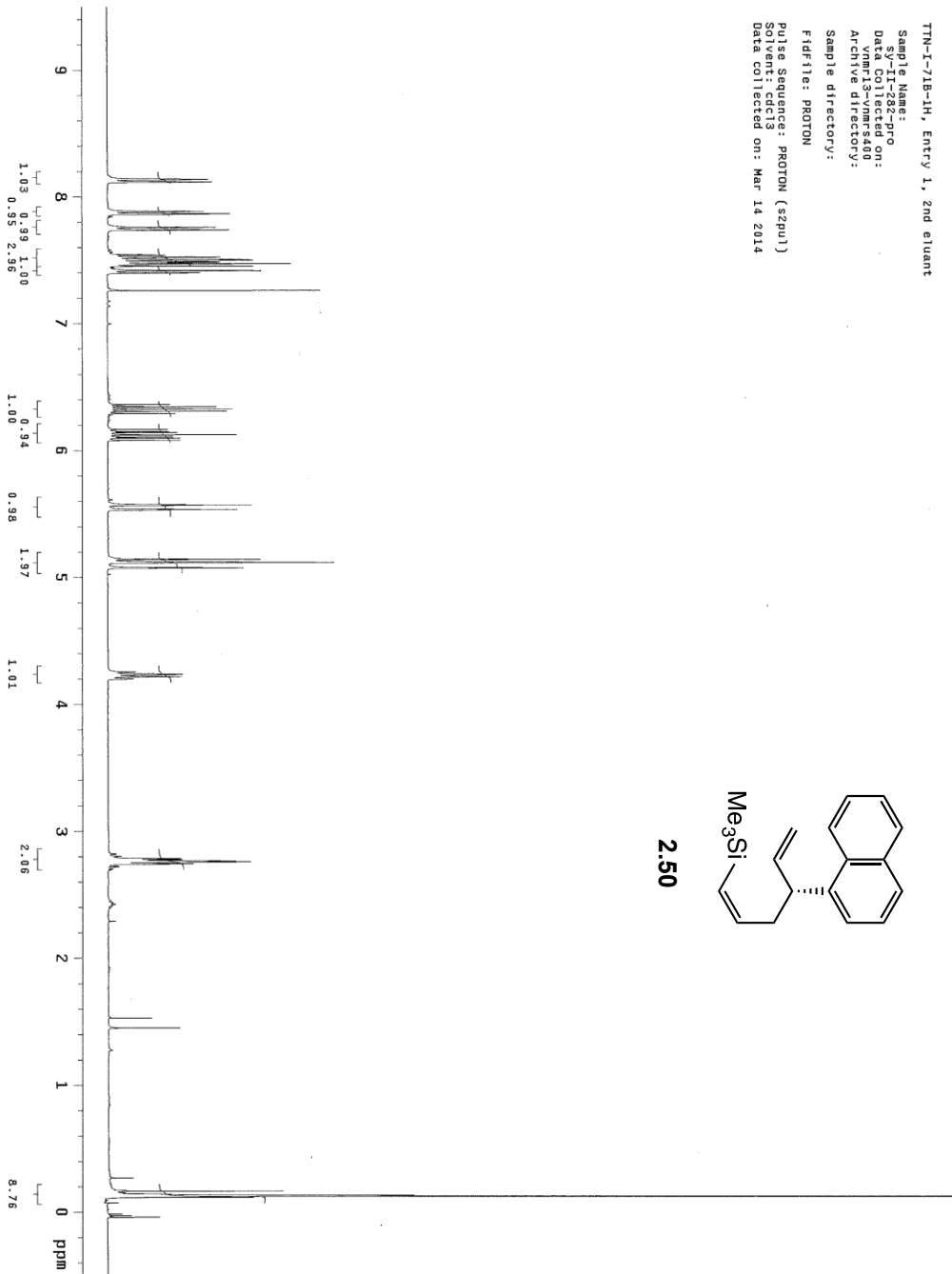


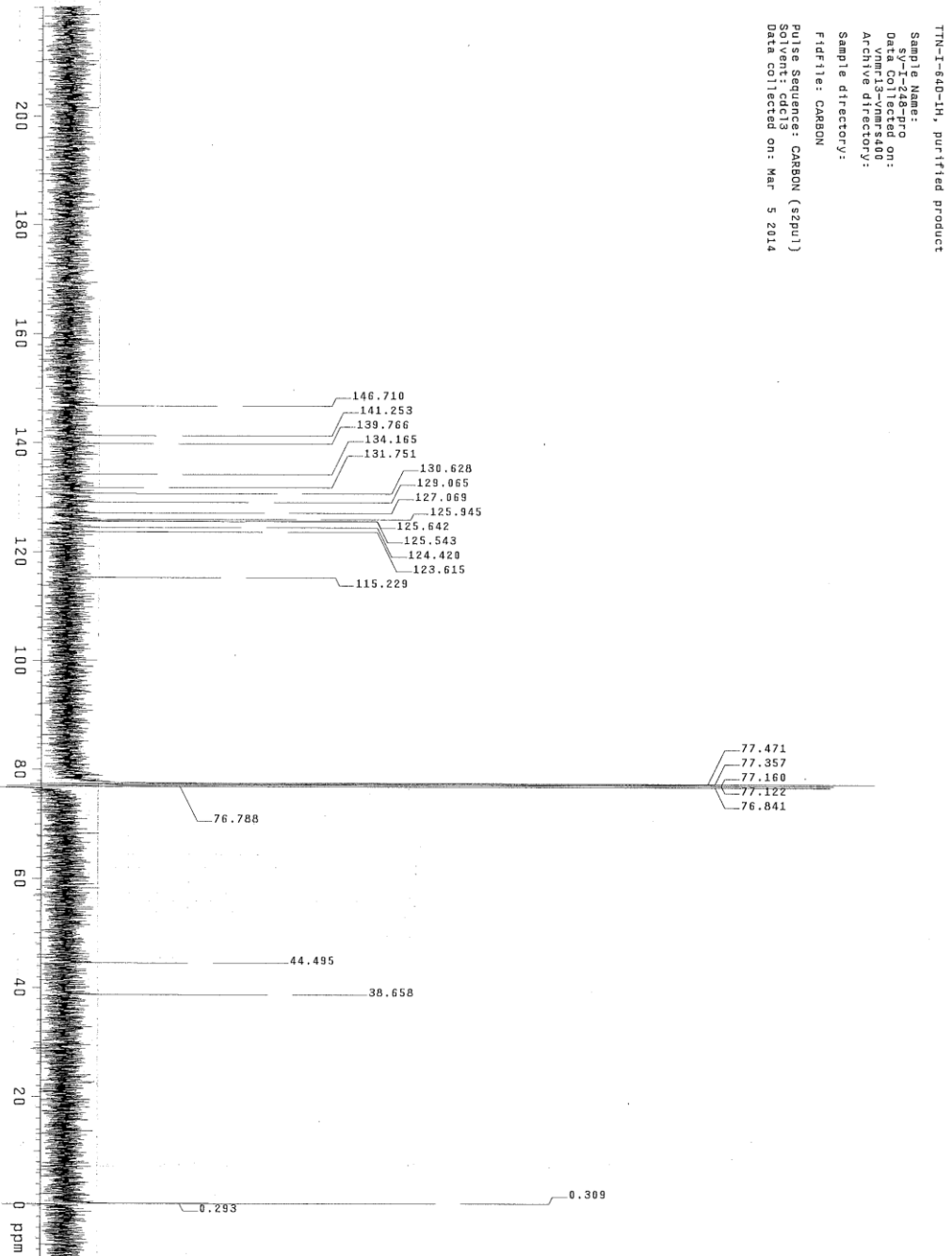
TM-1-718-H, Entry 1, 2nd eluant

Sample Name:
 vnmr13
 Data Collected on:
 vnmr13-vmr3480
 Archive directory:
 Sample directory:
 F1df11e: PROTON
 Pulse Sequence: PROTON (g2pu1)
 Solvent: CDCl3
 Data collected on: Mar 14 2014



2.50

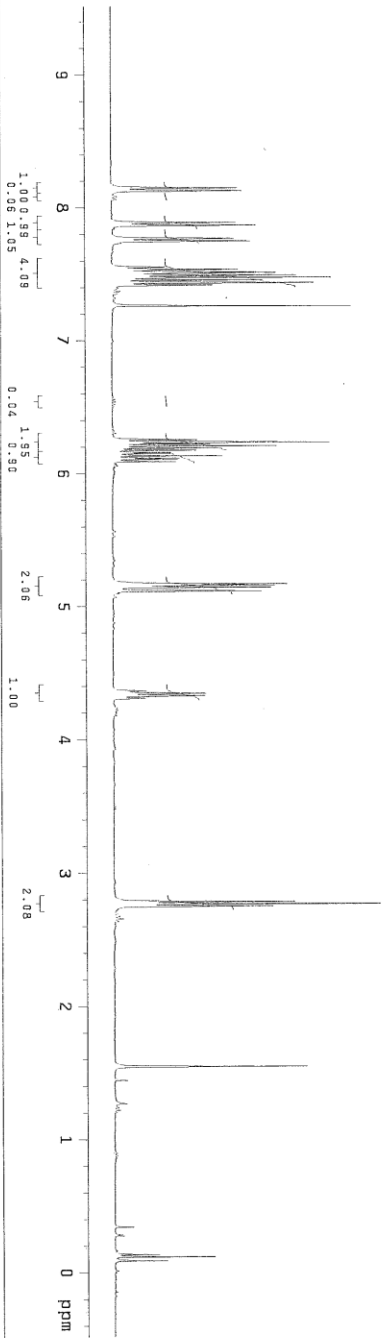
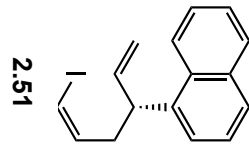


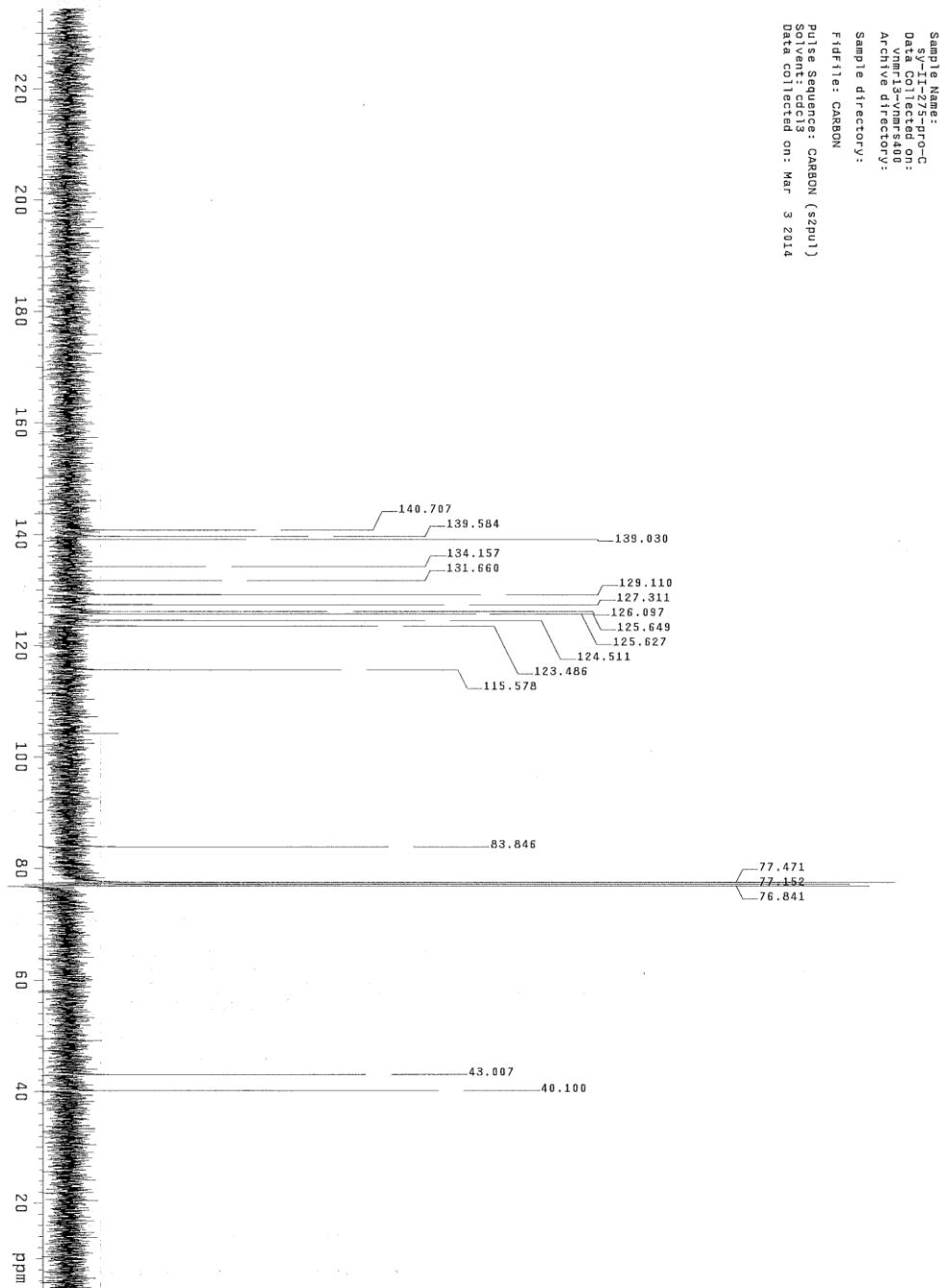


TTN-I-64b-1H, purified product

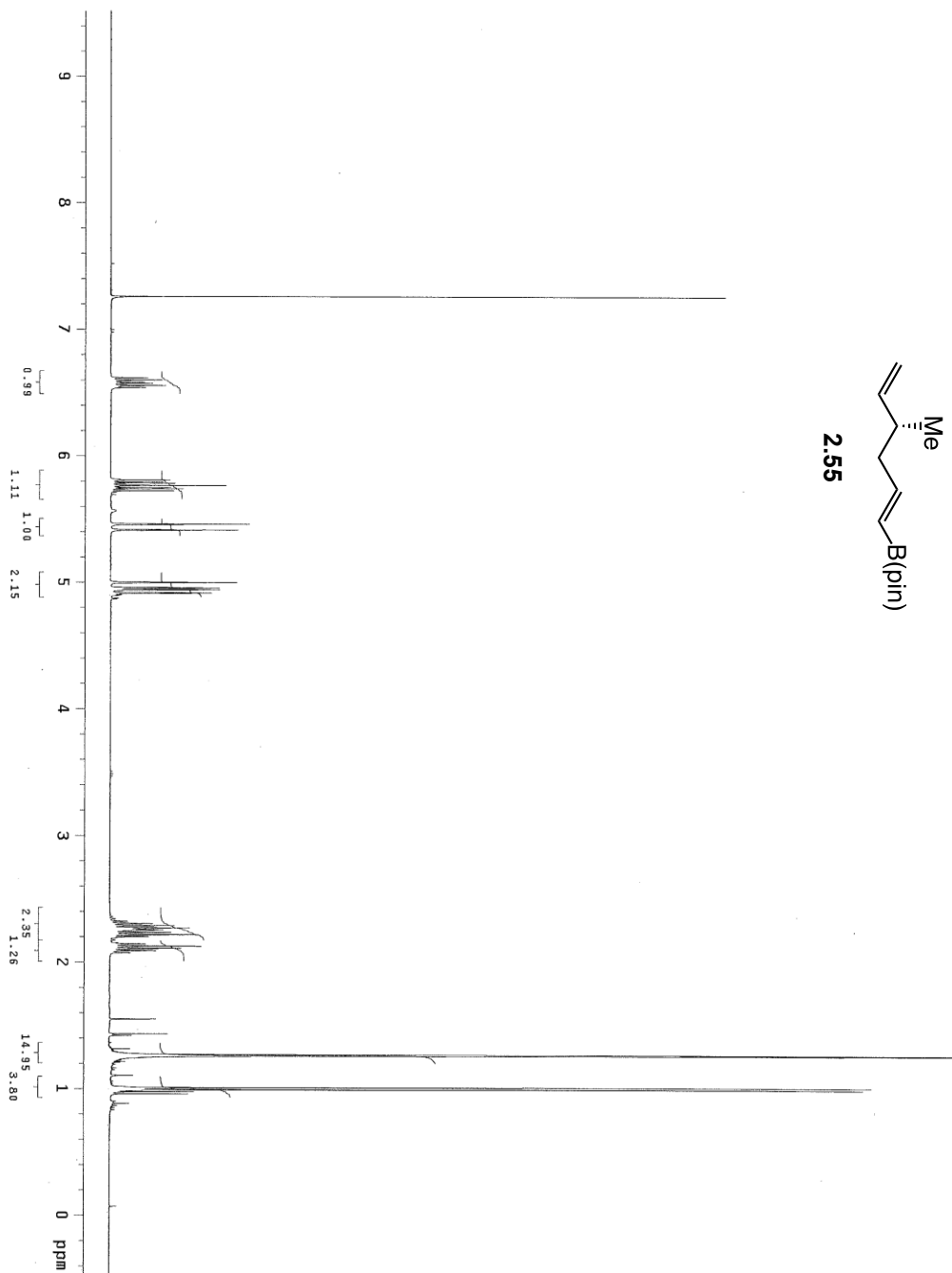
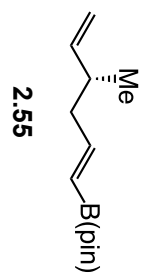
Sample Name:
Data Collected on:
vnmr13-vnmr400
Archive directory:
Sample directory:
Fidfile: CARBON
Pulse Sequence: CARBON (zgpg1)
Solvent: CDCl3
Data collected on: Mar 5 2014

LKA-II-1060-C
Sample Name: -
Data Collected on: vnmr13-vnmr540
Archive directory: /home/ahn
Sample ID: LKA-II-1060-C_20140730_01
FID File: PROTON
Pulse Sequence: PROTON (s2pu1)
SFO
Data collected on: Jul 31 2014

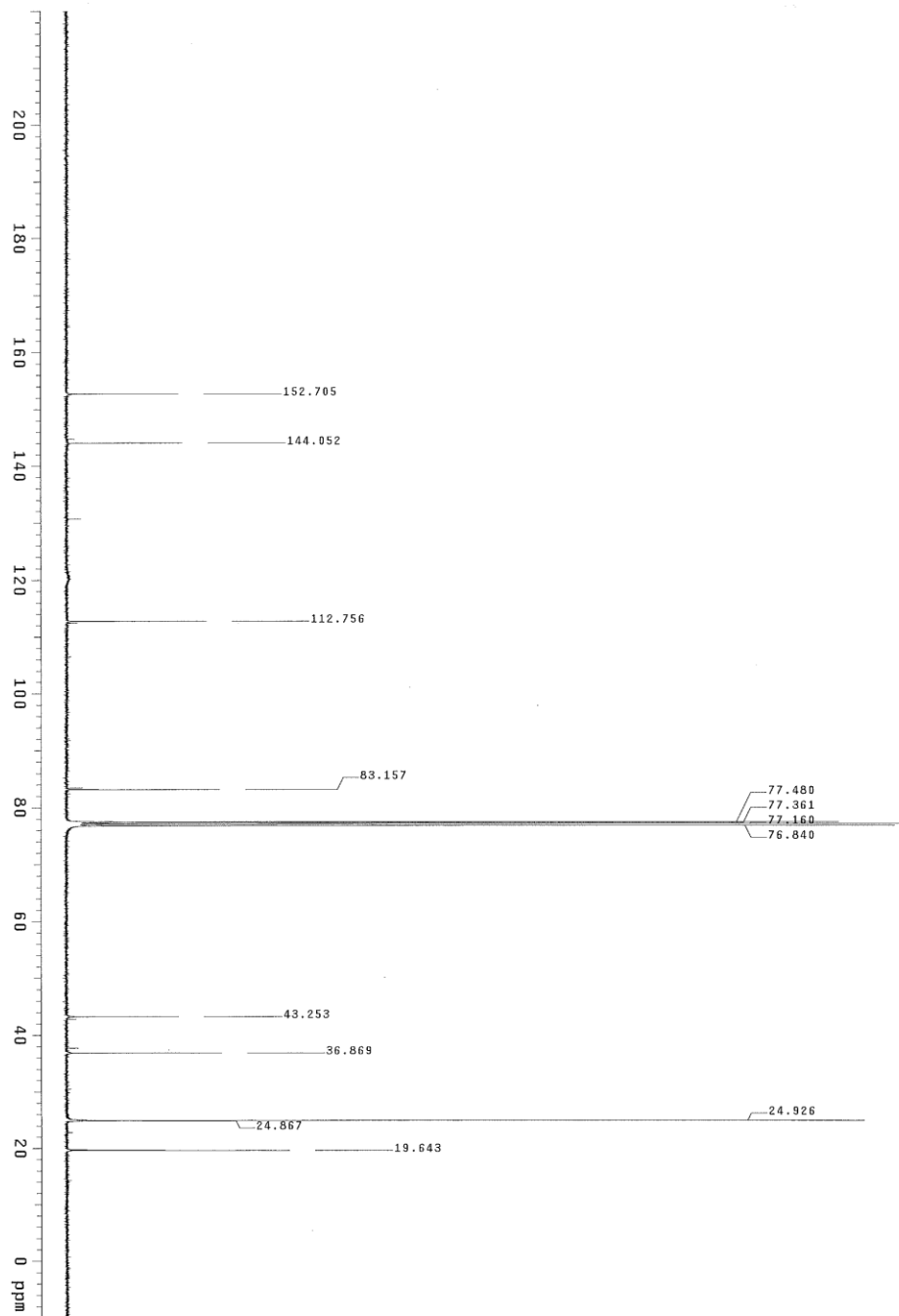




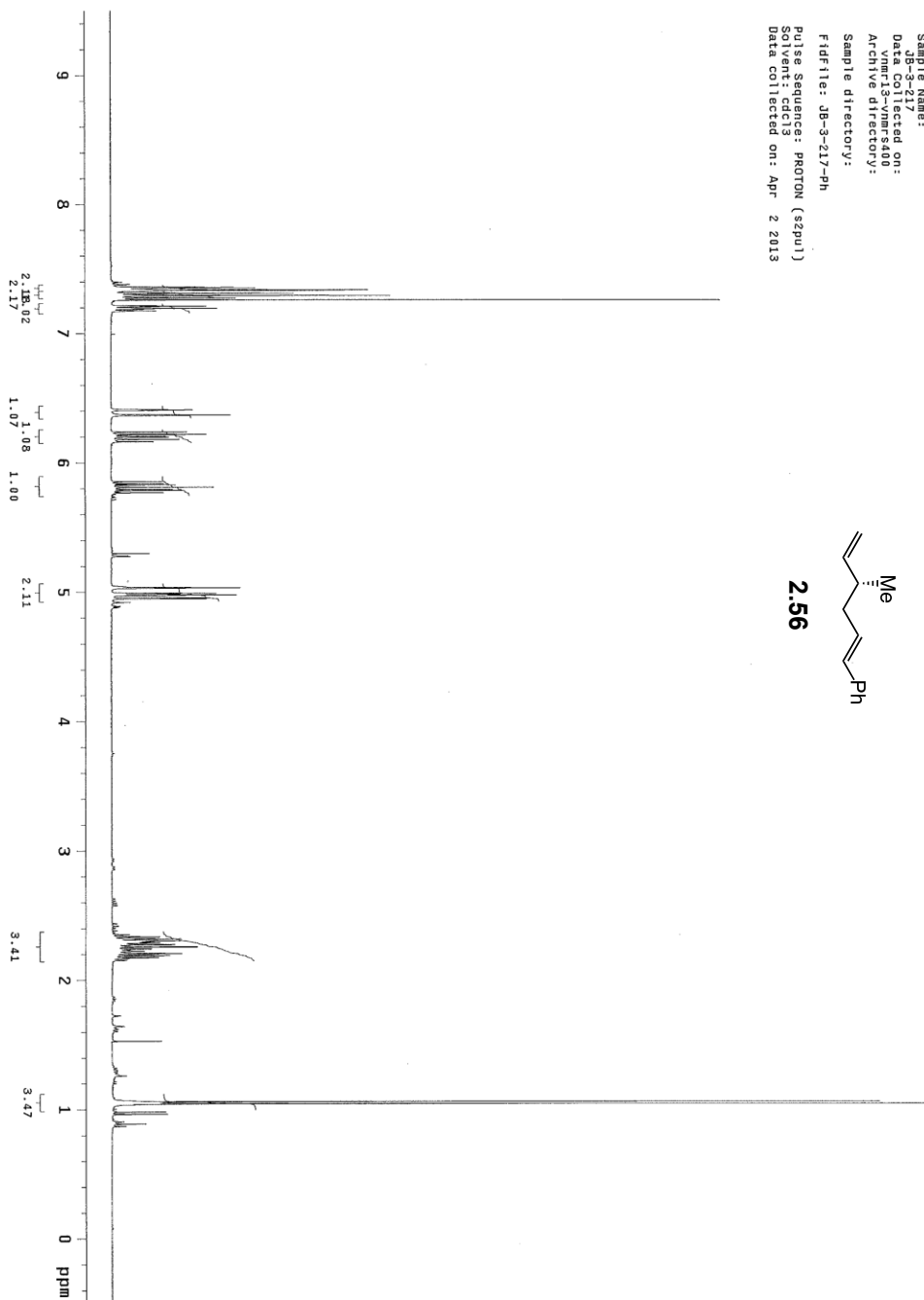
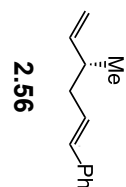
5B-3-194-2d4



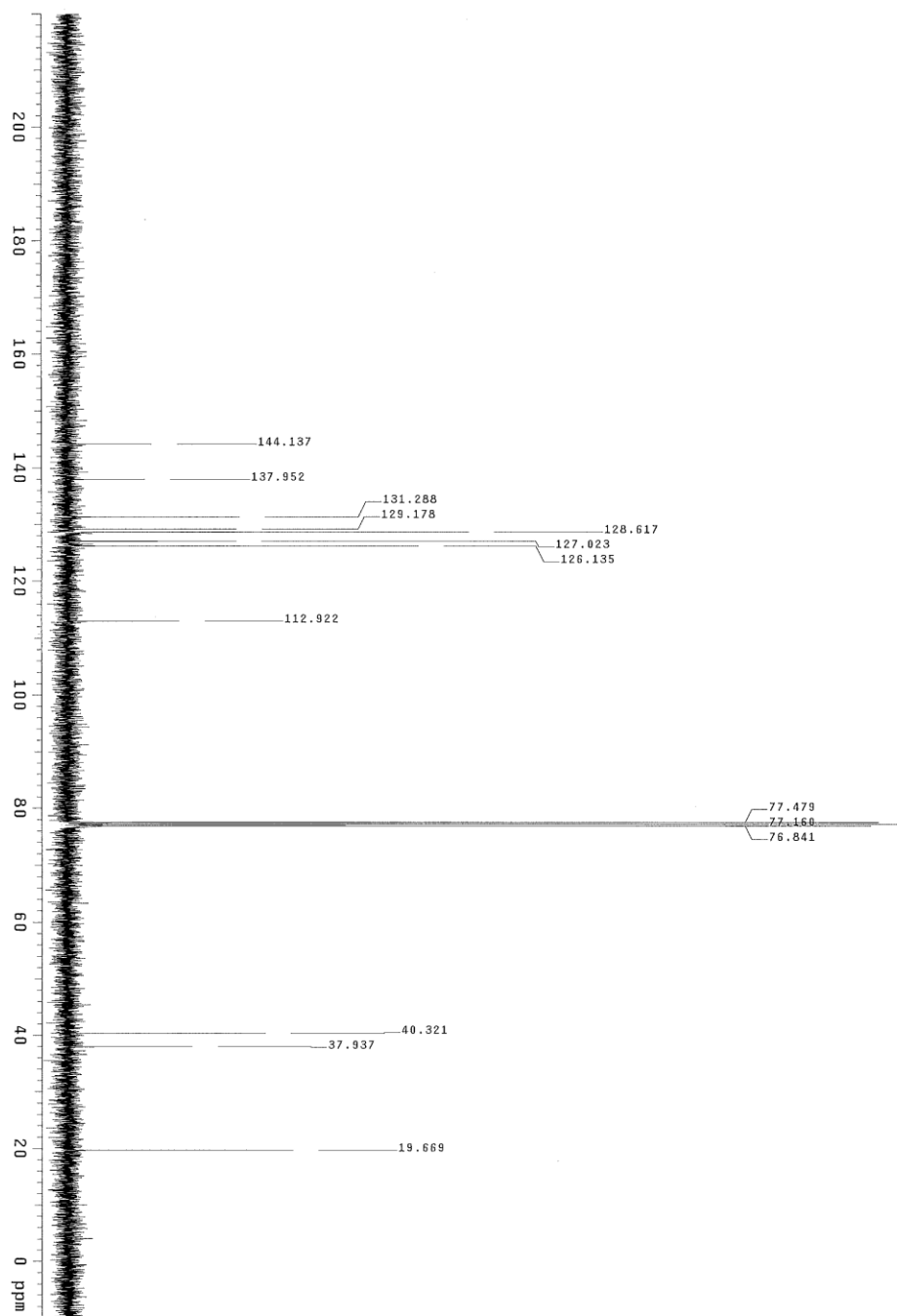
JR-3-74-2



Sample Name: 40-3-21-13
Data Collected on: vnmr13-vnmr3400
Archive directory:
Sample directory:
Fidfile: j8-3-21-13-ph
Pulse Sequence: PROTON (g2pul)
Solvent: cdcl3
Data collected on: Apr 2 2013



SY- JB-3-217-PH-C

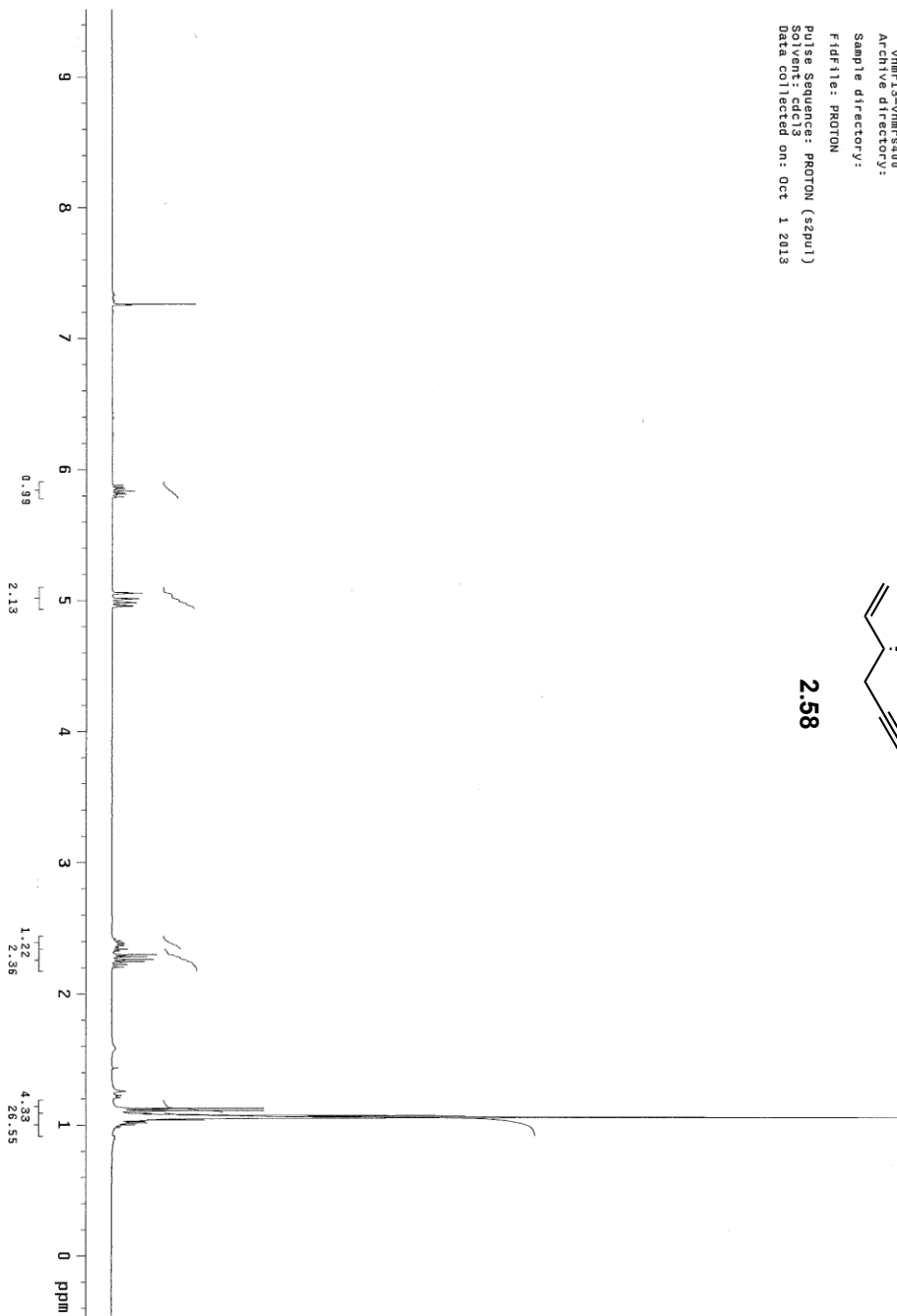


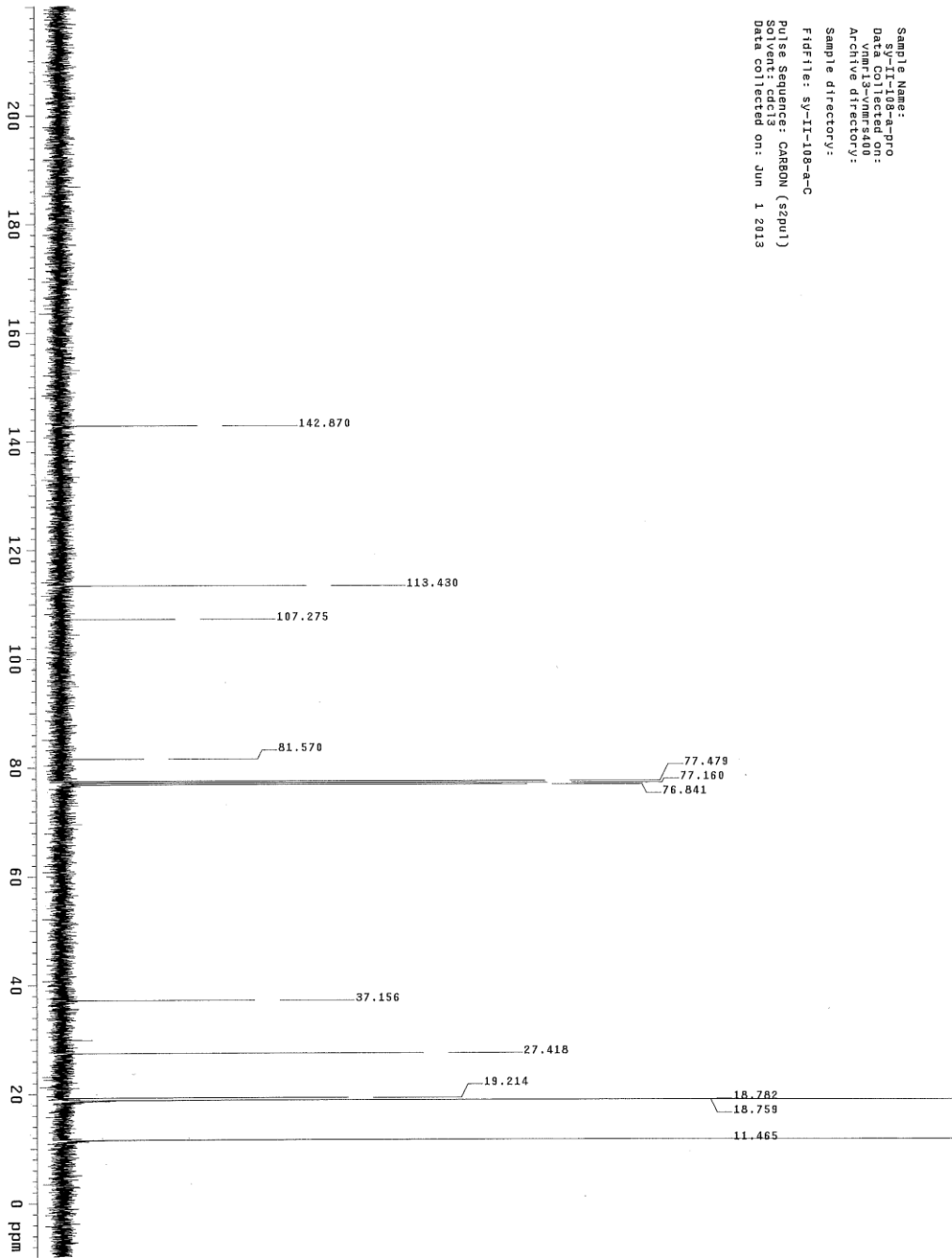
MJK-II-125A-1H, after work-up

Sample Name:
 MJK-II-125A-1H
 Data Collected on:
 vnmr13-vnmr400
 Archive directory:

Sample directory:

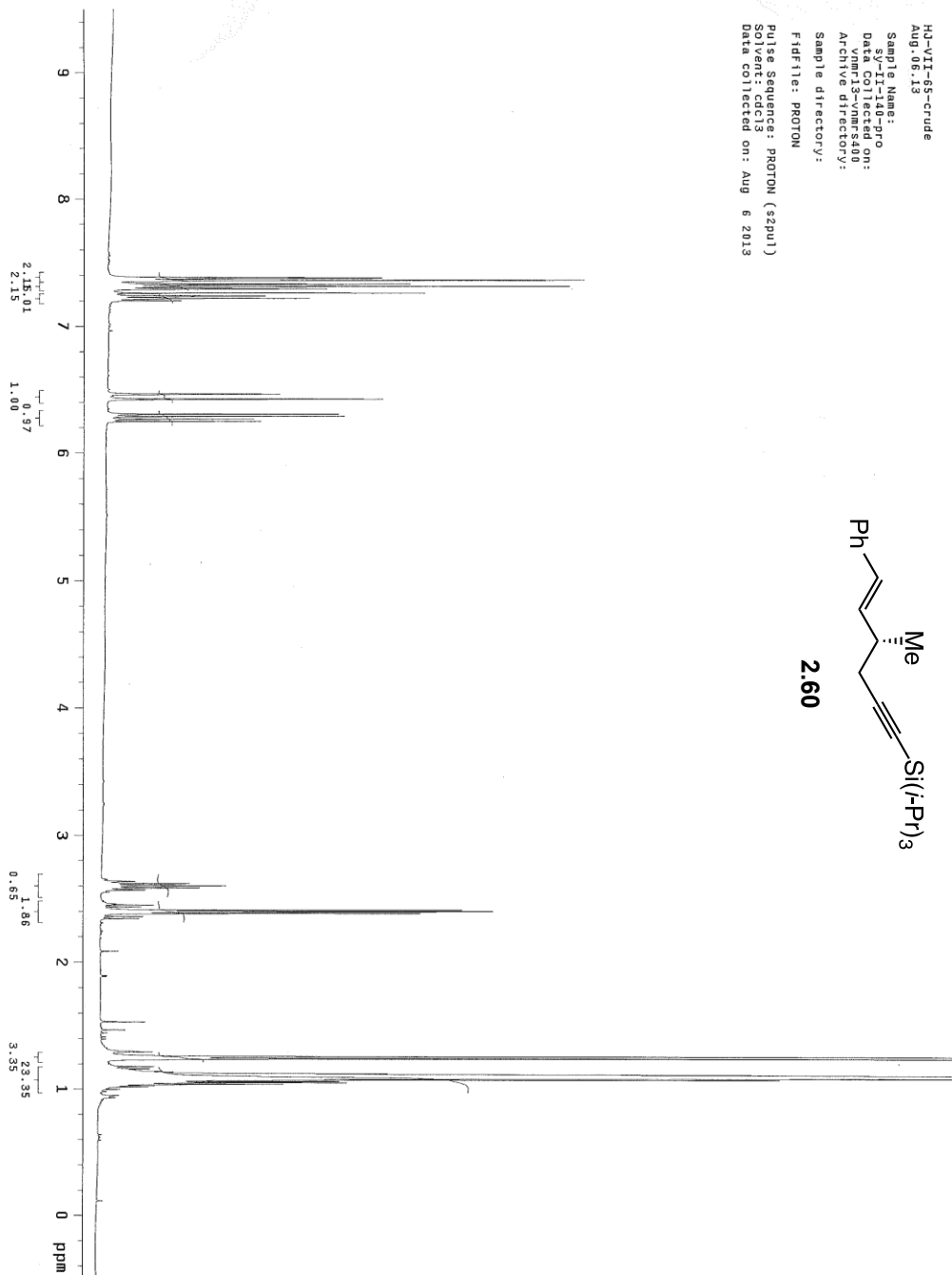
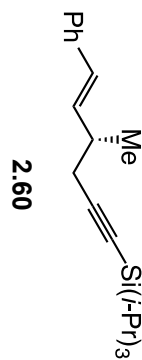
Fidfile: PROTON
 Pulse Sequence: PROTON (zpg1)
 Solvent: CDCl3
 Data collected on: Oct 1 2013



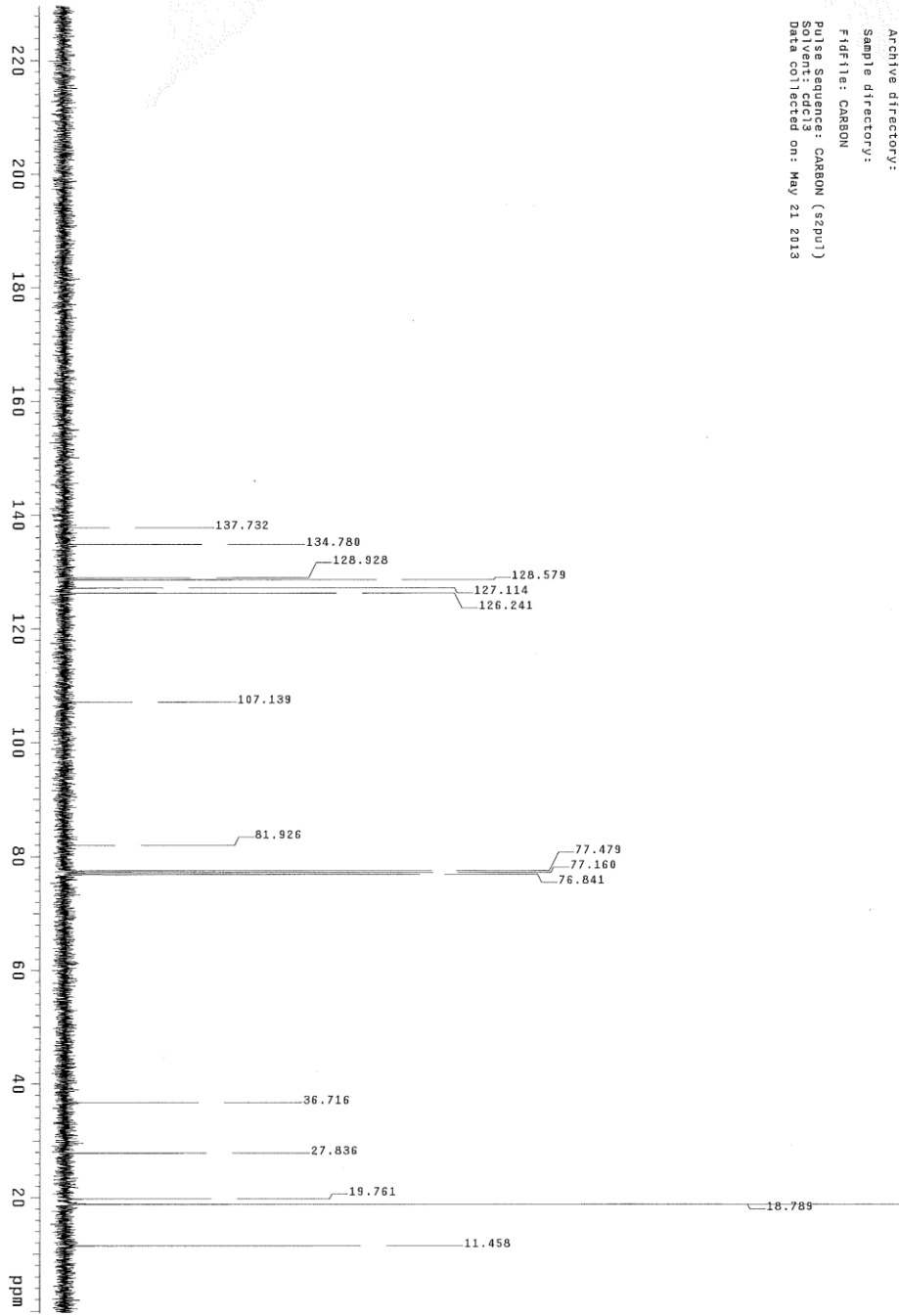


Sample Name: sy-II-108-a-pro
Data Collected on: 2013 Jun 1 14:40
Archive directory:
Sample directory:
Fidfile: sy-II-108-a-C
Pulse Sequence: CARBON (s2pu1)
Solvent: cdcl3
Data collected on: Jun 1 2013

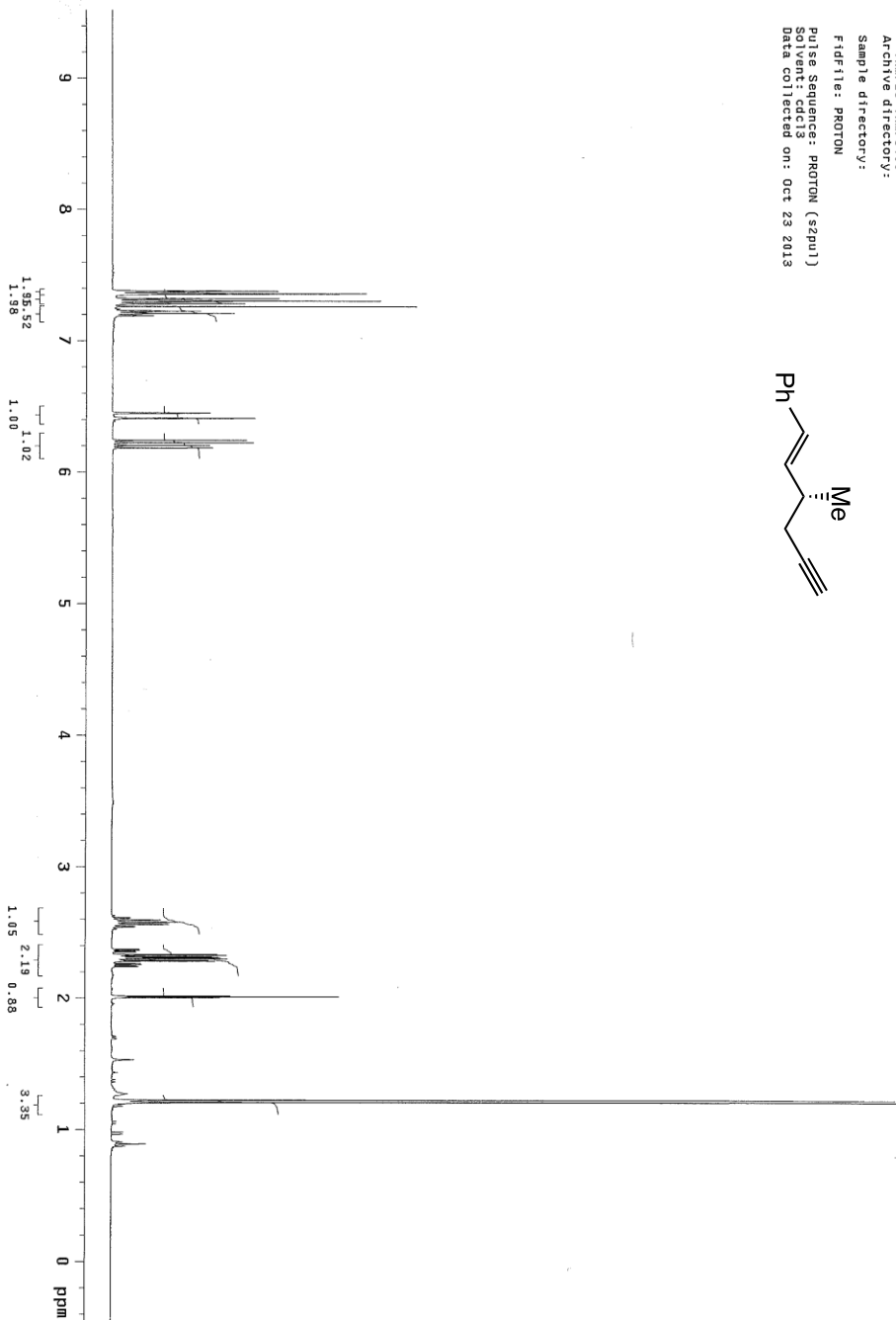
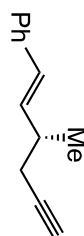
HJ-VII-65-crude
 Aug. 06.13
 Sample Name:
 Data Collected on:
 Vnmr13-vnmr5400
 Archive directory:
 Sample directory:
 F1dir1: PROTON
 Pulse Sequence: PROTON (zgpg3)
 Solvent:
 Data collected on: Aug 6 2013

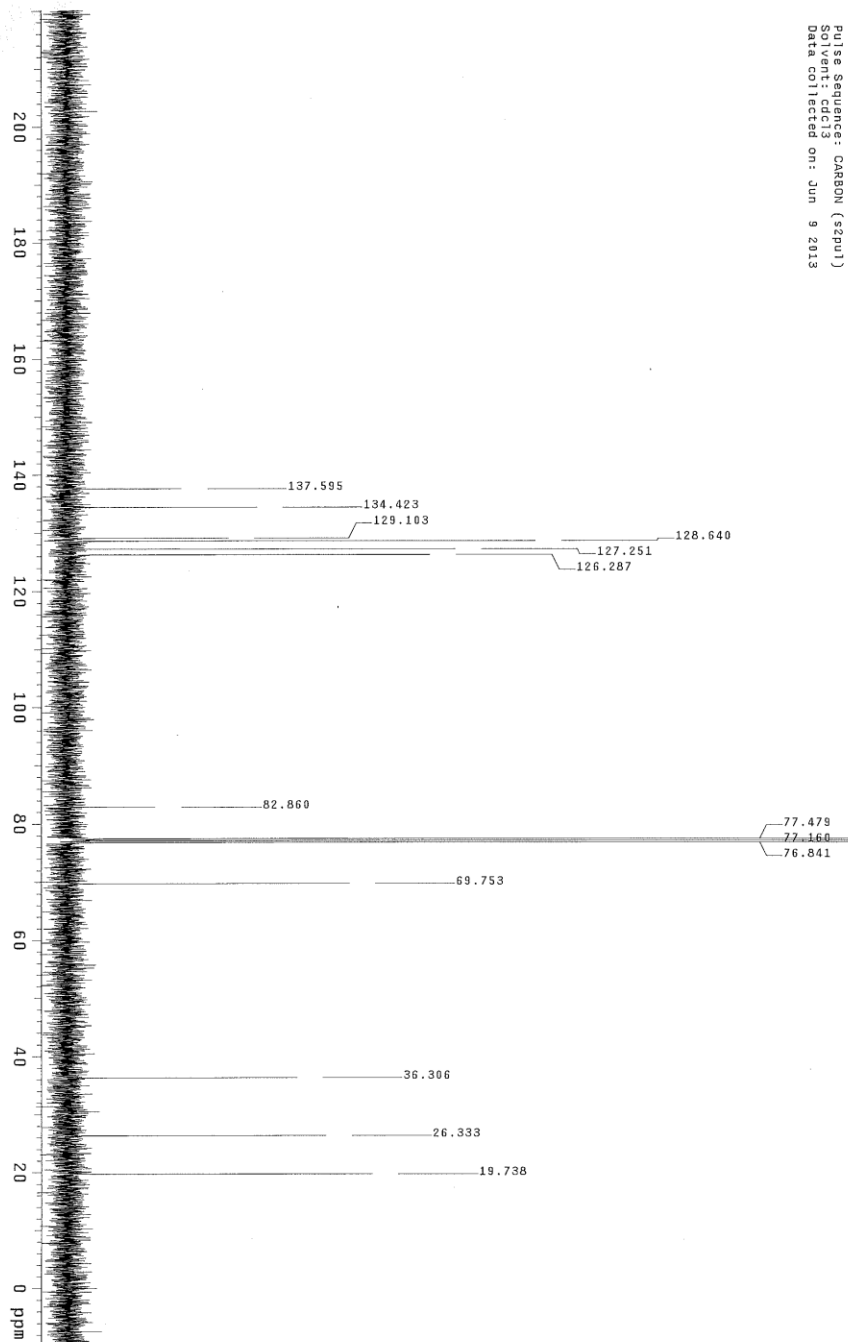


Sample Name: 5y-II-90-pur
Data Collected on: 5/21/13
Archive directory:
Sample directory:
Fidfile: CARBON
Pulse Sequence: CARBON (szpu1)
Solvent: cdcl3
Data collected on: May 21 2013

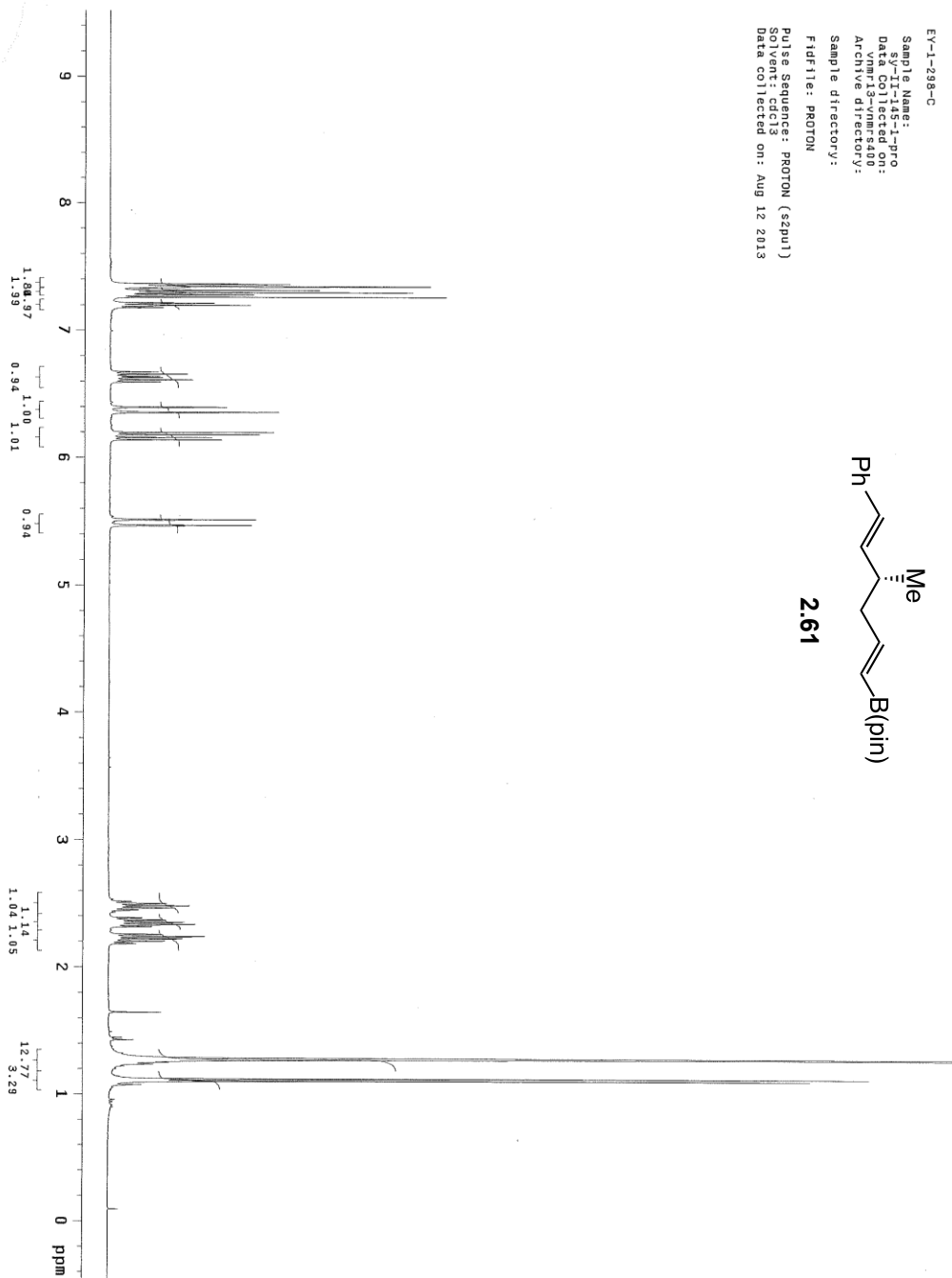
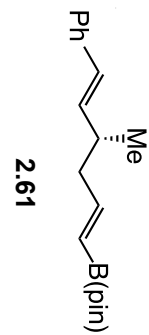


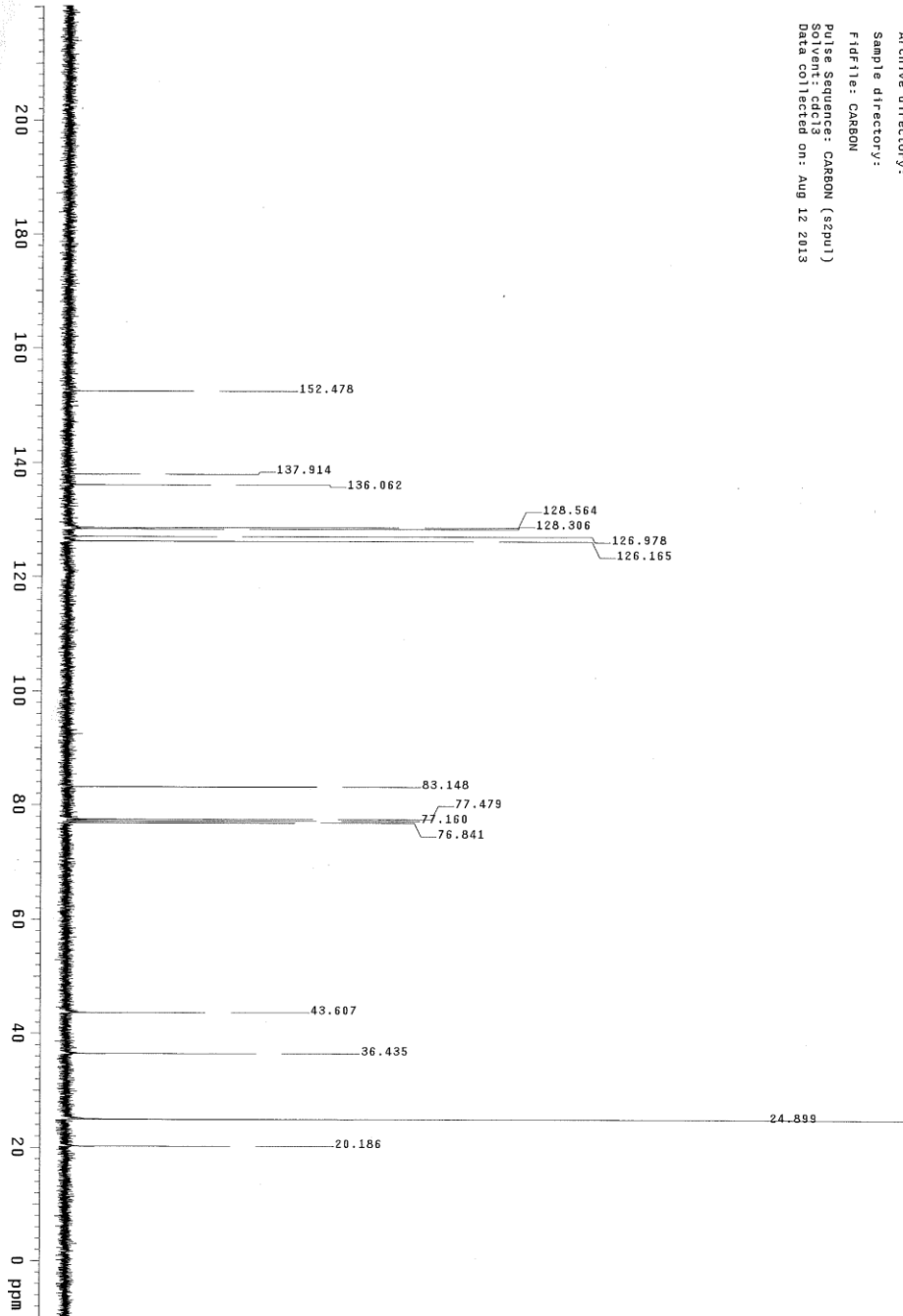
new experiment
Sample Name: sy-11-194-mix
Data Collected on: 11/19/11
Archive directory:
Sample directory:
Fidfile: PROTON
Pulse Sequence: PROTON (szpu1)
Solvent: cdcl3
Data collected on: Oct 23 2013



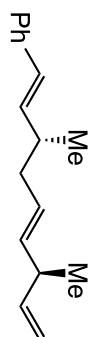


EV-1-298-C
 Sample Name: -
 Data Collected on: -
 vnmr13-vnmr-s400
 Archive directory: -
 Sample directory: -
 F1F1file: PROTON
 Pulse Sequence: PROTON (szpu1)
 Date collected on: Aug 12 2013



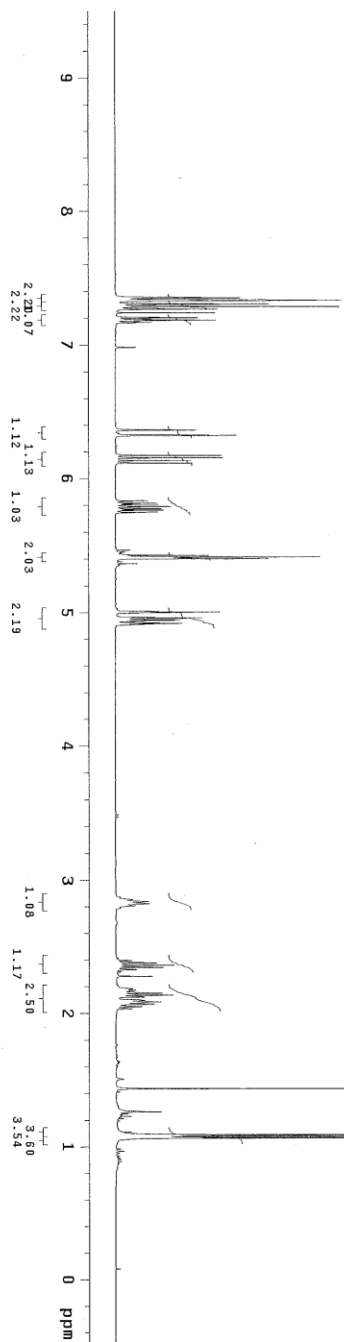


EY-1-298-C
Sample Name: EY-1-298-C
File Path: EY-1-298-C
Data File: EY-1-298-C
Vmr13-Vmr1400
Archive directory:
Sample directory:
File: CARBON
Pulse Sequence: CARBON (szpu)
Data collected on: Aug 12 2013

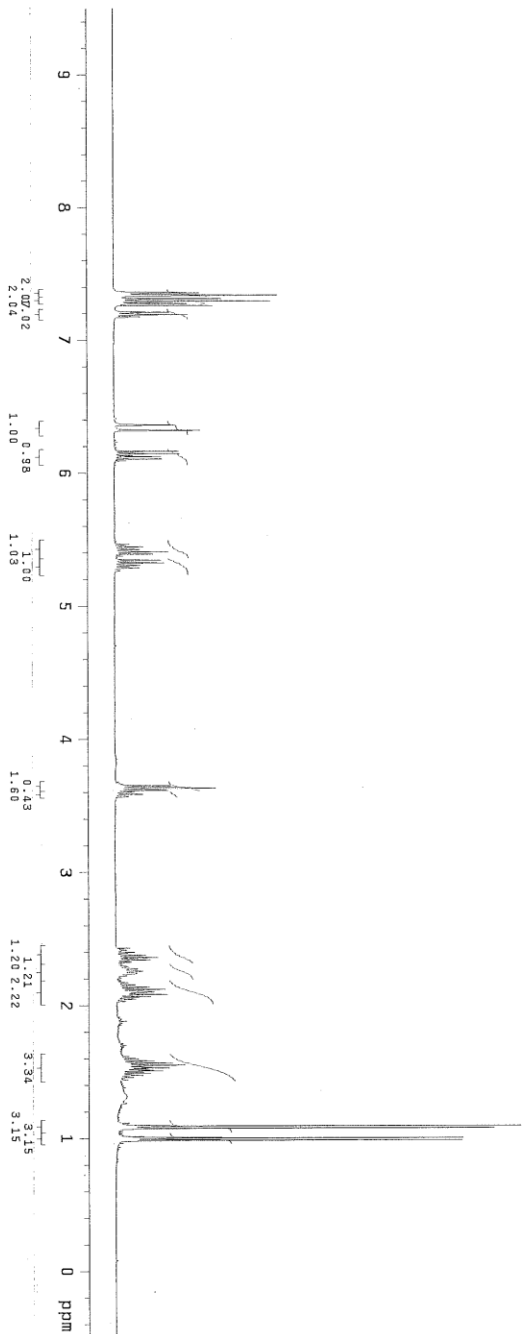
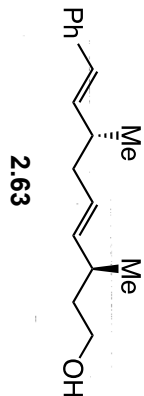


2.62

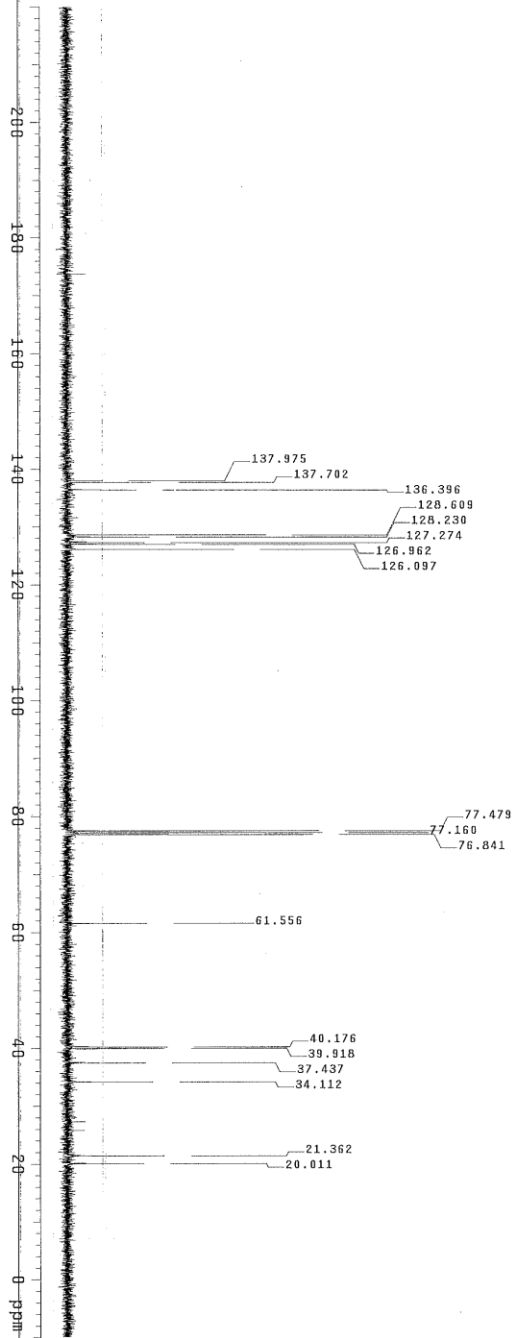
Sample Name: 2.62
 Date Collected: 08/19/2013
 Vnmr3-vmr5400
 Archive directory:
 Sample directory:
 F1dfiles: PROTON
 Pulse Sequence: PROTON (szpu1)
 Data Collected on: Aug 19 2013



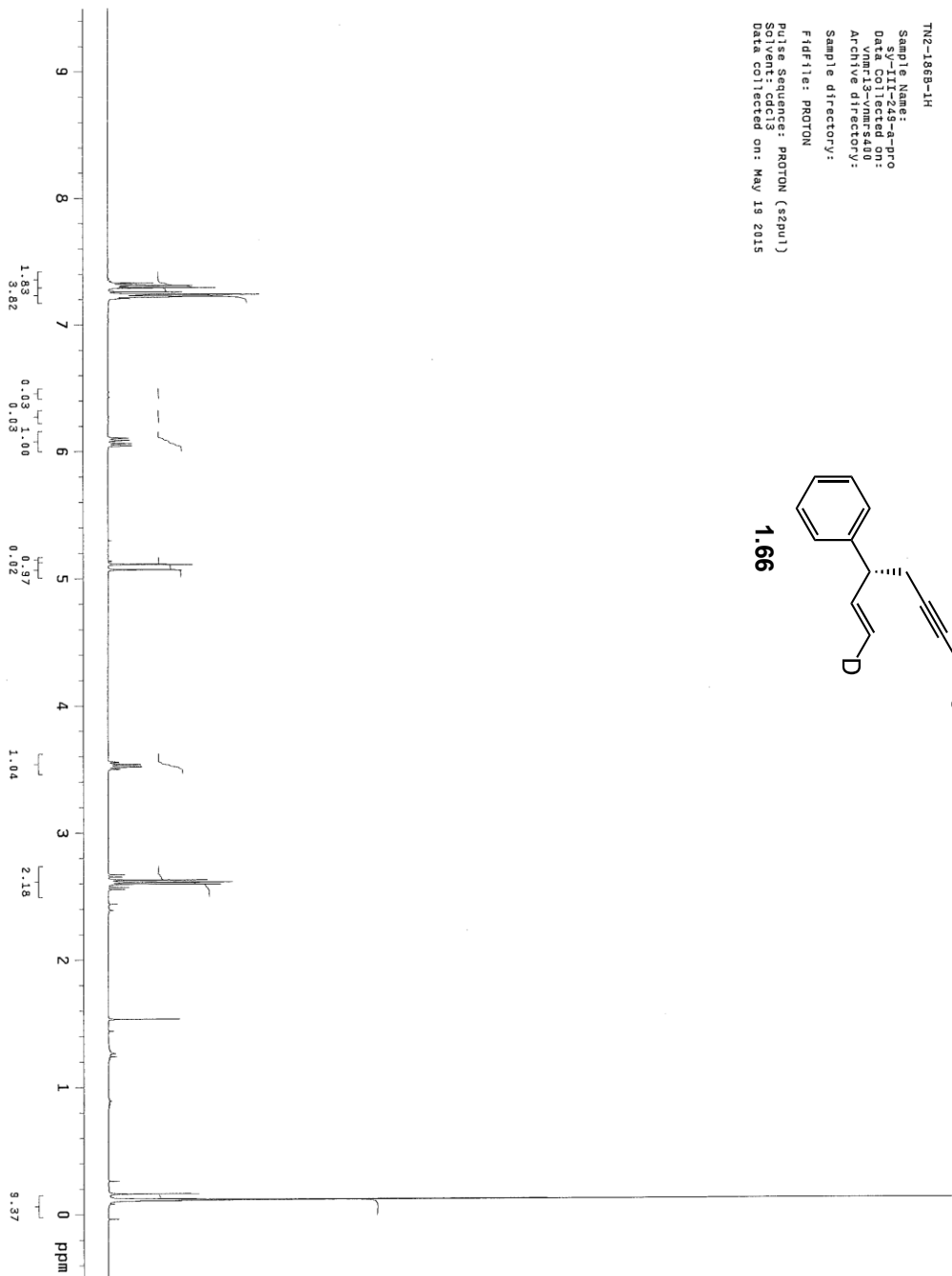
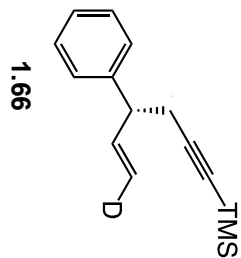
BL-1-023-341057
 Sample Name: -
 Date Collected: -
 Vnmr13-vnmr-s400
 Archive directory: -
 Sample directory: -
 F1file: PROTON
 Pulse Sequence: PROTON (szpu1)
 Date Collected on: Aug 2 2014

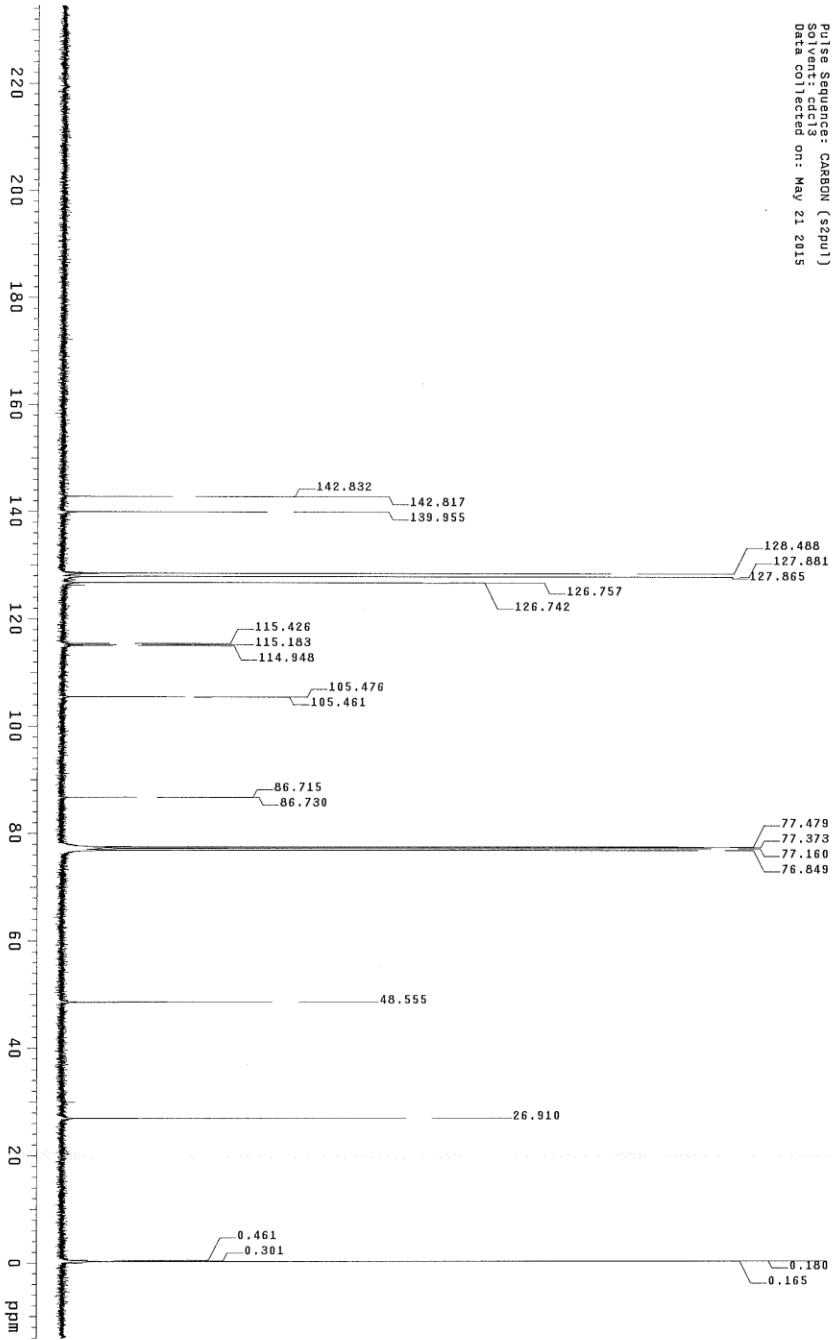


BL-I-023-341057
Sample Name: 5-pro...
Data Collected on: Vnmr3-vnmrs400
Archive directory:
Sample directory:
Fidfile: CARBON
Pulse Sequence: CARBON (szpu1)
Solvent: CDCl3
Data collected on: Aug 2 2014



TN2-1069-1H
 Sample Name: sy-111-249-a-pro
 Data Collected on: 11/14/11
 Archive directory:
 Sample directory:
 FIDfile: PROTON
 Pulse Sequence: PROTON (szpu1)
 Solvent: cdcl3
 Data collected on: May 19 2015





Chapter Three

NHC–Cu-Catalyzed Enantioselective Allylic Substitutions with Methylenediboron to Generate Tertiary and Quaternary Carbon Stereogenic Centers

3.1. Introduction

Copper-catalyzed enantioselective allylic substitution (EAS) reactions¹ are among the most versatile classes of transformations in organic chemistry: such processes deliver enantiomerically enriched products bearing a stereogenic center adjacent to a functionalizable alkene from readily accessible allylic electrophiles with “hard” nucleophiles. These processes may involve various organometallic reagents (e.g., Zn-, Mg-, or Al-based) and can be promoted by Cu complexes derived from chiral O-, N-, or P-based ligands or N-heterocyclic carbenes (NHCs). Several applications in total synthesis have demonstrated their utility.² While the last decade has seen considerable

(1) For reviews on Cu-catalyzed allylic substitution reactions with “hard” nucleophiles (a) Hoveyda, A. H.; Hird, A. W.; Kacprzynski, M. A. *Chem. Commun.* **2004**, 1779–1785. (b) Yorimitsu, H.; Oshima, K. *Angew. Chem., Int. Ed.*, **2005**, *44*, 4435–4439. (c) Kar, A.; Argade, N. P. *Synthesis*, **2005**, 2995–3022. (d) Alexakis, A.; Malan, C.; Lea, L.; Tissot-Croset, K.; Polet, D.; Falciola, C. *Chimia*, **2006**, *60*, 124–130. (e) Falciola, C. A.; Alexakis, A. *Eur. J. Org. Chem.* **2008**, *22*, 3765–3780. (f) Yokobori, U.; Ohmiya, H.; Sawamura, M. *Organometallics*, **2012**, *31*, 7909–7913.

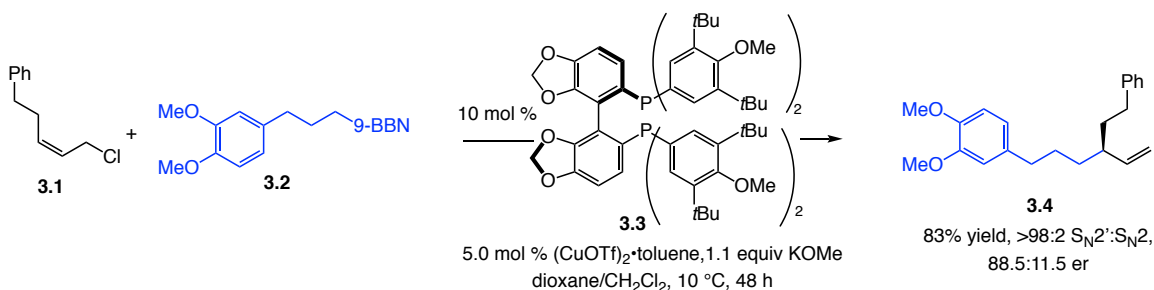
(2) For a recent review regarding applications of catalytic EAS reactions to natural product synthesis, see: Calvo, B. C.; Buter, J.; Minnaard A. J. in *Copper-Catalyzed Asymmetric Synthesis*, A. Alexakis, N. Krause, S. Woodward, Eds. Wiley-VCH, Weinheim, 2014, pp. 373–447.

developments in Cu-catalyzed EAS with organometallic reagents, there are still shortcomings that need to be addressed in order to achieve a broad scope with these important transformations. One major drawback is the sensitivity of common organometallic species to air and moisture: mandating their fresh preparation to ensure quality and reproducibility of the results. Additionally, the functional group compatibility of most organometallic reagents is poor, resulting in difficulty in incorporating many desired functionalities or requiring a series of cumbersome protecting group manipulations.

To remedy these fundamental limitations, organoboron nucleophiles have been adopted in this area because of their robustness and functional group tolerance. The first examples of enantioselective allylic substitution involving trialkylboranes were published by Sawamura and co-workers in 2012.³ As shown in Scheme 3.1, unlike previous reactions utilizing allylic phosphates,⁴ the enantioselective variant employed allylchlorides as the electrophiles. Under this protocol, alkyl addition products were obtained in the presence of 10 mol % of an *in situ* generated bisphosphine–Cu complex derived from chiral ligand **3.3** in 83% yield and 88.5:11.5 er as a single regioisomer (>98:2 S_N2':S_N2) after 48 h at 10 °C.

(3) Shido, Y.; Yoshida, M.; Tanabe, M.; Ohmiya, H.; Sawamura, M. *J. Am. Chem. Soc.* **2012**, *134*, 18573–18576.

(4) (a) Nagao, K.; Yokobori, U.; Makida, Y.; Ohmiya, H.; Sawamura, M. *J. Am. Chem. Soc.* **2012**, *134*, 8982–8987. (b) Ohmiya, H.; Yokobori, U.; Makida, Y.; Sawamura, M. *Org. Lett.* **2011**, *13*, 6312–6315. (c) Yokobori, U.; Ohmiya, H.; Sawamura, M. *Organometallics* **2012**, *31*, 7909–7913.

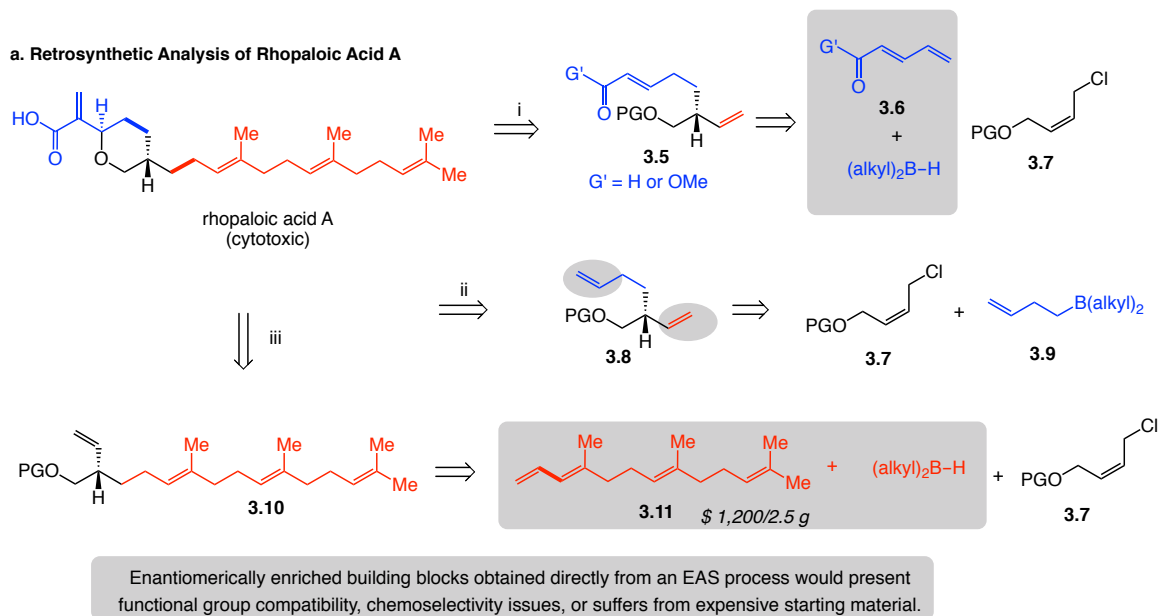
Scheme 3.1. EAS Reaction with Alkylborane Reagents

We sought to develop our own method to address these shortcomings as we considered synthesis of natural product rhopaloic acid **A** employing EAS reactions with alkylborane reagents (Scheme 3.2a). In each of the routes, the construction of the stereogenic center requires EAS reactions with allylchloride **3.7**. In route (i), preparation of enantiomerically enriched **3.5** called for an organoboron reagent that required site-selective hydroboration of a somewhat sensitive dienyl aldehyde **3.6** (or an ester-derivative). An alternative route (ii) through diene **3.9**, accessible by previously reported EAS methods,⁵ would demand the differentiation of two terminal olefins, likely to result in the generation of difficult-to-separate isomeric mixtures. Another possible route (iii) is to utilize a more expensive diene **3.11** (\$ 1,200/ 2.5 g) derived from farnesol. Instead, we turned our attention to the much less reactive, but functional group tolerant methylene diboron **3.13**. As shown in Scheme 3.2b, we proposed a new EAS reaction protocol utilizing allylic phosphate **3.12** and methylene diboron **3.13**. Such processes would not only involve an organoboron reagent as a starting material, but would deliver products containing a versatile C–B(pin) bond as well. We imagined a subsequent sequence entailing hydroboration of the EAS product **3.14** to furnish **3.15** with differentiable C–B bonds that could then be converted chemoselectively into **3.19** by a pair of catalytic

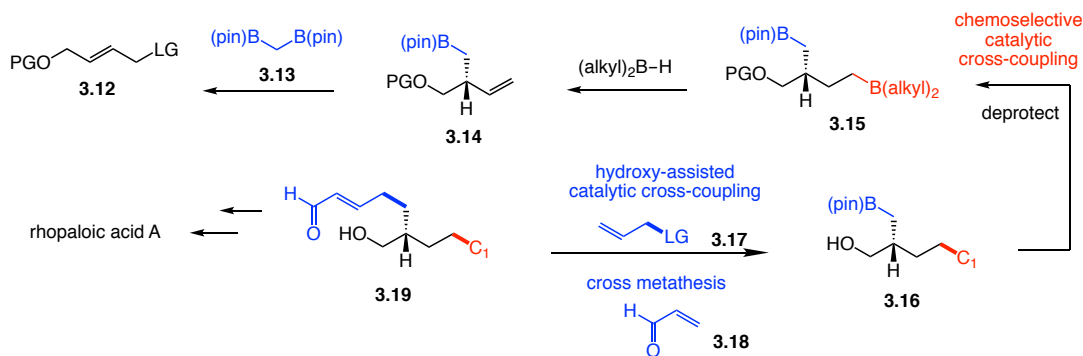
(5) For example, see: (a) Tissot-Croset, K.; D. Polet, Alexakis, A. *Angew. Chem. Int. Ed.* **2004**, *43*, 2426–2428; *Angew. Chem.* **2004**, *116*, 2480–2482. (b) López, F.; van Zijl, A. W.; Minnaard, A. J.; Feringa, B. L.; *Chem. Commun.* **2006**, 409–411.

cross-coupling reactions followed by cross metathesis with acrolein **3.18**. The first cross-coupling would chemoselectively react with the more reactive the alkylborane, and the second one could be directed by the neighboring hydroxy group, that could then be readily transformed to the pyran motif.

Scheme 3.2. Problems Associated with the Application of Catalytic EAS to the Synthesis of Rhopaloic Acid A and an Alternative Route.



b. Proposed Strategy Involving Three Catalytic C–C bond Forming Processes

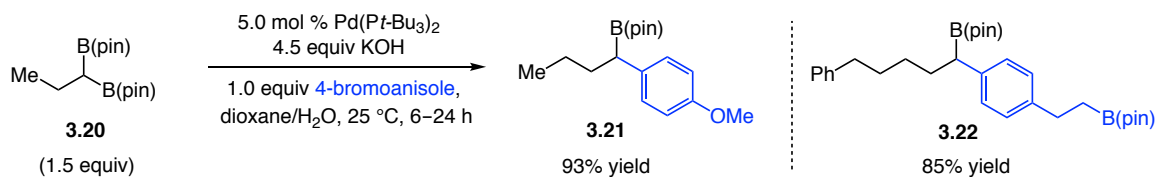


3.2. Background

Methylenediboron **3.13**, a member of a class of compounds developed by

Matteson⁶ and co-workers, has been the focus of several studies following the pioneering work by Endo and Shibata.⁷ Suzuki cross-coupling reactions with alkyl boronate compounds are known to suffer from slow transmetalation, β -hydride elimination as well as protodeboration. However, the Shibata group demonstrated that the Suzuki cross-coupling of geminal diboron reagents such as **3.20**, proceeds at room temperature without the need for a large excess of the boron reagent (Scheme 3.3). Additionally, the second B(pin) group does not undergo further cross-coupling even in the presence of excess aryl iodide. Furthermore, in the formation of **3.22**, the aryl bromide reacts selectively with the geminal diboron over the unsubstituted alkyl-B(pin).

Scheme 3.3 Catalytic Suzuki Cross-Coupling with Geminal Diboron Reagents



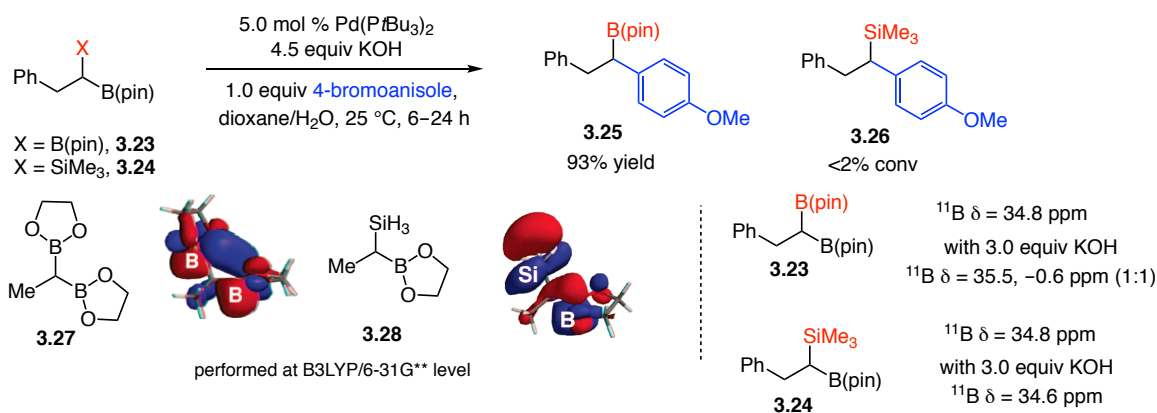
The authors propose that the transmetalation is able to occur at lower temperatures in part due to the ability of the B(pin) moiety to stabilize the negative charge built up at the α -C in the transition state of transmetalation through hyperconjugation into the empty p orbital of the vicinal B atom.^{7a} To probe this stabilizing effect, the analogous α -silyl boryl reagent **3.24** was subjected to the same cross-coupling conditions, but <2% conversion to the desired product **3.26** was observed (Scheme 3.4). DFT calculations were used to create a LUMO map for both the diboron

(6) Matteson, D. S.; Moody, R. J. *Organometallics* **1982**, *1*, 20–28.

(7) (a) Endo, K.; Ohkubo, T.; Hirokami, M.; Shibata, T. *J. Am. Chem. Soc.* **2010**, *132*, 11033–11035. (b) Endo, K.; Ohkubo, T.; Shibata, T. *Org. Lett.* **2011**, *13*, 3368–3371. (c) Endo, K.; Ohkubo, T.; Ishioka, T.; Shibata, T. *J. Org. Chem.* **2012**, *77*, 4826–4831. (d) Endo, K.; Ishioka, T.; Ohkubo, T.; Shibata, T. *J. Org. Chem.* **2012**, *77*, 7223–7231. (e) Endo, K.; Ishioka, T.; Shibata, T. *Synlett* **2014**, *25*, 2184–2188. for related investigations, see: (f) Z.-Q. Zhang, C.-T. Yang, L.-J. Liang, B. Xiao, X. Lu, J.-H. Liu, Y.-Y. San, T. B. Marder, Y. Fu, *Org. Lett.* **2014**, *16*, 6342–6345.

and borosilane reagents. As shown in Scheme 3.4, the LUMO of **3.27** is distributed across the B–C–B bonds whereas in **3.28**, the LUMO is delocalized around the boron and silicon atoms. The distribution of the LUMO in **3.27** lowers its energy and allows for a more facile formation of the borate species, which then participates in transmetalation. ^{11}B NMR of **3.23** and **3.24** point to the formation of a borate species generated from **3.23** when 3.0 equiv KOH is added (1:1 signals at 35.5 and -0.6 ppm), whereas **3.24** produces one signal at 34.6 ppm, indicating that the corresponding borate is not formed.

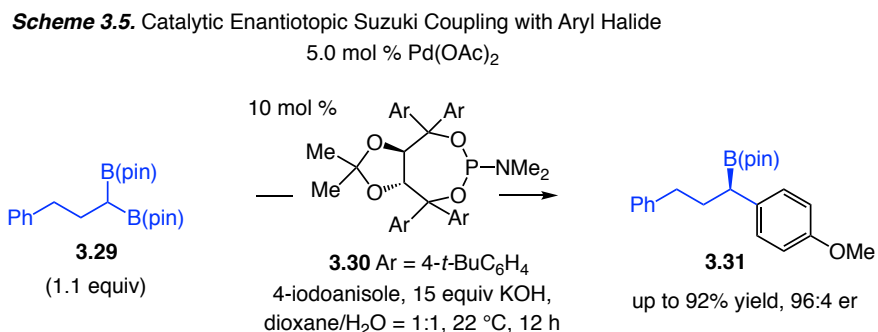
Scheme 3.4 Catalytic Suzuki Cross-Coupling with A Geminal Diboron Reagent and α -Silyl-substituted Alkyl–B(pin)



Morken and co-workers demonstrated the first enantioselective Pd-catalyzed Suzuki cross-coupling of symmetric geminal diboron compounds (Scheme 3.5).⁸ The reaction, catalyzed by 5.0 mol % Pd(OAc)₂ and 10 mol % of phosphoramidite ligand **3.30** with 15 equiv KOH, allows for the enantioselective cross-coupling of diboron reagents with a range of aryl halides in up to 92% yield and 96:4 er. The authors proposed that the transmetalation occurs with inversion in a stereospecific fashion based on the results of a ^{10}B -labeled experiment. The Morken group also published a desymmetrization reaction of symmetric geminal diboron compounds with alkenyl halides leading to the formation

(8) C. Sun, B. Potter, J. P. Morken, *J. Am. Chem. Soc.* **2014**, *136*, 6534–6537.

of enantiomeric enriched allylic boronate in the same year.⁹

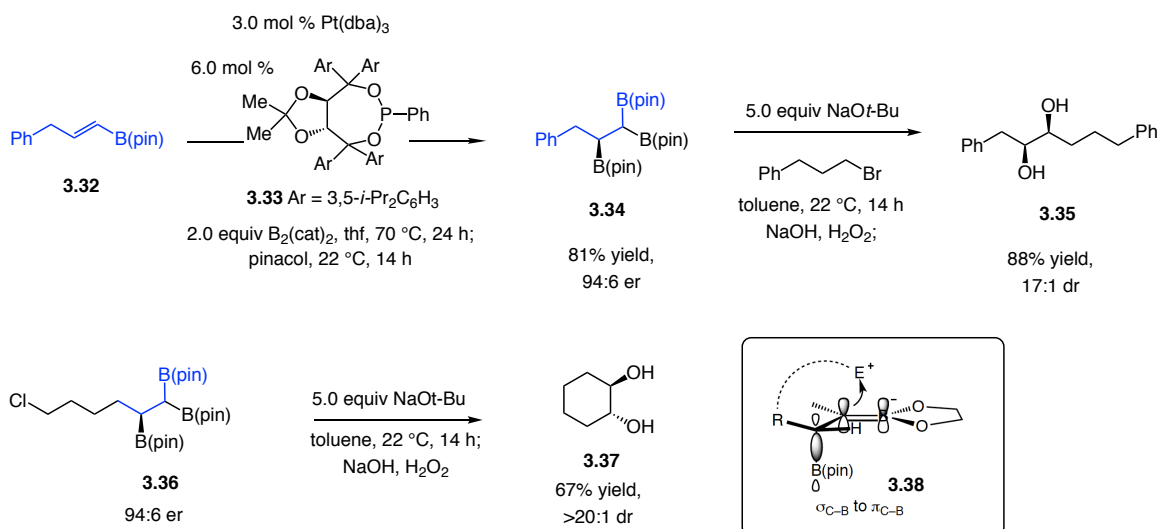


In 2014, the Morken group also demonstrated that a deborylation/alkylation could be performed with a diboron reagent in the presence of NaO*t*-Bu and an alkyl halide.¹⁰ In the same year, the Morken laboratory also published a protocol involving an enantioselective diboration of alkenyl boronic acid pinacol esters followed by selective deborylative alkylation of the tris(boronate) products to generate the vicinal diboron product (Scheme 3.6).¹¹ In the presence of 3.0 mol % Pt(dba)₃ and 6.0 mol % of chiral phosphite ligand **3.33**, a range of *E*-alkyl-substituted alkenyl-B(pin) substrates, for example **3.32**, undergo diboration with B₂(cat)₂ in 67–82% yield and up to 95:5 er. Deborylative/alkylation occurs in the presence of 5.0 equiv NaO*t*-Bu in toluene at room temperature with both primary and secondary alkyl halides. After oxidation, syn-diol **3.35** was obtained in high diastereoselectivity and enantioselectivity. Of note, intramolecular alkylation, however, provides access to anti-diol **3.37** in good yield and high diastereoselectivity, suggesting the formation of the C–C bond and the vicinal C–B bond occurs in an anti-fashion through **3.38**.

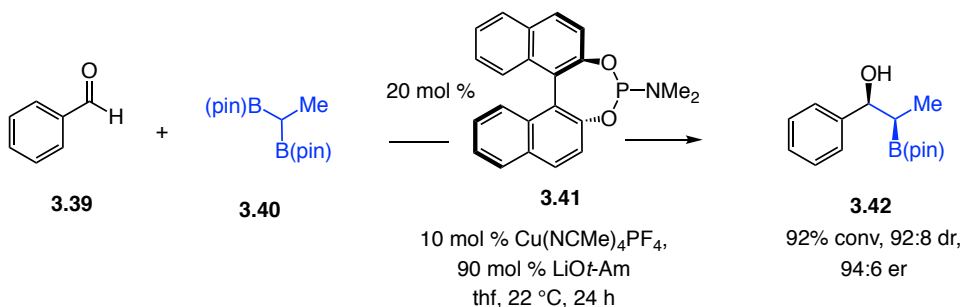
(9) B. Potter, A. A. Szymaniak, E. K. Edelstein, J. P. Morken, *J. Am. Chem. Soc.* **2014**, *136*, 17918–17921.

(10) Hong, K.; Liu, X.; Morken, J. P. *J. Am. Chem. Soc.* **2014**, *136*, 10581–10584.

(11) Coombs, J.R.; Zhang, L.; Morken, J. P. *J. Am. Chem. Soc.* **2014**, *136*, 16140–16143.

Scheme 3.6. Enantioselective Synthesis of Tris(boronate) and Diastereoselective Alkylation

The Meek group reported a Cu-catalyzed enantio- and diastereoselective synthesis of 1,2-hydroxyboronates through methyleneboryl addition to aldehydes (Scheme 3.7).¹² Reactions are promoted by a readily available chiral monodentate phosphoramidite-Cu complex derived from **3.41** in the presence of an alkyl 1,1-diboron reagent **3.40**. Products contain two contiguous stereogenic centers and are obtained in up to 91% yield, >98:2 dr., and 98:2 er in high syn selectivity. In 2015, they also reported a method involving Ag-catalyzed diastereoselective synthesis of anti-1,2-hydroxyboronates.¹³

Scheme 3.7. Catalytic Diastereo- and Enantioselective Formation of 1,2-Hydroxyboronates

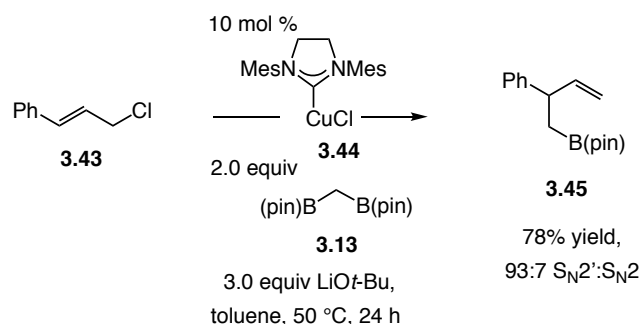
More recently, the Cho and Fu group disclosed the NHC-Cu-catalyzed allylic

(12) Joannou, M. V.; Moyer, B. S.; Meek, S. J. *J. Am. Chem. Soc.* **2015**, *137*, 6176–6179.

(13) Joannou, M. V.; Moyer, B. S.; Goldfogel, M. J.; Meek, S. J. *Angew. Chem. Int. Ed.* **2015**, *54*, 14141–14145; *Angew. Chem.* **2015**, *127*, 14347–14351.

substitution of geminal diboron reagents separately (Scheme 3.8).¹⁴ Reaction of allylic chlorides and diboron reagents, catalyzed by NHC–Cu complex **3.44**, occur at 50 °C in toluene to afford racemic primary alkyl–B(pin) products in 55–86% yield. After disclosure of our EAS method, the Niu group reported a Ir-catalyzed EAS protocol to form S_N2' products from allylic carbonates with diboron reagent **3.13**.¹⁵ However, alkyl substrates suffered from poor reaction efficiency.

Scheme 3.8. Catalytic Allylic Substitution with a Methyleneboron Reagent



3.3. Catalytic Enantioselective Allylic Substitutions with Methyleneboron

3.3.1. Screening of Reaction Conditions for Methyleneboron Additions to 1,2-Disubstituted Allylic Phosphates

We sought to identify a Cu-catalyzed allylic substitution protocol with methylene diboron **3.13** and allylic phosphates to achieve enantioselective formation of **3.45**.¹⁶ This product contains an alkyl–B(pin) which can be further elaborated to versatile functional groups (Scheme 3.9). Upon ligand screening, we found that NHC ligands derived from **3.48–3.50** and bisphosphine ligands **3.51** and **3.52** all favored the formation of the undesired S_N2 product **3.47**. Only the

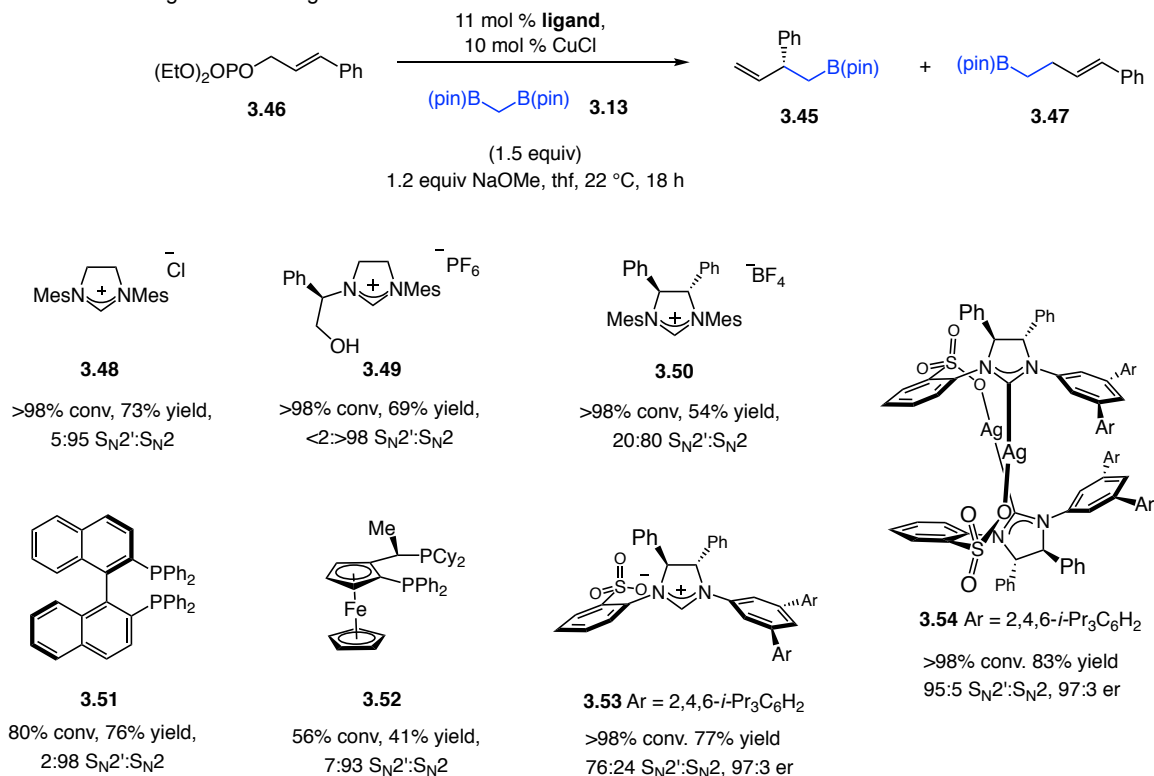
(14) (a) Kim, J.; Park, S.; Park, J.; Cho, S. H. *Angew. Chem., Int. Ed.* **2016**, *55*, 1498–1501. (b) Zhang, Z.-Q.; Zhang, B.; Lu, X.; Liu, J.-H.; Lu, X.-Y.; Xiao, B.; Fu, Y. *Org. Lett.* **2016**, *18*, 952–955.

(15) Zhan, M.; Li, R.-Z.; Mou, Z.-D.; Cao, C.-G.; J Liu, J.; Chen, Y.; Niu, D. *ACS Catal.* **2016**, *6*, 3381–3386.

(16) Shi, Y.; Hoveyda, A. H. *Angew. Chem. Int. Ed.* **2016**, *55*, 3455–3458.

sulfonate-bearing NHC ligand derived from imidazolium salt **3.53** furnished the desired S_N2' product **3.45**. To achieve higher regioselectivity, NHC–Ag complex **3.54** was employed in the reaction, **3.44** was generated in 83% yield, 95:5 S_N2' : S_N2 , 97:3 er.

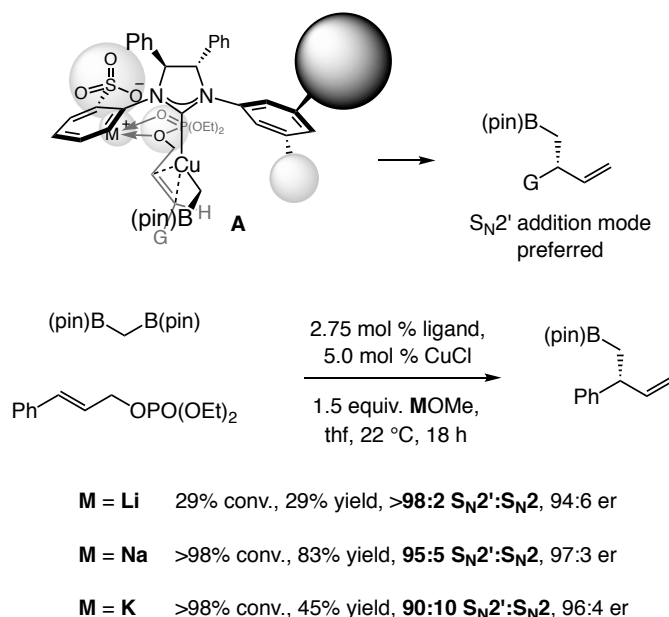
Scheme 3.9. Ligand Screening



A distinct feature of the sulfonate-containing chiral NHC ligands (see **3.54** and **3.51**) is that the Cu complexes promote highly S_N2' -selective reactions (see Scheme 3.9 and Scheme 3.10). This is congruent with the most recent mechanistic and computational studies, revealing that the active species is likely a monodentate system wherein the sulfonate group, without the geometric constraints of chelation with the Cu center, is oriented anti to the proximal phenyl substituent on the NHC backbone (A, Scheme 3.10). Formation of an alkali metal bridge between the anionic tether of the chiral catalyst and the Lewis basic phosphate unit can engender a well-defined transition structure with the

Cu–C bond disposed for S_N2' addition. There is indeed measurable dependence of branch selectivity on the identity of the base used (Scheme 3.10). With the more Lewis acidic lithium salt, there was >98% S_N2' selectivity, albeit at lower yield owing to solubility issues. More of the achiral isomer was generated with the less Lewis acidic and larger potassium methoxide.

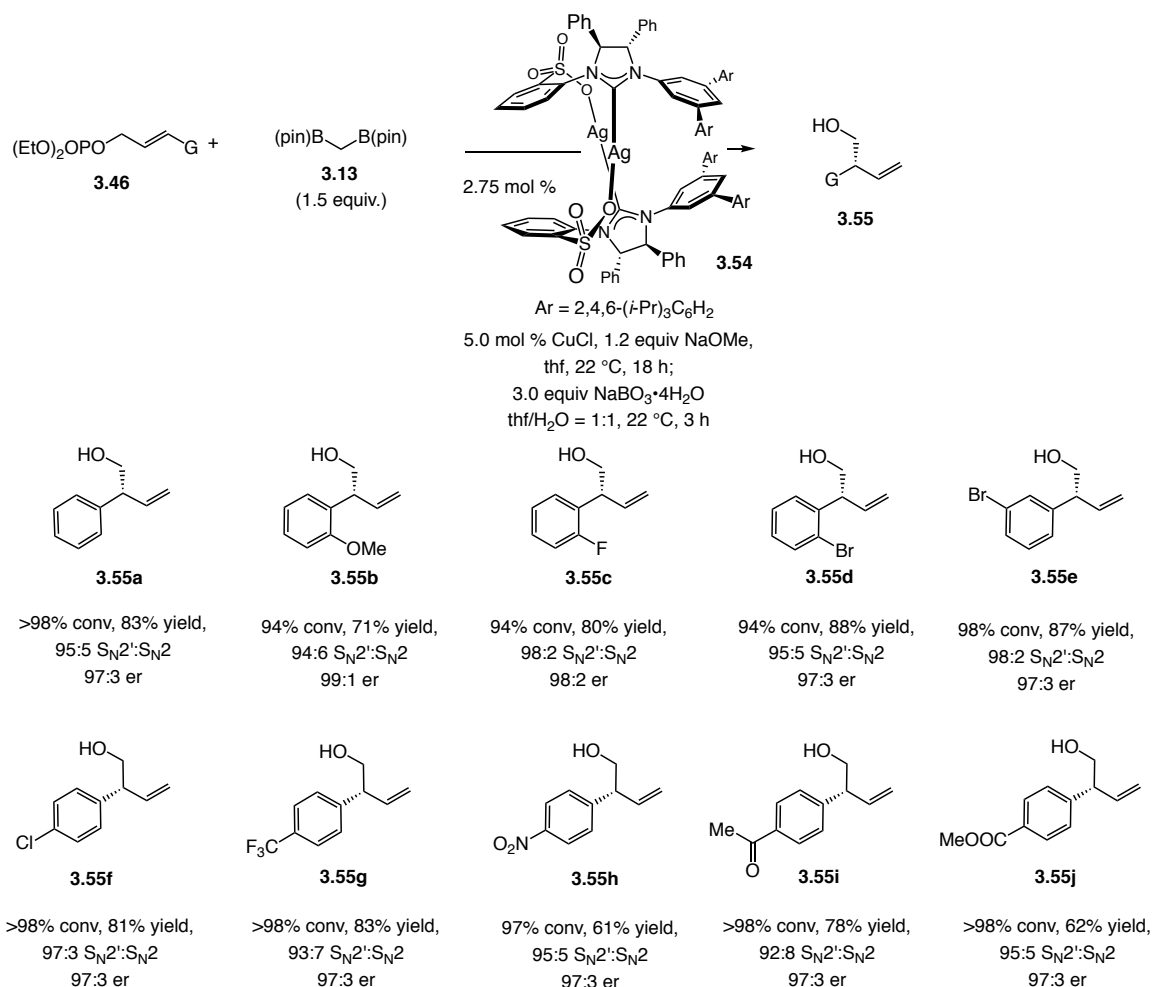
Scheme 3.10. Role of Counter Ion



The method has a considerable scope (Scheme 3.11). Various aryl-substituted substrates, including those with an electron-donating or -withdrawing substituent, regardless of position (**3.55a–3.55j**), were converted into the corresponding primary alcohols in 61–95% yield (after oxidation), 88:12 to >98:2 S_N2'/S_N2 selectivity, and 85:15–99:1 er. There were no complications due to other competitive electrophilic sites, such as the aryl ketone unit in **3.55i**. Such a functional group is not compatible in NHC–Cu-catalyzed transformations with propargyl–B(pin).¹⁷ In that case, competitive propargyl addition to the reactive carbonyl group was observed.

(17) Shi, Y.; Jung, B.; Torker, S.; Hoveyda, A. H. *J. Am. Chem. Soc.* **2015**, *137*, 8948–8964.

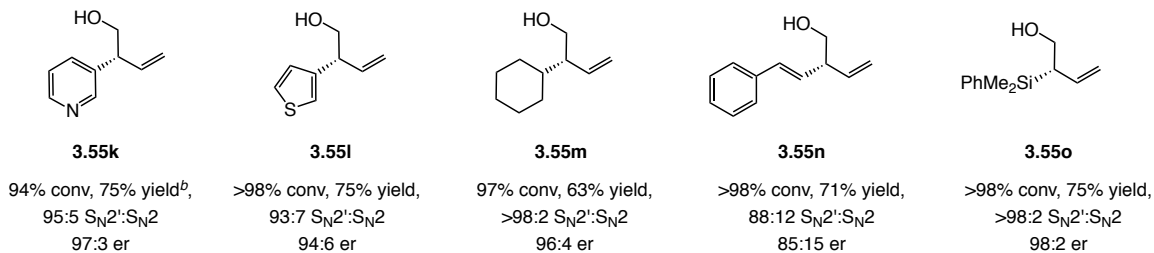
Scheme 3.11. Scope of Catalytic EAS with a Methyleneboron Reagent



As shown in Scheme 3.12, The Cu catalyst remained operative in the presence of Lewis basic heterocyclic moieties that can potentially deactivate the catalyst: pyridyl- and thienyl-substituted **3.55k** and **3.55l** were obtained with similar efficiency and selectivity. Alkyl-substituted allylic phosphates (e.g., **3.55m**) were suitable. The reaction with a 1,3-dienyl substrate was somewhat less S_N2'- and enantioselective but none of the side products from the formation of the S_N2'' addition by-product could be detected (**3.55n**). However, employing NHC–Ag complex **3.56** (as in Scheme 3.13), **3.55n** can be furnished in higher enantioselectivity (95:5 er). Allylsilane **3.55o** can be also generated in 75% yield, >98:2 S_N2'/S_N2 selectivity and 98:2 er, which may be utilized in

stereoselective synthesis.

Scheme 3.12. Catalytic EAS Reactions with Heteroaryl-, Alkyl-, Alkenyl- and Silyl-Substituted Allylic Phosphates^a



^a Yields of isolated and purified S_N2' product. ^b Yield of isolated mixture of S_N2' and S_N2 products.

3.3.2. Application to the Synthesis of Rhopaloic Acid A

We then probed the feasibility of the application of this process to the synthesis of rhopaloic acid A (Scheme 3.13).¹⁸ Organoboron compound **3.57** was purified by column chromatography on silica gel and isolated in 89% yield, >98:2 S_N2'/S_N2 selectivity, and 96:4 er; in this case, the Cu complex derived from **3.56** gave higher enantioselectivity (84:16 er with **3.54**). Improvement of enantioselectivity in EAS reactions with disubstituted allylic phosphates with large boron-based nucleophile was also observed by switching the substitution pattern of the N-aryl group on the sulfonate-containing NHC ligands: NHC–Cu complex with 2,5-substitution delivered the EAS products with a tertiary stereogenic center in higher enantioselectivity than the ones with 3,5-substitution pattern. Moreover, the utility of this sulfonate-based NHC ligand was also highlighted in the synthesis of plakinic acid A.¹⁹

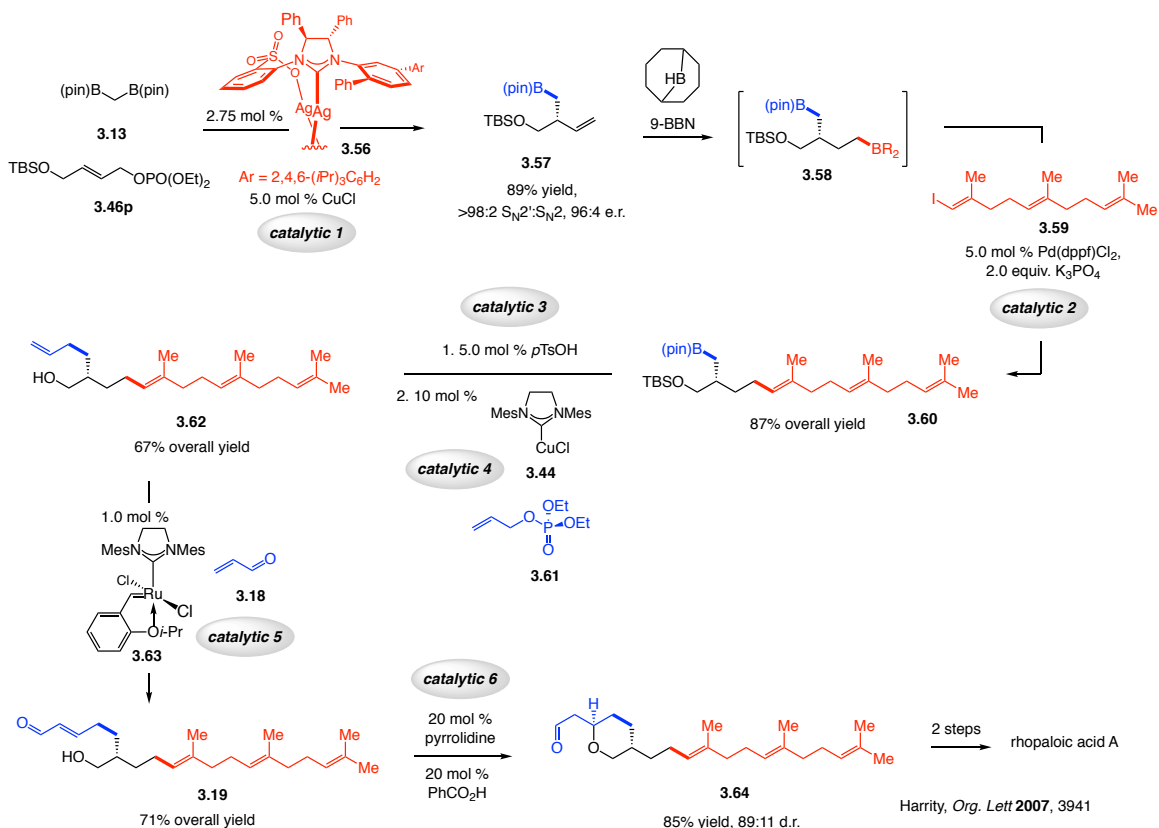
Hydroboration afforded diboron product **3.58**, which was used crude and

(18) a) Yanai, M.; Ohta, S.; Ohta, E.; Ikegami, S. *Tetrahedron* **1998**, *54*, 15607–15612. b) Ohta, S.; Uno, M.; Yoshimura, M.; Hiraga, Y.; Ikegami, S. *Tetrahedron Lett.* **1996**, *37*, 2265–2266. For previous studies regarding the synthesis of rhopaloic acids, see: c) Snider, B. B.; He, F. *Tetrahedron Lett.* **1997**, *38*, 5453–5454. d) Takagi, R.; Sasaoka, A.; Kojima, S.; Ohkata, K. *Chem. Commun.* **1997**, 1887–1888. e) Takagi, R.; Sasaoka, A.; Nishitani, H.; Kojima, S.; Hiraga, Y.; Ohkata, K. *J. Chem. Soc. Perkin Trans. 1* **1998**, 925–934. f) Nishitani, H.; Sasaoka, A.; Tokumasu, M.; Ohkata, K. *Heterocycles* **1999**, *50*, 35–38. g) Kadota, K.; Ogasawara, K. *Heterocycles* **2003**, *59*, 485–490. h) Brioche, J. C. R.; Goodenough, K. M.; Whatrup, D. J.; Harrity, J. P. A. *Org. Lett.* **2007**, *9*, 3941–3943. i) Brioche, J. C. R.; Goodenough, K. M.; Whatrup, D. J.; Harrity, J. P. A. *J. Org. Chem.* **2008**, *73*, 1946–1953.

(19) ref.17. also see discussion in Chapter 2.4.1.

subjected to a Pd-catalyzed cross-coupling²⁰ with *E*-alkenyl iodide **3.59**²¹, affording **3.60** in >98% chemoselectivity and 87% yield. Removal of the silyl ether and NHC–Cu-catalyzed C–C bond formation with the alkyl–B(pin) moiety of **3.60** and commercially available allyl phosphate **3.61** delivered tetraene **3.62** in 67% overall yield. As noted earlier, this latter process strongly benefited from the proximal hydroxyl group: there was <2% C–C bond formation with silyl ether **3.60**. Cross-metathesis with Ru complex **3.63** and acrolein **3.18** led to enal **3.19** (71% overall yield). Intramolecular conjugate addition delivered pyran **3.64**, which has previously been converted into rhopaloic acid A in 85% yield and 89:11 diastereomeric ratio.

Scheme 3.13. Application to the Synthesis of Rhopaloic Acid A



(20) a) Miyaura, N.; Suzuki, A. *Chem. Rev.* **1995**, *95*, 2457–2483. b) Chemler, S. R.; Trauner, D.; Danishefsky, S. J. *Angew. Chem. Int. Ed.* **2001**, *40*, 4544–4568; *Angew. Chem.* **2001**, *113*, 4676–4701.

(21) a) Sulake, R. S.; Lin, H.-H.; Hsu, C.-Y.; Weng, C.-F.; Chen, C. *J. Org. Chem.* **2015**, *80*, 6044–6051. b) Wipf, P.; Lim, S. *Angew. Chem. Int. Ed. Engl.* **1993**, *32*, 1068–1071; *Angew. Chem.* **1993**, *105*, 1095–1097. See the Supporting Information for details.

3.3.3 Screening of Reaction Conditions for Methyleneboryl Additions to Trisubstituted Allylic Phosphates and DFT Calculations

As shown above, we found out **3.54** is the optimal ligand for constructing a tertiary stereogenic center with 1,2-disubstituted alkenes. However, when we tried to elaborate this protocol to generate a quaternary stereogenic center from an *E*-trisubstituted olefin **3.65**, it was not surprising to find out that **3.54**, which afforded good selectivity in EAS reactions with a propargyl-B(pin),¹⁷ delivered low yield and low selectivity (entry 1, 48:52 S_N2':S_N2 selectivity), albeit in a moderate er (20:80 er). When switching to NHC-Ag complexes with ortho-substitution, increasing the size of ortho-substituted ligands led to lower enantioselectivity and more drastically lower S_N2' selectivity (Table 3.1, **3.68–3.70**, entry 2–4). When NHC ligands with a 2,5-disubstituted N-aryl group, **3.71** and **3.72**, were applied in the system, improved S_N2' selectivities were observed (entry 5, 6) albeit with low enantioselectivities. Increasing the steric bulk of the ligand or lowering the temperature did not yield higher enantioselectivity due to the more sterically-encumbered nucleophile and lower reactivity of methylenediboron (<2% detection of the desired product if the EAS reaction was carried out at 4 °C). It was also worth mentioning that free CuCl promoted generation of the S_N2 byproduct. Thus, in this case the use of NHC-Cu catalyst with the proper binding pocket was crucial to get high S_N2' selectivity and enantioselectivity at the same time.²²

We went on to explore the impact of the stereochemistry of the electrophile with *Z*-**3.66**. A higher enantioselectivity was observed with ligand **3.72** (90:10 er, Table 3.1, entry 9). By altering the N-aryl group to have a more sterically-demanding ortho

(22) see discussions in Chapter 1.

substituent (**3.72** vs. **3.73**), EAS product **3.67** was generated more efficiently with a high enantiomeric ratio (80% yield, 92:8 er, entry 10).

Table 3.1. EAS Reactions with Methylene Di-B(pin) to Generate Quaternary Stereogenic Centers

entry	substrate	ligand	conv (%) ^b ; yield (%) ^c	S _N 2':S _N 2 ^b	er ^d
1	(<i>E</i>)- 3.65	3.54	84; 32	48:52	20:80
2	(<i>E</i>)- 3.65	3.68	72; 56	93:7	84:16
3	(<i>E</i>)- 3.65	3.69	79; 69	93:7	81:19
4	(<i>E</i>)- 3.65	3.70	65; 25	39:61	68:32
5	(<i>E</i>)- 3.65	3.71	72; 60	98:2	62:38
6	(<i>E</i>)- 3.65	3.72	73; 52	98:2	64:36
7	(<i>Z</i>)- 3.66	3.54	72; 12	19:81	54:46
8	(<i>Z</i>)- 3.66	3.71	70; 36	57:43	76:24
9	(<i>Z</i>)- 3.66	3.72	86; 76	93:7	90:10
10	(<i>Z</i>)- 3.66	3.73	95; 80	98:2	92:8

3.68 Ar = Mes
3.69 Ar = 2,6-Et₂C₆H₃
3.70 Ar = 2,4,6-*i*-Pr₃C₆H₂

3.54 Ar = 3,5-(2,4,6-*i*-Pr₃C₆H₂)₂C₆H₃
3.71 Ar = 2-Me,5-*t*BuC₆H₃
3.72 Ar = 2-Ph,5-*t*BuC₆H₃
3.73 Ar = 2-(3,5-Me₂C₆H₃),5-*t*BuC₆H₃

^a Reactions performed under N₂ atm. ^b Conversion (allylic phosphate consumption) and group (propargyl/allenyl addition) selectivities ($\pm 2\%$) were determined by analysis of 400 MHz ¹H NMR spectra of product mixtures prior to purification. Site selectivities were determined by analysis of 400 MHz ¹H NMR spectra of purified material. ^c Yield ($\pm 5\%$) of S_N2' addition products after silica gel chromatography. ^d Enantioselectivity ($\pm 1\%$) determined by HPLC analysis. See the Supporting Information for experimental and analytical details.

As shown in Figure 3.1, the stereochemical models obtained by DFT calculations provided a rationale for the higher enantiomeric ratio utilizing *Z*-trisubstituted substrates (see **3.76**, **3.77**) than its *E* counterpart (**3.74**, **3.75**) in EAS reactions catalyzed by NHC-Cu species derived from ligand **3.72**. In all the transition states, the large B(pin) was oriented away from the large phenyl substituent on the allylic phosphate to avoid a potentially severe steric interaction. With *E*-**3.65**, the major mode of addition **3.74** suffered from a steric interaction between the ortho substituent and the methylene-B(pin) group in the right front quadrant, while the methyl group on the substrate would have steric interaction with the meta-substituent of the N-aryl ring causing it to rotate to the

back in order to alleviate the steric strain in the front. Thus, this mode of addition was also disfavored, causing the erosion of enantioselectivity. In the minor pathway **3.75** for addition to *E*-**3.65**, the B(pin) group was oriented to the left to avoid a steric interaction with the phenyl group, thus inducing a steric strain with the sulfonate N-aryl ring. However, in this case, the steric strain could not be alleviated by rotating to the back due to hindrance from the phosphate group. The energy difference between these two modes of addition was not large enough to induce high er (1.9 kcal/mol). However, in the case with *Z*-**3.66**, there was a lack of disfavoring interactions between the catalyst and the substrate attributable to the different orientations of the B(pin) moiety and the phosphate group in the major mode of addition **3.76**. However, in the minor pathway **3.75**, steric strain between the B(pin) and ortho substituent, and also between the meta substituent and the methyl group on the allylic phosphate, disfavored this mode of addition. When increasing the size of the ortho substituent, this mode of addition suffered increased severe interaction between the ortho substituent and the B(pin) moiety, thus increasing the enantioselectivity of the product (compare 90:10 er with **3.72**, 92:8 er with **3.73**). Moreover, the large phenyl group on the substrate experienced steric repulsion with the sulfonate N-aryl ring due to the *Z*-substitution pattern of the substrate, further destabilizing this transition state. The large energy gap between **3.76** and **3.77** contributes to the higher er obtained in EAS reaction with *Z*-**3.66**.

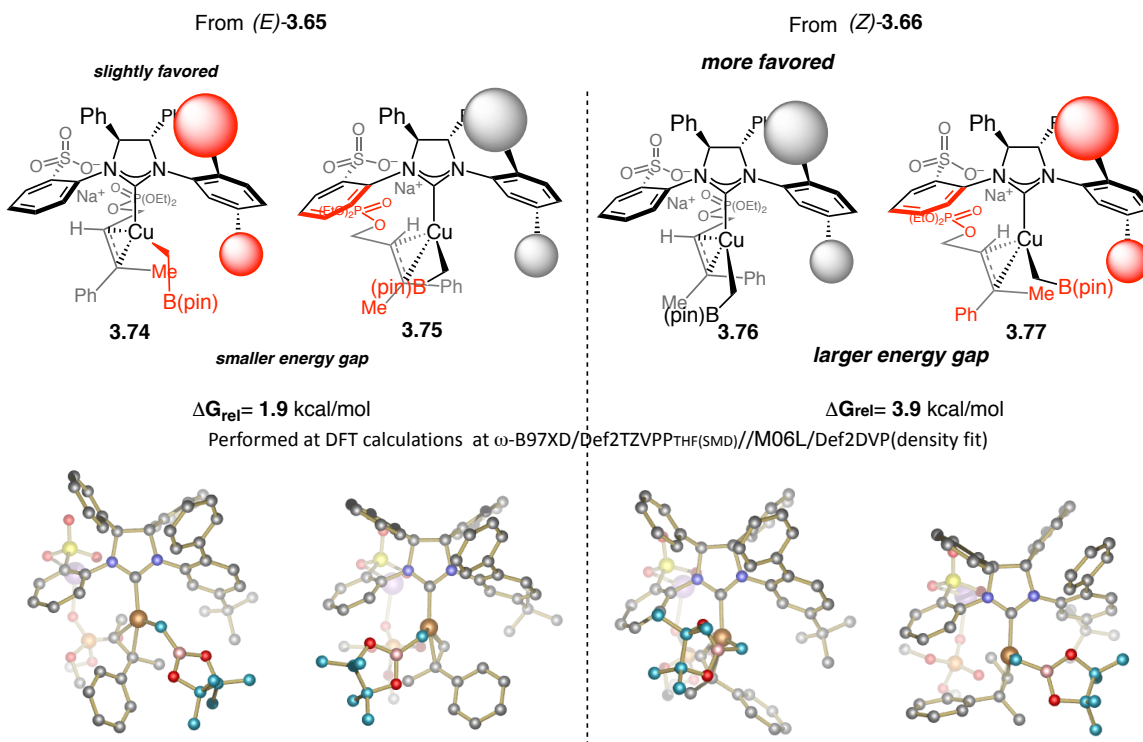
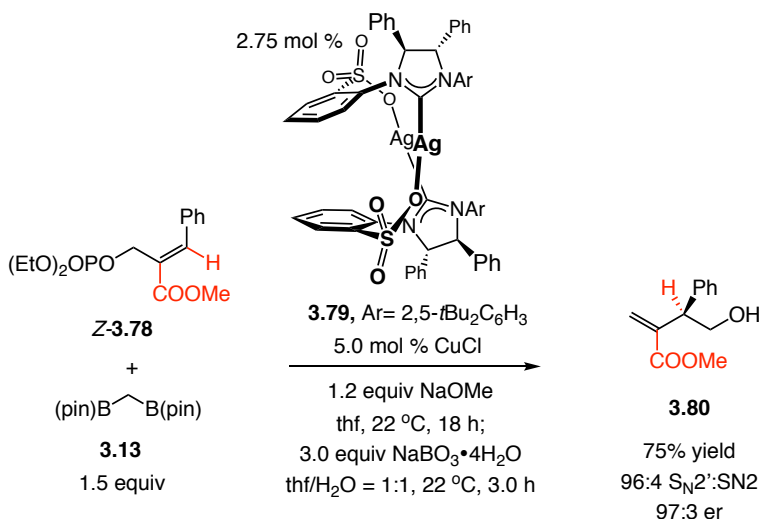


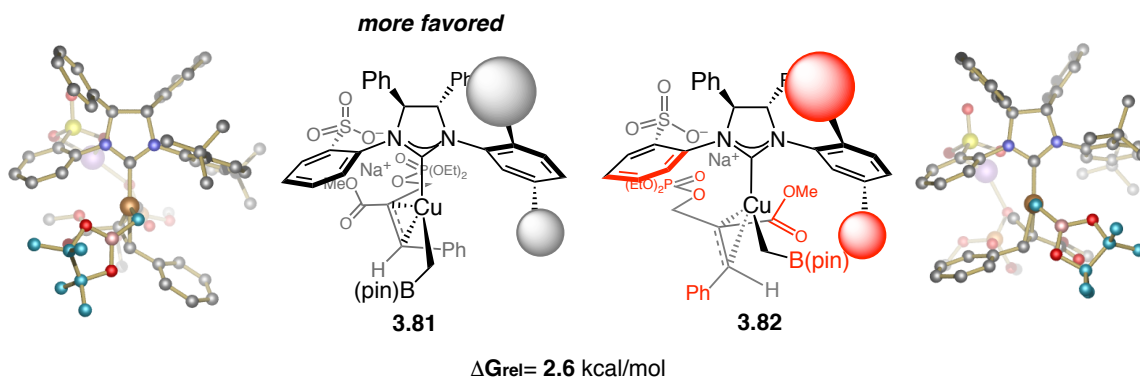
Figure 3.1. Stereochemical Models Account for Higher Enantioselectivity with *Z*- in Comparison to *E*-Allylic Phosphates

Another type of NHC–Cu complex with 2,5-substitution yielded high S_N2' selectivity and *er* when we explored EAS reactions to form a tertiary stereogenic center employing β -ester-substituted *Z*-allylic phosphates with methylenediboron **3.13** as shown in Scheme 3.14. Sulfonate-bearing NHC–Cu catalyst derived from **3.79** delivered the desired product **3.80** in 75% yield, 96% branched selectivity and a 97:3 enantiomeric ratio.

Scheme 3.14. EAS Reactions to Generate a Tertiary Stereogenic Center Employing *Z*-Trisubstituted Allylic Phosphates



The stereochemical model obtained with DFT calculations (Figure 3.2), illustrated that the minor pathway (**3.82**) suffered from the steric repulsion between the *N*-aryl ring and the phenyl substituent on the substrate. Furthermore, this mode of addition was also destabilized by the steric strain between the B(pin) group and ortho substituent on the *N*-aryl ring. Another destabilizing interaction comes from the β -ester group and meta-substituent. Thus high enantiomeric ratio was attributed to the large energy gap between the two modes of addition.

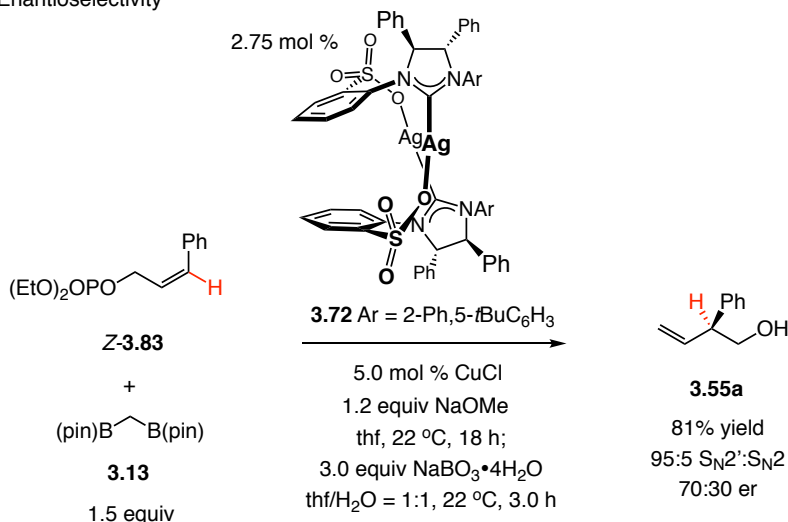


Performed at DFT calculations at ω -B97XD/Def2TZVP_{THF}(SMD)//bp86-631G*/Def2DVP

Figure 3.2. Stereochemical Models for EAS Reactions Employing *Z*-Allylic Phosphates with β -Ester Group

The trisubstituted substrates were required to achieve a high enantioselectivity in EAS reactions promoted by this type of sulfonate-based NHC with 2,5-substitution. As shown by the stereochemical models in Figure 3.1 and 3.2, the methyl group of **3.74** and the β -ester group on **3.76** played an important role in the differentiation of two modes of addition. Consequently, only 70:30 er was obtained when disubstituted allylic phosphate **Z-3.83** was examined in the EAS reactions catalyzed by NHC–Cu complex derived from **3.72** (Scheme 3.15).

Scheme 3.15. The Necessity of Trisubstituted Z-Allylic Phosphates for High Enantioselectivity



3.4. Conclusions

A catalytic EAS method for the site- and enantioselective addition of commercially available methylenediboron to disubstituted allylic phosphates was developed. Transformations were facilitated by a sulfonate-containing NHC–Cu complex and products are obtained in 63–95% yield, 88:12 to >98:2 S_N2'/S_N2 selectivity, and 85:15–99:1 enantiomeric ratio. The utility of the approach is highlighted by the application to the formal synthesis of the cytotoxic natural product rhopaloic acid A. Catalytic EAS methods of methylenediboron addition to Z-trisubstituted allylic

phosphates were also disclosed. DFT calculations provided insight to the stereochemical models and explain the rationales behind employing *Z*-trisubstituted allylic phosphates as the starting materials.

3.5. Experimentals

General

Infrared (IR) spectra were recorded on a Bruker FT-IR Alpha (ATR mode) spectrophotometer, λ_{max} in cm^{-1} . Bands are characterized as broad (br), strong (s), medium (m), and weak (w). ^1H NMR spectra were recorded on a Varian Unity INOVA 400 (400 MHz) or Varian Unity INOVA 600 (600 MHz) spectrometer. Chemical shifts are reported in ppm from tetramethylsilane with the solvent resonance as the internal standard (CDCl_3 : δ 7.26 ppm). Data are reported as follows: chemical shift, integration, multiplicity (s = singlet, d = doublet, t = triplet, q = quartet, br = broad, m = multiplet), and coupling constant (Hz). ^{13}C NMR spectra were recorded on a Varian Unity INOVA 400 (100 MHz) spectrometer with complete proton decoupling. Chemical shifts are reported in ppm from tetramethylsilane with the solvent resonance as the internal standard (CDCl_3 : δ 77.16 ppm). High-resolution mass spectrometry was performed on a JEOL AccuTOF DART (positive mode) at the Mass Spectrometry Facility, Boston College. Enantiomer ratios were determined by GC analysis (Alltech Associated Chiraldex B-DM (30 m x 0.25 mm), Chiraldex G-TA (30 m x 0.25 mm), and Betadex 120 column (30 m x 0.25 mm)), or HPLC analysis (Chiral Technologies Chiralpak AZ-H (4.6 x 250 mm) comparison with authentic racemic materials. Specific rotations were measured on an ATAGO[®] AP-300 Automatic Polarimeter or a Rudolph Research Analytical Autopol IV Polarimeter. Melting points were measured on a Thomas Hoover capillary melting point apparatus and are uncorrected.

Unless otherwise noted, all reactions were carried out with distilled and degassed solvents under an atmosphere of dry N_2 in oven- (135 °C) or flame-dried glassware with standard dry box or vacuum-line techniques. Solvents were purified under a positive pressure of dry argon by a modified Innovative Technologies purification system: toluene, benzene and hexanes were purified through a copper oxide and alumina column; CH_2Cl_2 and Et_2O were purged with Ar and purified by passage through two alumina columns. Tetrahydrofuran (Aldrich Chemical Co.) was purified by distillation from sodium benzophenone ketyl immediately prior to use unless otherwise specified. All work-up and purification procedures were carried out with reagent grade solvents (purchased from Fisher Scientific, Inc.) in air.

Reagents

Allyl phosphate was purchased from Aldrich and used as received.

Benzoic acid (BzOH) was purchased from Aldrich and used as received.

[1,1'-Bis(diphenylphosphino)ferrocene]palladium(II) dichloride (PdCl₂(dppf)) was purchased from TCI chemicals and used as received.

Bis[(pinacolato)boryl]methane (CH₂B₂(pin)₂) was purchased from TCI chemicals and used as received.

1,3-Bis(2,4,6-trimethylphenyl)imidazolinium chloride (SIMes) was purchased from Aldrich and used as received.

9-Borabicyclo[3.3.1]nonane dimer (9-BBN) was purchased from Aldrich and used as received.

(E)-4-[(*tert*-Butyldimethylsilyloxy)but-2-en-1-yl] diethyl phosphate (3.46p)²³

Copper (I) chloride (CuCl) was purchased from Strem and used as received.

(E)-Diethyl 3-(2-bromophenyl)prop-2-enyl phosphate (3.46d)²⁴

(E)-Diethyl 3-(3-bromophenyl)prop-2-enyl phosphate (3.46e)²⁵

(E)-Diethyl 3-(4-chlorophenyl)prop-2-enyl phosphate (3.46f)²⁵

(E)-Diethyl 3-cyclohexylprop-2-enyl phosphate (3.46m)²⁵

(E)-Diethyl 3-(2-fluorophenyl)prop-2-enyl phosphate (3.46c)²⁴

(E)-Diethyl 3-(2-methoxyphenyl)prop-2-enyl phosphate (3.46b)²⁵

(E)-Diethyl 3-(4-nitrophenyl)prop-2-enyl phosphate (3.46h)²⁶

(E)-Diethyl 3-phenylprop-2-enyl phosphate (3.46a)²⁷

(E)-Diethyl (3-(pyridin-3-yl)allyl) phosphate (3.46k)²⁷

(E)-Diethyl (3-(thiophen-3-yl)allyl) phosphate (3.46l)²⁷

(E)-Diethyl 3-(4-trifluoromethylphenyl)prop-2-enyl phosphate (3.46g)²⁴

(E)-3-[Dimethyl(phenyl)silyl]prop-2-enyl diethyl phosphate (3.46o)²⁷

Imidazolinium salts 3.49, 3.50 were prepared according to previously reported procedures.²⁸

(23) L. B. Delves, D. J. Vyas, M. Oestreich, *Angew. Chem. Int. Ed.* **2013**, *52*, 4650–4653.

(24) B. Jung, A. H. Hoveyda, *J. Am. Chem. Soc.* **2012**, *134*, 1490–1493.

(25) K. Akiyama, F. Gao, A. H. Hoveyda, *Angew. Chem. Int. Ed.* **2010**, *49*, 419–423.

(26) C. A. Luchaco-Cullis, H. Mizutani, K. E. Murphy, A. H. Hoveyda, *Angew. Chem. Int. Ed. Engl.* **2001**, *40*, 1456–1460.

(27) Y. Shi, B. Jung, S. Torker, A. H. Hoveyda, *J. Am. Chem. Soc.* **2015**, *127*, 6877–6882.

(1*E*,5*E*)-1-Iodo-2,6,10-trimethylundeca-1,5,9-triene (**3.59**) was prepared according to previously reported procedures.²⁹

Lithium methoxide (LiOMe) was purchased from Aldrich and used as received.

Methanol was purchased from Acros and purified by distillation from Na (Aldrich) prior to use.

Methyl (*E*)-4-(3-((diethoxyphosphoryl)oxy)prop-1-en-1-yl)benzoate (3.46j**)¹⁷**

NHC–Ag complex 3.54 and **3.56** were prepared according to a previously reported procedure.³⁰

Palladium (II) Acetate (Pd(OAc)₂) was purchased from Strem and used as received.

Potassium *t*-butoxide (KO*t*-Bu) was purchased from Strem and used as received.

Potassium methoxide (KOMe) was purchased from Aldrich and used as received.

Pyrrolidine was purchased from Aldrich and used as received.

Ruthenium complex (3.63) was purchased from Aldrich and used as received.

Sodium perborate tetrahydrate (NaBO₃•4H₂O) was purchased from Aldrich and used as received.

Sodium methoxide (NaOMe) was purchased from Strem and used as received.

Silver (I) Acetate (AgOAc) was purchased from Aldrich and used as received.

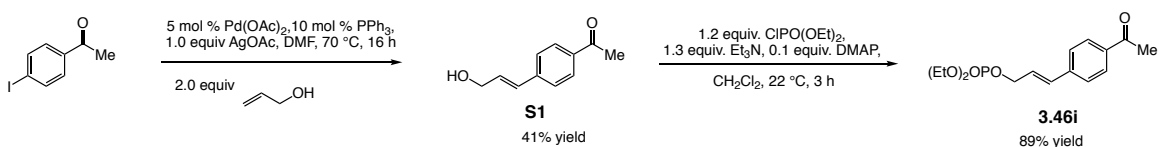
***p*-Toluenesulfonic acid (*p*-TsOH)** was purchased from Aldrich and used as received.

Triethylamine (Et₃N) was purchased from Fisher Scientific, Inc. and distilled over CaH₂ prior to use.

Tripotassium phosphate (K₃PO₄) was purchased from Fisher Scientific, Inc. and distilled over CaH₂ prior to use.

Characterization Data for Allylic Phosphates Not Previously Reported

Scheme S1. Preparation of Allylic Phosphate **3.46i**



(*E*)-3-(4-Acetylphenyl)allyl diethyl phosphate (3.46i): IR (neat): 2985 (w), 2932 (w), 1681 (s), 1603 (m), 1563 (w), 1360 (w), 1266 (s), 1182 (w), 1166 (w), 1101 (w), 1028 (s), 975 (s), 853 (w), 801 (w), 594 (w) cm⁻¹; **¹H NMR (CDCl₃, 600 MHz):** δ 7.90 (2H, d, *J* =

(28) a) J. J. Van Veldhuizen, J. E. Campbell, R. E. Guidici, A. H. Hoveyda, *J. Am. Chem. Soc.* **2005**, *127*, 6877–6882; b) K.-s. Lee, A. H. Hoveyda, *J. Org. Chem.* **2009**, *74*, 4455–4462.

(29) R. S. Sulake, H.-H. Lin, C.-Y. Hsu, C.-F. Weng, C. Chen, *J. Org. Chem.* **2015**, *80*, 6044–6051.

(30) T. L. May, M. K. Brown, A. H. Hoveyda, *Angew. Chem. Int. Ed.* **2008**, *47*, 7358–7362.

8.4 Hz), 7.45 (2H, d, $J = 8.4$ Hz), 6.70 (1H, d, $J = 15.6$ Hz), 6.40 (1H, dt, $J = 15.6, 6.0$ Hz), 4.70 (2H, t, $J = 8.4$ Hz), 4.15–4.10 (4H, m), 2.57 (3H, s), 1.33 (6H, t, $J = 7.2$ Hz; ^{13}C NMR (CDCl_3 , 150 MHz): δ 197.5, 140.7, 136.6, 132.3, 128.9, 126.8, 126.6 (d, $J_{\text{CP}} = 6.9$ Hz), 67.5 (d, $J_{\text{CP}} = 4.7$ Hz), 64.0 (d, $J_{\text{CP}} = 5.7$ Hz), 26.7, 16.2 (d, $J_{\text{CP}} = 6.9$ Hz). HRMS (ESI^+): Calcd for $\text{C}_{15}\text{H}_{22}\text{O}_5\text{P}_1$ $[\text{M}+\text{H}]^+$: 313.1205; Found: 313.1217.

Representative Procedure for NHC–Cu-Catalyzed Enantioselective Methylene-Boryl Addition to Disubstituted Allylic Phosphates

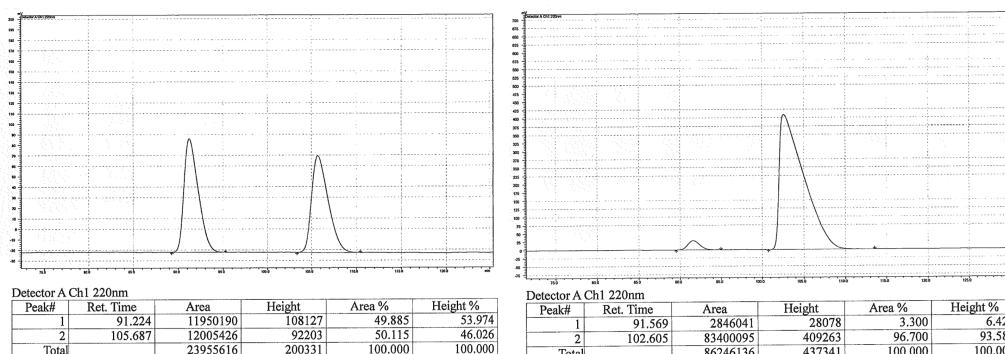
An oven-dried 1-dram vial equipped with a stir bar was charged with NHC–Ag complex **3.54** (4.8 mg, 5.5 μmol), NaOMe (6.5 mg, 150 μmol), and CuCl (0.5 mg, 5.0 μmol) in a nitrogen-filled glove box. The vial was sealed with a cap (phenolic open top cap with a red PTFE/white silicon septum) and electrical tape, and removed from the glove box. Tetrahydrofuran (thf; 0.50 mL) was added and the mixture was allowed to stir for 2 h under N_2 at 22 $^\circ\text{C}$ (the mixture became bright-yellow solution). The mixture of allylic phosphate **3.46a** (28 mg, 0.10 mmol) and bis[(pinacolato)boryl]methane **1** (40 mg, 0.15 mmol) in thf (0.5 mL) was added to the mixture slowly through a syringe. The resulting mixture was allowed to stir at 22 $^\circ\text{C}$ for 18 h. The mixture was passed through a short plug of silica gel (4 cm x 1 cm) and eluted with Et_2O . The organic layer was concentrated *in vacuo*, resulting in a yellow oily residue, which was diluted with thf (0.5 ml) and water (0.5 ml), then $\text{NaBO}_3 \cdot 4\text{H}_2\text{O}$ (78mg, 0.3 mmol) was added and the mixture was allowed to stir at 22 $^\circ\text{C}$ for 3 h. The mixture was washed with Et_2O (1.0 ml) three times and the combined organic layers was passed through a short plug of MgSO_4 , concentrated and purified by silica gel chromatography (6:1 hexanes/ Et_2O , $R_f = 0.18$) to afford 12.3 mg of the desired product **3.55a** as colorless oil (0.083 mmol, 83% yield).

Characterization Data for Alcohols with a Tertiary Carbon Stereogenic Center

(R)-2-Phenylbut-3-en-1-ol (3.55a). IR (neat): 3353 (br, s), 2925 (w), 2873 (w), 1637 (w), 1601 (w), 1493 (w), 1452 (w), 1051 (m), 1027 (m), 916 (m), 755 (m), 698 (s), 679 (m), 593 (w), 537 (m) cm^{-1} ; ^1H NMR (CDCl_3 , 400 MHz): δ 7.35–7.31 (2H, m), 7.26–7.22 (3H, m), 6.00 (1H, ddd, $J = 18.0, 10.4, 8.0$ Hz), 5.22–5.15 (2H, m), 3.82 (1H, d, $J = 6.8$ Hz), 3.81 (1H, d, $J = 6.8$ Hz), 3.52 (1H, q, $J = 7.2$ Hz), 1.54 (1H, s); ^{13}C NMR (CDCl_3 , 100 MHz): δ 140.7, 138.3, 128.9, 128.1, 127.1, 117.3, 66.2, 52.7. HRMS (ESI^+): Calcd for $\text{C}_{10}\text{H}_{11}$ $[\text{M}+\text{H}-\text{H}_2\text{O}]^+$: 131.0854; Found: 131.0861. Specific rotation: $[\alpha]_{\text{D}}^{20.0} -36.0$ (c 0.25, CHCl_3) for an enantiomerically enriched sample of 97:3 e.r. Based on reported optical rotation value ($[\alpha]_{\text{D}}^{26} +19$ (c 0.81, CHCl_3) for 33:67 er), the absolute stereochemistry of the major enantiomer is assigned to be *R*.³¹

(31) K. B. Selim, K. Yamada, K. Tomioka, *Chem. Commun.* **2008**, 5140–5142.

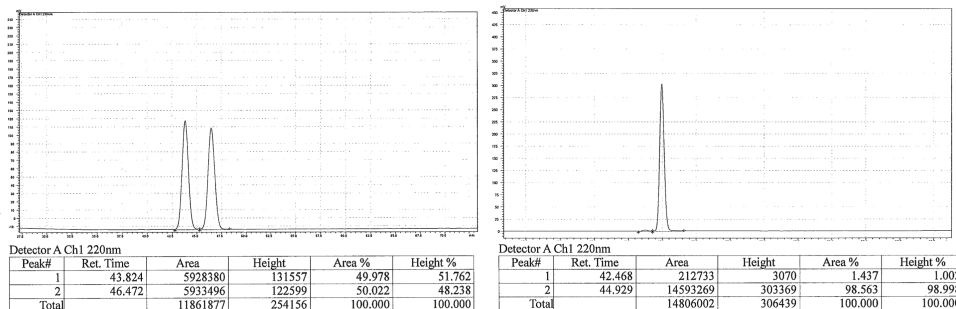
Enantiomeric purity was determined by HPLC analysis in comparison with authentic racemic material; Chiralpak AZ-H column, 99.5:0.5 hexanes/*i*PrOH, 0.5 mL/min, 220 nm.



Retention Time	Area	Area%	Retention Time	Area	Area%
91.224	11050190	49.885	91.569	2846041	3.300
105.687	120005426	50.115	102.605	83400095	96.700

(R)-2-(2-Methoxyphenyl)but-3-en-1-ol (3.55b): IR (neat): 3379 (br, s), 2937 (w), 2836 (w), 1636 (w), 1597 (w), 1585 (w), 1491 (s), 1462 (m), 1438 (m), 1288 (w), 1240 (w), 1187 (w), 1168 (w), 1109 (w), 1051 (s), 1026 (s), 996 (m), 915 (m), 751 (s), 670 (m) cm^{-1} ; $^1\text{H NMR}$ (CDCl_3 , 400 MHz): δ 7.26-7.21 (1H, m), 7.20 (1H, m), 6.94 (1H, t, $J = 7.6$ Hz), 6.89 (1H, d, $J = 8.4$ Hz), 6.12-6.03 (1H, m), 5.22-5.17 (2H, m), 3.87 (1H, q, $J = 7.2$ Hz), 3.86-3.80 (5H, m), 1.61 (1H, s); $^{13}\text{C NMR}$ (CDCl_3 , 100 MHz): δ 157.3, 138.0, 129.0, 128.5, 128.0, 120.9, 117.0, 111.0, 65.3, 55.6, 45.9. HRMS (ESI $^+$): Calcd for $\text{C}_{11}\text{H}_{13}\text{O}_1$ $[\text{M}+\text{H}-\text{H}_2\text{O}]^+$: 161.0966; Found: 161.0968. Specific rotation: $[\alpha]_{\text{D}}^{20.0} -25.2$ (c 0.85, CHCl_3) for an enantiomerically enriched sample of 99:1 e.r.

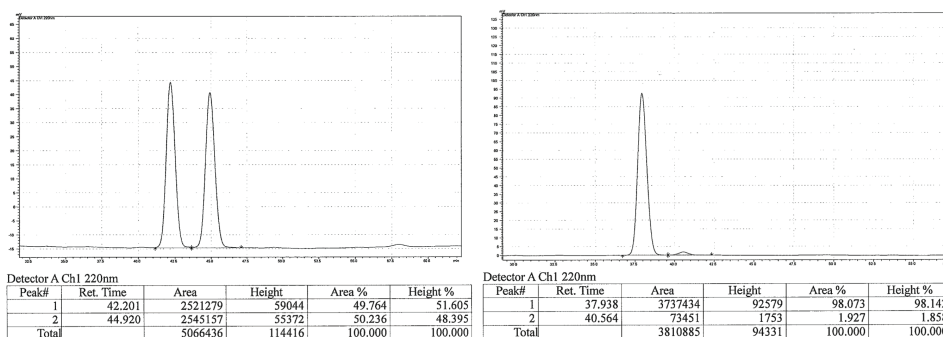
Enantiomeric purity was determined by HPLC analysis in comparison with authentic racemic material; Chiralpak AZ-H column, 99.0:1.0 hexanes/*i*PrOH, 0.5 mL/min, 220 nm.



Retention Time	Area	Area%	Retention Time	Area	Area%
43.824	5928380	49.978	42.468	212733	1.437
46.472	5933496	50.022	44.929	14593269	98.563

(R)-2-(2-Fluorophenyl)but-3-en-1-ol (3.55c): IR (neat): 3358 (br, s), 2938 (w), 1638 (w), 1583 (w), 1490 (s), 1454 (m), 1418 (w), 1228 (s), 1175 (w), 1055 (s), 1036 (s), 993 (m), 919 (s), 824 (w), 806 (w), 665 (w), 602 (w), 479 (w) cm^{-1} ; **^1H NMR (CDCl_3 , 400 MHz):** δ 7.27–7.20 (2H, m), 7.14–7.10 (1H, m), 7.07–7.03 (1H, m), 6.08–6.00 (1H, m), 5.23 (1H, d, $J = 10.8$ Hz), 5.13 (1H, $J = 17.2$ Hz), 3.86 (3H, app.s), 1.58 (1H, s); **^{13}C NMR (CDCl_3 , 100 MHz):** δ 161.0 (d, $J_{CF} = 244.4$ Hz), 137.0, 129.3 (d, $J_{CF} = 4.5$ Hz), 128.5 (d, $J_{CF} = 8.4$ Hz), 127.7 (d, $J_{CF} = 15.2$ Hz), 124.4 (d, $J_{CF} = 3.0$ Hz), 117.8, 115.9 (d, $J_{CF} = 22.0$ Hz), 65.1, 46.2. **HRMS (ESI^+):** Calcd for $\text{C}_{10}\text{H}_{10}\text{F}$ [$\text{M}+\text{H}-\text{H}_2\text{O}$] $^+$: 149.0767; Found: 149.0773. Specific rotation: $[\alpha]_{\text{D}}^{20.0} -34.2$ (c 0.89, CHCl_3) for an enantiomerically enriched sample of 98:2 er.

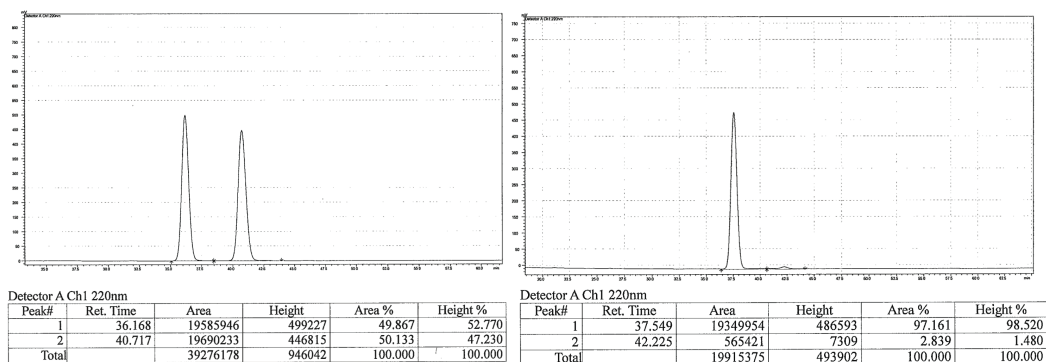
Enantiomeric purity was determined by HPLC analysis in comparison with authentic racemic material; Chiralpak AZ-H column, 99.0:1.0 hexanes/*i*PrOH, 0.5 mL/min, 220 nm



Retention Time	Area	Area%	Retention Time	Area	Area%
42.201	2521279	49.764	37.938	3737434	98.073
44.920	2545157	50.236	40.564	73451	1.927

(R)-2-(2-Bromophenyl)but-3-en-1-ol (3.55d): IR (neat): 3353 (br, s), 3080 (w), 2928 (w), 2874 (w), 1730 (w), 1637 (w), 1469 (m), 1437 (w), 1417 (w), 1373 (w), 1222 (w), 1021 (s), 992 (s), 918 (s), 832 (w), 750 (s), 724 (m), 646 (m), 600 (w) cm^{-1} ; **^1H NMR (CDCl_3 , 400 MHz):** δ 7.59 (1H, $J = 8.0$ Hz), 7.32–7.28 (2H, m), 7.13–7.08 (1H, m), 5.99 (1H, ddd, $J = 17.6, 10.0, 6.8$ Hz), 5.27 (1H, dd, $J = 10.4$ Hz), 5.23 (1H, d, $J = 17.6$ Hz), 4.11 (1H, $J = 6.8$ Hz), 3.91–3.87 (2H, m), 1.56 (1H, s); **^{13}C NMR (CDCl_3 , 100 MHz):** δ 139.8, 137.1, 133.4, 128.9, 128.5, 127.8, 125.3, 118.0, 65.1, 50.7. **HRMS (ESI^+):** Calcd for $\text{C}_{10}\text{H}_{10}\text{Br}$ [$\text{M}+\text{H}-\text{H}_2\text{O}$] $^+$: 208.9966; Found: 208.9964. Specific rotation: $[\alpha]_{\text{D}}^{20.0} -11.9$ (c 1.33, CHCl_3) for an enantiomerically enriched sample of 97:3 er.

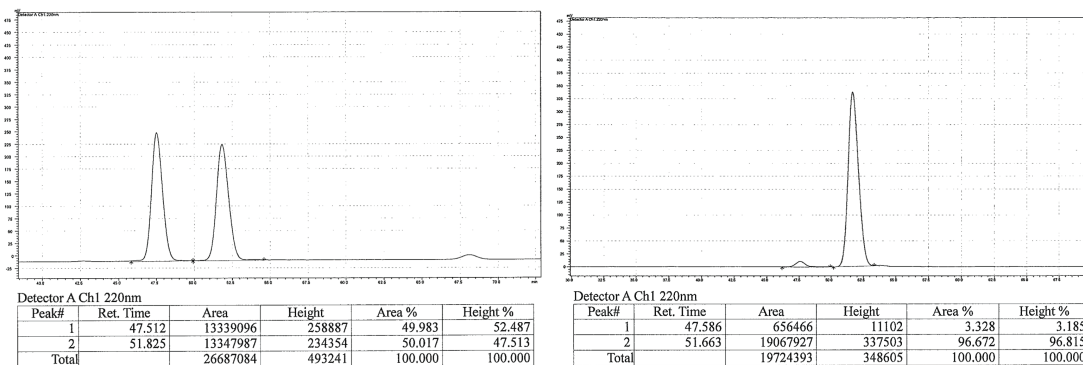
Enantiomeric purity was determined by HPLC analysis in comparison with authentic racemic material; Chiralpak AZ-H column, 99.0:1.0 hexanes/*i*PrOH, 0.5 mL/min, 220 nm.



Retention Time	Area	Area%	Retention Time	Area	Area%
36.168	19585946	49.867	37.549	19349954	97.161
40.717	19690233	50.133	42.225	565421	2.839

(R)-2-(3-Bromophenyl)but-3-en-1-ol (3.55e): IR (neat): 3333 (br, s), 2925 (w), 2874 (w), 1638 (w), 1593 (m), 1566 (m), 1474 (m), 1426 (m), 1299 (w), 1187 (w), 1127 (w), 1071 (s), 1053 (s), 1027 (s), 996 (s), 919 (s), 878 (m), 836 (w), 804 (w), 779 (s), 693 (s), 656 (m), 435 (m) cm^{-1} ; **^1H NMR (CDCl_3 , 400 MHz):** δ 7.39–7.37 (2H, m), 7.23–7.16 (2H, m), 5.96 (1H, ddd, $J = 17.2, 9.6, 6.8$ Hz), 5.24 (1H, d, $J = 9.6$ Hz), 5.19 (1H, d, $J = 16.8$ Hz), 3.82 (2H, app. d, $J = 7.2$ Hz), 3.50 (1H, app. q, $J = 7.2$ Hz), 1.56 (1H, s); **^{13}C NMR (CDCl_3 , 100 MHz):** δ 143.2, 137.6, 131.2, 130.4, 130.2, 126.8, 122.9, 117.8, 66.0, 52.2. **HRMS (ESI $^+$):** Calcd for $\text{C}_{10}\text{H}_{10}\text{Br}$ $[\text{M}+\text{H}-\text{H}_2\text{O}]^+$: 208.9966; Found: 208.9957. Specific rotation: $[\alpha]_{\text{D}}^{20.0} -39.5$ (c 1.32, CHCl_3) for an enantiomerically enriched sample of 97:3 e.r.

Enantiomeric purity was determined by HPLC analysis in comparison with authentic racemic material; Chiralpak AZ-H column, 99.0:1.0 hexanes/*i*PrOH, 0.5 mL/min, 220 nm.

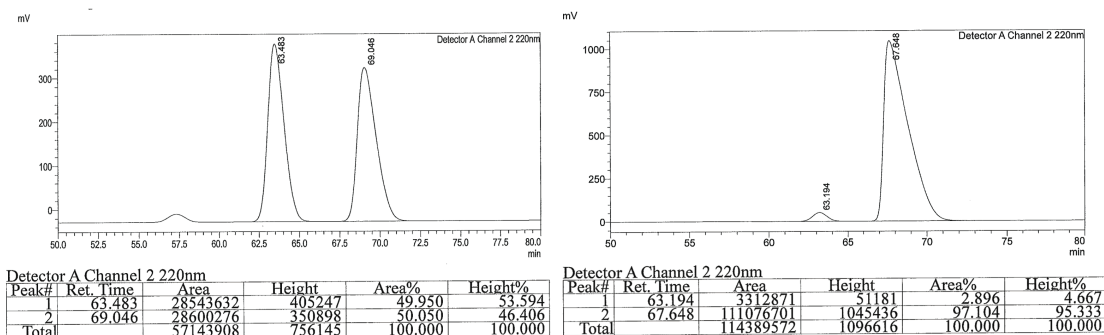


Retention Time	Area	Area%	Retention Time	Area	Area%
47.512	13339096	49.983	47.586	656466	3.328
51.825	13347987	50.017	51.663	19067927	96.672

47.512	13339096	49.983	47.586	656466	3.328
51.825	13347987	50.017	51.663	19067927	96.672

(R)-2-(4-Chlorophenyl)but-3-en-1-ol (3.55f): IR (neat): 3345 (br, s), 2926 (w), 2876 (w), 1637 (w), 1490 (s), 1406 (m), 1297 (w), 1181 (w), 1091 (s), 1053 (s), 1030 (s), 1014 (s), 993 (s), 919 (s), 870 (w), 824 (w), 784 (m), 723 (m), 625 (m), 540 (s), 521 (s), 457 (w) cm^{-1} ; **^1H NMR (CDCl_3 , 400 MHz):** δ 7.33–7.29 (2H, m), 7.19–7.16 (2H, m), 5.97 (1H, ddd, $J = 17.6, 10.0, 7.2$ Hz), 5.23 (1H, app. dt, $J = 10.4, 1.2$ Hz), 5.17 (1H, app. dt, $J = 17.2, 1.2$ Hz), 3.81 (2H, app. d, $J = 7.2$ Hz), 3.51 (1H, app. q, $J = 7.2$ Hz), 1.50 (1H, s); **^{13}C NMR (CDCl_3 , 100 MHz):** δ 139.3, 137.8, 132.8, 129.5, 129.0, 117.6, 66.0, 51.9. **HRMS (ESI^+):** Calcd for $\text{C}_{10}\text{H}_{10}\text{Cl}$ $[\text{M}+\text{H}-\text{H}_2\text{O}]^+$: 165.0471; Found: 165.0470. Specific rotation: $[\alpha]_{\text{D}}^{20.0} -49.5$ (c 0.58, CHCl_3) for an enantiomerically enriched sample of 97:3 e.r.

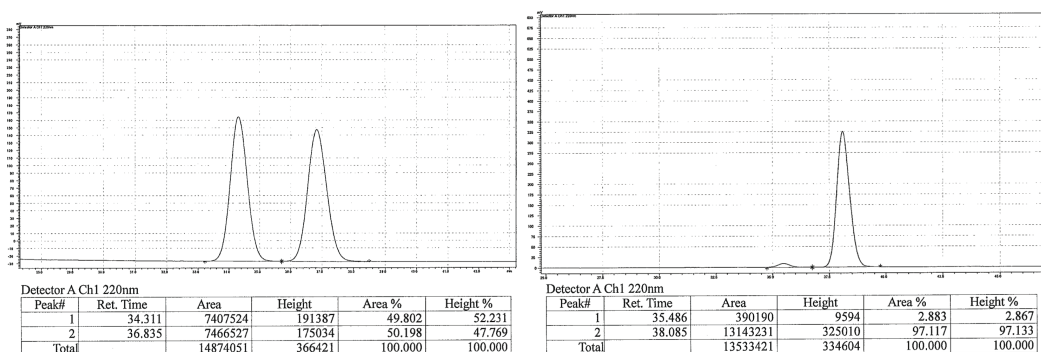
Enantiomeric purity was determined by HPLC analysis in comparison with authentic racemic material; Chiralpak AZ–H column, 99.0:1.0 hexanes/*i*PrOH, 0.5 mL/min, 220 nm.



Retention Time	Area	Area%	Retention Time	Area	Area%
63.483	28543632	49.950	63.194	3312871	2.896
69.046	28600276	50.050	67.648	111076701	97.104

(R)-2-(4-(Trifluoromethyl)phenyl)but-3-en-1-ol (3.55g): IR (neat): 3344 (br, s), 2923 (m), 2853 (w), 1731 (w), 1619 (w), 1554 (w), 14612 (w), 1377 (w), 1325 (s), 1261 (w), 1164 (m), 1124 (s), 1068 (s), 1018 (m), 922 (w), 839 (w), 738 (w), 605 (w) cm^{-1} ; **^1H NMR (CDCl_3 , 400 MHz):** δ 7.60 (2H, d, $J = 8.0$ Hz), 7.37 (2H, d, $J = 8.0$ Hz), 6.00 (1H, ddd, $J = 17.6, 10.0, 7.2$ Hz), 5.26 (1H, d, $J = 10.0$ Hz), 5.20 (1H, dd, $J = 17.2, 0.8$ Hz), 3.86 (2H, d, $J = 7.2$ Hz), 3.60 (1H, app. q, $J = 7.2$ Hz), 1.57 (1H, s); **^{13}C NMR (CDCl_3 , 100 MHz):** 145.0, 137.4, 129.4 (q, $J_{\text{CF}} = 31.9$ Hz), 128.5, 125.8 (q, $J_{\text{CF}} = 3.8$ Hz), 124.3 (q, $J_{\text{CF}} = 270.2$ Hz), 118.0, 65.9, 52.4. **HRMS (ESI^+):** Calcd for $\text{C}_{11}\text{H}_{10}\text{F}_3$ $[\text{M}+\text{H}-\text{H}_2\text{O}]^+$: 199.0735; Found: 199.0737. Specific rotation: $[\alpha]_{\text{D}}^{20.0} 11.7$ (c 1.09, CHCl_3) for an enantiomerically enriched sample of 97:3 e.r.

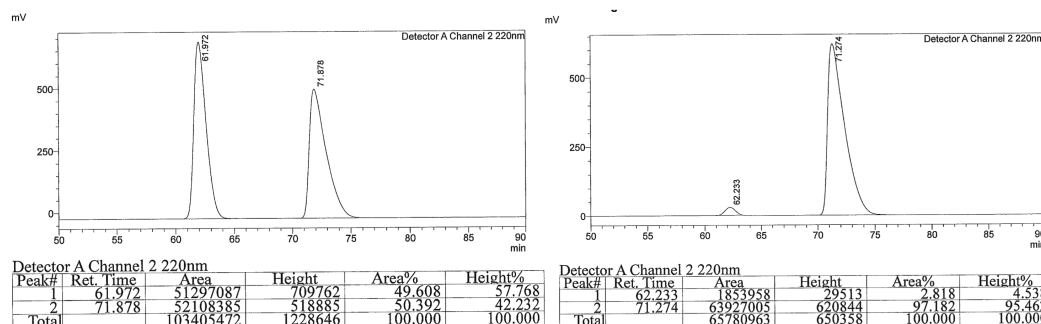
Enantiomeric purity was determined by HPLC analysis in comparison with authentic racemic material; Chiralpak AZ–H column, 99.0:1.0 hexanes/*i*PrOH, 0.5 mL/min, 220 nm.



Retention Time	Area	Area%	Retention Time	Area	Area%
34.311	7407524	49.802	35.486	390190	2.883
36.835	7466527	50.198	38.085	13143231	97.117

(R)-2-(4-Nitrophenyl)but-3-en-1-ol (3.55h): IR (neat): 3374 (br, s), 2927 (w), 2877 (w), 1638 (w), 1597 (m), 1514 (s), 1411 (w), 1342 (s), 1182 (w), 1109 (w), 1052 (m), 1014 (m), 994 (m), 923 (m), 850 (s), 827 (m), 779 (w), 751 (m), 702 (s), 535 (w) cm^{-1} ; ^1H NMR (CDCl_3 , 400 MHz): δ 8.18 (2H, d, $J = 8.8$ Hz), 7.42 (2H, d, $J = 8.8$ Hz), 5.99 (1H, ddd, $J = 17.6, 10.0, 7.2$ Hz), 5.28 (1H, d, $J = 10.4$ Hz), 5.20 (1H, d, $J = 17.2$ Hz), 3.88 (2H, d, $J = 7.6$ Hz), 3.65 (1H, app. q, $J = 7.2$ Hz), 1.86 (1H, br); ^{13}C NMR (CDCl_3 , 100 MHz): δ 148.7, 147.1, 136.8, 129.1, 124.0, 118.5, 65.7, 52.3. HRMS (ESI^+): Calcd for $\text{C}_{10}\text{H}_{12}\text{O}_3\text{N}$ $[\text{M}+\text{H}]^+$: 194.0817; Found: 194.0811. Specific rotation: $[\alpha]_D^{20.0} -62.8$ (c 0.78, CHCl_3) for an enantiomerically enriched sample of 97:3 e.r.

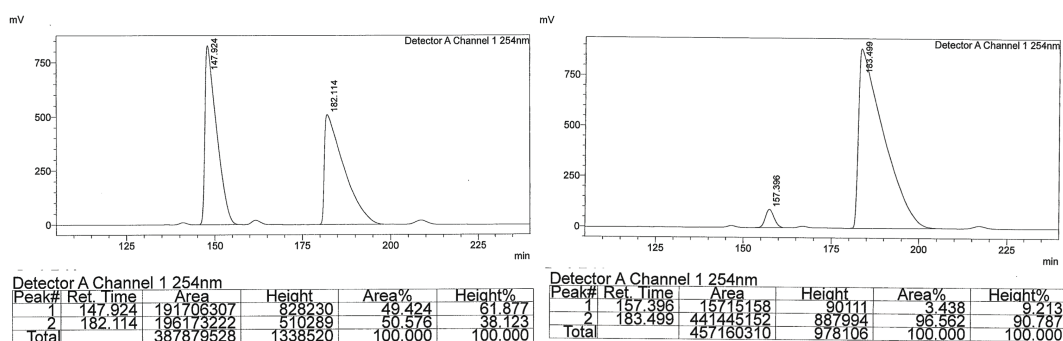
Enantiomeric purity was determined by HPLC analysis in comparison with authentic racemic material; Chiralpak AZ–H column, 96.0:4.0 hexanes/*i*PrOH, 0.5 mL/min, 220 nm.



Retention Time	Area	Area%	Retention Time	Area	Area%
61.972	51297087	49.608	62.233	1853958	2.818
71.878	52108385	50.392	71.274	63927005	97.182

(R)-1-(4-(1-Hydroxybut-3-en-2-yl)phenyl)ethan-1-one (3.55i): IR (neat): 3423 (br, s), 2924 (m), 2827 (w), 1679 (s), 1605 (s), 1459 (w), 1411 (m), 1359 (m), 1307 (w), 1270 (s), 1184 (w), 1115 (w), 1056 (m), 1017 (m), 996 (w), 959 (w), 835 (w) cm^{-1} ; $^1\text{H NMR}$ (CDCl_3 , 400 MHz): δ 7.94–7.91 (2H, m), 7.35–7.33 (2H, m), 6.00 (1H, ddd, $J = 17.6$, 10.0, 7.2 Hz), 5.25 (1H, d, $J = 10.4$ Hz), 5.20 (1H, d, $J = 17.6$ Hz), 3.86 (2H, d, $J = 5.2$ Hz), 3.61 (1H, q, $J = 7.2$ Hz), 2.59 (3H, s), 1.59 (1H, s); $^{13}\text{C NMR}$ (CDCl_3 , 100 MHz): δ 197.9, 146.5, 137.5, 136.0, 128.9, 128.4, 118.0, 65.9, 52.6, 26.7. HRMS (ESI $^+$): Calcd for $\text{C}_{12}\text{H}_{15}\text{O}_2$ $[\text{M}+\text{H}]^+$: 191.1072; Found: 191.1073. Specific rotation: $[\alpha]_{\text{D}}^{20.0} -55.6$ (c 0.73, CHCl_3) for an enantiomerically enriched sample of 97:3 e.r.

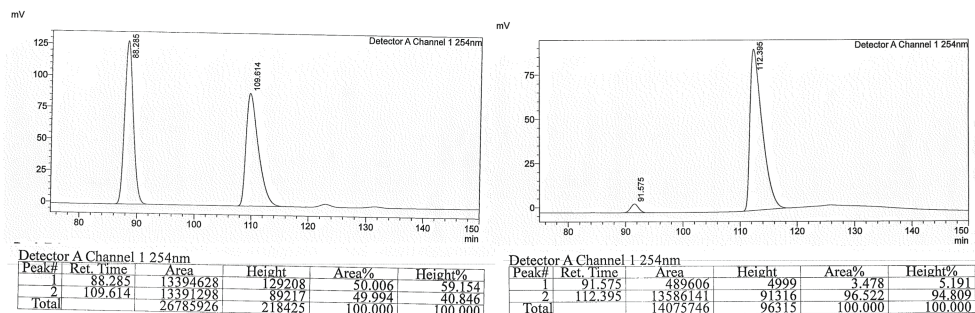
Enantiomeric purity was determined by HPLC analysis in comparison with authentic racemic material; Chiralpak AZ-H column, 96.0:4.0 hexanes/*i*PrOH, 0.5 mL/min, 254 nm.



Retention Time	Area	Area%	Retention Time	Area	Area%
147.924	191706307	49.424	157.396	15715158	3.438
182.114	196173222	50.576	183.499	441445152	96.562

Methyl (R)-4-(1-hydroxybut-3-en-2-yl)benzoate (3.55j): IR (neat): 3419 (br, s), 2951 (w), 2878 (w), 1718 (s), 1637 (w), 1609 (m), 1574 (w), 1436 (m), 1413 (w), 1312 (m), 1277 (s), 1181 (m), 1110 (s), 1054 (m), 1019 (m), 996 (w), 966 (w), 920 (w), 769 (m), 709 (m) cm^{-1} ; $^1\text{H NMR}$ (CDCl_3 , 600 MHz): δ 8.01 (2H, $J = 8.4$ Hz), 7.32 (2H, $J = 8.4$ Hz), 6.00 (1H, ddd, $J = 17.4$, 9.6, 7.2 Hz), 5.25 (1H, app. d, $J = 10.2$ Hz), 5.20 (1H, app. d, $J = 18.0$ Hz), 3.91 (3H, s), 3.85 (2H, d, $J = 6.6$ Hz), 3.60 (1H, q, $J = 7.2$ Hz), 1.52 (1H, s); $^{13}\text{C NMR}$ (CDCl_3 , 100 MHz): δ 167.1, 146.2, 137.6, 130.2, 129.0, 128.2, 117.9, 66.0, 52.6, 52.2. HRMS (ESI $^+$): Calcd for $\text{C}_{12}\text{H}_{15}\text{O}_3$ $[\text{M}+\text{H}]^+$: 207.1021; Found: 207.1025. Specific rotation: $[\alpha]_{\text{D}}^{20.0} -51.7$ (c 1.05, CHCl_3) for an enantiomerically enriched sample of 97:3 e.r.

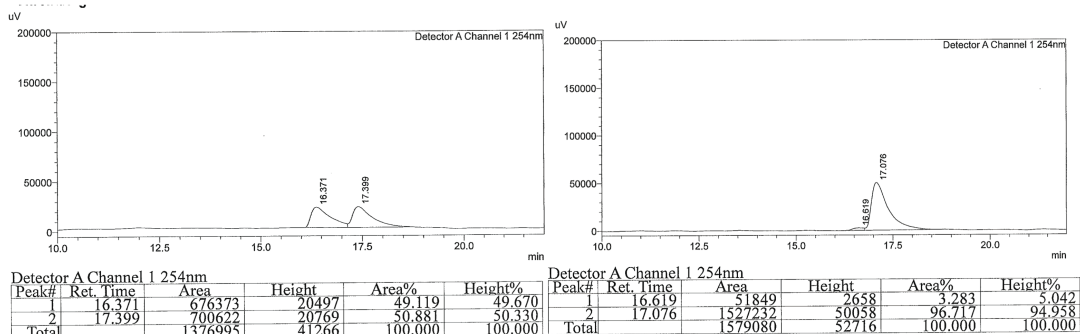
Enantiomeric purity was determined by HPLC analysis in comparison with authentic racemic material; Chiralpak AZ-H column, 96.0:4.0 hexanes/*i*PrOH, 0.5 mL/min, 254 nm.



Retention Time	Area	Area%	Retention Time	Area	Area%
88.285	13394628	50.006	91.575	489606	3.478
109.614	13391298	49.994	112.395	13586141	96.522

(R)-2-(Pyridin-3-yl)but-3-en-1-ol (3.55k): IR (neat): 3222 (br, s), 3081 (w), 2922 (w), 2868 (w), 1638 (w), 1592 (w), 1479 (m), 1425 (m), 1369 (w), 1060 (s), 1028 (s), 994 (m), 918 (s), 810 (m), 785 (m), 713 (s), 633 (m), 400 (m) cm^{-1} ; $^1\text{H NMR}$ (CDCl_3 , 600 MHz): δ 8.49–8.47 (2H, m), 7.57 (1H, dt, $J = 7.8, 1.8$ Hz), 7.27–7.25 (1H, m), 6.00 (1H, ddd, $J = 18.0, 10.2, 7.2$ Hz), 5.26 (1H, td, $J = 10.2, 1.2$ Hz), 5.19 (1H, td, $J = 17.4, 1.2$ Hz), 3.87–3.86 (1H, m), 3.56 (1H, q, $J = 7.2$ Hz), 1.95 (1H, s); $^{13}\text{C NMR}$ (CDCl_3 , 100 MHz): δ 149.8, 148.2, 137.3, 136.7, 135.6, 123.7, 118.0, 65.8, 50.0. HRMS (ESI⁺): Calcd for $\text{C}_9\text{H}_{12}\text{NO}$ $[\text{M}+\text{H}]^+$: 150.0919; Found: 150.0921. Specific rotation: $[\alpha]_D^{20.0} -20.6$ (c 0.67, CHCl_3) for an enantiomerically enriched sample of 97:3 e.r.

Enantiomeric purity was determined by HPLC analysis in comparison with authentic racemic material before oxidation; Chiralpak AZ–H column, 98.0:2.0 hexanes/ *i*PrOH, 1.0 mL/min, 254 nm.

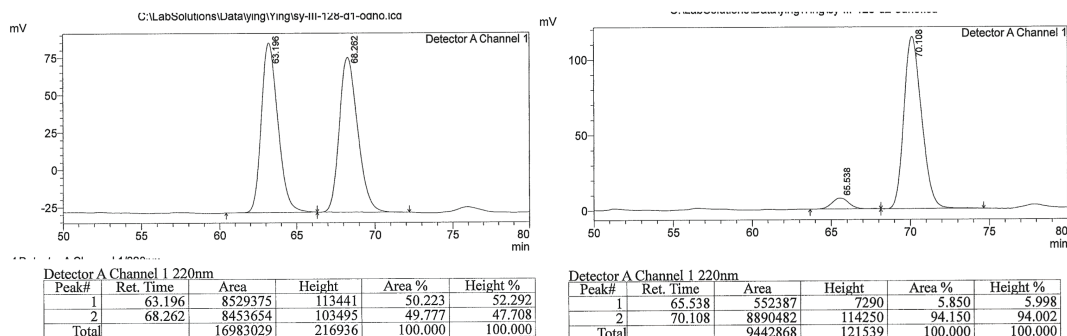


Retention Time	Area	Area%	Retention Time	Area	Area%
16.371	676373	49.119	16.619	51849	3.283
17.399	700622	50.881	17.076	1527232	96.717

(R)-2-(Thiophen-3-yl)but-3-en-1-ol (3.55l): IR (neat): 3392 (br, s), 2923 (s), 2853 (m), 1733 (w), 1639 (w), 1461 (m), 1414 (m), 1382 (m), 1259 (m), 1156 (m), 1079 (s), 1030 (s), 993 (s), 965 (m), 921 (s), 840 (m), 783 (s), 714 (m), 632 (m), 482 (w) cm^{-1} ; $^1\text{H NMR}$ (CDCl_3 , 500 MHz): δ 7.32 (1H, dd, $J = 5.2, 3.2$ Hz), 7.08–7.07 (1H, m), 7.00 (1H, dd, J

= 5.2, 1.2 Hz), 5.97 (1H, ddd, $J = 17.2, 10.0, 7.2$ Hz), 5.24–5.17 (2H, m), 3.86–3.76 (2H, m), 3.65 (1H, q, $J = 7.2$ Hz), 1.57 (1H, s); ^{13}C NMR (CDCl_3 , 100 MHz): δ 141.2, 138.0, 127.2, 126.1, 121.3, 117.4, 65.9, 48.2. HRMS (ESI⁺): Calcd for $\text{C}_8\text{H}_9\text{S}$ $[\text{M}+\text{H}-\text{H}_2\text{O}]^+$: 137.0425; Found: 137.0420. Specific rotation: $[\alpha]_{\text{D}}^{20.0} -13.6$ (c 0.87, CHCl_3) for an enantiomerically enriched sample of 94:6 e.r.

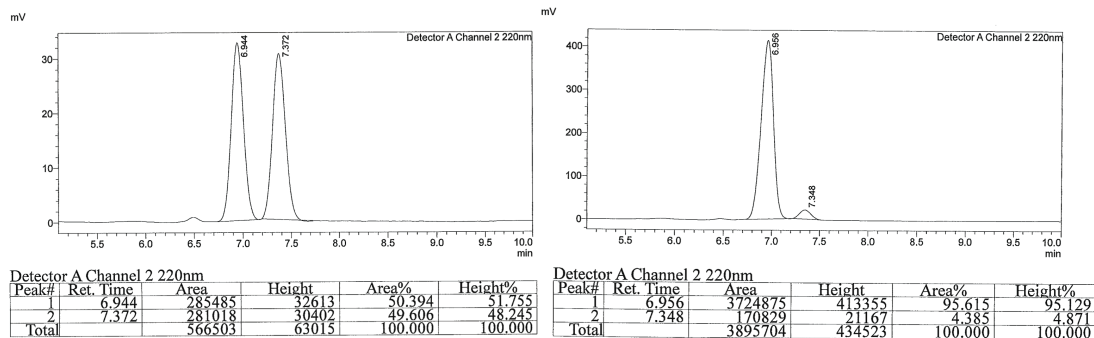
Enantiomeric purity was determined by HPLC analysis in comparison with authentic racemic material before oxidation; Chiralpak AZ–H column, 99.0:1.0 hexanes/*i*PrOH, 0.5 mL/min, 220 nm.



Retention Time	Area	Area%	Retention Time	Area	Area%
63.196	8529375	50.223	65.538	552387	5.850
68.262	8453654	49.777	70.108	8890482	94.150

(R)-2-Cyclohexylbut-3-en-1-ol (3.55m): IR (neat): 3358 (br, s), 2923 (s), 2852 (m), 1449 (w), 1055 (w), 1016 (w), 997 (w), 913 (w) cm^{-1} ; ^1H NMR (CDCl_3 , 400 MHz): δ 5.63 (1H, dt, $J = 16.8, 10.0$ Hz), 5.19 (1H, dd, $J = 10.4, 2.0$ Hz), 5.11 (1H, dd, $J = 17.2, 2.0$ Hz), 3.70 (1H, dd, $J = 10.4, 4.8$ Hz), 3.44 (1H, dd, $J = 10.4, 9.2$ Hz), 2.07–2.00 (1H, m), 1.73–1.62 (5H, m), 1.43 (1H, s), 1.37–1.31 (1H, m), 1.27–1.10 (3H, m), 1.07–0.93 (2H, m); ^{13}C NMR (CDCl_3 , 100 MHz): δ 138.9, 118.3, 63.6, 53.2, 38.7, 31.3, 30.4, 26.7, 26.6, 26.5. HRMS (ESI⁺): Calcd for $\text{C}_{10}\text{H}_{19}\text{O}$ $[\text{M}+\text{H}]^+$: 155.1426; Found: 155.1432. Specific rotation: $[\alpha]_{\text{D}}^{20.0} -10.8$ (c 0.65, CHCl_3) for an enantiomerically enriched sample of 96:4 e.r.

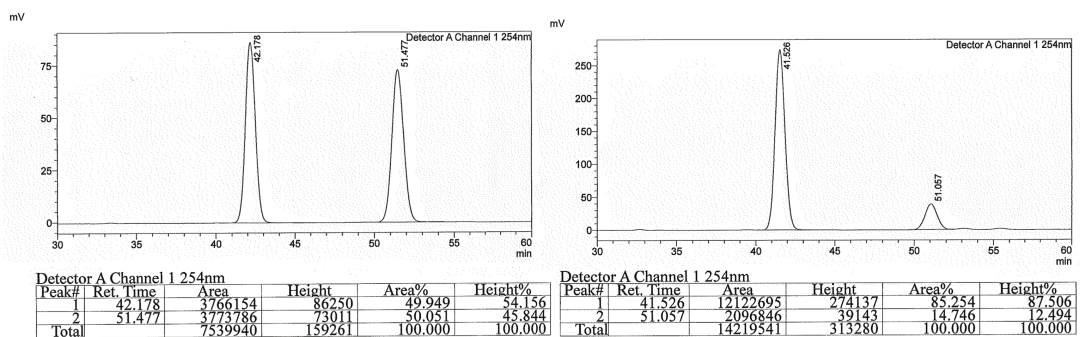
Enantiomeric purity was determined by HPLC analysis in comparison with authentic racemic material after benzylation; Chiralpak AZ–H column, 99.0:1.0 hexanes/*i*PrOH, 1.0 mL/min, 220 nm.



Retention Time	Area	Area%	Retention Time	Area	Area%
6.944	285485	50.394	6.956	3724875	95.615
7.372	282018	49.606	7.348	170829	4.385

(*R,E*)-4-Phenyl-2-vinylbut-3-en-1-ol (3.55n): IR (neat): 3349 (br, s), 3080 (w), 3059 (w), 3025 (w), 2926 (w), 2872 (w), 1637 (w), 1598 (w), 1493 (w), 1448 (w), 1415 (w), 1028 (m), 990 (m), 965 (s), 915 (s), 862 (w), 842 (w), 746 (s), 691 (s), 601 (w), 508 (w) cm^{-1} ; $^1\text{H NMR}$ (CDCl_3 , 400 MHz): δ 7.38 (2H, d, $J = 7.2$ Hz), 7.31 (2H, app. t, $J = 7.2$ Hz), 7.25–7.21 (1H, m), 6.51 (1H, d, $J = 16.0$ Hz), 6.14 (1H, dd, $J = 16.0, 8.0$ Hz), 5.89–5.80 (1H, m), 5.25–5.21 (2H, m), 3.66 (2H, d, $J = 6.8$ Hz), 3.18–3.11 (1H, m), 1.59 (1H, s); $^{13}\text{C NMR}$ (CDCl_3 , 100 MHz): δ 137.5, 137.1, 132.4, 128.70, 128.68, 128.63, 126.4, 117.4, 65.4, 50.2. HRMS (ESI $^+$): Calcd for $\text{C}_{12}\text{H}_{13}$ $[\text{M}+\text{H}-\text{H}_2\text{O}]^+$: 157.1017; Found: 157.1014; specific rotation: $[\alpha]_{\text{D}}^{20.0} -43.8$ (c 0.84, CHCl_3) for an enantiomerically enriched sample of 85:15 e.r.

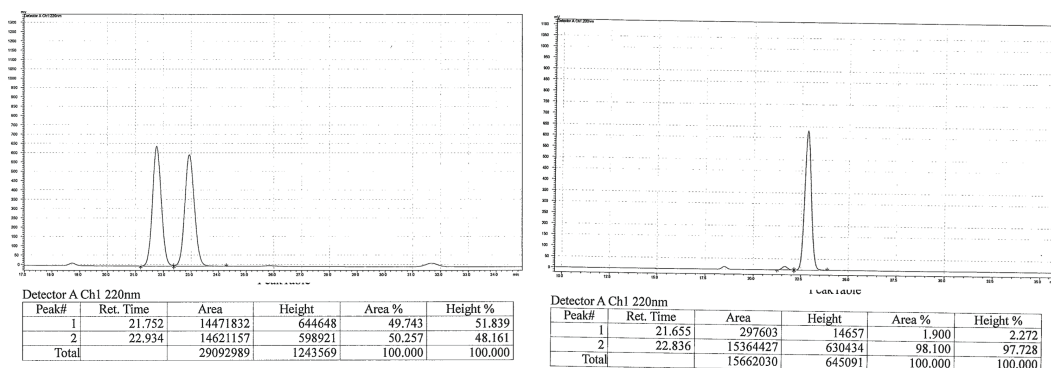
Enantiomeric purity was determined by HPLC analysis in comparison with authentic racemic material; Chiralpak AZ-H column, 99.0:1.0 hexanes/*i*PrOH, 0.5 mL/min, 254 nm.



Retention Time	Area	Area%	Retention Time	Area	Area%
42.178	3766154	49.949	41.526	12122695	85.254
51.477	3773786	50.051	51.057	2096846	14.746

(S)-2-(Dimethyl(phenyl)silyl)but-3-en-1-ol (3.55o): IR (neat): 3347(br, s), 2956 (w), 2868 (w), 1627 (w), 1427 (w), 1412 (w), 1301 (w), 1248 (m), 1111(m), 1049 (m), 993 (m), 896 (m), 832 (s), 812 (s), 793 (s), 775 (m), 759 (m), 729 (s), 698 (s), 653 (s), 594 (w), 469 (m), 417 (m) cm^{-1} ; **^1H NMR (CDCl_3 , 500 MHz):** δ 7.50–7.48 (2H, m), 7.39–7.33 (3H, m), 5.69 (1H, dt, $J = 17.6, 10.4$ Hz), 5.08 (1H, d, $J = 10.4$ Hz), 5.02 (2H, 1H, d, $J = 10.4$ Hz), 3.74–3.65 (2H, m), 2.15 (1H, td, $J = 10.0, 4.8$ Hz), 1.47 (1H, s), 0.32 (6H, s); **^{13}C NMR (CDCl_3 , 100 MHz):** δ 136.84, 136.75, 134.4, 129.4, 128.0, 115.6, 62.4, 39.7, –4.13, –4.81. **HRMS (ESI $^+$):** Calcd for $\text{C}_{12}\text{H}_{17}\text{Si}$ $[\text{M}+\text{H}-\text{H}_2\text{O}]^+$: 189.1100; Found: 189.1106. Specific rotation: $[\alpha]_{\text{D}}^{20.0}$ –4.22 (c 1.47, CHCl_3) for an enantiomerically enriched sample of 98:2 e.r.

Enantiomeric purity was determined by HPLC analysis in comparison with authentic racemic material; Chiralpak AZ–H column, 99.0:1.0 hexanes/*i*PrOH, 0.5 mL/min, 220 nm.



Retention Time	Area	Area%	Retention Time	Area	Area%
21.752	14471832	49.743	21.655	297603	1.900
22.934	14621157	50.257	22.836	15364427	98.100

Formal Synthesis of Rhopaloic Acid A

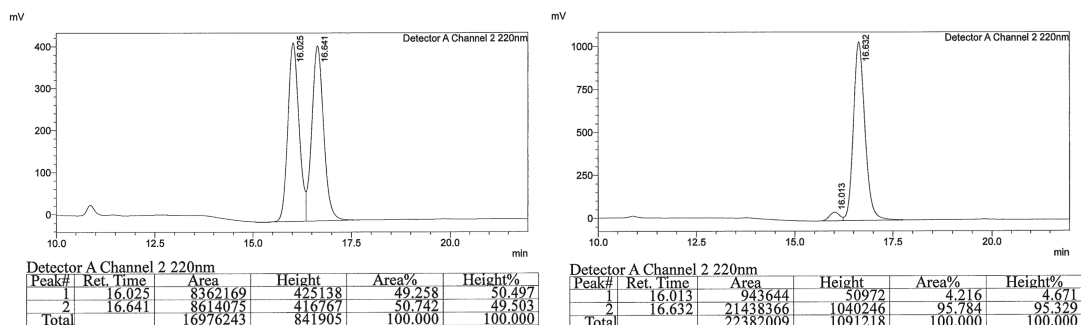
NHC–Cu-Catalyzed EAS with Allylic Phosphate 3.46p

A 100-mL oven-dried flask equipped with a stir bar was charged with NHC–Ag complex **3.56** (35 mg, 55 μmol), NaOMe (65 mg, 1.20 mmol), and CuCl (5.0 mg, 50 μmol) in an N_2 -filled glove box. The vial was sealed with a septum and electrical tape, and removed from the glove box. Tetrahydrofuran (5.0 mL) was added and the mixture was allowed to stir for 2 h under N_2 at 22 $^\circ\text{C}$. The solution became bright yellow. Bis[(pinacolato)boryl]methane **3.13** (400 mg, 1.5 mmol) and allylic phosphate **3.46p** (338 mg, 1.0 mmol) dissolved in thf (5.0 mL) was added through a syringe and the resulting solution was allowed to stir at 22 $^\circ\text{C}$ for 6 h. The solution was then passed through a short plug of silica gel and eluted with Et_2O . The organic layer was concentrated *in vacuo*,

resulting in yellow oil that was purified by silica gel chromatography (20:1 hexanes/Et₂O, R_f 0.19) to afford 290 mg of **3.57** (>98:2 S_N2'/S_N2) as pale yellow oil (0.89 mmol, 89% yield).

(R)-tert-Butyldimethyl((2-((4,4,5,5-tetramethyl-1,3,2-dioxaborolan-2-yl)methyl)but-3-en-1-yl)oxy)silane (3.57): IR (neat): 2978 (w), 2956 (w), 2929 (w), 2888 (w), 2857(w), 1471 (w), 1407 (w), 1368 (s), 1317 (s), 1253 (s), 1213 (w), 1145 (s), 1095 (s), 1004 (w), 969 (w), 888 (w), 834 (s), 774 (s), 667 (m) cm⁻¹; ¹H NMR (CDCl₃, 400 MHz): δ 5.78 (1H, ddd, *J* = 18.0, 10.4, 7.6 Hz), 5.03 (1H, app. d, *J* = 17.2 Hz), 4.97 (1H, app. d, *J* = 10.8 Hz), 3.49 (2H, d, *J* = 6.4 Hz), 2.50–2.41 (1H, m), 1.23 (12H, d, *J* = 2.4 Hz), 0.96 (1H, dd, *J* = 15.6, 10.0 Hz), 0.88 (9H, s), 0.79 (1H, dd, *J* = 16.0, 9.2 Hz), 0.03 (6H, s); ¹³C NMR (CDCl₃, 150 MHz): δ 141.7, 114.2, 83.3, 68.2, 42.1, 26.1, 25.1, 24.9, -5.1, -5.2. HRMS (ESI⁺): Calcd for C₁₇H₃₆BO₃Si [M+H]⁺: 327.2527; Found: 327.2527. Specific rotation: [α]_D^{20.0} 7.89 (*c* 0.84, CHCl₃) for an enantiomerically enriched sample of 96:4 e.r.

Enantiomeric purity was determined by HPLC analysis in comparison with authentic racemic material after desilylation and benzooylation of the resulting alcohol; Chiralpak AZ–H column, 97.0:3.0 hexanes/*i*PrOH, 0.3 mL/min, 220 nm.



Retention Time	Area	Area%	Retention Time	Area	Area%
16.025	8362169	49.258	16.013	50972	4.216
16.641	8614075	50.742	16.632	1040246	95.784

Phosphine–Palladium Catalyzed Suzuki Cross-Coupling³² with Alkenyl Iodide

A 4-dram vial with a stir bar was charged with alkyl–B(pin) **3.57** (290 mg, 0.89 mmol) and a solution of 9-BBN dimer (119 mg, 0.97 mmol) in thf (0.5 ml). After 12 h, the mixture was transferred to a 25 mL flask under nitrogen atmosphere containing PdCl₂(dppf)₂ (36 mg, 0.045 mmol), K₃PO₄ (378 mg, 1.78 mmol), alkenyl iodide **3.59** (308 mg, 0.97 mmol) and 3 mL dmf. Then 150 μL deionized water (sparged with nitrogen) was transferred to the flask and the mixture was allowed to stir at 50 °C for 24 h. At this time, the reaction was quenched by addition of a saturated solution of NH₄Cl

(32) S. R. Chemler, D. Trauner, S. J. Danishefsky, *Angew. Chem. Int. Ed.* **2001**, *40*, 4544–4568.

and the inorganic layer was washed with Et₂O (5.0 mL, three times). The combined organic layer was concentrated *in vacuo* and purified by silica gel chromatography (20:1 hexanes/Et₂O, R_f = 0.25) to afford **3.60** as colorless oil (402 mg, 87% yield). **tert-Butyldimethyl(((R,5E,9E)-6,10,14-trimethyl-2-((4,4,5,5-tetramethyl-1,3,2-dioxaborolan-2-yl)methyl)pentadeca-5,9,13-trien-1-yl)oxy)silane (3.60)**: IR (neat): 2956 (s), 2927 (s), 2855 (s), 1447 (m), 1372 (s), 1317 (m), 1252 (m), 1146 (s), 1093 (s), 969 (w), 8356 (s), 813 (w), 774 (s) cm⁻¹; ¹H NMR (CDCl₃, 400 MHz): δ 5.14–5.07 (3H, m), 3.50 (1H, dd, *J* = 10.0, 5.6 Hz), 3.44 (1H, dd, *J* = 9.6, 6.4 Hz), 2.10–2.03 (4H, m), 1.99–1.95 (6H, m), 1.77–1.71 (1H, m), 1.67 (3H, s), 1.59 (9H, s), 1.53–1.43 (2H, m), 1.23 (12H, s), 0.88 (9H, s), 0.82–0.76 (2H, m), 0.03 (6H, s); ¹³C NMR (CDCl₃, 100 MHz): δ 135.0, 134.7, 131.3, 125.1, 124.6, 124.5, 82.9, 62.6, 39.90, 39.87, 36.9, 33.6, 27.0, 26.9, 26.8, 26.1, 25.8, 25.6, 25.0, 24.9, 18.5, 17.8, 16.13, 16.10, –5.2. HRMS (ESI⁺): Calcd for C₃₁H₆₀BO₃Si [M+H]⁺: 519.4405; Found: 519.4422. Specific rotation: [α]_D^{20.0} 2.61 (*c* 1.15, CHCl₃) for an enantiomerically enriched sample of 96:4 e.r.

Deprotection/NHC–Cu-catalyzed Allylic Substitution to Obtain 3.62

To a solution of alkyl-B(pin) **3.60** (402 mg, 0.77 mmol) in anhydrous methanol (1.0 ml) was added *p*-TsOH (6.6 mg, 0.039 mmol) at 22 °C and the mixture was allowed to stir for 2 h. The resulting solution was concentrated *in vacuo* to remove methanol. A 4-dram vial was charged with CuCl (19 mg, 0.19 mmol), imidazolinium salt (26 mg, 0.076 mmol), KO^{*t*}Bu (129 mg, 1.2 mmol) and thf (5.0 ml) was allowed to stir at 22 °C for 2 h. Then the crude of desilylation and allyl phosphate (224 mg, 1.2mol) in thf (2.0 ml) was transferred to the vial and the reaction mixture was allowed to stir at 70 °C for 24 h. The reaction was then quenched by passing the solution through a short plug of silica gel, after which it was washed with Et₂O (20 ml), concentrated *in vacuo* to afford a pale yellow oily residue, which was purified by silica gel chromatography (6:1 hexanes/Et₂O, R_f = 0.30) to deliver alcohol **3.62** as colorless oil (165 mg, 0.51 mmol, 67% yield). **(R,5E,9E)-2-(But-3-en-1-yl)-6,10,14-trimethylpentadeca-5,9,13-trien-1-ol (3.62)**: IR (neat): 3323 (s), 2966 (m), 2917 (s), 2855 (s), 1641 (w), 1449 (m), 1379 (m), 1202 (w), 1107 (w), 1032 (s), 993 (s), 908 (s), 833 (m), 743 (w) cm⁻¹; ¹H NMR (CDCl₃, 400 MHz): δ 5.87 (1H, m), 5.14–5.08 (1H, m), 5.05–4.99 (1H, m), 4.95 (1H, dt, *J* = 10.0, 0.8 Hz), 3.57 (2H, d, *J* = 4.8 Hz), 2.12–2.05 (6H, m), 2.03–1.95 (6H, m), 1.68 (3H, s), 1.60 (9H, s), 1.54–1.33 (5H, m); ¹³C NMR (CDCl₃, 100 MHz): δ 139.1, 135.4, 135.1, 131.4, 124.6, 124.5, 124.3, 114.6, 65.5, 39.9, 39.7, 31.6, 31.3, 31.1, 30.3, 26.9, 26.8, 25.5, 25.3, 17.8, 16.18, 16.16. HRMS (ESI⁺): Calcd for C₂₂H₃₉O [M+H]⁺: 319.3001; Found: 319.3008. Specific rotation: [α]_D^{20.0} –3.74 (*c* 0.80, CHCl₃) for an enantiomerically enriched sample of 96:4 e.r.

Catalytic Cross-Metathesis with Acrolein³³

In a 1-dram vial with a stir bar was charged with alkene **3.62** (16 mg, 0.051 mmol) and acrolein (67 μ l, 1.02 mmol). A solution of Ru complex **3.63** (0.01 M in CH₂Cl₂, 0.5 mL, 0.005 mmol, 1.0 mol %) was introduced and the mixture was allowed to stir at 22 °C for 0.5 h under nitrogen atmosphere. Then the mixture was flushed through a short plug of silica gel with Et₂O and concentrated *in vacuo* and purified by silica gel chromatography (6:1 hexanes/Et₂O, R_f = 0.35 to 1:1 hexanes/Et₂O) to afford α,β -unsaturated aldehyde **3.19** (>98:2 *E/Z*) as colorless oil (13.5 mg, 71% yield). **(R,2E,9E,13E)-6-(Hydroxymethyl)-10,14,18-trimethylnonadeca-2,9,13,17-tetraenal (3.19)**: IR (neat): 2962 (m), 2917 (s), 2870 (m), 2851 (m), 2184 (w), 2138 (w), 2033 (w), 1691 (s), 1636 (w), 1449 (w), 1379 (w), 1131 (w), 1102 (w), 1035 (w), 1023 (w) cm⁻¹; ¹H NMR (CDCl₃, 400 MHz): δ 9.51 (1H, d, *J* = 8.0 Hz), 6.86 (1H, dt, *J* = 15.6, 6.4 Hz), 6.14 (1H, ddt, *J* = 16.0, 8.0, 1.6 Hz), 5.13–5.07 (3H, m), 3.63 (1H, *J* = 10.4, 4.0 Hz), 2.37 (2H, *J* = 6.0 Hz), 2.10–1.95 (10H, m), 1.68 (3H, d, *J* = 1.2 Hz), 1.60 (9H, s), 1.58–1.34 (5H, m); ¹³C NMR (CDCl₃, 100 MHz): δ 194.2, 158.8, 135.7, 135.2, 133.1, 131.5, 124.5, 124.25, 124.20, 65.2, 39.9, 39.8, 39.7, 31.0, 30.3, 29.4, 26.9, 26.7, 25.9, 25.3, 17.8, 16.22, 16.17. HRMS (ESI⁺): Calcd for C₂₃H₃₉O₂ [M+H]⁺: 374.2950; Found: 374.2957. Specific rotation: $[\alpha]_D^{20.0}$ –3.17 (*c* 0.80, CHCl₃) for an enantiomerically enriched sample of 96:4 e.r.

Catalytic Oxa-Michael Addition³⁴

To a solution of aldehyde **3.19** (32.3 mg, 0.078 mmol) in CH₂Cl₂ (3.0 mL, 0.026 M) was added dropwise a 1:1 mixture of pyrrolidine/BzOH (0.28 mL, 0.054 M in CH₂Cl₂) at 22 °C. After the solution was allowed to stir for 1 h at 22 °C, it was diluted with hexanes (30.0 mL), filtered through a short pad of silica gel (hexanes/EtOAc, 3/1), and concentrated *in vacuo*. The resulting residue was purified by silica gel chromatography (5:1 hexanes/Et₂O, R_f 0.36) to afford aldehyde **3.64** (31.6 mg, diastereoisomer ratio 8:1) as colorless oil. **2-((2R,5S)-5-((3E,7E)-4,8,12-Trimethyltrideca-3,7,11-trien-1-yl)tetrahydro-2H-pyran-2-yl)acetaldehyde (3.64)**: IR (neat): 3070 (w), 2958 (w), 2899 (w), 2173 (w), 1626 (w), 1487 (w), 1427 (w), 1411 (w), 1317 (w), 1248 (m), 1112 (m), 1040 (w), 998 (w), 942 (w), 899 (w), 836 (s), 813 (s), 778 (m), 758 (s), 723 (s), 697 (s), 642 (m), 548 (w), 469 (m) cm⁻¹; ¹H NMR (CDCl₃, 600 MHz): δ 9.79 (1H, t, *J* = 2.4 Hz), 5.11–5.07 (3H, m), 3.94–3.91 (1H, m), 3.78–3.73 (1H, m), 3.06 (1H, t, *J* = 10.8 Hz), 2.58 (1H, ddd, *J* = 16.8, 7.8, 3.0 Hz), 2.47 (1H, ddd, *J* = 16.2, 4.8, 1.8 Hz), 2.09–2.04 (4H, m), 2.00–1.96 (6H, m), 1.68–1.67 (4H, m), 1.60 (9H, d), 1.57–1.54 (1H, m), 1.37 (1H, qd, *J* = 10.8, 3.0 Hz), 1.21–1.11 (2H, m); ¹³C NMR (CDCl₃, 150 MHz): δ 201.6, 135.5, 135.1,

(33) Killen, J. C.; Leonard, J.; Aggarwal, V. K. *Synlett*. **2010**, 4, 579–582.

(34) Lee, K. ; Kim, H.; Hong, J. *Org Lett*. **2011**, 13, 2722–2725.

131.4, 124.5, 124.29, 124.25, 73.8, 73.2, 50.1, 39.9, 39.8, 35.2, 32.7, 31.9, 30.3, 26.9, 26.1, 25.8, 25.1, 17.8, 16.2, 16.1. **HRMS (ESI⁺)**: Calcd for C₁₇H₂₇Si₂ [M+H]⁺: 287.1651; Found: 287.1654. Specific rotation: $[\alpha]_{\text{D}}^{20.0} = -1.97$ (*c* 0.65, CHCl₃) for an enantiomerically enriched sample of 96:4 e.r.

¹H NMR and ¹³C NMR Spectra

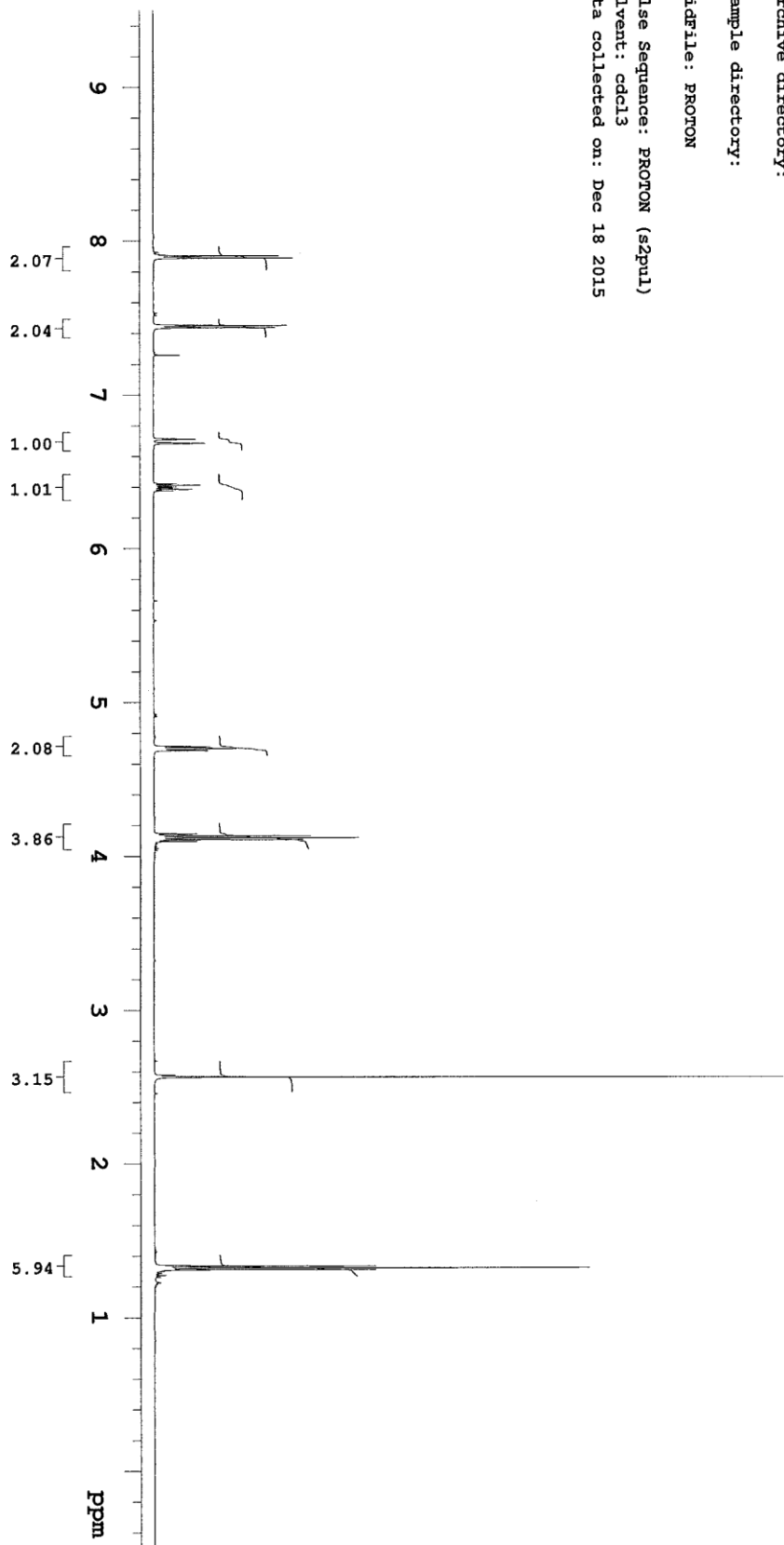
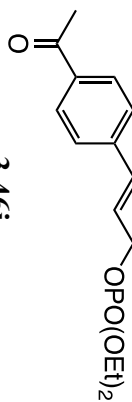
XCF-11-110-2

Sample Name: sy-11-191-b-pro
Data Collected on: nmr19-vnmrs600
Archive directory:

Sample directory:

Fidfile: PROTON

Pulse Sequence: PROTON (s2pu1)
Solvent: cdcl3
Data collected on: Dec 18 2015



XCF-1I-110-2

Sample Name:

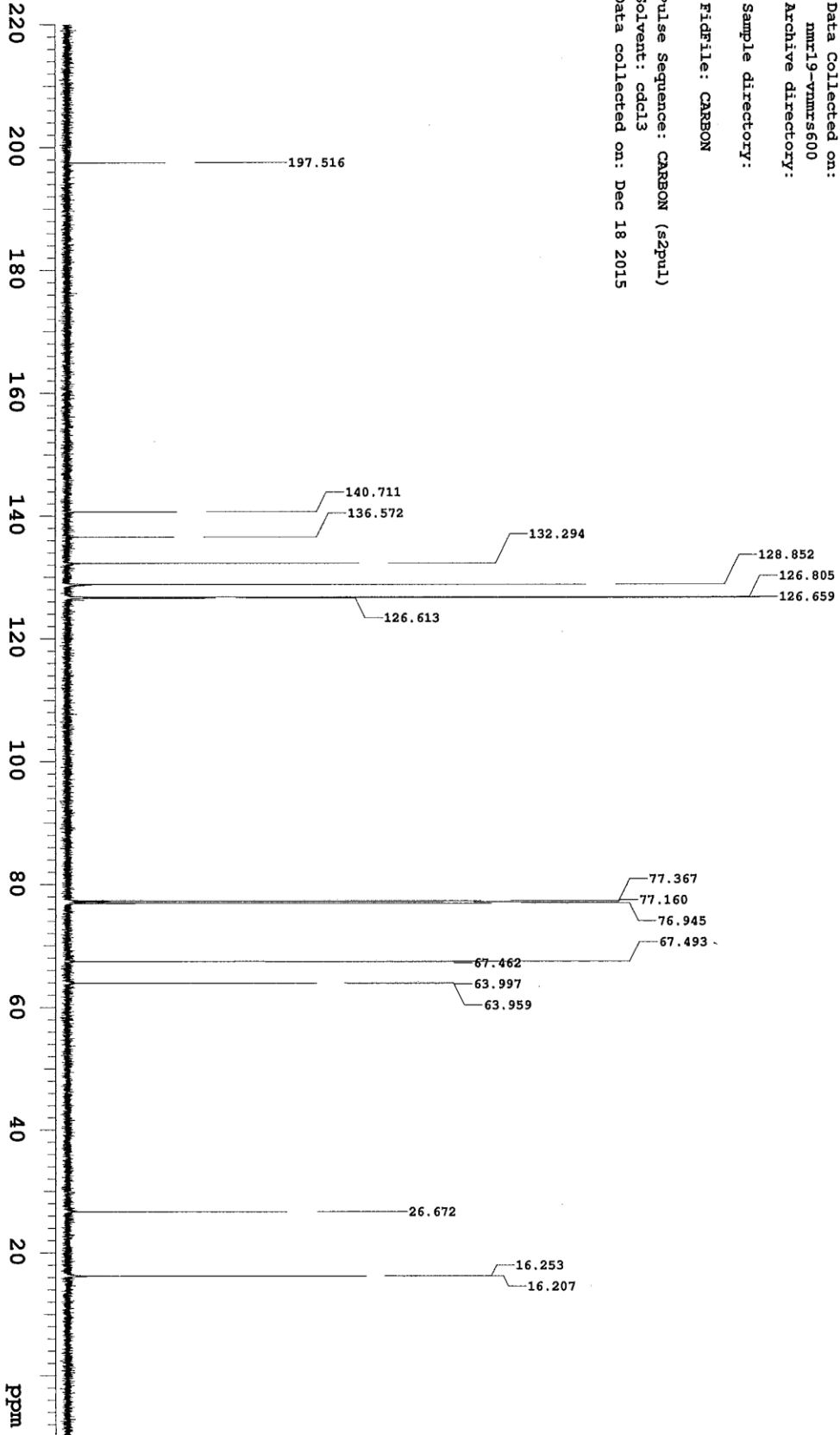
Data Collected on:
nmr19-vnmrs600

Archive directory:

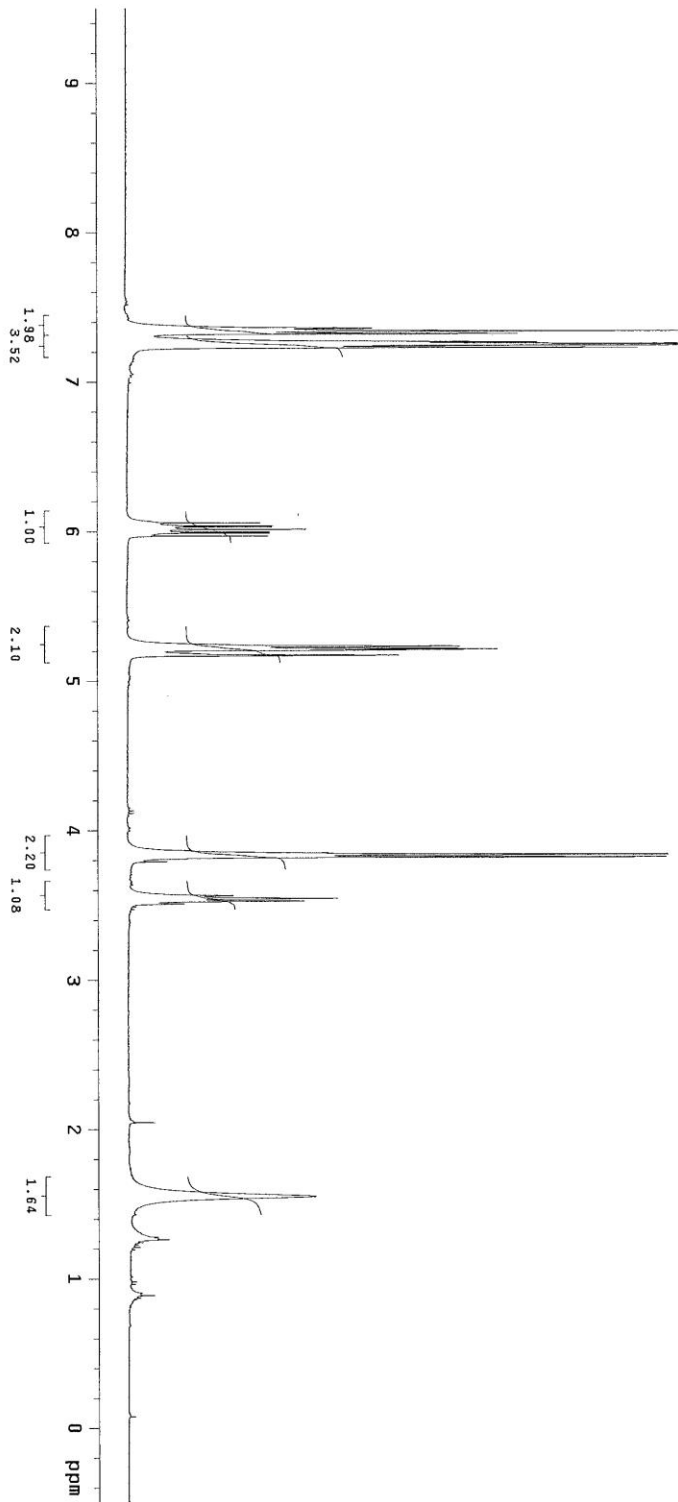
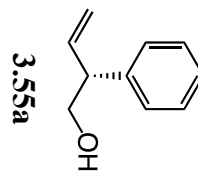
Sample directory:

FIDFile: CARBON

Pulse Sequence: CARBON (s2pu1)
Solvent: cdd13
Data collected on: Dec 18 2015

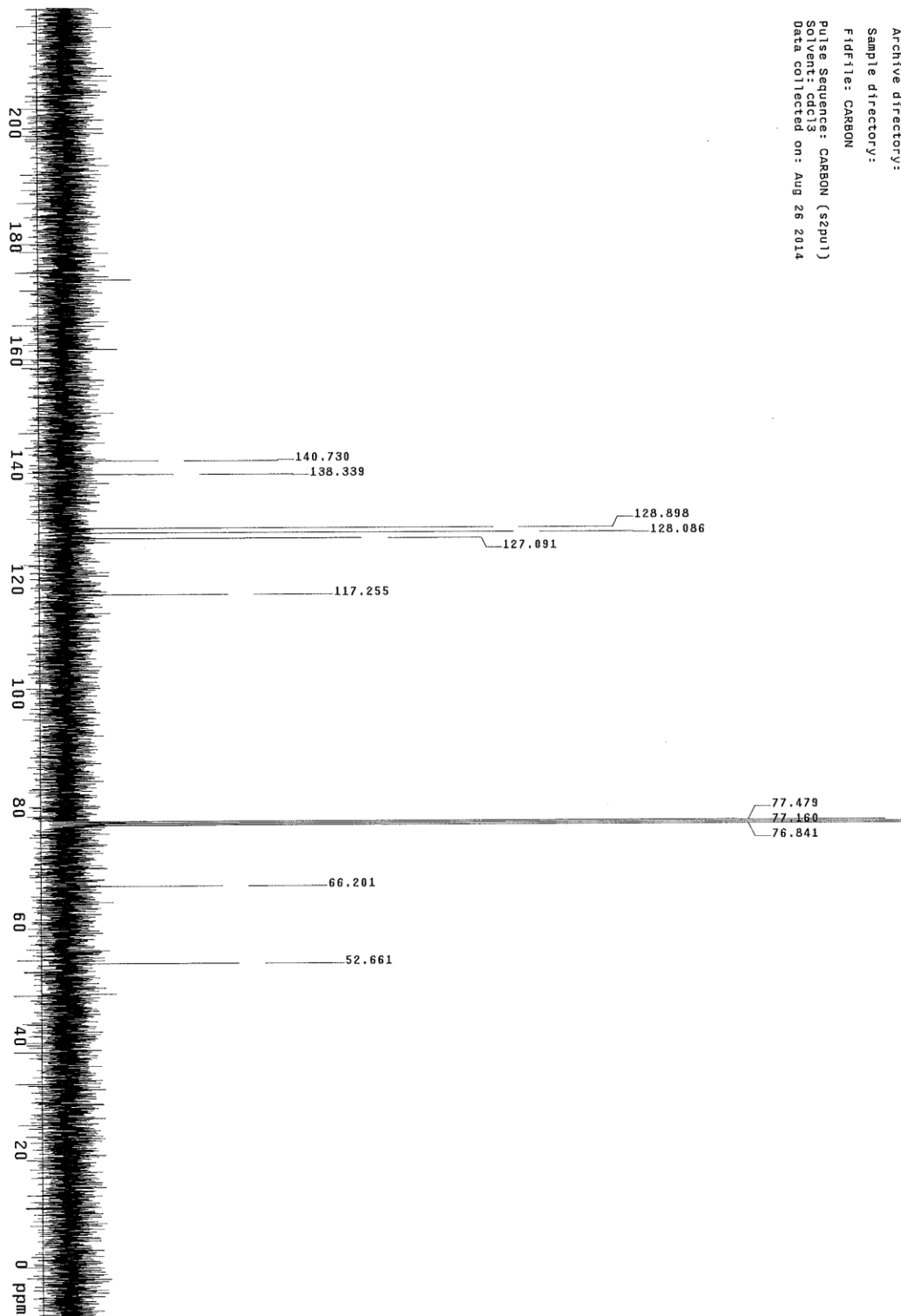


NM-5-121crude
 Sample Name: SY-II-119-a1-pro
 Data Collected on: Vnmr13-vnmrs400
 Archive directory:
 Sample directory:
 F1file: PROTON
 Pulse Sequence: PROTON (s2pu1)
 Solvent: cdcl3
 Data collected on: Aug 26 2014

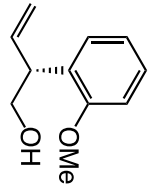


MJK-III-260A-1H, purified

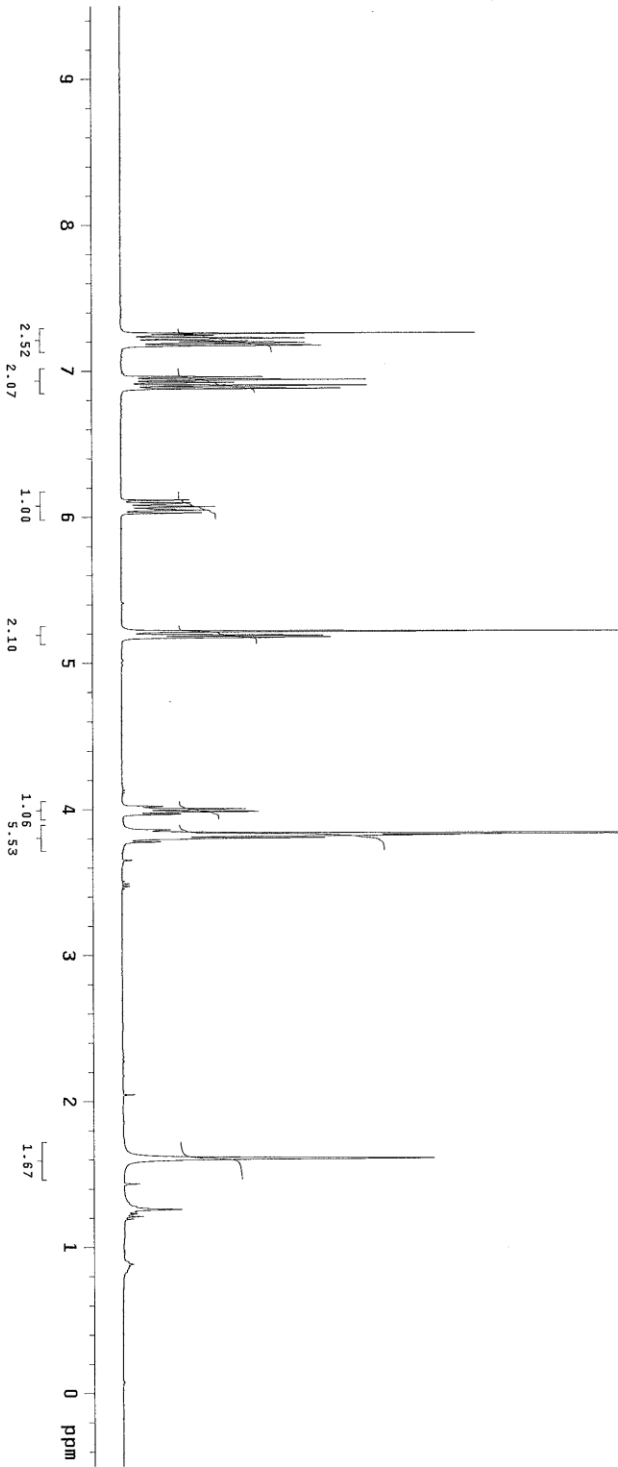
Sample Name: sy-ii-119-a1-pro
Data Collected on: vnmr13-vnmr540
Archive directory:
Sample directory:
Fid file: CARBON
Pulse Sequence: CARBON (szpu1)
Solvent: cdc13
Data collected on: Aug 26 2014



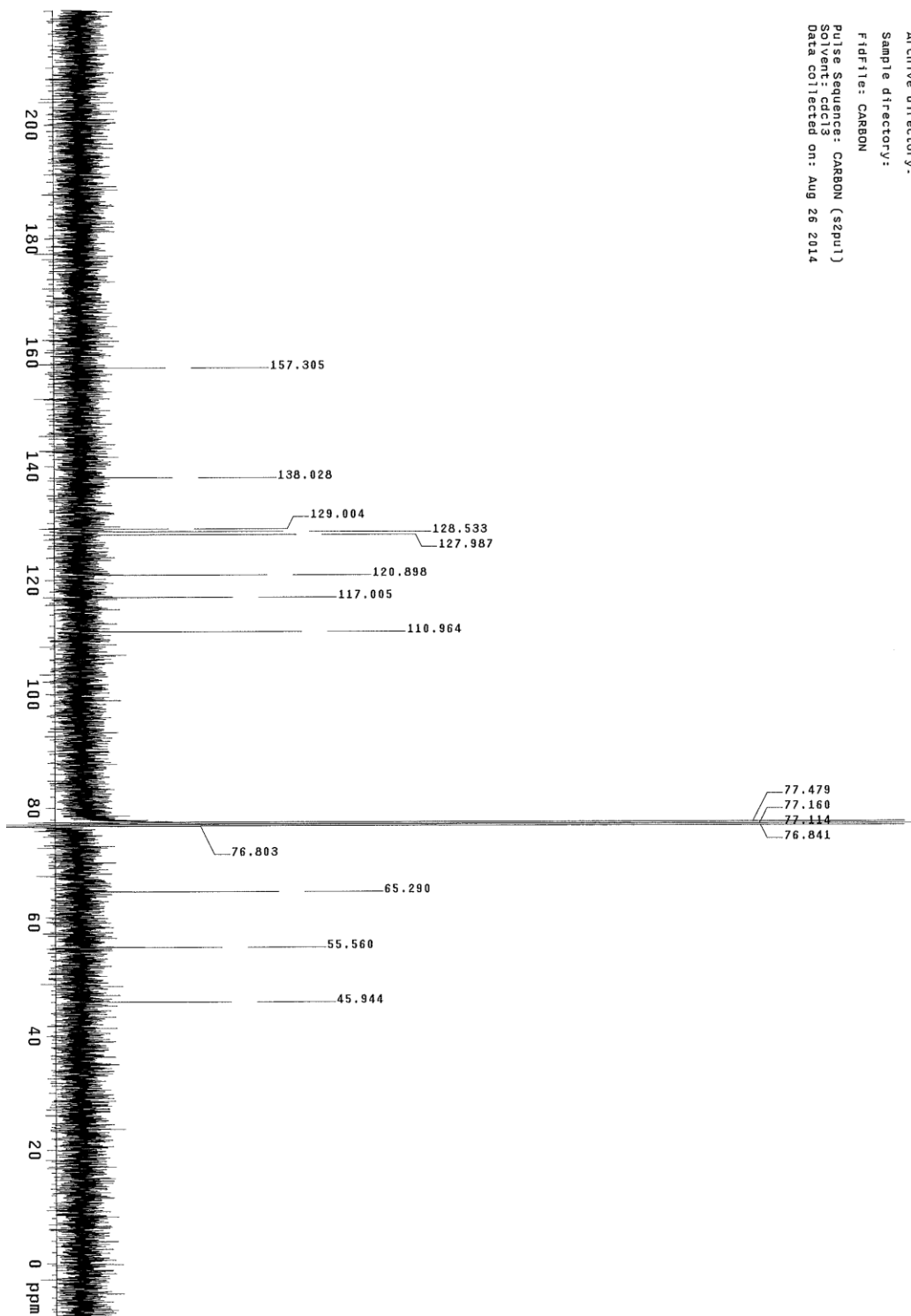
Sample Name: gy-III-119-41-pro
Data Collected on: vnmr13-vnmr1400
Archive directory:
Sample directory:
Fid-file: PROTON
Pulse Sequence: PROTON (szpu1)
Solvent: cdcl3
Data Collected on: Aug 26 2014



3.55b

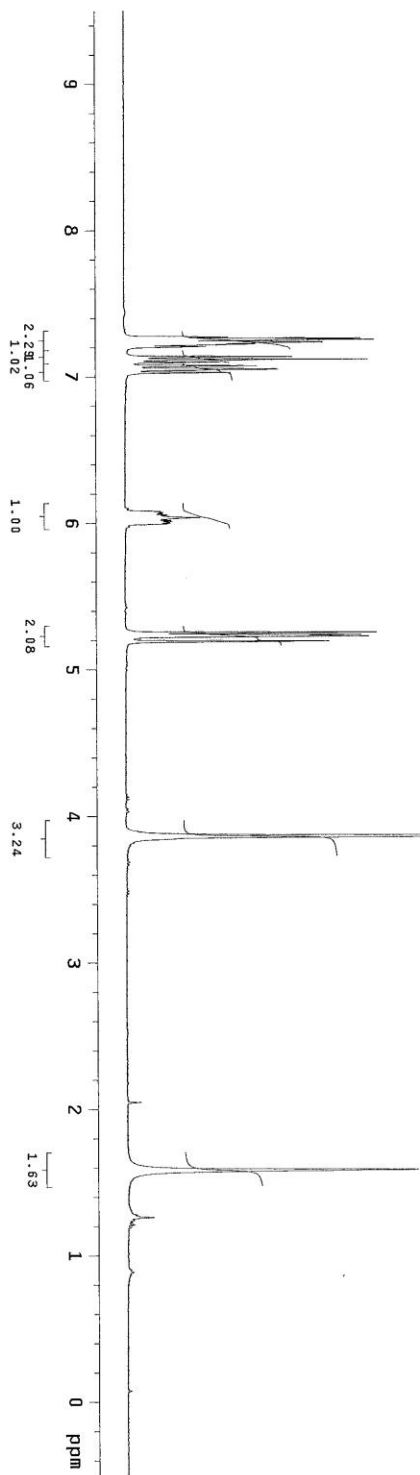
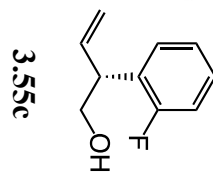


Sample Name: sy-111-119-d1-pro
Date Collected on: vhm-13-vhm-s400
Archive directory:
Sample directory:
Fidfile: CARBON
Pulse Sequence: CARBON (s2p11)
Solvent: cdc3
Data Collected on: Aug 26 2014

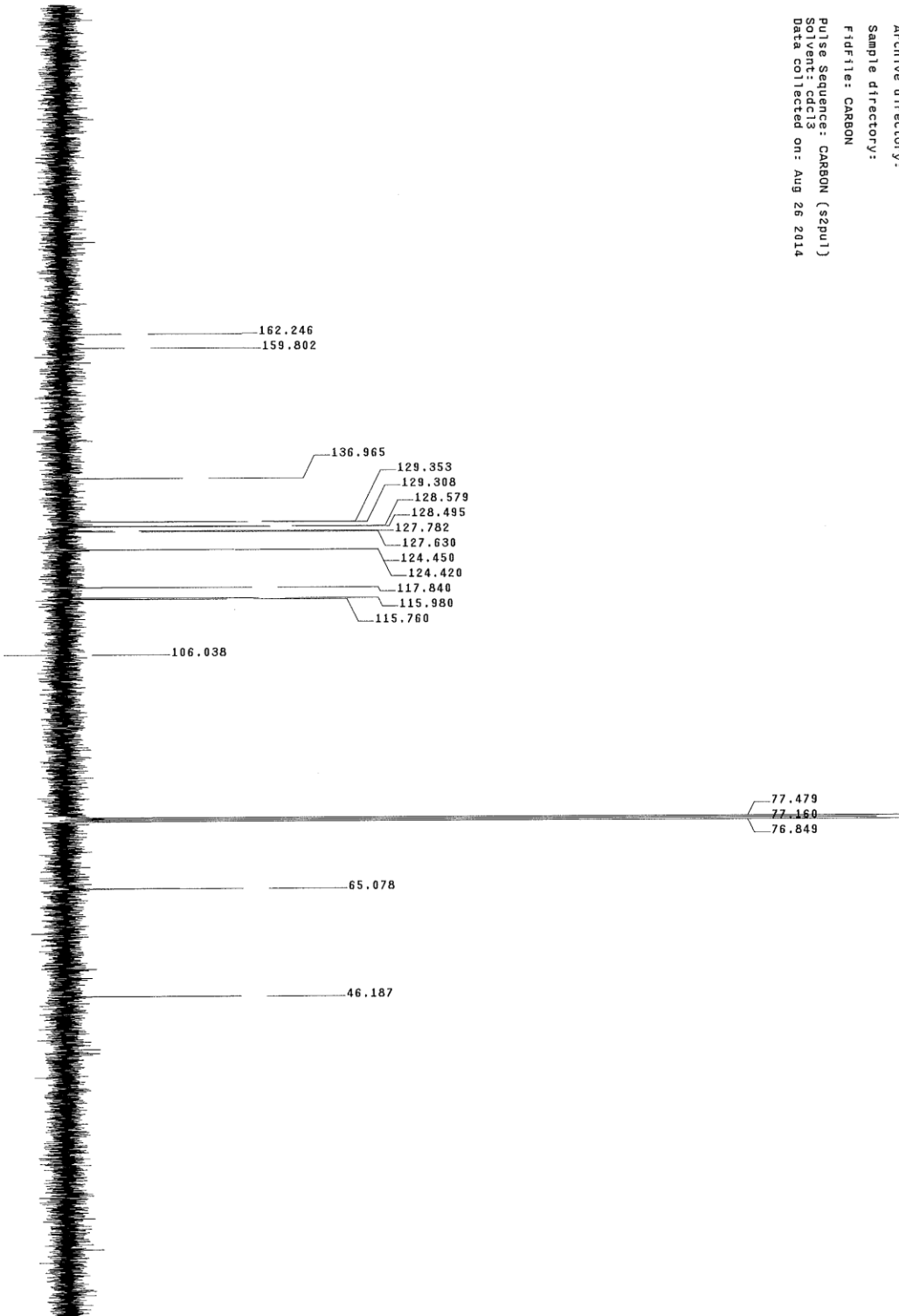


MOK-III-260A-1H, purified

Sample Name: sy-III-119-bi-pro
Data Collected on: vnmr-13-vnmr-s400
Archive directory: Sample directory:
Fidfile: PROTON
Pulse Sequence: PROTON (s2pu1)
Solvent: cdcl3
Data collected on: Aug 26 2014

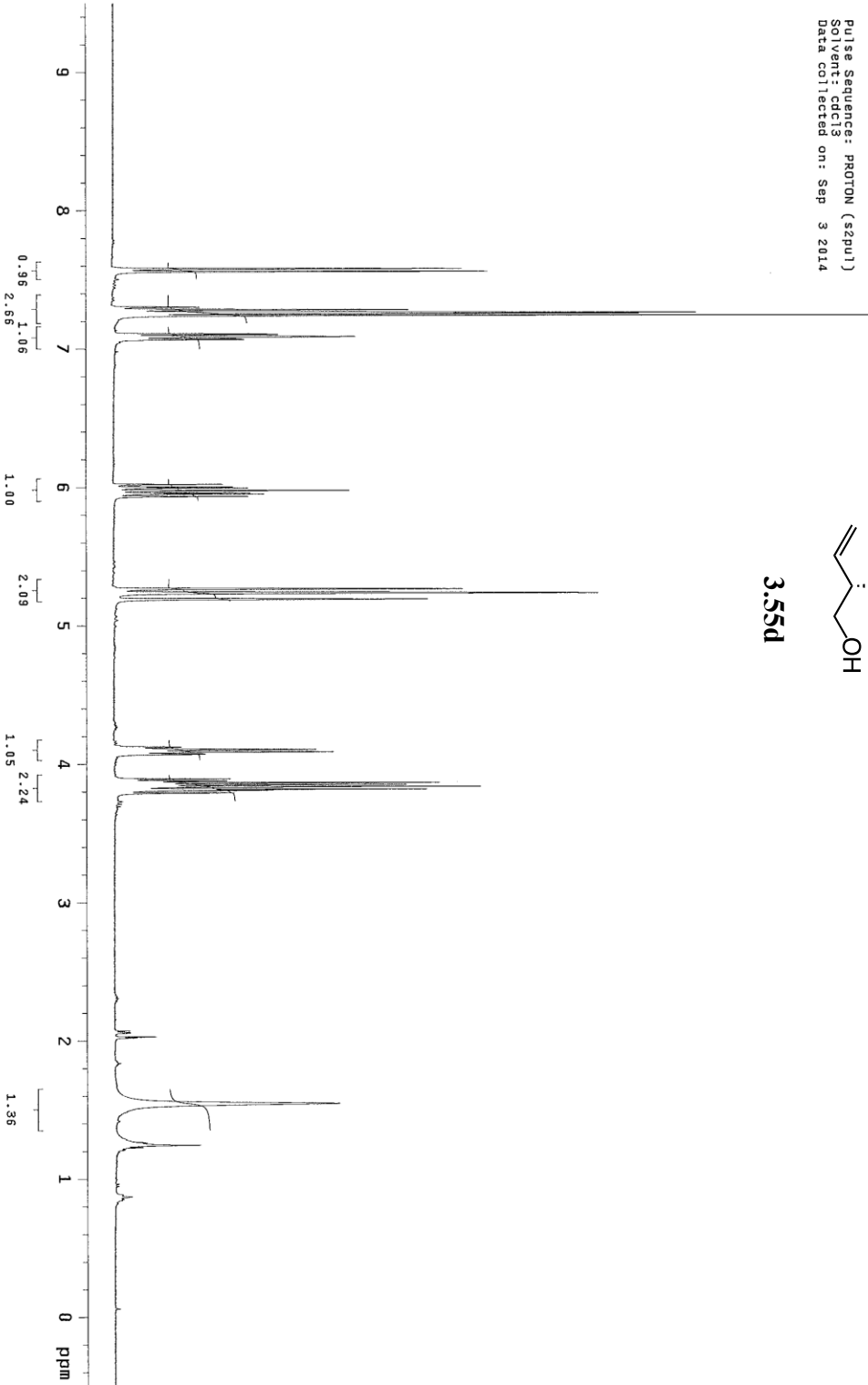
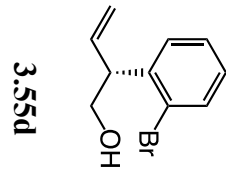


MJK-II-260A-1H, purified
Sample Name: sy-II-119-b1-pro
Data Collected on: Vnmr1s-vnmr5400
Archive directory:
Sample directory:
Fid file: CARBON
Pulse Sequence: CARBON (s2pu1)
Solvent: cdcl3
Data collected on: Aug 26 2014

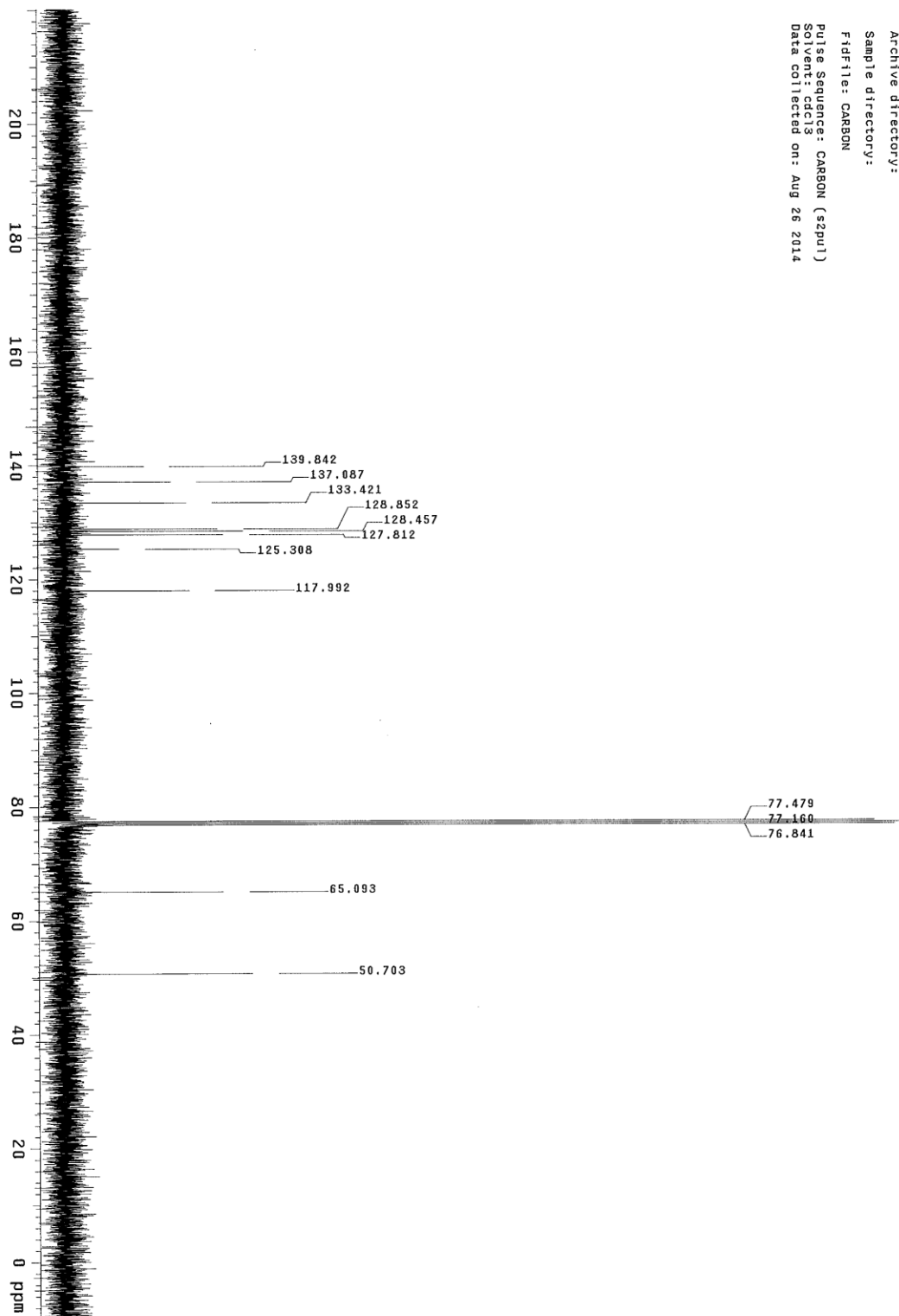


STANDARD FLUORINE PARAMETERS

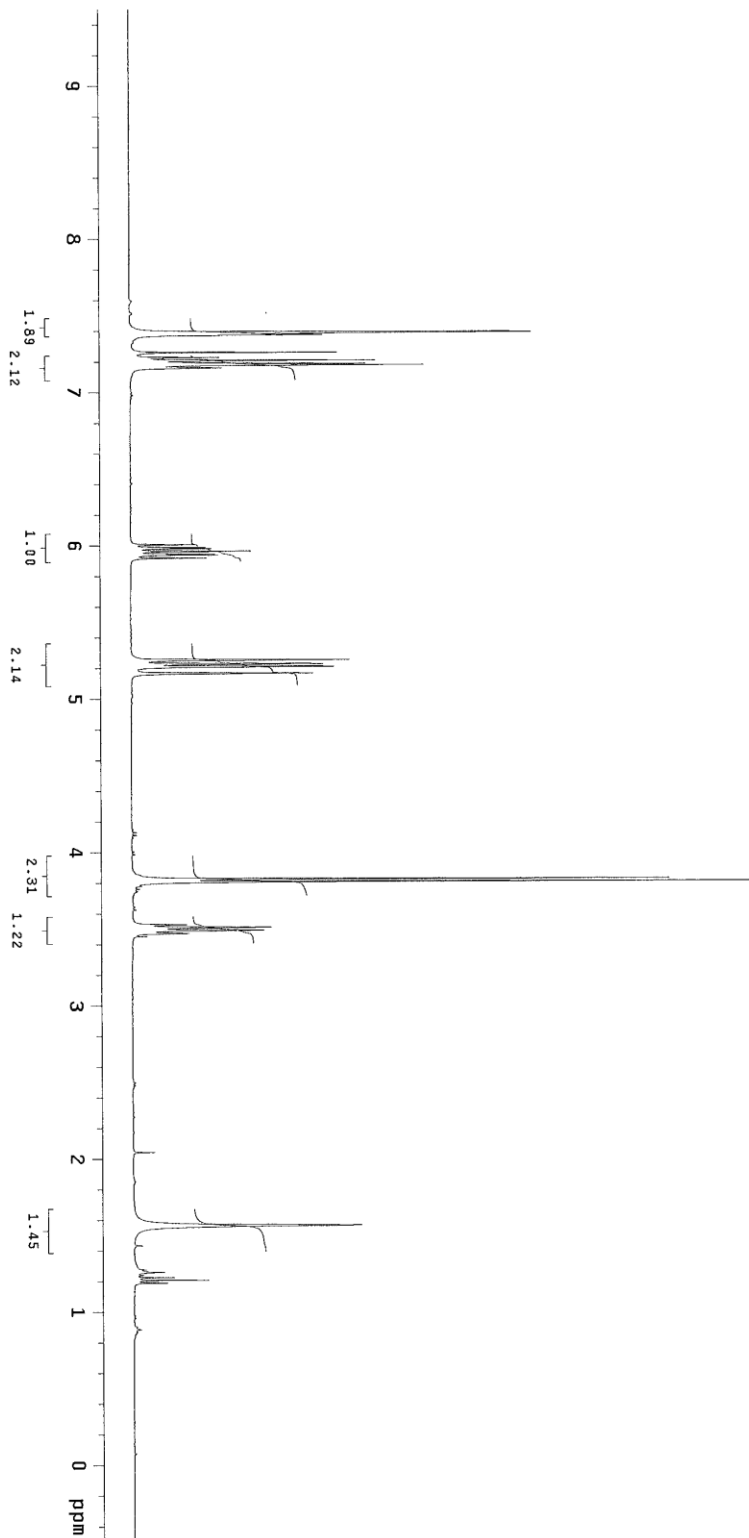
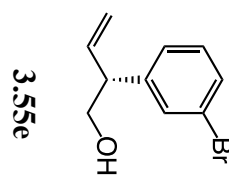
Sample Name: s3-11-13-c2-oxi-pro
Data File: vmp13-vmpf40
Archive directory:
Sample directory:
Fidfile: PROTON
Pulse Sequence: PROTON (szpu1)
Signal(s) used:
Data collected on: Sep 3 2014



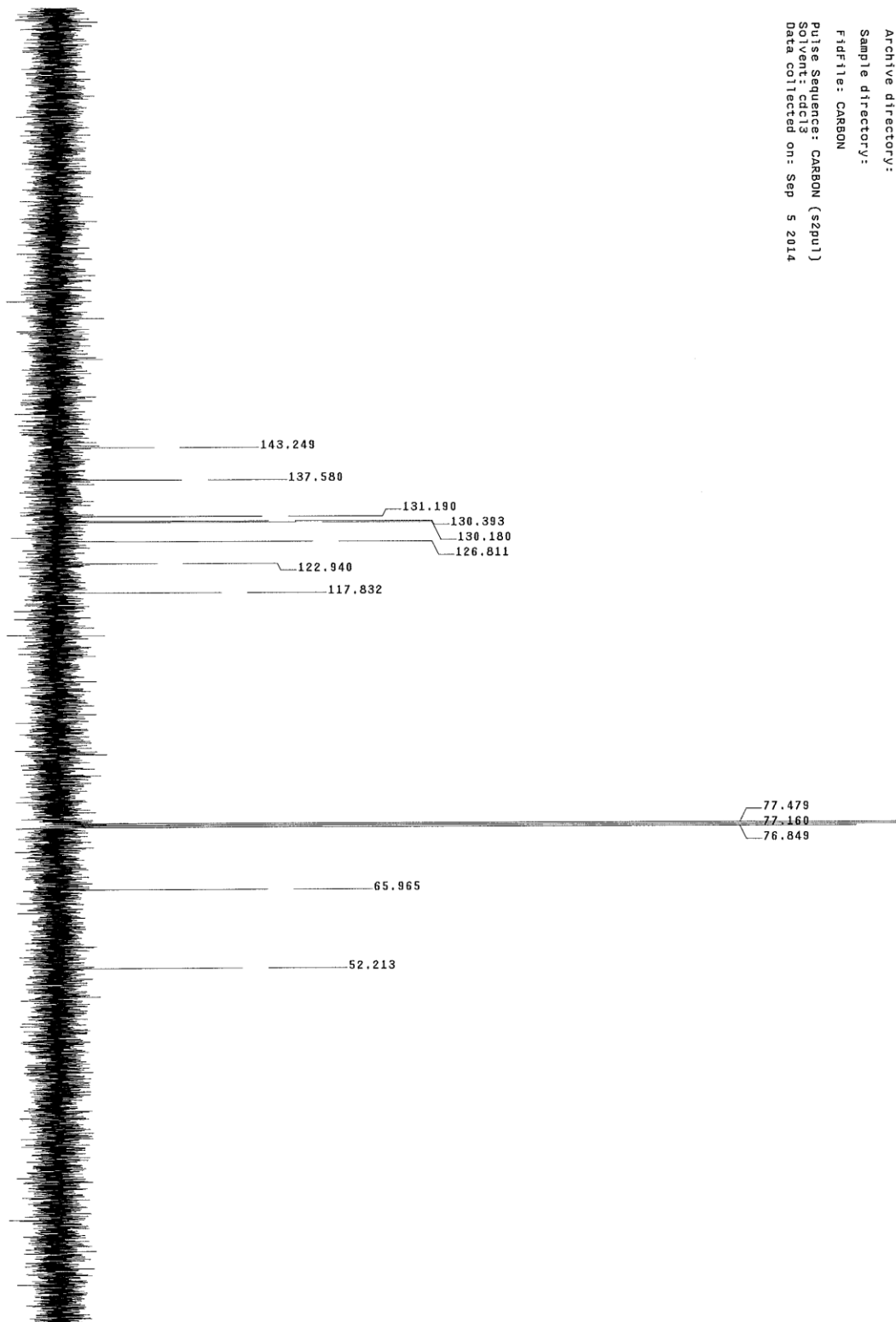
Sample Name: sy-ii-119-cl-pro
Data Collected on: vnm-13-vnm-s400
Archive directory:
Sample directory:
Fidfile: CARBON
Pulse Sequence: CARBON (szpu1)
Solvent: cdcl3
Data collected on: Aug 26 2014



Sample Name: sy-II-122-cl-pro
 Data Collected on: Thu Jul 10 14:40
 Archive directory:
 Sample directory:
 F1dF11e: PROTON
 Pulse Sequence: PROTON (s2pu1)
 Solvent: cdcl3
 Data collected on: Sep 5 2014



Sample Name: sy-11-12-c1-pro
Data Collected on: 09/05/2014
Archive Path: /data/09/05/2014
Archive directory:
Sample directory:
Fid file: CARBON
Pulse Sequence: CARBON (szpu1)
Solvent: cdcl3
Data collected on: Sep 5 2014



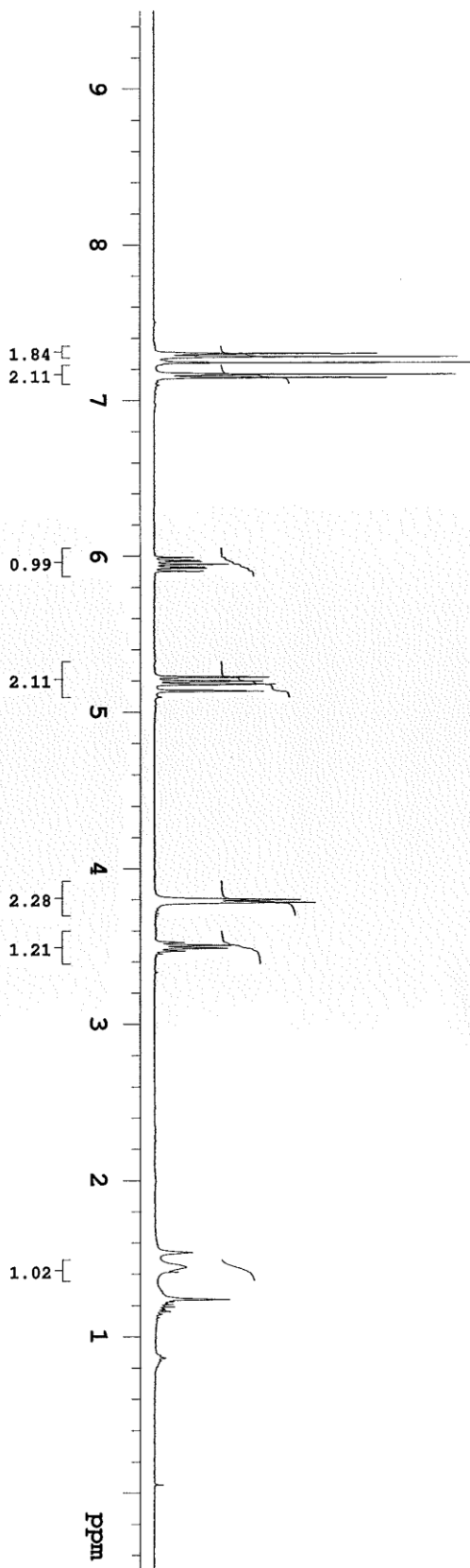
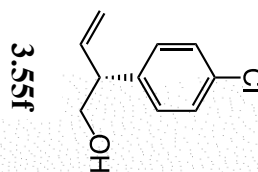
H¹-IX-59-crude5
Jan. 07.16

Sample Name:
sy-III-Cl-boh
Data Collected on:
nmr13-vnmrs400
Archive directory:

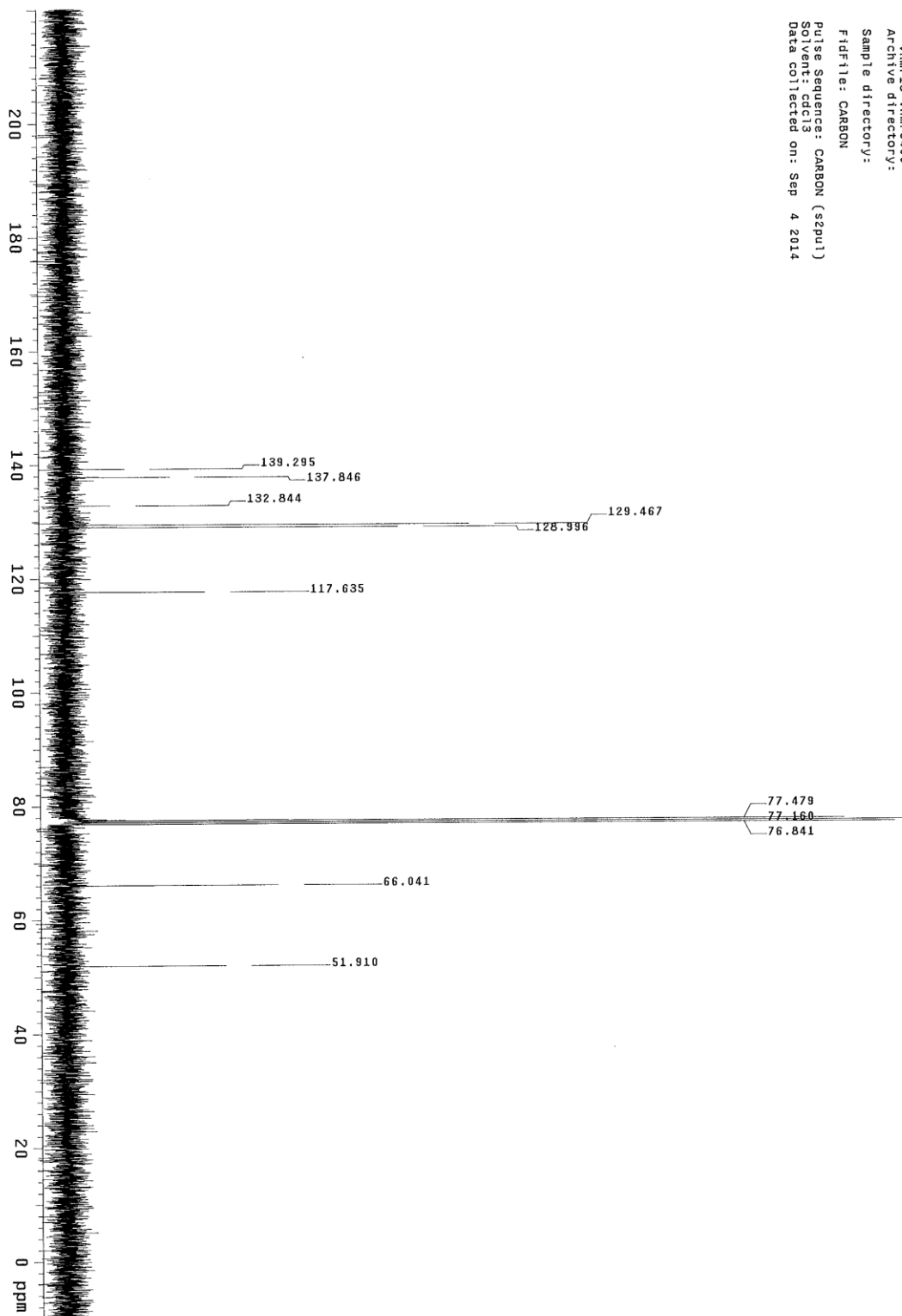
Sample directory:

FidFile: PROTON

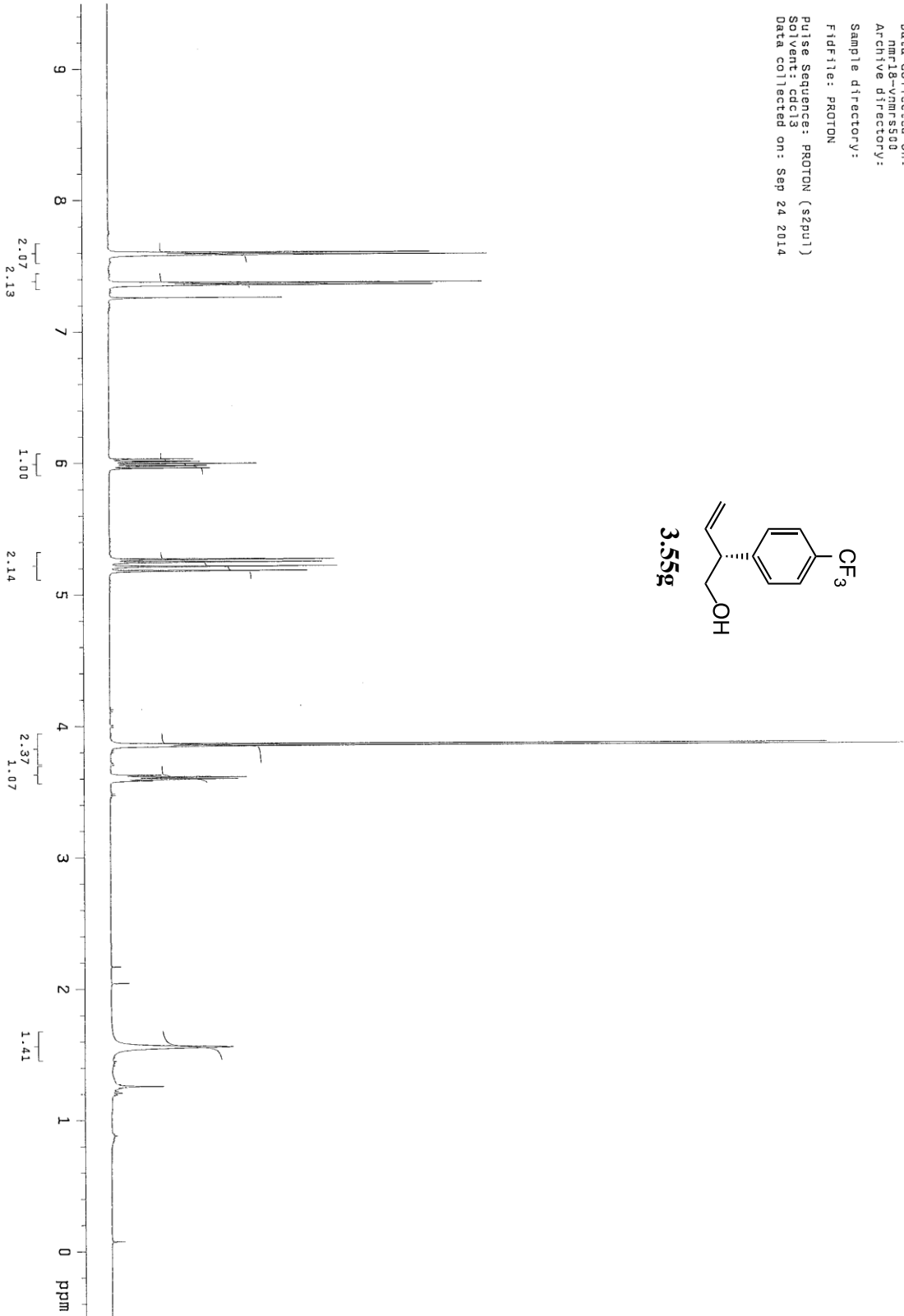
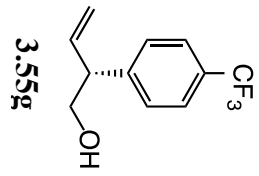
Pulse Sequence: PROTON (s2pul)
Solvent: cdcl3
Data collected on: Jan 7 2016



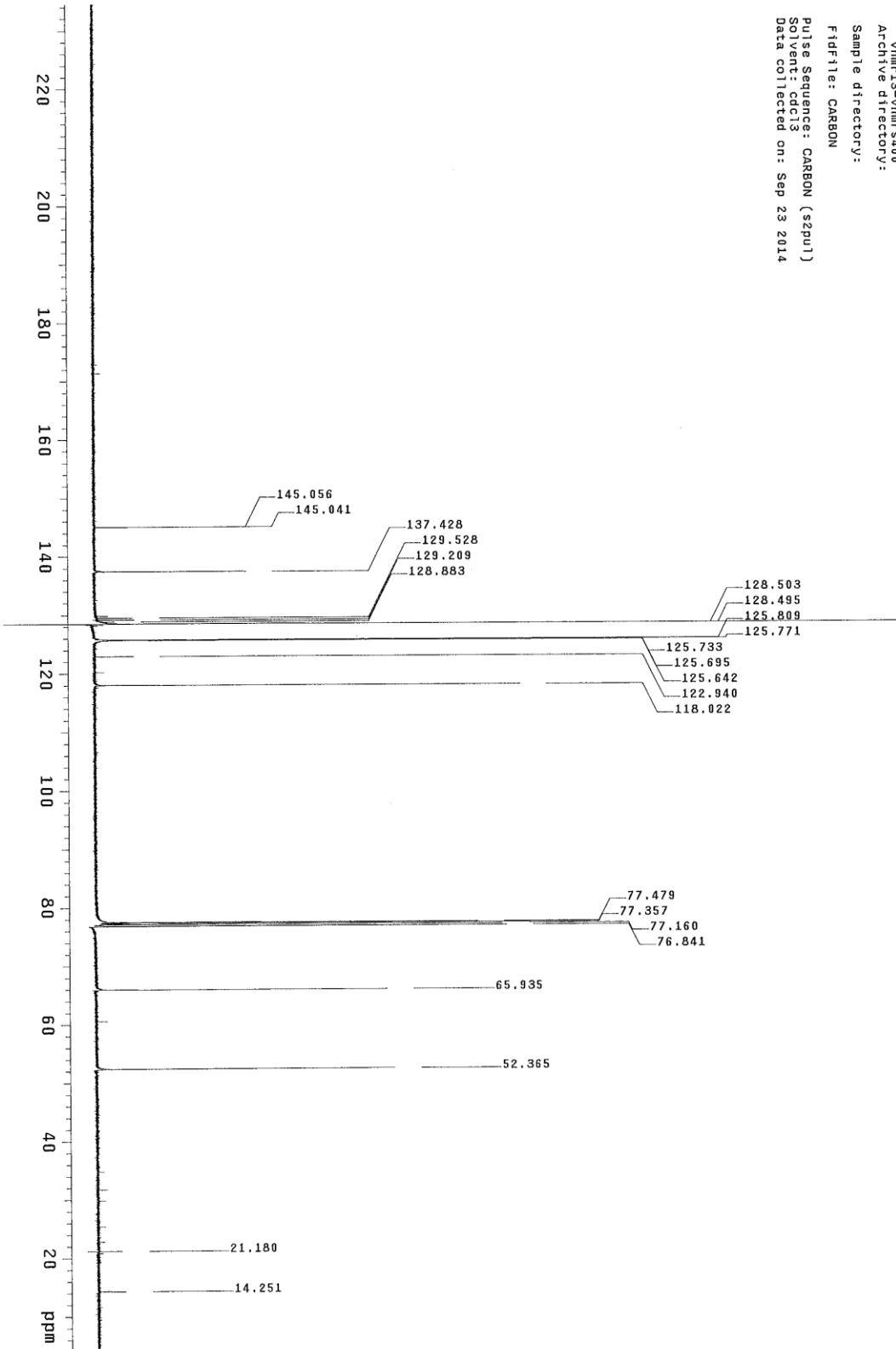
Sample Name: sp-11-11-20-01-pro
Data Collected on: vnmr13-vnmrs400
Archive directory:
Sample directory:
Fidfile: CARBON
Pulse Sequence: CARBON (szpu1)
Solvent: cdcl3
Data collected on: Sep 4 2014



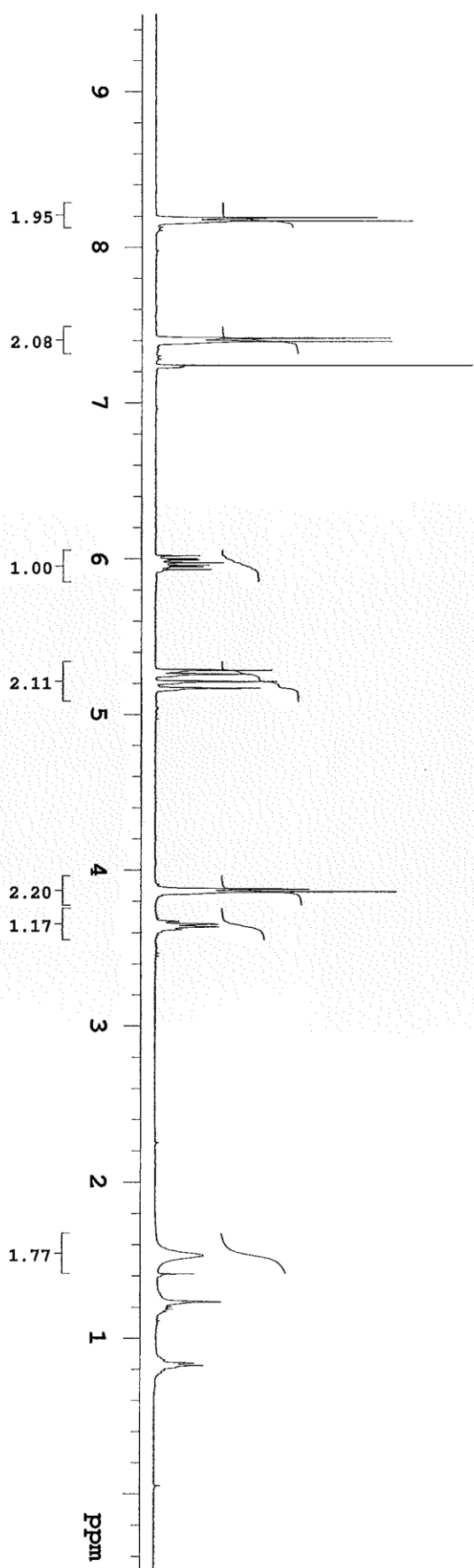
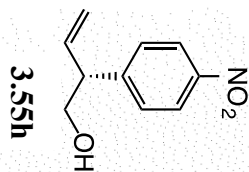
Sample Name: sy-111-128-a1-pro
Data Collected On: mri18-vnmr-s00
Archive directory:
Sample directory:
Fidfile: PROTON
Pulse Sequence: PROTON (s2pu1)
Solvent: cdcl3
Data collected on: Sep 24 2014



Sample Name: sv-III-128-a1-pro
Data Collected on: vnmr-13-vnmr5400
Archive directory:
Sample directory:
FidFile: CARBON
Pulse Sequence: CARBON (s2pu1)
Solvent: dcd13
Data collected on: Sep 23 2014



Sample Name: sy-III-no2-boh
Data Collected on: nmr13-vnmrs400
Archive directory:
Sample directory:
Fidfile: PROTON
Pulse Sequence: PROTON (s2pu1)
Solvent: cdcl3
Data collected on: Jan 7 2016



XCF-II-141-3

Sample Name:

sy-III-NO2-p_OH_

Data Collected on:

nmr19-vnmr5600

Archive directory:

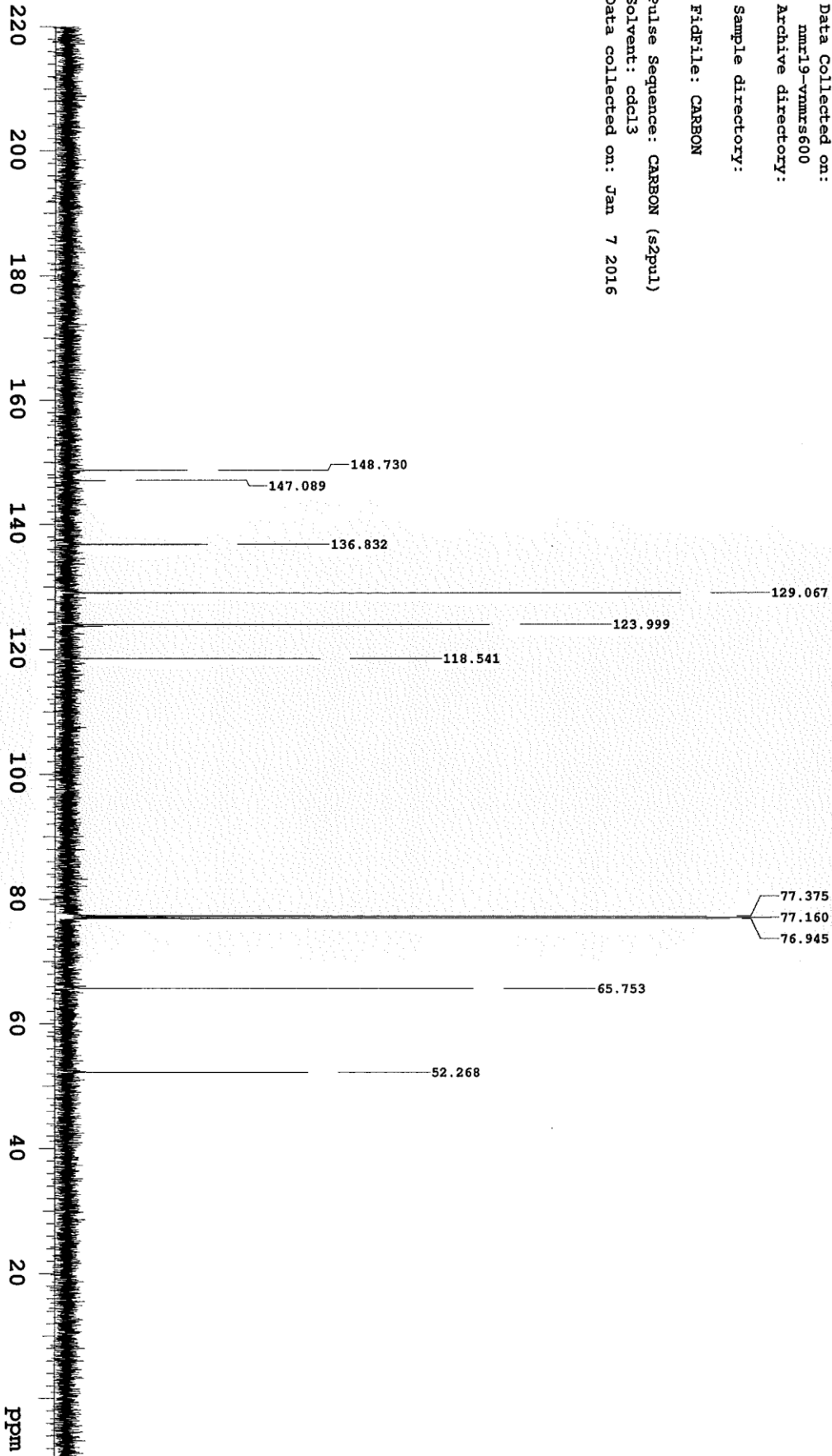
Sample directory:

FidFile: CARBON

Pulse Sequence: CARBON (s2pu1)

Solvent: cdcl3

Data collected on: Jan 7 2016



Agilent Technologies

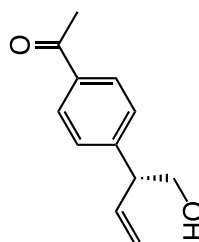
MJK-V-127A-1H, purified

Sample Name:
 sy-III-239-b1-pro
 Data Collected on:
 vnmr13-vnmrs400
 Archive directory:

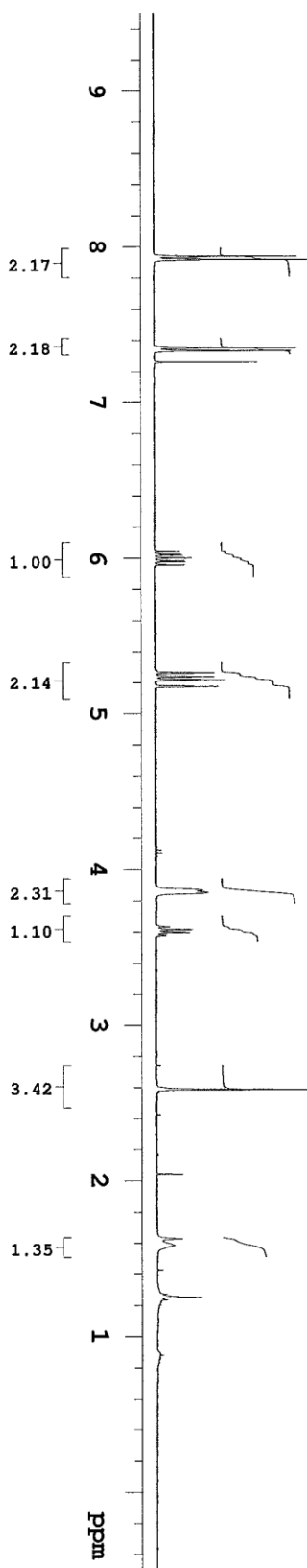
Sample directory:

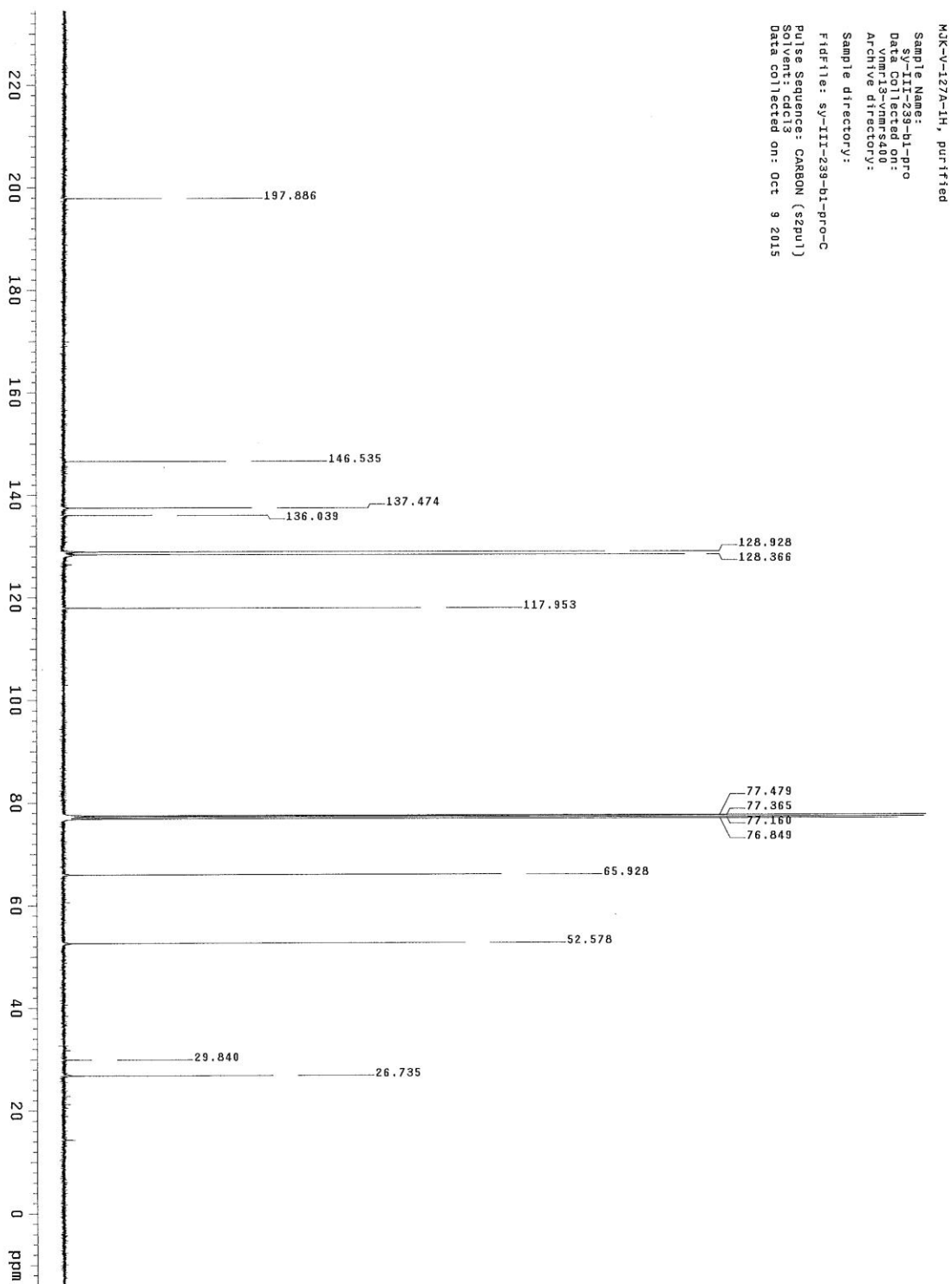
FidFile: sy-III-239-b1-pro

Pulse Sequence: PROTON (s2pul1)
 Solvent: cdcl3
 Data collected on: Oct 9 2015



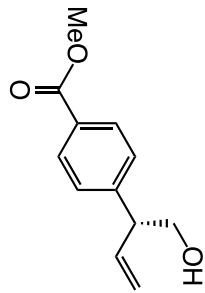
121





FV-I-264-13C
E-Cinn Imine
12/16/15

Sample Name:
sy-FV-45-5me2-1h-III-229-91-Pr2
Data Collected on:
nmr19-vmmr600
Archive directory:



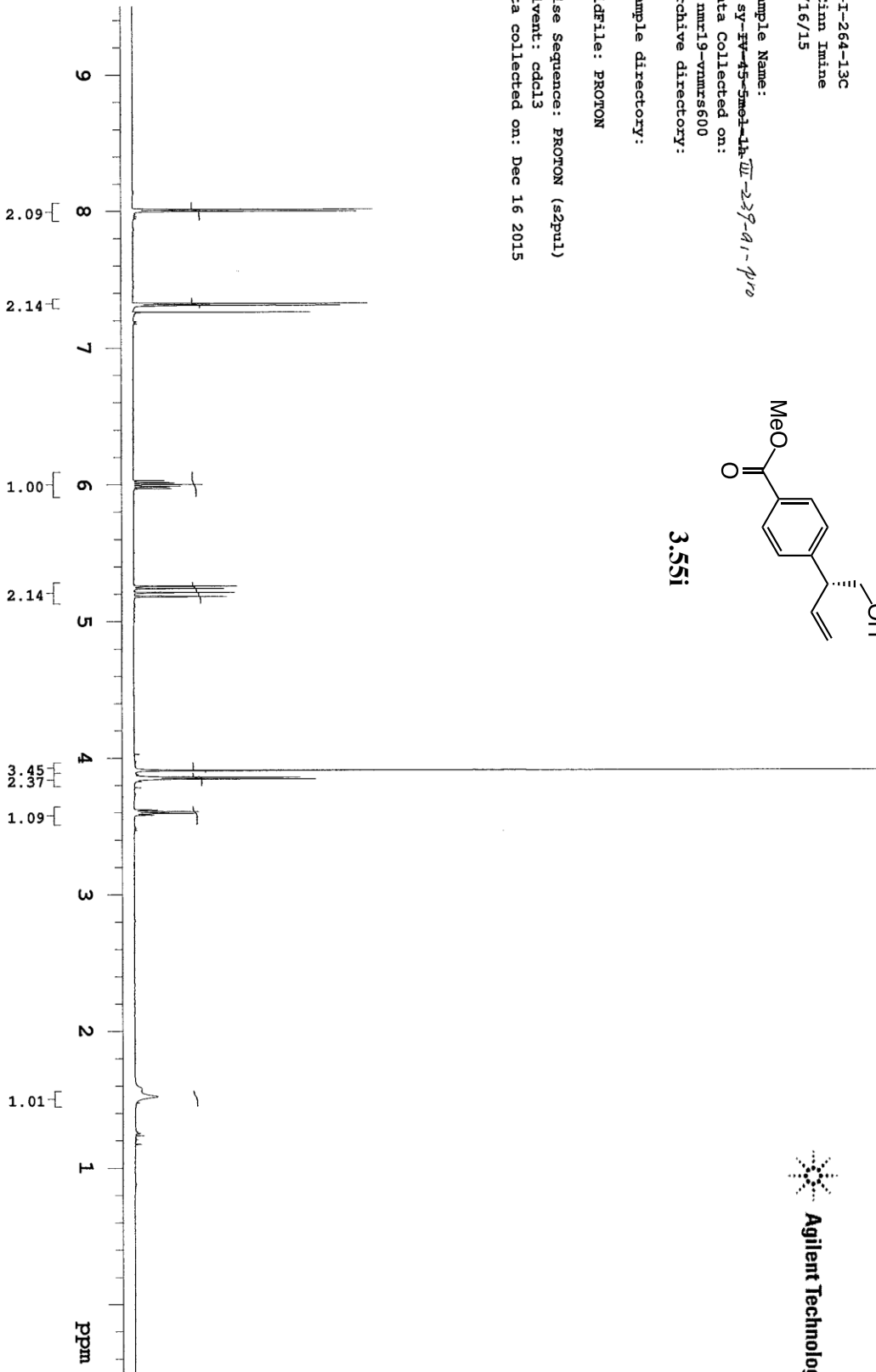
Sample directory:

FidFile: PROTON

Pulse Sequence: PROTON (s2pu1)

Solvent: cdcl3

Data collected on: Dec 16 2015



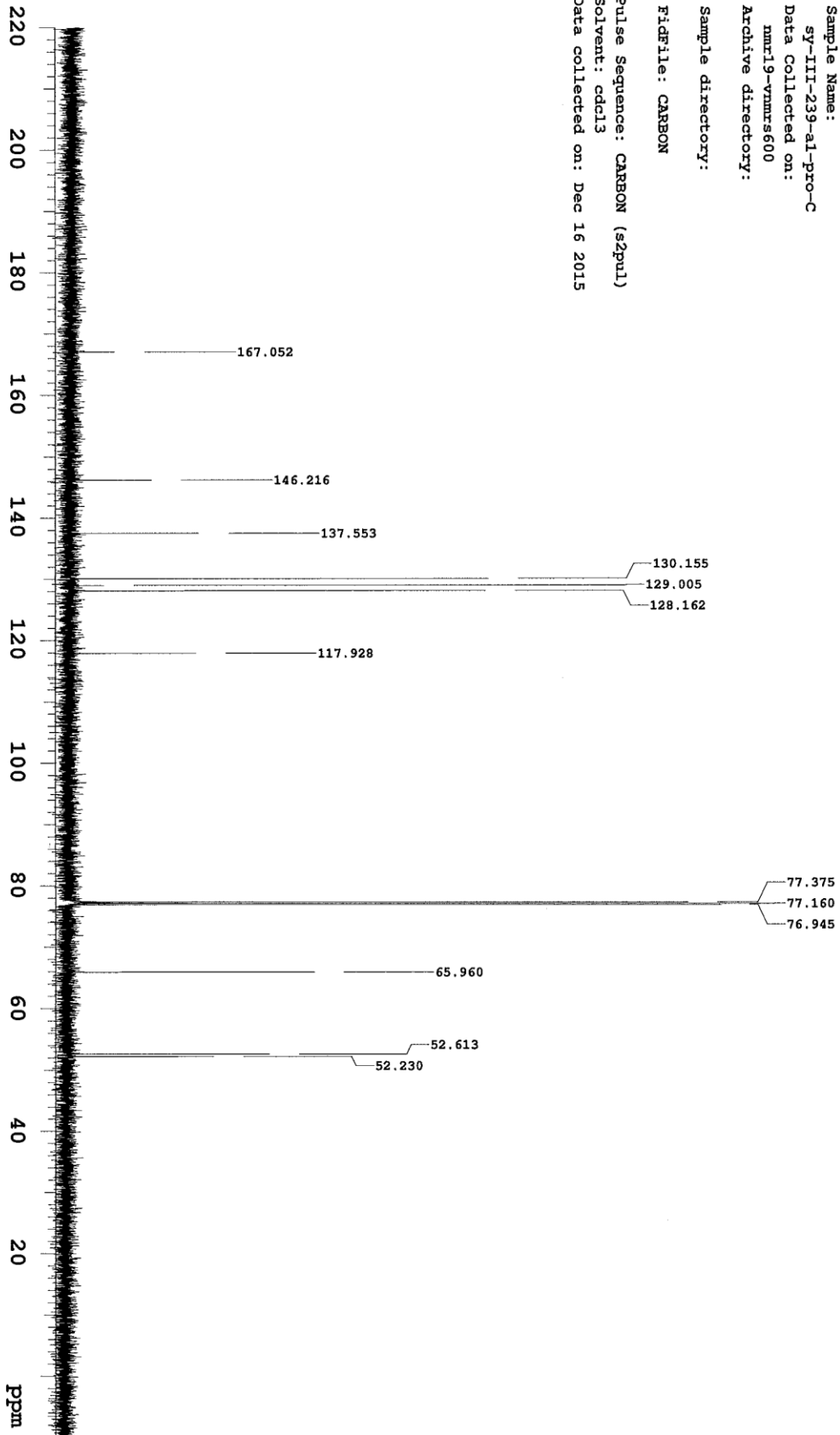
FV-I-264-13C
H-Cinn Imine
12/16/15

Sample Name:
sy-III-239-a1-pro-C
Data Collected on:
nmr19-vnmrs600
Archive directory:

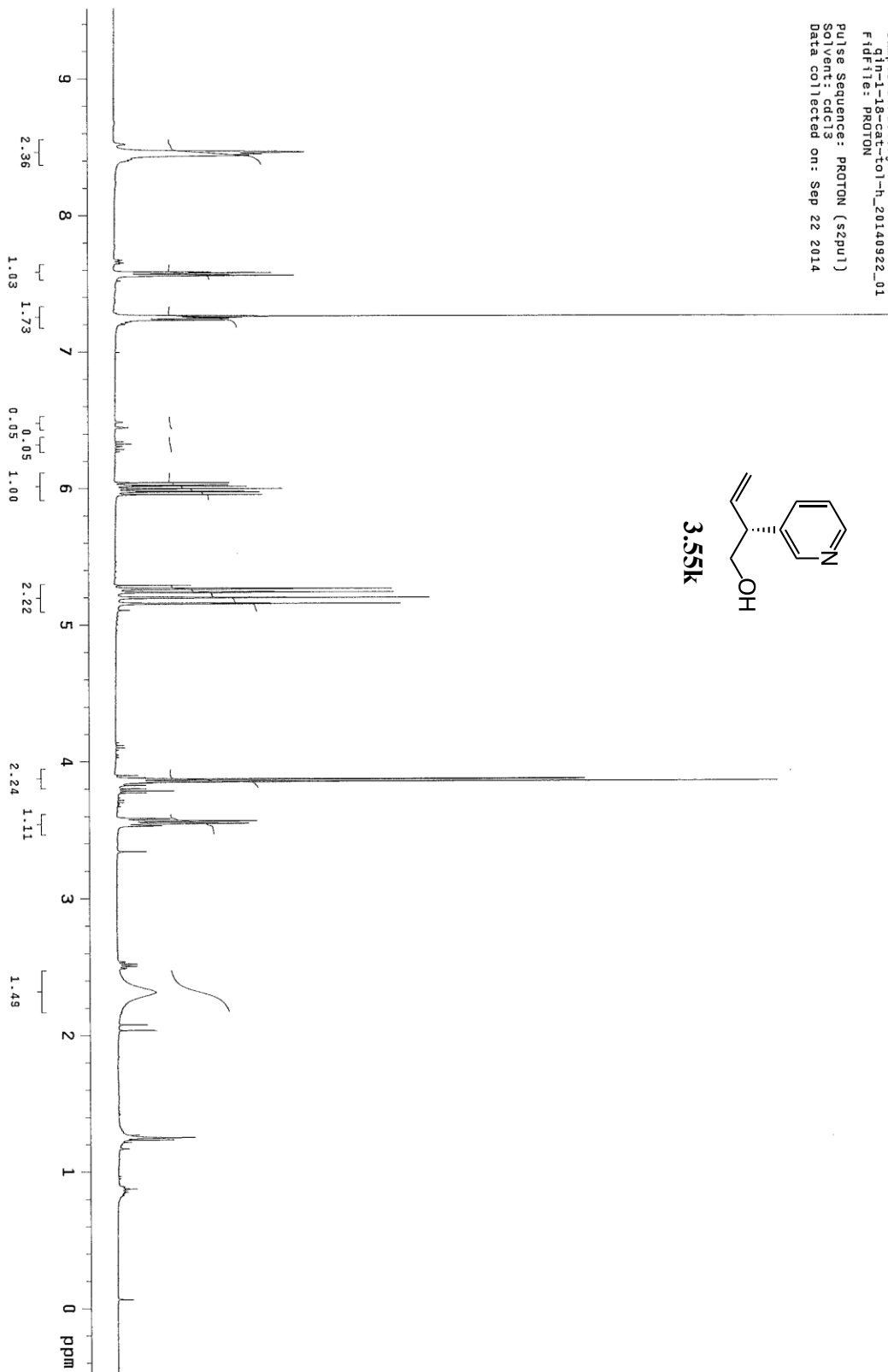
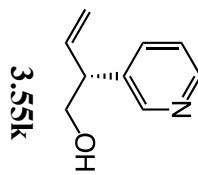
Sample directory:

FidFile: CARBON

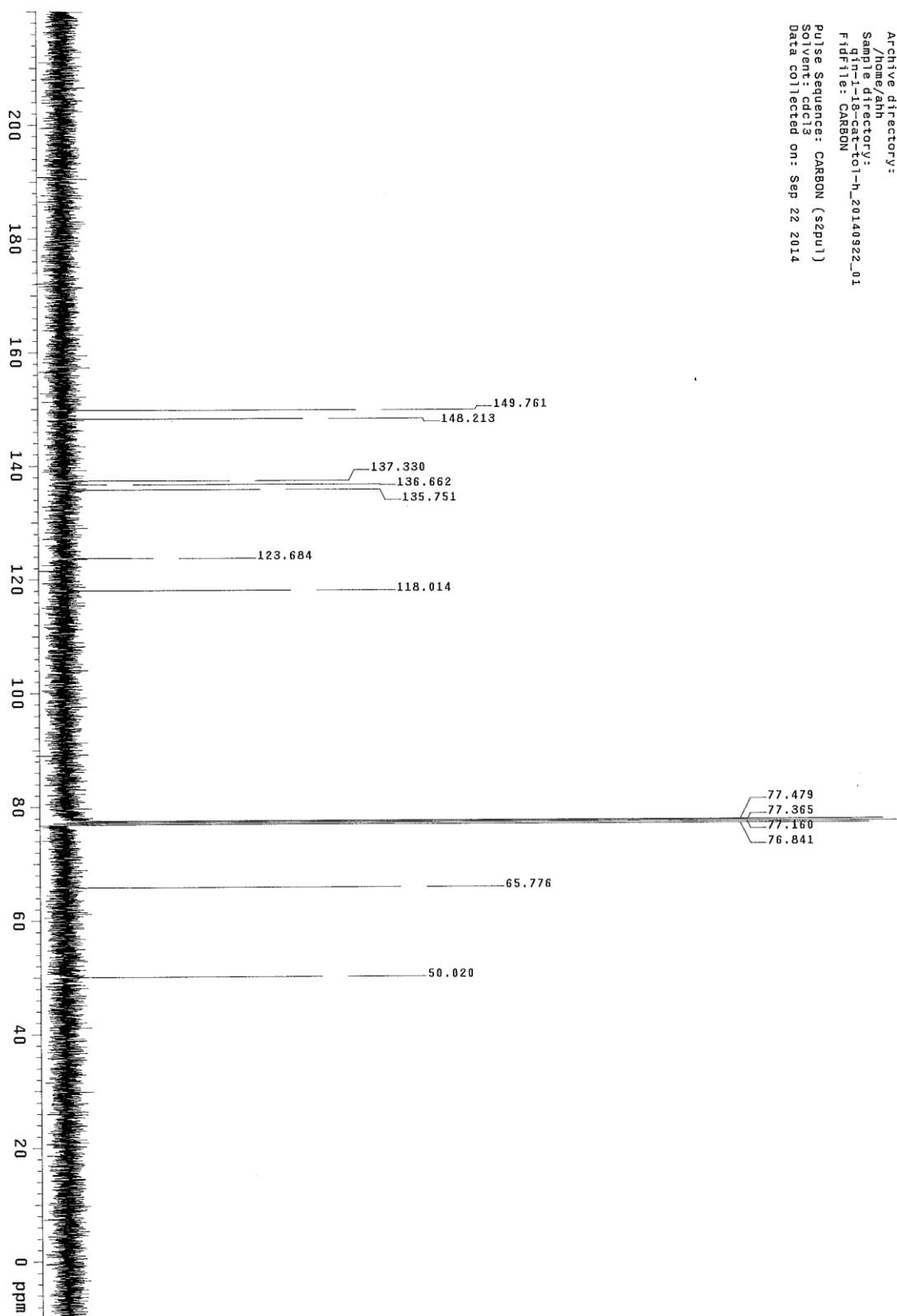
Pulse Sequence: CARBON (s2pul)
Solvent: cdcl3
Data collected on: Dec 16 2015



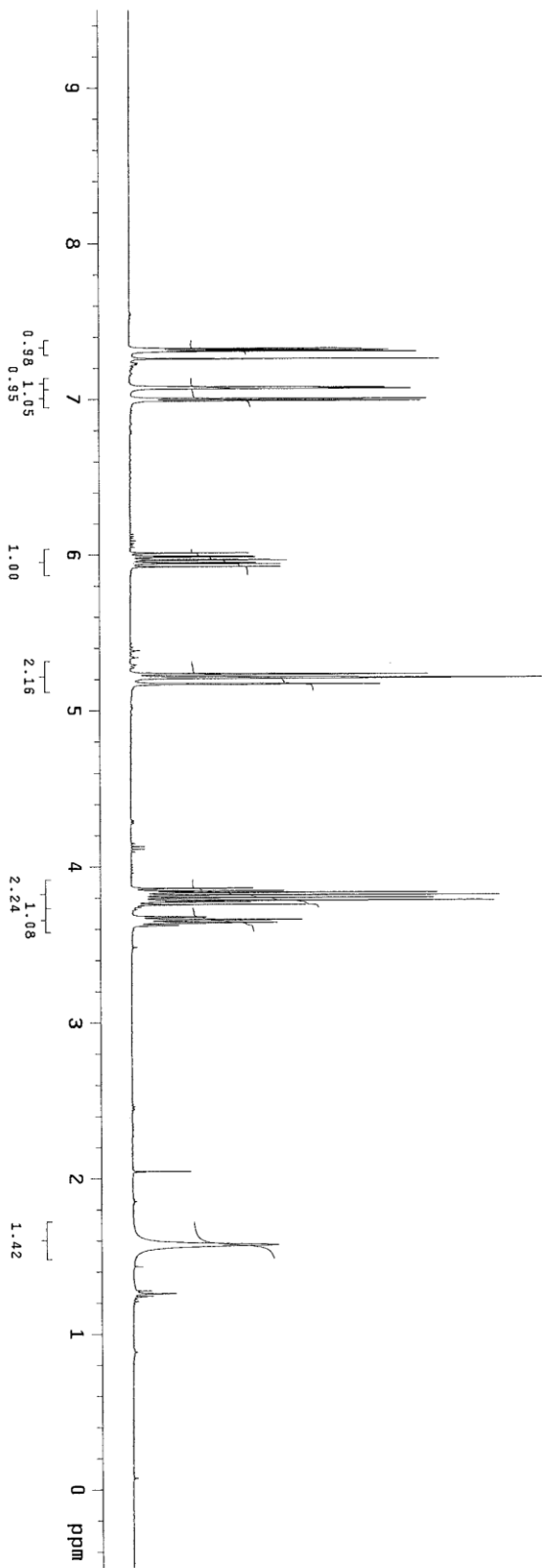
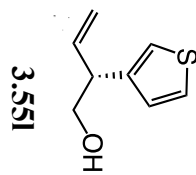
Sample Name: SY-TII-128-cl-pro
 Data Collected on: vnmr13-vnmrs400
 Archive directory: /home/ahh
 Sample directory: qh-18-cat-to1-h_20140922_01
 Fdfile: PROTON
 Pulse Sequence: PROTON (szpu1)
 Solvent: cdcl3
 Data collected on: Sep 22 2014



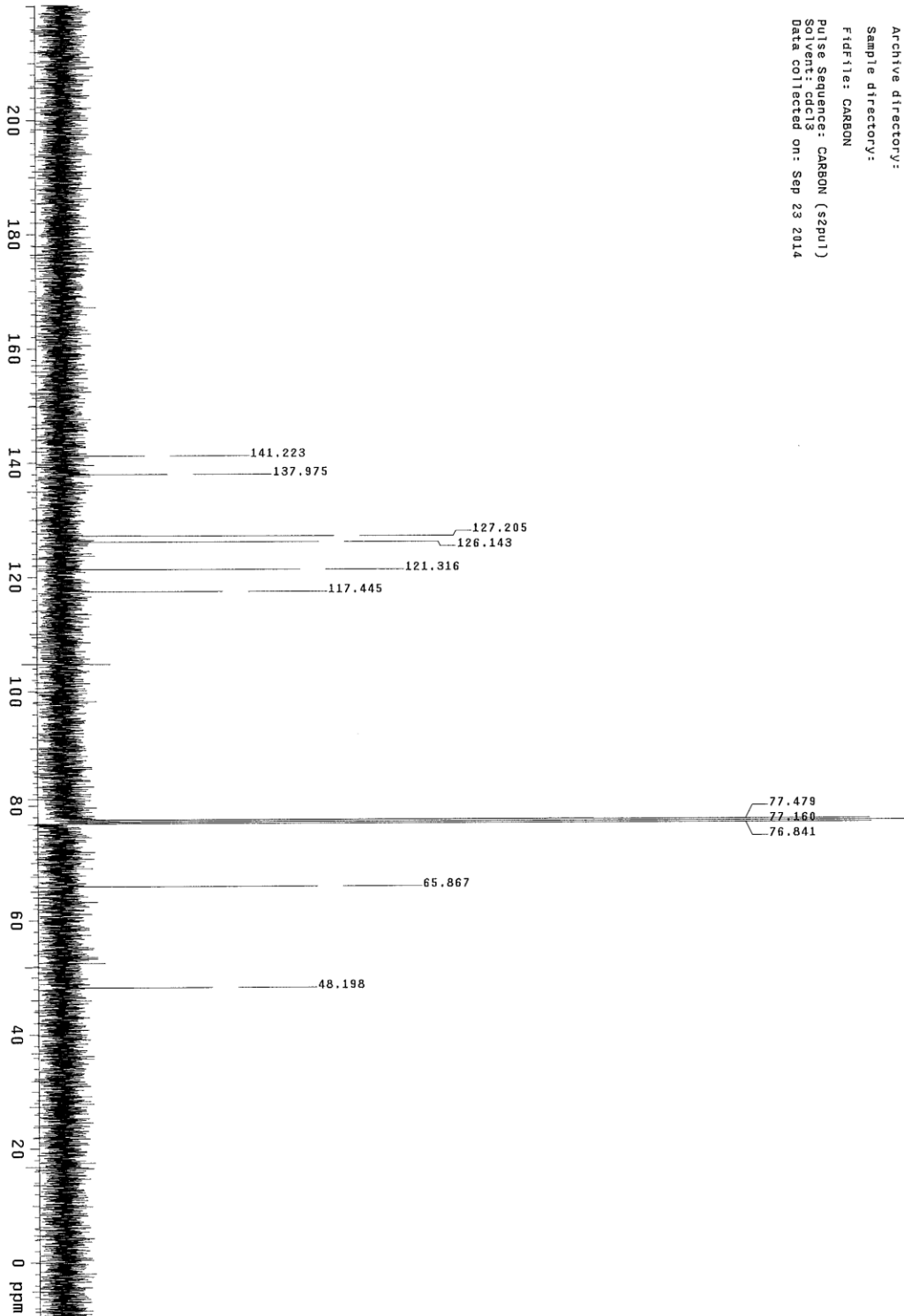
--SY-11-128-cl-pro
Data Collected on:
vnmr13-vnmr5400
Archive directory:
/home/anh
Sample directory:
q1h-18-cat-1-h_20140922_01
FidFile: CARBON
Pulse Sequence: CARBON (zgpg1)
Solvent: cdcl3
Data collected on: Sep 22 2014



Sample Name: sy-III-128-d2-pro
Data Collected on: 09/23/2014 13:40
Archive directory:
Sample directory:
FIDFile: sy-III-128-d2-pro
Pulse Sequence: PROTON (s2pu1)
Solvent: cdcl3
Data collected on: Sep 23 2014

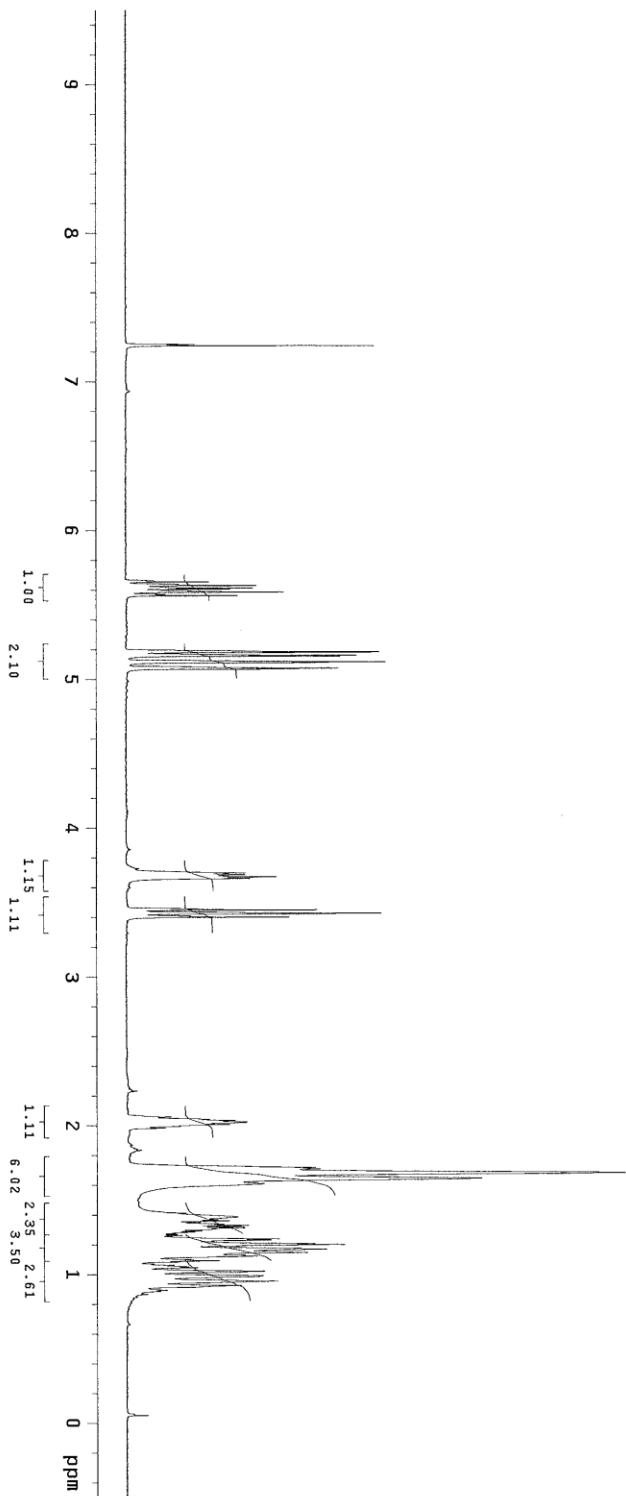
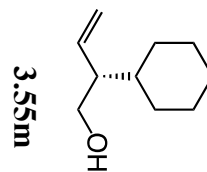


Sample Name: SY-III-128-d2-pro
Data Collected on: VMMS-VMMS408
Archive directory: Sample directory:
Fidfile: CARBON
Pulse Sequence: CARBON (s2pu1)
Solvent: cdc13
Data collected on: Sep 23 2014



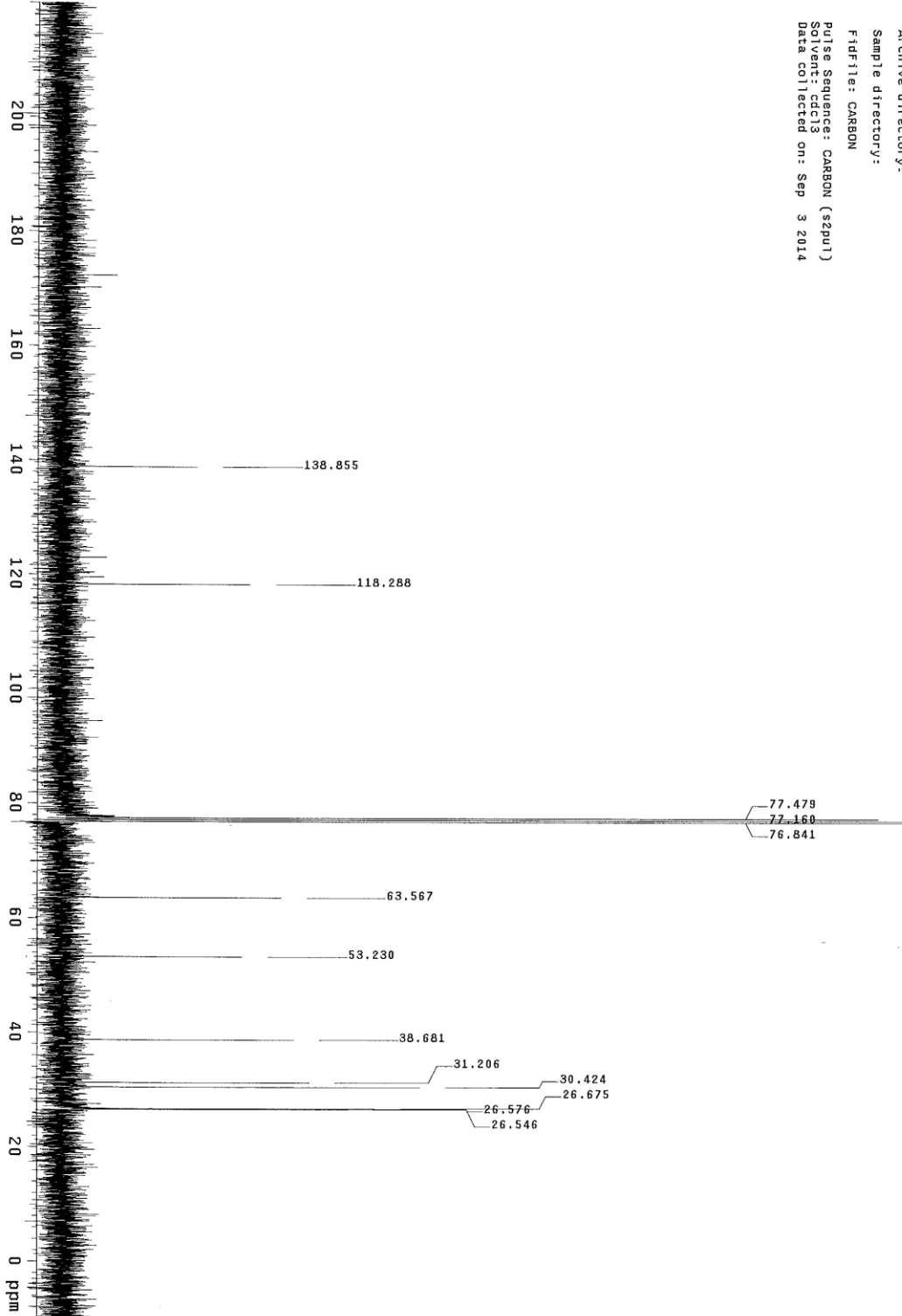
STANDARD FLUORINE PARAMETERS

Sample Name: SY-IT-120-C2-oxi-pro
 Date Collected on: Vnmr13-vnmr5400
 Archive directory:
 Sample directory:
 F1dfile: PROTON
 Pulse Sequence: PROTON (szpu1)
 Solvent: cdcl3
 Data collected on: Sep 3 2014

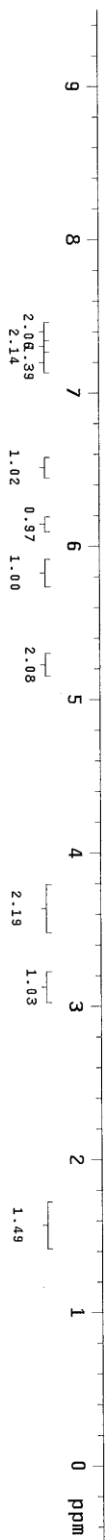
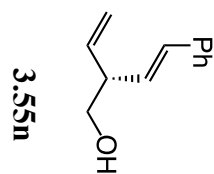


STANDARD FLUORINE PARAMETERS

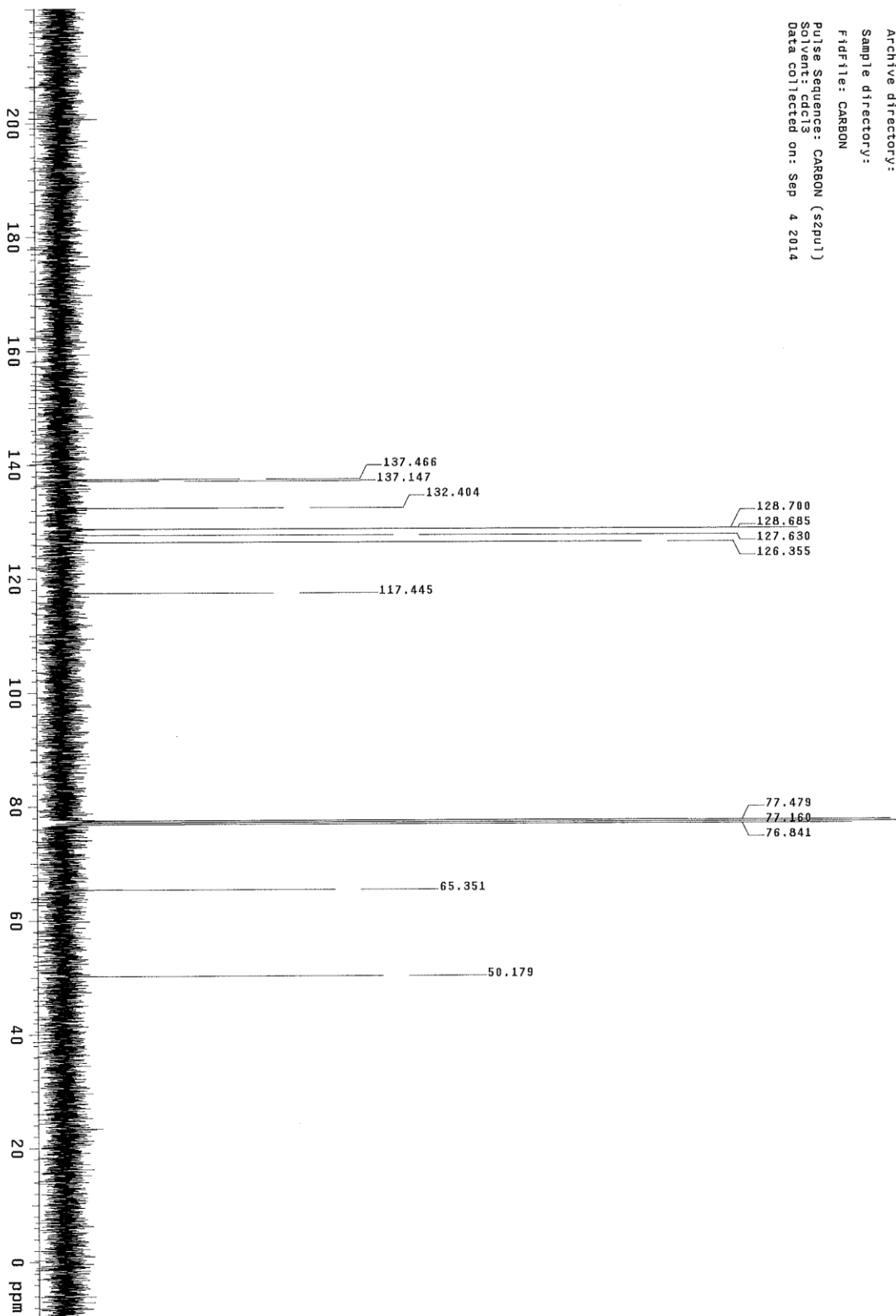
Sample Name: sy-11-120-cl-oxi-pro
Data Collected on: vnmr13-vnmrs400
Archive directory:
Sample directory:
Fidfile: CARBON
Pulse Sequence: CARBON (szpu1)
Solvent: cdcl3
Data collected on: Sep 3 2014



Sample Name: sv-111-122-al-pro
 Data Collected on: vnmr13-vnmrs400
 Archive directory:
 Sample directory:
 F1dfile: PROTON
 Pulse Sequence: PROTON (szpu1)
 Solvent: cdcl3
 Data collected on: Sep 4 2014



Sample Name: sy-11-12-ai-pro
Data Collected on: vnmr3-vnmr5400
Archive directory:
Sample directory:
Fidfile: CARBON
Pulse Sequence: CARBON (zgpg1)
Solvent: cdcl3
Data collected on: Sep 4 2014



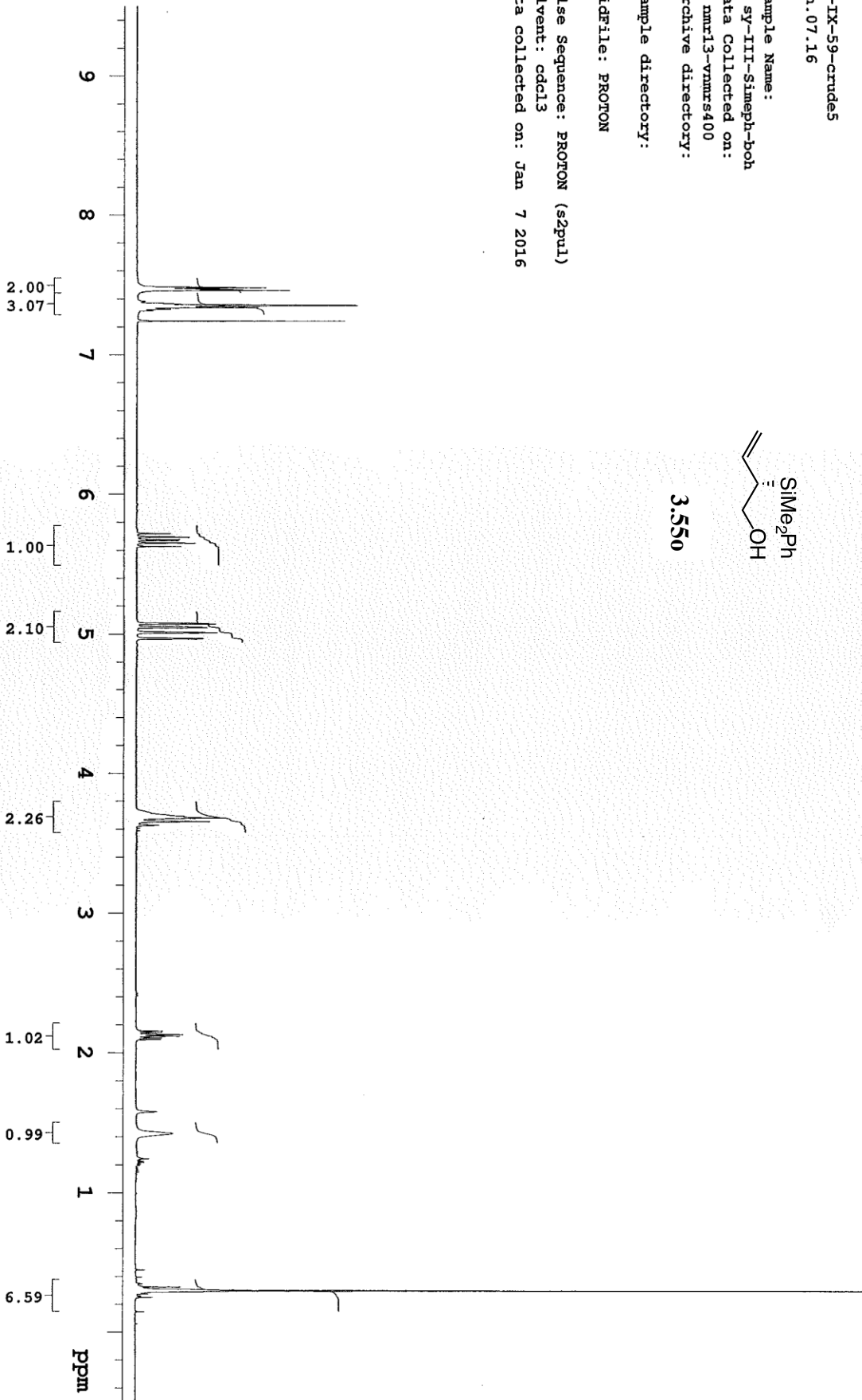
HJ-IX-59-crudes
Jan. 07.16

Sample Name:
sy-III-Simeph-boh
Data Collected on:
nmr13-vmmrs400
Archive directory:

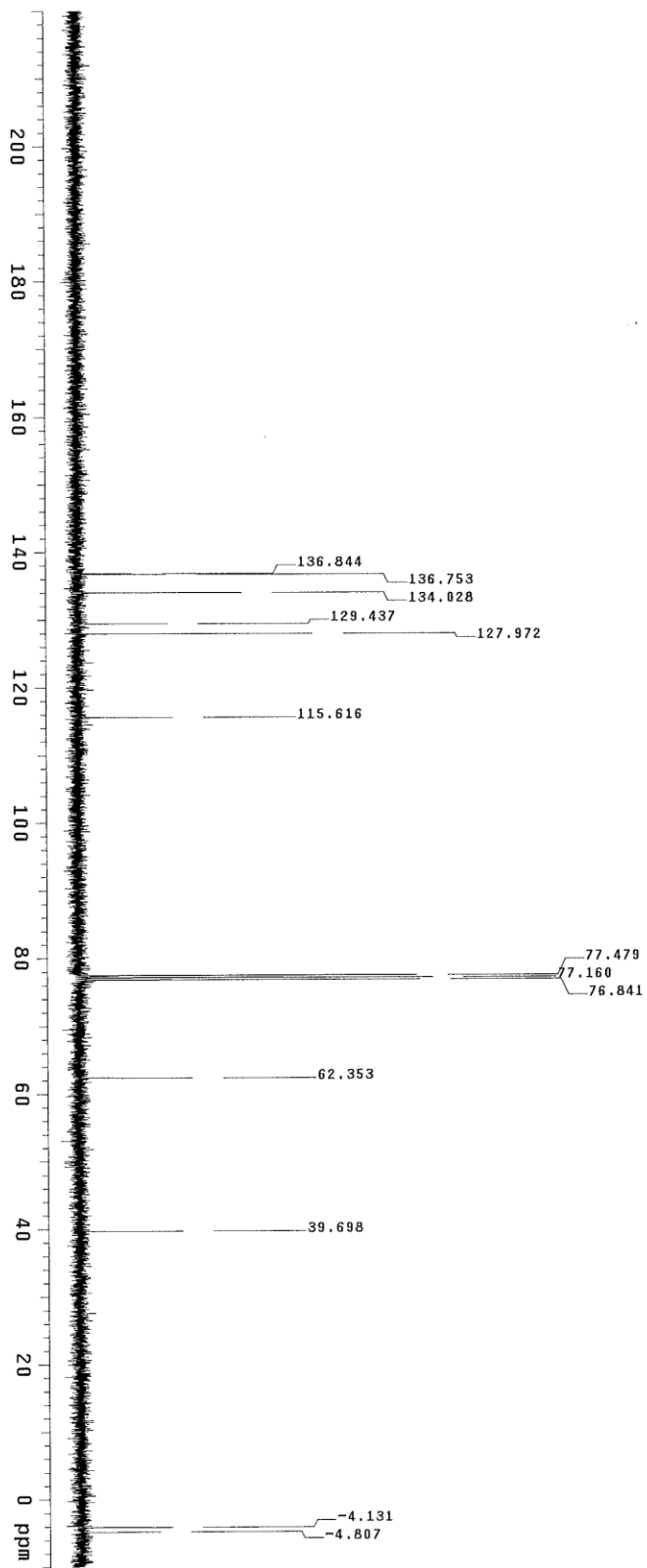
Sample directory:

FidFile: PROTON

Pulse Sequence: PROTON (s2pu1)
Solvent: cdcl3
Data collected on: Jan 7 2016



sv-III-120-d1-pro
Data Collected on:
vnmr13-vnmr540
Archive directory:
Sample directory:
F1DF11e: CARBON
Pulse Sequence: CARBON (szpu1)
Solvent: cdcl3
Data collected on: Sep 4 2014



Sample Name: sy-IV-62-pro
Data Collected on: mmr13-vnmrs400
Archive directory:

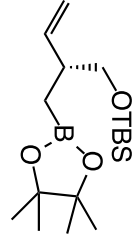
Sample directory:

F1DF1le: PROTON

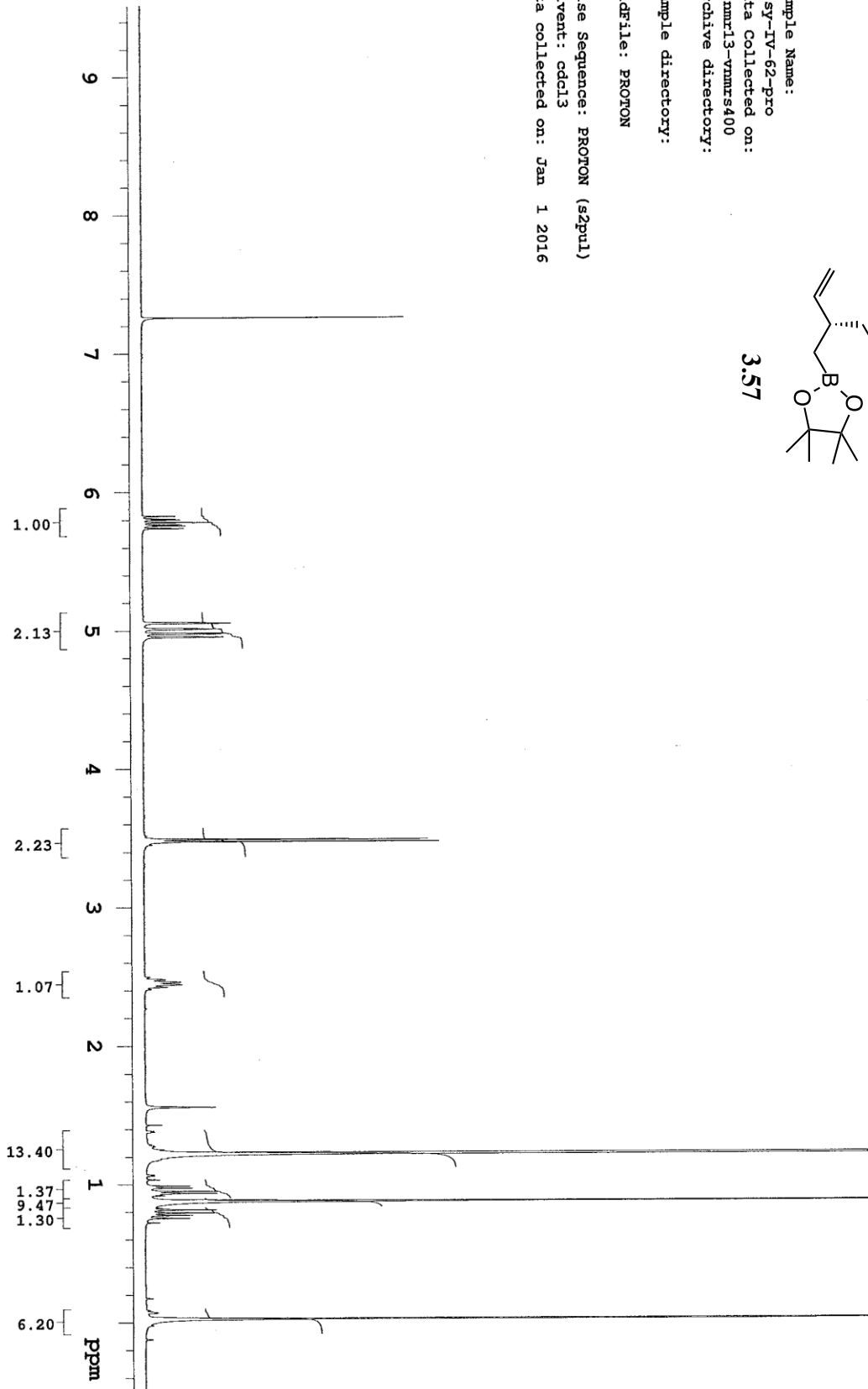
Pulse Sequence: PROTON (szpul)

Solvent: cdcl3

Data collected on: Jan 1 2016



3.57



MM-6-236crude2weeks

Sample Name:

Data Collected on:

nmr19-vmr600

Archive directory:

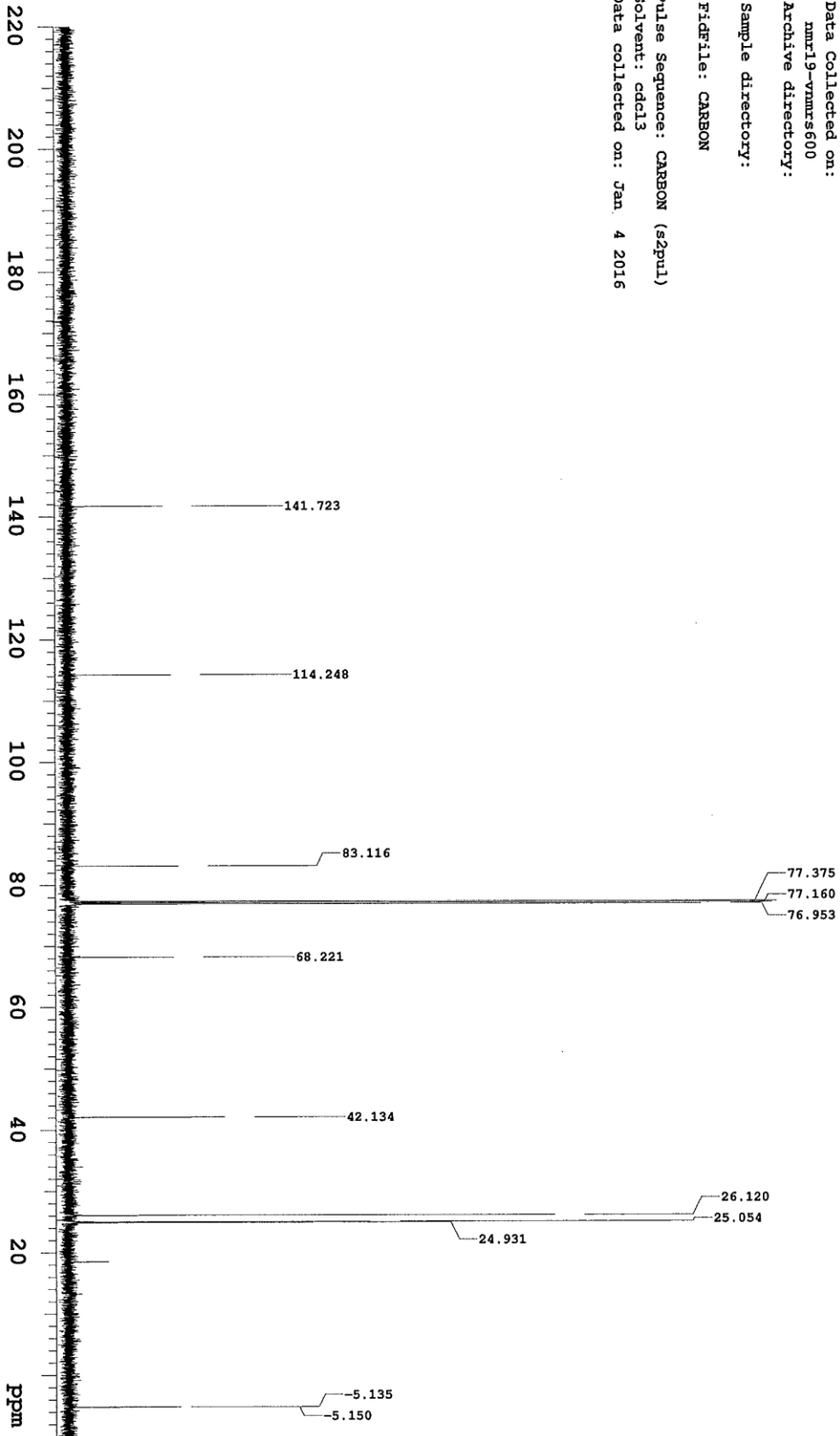
Sample directory:

F1File: CARBON

Pulse Sequence: CARBON (s2pul)

Solvent: cdcl3

Data collected on: Jan. 4 2016



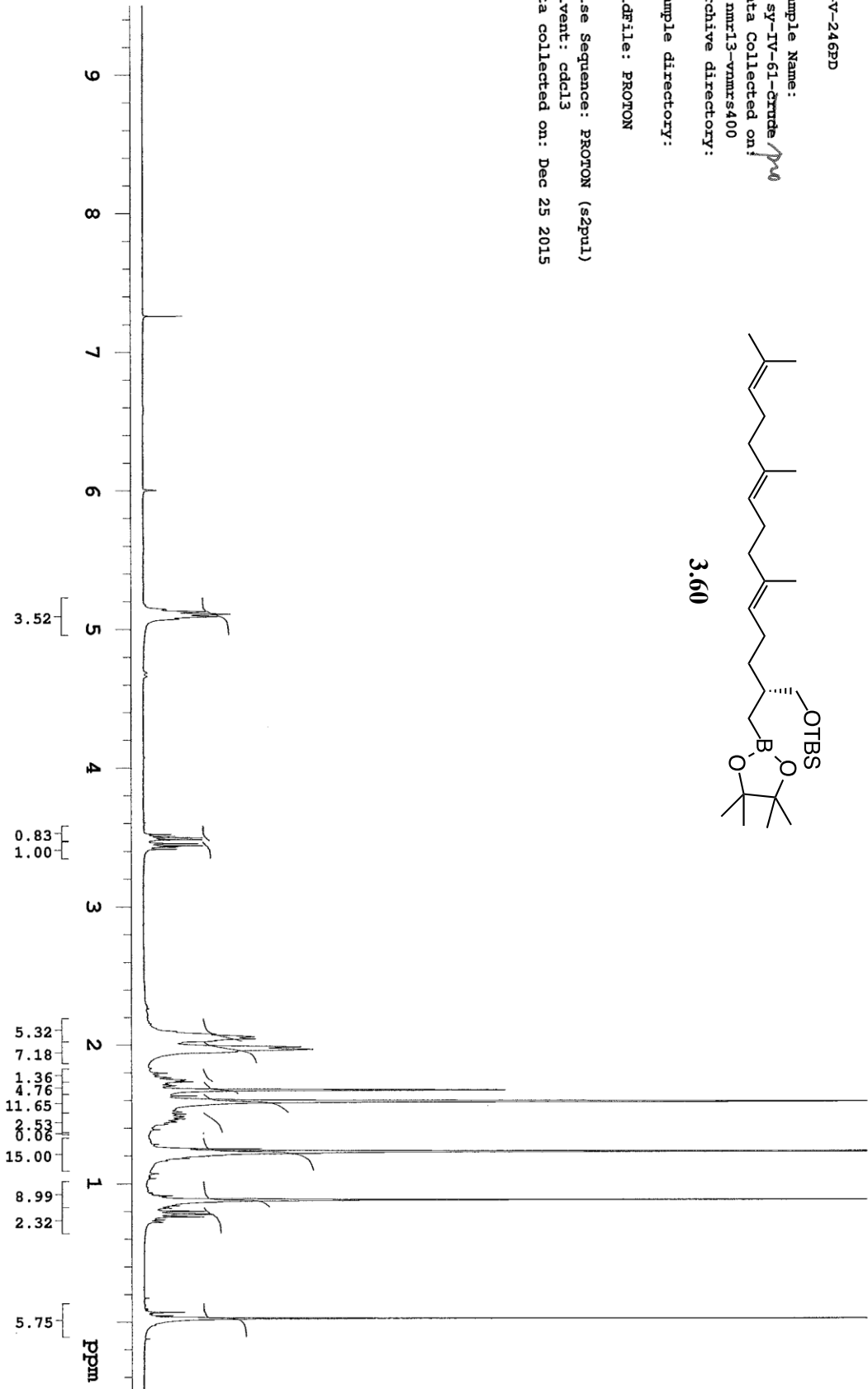
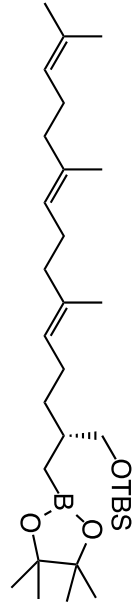
SR-V-246PD

Sample Name:
 sy-IV-61-Grude *pu*
 Data Collected on:
 nm13-vnmrs400
 Archive directory:

Sample directory:

F1F1file: PROTON

Pulse Sequence: PROTON (s2pu1)
 Solvent: cdcl3
 Data collected on: Dec 25 2015



SR-V-246PD

Sample Name:

sy-IV-61-crude

Data Collected on:

nmr13-vnmr5400

Archive directory:

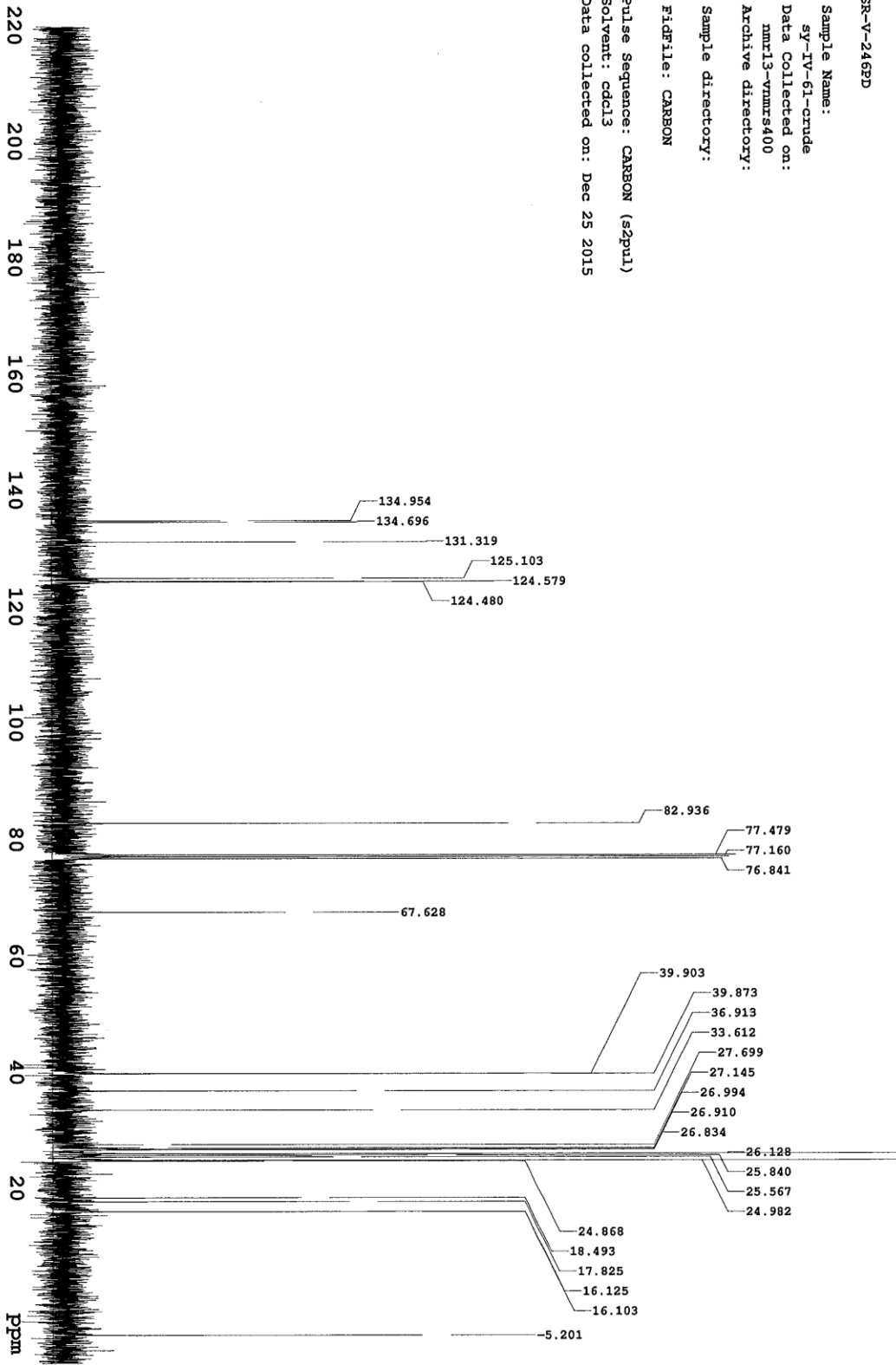
Sample directory:

F1dFile: CARBON

Pulse Sequence: CARBON (szpul)

Solvent: cdcl3

Data collected on: Dec 25 2015



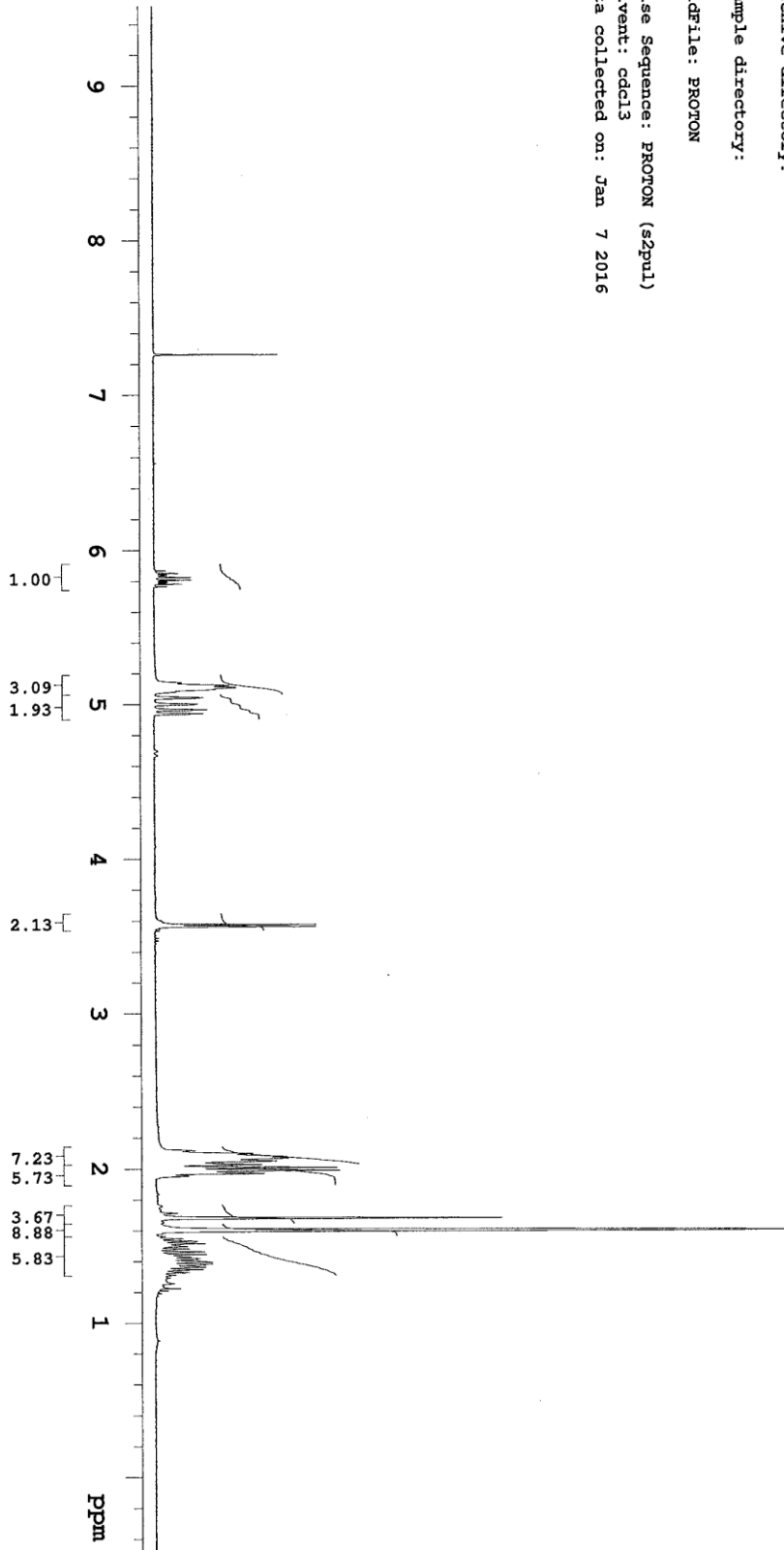
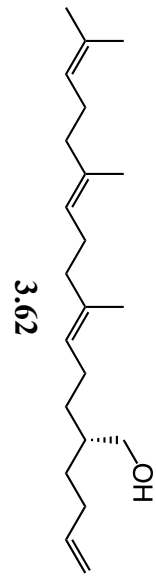
KS-01172H11quid

Sample Name:
sy-IV-72-d-pro
Data Collected on:
nmr13-vnmrs400
Archive directory:

Sample directory:

FidFile: PROTON

Pulse Sequence: PROTON (s2pul)
Solvent: cdcl3
Data collected on: Jan 7 2016



MJK-V-223B-19F, crude

Sample Name:

sy-IV_72-pro

Data Collected on:

nmr13-vmmrs400

Archive directory:

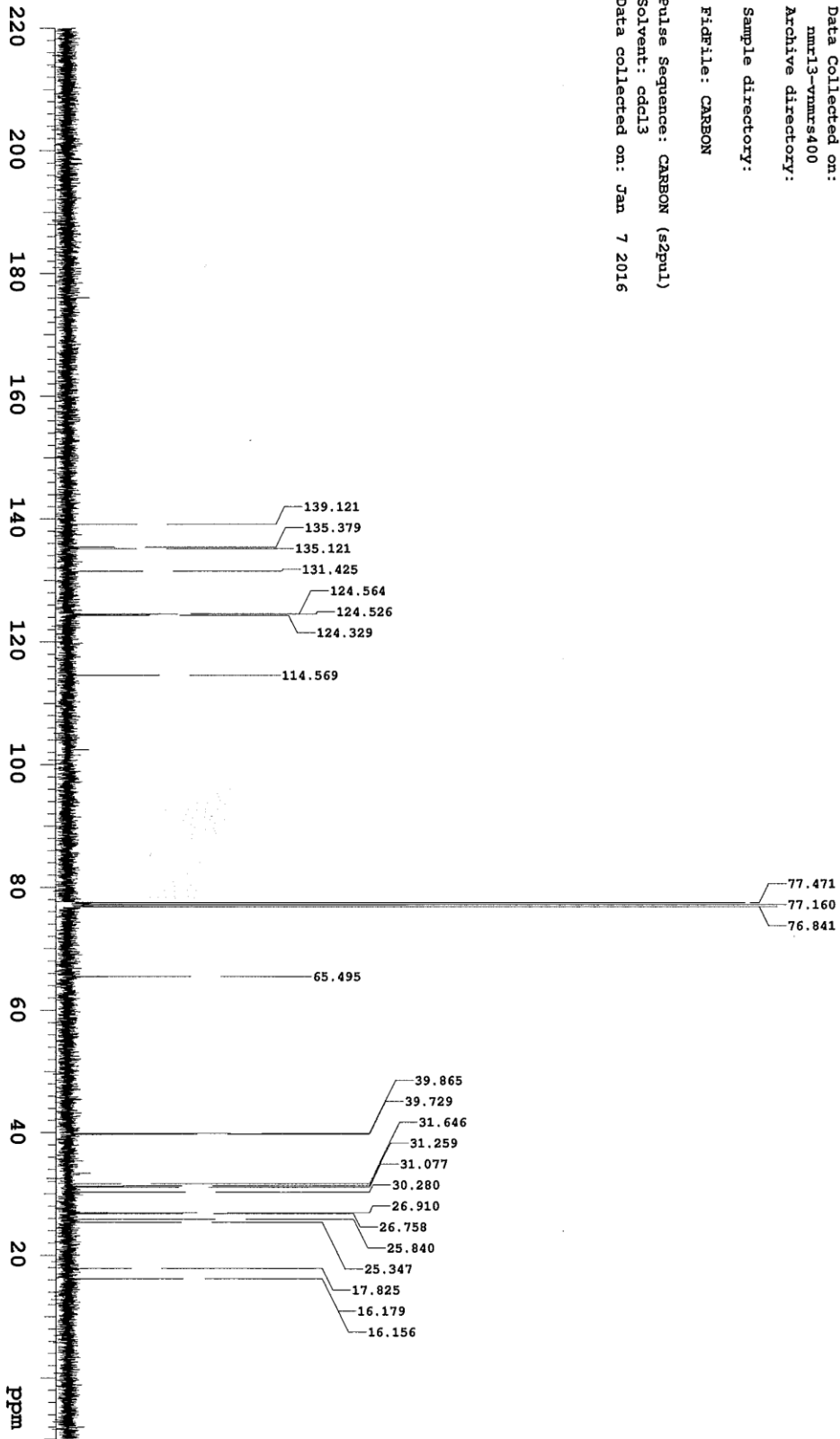
Sample directory:

Fidfile: CARBON

Pulse Sequence: CARBON (s2pul)

Solvent: cdcl3

Data collected on: Jan 7 2016

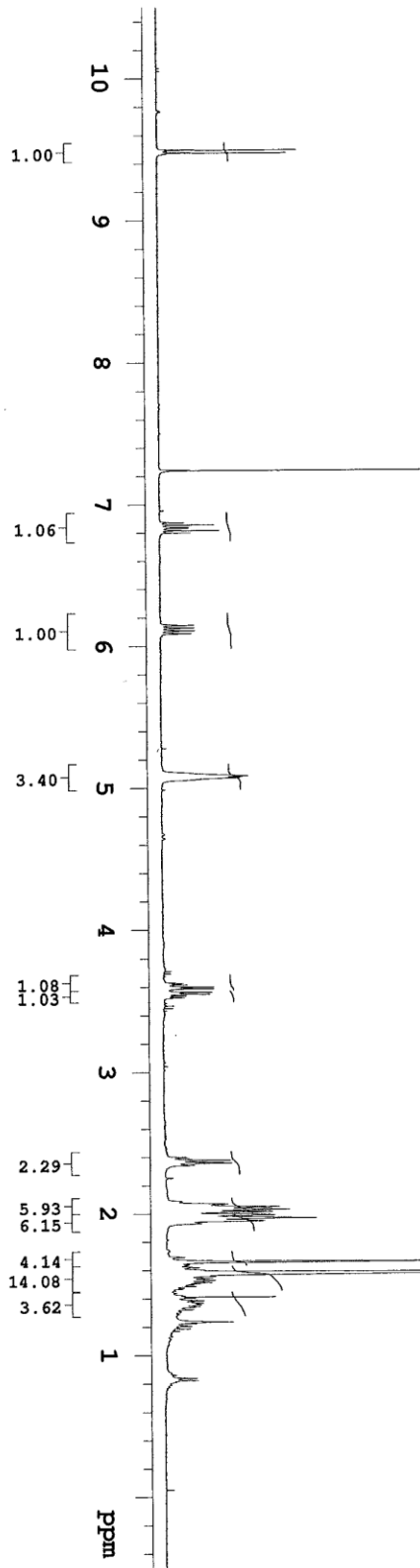
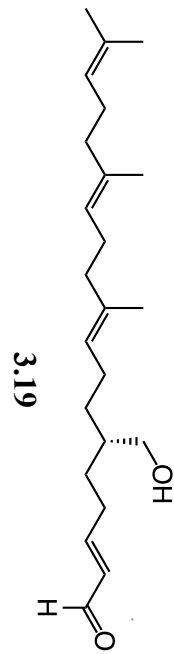


XS-01172H1iquid

Sample Name:
sy-IV-74-2-pro
Data Collected on:
mmr13-vmmrs400
Archive directory:
Sample directory:

FidFile: PROTON

Pulse Sequence: PROTON (s2pul)
Solvent: cdcl3
Data collected on: Jan 8 2016



TN3-128A1-13C

Sample Name:

SY-IV-57-a-pro-C

Data Collected on:

mmr19-vmmr600

Archive directory:

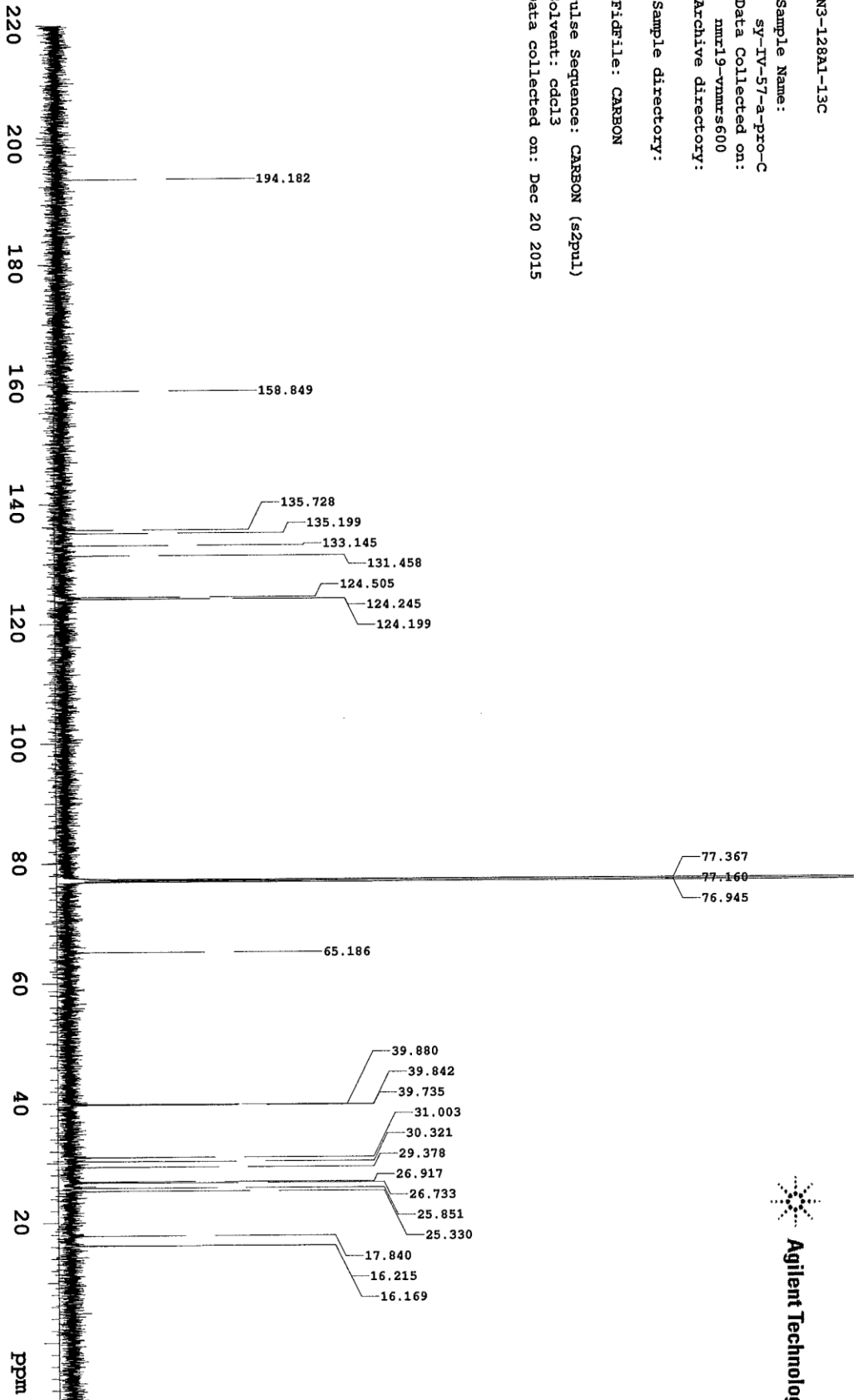
Sample directory:

FidFile: CARBON

Pulse Sequence: CARBON (s2pul)

Solvent: cdcl3

Data collected on: Dec 20 2015



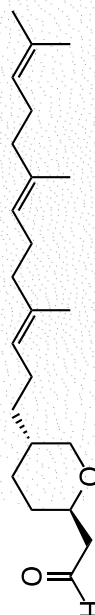
EV-III-049-C
 Chloro Allyl Spin Addn - tBu cat
 1/8/16

Sample Name:
 sy-IV-75-pro
 Data Collected on:
 nmr19-vmmrs600
 Archive directory:

Sample directory:

File: sy-IV-75-pro

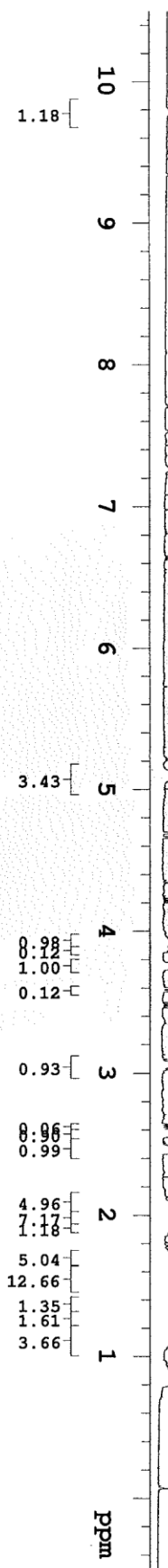
Pulse Sequence: PROTON (s2pul)
 Solvent: cdcl3
 Data collected on: Jan 8 2016



3.64



Agilent Technologies



TM3-128A1-13C

Sample Name:

sy6-IV-75-pro-C

Data Collected on:

nmr19-vnmr5600

Archive directory:

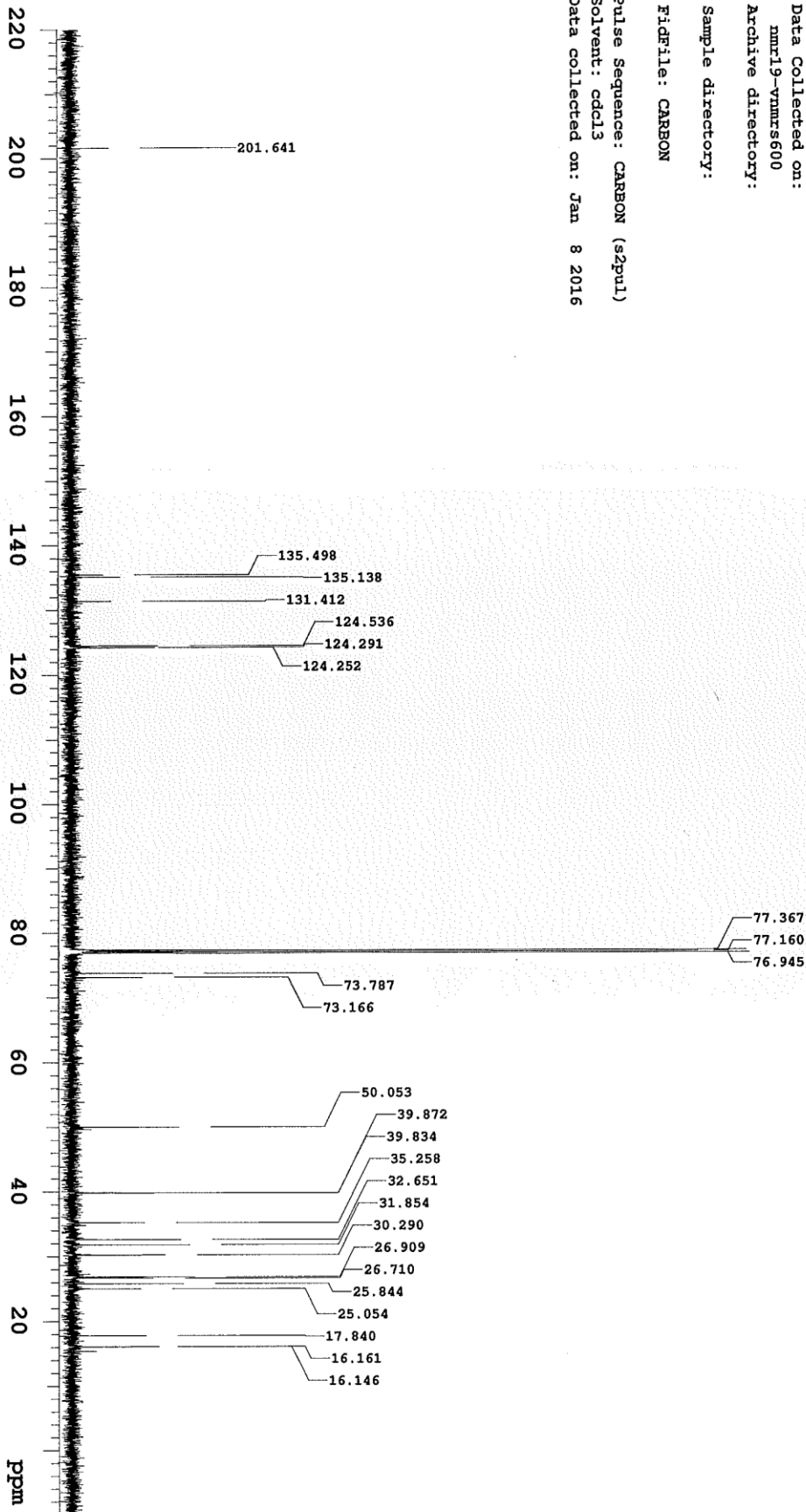
Sample directory:

FidFile: CARBON

Pulse Sequence: CARBON (s2pu1)

Solvent: cdcl3

Data collected on: Jan 8 2016



Chapter Four

Enantioselective NHC–Cu-Catalyzed Prenyl Conjugate Additions to Enoates

4.1. Introduction

Prenyl groups are commonly occurring in biologically important natural products.¹ Furthermore, functionalization of a prenyl unit can be performed in a number of ways, leading to the formation of a number of desirable derivatives (Figure 4.1). Prenylation of proteins is a well-known lipid modification that plays an important role in promoting membrane translocation, and is crucial for protein-protein interaction and cellular signal transduction.² Therefore, design and development of methods for efficient preparation of enantiomerically enriched prenyl-containing molecules is a compelling objective of research in organic chemistry.

(1) Recent reviews: (a) Williams, R. M.; Stocking, E. M.; Sanz-Cervera, J. F. *Top. Curr. Chem.* **2000**, *209*, 97–173. (b) Li, S. *Nat. Prod. Rep.* **2010**, *27*, 57–78.

(2) Zhang, F. L.; Casey, P. J. *Annu. Rev. Biochem.* **1996**, *65*, 241–69.

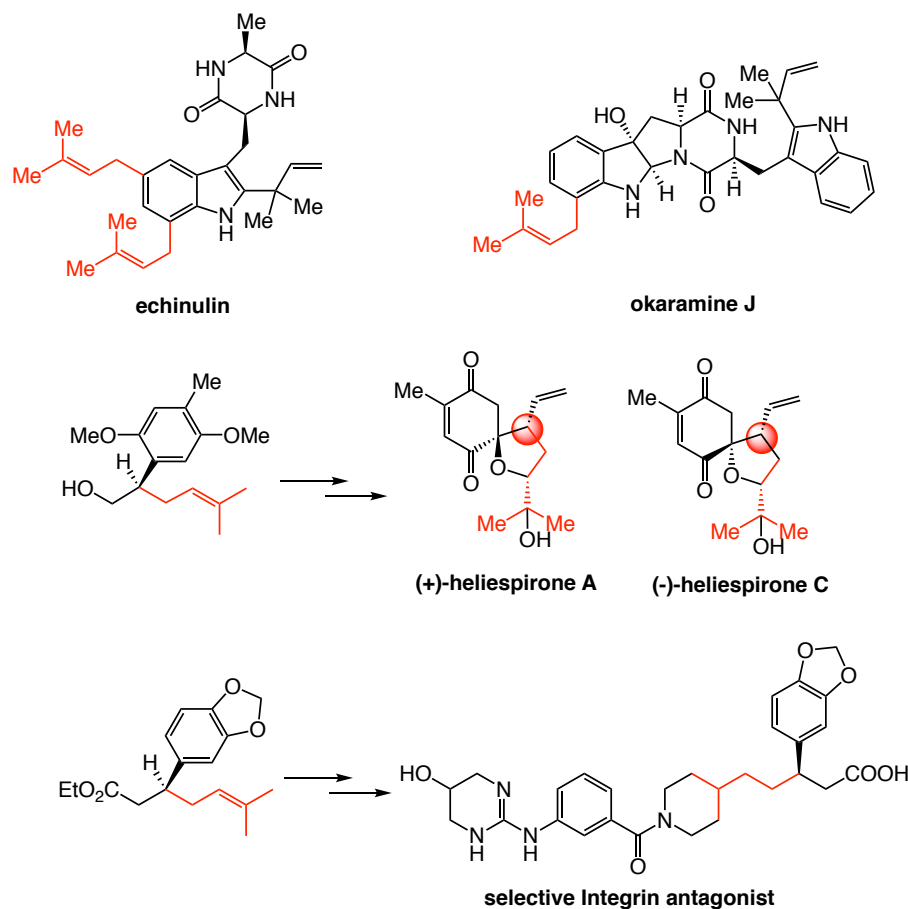


Figure 4.1. Prenylated Natural Products and Natural Products/Pharmaceuticals Derived from Prenylated Compounds

Cu-catalyzed enantioselective conjugate addition (ECA)³ reactions have been developed as a convenient method to generate stereogenic centers at the β position to carbonyl groups. Cu-catalyzed ECA methods may involve the use of Grignard reagent,⁴

(3) Recent reviews: (a) *Copper-Catalyzed Asymmetric Synthesis*; Alexakis, A.; Krause, N.; Woodward, S. Eds; VCH: Weinheim, 2004, pp 33–68. (b) *Catalytic Asymmetric Conjugate Reactions*; Córdova, A., Ed.; Wiley-VCH: Weinheim, Germany, 2010; pp 71–168. (c) Wang, S.-Y.; Loh, T.-P. *Chem. Commun.* **2009**, 46, 8694–8703. (d) Harutyunyan, S. R.; den Hartog, T.; Geurts, K.; Minnaard, A. J.; Feringa, B. L. *Chem. Rev.* **2008**, *108*, 2824–2852. (e) López, F.; Minnaard, A. J.; Feringa, B. L. *Acc. Chem. Res.* **2007**, *40*, 179–188. (f) Alexakis, A.; Bäckwall, J. E.; Krause, N.; Pa mies, O.; Diéguez, M. *Chem. Rev.* **2008**, *108*, 2796–2823. (g) Christoffers, J.; Koripelly, G.; Rösiak, A.; Rossle, M. *Synthesis* **2007**, 1279–1300. (h) von Zezschwitz, P. *Synthesis* **2008**, 1809–1831.

(4) For recent examples, see: (a) Wilsily, A.; Lou, T.; Fillion, E. *Synthesis* **2009**, 2066–2072. (b) Bos, P. H.; Maciá, B.; Fernández-Ibañez, M. A.; Minnaard, A. J.; Feringa, B. L. *Org. Biomol. Chem.* **2010**, *8*, 47–49. (c) Palais, L.; Babel, L.; Quintard, A.; Belot, S.; Alexakis, A. *Org. Lett.* **2010**, *12*, 1988–1991. (d) Endo, K.; Ogawa, M.; Shibata, T. *Angew. Chem., Int. Ed.* **2010**, *49*, 2410–2413. (e) Superchi, S.; Marchitello, V.; Pisani, L.; Scafato, P. *Chirality* **2011**, *23*, 761–767. (f) Drissi-Amraoui, S.; Morin, M. S. T.; Crévisy, C.; Baslé, O.; de Figueiredo, R. M.; Mauduit, M.; Campagne, J.-M. *Angew. Chem., Int. Ed.*

an organozinc reagent, or an organoaluminum species. However, these protocols are typically used to introduce an alkyl moiety. Related transformations involving an alkenyl and aryl metal reagents⁵ have been developed as well. And yet, ECA of an allyl group, a class of valuable reactions, remains underdeveloped.⁴⁻⁸ Boron-based reagents^{8-9,12} have only been introduced recently as partners in Cu-catalyzed ECA, offering a more practical, functional group tolerant and milder alternative to the corresponding organometallic entities. We envisioned that if we can achieve enantioselective Cu-catalyzed prenyl conjugate additions to enoates, we may easily access synthetically useful motifs for the synthesis of natural products and pharmaceuticals (Figure 4.1).

4.2. Background

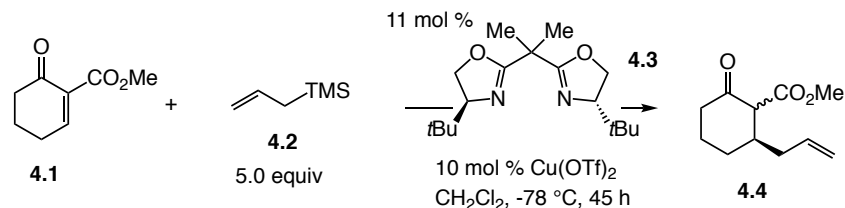
4.2.1 Catalytic Enantioselective Allyl Conjugate Additions to Cyclic α,β -Unsaturated Diesters

In 2008, Snapper and co-workers disclosed the first Cu-catalyzed enantioselective Hosomi-Sakurai conjugate allyl additions to cyclic unsaturated ketoesters with allyltrimethylsilane (Scheme 4.1).⁶ The desired product were obtained in high yields and up to >99:1 er. Cyclic enones with different substitution patterns were explored as well. Five- and eight-membered ring electrophiles proved to be suitable substrates, as they were converted to ECA products in 85:15–>98:2 er.

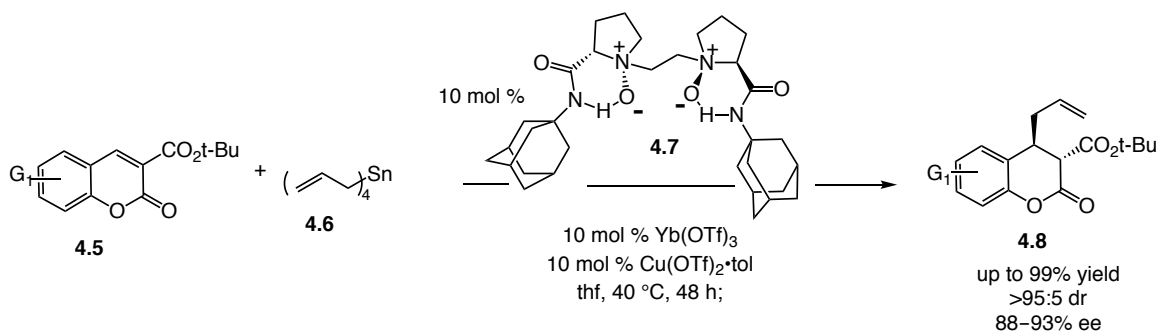
2015, 54, 11830–11834. (g) Drissi-Amraoui, S.; Schmid, T. E.; Lauberteaux, J.; Crévisy, C.; Baslé, O.; de Figueiredo, R. M.; Halbert, S.; Gérard, H.; Mauduit, M.; Campagne, J.-M. *Adv. Synth. Catal.* **2016**, 358, 2519–2540.

(5) (a) Chong, Q.; Yue, Z.; Zhang, S.; Ji, C.; Cheng, F.; Zhang, H.; Hong, X.; Meng, F. *ACS Catalysis* **2017**, 7, 5693–5698. Cu-catalyzed ECA protocol with aryl boron reagent involving one example of alkenyl addition: (b) Takatsu, K.; Shintani, R.; Hayashi, T. *Angew. Chem., Int. Ed.* **2011**, 50, 5548–5552.

(6) Shizuka, M.; Snapper, M. L. *Angew. Chem., Int. Ed.* **2008**, 47, 5049–5051.

Scheme 4.1. Enantioselective Hosomi-Sakurai Conjugate Allylation of Cyclic Unsaturated Ketosesters

In 2011, Feng and co-workers reported a catalytic diastereoselective and enantioselective allyl conjugate addition reaction to coumarins.⁷ High yields and stereoselectivities were obtained through a dual activation strategy: N,N' -dioxide **4.7** used in combination with $\text{Yb}(\text{OTf})_3$, serves to activate the electrophile, coumarin **4.5**. In situ transmetalation from tetraallyltin **4.6** to $\text{Cu}(\text{OTf})_2 \cdot \text{tol}$ serves to generate the more nucleophilic species.

Scheme 4.2. Catalytic Asymmetric Conjugate Allylation of Coumarins

4.2.2 Catalytic Enantioselective Allyl Conjugate Additions to Acyclic α,β -Unsaturated Diesters

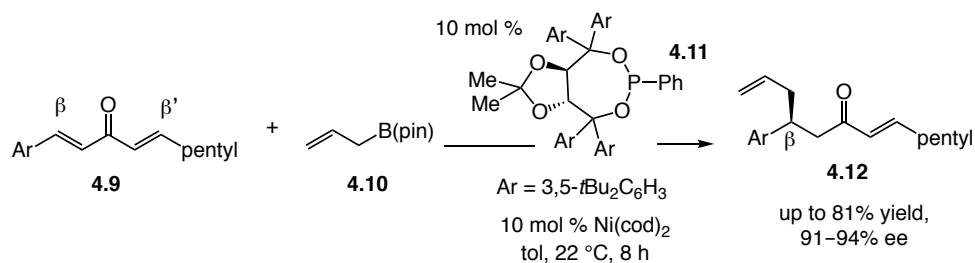
The Morcken group pioneered the Ni-catalyzed enantioselective conjugate addition of allylboronic acid pinacol ester to dialkylidene ketones.⁸ Reactions proceeded highly efficiently and favors allylation at benzyldiene positions with $\beta:\beta'$ ratios ranging from 5.1:1 to 49:1, and in up to 97:3 er. In 2011, the same research group showed that Pd-

(7) Kuang, Y.; Liu, X.; Chang, L.; Wang, M.; Lin, L.; Feng, X. *Org. Lett.* **2011**, *13*, 3814–3817.

(8) (a) Sieber, J. D.; Liu, S.; Morcken, J. P. *J. Am. Chem. Soc.* **2007**, *129*, 2214–2215. (b) Sieber, J. D.; Morcken, J. P. *J. Am. Chem. Soc.* **2008**, *130*, 4978–4983.

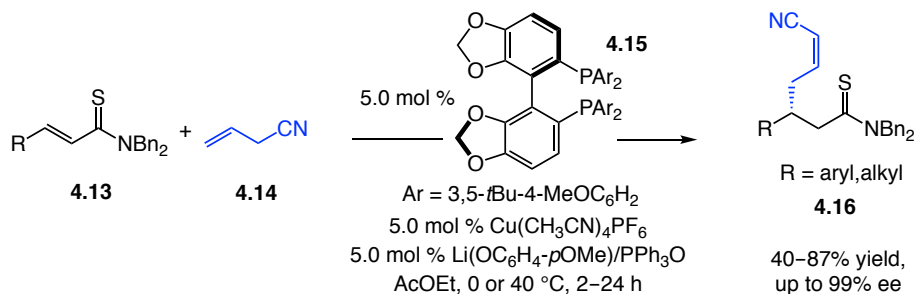
based catalysts may be used to promote ECA reactions with methylidene ketones.⁹

Scheme 4.3. Ni-Catalyzed Enantioselective Conjugate Allylation of Activated Enones



In 2011, Shibasaki et al. reported on Cu-catalyzed enantioselective conjugate additions of allyl cyanide to unsaturated thioamides, leading to the formation of a wide range of Z-alkenyl cyanide products.¹⁰ Both aryl- and alkyl-thioamides are suitable substrates for the transformations. Reactions proceeded through deprotonation of allyl cyanide/formation of an allyl copper catalyst, followed by enantioselective additions to thioamides **4.13**. Products were then obtained in high yield and with exceptional enantioselectivity. It is worth mentioning that triphenylphosphine-oxide serves as a “hard” Lewis base to enhance the Brønsted basicity of Li(OC₆H₄-pOMe) through a hard–hard interaction with the Li cation.

Scheme 4.4. Cu-Catalyzed Conjugate Additions of Allyl Cyanide to α,β -Unsaturated Thioamides



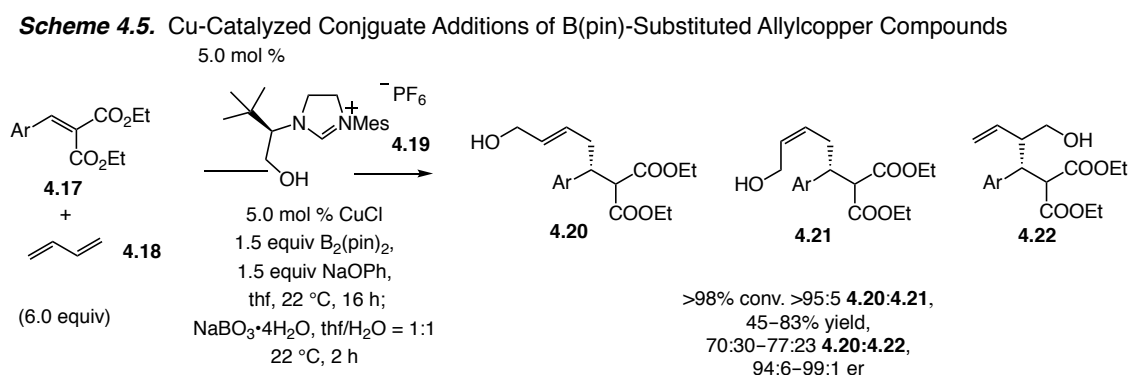
4.2.3 Catalytic Enantioselective Conjugate Additions to Acyclic α,β -Unsaturated

Dieters with Boron-Based Nucleophiles

(9) Brozek, L. A.; Sieber, J. D.; Morken, J. P. *Org. Lett.* **2011**, *13*, 995–997.

(10) Yanagida, Y.; Yazaki, R.; Kumagai, N.; Shibasaki, M. *Angew. Chem., Int. Ed.* **2011**, *50*, 7910–7914.

In 2016, following the development of enantioselective 1,6-conjugate propargyl and allyl additions to dienones,¹¹ we reported a multicomponent reaction protocol to facilitate the transformation of an *in situ* B(pin)-substituted allylcopper compound to α,β -unsaturated diesters.¹² Products were obtained in 45–83% yield, over 95% α selectivity (**4.20**:**4.21**), 94:6–99:1 er. Reactions involving butadiene and isoprene, which are common feedstock, enoates and B₂(pin)₂ were promoted by a NHC–Cu catalyst derived from an imidazolium salt **4.19**. A stereochemical model was proposed for this transformation: the sodium cation bridges the catalyst alkoxy group and the carbonyl groups on the substrate, which not only serves to rigidify the transition state and also lowers the activation barrier by stabilizing the negative charge accommodated during the C–C bond formation step.



Very recently, Meng reported a reaction protocol regarding ECA reactions of allenyl–B(pin) compounds to α,β -unsaturated diesters **4.23**.¹³ Alkyl as well as aryl-substituted enoates are suitable substrates for this transformation. An alkoxy-based

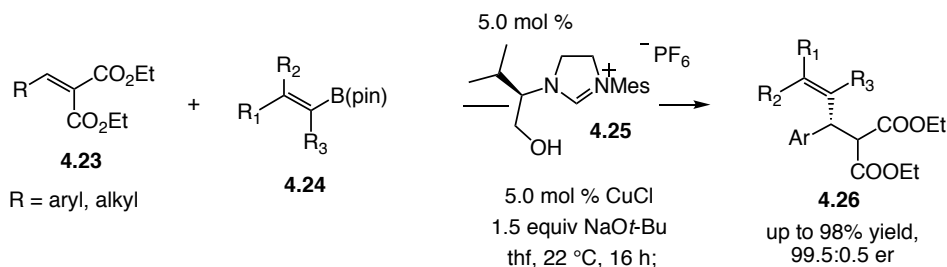
(11) Meng, F.; Li, X.; Torker, S.; Shi, Y.; Shen, X.; Hoveyda, A. H. *Nature* **2016**, 537, 387–393.

(12) Li, X.; Meng, F.; Torker, S.; Shi, Y.; Hoveyda, A. H. *Angew. Chem., Int. Ed.* **2016**, 55, 9997–10002.

(13) Chong, Q.; Yue, Z.; Zhang, S.; Ji, C.; Cheng, F.; Zhang, H.; Hong, X.; Meng, F. *ACS Catal.* **2017**, 7, 5693–5698.

NHC–Cu catalyst serves as the catalyst and a variety of functionalized alkenyl units were used.

Scheme 4.6. Cu-Catalyzed Conjugate Additions of Alkenyl-B(pin)

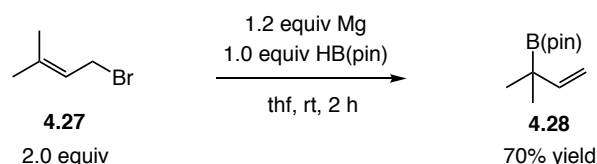


4.3. Cu-Catalyzed Enantioselective Prenyl Conjugate Additions to Acyclic α,β -Unsaturated Diesters

4.3.1 Catalyst Screening and Reaction Optimizations

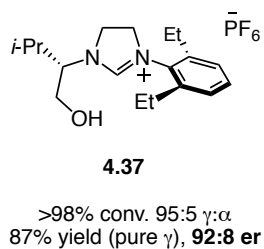
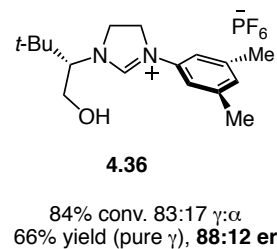
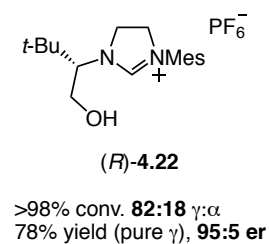
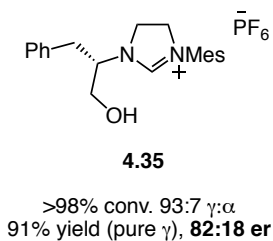
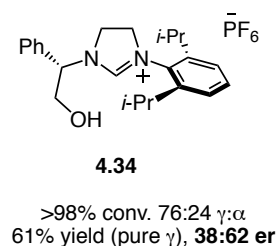
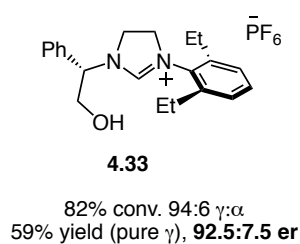
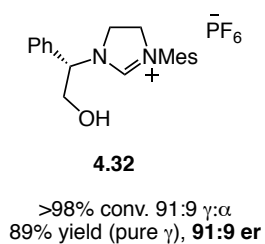
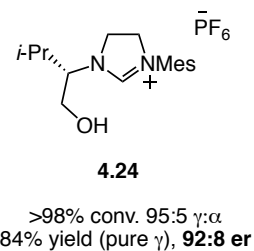
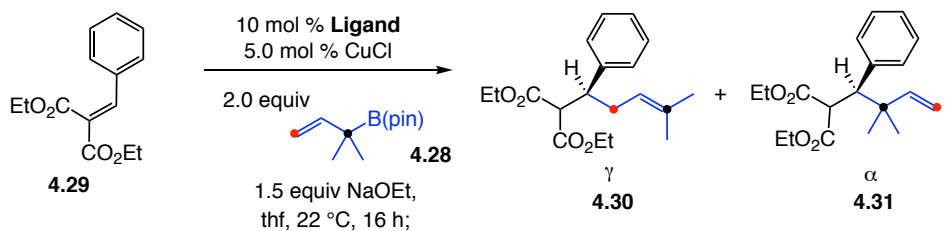
We decided to utilize 3,3-dimethylallyl B(pin) **4.28** to introduce the prenyl unit to a stereogenic center. The requisite organoboron compound (**4.28**) is easily accessible from relatively inexpensive starting materials (Scheme 4.7).

Scheme 4.7. Preparation of 3,3-Dimethylallyl–B(pin)

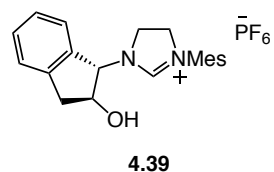
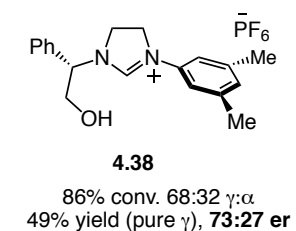


As shown in Scheme 4.8, prenyl addition to enoate **4.29** affords diester **4.30** in 84% yield, 92:8 er with 95:5 $\gamma:\alpha$ ratio. The transformation was performed with 5.0 mol % NHC–Cu complex derived from 10 mol % valinol-based **4.24**, 5.0 mol % CuCl and 1.5 equivalent of sodium ethoxide in thf at 22 °C for 18 h. 10 mol % of ligand was needed to avoid complication arising from the generation of **4.31** presumably by background reaction promoted by (prenyl)CuOEt (Scheme 4.9). Switching the N-alkyl substituent of the NHC ligand from isopropyl group to a phenyl group **4.32** delivers the desired product

in 89% yield, 91:9 er with slight decrease of group-selectivity (91:9 γ : α ratio). Increasing the size of ortho-substituent on the N-aryl ring to Et group led to a slight increase in the enantioselectivity (92.5:7.5 er vs 91:9 er, **4.33** vs. **4.32**). However, further increasing the size of ortho substituent on N-aryl ring from Et to *i*-Pr group led to detrimental effect on the enantioselectivity (38:62 er vs 92.5:7.5 er, **4.34** vs. **4.33**), favoring the generation of alternative enantiomer of the product. Switching to phenylalaninol-based NHC ligand **4.35** cause the enantiomeric ratio to drop to 82:18 er. Desired product **4.30** with 95:5 er was obtained when a NHC ligand derived from *tert*-leucinol (*R*)-**4.22** was used. However, drop of regioselectivity was also observed (cf. 82:18 vs. 91:9 γ : α selectivity, (*R*)-**4.22** vs. **4.32**). Changing the substitution pattern of N-aryl ring from ortho to meta led to a lower yield, regioselectivity and enantioselectivity (cf. 88:12 er vs 95:5 er, **4.36** vs. (*R*)-**4.22**; 73:27 er vs 91:9 er, **4.38** vs. **4.32**). When NHC ligand derived from *trans*-1-amino-2-indanol-based imidazolium salt **4.39** was utilized in the reaction conditions, **4.30** was obtained in 92% yield with 96:4 group selectivity and 95:5 enantioselectivity. Decreasing the loading of **4.39** from 10 mol % to 6.0 mol %, ECA reaction afforded **4.30** in a slightly lower yield (85% yield vs. 92% yield) with no obvious drop of group selectivity and enantioselectivity.

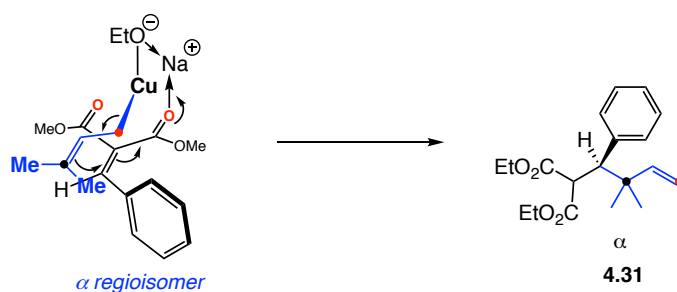
Scheme 4.8. Ligand Screening for Prenyl Conjugate Additions

ligand = 6.0 mol %
 >98% conv. **78:22** γ : α
 74% yield (pure γ), **92:8 er**

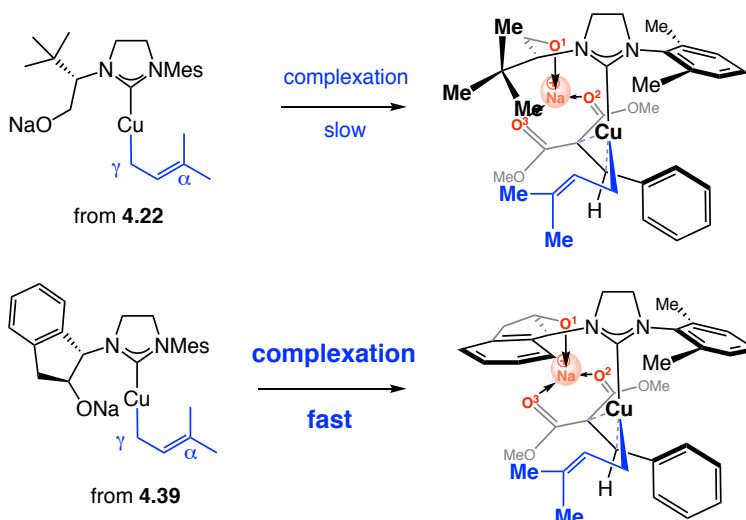


>98% conv. **96:4** γ : α
 92% yield (pure γ), **95:5 er**

Ligand = 6.0 mol %
 92% conv. **96:4** γ : α
 85% yield (pure γ), **95:5 er**

Scheme 4.9. Formation of Regioisomer Promoted by Unbound CuOEt

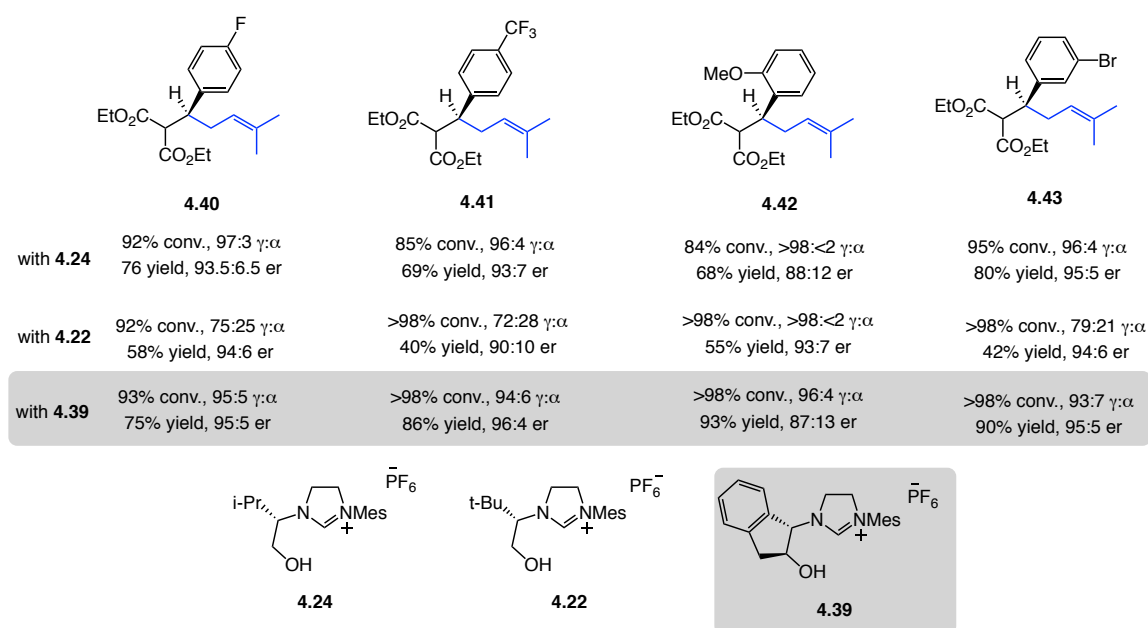
However, a drastic decrease in regio- and enantioselectivity was observed, when lower catalyst loading of sterically-demanding ligand **4.22** was utilized; product was obtained in only 78:22 γ : α ratio with 92:8 er when lowering the catalyst loading of **4.22** to 6.0 mol %. However, product could be obtained in high regio- and enantioselectivity when 6.0 mol % of ligand **4.39** was used. We surmised that the bulky *t*-Bu group in **4.22** might elevate the barrier complexation step, as shown in Scheme 4.10, as compared to the sterically less demanding phenyl unit of the indanyl group in **4.36**, thus the background reaction (Scheme 4.9).

Scheme 4.10. Comparison of the Rate of of the Complexation Step

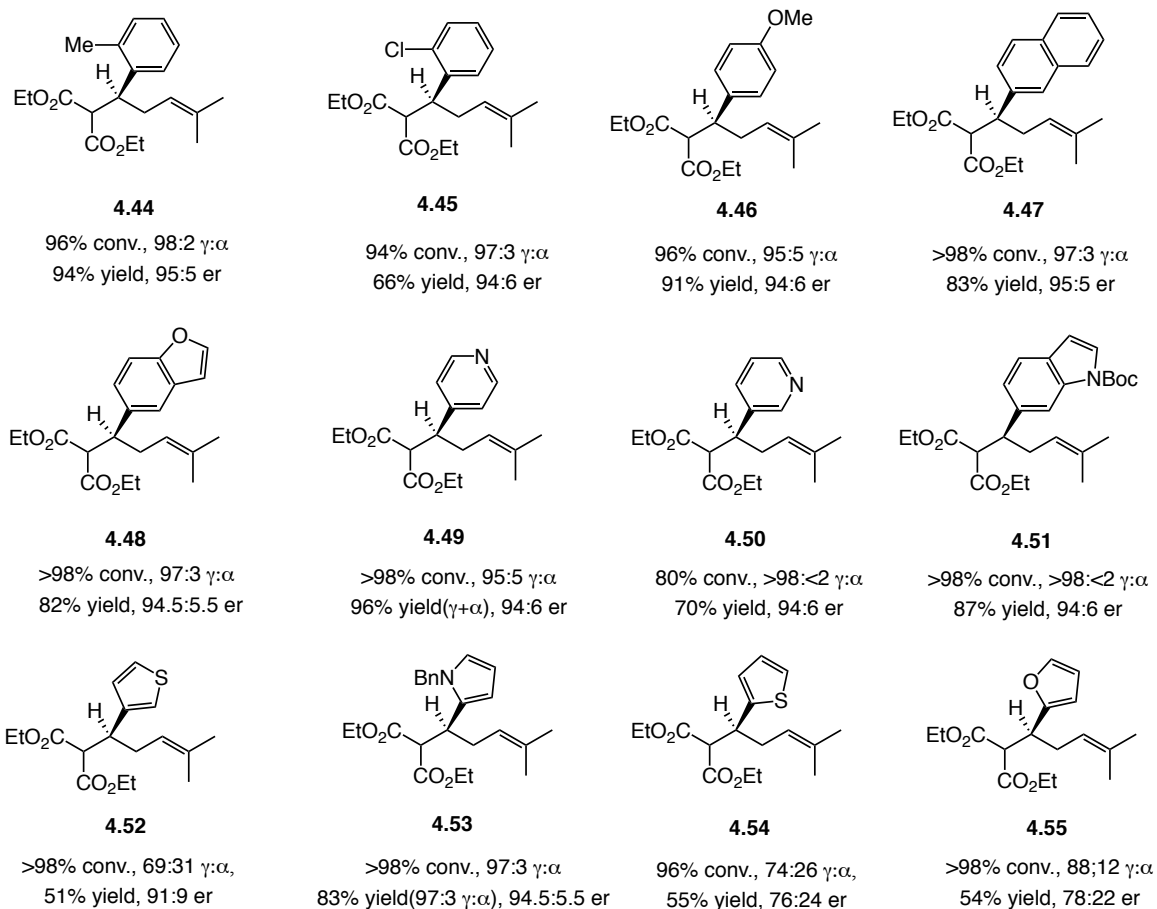
4.3.2 Scope of Enantioselective Prenyl Conjugate Additions

A range of aryl-substituted substrates with electron-donating and electron-withdrawing group were employed in the ECA reaction conditions (Scheme 4.11). Conjugate addition products were obtained in higher yield, $\gamma:\alpha$ ratio and enantioselectivity with the use of **4.39** as compared to **4.24** or **4.22**. Sterically-demanding substrate with an electron-donating group led to lower enantioselectivity (cf. **4.42**). In this case, **4.22** afforded higher enantioselectivity albeit in lower yield.

Scheme 4.11. Scope with Electron-Deficient and Electron-Donating Enoates



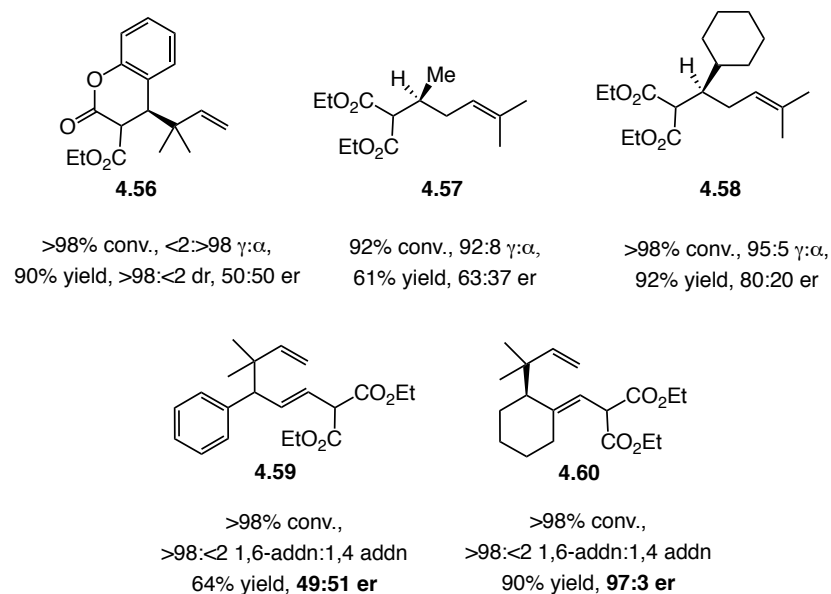
As shown in Scheme 4.12, enoates with an electron-donating group (see **4.46**), or a sterically hindered aryl substituent (see **4.44**) or a halogen-containing aryl group (see **4.45**) are all suitable substrates. In the case of heteroaryl substrates, high enantioselectivities and yields were obtained with the use of ligand **4.39**; however, less congested heteroaryl enoates with the heteroatom at the 2-positions led to a dramatic drop in enantioselectivity (76:24 er and 78:22 er for **4.54** and **4.55**).

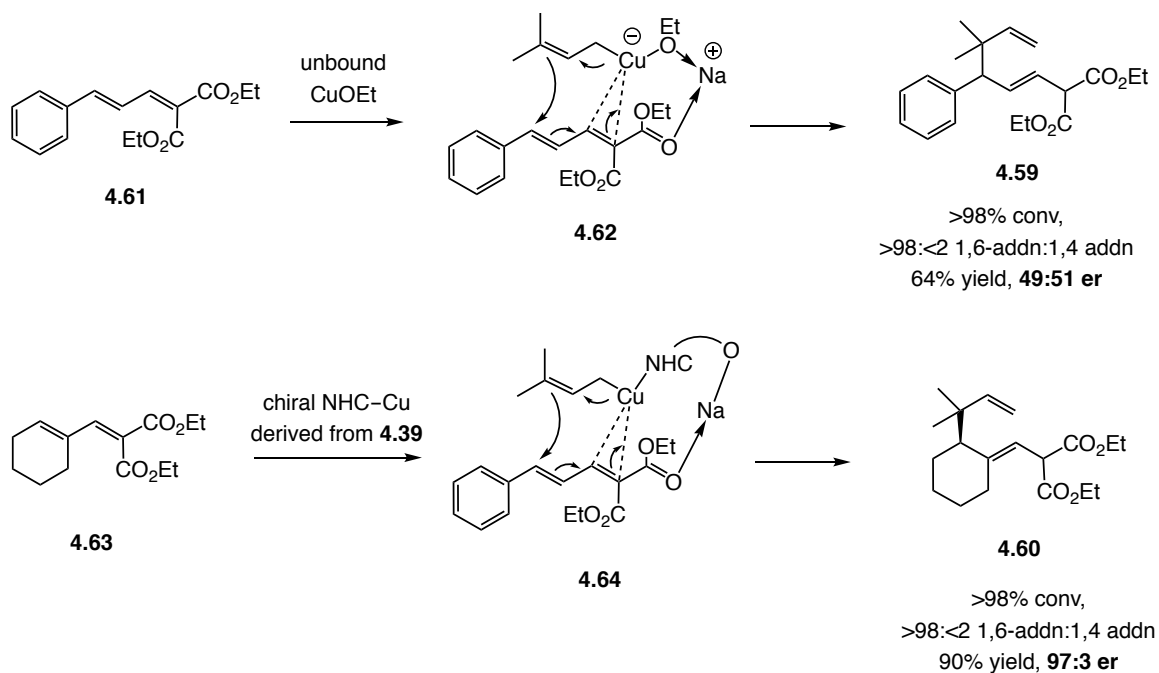
Scheme 4.12. Scope with Aryl- and Heteroaryl-Substituted Enoates Catalyzed by NHC–Cu complex Derived from **4.39**

As shown in Scheme 4.13, prenyl conjugate additions to coumarin led to the generation of racemic compound with >98% α selectivity (see **4.56**). The complete formation of the undesired regioisomer is probably due to the background reaction which outcompetes the desired reaction. ECA reactions employing alkyl-substituted substrates proceeded efficiently, however with lower enantioselectivities (63:37 er and 80:20 er see **4.57** and **4.58**). When alkenyl-substituted substrates were utilized in the reaction conditions, >98% conversion to 1,6-conjugate addition product (see **4.59** and **4.60**). It is worth mentioning that ECA reaction with an alkyl-substituted dienoate led to product with near perfect enantioselective while the formation of racemic product was observed starting with a less sterically demanding and electronically activated aryl-substituted

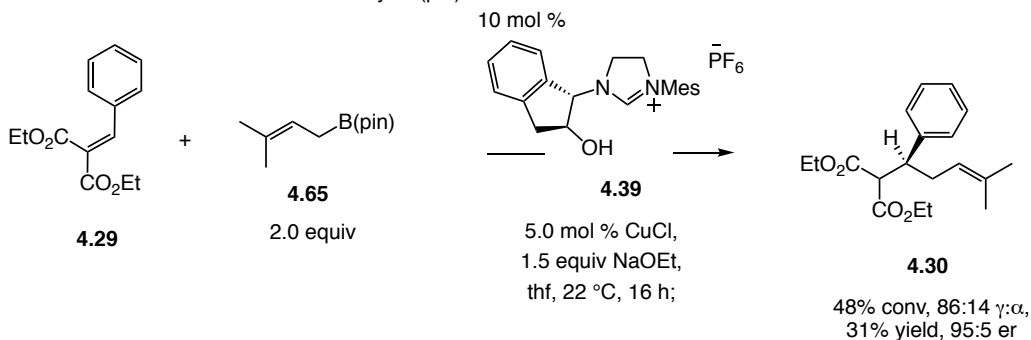
dienoates (97:3 er vs. 49:51 er, **4.60** vs. **4.59**). These dramatic difference in enantioselectivities might be due to the faster rate of 1,6-conjugate addition promoted by unbound (prenyl)CuOEt with electronically-activated **4.61**; while high enantioselective product could be obtained with less activated **4.63**, promoted by NHC-Cu catalyst derived from the chiral ligand **4.39** (Scheme 4.14).

Scheme 4.13. Scope with Coumarin, Alkyl-, Alkenyl-Substituted Enoates Catalyzed by NHC-Cu Complex Derived from **4.39**

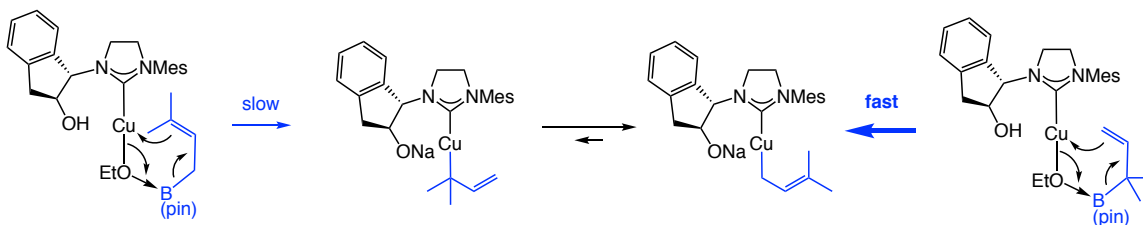


Scheme 4.14. 1,6-Conjugate Addition with Alkenyl-Substituted Enoates Catalyzed by (Prenyl)CuOEt and NHC-Cu Complex Derived from **4.39**

As shown in Scheme 4.15, when prenyl B(pin) reagent **4.61** was employed in the ECA reaction instead of **4.28**, **4.29** was obtained in only 31% yield, 95:5 er, indicating the inefficient transmetalation of **4.65** with CuCl in a γ -addition fashion (Scheme 4.16).¹⁴

Scheme 4.15. ECA Reaction with Prenyl-B(pin)

(14) Ardolino, M. J.; Morken, J. P. *J. Am. Chem. Soc.* **2014**, *136*, 7092–7100.

Scheme 4.16. Transmetalation with Prenyl-B(pin) and 1,1-Dimethylallyl-B(pin)

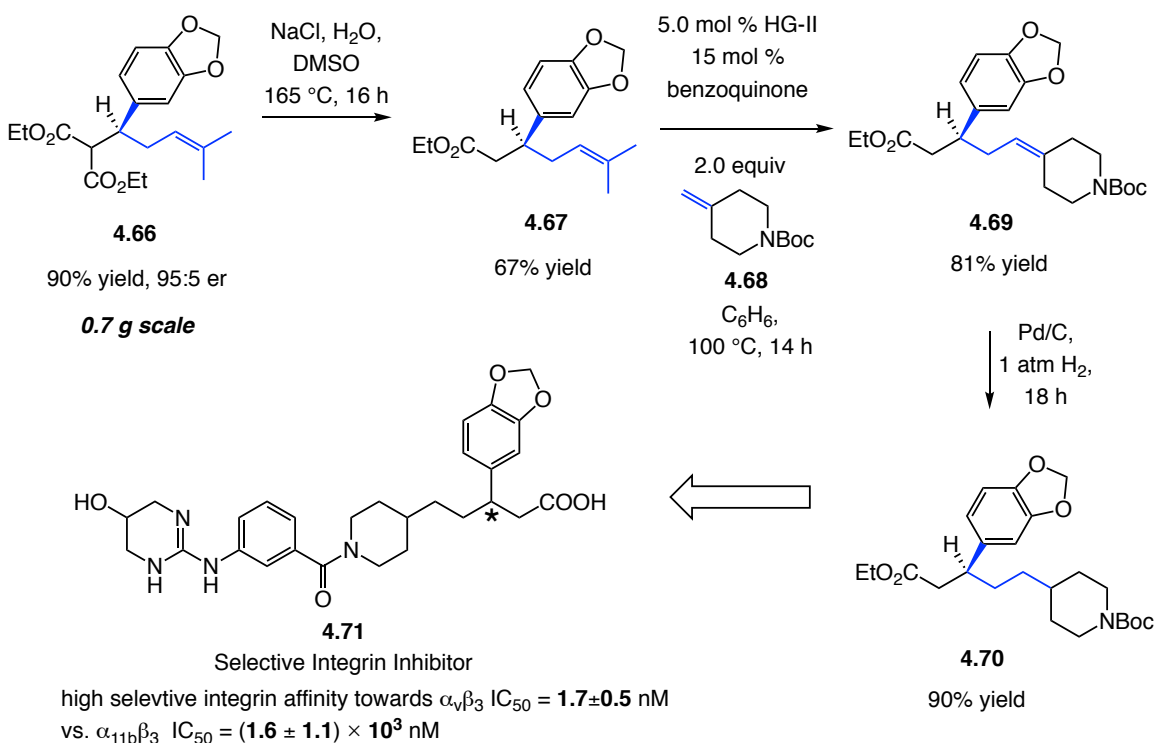
4.3.3 Functionalization and Application to the Synthesis of a Selective Integrin

Antagonist

At this stage, we carried on the formal synthesis of **4.71** reported as a selective integrin antagonist.¹⁵ As shown in Scheme 4.16, ECA product **4.66** was obtained in 90% yield and 95:5 er in 0.7 g scale. Followed by decarboxylation, **4.67** was generated in 67% yield, which underwent Ru-catalyzed cross metathesis with a 1,1-disubstituted alkene **4.68** in the presence of 15 mol % benzoquinone. It is worth mentioning the prenyl group is crucial for the promoting the generation of the trisubstituted olefin **4.69** by site-selective formation of the Ru-metallacyclobutane complex following the initiation of cross metathesis of Ru-based catalyst with **4.68**.¹⁶ Hydrogenation of **4.69** gave the desired product **4.70** which can be further elaborated to **4.71** as the target molecule.

(15) De Corte, B. L.; Kinney, W. A.; Liu, L.; Ghosh, S.; Brunner, L.; Hoekstra, W. J.; Santulli, R. J.; Tuman, R. W.; Baker, J.; Burns, C.; Proost, J. C.; Tounge, B. A.; Damiano, B. P.; Maryanoff, B. E.; Johnson, D. L.; Galembo, R. A. *Bio. Med. Chem. Lett.* **2004**, *14*, 5227–5232.

(16) Wang, Z. J.; Jackson, W. R.; Andrea J. Robinson, A. J. *Org. Lett.* **2013**, *15*, 3006–3009.

Scheme 4.17. Application to the Synthesis of a Selective Integrin Inhibitor

4.3.4 Stereochemical Models by DFT Calculations

As shown in Figure 4.2, DFT calculations provided the rationale for the high enantioselectivity obtained with **4.39**. During the C–C bond forming step, the copper center coordinated with the enoate with the alkoxy group, which served as a secondary binding site with the enoate through a cation metal bridge. In the major mode of addition **4.72**, the aryl group was situated beneath the N-aryl ring on the catalyst and benefited from the edge to face π -interaction. However, the minor mode of **4.73** suffered from the steric interaction between the prenyl group and the ortho-substituted N-aryl ring. The stereochemical model provided an explanation for the low enantioselectivity for alkyl substrates (63:37 er and 80:20 er, **4.57** and **4.58**, Scheme 4.13) and heteroaryl cases (76:24 er and 73:27 er for **4.54** and **4.55**, Scheme 4.12): complete or partial loss of the

favoring edge to face CH- π -interaction raised the energy barrier for the major pathway, causing the erosion of enantioselectivity.

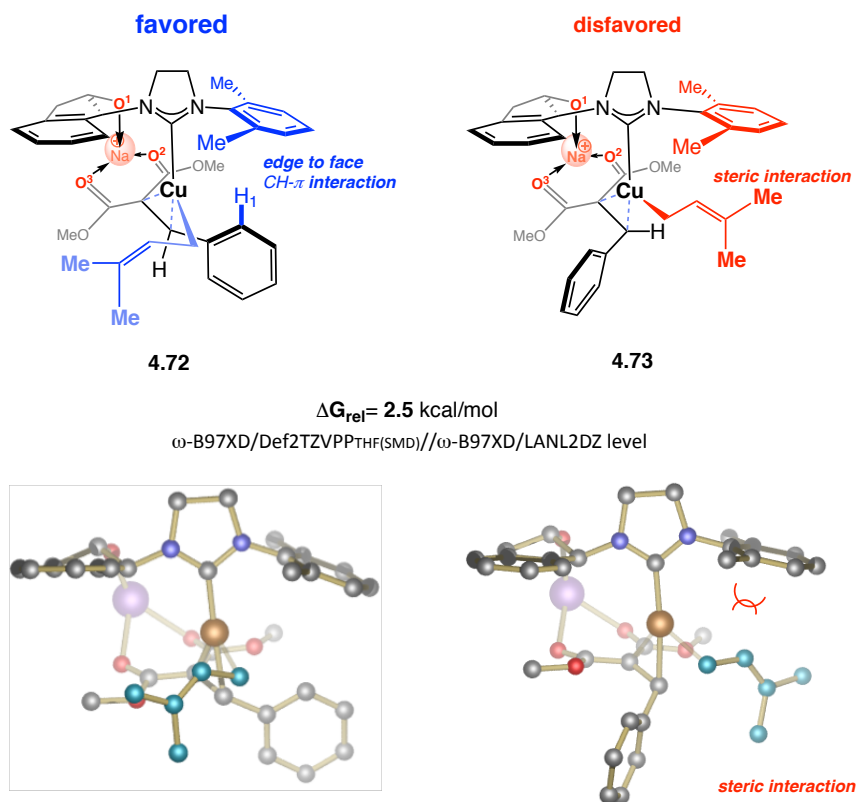


Figure 4.2. Stereochemical Model for Prenyl Conjugate Additions with **4.39**

4.4. Conclusions

An efficient catalytic protocol for generation of prenyl-bearing tertiary carbon stereogenic centers from aryl-substituted enoate was achieved in the presence of chiral NHC-Cu complex. A range of aryl and heteroaryl-substituted substrate were suitable substrates, the corresponding prenyl conjugate addition products were generated in up to 94% yield and 95:5 enantioselectivity. The utility of the current method has been shown in the application to the synthesis of a selective integrin antagonist. DFT calculations provided a stereochemical model for the ECA reaction employing NHC-Cu catalyst derived from **4.39**.

4.5. Experimentals

General. Infrared (IR) spectra were recorded on a Bruker FT-IR Alpha (ATR mode) spectrophotometer, λ_{max} in cm^{-1} . Bands are characterized as broad (br), strong (s), medium (m), and weak (w). ^1H NMR spectra were recorded on a Varian Unity INOVA 400 (400 MHz) spectrometer. Chemical shifts are reported in ppm from tetramethylsilane with the solvent resonance as the internal standard (CDCl_3 : δ 7.26 ppm). Data are reported as follows: chemical shift, integration, multiplicity (s = singlet, d = doublet, t = triplet, q = quartet, br s = broad singlet, m = multiplet app = apparent), and coupling constants (Hz). ^{13}C NMR spectra were recorded on a Varian Unity INOVA 400 (100 MHz) spectrometer with complete proton decoupling. Chemical shifts are reported in ppm from tetramethylsilane with the solvent resonance as the internal standard (CDCl_3 : δ 77.16 ppm). High-resolution mass spectrometry was performed on a Micromass LCT ESI-MS (positive mode) at the Mass Spectrometry Facility, Boston College. Elemental microanalyses were performed at Robertson Microlit Laboratories (Madison, NJ). Enantiomeric ratios were determined by high-performance liquid chromatography (HPLC) with a Shimadzu chromatograph (Chiral Technologies Chiralcel OB-H (4.6 x 250 mm), Chiral Technologies Chiralcel OJ-H (4.6 x 250 mm)) in comparison with authentic racemic materials. Optical rotations were measured on a Rudolph Research Analytical Autopol IV Polarimeter. Unless otherwise noted, all reactions were carried out with distilled and degassed solvents under an atmosphere of dry N_2 in oven- (135 °C) or flame-dried glassware with standard dry box or vacuum-line techniques. Dichloromethane (Fisher Scientific, Inc.) was purified by being passed through two alumina columns under a positive pressure of dry argon by a modified Innovative

Technologies purification system. Tetrahydrofuran (Aldrich Chemical Co.) was purified by distillation from sodium benzophenone ketyl immediately prior to use unless otherwise specified. Methanol (Aldrich Chemical Co.) was distilled over CaH₂. All work-up and purification procedures were carried out with reagent grade solvents (purchased from Doe & Ingalls) under air.

Reagents

Copper (I) chloride: purchased from Strem Chemicals Inc. and used as received.

Diethyl benzylidenemalonate (3.29): purchased from Aldrich Chemical Co. and used as received.

Enoate (substrate for **4.40–4.55**): prepared according to previously reported procedures.¹⁷

Imidazolinium salts (4.32–4.38,¹⁸ 4.39^{5b}): prepared according to previously reported procedures.

Ruthenium complex (HG-II) was purchased from Aldrich and used as received.

Sodium methoxide (NaOEt) was purchased from Strem and used as received.

Procedure for NHC–Cu-Catalyzed Additions to Enoates (Scheme 4.8 and 4.10):

In an N₂-filled glove box, an oven-dried vial (4 mL) with a magnetic stir bar was charged with imidazolinium salt **4.39** (2.8 mg, 0.0060 mmol), CuCl (0.5 mg, 0.005 mmol), NaOEt (10.2 mg, 0.150 mmol) and tetrahydrofuran (thf, 1.0 mL). The vessel was sealed with a cap (phenolic open top cap with red PTFE/white silicone septum) and the solution was allowed to stir at 22 °C for 3.0 h. 1,1-Dimethylallyl–B(pin) **4.28** (29.4 mg, 0.150 mmol) was added to the solution, causing it to turn dark brown immediately. The mixture was allowed to stir at 22 °C for 10 min under an atmosphere of N₂. enoate **4.29** (24.8 mg, 0.100 mmol) were added through a syringe. The vial was re-sealed with a cap (phenolic open top cap with red PTFE/white silicone septum) and removed from the glove box. The

(17) Allen, C. F. H.; Spangler, F. W. *Org. Syn.* **1945**, 25, 42.

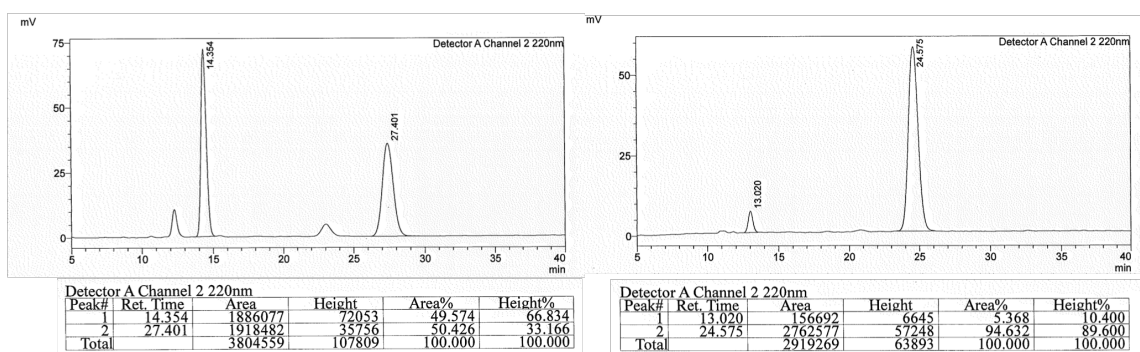
(18) Clavier, H.; Coutable, L.; Toupet, L.; Guillemin, J.-C.; Mauduit, M. J. *J. Organomet. Chem.* **2005**, 690, 5237–5254.

resulting solution was allowed to stir at 22 °C for 16 hours before the reaction was quenched by passing the mixture through a short plug of silica gel and eluted with Et₂O. The filtrate was concentrated *in vacuo* to provide yellow oil, which was purified by silica gel chromatography (hexanes/ethyl acetate = 75:1 to 60:1) to afford the **4.30** as colorless oil (27.0 mg, 0.085 mmol, 85% yield).

Characterization Data for Diesters with a *Tertiary Carbon Stereogenic Center*

Diethyl (*S*)-2-(4-methyl-1-phenylpent-3-en-1-yl)malonate (4.30). IR (neat): 3030 (w), 2980 (w), 2931 (w), 1752 (s), 1729 (s), 1496 (w), 1453 (m), 1368 (m), 1310 (m), 1248 (s), 1175 (s), 1146 (s), 1112 (m), 1096 (m), 1031 (s), 861 (w), 757 (m), 699 (s), 574 (w) cm⁻¹; ¹H NMR (CDCl₃, 400 MHz): δ 7.30–7.27 (2H, m), 7.22–7.19 (3H, m), 4.93 (1H, t, *J* = 8.0 Hz), 4.26 (2H, q, *J* = 7.2 Hz), 3.93–3.88 (2H, m), 3.72 (1H, d, *J* = 10.4 Hz), 3.44 (1H, td, *J* = 10.0, 4.4 Hz), 2.50–2.43 (1H, m), 2.36–2.29 (1H, m), 1.60 (3H, s), 1.49 (3H, s), 1.32 (3H, t, *J* = 7.2 Hz), 0.96 (3H, t, *J* = 7.2 Hz); ¹³C NMR (CDCl₃, 100 MHz): δ 168.7, 168.0, 141.1, 133.8, 128.5, 128.2, 126.8, 121.0, 61.6, 61.2, 58.1, 46.0, 32.9, 25.8, 17.8, 14.2, 13.8. HRMS (ESI⁺): Calcd for C₁₉H₂₇O₄ [M+H]⁺: 319.1909; Found: 319.1912. Specific rotation: [α]_D^{20.0} -7.89 (*c* 1.85, CHCl₃) for an enantiomerically enriched sample of 95:5 e.r.

Enantiomeric purity was determined by HPLC analysis in comparison with authentic racemic material; Chiralpak OZ-H column, 99.0:1.0 hexanes/*i*PrOH, 1.0 mL/min, 220 nm.

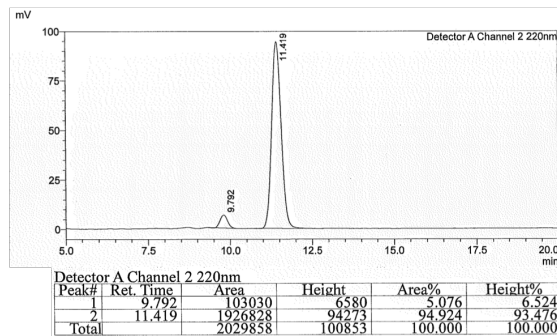
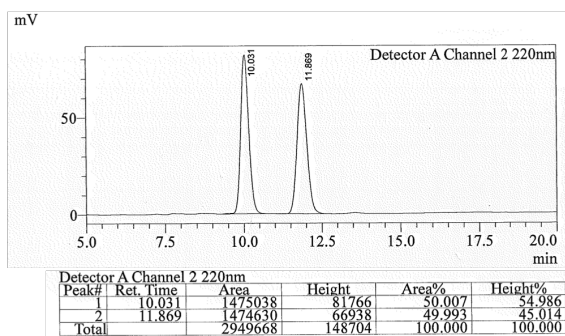


Retention Time	Area	Area%	Retention Time	Area	Area%
14.354	1886077	49.574	13.020	156692	5.368
27.401	1918482	50.426	24.575	2762577	94.632

Diethyl (*S*)-2-(1-(4-fluorophenyl)-4-methylpent-3-en-1-yl)malonate (4.40): IR (neat): 2980 (w), 2931 (w), 1752 (s), 1730 (s), 1605 (w), 1509 (s), 1446 (w), 1368 (m), 1307 (m), 1223 (s), 1175 (s), 1147 (s), 1098 (s), 1031 (s), 860 (w), 831 (s), 570 (w), 546 (w) cm⁻¹;

^1H NMR (CDCl_3 , 400 MHz): δ 7.16–7.13 (2H, m), 6.94 (2H, t, $J = 8.8$ Hz), 4.87 (1H, t, $J = 7.2$ Hz), 4.23 (2H, q, $J = 7.2$ Hz), 3.90 (2H, qd, $J = 7.2$, 1.2 Hz), 3.64 (1H, d, $J = 11.2$ Hz), 3.40 (1H, td, $J = 10.4$, 4.8 Hz), 2.45–2.38 (1H, m), 2.29–2.21 (1H, m), 1.57 (3H, s), 1.45 (3H, s), 1.29 (3H, t, $J = 7.2$ Hz), 0.97 (3H, t, $J = 7.2$ Hz); **^{13}C NMR (CDCl_3 , 100 MHz):** δ 168.5, 167.9, 161.8 (d, $J_{CF} = 243.6$ Hz), 136.8 (d, $J_{CF} = 3.1$ Hz), 134.1, 130.0 (d, $J_{CF} = 7.6$ Hz), 120.7, 115.1 (d, $J_{CF} = 21.2$ Hz), 61.7, 61.3, 58.1, 45.2, 33.0, 25.8, 17.8, 14.2, 13.9. **HRMS (DART⁺):** Calcd for $\text{C}_{19}\text{H}_{26}\text{O}_4\text{F}$ $[\text{M}+\text{H}]^+$: 337.1815; Found: 337.1816. Specific rotation: $[\alpha]_{\text{D}}^{20.0} -5.66$ (c 1.16, CHCl_3) for an enantiomerically enriched sample of 95:5 e.r.

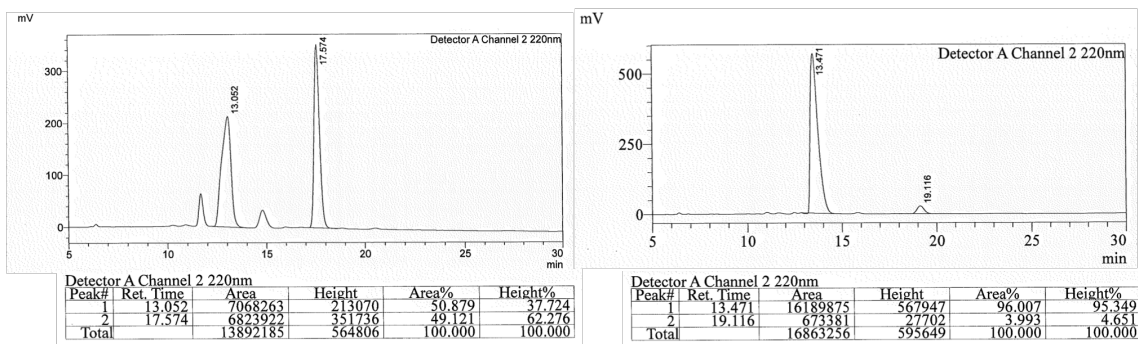
Enantiomeric purity was determined by HPLC analysis in comparison with authentic racemic material; Chiralpak OZ–H column, 99.0:1.0 hexanes/*i*PrOH, 1.0 mL/min, 220 nm.



Retention Time	Area	Area%	Retention Time	Area	Area%
10.031	1475038	50.007	9.792	103030	5.076
11.869	1474630	49.993	11.419	1926828	94.924

Diethyl (*S*)-2-(4-methyl-1-(4-(trifluoromethyl)phenyl)pent-3-en-1-yl)malonate (4.41): **IR (neat):** 2981 (w), 2931 (w), 1752 (s), 1731 (s), 1619 (w), 1447 (w), 1421 (w), 1370 (w), 1324 (s), 1250 (s), 1162 (s), 1113 (s), 1068 (s), 1033 (s), 1018 (s), 833 (s), 732 (w), 610 (m), 444 (w) cm^{-1} ; **^1H NMR (CDCl_3 , 400 MHz):** δ 7.52 (2H, d, $J = 8.0$ Hz), 7.31 (2H, d, $J = 8.0$ Hz), 4.86 (1H, t, $J = 7.2$ Hz), 4.24 (2H, q, $J = 7.2$ Hz), 3.90 (2H, q, $J = 7.2$ Hz), 3.70 (1H, d, $J = 10.4$ Hz), 3.52–3.45 (1H, m), 2.48–2.42 (1H, m), 2.34–2.26 (1H, m), 1.58 (3H, s), 1.44 (3H, s), 1.29 (3H, t, $J = 7.2$ Hz), 0.94 (3H, t, $J = 7.2$ Hz); **^{13}C NMR (CDCl_3 , 100 MHz):** δ 168.3, 167.7, 145.48, 148.47, 134.6, 129.2 (q, $J_{CF} = 31.9$ Hz), 128.9, 125.2 (q, $J_{CF} = 3.8$ Hz), 120.3, 61.9, 61.5, 57.6, 45.7, 32.7, 25.8, 17.8, 14.2, 13.8. **HRMS (DART⁺):** Calcd for $\text{C}_{20}\text{H}_{26}\text{F}_3\text{O}_4$ $[\text{M}+\text{H}]^+$: 387.1783; Found: 387.1782. Specific rotation: $[\alpha]_{\text{D}}^{20.0} -11.2$ (c 2.97, CHCl_3) for an enantiomerically enriched sample of 96:4 e.r.

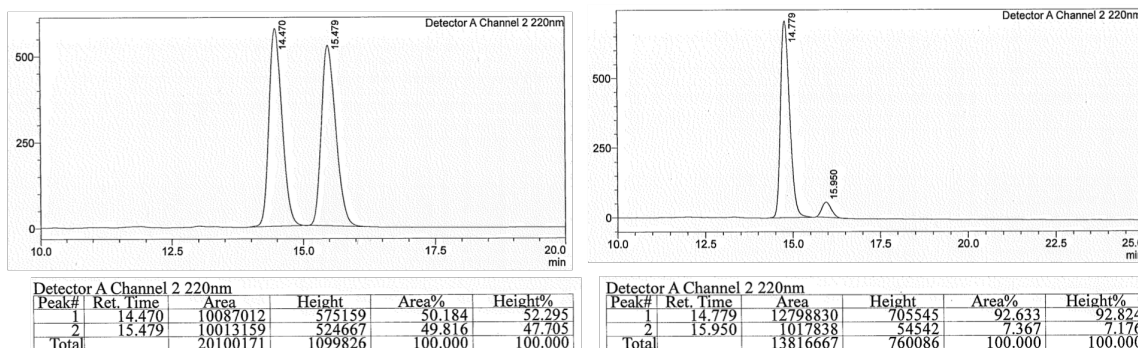
Enantiomeric purity was determined by HPLC analysis in comparison with authentic racemic material; Chiralpak OD–H column, 99.0:1.0 hexanes/*i*PrOH, 0.5 mL/min, 220 nm



Retention Time	Area	Area%	Retention Time	Area	Area%
13.052	7068263	50.879	13.471	16189875	96.007
17.574	6823922	49.121	19.116	673381	3.993

Diethyl (S)-2-(1-(2-methoxyphenyl)-4-methylpent-3-en-1-yl)malonate (4.42): IR (neat): 2979 (w), 2931 (w), 1752 (s), 1730 (s), 1600 (w), 1586 (w), 1493 (m), 1462 (m), 1440 (m), 1368 (m), 1307 (s), 1242 (s), 1175 (s), 1146 (s), 1117 (m), 1096 (m), 1027 (s), 861 (w), 751 (s), 523 (w) cm^{-1} ; $^1\text{H NMR}$ (CDCl_3 , 400 MHz): δ 7.15 (1H, td, $J = 7.6$, 1.6 Hz), 7.06 (1H, dd, $J = 7.6$, 1.6 Hz), 6.84–6.80 (2H, m), 4.92 (1H, t, $J = 7.2$ Hz), 4.21 (2H, q, $J = 7.2$ Hz), 4.00 (1H, d, $J = 10.8$ Hz), 3.91–3.85 (2H, m), 3.82 (3H, s), 3.70 (1H, td, $J = 10.4$, 4.8 Hz), 2.51–2.44 (1H, m), 2.39–2.33 (1H, m), 1.55 (3H, s), 1.44 (3H, s), 1.27 (3H, t, $J = 7.2$ Hz), 0.94 (3H, t, $J = 7.2$ Hz); $^{13}\text{C NMR}$ (CDCl_3 , 100 MHz): δ 169.1, 168.5, 157.9, 133.2, 130.2, 129.0, 127.9, 121.8, 120.3, 110.8, 61.4, 61.0, 56.1, 55.4, 30.8, 25.8, 17.7, 14.3, 13.9. HRMS (DART⁺): Calcd for $\text{C}_{20}\text{H}_{29}\text{O}_5$ $[\text{M}+\text{H}]^+$: 349.2015; Found: 349.2007. Specific rotation: $[\alpha]_{\text{D}}^{20.0} -5.50$ (c 1.09, CHCl_3) for an enantiomerically enriched sample of 93:7 er.

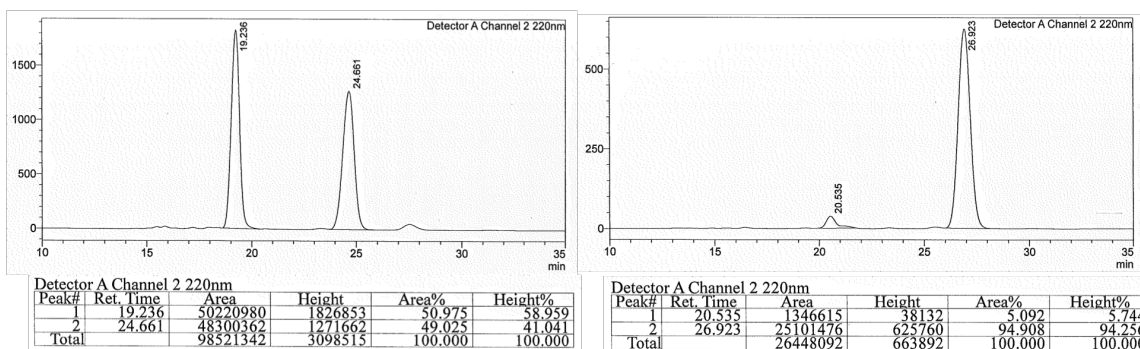
Enantiomeric purity was determined by HPLC analysis in comparison with authentic racemic material; Chiralpak OD–H column, 99.0:1.0 hexanes/*i*PrOH, 0.5 mL/min, 220 nm.



Retention Time	Area	Area%	Retention Time	Area	Area%
14.470	10087012	50.184	14.779	12798830	92.633
15.479	10013159	49.816	15.950	1017838	7.367

Diethyl (S)-2-(1-(3-bromophenyl)-4-methylpent-3-en-1-yl)malonate (4.43): IR (neat): 2979 (w), 2931 (w), 1752 (s), 1730 (s), 1594 (w), 1567 (w), 1474 (w), 1446 (w), 1429 (w), 1368 (m), 1302 (m), 1247 (s), 1176 (s), 1147 (s), 1112 (m), 1096 (m), 1074 (m), 1030 (s), 997 (w), 784 (m), 662 (w), 440 (w) cm^{-1} ; $^1\text{H NMR}$ (CDCl_3 , 400 MHz): δ 7.33–7.31 (2H, m), 7.13–7.11 (2H, m), 6.84–6.80 (2H, m), 4.88 (1H, t, $J = 7.2$ Hz), 4.23 (2H, q, $J = 7.2$ Hz), 3.92 (2H, q, $J = 7.2$ Hz), 3.65 (1H, d, $J = 10.8$ Hz), 3.38 (1H, td, $J = 10.0, 4.8$ Hz), 2.45–2.39 (1H, m), 2.30–2.23 (1H, m), 1.59 (3H, s), 1.46 (3H, s), 1.29 (3H, t, $J = 7.2$ Hz), 0.97 (3H, t, $J = 7.2$ Hz); $^{13}\text{C NMR}$ (CDCl_3 , 100 MHz): δ 168.4, 167.8, 143.6, 134.5, 131.6, 130.0, 129.8, 127.3, 122.3, 120.5, 61.8, 61.4, 57.7, 45.6, 32.7, 25.8, 17.8, 14.2, 13.9. HRMS (DART^+): Calcd for $\text{C}_{19}\text{H}_{26}\text{BrO}_4$ $[\text{M}+\text{H}]^+$: 397.1014; Found: 397.1009. Specific rotation: $[\alpha]_{\text{D}}^{20.0} -12.0$ (c 2.39, CHCl_3) for an enantiomerically enriched sample of 95:5 e.r.

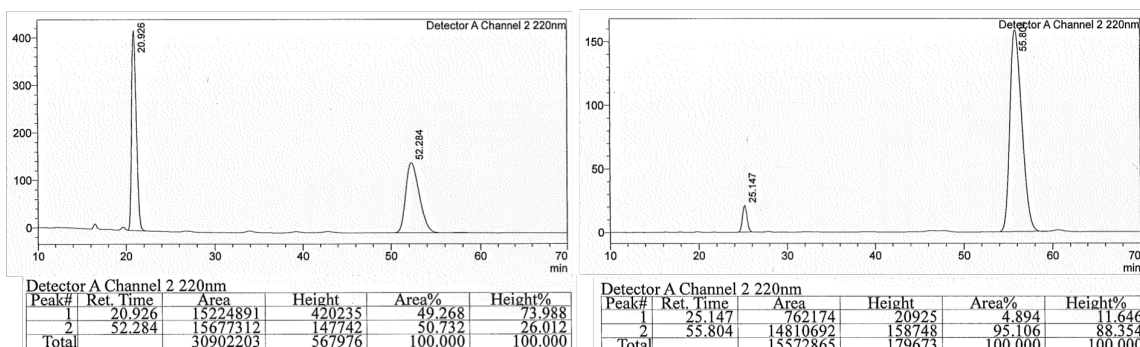
Enantiomeric purity was determined by HPLC analysis in comparison with authentic racemic material; Chiralpak OZ–H column, 99.0:1.0 hexanes/*i*PrOH, 0.5 mL/min, 220 nm.



Retention Time	Area	Area%	Retention Time	Area	Area%
19.236	50220980	50.975	20.535	1346615	5.092
24.661	48300362	49.025	26.923	25101476	94.908

Diethyl (S)-2-(4-methyl-1-(*o*-tolyl)pent-3-en-1-yl)malonate (4.44): IR (neat): 2978 (w), 2928 (w), 2856 (w), 1753 (s), 1731 (s), 1493 (w), 1464 (w), 1446 (w), 1368 (s), 1307 (s), 1250 (s), 1175 (s), 1146 (s), 1114 (m), 1096 (m), 1032 (s), 861 (w), 756 (m), 726 (m), 594 (w), 455 (w) cm^{-1} ; $^1\text{H NMR}$ (CDCl_3 , 400 MHz): δ 7.13–7.12 (2H, m), 7.10–7.05 (2H, m), 4.90 (1H, t, $J = 7.2$ Hz), 4.24 (2H, q, $J = 7.2$ Hz), 3.85 (2H, q, $J = 7.2$ Hz), 3.81–3.72 (2H, m), 2.45–2.38 (1H, m), 2.35 (3H, s), 2.26–2.18 (1H, m), 1.57 (3H, s), 1.44 (3H, s), 1.30 (3H, t, $J = 7.2$ Hz), 0.90 (3H, t, $J = 7.2$ Hz); $^{13}\text{C NMR}$ (CDCl_3 , 100 MHz): δ 168.8, 168.1, 139.8, 137.1, 133.9, 130.3, 126.5, 126.4, 125.9, 120.7, 61.6, 61.2, 57.9, 40.2, 33.3, 25.8, 20.1, 17.7, 14.3, 13.7. HRMS (ESI^+): Calcd for $\text{C}_{20}\text{H}_{29}\text{O}_4$ $[\text{M}+\text{H}]^+$: 333.2066; Found: 333.2057. Specific rotation: $[\alpha]_{\text{D}}^{20.0} -21.8$ (c 2.17, CHCl_3) for an enantiomerically enriched sample of 95:5 e.r.

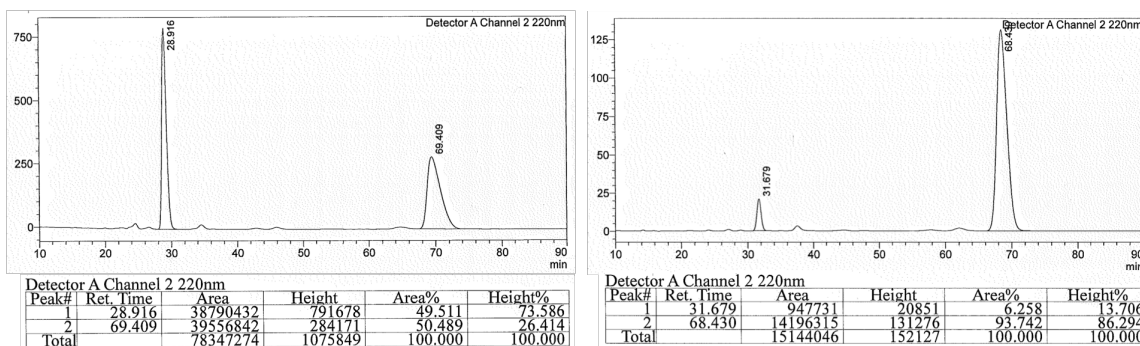
Enantiomeric purity was determined by HPLC analysis in comparison with authentic racemic material; Chiralpak OZ-H column, 99.0:1.0 hexanes/*i*PrOH, 0.5 mL/min, 220 nm.



Retention Time	Area	Area%	Retention Time	Area	Area%
20.926	15224891	49.268	25.147	762174	4.894
52.284	15677312	50.732	55.804	14810692	95.106

Diethyl (S)-2-(1-(2-chlorophenyl)-4-methylpent-3-en-1-yl)malonate (4.45): IR (neat): 2980 (w), 2932 (w), 1731 (s), 1476 (w), 1443 (w), 1369 (m), 1305 (m), 1247 (s), 1176 (s), 1148 (s), 1110 (m), 1096 (m), 1035 (s), 862 (w), 754 (s), 456 (m) cm^{-1} ; $^1\text{H NMR}$ (CDCl_3 , 400 MHz): δ 7.32 (1H, d, $J = 7.2$ Hz), 7.20–7.17 (2H, m), 7.17–7.09 (1H, m), 4.93 (1H, tt, $J = 7.2, 1.2$ Hz), 4.24 (2H, q, $J = 7.6$ Hz), 3.85 (2H, q, $J = 7.2$ Hz), 4.10 (1H, s, br), 3.98–3.88 (2H, m), 2.86–2.82 (1H, m), 2.48–2.38 (2H, m), 1.57 (3H, s), 1.42 (3H, s), 1.28 (3H, t, $J = 7.2$ Hz), 0.98 (3H, t, $J = 7.2$ Hz); $^{13}\text{C NMR}$ (CDCl_3 , 100 MHz): δ 168.4, 167.8, 138.8, 134.8, 134.5, 129.8, 127.8, 126.7, 120.2, 61.7, 61.4, 56.6, 31.7, 29.8, 25.8, 17.7, 14.2, 13.8. **HRMS (ESI $^+$):** Calcd for $\text{C}_{19}\text{H}_{26}\text{ClO}_4$ $[\text{M}+\text{H}]^+$: 353.1520; Found: 353.1515. Specific rotation: $[\alpha]_{\text{D}}^{20.0} -5.84$ (c 1.09, CHCl_3) for an enantiomerically enriched sample of 94:6 er.

Enantiomeric purity was determined by HPLC analysis in comparison with authentic racemic material; Chiralpak OZ-H column, 99.0:1.0 hexanes/*i*PrOH, 0.5 mL/min, 220 nm.

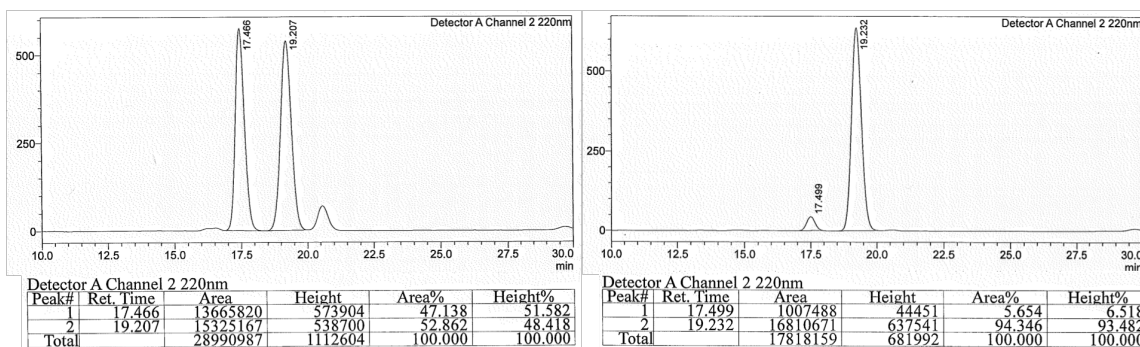


Retention Time	Area	Area%	Retention Time	Area	Area%
28.916	38790432	49.511	31.679	947731	6.258
			68.430	14196315	93.742

69.409	39556842	50.489	68.430	14196315	93.742
--------	----------	--------	--------	----------	--------

Diethyl (S)-2-(1-(4-methoxyphenyl)-4-methylpent-3-en-1-yl)malonate (4.46): IR (neat): 2979 (w), 2933 (w), 1752 (s), 1729 (s), 1611 (w), 1512 (s), 1463 (w), 1444 (w), 1368 (m), 1303 (m), 1246 (s), 1177 (s), 1146 (s), 1113 (s), 1096 (m), 1033 (s), 861 (w), 828 (s), 573 (w), 551 (m) cm^{-1} ; $^1\text{H NMR}$ (CDCl_3 , 400 MHz): δ 7.10 (2H, d, $J = 8.4$ Hz), 6.79 (2H, d, $J = 8.8$ Hz), 4.89 (1H, tt, $J = 7.2, 1.2$ Hz), 4.22 (2H, q, $J = 7.2$ Hz), 3.89 (2H, qd, $J = 7.2, 1.6$ Hz), 3.77 (3H, s), 3.63 (1H, d, $J = 11.2$ Hz), 3.36 (1H, td, $J = 10.0, 4.8$ Hz), 2.44–2.37 (1H, m), 2.29–2.22 (1H, m), 1.58 (3H, s), 1.47 (3H, s), 1.28 (3H, t, $J = 7.2$ Hz), 0.97 (3H, t, $J = 7.2$ Hz); $^{13}\text{C NMR}$ (CDCl_3 , 100 MHz): δ 168.7, 168.1, 158.4, 133.7, 133.1, 129.5, 121.2, 113.6, 61.6, 61.2, 58.3, 55.3, 45.2, 33.0, 25.8, 17.8, 14.2, 13.9. HRMS (ESI^+): Calcd for $\text{C}_{20}\text{H}_{29}\text{O}_5$ $[\text{M}+\text{H}]^+$: 349.2028; Found: 349.2015. Specific rotation: $[\alpha]_{\text{D}}^{20.0} -7.27$ (c 1.54, CHCl_3) for an enantiomerically enriched sample of 94:6 e.r.

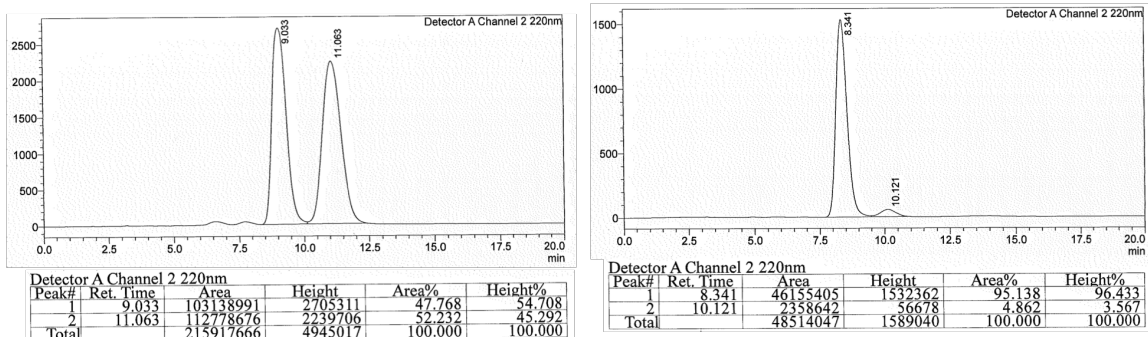
Enantiomeric purity was determined by HPLC analysis in comparison with authentic racemic material; Chiralpak OZ–H column, 99.0:1.0 hexanes/*i*PrOH, 0.5 mL/min, 220 nm.



Retention Time	Area	Area%	Retention Time	Area	Area%
17.466	13665820	47.138	17.499	1007488	5.654
19.207	15325167	52.862	19.232	16810671	94.346

Diethyl (S)-2-(4-methyl-1-(naphthalen-2-yl)pent-3-en-1-yl)malonate (4.47): IR (neat): 3055 (w), 2979 (w), 2931 (w), 1751 (s), 1728 (s), 1600 (w), 1508 (w), 1445 (w), 1368 (m), 1302 (m), 1246 (s), 1174 (s), 1145 (s), 1112 (m), 1095 (m), 1029 (s), 856 (s), 817 (s), 746 (s), 662 (w), 477 (s) cm^{-1} ; $^1\text{H NMR}$ (CDCl_3 , 400 MHz): δ 7.80–7.75 (3H, m), 7.64 (1H, s), 7.47–7.41 (2H, m), 7.36 (1H, td, $J = 8.4, 1.2$ Hz), 4.93 (1H, t, $J = 7.2$ Hz), 4.26 (2H, q, $J = 7.2$ Hz), 3.87–3.78 (3H, m), 3.61 (1H, td, $J = 11.2, 4.4$ Hz), 2.56–2.50 (1H, m), 2.46–2.38 (1H, m), 1.55 (3H, s), 1.48 (3H, s), 1.31 (3H, t, $J = 7.2$ Hz), 0.85 (3H, t, $J = 7.2$ Hz); $^{13}\text{C NMR}$ (CDCl_3 , 100 MHz): δ 168.6, 168.0, 138.7, 133.9, 133.4, 132.6, 127.9, 127.7, 127.4, 126.6, 126.0, 125.6, 121.0, 61.7, 61.2, 58.1, 46.0, 32.8, 25.8, 17.9, 14.3, 13.8. HRMS (DART^+): Calcd for $\text{C}_{23}\text{H}_{29}\text{O}_4$ $[\text{M}+\text{H}]^+$: 369.2066; Found: 369.2061. Specific rotation: $[\alpha]_{\text{D}}^{20.0} -18.6$ (c 2.05, CHCl_3) for an enantiomerically enriched sample of 95:5 e.r.

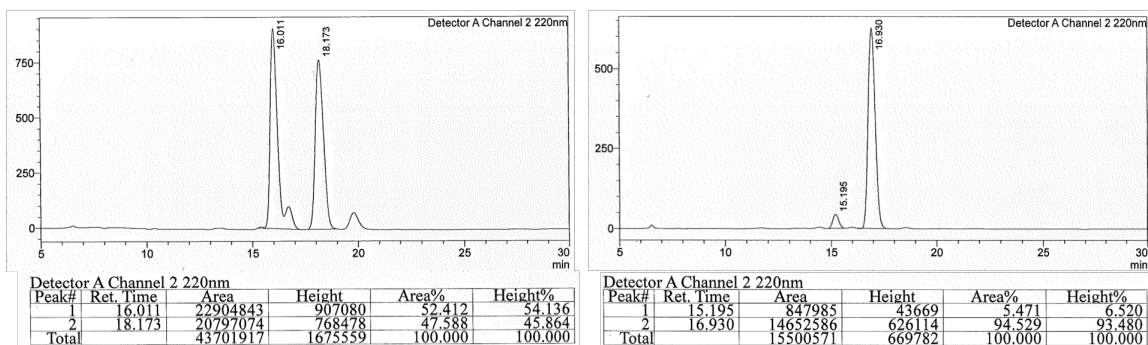
Enantiomeric purity was determined by HPLC analysis in comparison with authentic racemic material; Chiralpak OZ–H column, 99.0:1.0 hexanes/*i*PrOH, 1.0 mL/min, 220 nm.



Retention Time	Area	Area%	Retention Time	Area	Area%
9.033	101138991	47.768	8.341	46155405	95.138
11.063	112778676	52.232	10.121	2358642	4.862

Diethyl (S)-2-(1-(benzofuran-5-yl)-4-methylpent-3-en-1-yl)malonate (4.48): IR (neat): 2979 (w), 2930 (w), 1751 (s), 1728 (s), 1468 (m), 1445 (m), 1368 (m), 1301 (m), 1248 (s), 1175 (s), 1148 (s), 1128 (s), 1111 (s), 1096 (m), 1030 (s), 880 (m), 861 (m), 811 (m), 769 (m), 738 (s), 650 (w), 442 (m) cm^{-1} ; $^1\text{H NMR}$ (CDCl_3 , 600 MHz): δ 7.57 (1H, d, $J = 2.0$ Hz), 7.42 (1H, d, $J = 1.6$ Hz), 7.39 (1H, d, $J = 8.8$ Hz), 7.13 (1H, dd, $J = 8.4, 1.6$ Hz), 4.90 (1H, t, $J = 7.2$ Hz), 4.24 (2H, q, $J = 7.2$ Hz), 3.88–3.80 (2H, m), 3.72 (1H, d, $J = 10.4$ Hz), 3.51 (1H, td, $J = 10.0, 4.8$ Hz), 2.51–2.45 (1H, m), 2.38–2.30 (1H, m), 1.56 (3H, s), 1.47 (3H, s), 1.29 (3H, t, $J = 7.2$ Hz), 0.88 (3H, t, $J = 7.2$ Hz); $^{13}\text{C NMR}$ (CDCl_3 , 100 MHz): δ 168.7, 168.1, 154.1, 145.2, 135.6, 133.7, 127.4, 124.8, 121.1, 121.0, 111.0, 106.7, 61.6, 61.2, 58.6, 45.9, 33.3, 25.8, 17.8, 14.2, 13.8. **HRMS (ESI $^+$):** Calcd for $\text{C}_{21}\text{H}_{27}\text{O}_5$ $[\text{M}+\text{H}]^+$: 359.1858; Found: 359.1843. Specific rotation: $[\alpha]_{\text{D}}^{20.0} -12.7$ (c 1.91, CHCl_3) for an enantiomerically enriched sample of 94.5:5.5 e.r.

Enantiomeric purity was determined by HPLC analysis in comparison with authentic racemic material; Chiralpak OZ–H column, 99.0:1.0 hexanes/ *i*PrOH, 0.5 mL/min, 254 nm.

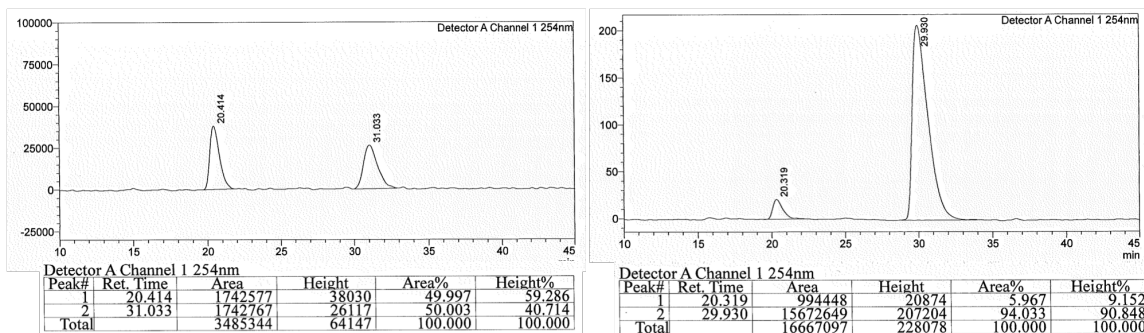


Retention Time	Area	Area%	Retention Time	Area	Area%
16.011	22904843	52.412	15.195	847985	5.471
18.173	20797074	47.588	16.930	14652586	94.529

16.011	22904843	52.412	15.195	847985	5.471
18.173	20797074	47.588	16.930	14652586	94.529

Diethyl (S)-2-(4-methyl-1-(pyridin-4-yl)pent-3-en-1-yl)malonate (4.49): IR (neat): 2980 (w), 2936 (w), 1728 (s), 1599 (m), 1559 (w), 1446 (m), 1416 (m), 1369 (m), 1300 (m), 1235 (s), 1174 (s), 1148 (s), 1128 (s), 1095 (m), 1071 (s), 1028 (s), 858 (m), 821 (m), 769 (m), 586 (m) cm^{-1} ; $^1\text{H NMR}$ (CDCl_3 , 600 MHz): δ 8.48 (2H, d, $J = 4.0$ Hz), 7.11 (2H, d, $J = 6.4$ Hz), 4.85 (1H, t, $J = 7.2$ Hz), 4.23 (2H, q, $J = 7.2$ Hz), 3.91 (2H, qd, $J = 7.2, 2.4$ Hz), 3.69 (1H, d, $J = 11.2$ Hz), 3.40 (1H, td, $J = 10.0, 4.8$ Hz), 2.45–2.39 (1H, m), 2.32–2.24 (1H, m), 1.57 (3H, s), 1.42 (3H, s), 1.28 (3H, t, $J = 7.2$ Hz), 0.96 (3H, t, $J = 7.2$ Hz); $^{13}\text{C NMR}$ (CDCl_3 , 100 MHz): δ 168.1, 167.5, 150.6, 149.7, 134.9, 123.9, 119.9, 61.9, 61.6, 56.9, 45.2, 32.3, 25.8, 17.8, 14.2, 13.8. HRMS (DART^+): Calcd for $\text{C}_{18}\text{H}_{26}\text{NO}_4$ $[\text{M}+\text{H}]^+$: 320.1862; Found: 320.1869. Specific rotation: $[\alpha]_{\text{D}}^{20.0} -8.57$ (c 1.19, CHCl_3) for an enantiomerically enriched sample of 94:6 e.r.

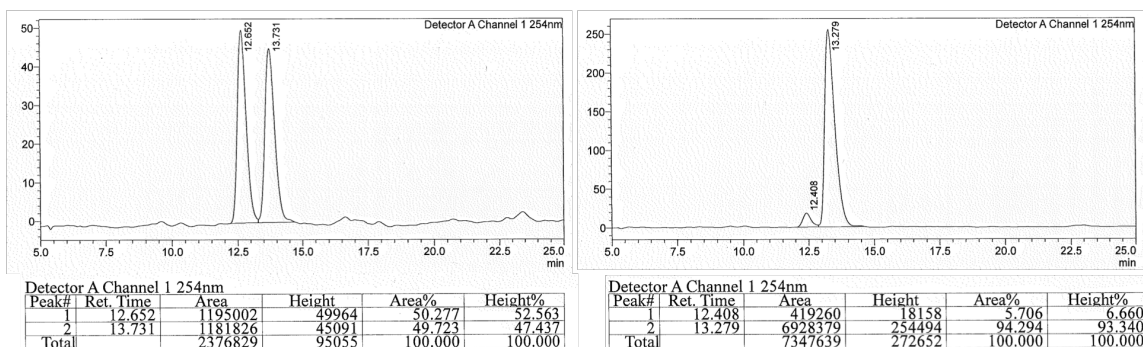
Enantiomeric purity was determined by HPLC analysis in comparison with authentic racemic material; Chiralpak OZ–H column, 95.0:5.0 hexanes/ *i*PrOH, 1.0 mL/min, 254 nm.



Retention Time	Area	Area%	Retention Time	Area	Area%
20.414	1742577	49.997	20.319	994448	5.967
31.033	1742767	50.003	29.930	15672649	94.033

Diethyl (S)-2-(4-methyl-1-(pyridin-3-yl)pent-3-en-1-yl)malonate (4.50): IR (neat): 2980 (w), 2933 (w), 1729 (s), 1572 (w), 1446 (m), 1426 (m), 1369 (m), 1302 (m), 1257 (s), 1240 (s), 1219 (s), 1173 (s), 1147 (s), 1111 (m), 1096 (m), 1024 (s), 861 (m), 809 (m), 715 (s), 627 (m) cm^{-1} ; $^1\text{H NMR}$ (CDCl_3 , 400 MHz): δ 8.43 (2H, m), 7.22 (1H, dt, $J = 7.6, 2.0$ Hz), 7.19 (1H, dd, $J = 7.6, 4.8$ Hz), 4.87 (1H, t, $J = 7.2$ Hz), 4.23 (2H, q, $J = 7.2$ Hz), 3.90 (2H, qd, $J = 7.2, 1.6$ Hz), 3.70 (1H, d, $J = 10.4$ Hz), 3.44 (1H, td, $J = 10.0, 4.4$ Hz), 2.48–2.41 (1H, m), 2.33–2.26 (1H, m), 1.57 (3H, s), 1.42 (3H, s), 1.28 (3H, t, $J = 7.2$ Hz), 0.96 (3H, t, $J = 7.2$ Hz); $^{13}\text{C NMR}$ (CDCl_3 , 100 MHz): δ 168.3, 167.7, 150.3, 148.3, 136.6, 135.8, 134.8, 123.2, 120.1, 61.9, 61.5, 57.3, 43.4, 32.6, 25.8, 17.8, 14.2, 13.9. HRMS (DART^+): Calcd for $\text{C}_{18}\text{H}_{26}\text{NO}_4$ $[\text{M}+\text{H}]^+$: 320.1862; Found: 320.1850. Specific rotation: $[\alpha]_{\text{D}}^{20.0} -5.42$ (c 1.61, CHCl_3) for an enantiomerically enriched sample of 94:6 e.r.

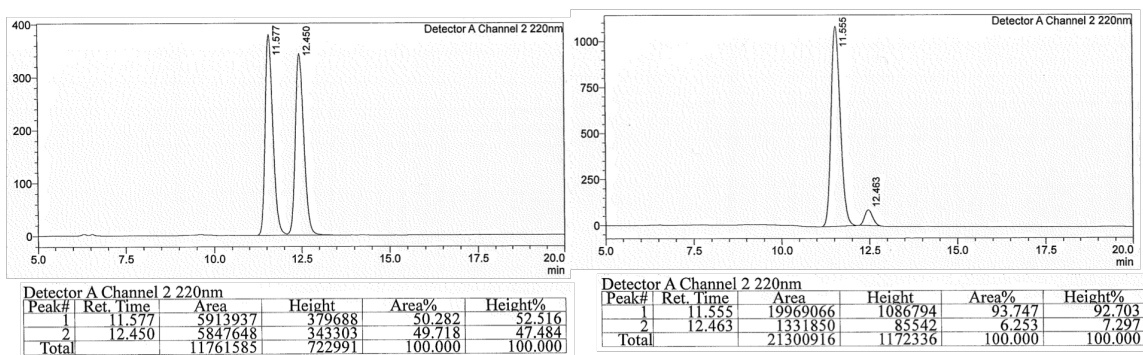
Enantiomeric purity was determined by HPLC analysis in comparison with authentic racemic material; Chiralpak OZ-H column, 95.0:5.0 hexanes/*i*PrOH, 1.0 mL/min, 254 nm.



Retention Time	Area	Area%	Retention Time	Area	Area%
12.652	1195002	50.277	12.408	419260	5.706
13.731	1181826	49.723	13.279	6928379	94.294

Diethyl (S)-2-(1-(1-(*tert*-butoxycarbonyl)-1*H*-indol-6-yl)-4-methylpent-3-en-1-yl)malonate (4.51): IR (neat): 2979 (w), 2932 (w), 1729 (s), 1529 (w), 1480 (w), 1439 (m), 1369 (m), 1335 (s), 1252 (s), 1211 (m), 1219 (s), 1170 (s), 1144 (s), 1128 (s), 1096 (m), 1078 (m), 1024 (s), 908 (m), 855 (m), 818 (m), 767 (m), 729 (s), 652 (m), 466 (w) cm^{-1} ; **^1H NMR (CDCl_3 , 400 MHz):** δ 8.02 (1H, s), 7.53 (1H, d, $J = 3.6$ Hz), 7.42 (1H, d, $J = 8.0$ Hz), 7.07 (1H, d, $J = 8.0$ Hz), 6.49 (1H, d, $J = 3.6$ Hz), 4.93 (1H, t, $J = 7.2$ Hz), 4.26-4.19 (2H, m), 3.86 (2H, q, $J = 7.2$ Hz), 3.75 (1H, d, $J = 10.4$ Hz), 3.55 (1H, td, $J = 10.0, 4.4$ Hz), 2.52-2.46 (1H, m), 2.41-2.34 (1H, m), 1.67 (9H, s), 1.56 (3H, s), 1.48 (3H, s), 1.29 (3H, t, $J = 7.2$ Hz), 0.93 (3H, t, $J = 7.2$ Hz); **^{13}C NMR (CDCl_3 , 100 MHz):** δ 168.8, 168.1, 149.8, 137.5, 135.4, 133.6, 129.5, 125.9, 123.6, 121.3, 120.5, 115.0, 107.2, 83.6, 61.6, 61.2, 58.5, 46.3, 33.2, 28.3, 25.8, 17.9, 14.2, 13.8. **HRMS (ESI $^+$):** Calcd for $\text{C}_{26}\text{H}_{39}\text{O}_6\text{N}_2$ $[\text{M}+\text{NH}_4]^+$: 475.2808; Found: 475.2811. Specific rotation: $[\alpha]_{\text{D}}^{20.0} -8.15$ (c 2.65, CHCl_3) for an enantiomerically enriched sample of 94:6 e.r.

Enantiomeric purity was determined by HPLC analysis in comparison with authentic racemic material; Chiralpak OD-H column, 99.0:1.0 hexanes/*i*PrOH, 0.5 mL/min, 220 nm.

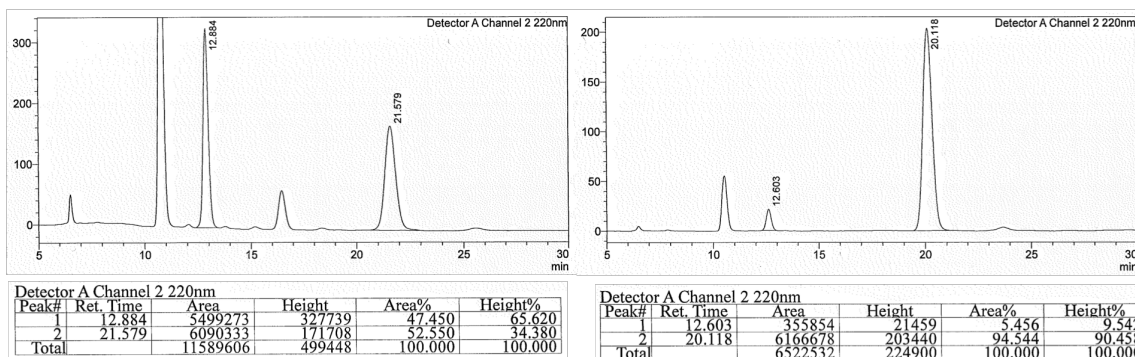


Retention Time	Area	Area%	Retention Time	Area	Area%
11.577	5913937	50.282	11.555	19969066	93.747
12.450	5847648	49.718	12.463	1331850	6.253

Diethyl (S)-2-(4-methyl-1-(thiophen-3-yl)pent-3-en-1-yl)malonate (4.52): IR (neat): 2979 (w), 2929 (w), 1751 (s), 1728 (s), 1446 (m), 1413 (w), 1368 (m), 1301 (m), 1255 (s), 1236 (s), 1174 (s), 1145 (s), 1112 (m), 1096 (m), 1030 (s), 904 (w), 858 (m), 836 (m), 782 (m), 657 (m), 428 (w) cm^{-1} ; **^1H NMR (CDCl_3 , 500 MHz):** δ 7.20 (1H, dd, $J = 4.8, 3.2$ Hz), 6.99 (1H, d, $J = 3.2$ Hz), 6.96 (1H, d, $J = 4.8$ Hz), 4.95 (1H, t, $J = 7.2$ Hz), 4.21 (2H, q, $J = 7.2$ Hz), 3.95 (2H, q, $J = 7.2$ Hz), 3.64 (1H, d, $J = 10.0$ Hz), 3.60–3.55 (1H, m), 2.45–2.39 (1H, m), 2.32–2.25 (1H, m), 1.61 (3H, s), 1.48 (3H, s), 1.28 (3H, t, $J = 7.2$ Hz), 1.02 (3H, t, $J = 7.2$ Hz); **^{13}C NMR (CDCl_3 , 100 MHz):** δ 168.6, 168.2, 141.8, 134.1, 61.6, 61.3, 57.8, 41.2, 32.7, 25.9, 17.7, 14.2, 13.9. **HRMS (DART⁺):** Calcd for $\text{C}_{17}\text{H}_{25}\text{SO}_4$ $[\text{M}+\text{H}]^+$: 325.1474; Found: 325.1486. Specific rotation: $[\alpha]_{\text{D}}^{20.0}$ 1.21 (c 0.99, CHCl_3) for an enantiomerically enriched sample of 91:9 e.r.

Diethyl (S)-2-(1-(1-benzyl-1H-pyrrol-2-yl)-4-methylpent-3-en-1-yl)malonate (4.53): IR (neat): 2979 (w), 2929 (w), 1750 (s), 1729 (s), 1496 (w), 1477 (w), 1452 (m), 1368 (m), 1300 (m), 1242 (s), 1176 (s), 1146 (s), 1096 (m), 1078 (m), 1028 (s), 861 (w), 778 (m), 705 (s), 622 (w), 613 (w), 443 (w) cm^{-1} ; **^1H NMR (CDCl_3 , 500 MHz):** δ 7.34–7.23 (3H, m), 7.08 (1H, d, $J = 7.6$ Hz), 6.52–6.50 (1H, m), 6.08 (1H, t, $J = 3.2$ Hz), 5.98–5.97 (1H, m), 5.20 (1H, d, $J = 8.0$ Hz), 5.02 (1H, d, $J = 8.0$ Hz), 4.79 (1H, t, $J = 7.2$ Hz), 4.19 (2H, q, $J = 7.2$ Hz), 3.97 (2H, q, $J = 7.2$ Hz), 3.60–3.51 (2H, m), 2.19 (2H, d, $J = 6.4$ Hz), 1.52 (3H, s), 1.41 (3H, s), 1.27 (3H, t, $J = 7.2$ Hz), 1.06 (3H, t, $J = 7.2$ Hz); **^{13}C NMR (CDCl_3 , 100 MHz):** δ 168.6, 168.3, 138.7, 133.9, 132.8, 128.68, 128.65, 127.4, 127.1, 120.9, 107.5, 106.5, 83.6, 61.6, 61.4, 58.1, 50.4, 36.3, 32.8, 25.9, 17.7, 14.2, 14.0. **HRMS (DART⁺):** Calcd for $\text{C}_{24}\text{H}_{32}\text{O}_4\text{N}$ $[\text{M}+\text{H}]^+$: 398.2331; Found: 398.2346. Specific rotation: $[\alpha]_{\text{D}}^{20.0}$ 1.69 (c 2.13, CHCl_3) for an enantiomerically enriched sample of 94.5:5.5 e.r.

Enantiomeric purity was determined by HPLC analysis in comparison with authentic racemic material; Chiralpak OZ–H column, 99.0:1.0 hexanes/*i*PrOH, 0.5 mL/min, 220 nm.

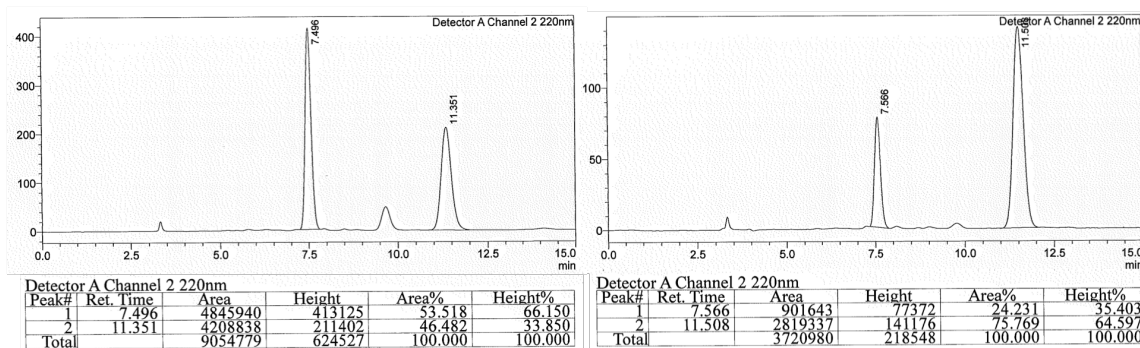


Retention Time	Area	Area%	Retention Time	Area	Area%
----------------	------	-------	----------------	------	-------

12.884	5499273	47.450	12.603	355854	5.456
21.579	6090333	52.550	20.118	6166678	94.544

Diethyl (S)-2-(4-methyl-1-(thiophen-2-yl)pent-3-en-1-yl)malonate (4.54): IR (neat): 2980 (w), 2930 (w), 1751 (s), 1730 (s), 1444 (w), 1368 (m), 1303 (m), 1259 (s), 1238 (s), 1149 (s), 1113 (m), 1096 (m), 1030 (s), 852 (m), 827 (m), 695 (s), 613 (w), 533 (w) cm^{-1} ; **^1H NMR (CDCl_3 , 400 MHz):** δ 7.14 (1H, d, $J = 5.2$ Hz), 6.88 (1H, d, $J = 5.2, 3.6$ Hz), 6.84 (1H, d, $J = 3.6$ Hz), 5.01 (1H, t, $J = 7.2$ Hz), 4.22 (2H, q, $J = 7.2$ Hz) 3.98 (2H, q, $J = 7.2$ Hz), 3.78–3.72 (1H, m), 3.65 (1H, d, $J = 10.4$ Hz), 2.52–2.46 (1H, m), 2.38–2.30 (1H, m), 1.63 (3H, s), 1.52 (3H, s), 1.28 (3H, t, $J = 7.2$ Hz), 1.06 (3H, t, $J = 7.2$ Hz); **^{13}C NMR (CDCl_3 , 100 MHz):** δ 168.3, 167.9, 144.5, 134.5, 126.4, 125.6, 124.0, 120.8, 61.7, 61.4, 58.7, 41.2, 33.8, 25.9, 17.9, 14.2, 13.9. **HRMS (DART⁺):** Calcd for $\text{C}_{17}\text{H}_{25}\text{SO}_4$ $[\text{M}+\text{H}]^+$: 325.1474; Found: 325.1473. Specific rotation: $[\alpha]_{\text{D}}^{20.0}$ 4.86 (c 1.07, CHCl_3) for an enantiomerically enriched sample of 76:24 e.r.

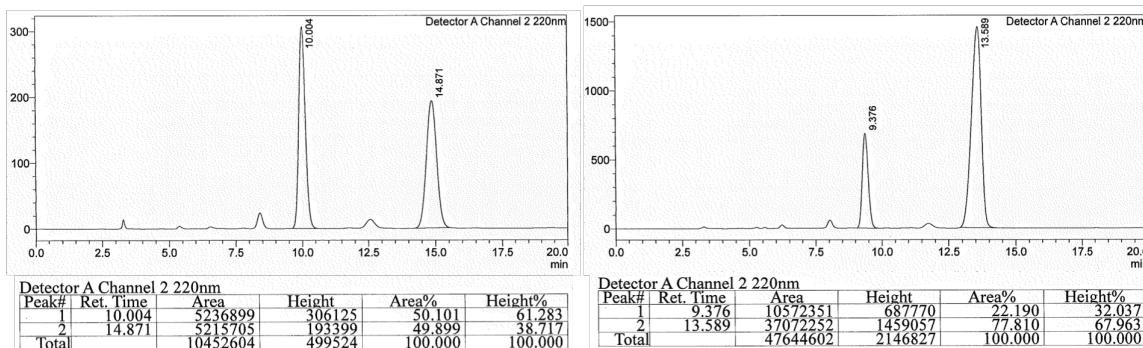
Enantiomeric purity was determined by HPLC analysis in comparison with authentic racemic material; Chiralpak OZ–H column, 99.0:1.0 hexanes/*i*PrOH, 1.0 mL/min, 220 nm.



Retention Time	Area	Area%	Retention Time	Area	Area%
7.496	4845940	53.518	7.566	901643	24.231
11.351	4208838	46.482	11.508	2819337	75.769

Diethyl (S)-2-(1-(furan-2-yl)-4-methylpent-3-en-1-yl)malonate (4.55): IR (neat): 2981 (w), 2931 (w), 1752 (s), 1731 (s), 1505 (w), 1446 (w), 1368 (m), 1303 (m), 1258 (s), 1239 (s), 1146 (s), 1112 (m), 1096 (m), 1031 (s), 1011 (s), 861 (m), 805 (m), 731 (s), 599 (m), 438 (w) cm^{-1} ; **^1H NMR (CDCl_3 , 400 MHz):** δ 7.30 (1H, t, $J = 0.8$ Hz), 6.25 (1H, t, $J = 2.0$ Hz), 6.05 (1H, d, $J = 3.2$ Hz), 4.98 (1H, t, $J = 7.2$ Hz), 4.21 (2H, q, $J = 7.2$ Hz), 4.01 (2H, qd, $J = 7.2, 2.0$ Hz), 3.70 (1H, d, $J = 9.6$ Hz), 3.57–3.51 (1H, m), 2.39 (1H, t, $J = 7.2$ Hz), 1.63 (3H, s), 1.51 (3H, s), 1.27 (3H, t, $J = 7.2$ Hz), 1.11 (3H, t, $J = 7.2$ Hz); **^{13}C NMR (CDCl_3 , 100 MHz):** δ 168.3, 168.1, 154.5, 142.5, 134.3, 120.7, 110.2, 107.1, 61.6, 61.4, 56.0, 39.4, 30.5, 25.9, 17.7, 14.2, 14.0. **HRMS (DART⁺):** Calcd for $\text{C}_{17}\text{H}_{25}\text{O}_5$ $[\text{M}+\text{H}]^+$: 309.1702; Found: 309.1712. Specific rotation: $[\alpha]_{\text{D}}^{20.0}$ -0.72 (c 1.11, CHCl_3) for an enantiomerically enriched sample of 78:22 e.r.

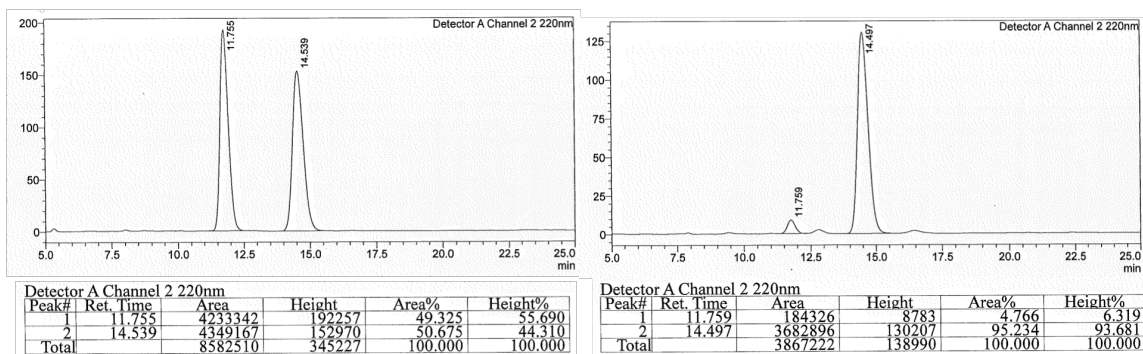
Enantiomeric purity was determined by HPLC analysis in comparison with authentic racemic material; Chiralpak OZ-H column, 99.0:1.0 hexanes/*i*PrOH, 1.0 mL/min, 220 nm.



Retention Time	Area	Area%	Retention Time	Area	Area%
10.004	5236899	50.101	9.376	10572351	22.190
14.871	5215705	49.899	13.589	37072252	77.810

Diethyl (S)-2-(1-(benzo[d][1,3]dioxol-5-yl)-4-methylpent-3-en-1-yl)malonate (4.62):
IR (neat): 2980 (w), 2917 (w), 1751 (s), 1729 (s), 1505 (m), 1488 (s), 1441 (m), 1368 (m), 1303 (m), 1243 (s), 1175 (s), 1147 (s), 1097 (s), 1036 (s), 934 (s), 900 (m), 859 (m), 810 (s), 644 (m), 444 (m) cm^{-1} ; **^1H NMR (CDCl_3 , 500 MHz):** δ 6.70–6.68 (2H, m), 6.63 (1H, dd, $J = 8.0, 2.0$ Hz), 5.91 (2H, s), 4.90 (1H, t, $J = 7.2$ Hz), 4.23 (2H, q, $J = 7.2$ Hz), 3.93 (2H, q, $J = 7.2$ Hz), 3.59 (1H, d, $J = 6.4$ Hz), 3.33 (1H, dt, $J = 10.0, 4.4$ Hz), 2.43–2.36 (1H, m), 2.26–2.18 (1H, m), 1.59 (3H, s), 1.49 (3H, s), 1.28 (3H, t, $J = 7.2$ Hz), 1.01 (3H, t, $J = 7.2$ Hz); **^{13}C NMR (CDCl_3 , 100 MHz):** δ 168.6, 168.0, 147.5, 146.3, 135.0, 133.8, 121.8, 121.0, 108.7, 108.0, 100.9, 61.6, 61.3, 58.3, 45.6, 32.9, 25.8, 17.9, 14.2, 14.0. **HRMS (DART⁺):** Calcd for $\text{C}_{20}\text{H}_{27}\text{O}_6$ $[\text{M}+\text{H}]^+$: 363.1808; Found: 363.1802. Specific rotation: $[\alpha]_{\text{D}}^{20.0} -1.01$ (c 2.17, CHCl_3) for an enantiomerically enriched sample of 95:5 e.r.

Enantiomeric purity was determined by HPLC analysis in comparison with authentic racemic material; Chiralpak OZ-H column, 99.0:1.0 hexanes/*i*PrOH, 1.0 mL/min, 220 nm.

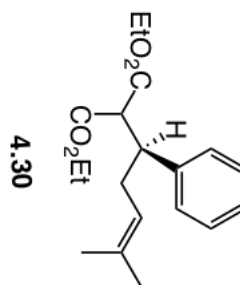
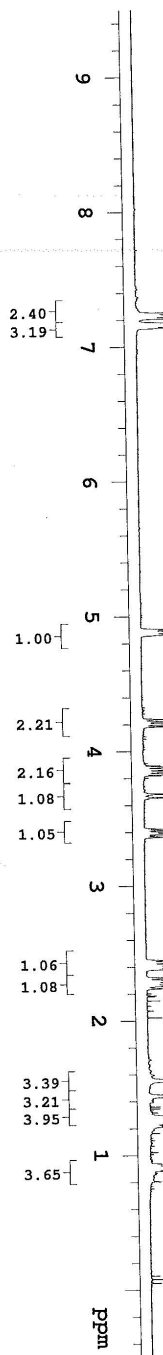


Retention Time	Area	Area%	Retention Time	Area	Area%
11.755	4233342	49.325	11.759	184326	4.766
14.539	4349167	50.675	14.497	3682896	95.234

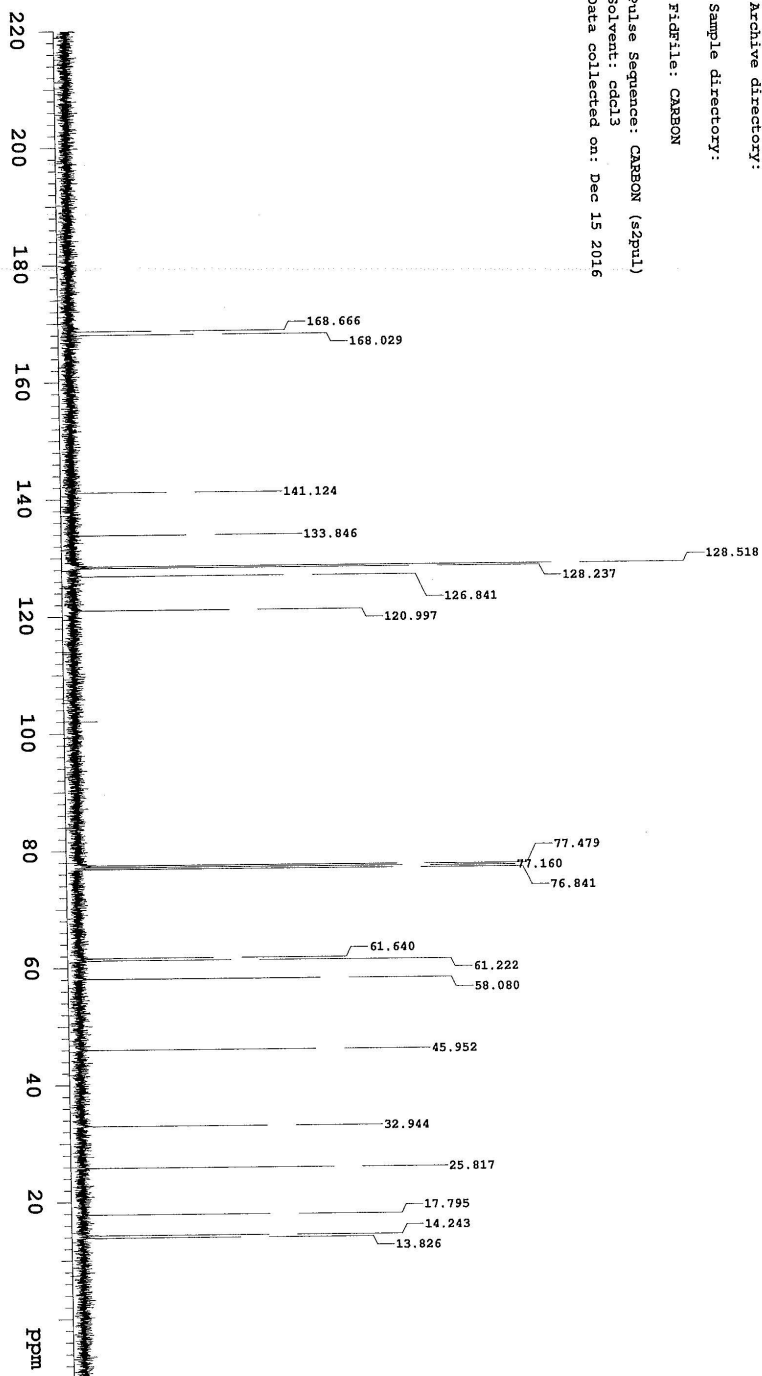
11.755	4233342	49.325	11.759	184326	4.766
14.539	4349167	50.675	14.497	3682896	95.234

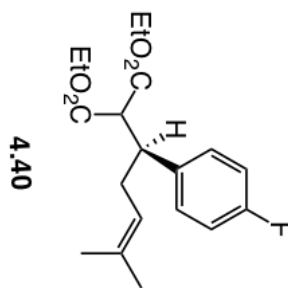
Ethyl (S)-3-(benzo[d][1,3]dioxol-5-yl)-6-methylhept-5-enoate (4.63): IR (neat): 2975 (w), 2912 (w), 1730 (s), 1503 (m), 1487 (s), 1440 (s), 1375 (m), 1347 (w), 1302 (w), 1240 (s), 1174 (s), 1142 (s), 1097 (m), 1037 (s), 935 (s), 902 (m), 857 (m), 808 (s), 727 (w), 639 (m), 438 (w) cm^{-1} ; $^1\text{H NMR}$ (CDCl_3 , 400 MHz): δ 6.72 (1H, d, $J = 8.0$ Hz), 6.69 (1H, d, $J = 1.6$ Hz), 6.64 (1H, dd, $J = 8.0, 1.6$ Hz), 5.92 (2H, s), 5.02 (1H, td, $J = 6.8, 1.2$ Hz), 4.03 (2H, qd, $J = 6.8, 0.8$ Hz) 3.06 (1H, m), 2.62 (1H, dd, $J = 15.6, 6.8$ Hz), 2.47 (1H, dd, $J = 15.2, 8.8$ Hz), 2.31–2.19 (2H, m), 1.65 (3H, s), 1.55 (3H, s), 1.16 (3H, t, $J = 7.2$ Hz); $^{13}\text{C NMR}$ (CDCl_3 , 100 MHz): δ 172.6, 147.6, 146.0, 138.3, 133.7, 121.8, 120.6, 108.2, 107.8, 100.9, 60.4, 42.4, 41.0, 35.3, 25.9, 18.0, 14.3. HRMS (DART⁺): Calcd for $\text{C}_{17}\text{H}_{23}\text{O}_4$ $[\text{M}+\text{H}]^+$: 291.1596; Found: 291.1601. Specific rotation: $[\alpha]_{\text{D}}^{20.0}$ 6.61 (c 1.21, CHCl_3) for an enantiomerically enriched sample of 95:5 e.r.

Sample Name: *59-IV-187-b-4pro*
 Data Collected on: *nmr13-vnmr5400*
 Archive directory:
 Sample directory:
 FIDFile: PROTON
 Pulse Sequence: PROTON (s2pul)
 Solvent: cdcl3
 Data collected on: Dec 15 2016



Sample Name:
sy-IV-187-b-pro-C
Data Collected on:
mm13-vmmr400
Archive directory:
Sample directory:
FIDFile: CARBON
Pulse Sequence: CARBON (s2pul)
Solvent: cdcl3
Data collected on: Dec 15 2016



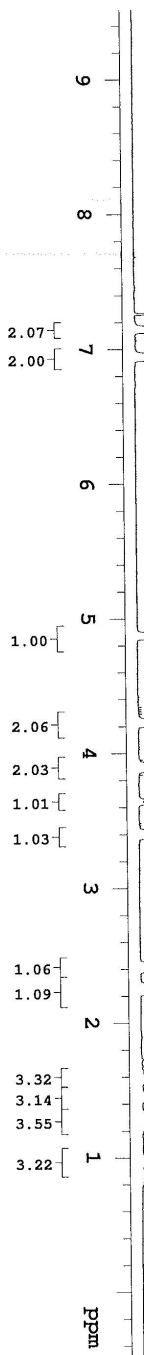


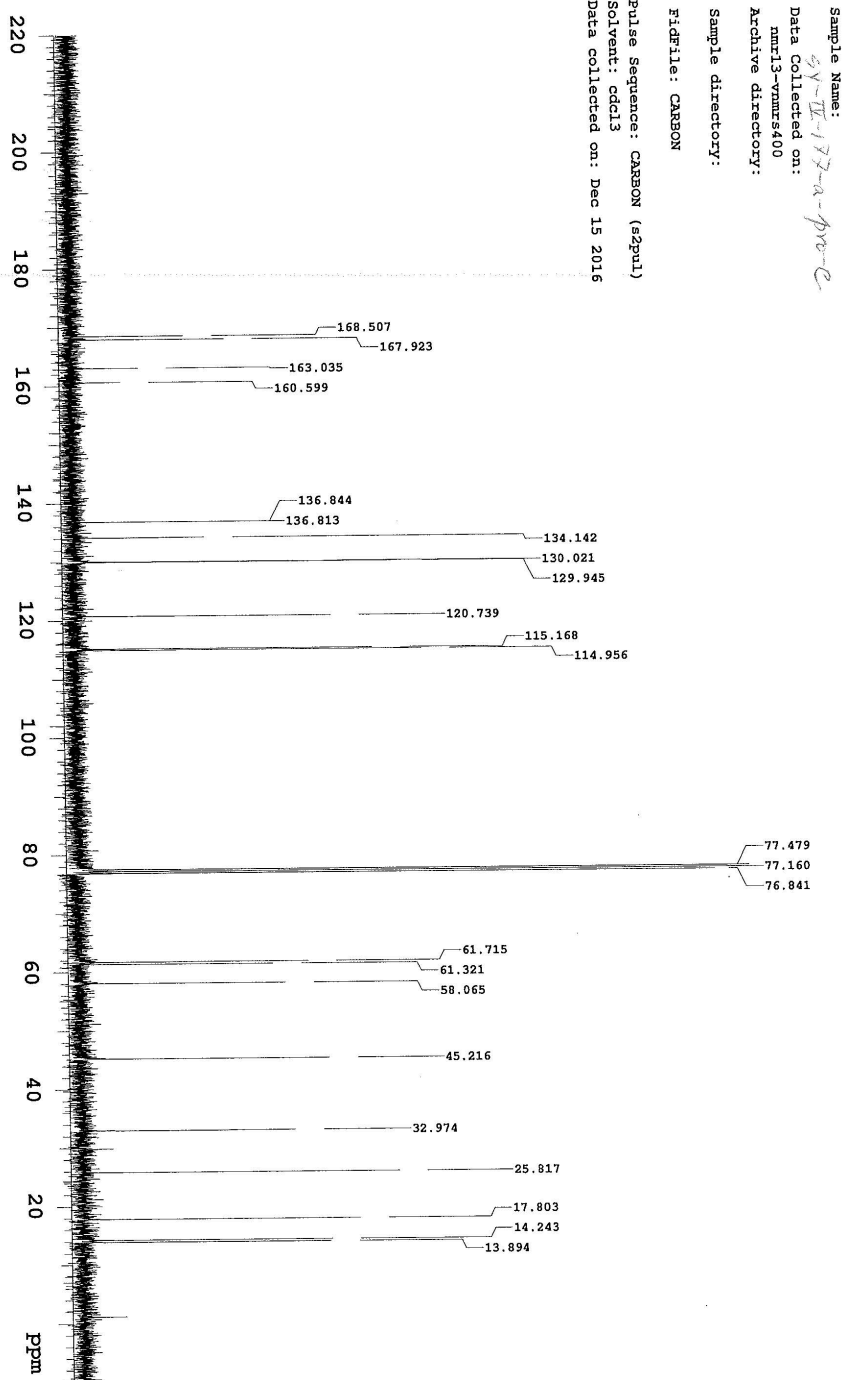
Sample Name: sy-IV-194-a-pro
 Data Collected on: nmr13-vnmr5400
 Archive directory:

Sample directory:

F1F1file: PROTON

Pulse Sequence: PROTON (s2pu1)
 Solvent: cdcl3
 Data collected on: Dec 28 2016



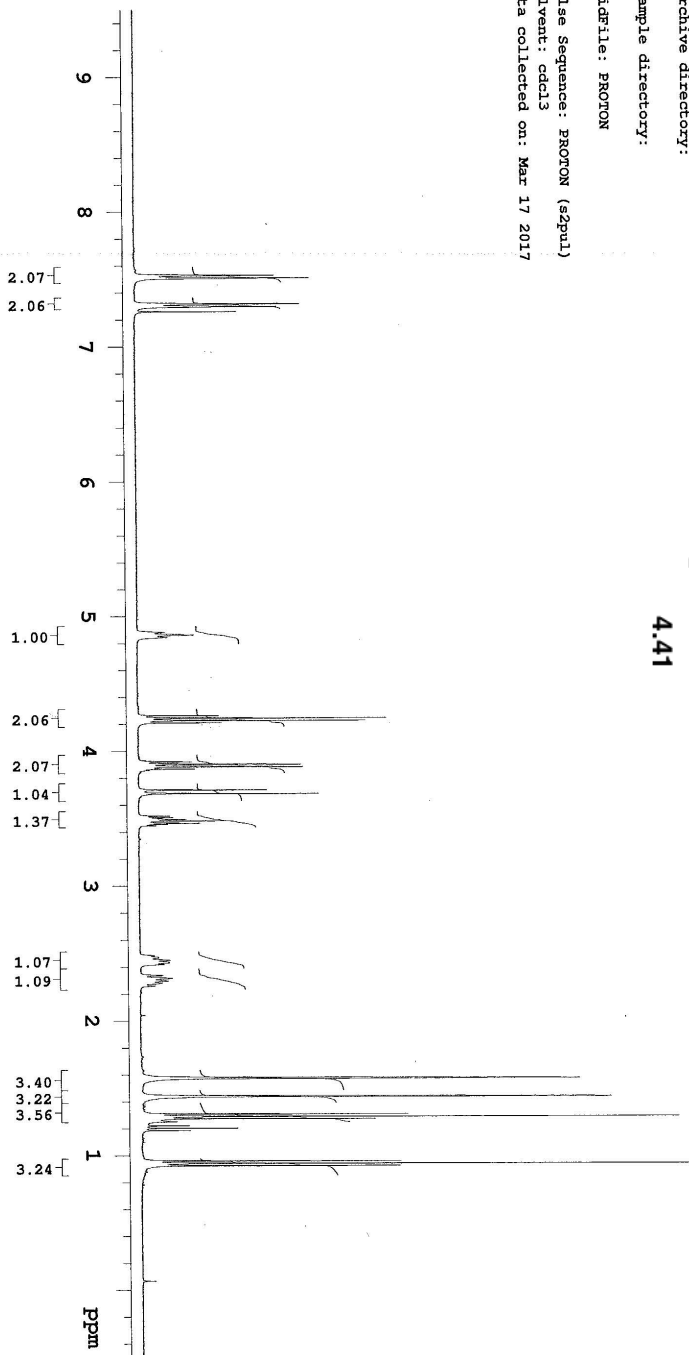
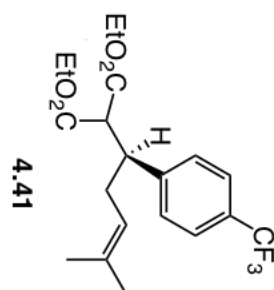


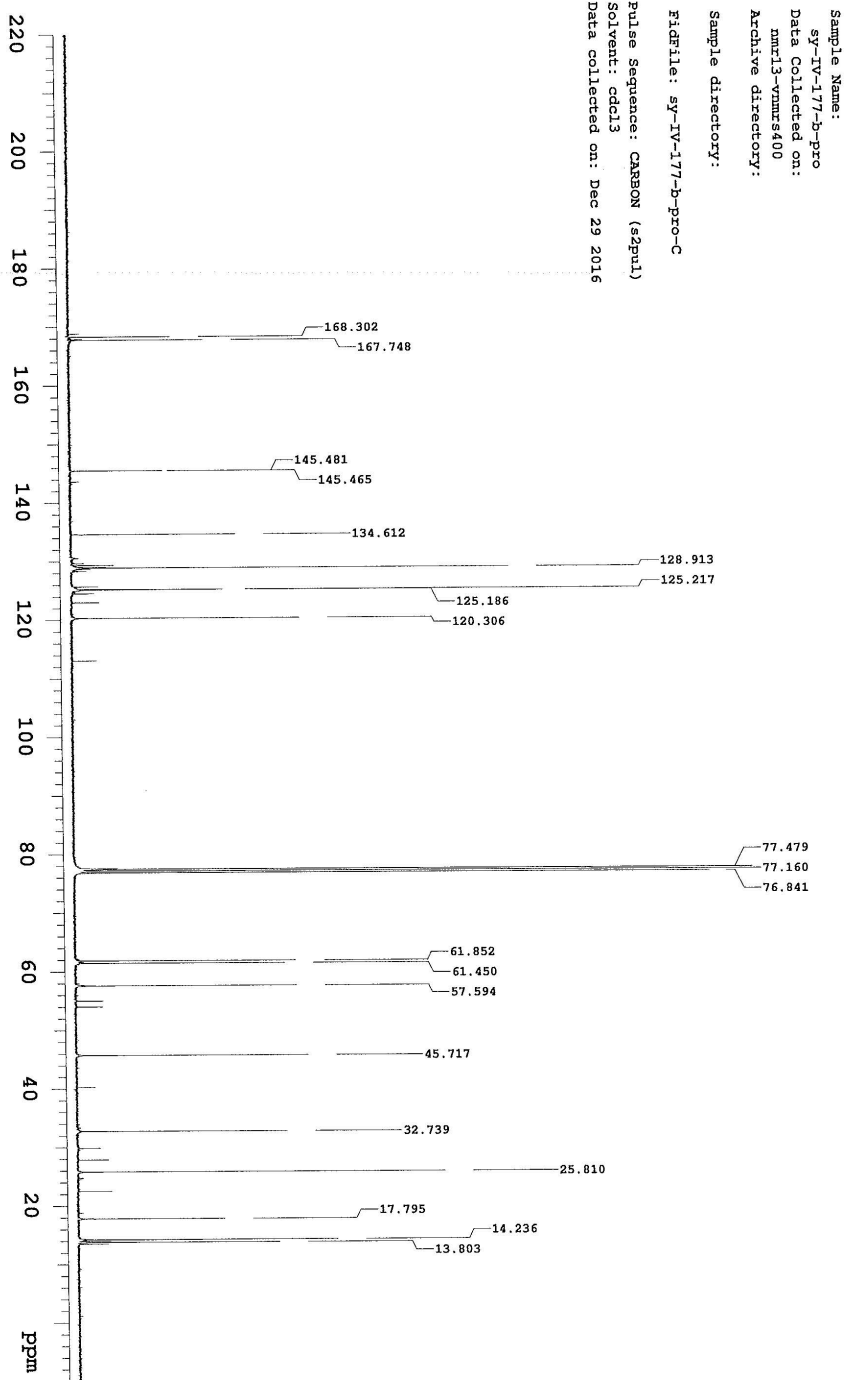
Sample Name:
 sy-1v-212-1-pro
 Data Collected on:
 mmr13-vnmrs400
 Archive directory:

Sample directory:

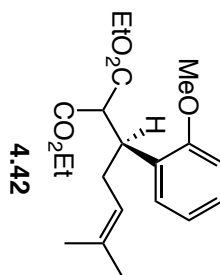
F1dFile: PROTON

Pulse Sequence: PROTON (s2pul)
 Solvent: cdcl3
 Data collected on: Mar 17 2017

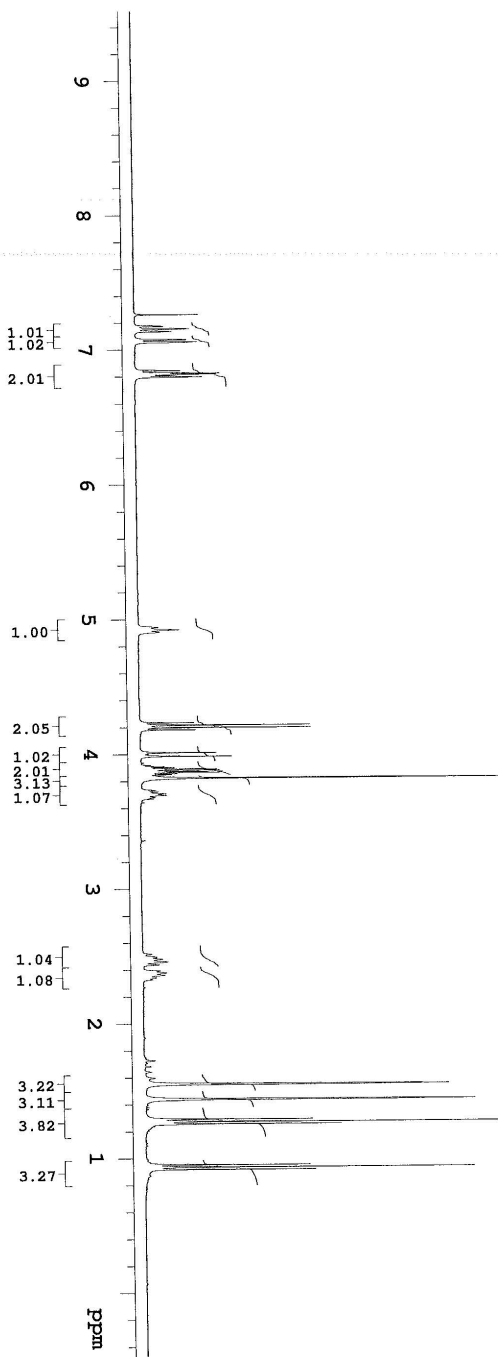




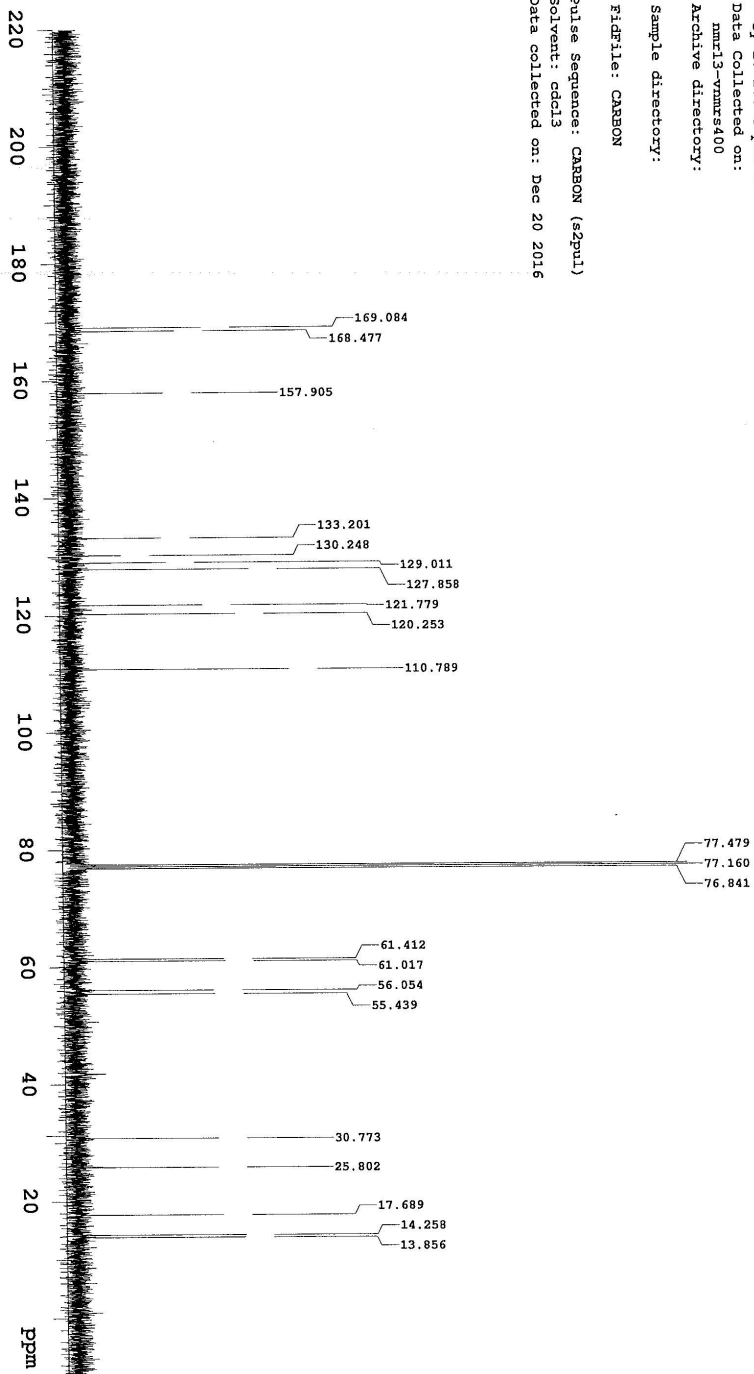
Sample Name: sy-iv-177-c-pro
 Data Collected on: mmr13-vmmrs400
 Archive directory:
 Sample directory:

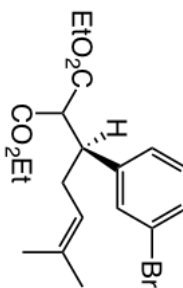


File: PROTON
 Pulse Sequence: PROTON (s2pu1)
 Solvent: cdcl3
 Data collected on: Dec 20 2016



Sample Name:
SY-IV-177-c-pro-C
Data Collected on:
mm13-vmars400
Archive directory:
Sample directory:
FidFile: CARBON
Pulse Sequence: CARBON (s2pul)
Solvent: cdcl3
Data collected on: Dec 20 2016

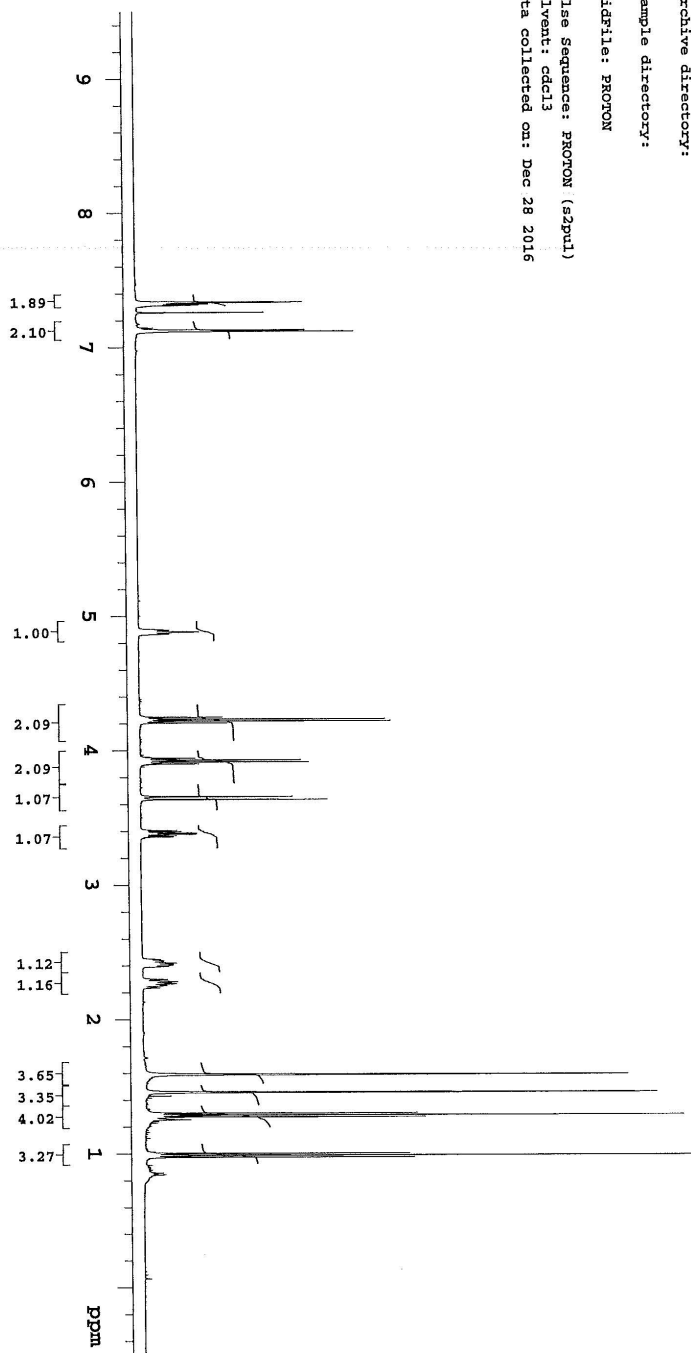


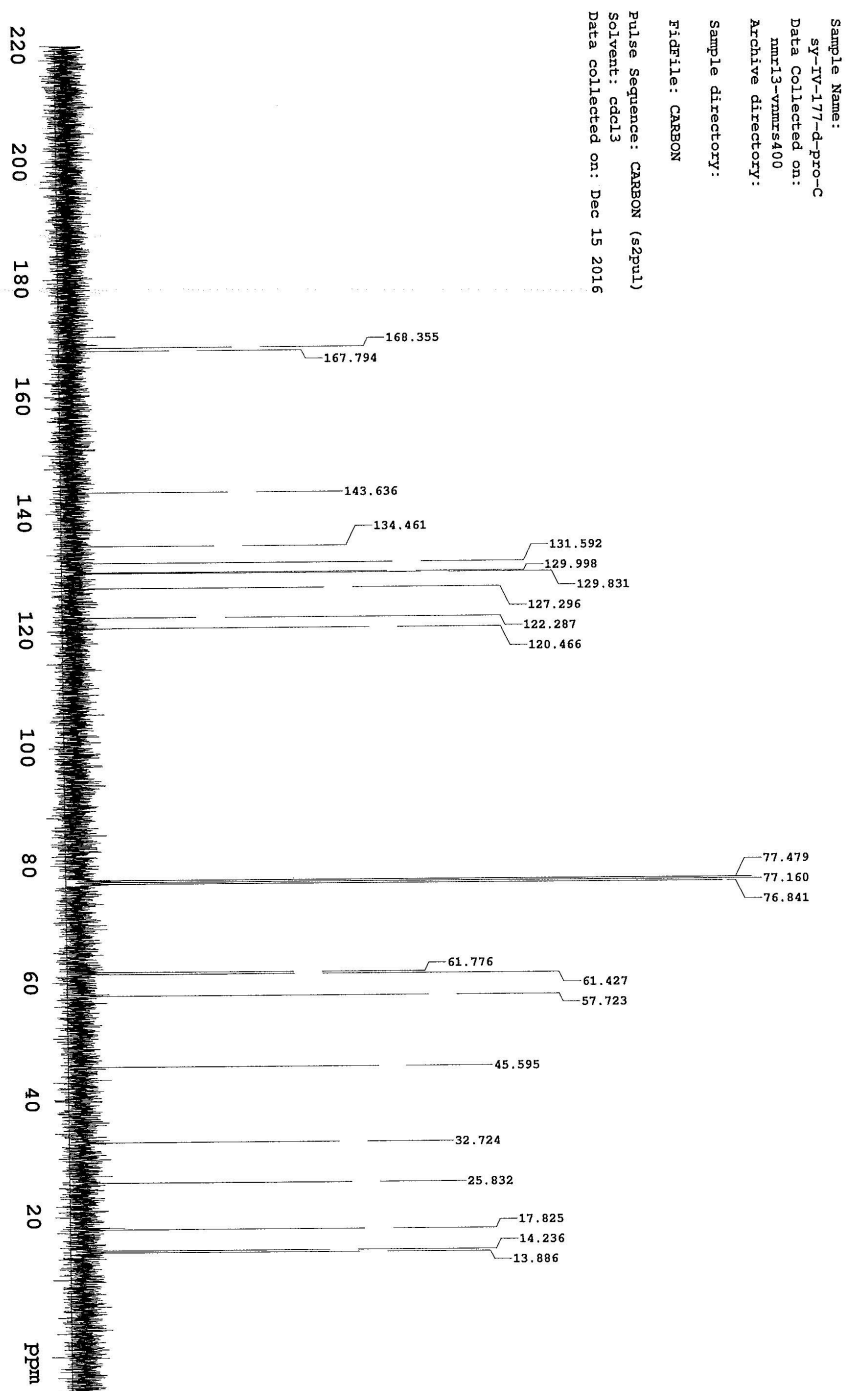


4.43

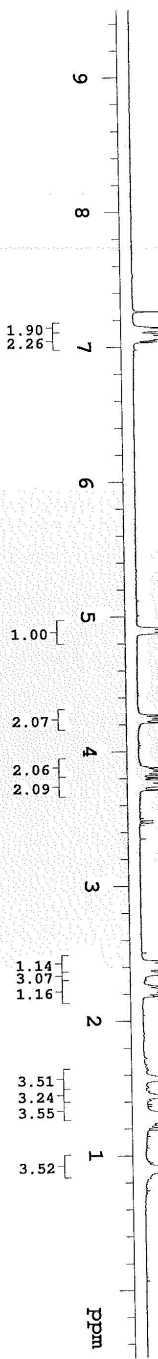
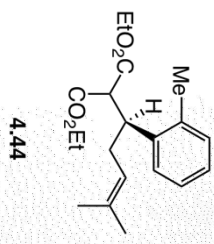


Sample Name: sy-IV-194-b-pro
 Data Collected on: mmx18-vnmr500
 Archive directory:
 Sample directory:
 Filefile: PROTON
 Pulse Sequence: PROTON (s2pul)
 Solvent: cdcl3
 Data collected on: Dec 28 2016

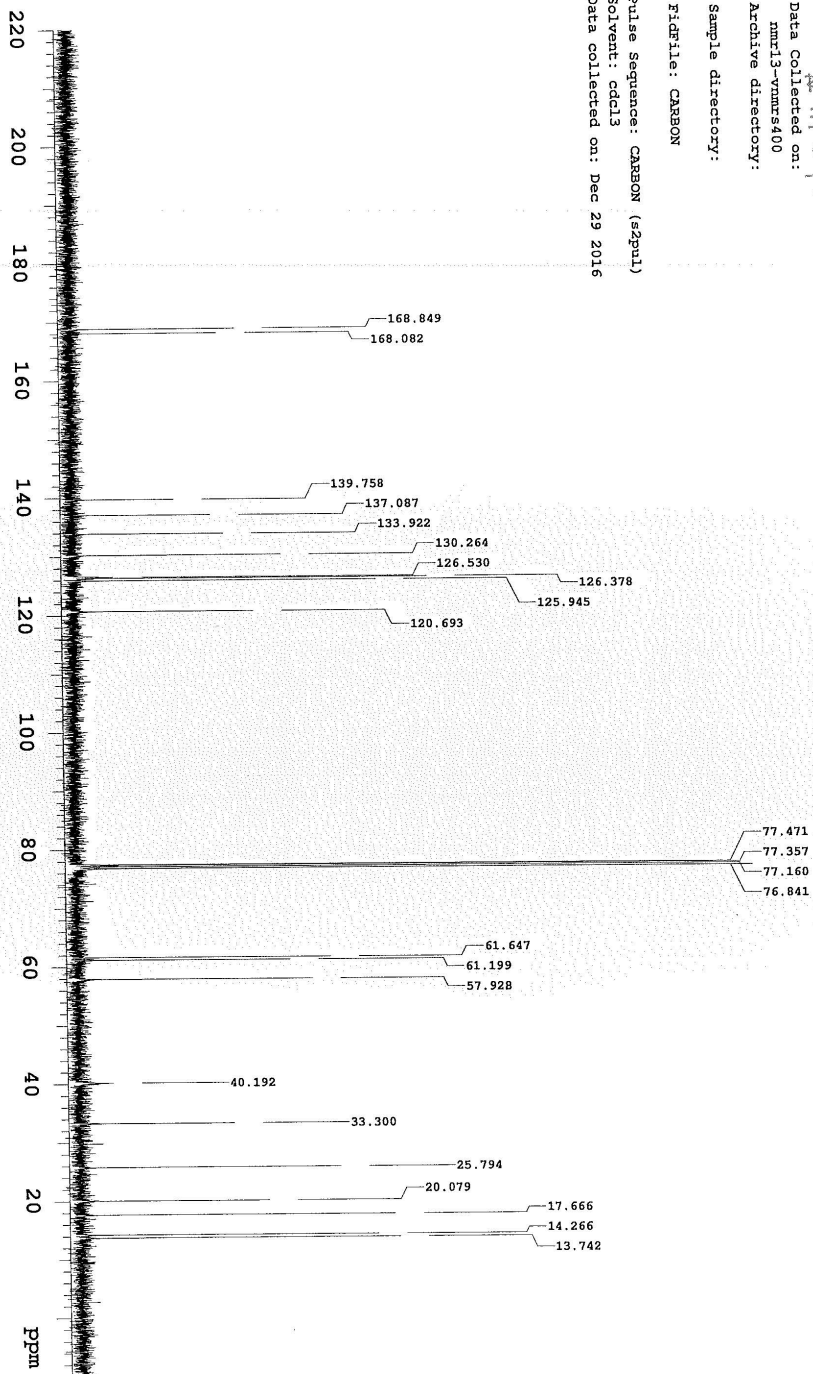


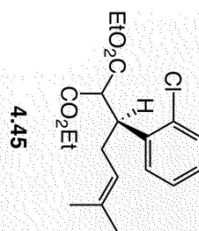


Sample Name:
 sy-IV-194-e-pro
 Data Collected on:
 nmr13-nmms400
 Archive directory:
 Sample directory:
 FIDfile: PROTON
 Pulse Sequence: PROTON (s2pu1)
 Solvent: cdcl3
 Data collected on: Dec 29 2016

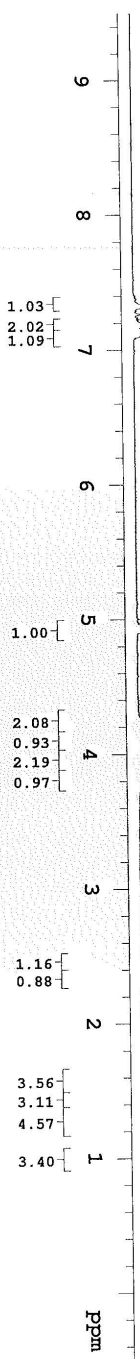


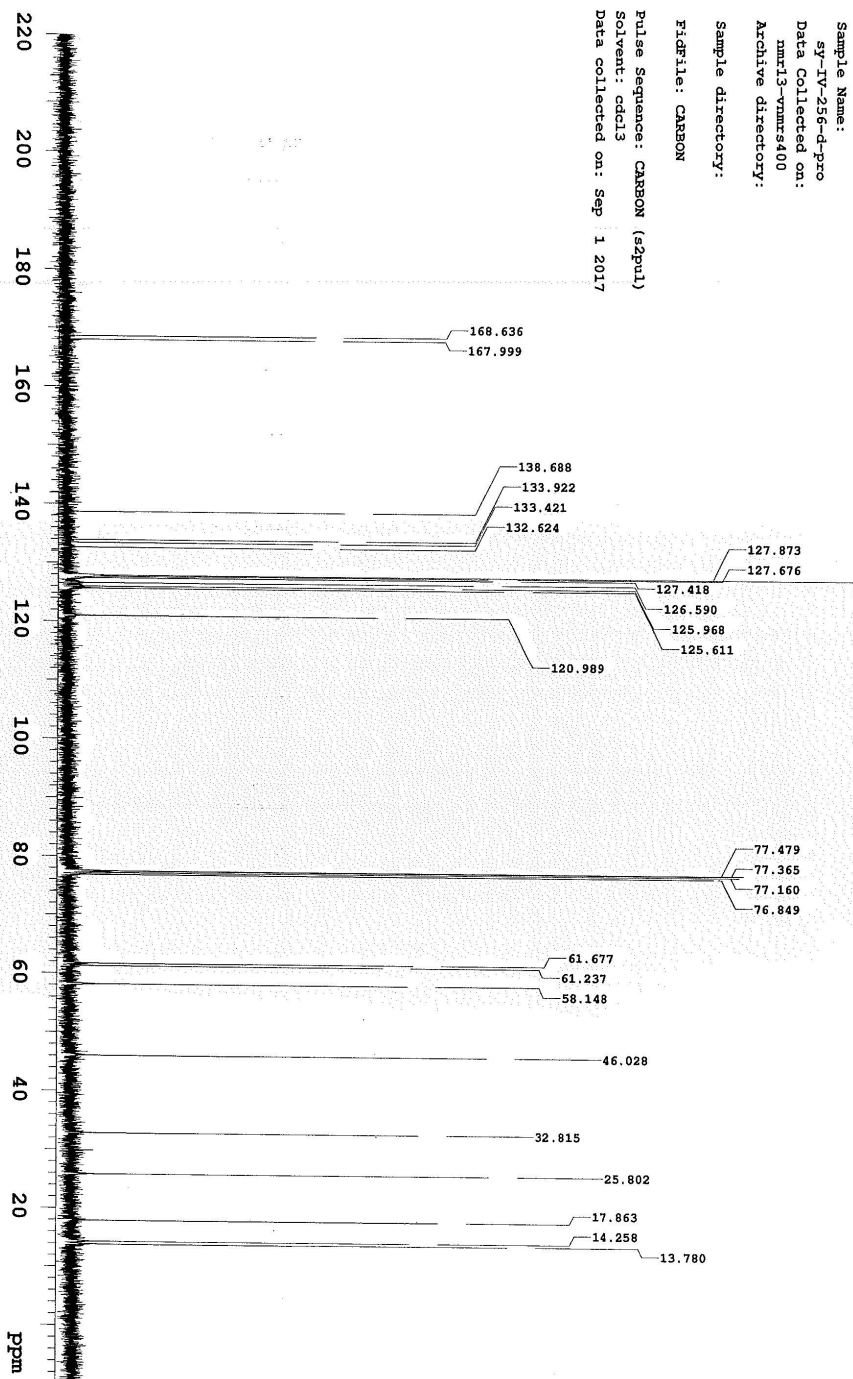
Sample Name: *11-19-0-AP-0-C*
Data Collected on: *11-19-0-AP-0-C*
nmr13-nmms400
Archive directory:
Sample directory:
Fidfile: CARBON
Pulse Sequence: CARBON (s2pu1)
Solvent: cdcl3
Data collected on: Dec 29 2016

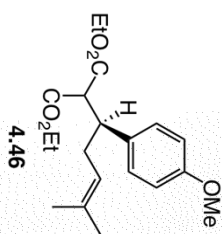




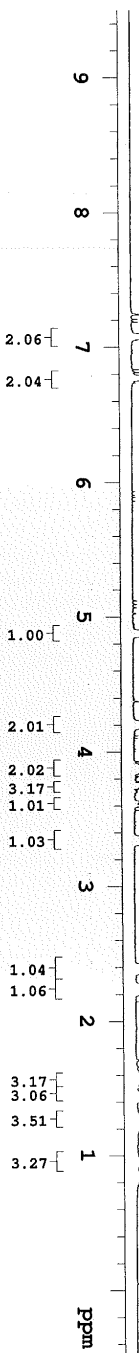
Sample Name:
 sy-IV-177-e-pro
 Data Collected on:
 nmr13-vnmrs400
 Archive directory:
 Sample directory:
 FILE: PROTON
 Pulse Sequence: PROTON (szpu1)
 Solvent: cdcl3
 Data collected on: Dec 29 2016



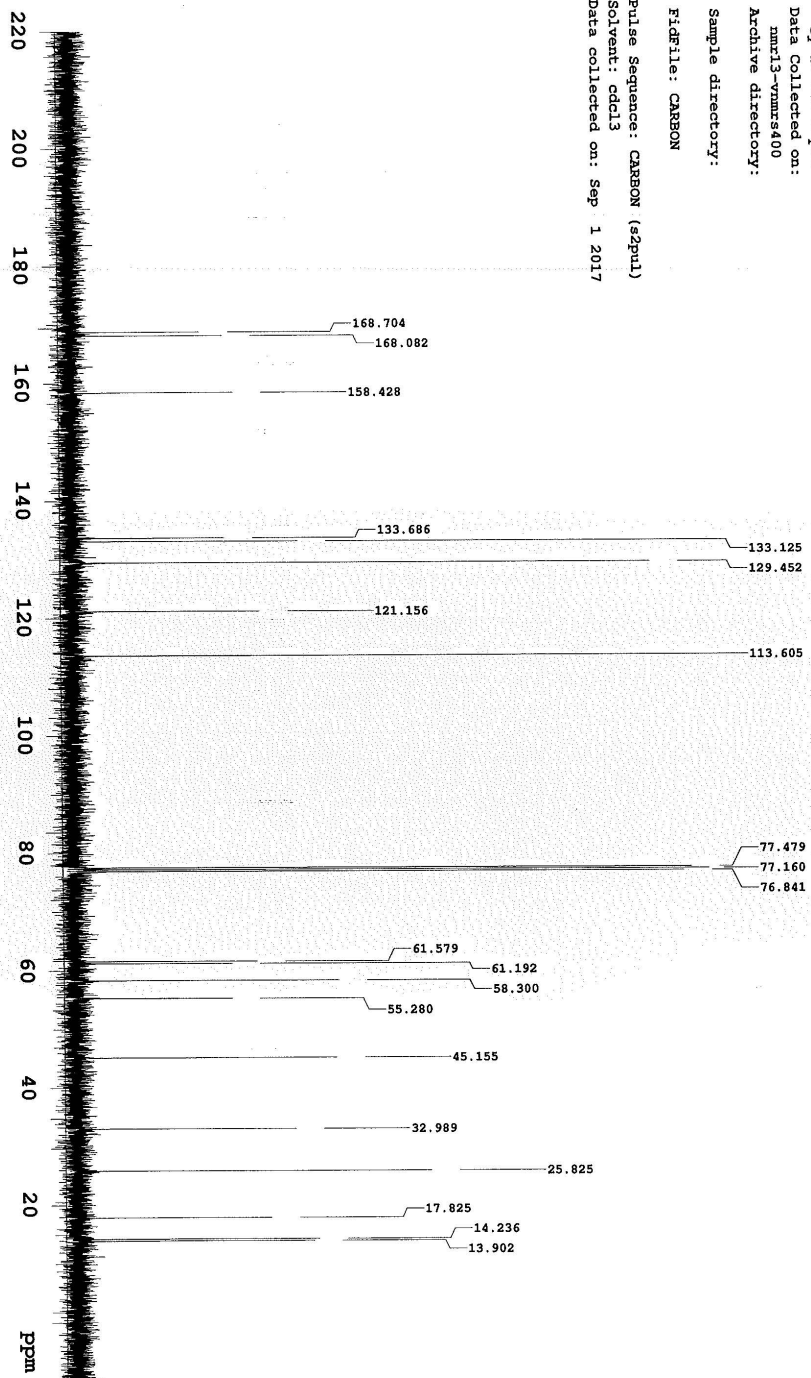




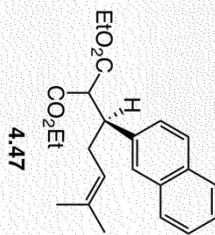
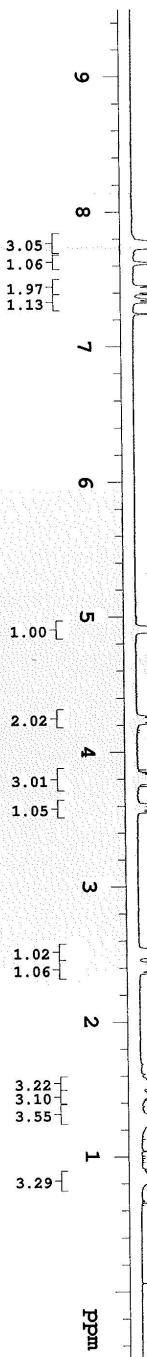
Sample Name: sy-IV-259-e-pro
 Data Collected on: nmr13-vnmr400
 Archive directory:
 Sample directory:
 Filefile: PROTON
 Pulse Sequence: PROTON (s2pu1)
 Solvent: cdcl3
 Data collected on: Sep 1 2017



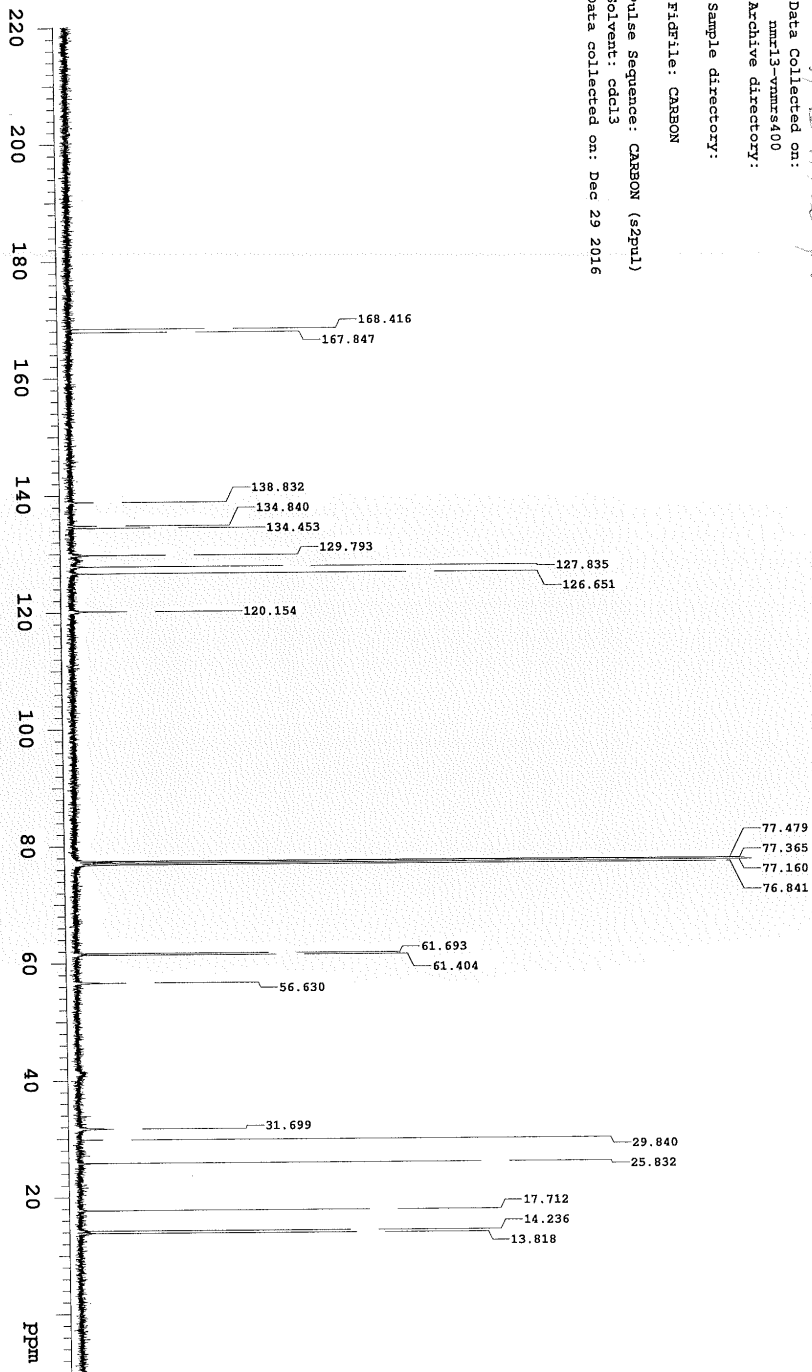
Sample Name: sy-IV-259-e-pro
Data Collected on: mm13-vnmrs400
Archive directory:
Sample directory:
FidFile: CARBON
Pulse Sequence: CARBON (s2pul1)
Solvent: cdcl3
Data collected on: Sep 1 2017



Sample Name: sy-IV-256-d-pro
 Data Collected on: nm13-vnmrs400
 Archive directory:
 Sample directory:
 FIDFile: sy-IV-256-d-pro
 Pulse Sequence: PROTON (s2pu1)
 Solvent: cdcl3
 Data collected on: sep 2 2017



Sample Name: *SY-III-172-E-40-C*
Data Collected on: *mm13-vmmrs400*
Archive directory:
Sample directory:
FidFile: CARBON
Pulse Sequence: CARBON (s2pul)
Solvent: cdcl3
Data collected on: Dec 29 2016

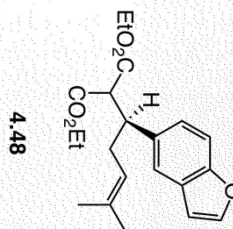
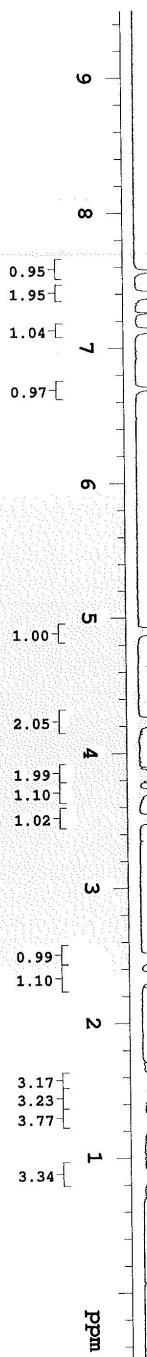


Sample Name:
 sy-1v-256-e-pro
 Data Collected on:
 nmr13-vnmrs400
 Archive directory:

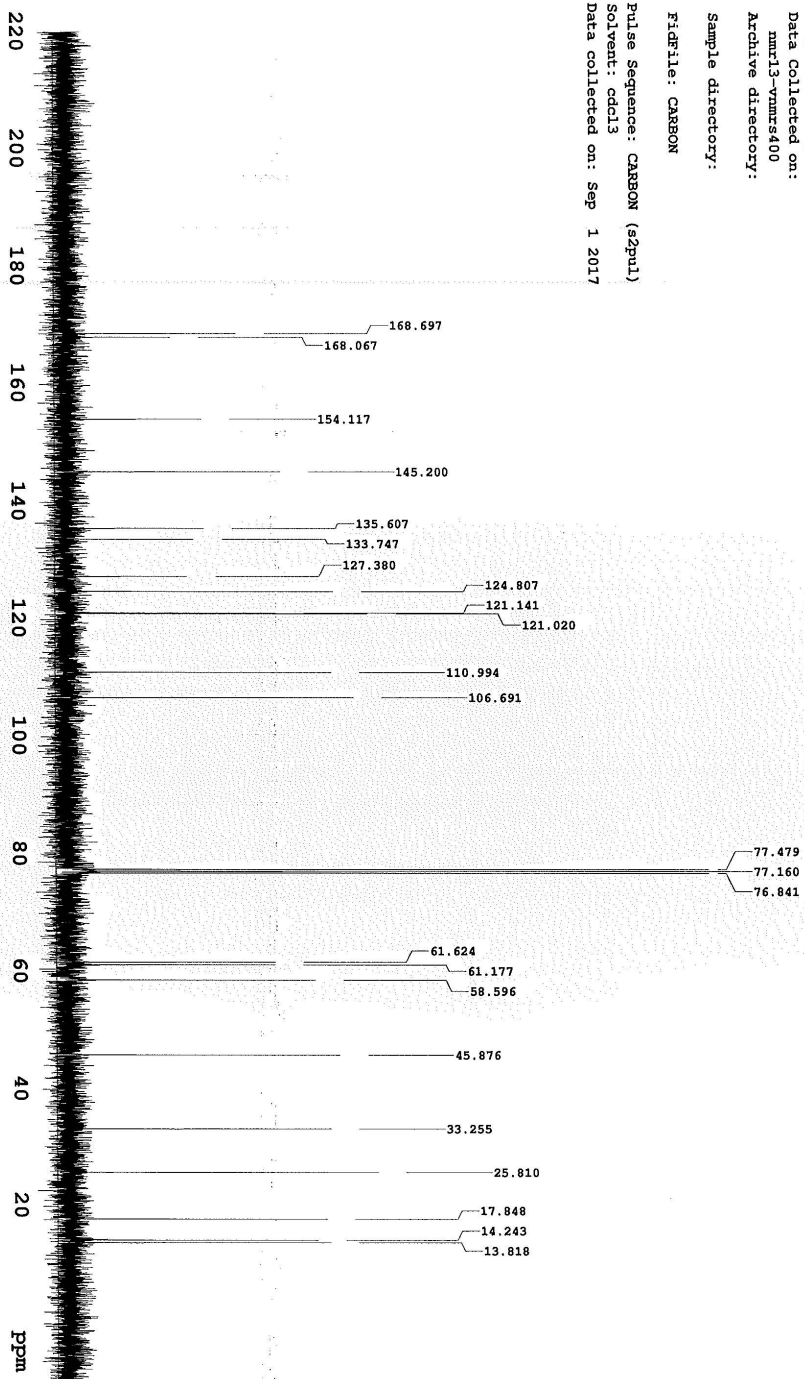
Sample directory:

F1: File: PROTON

Pulse Sequence: PROTON (s2pu1)
 Solvent: cdcl3
 Data collected on: Sep 1 2017



Sample Name: sy-IV-256-e-pro
Data Collected on: mmr13-vmr1s400
Archive directory:
Sample directory:
FIDFile: CARBON
Pulse Sequence: CARBON (s2pul)
Solvent: cdcl3
Data collected on: sep 1 2017

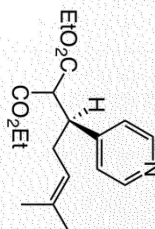


Sample Name:
 sy-1V-262-b-pro
 Data Collected on:
 mm13-vnmr5400
 Archive directory:

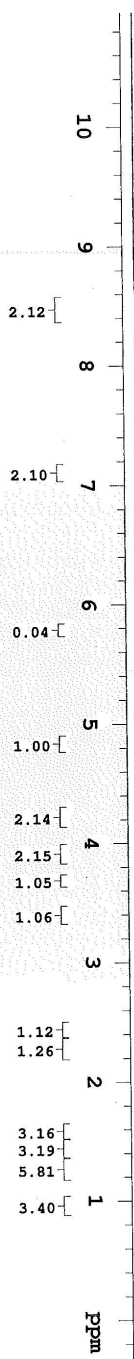
Sample directory:

FidFile: PROTON

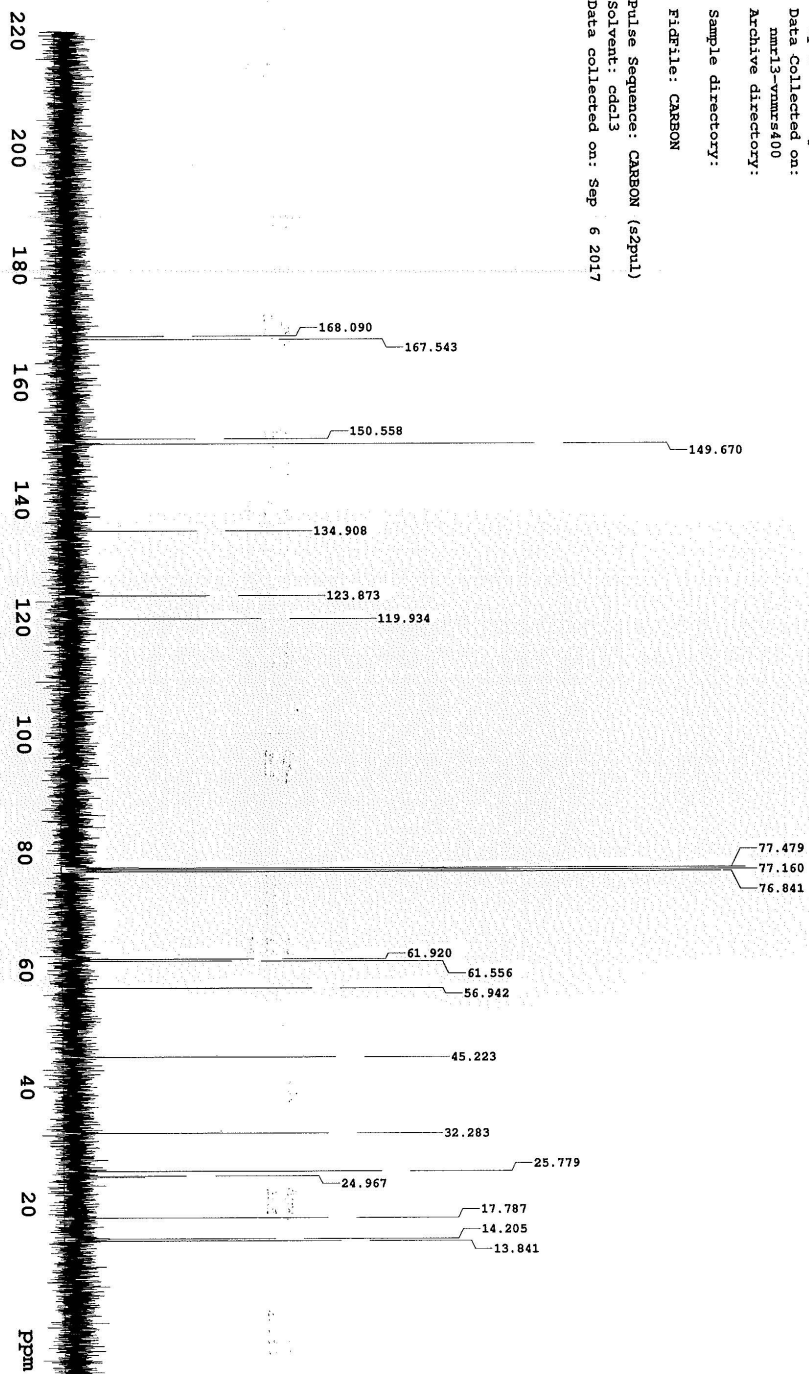
Pulse Sequence: PROTON (szpu1)
 Solvent: cdcl3
 Data collected on: Sep 6 2017



4.49



Sample Name: sy-IV-262-b-pro
Data Collected on: mm13-vmmr400
Archive directory:
Sample directory:
FidFile: CARBON
Pulse Sequence: CARBON (szpul)
Solvent: cdcl3
Data collected on: Sep 6 2017

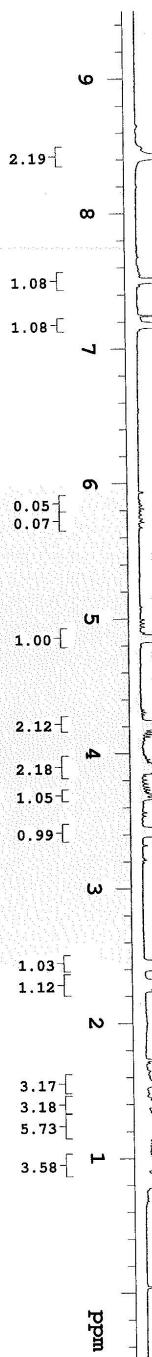
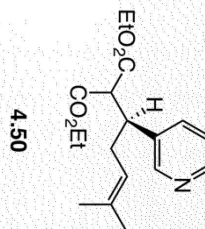


Sample Name:
 sy-IV-259-d-pro
 Data Collected on:
 mmr13-vmr400
 Archive directory:

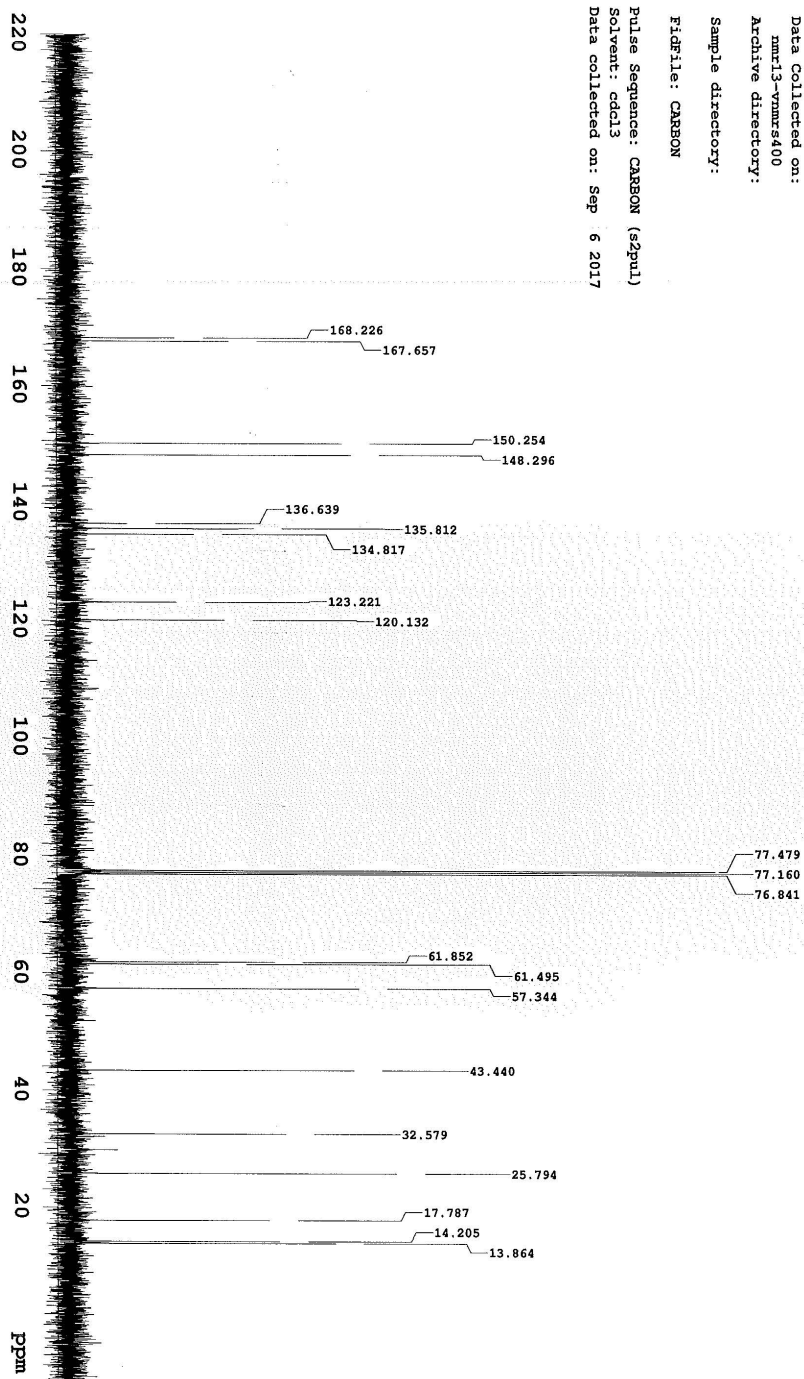
Sample directory:

File: PROTON

Pulse Sequence: PROTON (s2pu1)
 Solvent: cdcl3
 Data collected on: Sep 6 2017



Sample Name: SY-IV-259-d-pro
Data Collected on: mmr13-vmmr-s400
Archive directory:
Sample directory:
FIDFile: CARBON
Pulse Sequence: CARBON (s2pul)
Solvent: cdcl3
Data collected on: Sep 6 2017

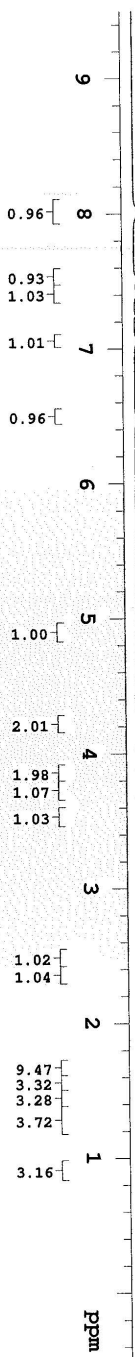
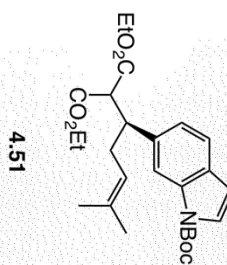


Sample Name:
 sy-IV-273-c-pro
 Data Collected on:
 mmr13-vmr400
 Archive directory:

Sample directory:

File: PROTON

Pulse Sequence: PROTON (s2pu1)
 Solvent: cdcl3
 Data collected on: Aug 22 2017



Probe tuning parameter

Sample Name:

SY-IV-223-c-pro-C

Data Collected on:

nmr13-vmr5400

Archive directory:

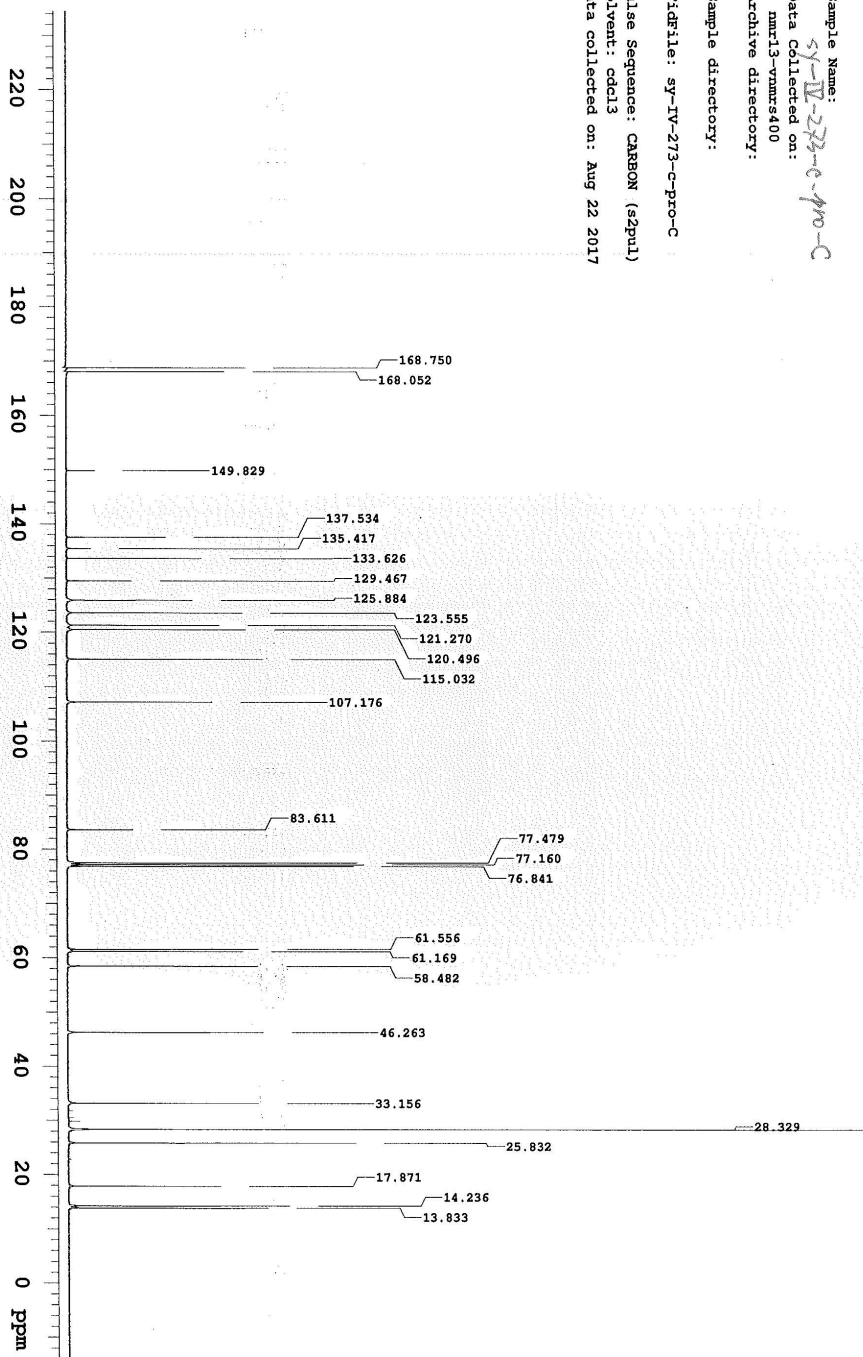
Sample directory:

FidFile: sy-IV-273-c-pro-C

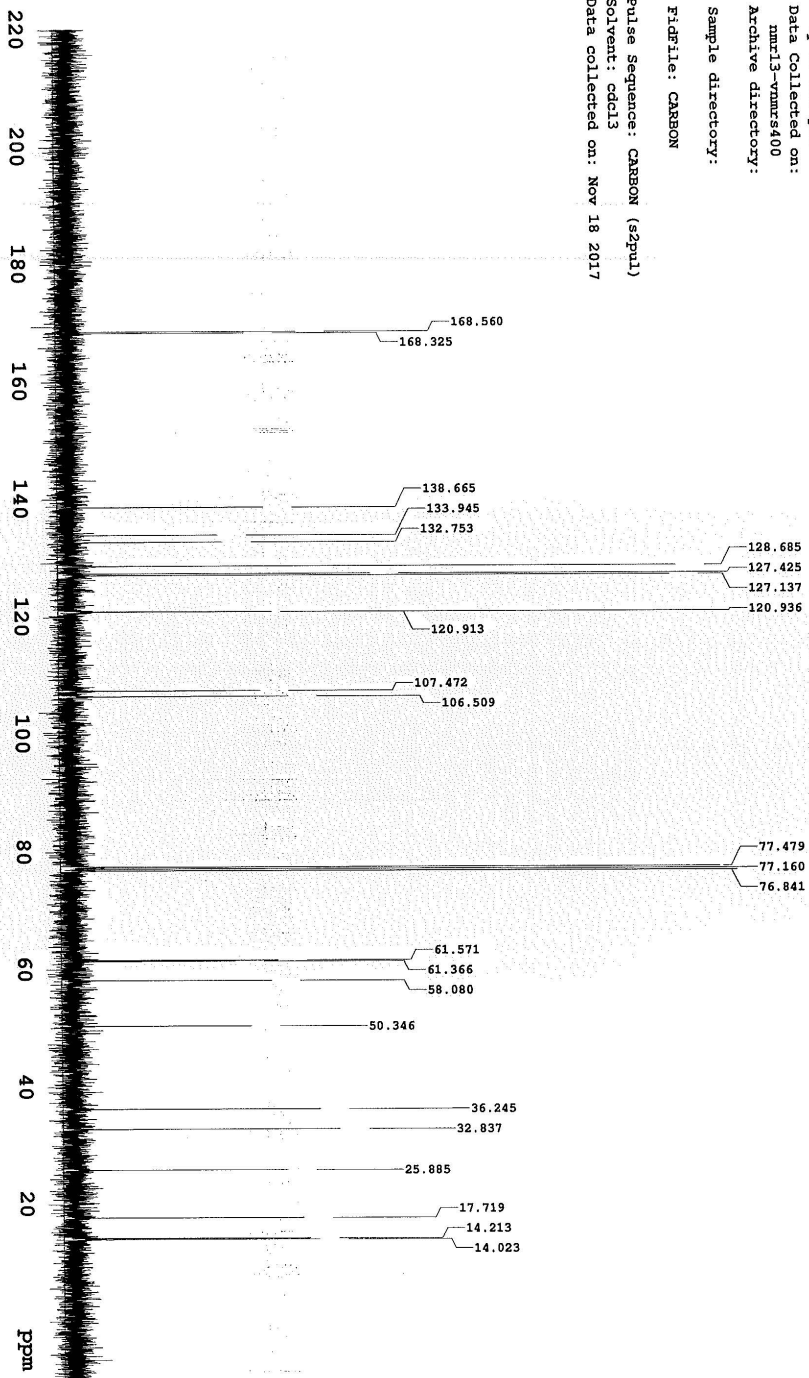
Pulse Sequence: CARBON (s2pul)

Solvent: cdcl3

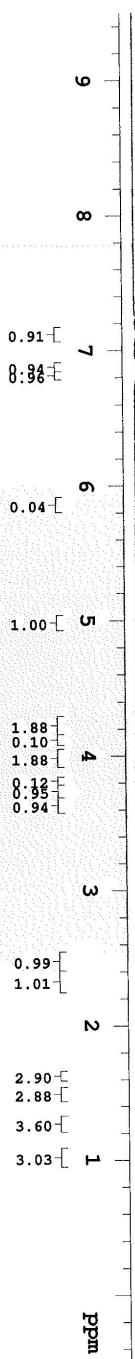
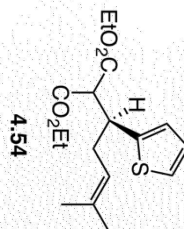
Data collected on: Aug 22 2017



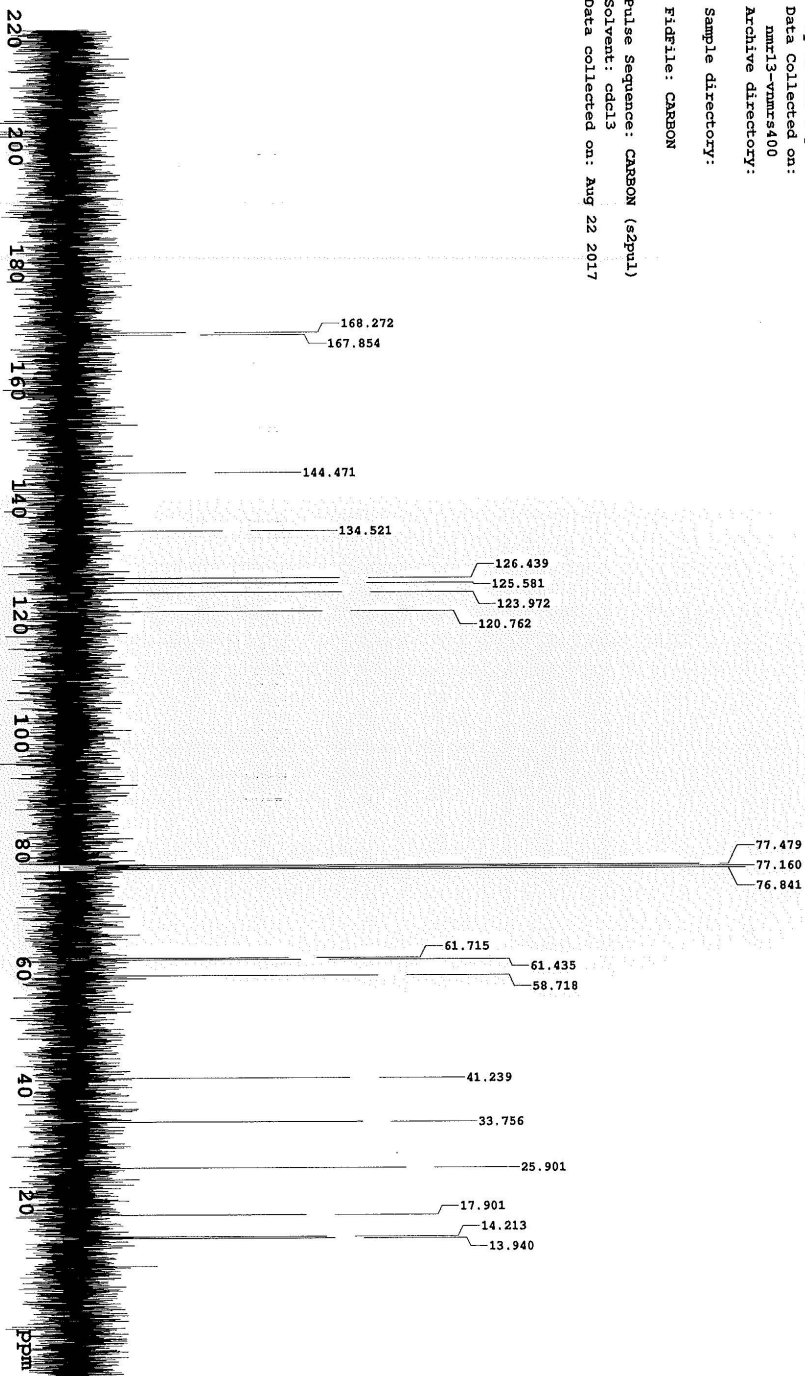
Sample Name: sy-IV-289-pro
Data Collected on: mmr13-vmmrs400
Archive directory:
Sample directory:
FIDFile: CARBON
Pulse Sequence: CARBON (szpul)
Solvent: cdcl3
Data collected on: Nov 18 2017

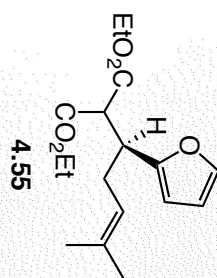


Sample Name: sy-IV-273-c-pro-C
 Data Collected on: mm13-vmmrs400
 Archive directory:
 Sample directory:
 FIDFile: PROTON
 Pulse Sequence: PROTON (s2pul)
 Solvent: cdcl3
 Data collected on: Aug 22 2017

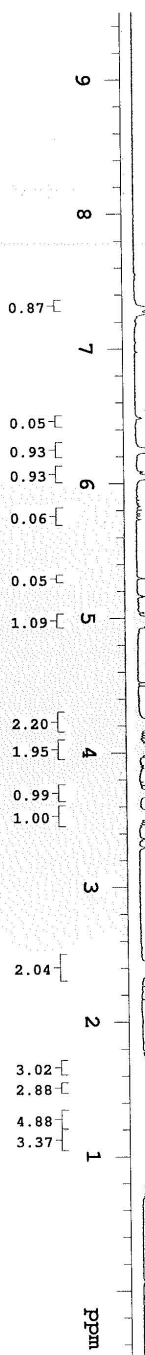


Sample Name: SY-IV-273-b-pro-C
Data Collected on: mmr13-vnmrs400
Archive directory:
Sample directory:
F1 file: CARBON
Pulse Sequence: CARBON (s2pu1)
Solvent: cdcl3
Data collected on: Aug 22 2017

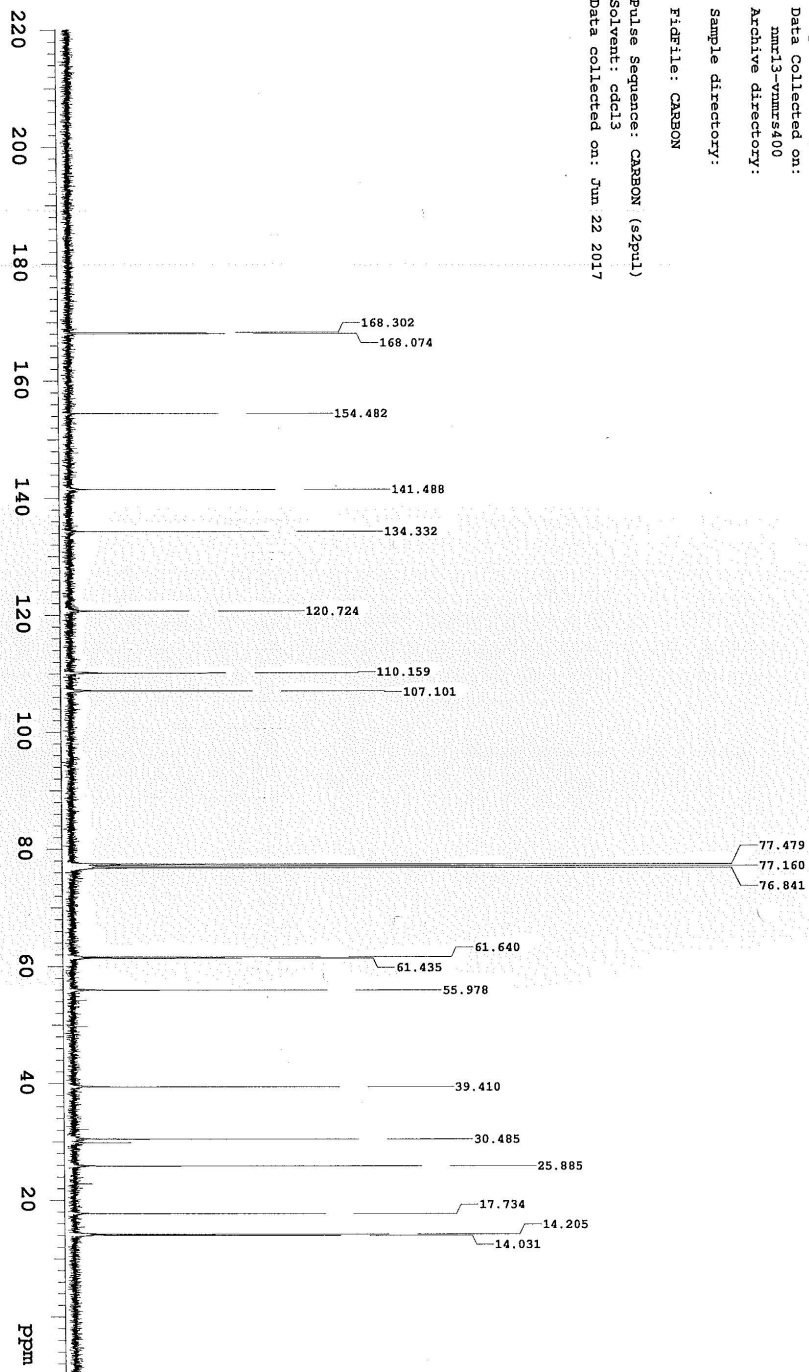




Sample Name: sy-IV-259-g-pro
 Data Collected on: nmr13-vmrms400
 Archive directory:
 Sample directory:
 FIDfile: PROTON
 Pulse Sequence: PROTON (s2pul)
 Solvent: cdcl3
 Data collected on: Jun 21 2017

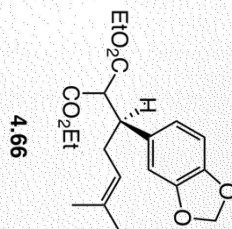
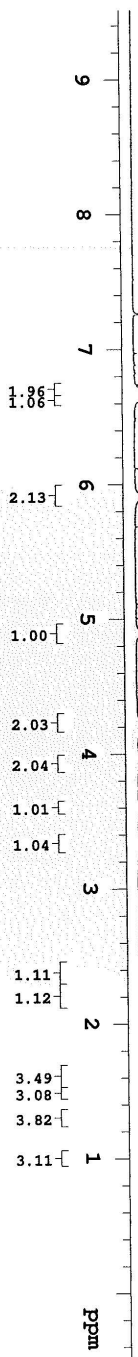


Sample Name: sy-IV-259-a-pro-C
Data Collected on: mmr13-vmmr9400
Archive directory:
Sample directory:
F1: FILE: CARBON
Pulse Sequence: CARBON (s2pm1)
Solvent: cdcl3
Data collected on: Jun 22 2017



Sample Name:
 sy-iv-282d-pro
 Data Collected on:
 mm14-vnmrs400
 Archive directory:
 Sample directory:

F1F1File: PROTON
 Pulse Sequence: PROTON (s2pu1)
 Solvent: cdcl3
 Data collected on: Sep 6 2017



Probe tuning parameter

Sample Name:

Data Collected on:

nmr14-ymmr5400

Archive directory:

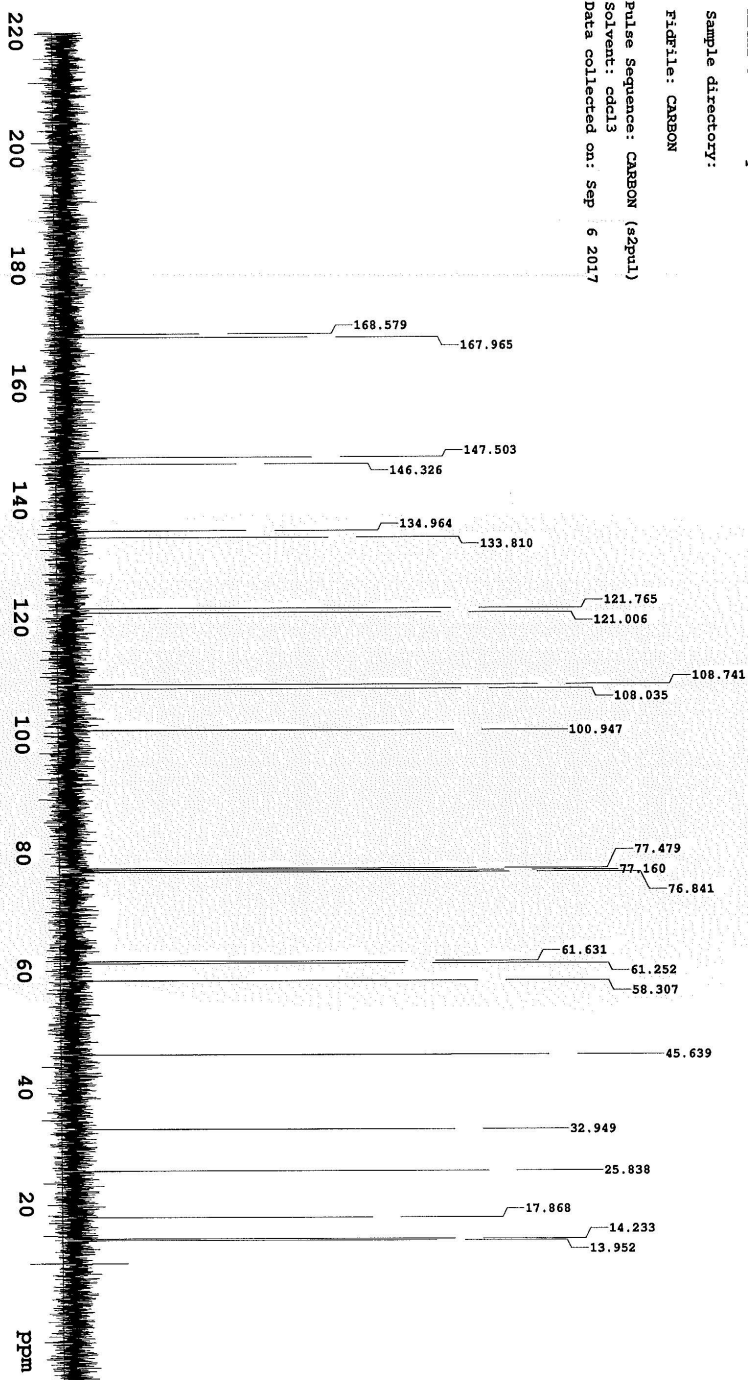
Sample directory:

F1:File: CARBON

Pulse Sequence: CARBON (s2pul)

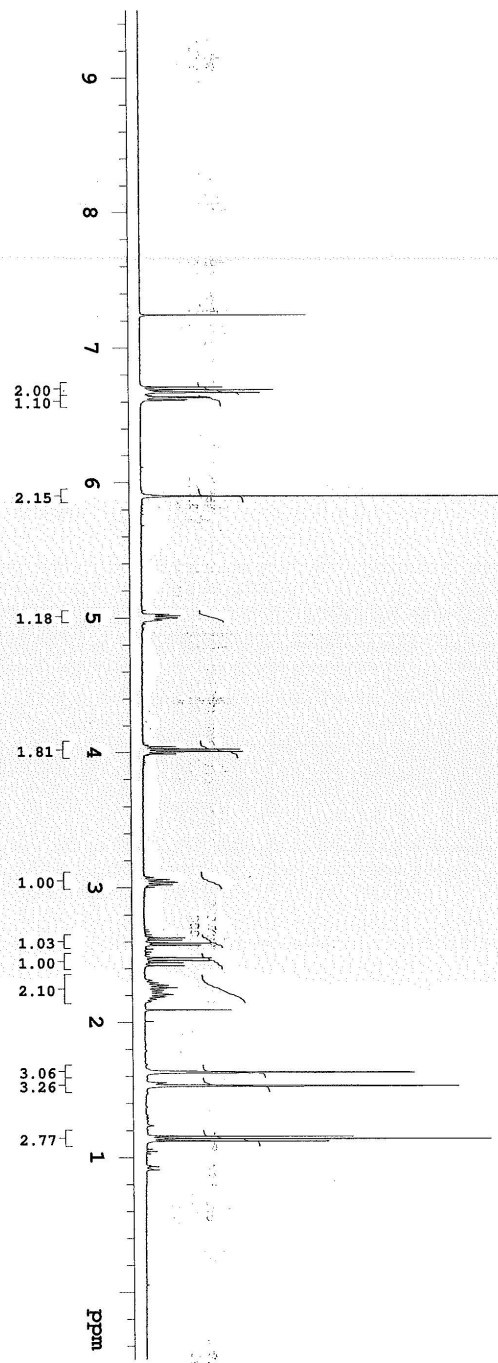
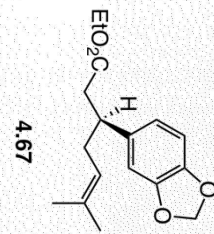
Solvent: cdcl3

Data collected on: Sep 6 2017



Sample Name: sy-IV-266-pro
 Data Collected on: mmr13-vmmr8400
 Archive directory:
 Sample directory:
 FIDFile: PROTON

Pulse Sequence: PROTON (sgpu1)
 Solvent: cdcl3
 Data collected on: Oct 18 2017



Sample Name:
sv-IV-266-pro
Data Collected on:
mmr13-vmmr5400
Archive directory:
Sample directory:
FIDFile: CARBON
Pulse Sequence: CARBON (s2pul)
Solvent: cdcl3
Data collected on: Oct 18 2017

